MTA doktori értekezés
tézises forma

A DNS-építőkövek dinamikájának szerepe a genomstabilitásban

Tóth Judit

Budapest

2021

Tartalomjegyzék

1 Az értekezésben bemutatott munka előzményei, szakmai hozzájárulás 4

2 Tudományterületi háttér 5

3 Célkitűzések 8

4 Alkalmazott módszertan és modellszervezetek 9

4.1 Molekuláris biológiai és géntechnológiai módszerek 9

4.1.1 Rekombináns fehérjék előállítása 9

4.1.2 mRNS és fehérjeexpressziós szintek vizsgálata 9

4.1.3 dNTP készlet mennyiségi meghatározása 9

4.1.4 Mikobakteriális géntechnológia, a *M. smegmatis* mutáns törzsek létrehozása 9

4.2 Fehérje szerkezet-funkció vizsgáló módszerek 9

4.2.1 Oldatbeli fehérjeszerkezet vizsgáló módszerek 9

4.2.2 Kinetikai módszerek 10

4.2.3 Termodinamikai módszerek 10

4.2.4 Elektroforézis technikák 10

4.2.5 Krisztallográfia, szerkezeti modellezés 11

4.2.6 Molekuláris dinamikai és kvantumkémiai számítások 11

5 Eredmények 12

5.1 A humán dUTPáz enzimatikus mechanizmusa 12

5.1.1 A hidrolízis ciklus kvantitatív kinetikai modellje 12

5.1.2 Az enzim és szubsztrát közötti π-π kölcsönhatás hozzájárul az átmeneti állapot stabilizálásához 15

5.1.3 A dUTPáz P-hurokszerű motívumot alkalmaz a katalitikus hatékonyság fokozására, és a nukleotid foszforiláltsági állapotainak megkülönböztetésére 18

5.1.4 Csereviszony a kooperativitás és a specificitás között az uracil-mentes DNS fenntartásáért 22

5.1.5 A P-hurokszerű motívum mutációi szétkapcsolják a protonátvitelt és a foszfáthasítást a dUTPáz katalizálta reakcióban 25

5.1.6 A dUTPáz rejtett aktív helye a fehérje kis amplitúdójú konformációs változásain keresztül érhető el 27

5.1.7 Inert kelátor? Az EDTA szorosan köti a dUTPázt, a Taq DNS polimerázt és a MutT enzimet, és gátolja a dUTPáz aktivitást 30

5.2 A dUTPáz élettani szerepe 33
5.2.1 A dUTPáz fehérje és a mikobaktérium-specifikus felszíni hurok nélkülözhetetlen a *M. smegmatis* életképességéhez 33
5.2.2 Fiziológiás funkciók szétválása a dUTPáz szupercsaládon belül: specializáció a dTTP bioszintézisére és a genomi integritás fenntartására 35
5.2.3 A dUTPáz génexpresszió-szabályozásban betöltött szerepének mechanizmusa 39
5.3 A dNTP készlet mérése és összefüggései a sejt életfolyamataival 43
5.3.1 Felhasználóbarát, nagy áteresztőképességű módszer fejlesztése a biológiai mintákból származó dNTP pontos mennyiségi meghatározására 43
5.3.2 A biológiai mintákban mért dNTP készletek és készletváltozások adatbázisa 47
6 Irányok és tervek 49
7 Az új tudományos eredmények tézises összefoglalása 51
8 Köszönetnyilvánítás 53
9 Rövidítésjegyzék 54
10 Irodalomjegyzék 55
10.1 A PhD fokozat megszerzése óta megjelent, az értekezés alapjául szolgáló levelező szerzős közlemények 55
10.2 A PhD fokozat megszerzése óta megjelent, az értekezéshez fel nem használt, de annak témájához kötődő saját közlemények 56
10.3 A PhD fokozat megszerzése óta megjelent, az értekezés témájához nem kötődő saját közlemények 57
10.4 Felhasznált irodalom 57
11 Függelék 68

1 Az értekezésben bemutatott munka előzményei, szakmai hozzájárulás

PhD munkám során, az USA-ban, elsajátítottam számos, az összetett működésű motor enzimek működési mechanizmusának vizsgálatához szükséges kísérleti technikát és egyfajta kinetikai, kvantitatív kutatói szemléletet. Ezekkel felvértezve, egy EMBO Long Term posztdoktori pályamunka keretében csatlakoztam az MTA Enzimológiai Intézet Genom Metabolizmus munkacsoportjához és kezdtem bele abba a kutatásba, amelynek eredményei jelentős részben az értekezés tárgyát képezik. A munkacsoport vezetője, Vértessy Beáta, előzőleg feltárta az *Escherichia coli* dUTPáz katalizálta nukleotidhidrolízis szerkezeti alapjait a posztdoktori munkája[1–3], majd a saját munkacsoportjával folytatott kutatómunka során[4]. A munkacsoport eredményesen tanulmányozta továbbá egy retrovirális (Mason-Pfizer majomvírus), nukleokapszid fehérjével fuzionált dUTPáz enzimatikus működését[5–7], és *Drosophila melanogaster* modellben a szerkezet-funkció vizsgálatokon kívül a dUTPáz élettani szerepét is[8,9]. Érkezésem előtt a munkacsoport figyelme a *Mycobacterium tuberculosis* (*M. tuberculosis*) baktérium dUTPáza felé fordult, amelynek nagyfelbontású szerkezetén dolgoztak éppen[10]. A *M. tuberculosis* a tuberkulózis kórokozója, és anyagcseréjében a dUTPáz kitüntetett szereppel bír. A téma potenciális orvosbiológiai jelentősége és újdonságereje miatt ebből a témából nyújtottam be az említett EMBO, és később, már saját kutatási eredményekre is alapozva, a nyertes NIH programgrant-pályázatomat is. Részben utóbbi forrásból létrehoztunk a Genom Metabolizmus laboratóriumban egy élvonalbeli gyorskinetikai platformot, amely lehetővé tette az elsajátított enzimkinetikai ismeretek itthoni használatát és továbbadását. Egy másik vonalon első doktoranduszhallgatóm, Pécsi Ildikó EMBO és FEMS ösztöndíjak keretében történt tanulmányútjainak nyomán meghonosítottuk a nem-patogén *Mycobacterium smegmatis* (*M. smegmatis*) modell rendszert, amely a DNS anyagcsere tárgyában jól modellezi a tuberkulózis kórokozóját.

Az eltelt 15 év során a dUTPáz példáján általános fehérje szerkezet-funkció összefüggéseket kutattam, a konkrét enzimre vonatkozó mechanizmuson túl mindig igyekeztem egy tágabb kontextusba helyezett üzenetet megfogalmazni. Ha a kutatási kérdés megválaszolásához nem volt megfelelő eszköz, akkor bizonyos esetekben azt is előállítottuk módszertani fejlesztéssel. Ugyanakkor a specifikus, intramolekuláris konformációváltozások vizsgálata felől a dNTP anyagcsere rendszerszintű vizsgálatai felé tolódott el a kutatási érdeklődésem. Részben annak is köszönhetően, hogy Vértessy Beátával tudatosan igyekeztünk egy általam elfoglalható, a tudományos közélet számára önállóan is értékelhető niche-t létrehozni. Erre szükség volt, mert amíg folyamatosan az együttműködés fontosságát és az interdiszciplináris munka hatékonyságát hangoztatjuk, addig a tudományértékelésben és -finanszírozásban az önálló produktumot díjazzuk. A Genom Metabolizmus Kutatócsoportban egy olyan modellt próbálunk megvalósítani, amelyben önálló témavezetéssel, emellett azonban szoros együttműködésben, közös és ezért stabilabb pénzügyi és szervezeti háttérrel folytatunk kutatásokat szorosan összefüggő, de megkülönböztethető témákon. Ez a típusú csoportfejlesztés tovább folyik újabb szakterületeken specializált kollégák pályázatképessé és önálló témavezetővé válásával és azzal a szándékkal, hogy a nagyobb csoporton belül képzelik el a tevékenységüket. Ezt a modellt a kutatás hatékony módjának látom.

2 Tudományterületi háttér

A DNS-t felépítő dezoxiribonukleotidok bioszintézise a megfelelő ribonukleozid-difoszfátból (ADP, GDP, CDP és UDP) a nukleobázisra nem-specifikus enzimek által, azonos kémiai reakciók láncolatában történik. Kivétel ez alól a dTTP, amelynek prekurzorai a vele azonos információtartalmat hordozó dezoxiuridin vegyületek. Egy külön enzimrendszer áll rendelkezésre annak a metilációs reakciónak a katalizálására, amely létrehozza a timint az uracilból. A metiláció a dUMP szintjén megy végbe, a dUMP termelés tehát limitáló „üvegnyak" a dTTP bioszintetikus folyamatban (1. ábra). dUMP többféle – taxonra jellemző – módon keletkezik az élő szervezetekben: dCMP-ből dezaminálással, dUTP-ből a foszfátlánc hidrolízisével vagy dCTP-ből a két előző reakció egy vagy két enzimen történő kombinálásával (1. ábra). Az élőlények nagy részében (pl. emlősök, *E. coli*) a dUMP keletkezés fő fluxusát a dCMP→dUMP útvonal képviseli. A dCTP→dUMP átalakulást katalizáló bifunkciós dCTP-dezamináz:dUTPáz enzim (Dcd:dut) ritkán fordul elő (pl. *Mycobacterium* sp., archeák), és a dCTP-dezamináz (Dcd) jelenléte sem általános. A dUTP→dUMP hidrolízist katalizáló dUTPáz enzim azonban szinte minden élőlényben megtalálható, sőt a vírusok többségében is[11,12].

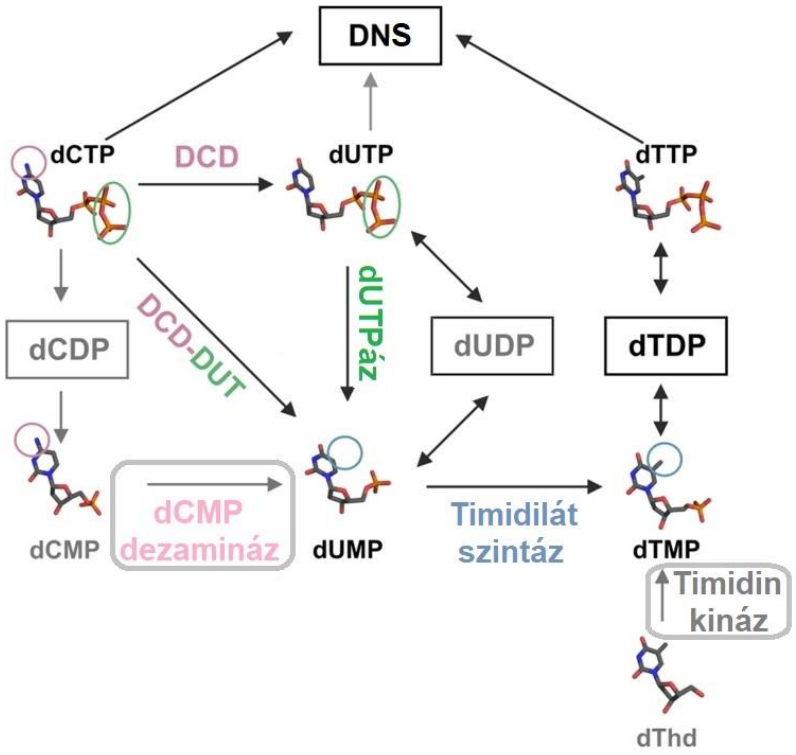

1. ábra: A timidilát bioszintézis útvonalai. A de novo szintézis útvonal a timidilát szintáz enzimen és obligát dUMP prekurzoron keresztül, míg a visszamentő útvonal a timidin kináz enzim segítségével alacsonyabb foszforiláltsági állapotú timidin származékokon keresztül történik. Azt a két reakciót, amely a Plasmodium és Mycobacterium fajokban hiányzik, szürke négyzettel jelöltem. Ezekben a fajokban mindenképpen dUTP-n keresztül keletkezik a dUMP, és ebből a dTTP.

Érdekes módon az összes felsorolt, a dUMP prekurzorhoz vezető útvonalat katalizáló enzim (dUTPáz, Dcd és Dcd:dut) szerkezetileg azonos felépítésű, rafináltan összefűzött homotrimer (2. ábra), és aktív centrumaik is nagyban konzerváltak egymás közt.

Közös jellemzőjük, hogy az átalakítandó pirimidin dezoxinukleotidot specifikusan kötik, és a megfelelő ribonukleotidot kizárják az aktív helyről. Ez a megfigyelés azt sejteti, hogy a dUMP keletkezés alapvető folyamata egy tőről származik, amelyből azután eltérő metabolikus stratégiák alakultak ki. A dUMP-t szubsztrátként használó timidilát szintézisnél ismét összeérnek az útvonalak (1. ábra), ez a lépés ugyanis rendkívül konzervált.

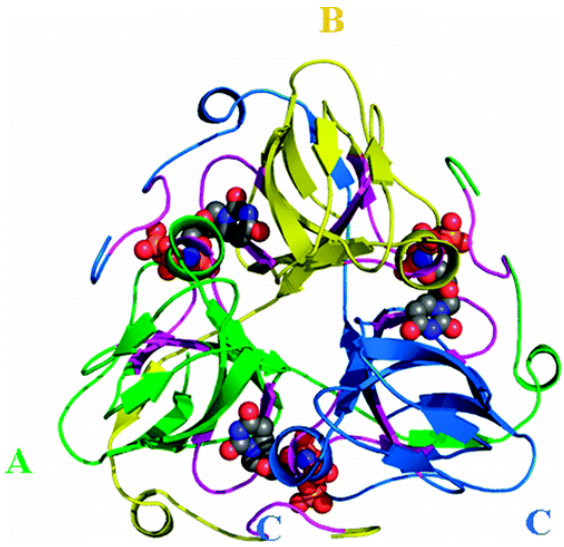

2. ábra: A dUTPáz homotrimer. A három alegység (A, B, C) három aktív helyet alkot szimmetrikus módon. Az egyes aktív helyeken kötött szubsztrátokat (térkitöltő modell) mindhárom alegység konzervált szekvenciamotívumai koordinálják (magentával jelölve). Bár minden alegység tartalmazza az összes szükséges motívumot a szubsztrát megkötéséhez, a trimerképződés elengedhetetlen ahhoz, hogy ezek a megfelelő pozícióba helyezkedjenek. (PDB azonosító: 2PY4)

Miért szükséges költséges módon timinnel helyettesíteni az uracilt a DNS-ben? A bázispárosodás szempontjából jelentéktelen a különbség e két bázis között és a DNS polimeráz szubsztrátként fogadja el mind a dUTP-t, mind a dTTP-t. A helyettesítés oka ugyanabban a kémiai átalakulásban keresendő, amelyet a fent bemutatott dCTP/dCMP-dezamináz enzimek katalizálnak: a citozin aminocsoportjának elvesztésében, vagyis uracillá történő átalakulásában. A sejtbéli körülmények között a reakció spontán is megtörténik, és ezzel a C→U átalakulással a DNS eredeti C:G bázispárjából a következő osztódásnál javítás hiányában T:A bázispár lesz. Ennek a súlyos, mutagén hibának a javítására létrejött egy uracilt felismerő és eltávolító mechanizmus, amely minden uracilt eltávolít a DNS-ből, az adeninnel szemben lévő, nem-mutagén uracilokat is. A timin metilcsoportja tehát egy megkülönböztető jelzés, használatával a citozin kémiai instabilitása mellett is lehetővé válik a bázispárosodásban rejlő információ hosszú távú megőrzése. Ez a megoldás azonban további következményeket is von maga után: a folyamatosan keletkező dUTP-től meg kell szabadulni. A dUTP/dTTP arányt alacsonyan kell tartani ahhoz, hogy a különben beépülő uracil ne terhelje túl a hibajavító rendszert. A folyamatosan keletkező dUTP eltávolítása a dNTP készletből a dUTPáz enzimcsalád segítségével történik minden ismert élőlényben. Enzimológiai és alkalmazott kutatási, gyógyászati szempontból is több érdekes aspektusa van ezeknek az enzimeknek. A foszfáthasítási és -transzferreakciók univerzálisak minden biológiai folyamatban, és számos tulajdonságuk a megfelelő katalitikus reakciókat végző enzimek többségében közös. Ilyen például a kétértékű Mg^{2+} ionok, illetve a foszfátláncot koordináló motívumok jelenléte és

alkalmazása a katalízisben. Alapkutatási szempontból szintén érdekes a dUTPáz szupercsaládra jellemző konzervált homotrimer szerkezet és az ebben rejlő allosztérikus lehetőségek (2. ábra). Érdekes az a mechanizmus, amellyel a dUTPázok a hidrolízist a α és a β foszfátcsoportok közé irányítják egy, a DNS polimerázokétól eltérő módon. Jelentős kérdés továbbá, hogy az egyes élőlényekben milyen szerepet játszanak még a mellett, hogy egyszerű lebontó anyagcsere-funkciót látnak el. Alkalmazott kutatási szempontból pedig azért tartanak érdeklődésre számot, mert a dUTPáz enzimcsalád ígéretesnek bizonyul a rákellenes és antimikrobiális terápiák célpontjaként is. A kemoterápiában gyakran alkalmazott fluoropirimidin antimetabolitok a timidilát szintáz enzimet gátolják, és ezzel megakadályozzák a dUMP -> dTMP „üvegnyakon" keresztüli, *de novo* dTTP bioszintézist (1. ábra). dTTP azonban a visszamentő útvonalakon is keletkezhet, ezért az antimetabolitok hatására nem fogy el teljesen a DNS szintézisre rendelkezésre álló dTTP készlet. A közvetített citotoxikus hatásban a dUTP/dTTP arány eltolódása is szerepet játszik[13]. Az osztódó sejt nem csak a dTTP-hiánnyal küzd, hanem a magas dUTP/dTTP arány következtében uracil épül be a képződő DNS-szálba, ami túlhajszolt DNS javítási ciklust indít be, és ez végül sejthalálhoz vezet[14]. Ezért, ha a timidilát szintézis gátlásával egyidejűleg a dUTPázt is gátolni lehet, akkor még inkább eltolható a sejtbéli dUTP/dTTP arány, és ezzel a kemoterápiás hatás fokozható. Ezt a hipotézist erősítette meg az a megfigyelés, hogy a dUTPáz-csendesítés érzékenyebbé tett egyes humán tumorsejtvonalakat a fluorodezoxiuridinre[15], ugyanakkor a dUTPáz túltermelése védő hatást fejtett ki a fluorouracil citosztatikus hatásával szemben[16–18]. Később, potens dUTPáz inhibitorok kifejlesztését[19–22] követően kimutatták, hogy a dUTPáz gátlása maximalizálja a fluoropirimidinek hatását HeLa sejtekben[23], nem-kissejtes tüdőrák sejtvonalakban (NSCLC)[24], vastagbélrák sejtekben[25], a legmakacsabb emlőrák sejtekben (triple-negative breast cancer)[26], és a tumorellenes aktivitást egérbe ültetett mellrák xenografton[21]. A dNTP bioszintézis egy általánosabb vonalán, klinikai minták elemzése szignifikáns korrelációt tárt fel az alacsony dUTPáz és a magas ribonukleotid reduktáz kombinációja, valamint a vastagbél- és emlőrákos betegek rossz prognózisa között[27]. Ugyanakkor a dUTPáz magas expressziós szintje megszüntette a ribonukelotid reduktáz túlműködés genomi instabilitást okozó hatását[27]. A dUTPáz gátlás, mint adjuváns terápia azóta II. fázisú klinikai vizsgálatig jutott, egyelőre mérsékelt sikerrel[28,29].

A rákellenes terápiák mellett a dUTPáz gátlása alkalmas lehet egyes fertőző betegségek, például a retrovirális fertőzések[12], a malária[30–32] és a tuberkulózis ellen is. A *Plasmodium falciparum* és a *M. tuberculosis* kórokozókban a dTMP bioszintézise a dUTPáz-aktivitásra támaszkodik (1. ábra). Mint fentebb említettem, a legtöbb szervezetben a dCMP dezaminázok biztosítják a dUMP-t a timidilát szintáz reakcióhoz, ezért ezekben a szervezetekben a dUTPáz-aktivitásból származó dUMP-ellátás kevésbé fontos. Az enterobaktériumokban, a mikobaktériumokban és a plazmódiumokban azonban a citozin dezamináció kizárólag a dCTP szintjén történik, amelynek az eredményeképpen keletkező dUTP-t a dUTPáz segítségével a dTTP szintézishez szükséges dUMP-vé kell alakítani (1. ábra), ezért a dUTPáz szerepe ezekben az élőlényekben kiemelt[14].

Mindezek a nagyrészt az itt bemutatott munkával párhuzamosan született eredmények folyamatos motivációt nyújtottak arra, hogy minél mélyrehatóbban megértsük a dUTPáz enzimatikus működését, ehhez kapcsolódó szerkezeti változásait és élettani szerepét.

3 Célkitűzések

A PhD megszerzése óta a genomanyagcsere témakörben levelező szerzőként közzétett és itt tárgyalt cikkeim célkitűzései a következők voltak:

1. A humán dUTPáz kvantitatív enzimkinetikai modelljének megalkotása, az enzimciklus részleteinek feltárása (Tóth *et al*, JBC 2007). Ez a munka szolgáltatta az alapot a további célok megfogalmazására, és azok kutatásának módszertani megvalósíthatóságára. A következő munkákban mindvégig a vizsgált enzimen túlmutató tágabb, alapvető enzimológiai összefüggések feltárására törekedtünk.
2. Az aktív helyen minden dUTPázban, illetve a legtöbb nukleotid hidrolázban megtalálható szubsztrát és enzim közötti aromás kölcsönhatás szerepének és jelentőségének feltárása az enzimkatalízisben (Pécsi *et al*, NAR 2010).
3. A P-hurok NTPázok enzimcsaládjának nevet adó motívum azonosítása és különös szerepének felderítése a dUTPázban, a hasonló módon kötődő dUTP (szubsztrát) és dUDP (nem-szubsztrát) megkülönböztetésének mechanizmusa (Pécsi *et al*, PNAS 2011, Lopata *et al*, ACS Catalysis 2015).
4. A dUTPázok fehérjeszerkezetében rejlő allosztérikus szabályozási lehetőségek vizsgálata (Szabó *et al*, SciRep 2016).
5. A spektroszkópiailag látszólag zárt nukleotidkötő zsebbe történő nukleotidkötés és az onnan történő termékfelszabadulás mechanizmusának vizsgálata (Lopata *et al*, JBC 2016)
6. A Mg^{2+}-mentes enzimaktivitás kivizsgálása (Lopata *et al*, Biomolecules 2019)
7. A mikobakteriális dUTPáz élettani szerepének vizsgálata (Pécsi *et al*, PLoS One 2012, Hirmondó *et al*, SciRep 2017)
8. A dUTPáz, mint génexpresszió-szabályozó fehérje kapcsolómechanizmusának felderítése (Szabó *et al*, 2014 NAR)
9. Megbízható és elérhető dNTP mérési módszer kifejlesztése (Szabó et al, NAR 2020)
10. Az irodalomban fellelhető dNTP mérések összegyűjtése és rendszerezése, mennyiségi dNTP-adatok előkészítése átfogó bioinformatikai analízishez (Pancsa *et al*, NAR 2021)

4 Alkalmazott módszertan és modellszervezetek

4.1 Molekuláris biológiai és géntechnológiai módszerek

4.1.1 Rekombináns fehérjék előállítása

A vizsgált fehérjéket kivétel nélkül elő lehetett állítani bakteriális heterológ expressziós rendszerben valamely standard *E. coli* BL21 törzsben. A mutáns fehérjéket kódoló klónokat jellemzően a mutációt tartalmazó primer vagy megaprimer segítségével hoztuk létre a QuikChange technikával, vagy PCR-t követő klónozással. A kovalens dUTPáz trimert több klónozási lépésben, monomer kazetták beépítésével hoztuk létre, ami az azonos szekvenciák rekombinációs hajlandósága miatt nagy kihívás volt. Az *E. coli*-ban termeltetett fehérjék tisztítását jellemzően affinitás-, ioncserélő és méretkizárásos kromatográfiával végeztük manuálisan vagy AKTA rendszeren.

4.1.2 mRNS és fehérjeexpressziós szintek vizsgálata

Az mRNS expressziós szinteket primerhatékonyság-vizsgálat után és több kontroll mRNS-hez viszonyítva qPCR technikával[33], a relatív fehérjeexpressziós szinteket pedig Western blottal határoztuk meg.

4.1.3 dNTP készlet mennyiségi meghatározása

A dNTP méréshez a sejtlizátum dNTP tartalmát metanolos extrakcióval nyertük ki[33]. Kezdetben radioaktívan jelzett dATP beépülésének mennyiségi meghatározásával[15,34], később qPCR készülékben a DNS-elongációs folyamat fluoreszcens nyomonkövetésével és ennek kinetikai elemzésével vizsgáltuk a biológiai mintában található különböző dNTP-k mennyiségét specifikus módon[35].

4.1.4 Mikobakteriális géntechnológia, a *M. smegmatis* mutáns törzsek létrehozása

A mikobakteriális genetikai kísérleteket *M. smegmatis* mc^2 155 törzsben végeztünk a Tanya Parish laboratóriumában (Queen Mary University of London) tanult technikákkal[36]. A mutáns törzseket homológ rekombinációval hoztuk létre, az ehhez szükséges vektorokat *E. coli*-ban állítottuk elő klónozással, majd elektrokompetenssé tett *M. smegmatis* sejtekbe elektroporáltuk. A mutáns, kétszeresen átkereszteződött (double cross over) törzseket kolónia-PCR-rel választottuk ki, és Southern-blot vizsgálattal ellenőriztük, majd legvégül a megfelelő genomrégió szekvenálásával. A komplementáló fehérjéket kódoló szekvenciákat episzomálisan vagy integrálódó vektorokon vittük be[33,37]. A spontán mutációs rátát David *et al.* szerint határoztuk meg[38], a mutációs spektrum vizsgálatához a rifampicinrezisztenciáért felelős *M. smegmatis* rpoB gén mutációs hot-spot régióját szekvenáltuk. A mutáns törzsek genomi uracil tartalmát a laboratóriumunkban fejlesztett qPCR alapú módszerrel mértük[39].

4.2 Fehérje szerkezet-funkció vizsgáló módszerek

4.2.1 Oldatbeli fehérjeszerkezet vizsgáló módszerek

Spektroszkópiai módszerek közül szerkezetvizsgálatra és a különböző fehérjekonformerek eloszlásának vizsgálatára CD- és fluoreszcencia-spektroszkópiát alkalmaztunk. Az intrinszik fluoreszcens jelet az egy-triptofános mutánsok helyspecifikusan, géntechnológiai úton bevitt triptofán oldallánca szolgáltatta. Az egy-triptofános fehérjék steady-state fluoreszcencia-spektrumainak, intenzitásának és oldószerkitettségének vizsgálata különböző apo és ligandumkötött állapotokban értékes információt szolgáltattak az

enzimmechanizmusra vonatkozóan. Az egyensúlyi állapotban definiált jelváltozások kiválóan alkalmasak az enzimreakciók részlépéseinek gyorskinetikai követésére is.

Flexibilis fehérjeszerkezeti elemek azonosítására és ezek a reakciómechanizmusban vagy fehérje-fehérje kölcsönhatásban játszott szerepének tisztázására limitált proteolízist, és azt követően fragmensanalízist (PAGE vagy MS) végeztünk[40,41].

4.2.2 Kinetikai módszerek

A steady-state mérésekben a dUTPáz reakcióban felszabaduló protonokat fenolvörös pH indikátorral, a dCTP dezamináz aktivitást pedig a dezoxicitidin és a dezoxiuridin moláris extinkciós együtthatóinak különbségét felhasználva detektáltuk kinetikai mérésekre optimalizált spektrofotométerben.

Az enzimmechanizmus részlépéseinek feltárására gyors- (tranziens) kinetikai módszereket alkalmaztunk, amelyekben a reaktánsok gyors összekeverése után, de a steady-state állapot beállta előtt vizsgálhatóak az egyedi részlépések. Ehhez stopped-flow készülékben nagy időfelbontásos fluoreszcencia-mérésekkel vizsgáltuk az egy-triptofános fehérjék elkülöníthető egyedi részlépéseit. A pH indikátor esszét is optimalizáltuk abszorbanciát követő stopped-flow vizsgálatokhoz, amellyel a protonfelszabadulási részlépés kinetikáját tudtuk nyomon követni. Alkalmaztunk még kémiai quenched-flow technikát is radioaktívan jelölt dUTP hidrolízisének közvetlen nyomon követésére.

A kísérletesen meghatározott sebességi és egyensúlyi állandókból felállított enzimmechanizmust kinetikai modellezéssel lehet szimulálni, illetve a koherenciáját tesztelni. Erre a célra a háttérben differenciálegyenletekkel működő, de felhasználóbarát Gepasi és Copasi szoftvereket használtuk. A kinetikai modellezés arra is alkalmas, hogy az enzimciklus részletes kvantitatív modelljének megalkotásához a kísérletileg nem vizsgálható paramétereket bizonyos értékhatárok között szimuláljuk, illetve a külső hatásokra adott válaszait modellezzük.

4.2.3 Termodinamikai módszerek

A fehérje–ligandum és fehérje–fehérje kölcsönhatások jellemzésére a spektroszkópiai módszereken kívül a fehérje hődenaturációt követő termális eltolódás módszert (ThermoFluor) és az izotermális titráló kalorimetriát (ITC) alkalmaztuk. Előző egy nagy áteresztőképességű, fluoreszcenciaváltozás követésén alapuló módszer, amely a különböző molekulákkal való kölcsönhatás a fehérje hőstabilitására gyakorolt hatásának vizsgálatára alkalmas. Ezzel a módszerrel gyorsan és kis anyagigénnyel lehet olyan kísérleti körülményeket találni, amelyek aztán alkalmasak a nagy anyagigényű de pontos termodinamikai paramétereket szolgáltató ITC mérésekhez.

4.2.4 Elektroforézis technikák

A standard fehérje minőségellenőrzésre és fragmensanalízisre használt SDS-PAGE-n kívül makromolekuláris kölcsönhatások és enzimaktivitás jellemzésére is használtunk gélelektroforézist. Az Stl-dUTPáz kölcsönhatás jellemzésére natív gélelektroforézist, az Stl fehérje funkcionális DNS kötésének vizsgálatára EMSA módszert alkalmaztunk[40]. Denaturáló 14%-os poliakrilamid-karbamid gélt (7,5 M karbamid) használtunk az oligonukleotidok egy bázispár pontosságú elválasztására[42], hogy demonstráljuk a Taq polimeráz exonukleáz aktivitását a fluoreszcens dNTP mérési módszerben.

4.2.5 Krisztallográfia, szerkezeti modellezés

Számos *M. tuberculosis* dUTPáz mutáns szerkezetét határoztuk meg különböző apo vagy ligandum-kötött állapotban röntgen-krisztallográfia segítségével (mtDUTH145W, 3HZA; mtDUTH145A, 3LOJ; mtDUTH21W, 4GCY). Az előkísérleteket kezdetben az ELTE-n Harmat Veronika segítségével, majd a Biostrukt laboratórium házi röntgenforrásánál végeztük, míg a nagyfelbontású adatokat valamely szinkrotron röntgenforrásnál gyűjtöttük (ESRF Grenoble; DESY, Hamburg). A szerkezetmeghatározást Leveles Ibolya és diákjai végezték. A homológia-modellezéseket a Swiss PDB Viewer segítségével, a legtöbb szerkezeti elemzést és a fehérjevariánsok tervezését pedig PyMol-lal végeztük. A bemutatott ábrák és cikkábrák szintén PyMol-lal készültek.

4.2.6 Molekuláris dinamikai és kvantumkémiai számítások

A nagy időfelbontású *in silico* molekuláris dinamikai módszereket és dokkolási technikákat alkalmazó kísérleteket együttműködésben végeztük szegedi (Jójárt Balázs) és külföldi (Rosta Edina) kollégáinkkal. Lopata Anna diákom mindkét említett kollégával szorosan együtt dolgozott, az *in silico* molekuláris dinamikai kísérletek jelentős részét ő végezte Rosta Edinánál az NIH-ben (Bethesda, USA), az Enzimológiai Intézetben, illetve Szegeden Jójárt Balázsnál. A kvantumkémiai számításokat Rosta Edina csoportja végezte.

5 Eredmények

5.1 A humán dUTPáz enzimatikus mechanizmusa

5.1.1 A hidrolízis ciklus kvantitatív kinetikai modellje

(Tóth *et al*, JBC 2007[43])

Korábban mások és a csoportunk is meghatározta a humán dUTPáz nagy felbontású kristályszerkezetét, amely fontos betekintést nyújtott a katalitikus mechanizmus szerkezeti alapjaiba[44,45] (3. ábra). A szerkezet ismerete azt is lehetővé tette, hogy olyan mutációkat tervezzünk, amelyek elősegítik a szerkezet-funkció összefüggések felderítését. A trimeren belül minden aktív hely két szomszédos alegység által kialakított kötőárokból alakul ki, amelyre a távoli, harmadik alegység C-terminális vége a szomszédos alegységet megkerülve ráhajlik (3. ábra A). Az α-β foszfoanhidrid kötés hasítása a katalitikus vízmolekula nukleofil támadásával történik. A katalitikus vízmolekulát egy konzervált aszpartát oldallánc (Asp102) koordinálja (3. ábra D panel). Korábban felvetésre került, hogy a nagy konformációs szabadsággal rendelkező C-terminus bezárása szükséges a kémiai lépés során[45,46].

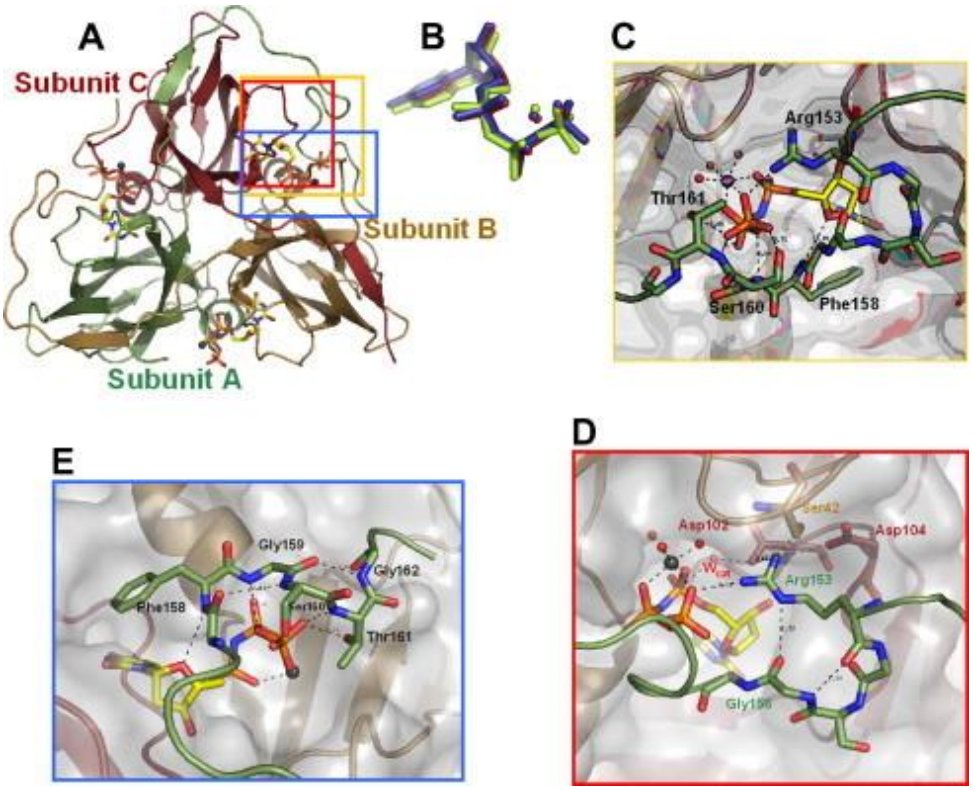

3. ábra: A humán dUTPáz kristályszerkezete α-β-imido-dUTP:Mg^{2+} komplexben. Az alegységeket színkódolt szalagmodellként, a ligandum molekulákat és Mg^{2+}-ionokat golyó-pálcika modellként ábrázoltuk. (A) A teljes trimer szerkezete. A színes téglalapok jelzik a C – E paneleken részletesen bemutatott régiókat. (B) Egymásra helyezett ligandum molekula komplexek a következő kristályszerkezetekből: humán dUTPáz:α-β-imidodUTP:Mg^{2+} (zöld), E. coli dUTPáz: α-β-imido-dUTP:Mg^{2+} (piros) és inaktív E. coli mutáns dUTPáz:dUTP:Mg^{2+} (kék). A szoros illeszkedés mutatja az aktív hely konzerváltságát. (C) A C-terminális kar kölcsönhatásai a ligandum molekulával. A ligandum szénatomjai sárga, a fehérje szénatomok az alegység szerinti színűek, a többi atom standard atomi színezéssel ábrázolva. A fehérje többi része szalagmodellként látható. A H-kötéseket szaggatott vonallal jeleztük. Figyeljük meg a C-terminális és a ligandum foszfátlánca között létrejövő interakciók nagy számát. (D) Közelkép a foszfátláncot koordináló kölcsönhatásokról az Arg153 oldalláncal és (E) a C-terminális hurok többi konzervált aminosav oldalláncával. Ábra forrása: Varga és mtsai, FEBS Letters 2007.

A modern farmakológia megköveteli a célenzimek pontos hatásmechanizmusának ismeretét, ezért a szerkezeti adatokat a humán dUTPáz oldatkinetikai vizsgálataival kívántuk kiegészíteni. A steady-state kinetikai paraméterek meghatározását dUTPázokban tipikusan a nukleotidhidrolízis során felszabaduló protonok pH-indikátorral való folyamatos követésével végzik. Ez a módszer azonban nem alkalmas az enzim konformációs változásainak felderítésére. Ez utóbbihoz az enzimatikus ciklus eseményeit érzékelő optikai jelre volt szükség. Ehhez egy belső triptofán-érzékelőt terveztünk, amely a továbbiakban nagyon hasznosnak bizonyult. Az aktív helyre ráhajló C-terminális karban cseréltünk ki egy konzervált fenilalanint triptofánra (F158W)[44], míg az enzim többi része nem tartalmazott triptofán oldalláncot vagy fluoreszcens kofaktort. Arra számítottunk, hogy a W158 kölcsönhatásba lép a dUTP uracilgyűrűjével, és szenzorként érzékeli az aktív hely nukleotid-kötött állapotát. Ez így is történt, a W158 fluoreszcens jele az enzimciklus minden lehetséges ligandumát képes fluoreszcencia jelintenzitás és hullámhossz maximum (λ_{max}) alapján megkülönböztetni (4. ábra).

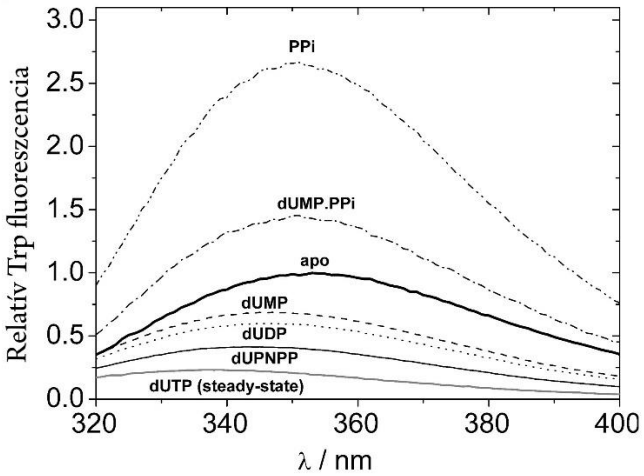

4. ábra: A humán dUTPáz W158 mutáns különböző, a reakcióciklus szempontjából releváns ligandumokkal alkotott komplexeinek fluoreszcencia spektruma

A benzolgyűrű indolcsoporttal történő mutációs helyettesítése nem zavarta meg az enzimaktivitást[44]. Minden feltétel adott volt tehát ahhoz, hogy az aktív hely W158 érzékelőjének segítségével tranziens kinetikai módszerekkel vizsgáljuk tovább az enzimreakciót. Ez a tudás elengedhetetlen a molekuláris mechanizmus funkcionális megértéséhez, és hozzájárulhat majdani inhibitorok gátlási mechanizmusának értelmezéséhez is. Megmutattuk, hogy a dUTPáz hidrolízis ciklusa legalább négy különböző enzimatikus lépésből áll: (i) gyors és reverzibilis szubsztrátkötés, (ii) az enzim-szubsztrát komplex izomerizációja a katalitikusan kompetens konformációvá, (iii) hidrolízis (kémiai) lépés, és (iv) a termékek gyors, random sorrendben történő felszabadulása (5. ábra).

A fluoreszcencia-alapú stopped-flow mérések a kémiai lépés, azaz a nukleotid α-β-foszfátcsoportjai között lévő kovalens kötés felhasadásának kinetikájába nem nyújtanak közvetlen betekintést. A kémiai lépés sebességét a radioaktív quench-flow technikával lehet legegyszerűbben meghatározni. Azonban az erre alkalmas γ^{32}P-jelzett dUTP nem kapható kereskedelmi forgalomban, ezért ennek előállítására új enzimatikus módszert dolgoztunk ki (6. ábra). Az előállított γ^{32}P-dUTP-vel végzett quench-flow kísérletek azt mutatták, hogy a kémiai lépés az enzimatikus ciklus sebességmeghatározó lépése (5. ábra).

Azt is megállapítottuk az indikátor-alapú esszé gyorskinetikára adaptálásának segítségével, hogy a proton felszabadulása egyidejű a sebességmeghatározó hidrolízislépéssel. Eredményeink a humán dUTPáz katalitikus ciklusának kvantitatív kinetikai modelljéhez és az enzim-ligandum kölcsönhatásban fontos szerepet betöltő C-terminális kar szerepének jobb megértéséhez vezettek.

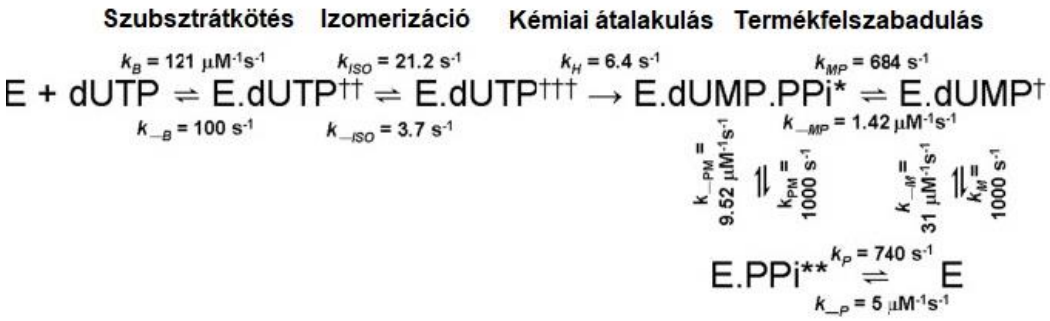

5. ábra: A humán dUTPáz enzimatikus mechanizmusa

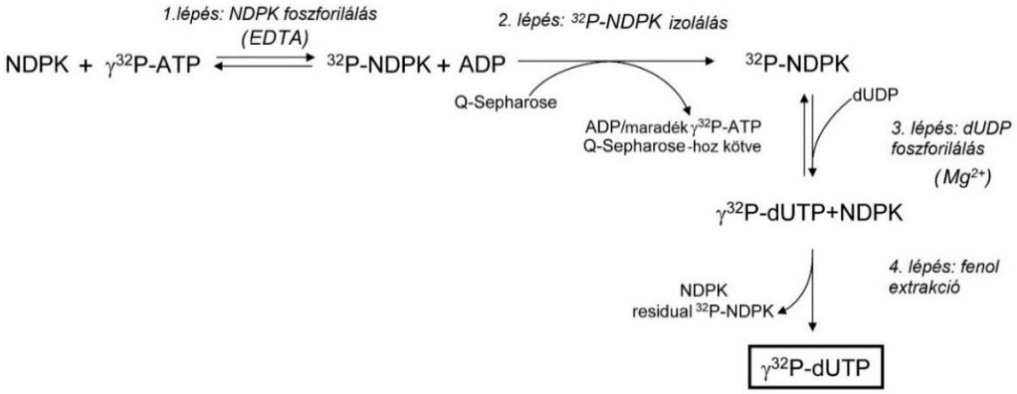

6. ábra: Enzimatikus radioaktív dNTP jelölési módszer. Az NDPK (nukleozid-difoszfát kináz) enzim szubsztrát promiszkuitása jóvoltából bármely, akár egzotikus dNTP jelölése lehetséges e módszerrel.

A dUTPáz gátlás ötlete nem sokkal e tanulmány kezdete előtt merült fel a fluoropirimidin típusú kemoterapeutikumok hatásának erősítésére[15]. Az 5-fluoro-dezoxiuridin származékok gyakran, vagy akár elsődlegesen alkalmazott kemoterápiás szerek az emésztőtraktus és egyes bőr- és mellrákos megbetegedések kezelésében (capecitabine, 5-fluorouracil, tegafur). Ezek a molekulák a szervezetben többek között 5-fluoro-dUTP-vé foszforilálódnak. Azt azonban nem lehetett tudni, hogy a szubsztrátra rendkívül specifikus dUTPáz képes-e a fluoro származék hidrolízisét is katalizálni, ezzel meggátolva annak beépülését a DNS-be. A dUTPáz enzimmechanizmusát vizsgáló kinetikai módszertárunkkal megállapítottuk, hogy a szubsztrát uracilgyűrűjén az 5F-szubsztitúció nem változtatja meg a dUTPáz által végzett dUTP-hidrolízis kinetikai mechanizmusát[47]. Ez az eredmény koherens a dUTPáz megfigyelt védőhatásával az 5-fluoro-dezoxiuridin származékokkal való kezeléssel szemben és az egyidejű dUTPáz gátlás, mint adjuváns terápia hatékonyságát támasztja alá.

5.1.2 Az enzim és szubsztrát közötti π-π kölcsönhatás hozzájárul az átmeneti állapot stabilizálásához

(Pécsi *et al* NAR 2010[48])

Az aromás kölcsönhatások jelentősége a makromolekulák konformációszabályozásában széles körben elfogadott[49] és tanulmányozott számos biológiai rendszerben (például a DNS kettős hélixben[50], a ribonukleoproteinekben[51] vagy a fehérjefeltekeredésben[52]). Ezekben az esetekben az intra- vagy intermolekuláris aromás átlapolás (más néven aromás π-π kölcsönhatás) hozzájárulása a szerkezeti stabilizációhoz erősségében összehasonlítható a hidrogénkötéssel[51]. A π-π kölcsönhatásoknak az enzimatikus katalízisben betöltött szerepe azonban kevesebb figyelmet kap, főként a flavoenzimek[53] és az N-glikozidos kötés nukleozid-hidroláz általi hasításának tanulmányozására korlátozódik[54]. Ez a két példa összehasonlítható abban az értelemben, hogy a π-π kölcsönhatásba lépő, a fehérjéből származó aromás gyűrű közvetlenül a kémiai reakció középpontjában található. A PDB adatbázisban elérhető szerkezetekben megvizsgáltuk, hogy a nukleotidot hidrolizáló enzimekben jellemző-e az aromás oldallánc az aktív centrumban, és azt találtuk, hogy nagyon gyakori. Ezeknek az oldalláncoknak a szerepét többnyire a szubsztrátkötésben látják (ABC transzporterek[55], kinezinek[56], kinázok[57], a 7. ábra A panel mutat ezekre példákat), a katalízisben betöltött szerepét azonban nem vizsgálták tekintettel a hidrolízis helye és a nukleotid aromás gyűrűje közötti viszonylag nagy fizikai és kémiai távolságra. Mi azonban azt gondoltuk az előbb tárgyalt enzimatikus mechanizmusról és a fehérjeszerkezetről szerzett ismereteink alapján, hogy a dUTPáz enzim C-terminális karjában lévő konzervált aromás aminosav (a F158, amelyet triptofán szenzorra cseréltünk) és a nukleotid bázis közötti π-π kölcsönhatásnak (7. ábra) katalitikus szerepe lehet az α és β foszfátcsoportok közötti hidrolízis reakcióban. Ennek az aromás kölcsönhatásnak korábban a szubsztrát megkötésében és esetleg a termék felszabadításában tulajdonítottak szerepet pusztán szerkezeti megfontolások alapján[45].

Hipotézisünk tesztelésére mutációkat hoztunk létre az emberi (hDUT) és a *M. tuberculosis* dUTPáz (mtDUT) konzervált aromás helyén (hDUTF158W, hDUTF158A, mtDUTH145W, mtDUTH145A). Ezeket a mutáns fehérjéket előállítottuk és kristályosítottuk (7. ábra), kinetikai és spektroszkópiás kísérleteket végeztünk rajtuk a változás hatásának feltárására. Azért használtunk két különböző enzimet, mert szerettük volna látni, hogy az aromás kölcsönhatás megszüntetése, illetve módosítása hasonló hatással jár-e a két enzimben annak ellenére, hogy az egyikben fenilalanin, a másikban pedig hisztidin van eredetileg a kérdéses pozícióban (7. ábra B panel). Továbbá az mtDUT kedvező kristályosodási tulajdonságai miatt bíztunk benne, hogy nagy felbontású szerkezeteket sikerül előállítani a mutánsokról, és azok segítenek majd az értelmezésben.

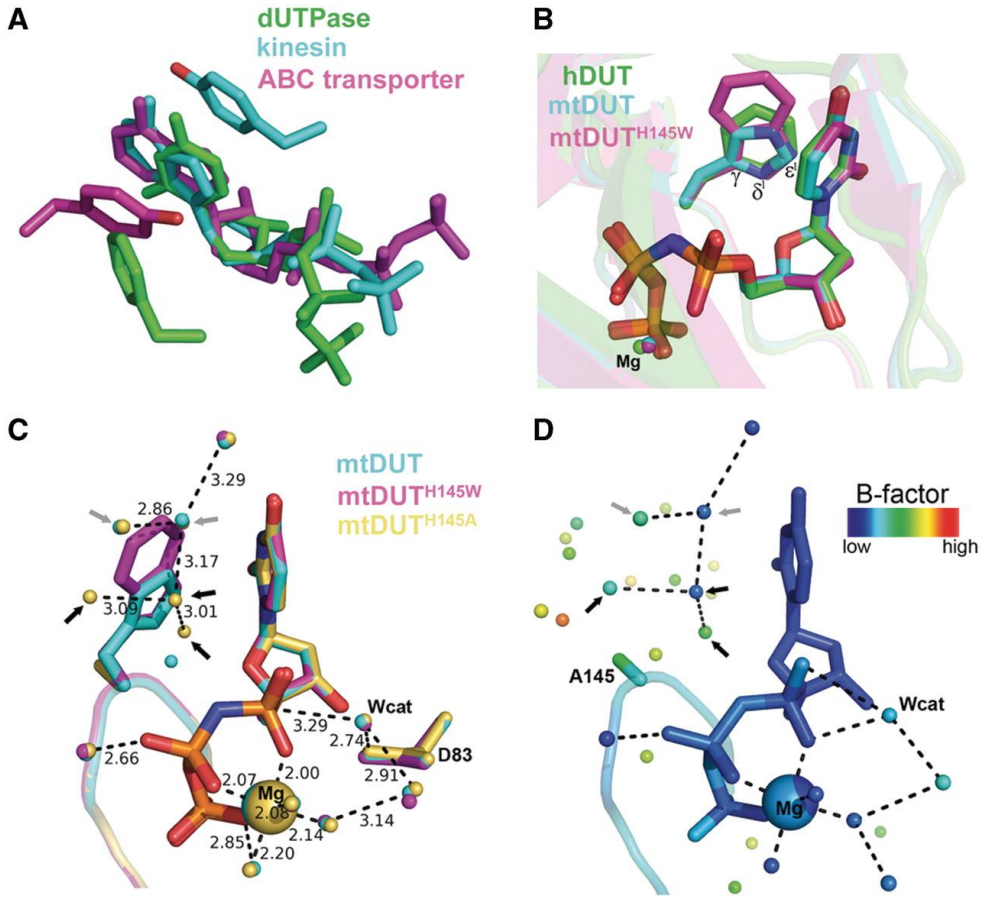

7. ábra: Az enzim és szubsztrát közötti aromás π–π átlapolás szerkezeti vonatkozásai a dUTPázban és más nukleotid hidrolázokban. (A) $\mathcal{A}$ különböző nukleotid-hidroláz családok képviselőinek PDB azonosítói: 2HQU, 2NCD és 1XEF. (B) A különböző aromás aminosavakat tartalmazó dUTPáz aktív hely-szerkezetek egymásra illesztése (Phe, His, Trp rendre a 2HQU, 2PY4 és a 3HZA PDB azonosítójú szerkezetekben) (C) Az újonnan előállított mutáns szerkezetek összeillesztése a vad típusú mtDUT szerkezetével. A szürke nyilak a csak az mtDUT -ban és az mtDUTH145A-ban, az mtDUTH145W -ban pedig nem megtalálható vízmolekulákra mutatnak, a fekete nyilak a csak az mtDUTH145A -ban megtalálható vízmolekulákra. A D83 az a katalitikus oldallánc, amely polarizálja a nukleofil támadó vízmolekulát (Wcat). (D) Ugyanaz a nézet, mint (C)-ben az mtDUTH145A aktív helyéről, B faktor alapján színezve. Vegyük észre a Trp-helyettesítő vízmolekulák viszonylag alacsony mobilitását a kristályszerkezetben. Az aromás elemek elvesztésekor megjelenő vízhálózat jól helyettesíti nagyjából egy indolgyűrű helyét, és jól illeszkedik a vad típusú kristályban megfigyelt H-kötési hálózatba. A katalitikus vízmolekula, valamint a többi konzervált oldallánc és a fém kofaktor egyformán helyezkedik el mindkét mutánsban, ami arra utal, hogy az mtDUTH145A aktivitásvesztése nem a katalitikus kölcsönhatási hálózat zavarainak eredménye. Az aromás gyűrűk terét elfoglaló vízhálózat modularitása magyarázza a különböző dUTPáz szekvenciákban megjelenő Phe/Trp/His/Tyr aminosavak cserélhetőségét is.

Az irodalomban megfogalmazott várakozásokkal ellentétben azt mutattuk ki, hogy az aromás kölcsönhatás megszüntetése csak kis mértékben befolyásolta a szubsztrát kötődését, miközben kifejezetten csökkentette a kémiai lépés sebességi állandóját (8. ábra), ami a katalitikus hatékonyság összességében 100-szoros csökkenését eredményezte.

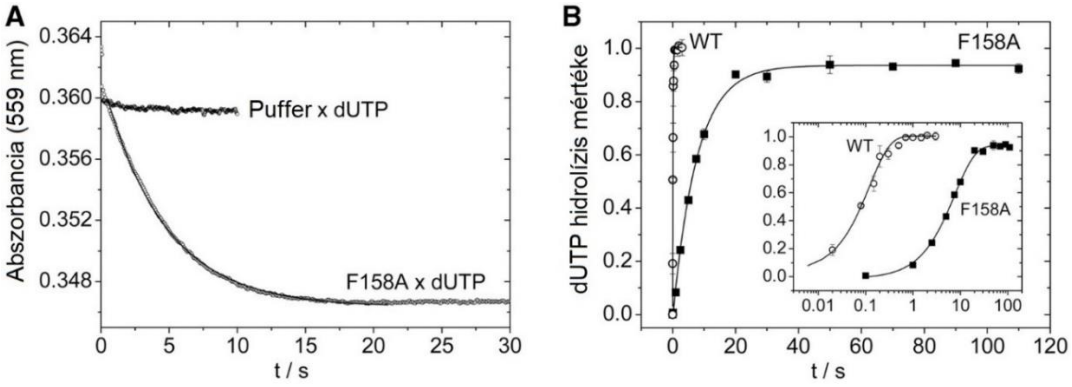

8. ábra: A protonfelszabadulás és a kémiai kötés felbomlása limitálja a megfigyelt steady-state sebességi állandókat a hDUTF158A mutánsban. (A) Protonfelszabadulást követő egyszeri átviteli időgörbe. 15 μM hDUTF158A vagy pufferrel, vagy szubsztöchiometrikus dUTP-vel keverve a stopped-flow készülékben. Az exponenciális illesztés eredménye k_{obs} = 0.23 ± 0.007 s^{-1}. (B) Egyszeri átviteli quench-flow időgörbe vad típusú hDUT vagy hDUTF158A radioaktív dUTP-vel való gyorskeverését követően. A betét ábra ugyanazt mutatja logaritmikus skálán.

A hidrolízis reakció nagy valószínűséggel asszociatív mechanizmussal megy végbe, amelyben az átmeneti komplex elektronban gazdag, különösen az α-foszfát csoport közelében. Kristályszerkezeti, kinetikai, optikai spektroszkópiai és termodinamikai számítási módszereket is alkalmazva javasoltuk a következő lehetséges mechanizmust, amellyel a sebességnövekedés elérhető ezzel a távoli π-π kölcsönhatással: mivel a dUTPáz az enzimciklusa során kísérleteink szerint nem megy át nagy konformációs változásokon, katalitikus hatása valószínűleg a nagy hatótávolságú elektrosztatikus stabilizációnak és/vagy az átmeneti állapot geometriai optimalizálásának köszönhető. Tanulmányunk azt mutatja, hogy a katalitikus elektrosztatikus hatás egyik fontos komponense a vizsgált aromás kölcsönhatásból származik, amely a reaktánsok komplexét gyengén, míg az átmeneti állapotot fokozottan stabilizálja. Ez a hatás a katalízisre azért sajátos, mivel az aromás kölcsönhatás által befolyásolt uracil viszonylag távol van az α-foszfátcsoport hidrolízisének helyétől. A különböző nukleotid-hidrolizáló enzimekben (például az ATPázok legtöbb családjában) található hasonló aromás kölcsönhatások sokasága felveti annak lehetőségét, hogy az általunk leírt jelenség a foszfoanhidrid hidrolízis enzimatikus katalízisének általános összetevője.

5.1.3 A dUTPáz P-hurokszerű motívumot alkalmaz a katalitikus hatékonyság fokozására, és a nukleotid foszforiláltsági állapotainak megkülönböztetésére

(Pécsi *et al*, PNAS 2011[58])

Rendkívül érdekesnek találtuk azt a kérdést, hogy a pirofoszfátot termelő nukleotid-hidrolázok hogyan különböztetik meg a nem-szubsztrát (d)NDP-t a szubsztrát (d)NTP-től, mindkettő tartalmazza ugyanis a hidrolizálandó α-β foszfoanhidrid kötést. A dUTPáz enzim jó alanynak tűnt ennek a kérdésnek a megvizsgálására, mivel specifikusan csak a dUTP hidrolízisét végzi az α- és β-foszfátok között pirofoszfátot és dUMP-t generálva, további kapcsolt reakciók nélkül. Az Mg:dUDP-hez és Mg:dUTP-analóghoz kötött enzimek kristályszerkezete szerencsésen rendelkezésre áll és összehasonlítható. Az összehasonlítás azonban nem ad magyarázatot arra, hogy a dUDP miért nem hidrolizálódik az enzimen, a felbontandó kötés és a nukleofil víz ugyanis mindkettőben ugyanazt a konformációt veszi fel (9. ábra B).

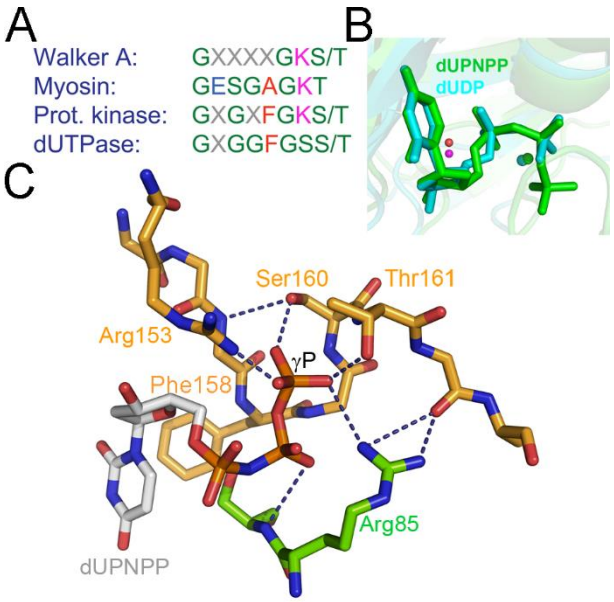

9. ábra: A dUTPáz P-hurokszerű C-terminális motívuma és ennek kölcsönhatásai a szubsztráttal. (A) Konszenzus P-hurok motívumok jól ismert P-hurok NTPázokból, összehasonlítva a dUTPázok P-hurokszerű szekvenciájával. A színezés a következő: poláris oldalláncok, zöld; apoláris, piros; negatív töltésű, kék; pozitív töltésű, magenta. (B) Két, dezoxiuridin-di- és trifoszfát-ligandumot tartalmazó dUTPáz-aktív hely egymásra illesztése (atomi színezés cián- és zöld szénnel, PDB azonosítók: 1SLH és 2HQU M. tuberculosis-ból, illetve Homo sapiens-ből). Az α-β–foszfátok helyzete azonos, és a katalitikus víz (narancssárga a tri- és magenta a difoszfát szerkezetben) és Mg^{2+} ionok (a hozzátartozó nukleotidoknak megfelelő színű gömbök) a helyükön vannak a feltételezett hidrolízishez mindkét szerkezetben. (C) A szubsztrát γ-foszfát koordinációja az általunk megváltoztatott aminosavak által. A homotrimer fehérjét (PDB azonosító: 2HQU) alegységek szerint színeztük (C alegység, atomszínezés narancssárga szénnel; B alegység atomi színezése zöld szénnel). A szaggatott vonalak a mutációk által részben felszámolt hidrogénkötéseket ábrázolják.

A dUTPáz sok más nukleotidkötő fehérjéhez hasonlóan egy konzervált hurok motívumot (V. motívum) tartalmaz a nukleotid foszfátláncának koordinálására. Az ezt a hurkot tartalmazó C-terminális kar nem része a globuláris enzimmagnak, kinyúlik a saját alegységéből, és a távolabbi aktív helyre hajlik rá, mint ahogyan azt már tárgyaltuk (2. ábra). A C-terminális karban található V. motívum szekvenciáját összehasonlítva a jól ismert P-hurokkal, vagy másnéven Walker A szekvenciával, észrevettük, hogy ezek számos

tulajdonságukban megegyeznek (9. ábra A). A népes, P-hurok NTPáz néven ismert, ATPáz és GTPáz enzimcsaládba tartoznak a kinázok, a citoszkeleton és DNS motorok, a membrán pumpák és transzporterek. Emlékeztetek itt arra, hogy a P-hurok NTPázok a nukleotidban a β-γ-foszfátok közötti hidrolízist katalizálják, míg a dUTPáz az α-β-foszfátok közötti foszfoanhidrid kötés hasadását segíti elő.

Korábban azt javasolták, hogy a dUTPáz C-terminális motívumának az aktív helyre záródása kedvezőtlen konformációt kényszerít a nukleotid-szubsztrátra, és ez lehet a felelős a katalízisért[59]. A dUPNPP szubsztrátanalóg azonban több olyan kristályszerkezetben is megőrzi ezt a kedvezőtlennek tűnő, feszült (akár gauche, akár transz) konformációt, amelyben a C-terminális kar rendezetlen és ezért nehezen elképzelhető, hogy bármilyen konformációt kényszerít a kötött ligandumra[4,6,45,60,61]. A sajátos feszült konformáció tehát függetlennek tűnik a C-terminális motívum konformációs merevségétől. Ezért nyitott maradt a kérdés, hogy ez a P-hurokszerű szekvencia hogyan járul hozzá a hidrolízis katalíziséhez.

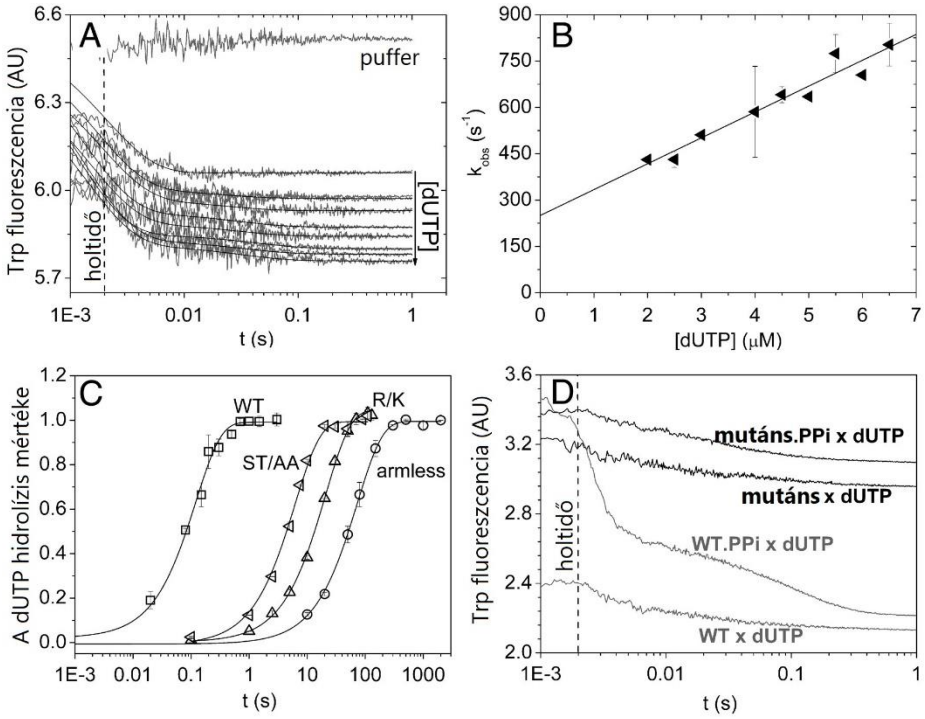

10. ábra: A P-hurok mutáns dUTPázok tranziens kinetikai vizsgálata. Az A és B panel a hDUT(ST/AA) dUTP-vel való reakciójának stopped-flow kísérleteit mutatja. (A) A fluoreszcencia időbeli változása különböző koncentrációjú dUTP 0,8 μM hDUT(ST/AA)-val való reakciójának kezdeti kötési fázisában. A sima vonalak a legjobb dupla exponenciális illeszkedések a kísérleti görbékhez. Az első exponenciálisból származó sebességi állandót (ez a gyors fázis, mely a teljes amplitúdó 95-98%-át reprezentálja) a B panelen ábrázoljuk a szubsztrát koncentráció függvényében. A második kis amplitúdójú exponenciális nem függ a koncentrációtól, k_{obs} = 29 ± 5-s^{-1} (SD n = 10). (B) A lineáris illesztés 84 ± 8 $\mu M^{-1}s^{-1}$ másodrendű kötési sebességi állandót és 250 ± 36 s^{-1} disszociációs sebességi állandót eredményezett. (C) Egyszeri átviteli γ^{32}P-dUTP hidrolízis quench-flow-val mérve. Mindegyik görbe egyetlen exponenciálissal illeszthető hidrolízis-sebességi állandót eredményezett a H-kötések elvesztésének függvényében drámaian csökkenő mértékben a különböző mutánsokban. (D) A termék PPi enzimmel alkotott komplexének disszociációját vizsgáltuk az idő függvényében dUTP chasing módszerrel, stopped-flow-ban, a vad típusú és a hDUT(ST/AA) enzimek esetében. Az chasing (üldözési) reakcióban a PPi disszociáció korlátozza a dUTP kötődési sebességét, amely követhető a vad típusú enzim esetében (szürke vonalak), míg a mutánsban nem figyelhető meg PPi disszociáció (fekete vonalak).

Annak érdekében, hogy betekintést nyerjünk a P-hurokszerű szekvencia dUTPáz-béli szerepébe, olyan P-hurok mutánsokat terveztünk, amelyek teljesen vagy részben elvesztették a kapcsolatot a szubsztrát nukleotid γ-foszfátjával. A megváltoztatni kívánt aminosavak szubsztrát-koordinációját a 9C ábra mutatja.

A mutációk részben (a Ser160Ala/Thr161Ala mutációkat hordozó hDUT(ST/AA) és az Arg153Lys mutációt hordozó hDUT(R/K) mutánsok) vagy teljesen (a Thr151Stop mutációt hordozó hDUTarmless mutáns) megzavarják a másodlagos interakciós hálózatot a γ-foszfát és a fehérje között. Ezeket a mutáns enzimeket kinetikai és ligandumkötési kísérleteknek vetettük alá két alapvető kérdést vizsgálva: egy P-hurokszerű motívum lehetséges hozzájárulása 1) a nukleozid-di- és trifoszfát-ligandumok megkülönböztetéséhez; 2) és a katalitikus hatékonysághoz.

Eredményeink azt mutatták, hogy a P-hurokszerű motívum mutánsai elvesztették a dUDP/dUTP diszkriminációs képességüket, és emellett a katalitikus hatékonyságuk a H-kötési hálózatba való beavatkozás mértékében csökkent, mégpedig a kémiai lépés sebességi állandójának csökkenésével, nem pedig a szubsztrátkötés akadályoztatása által (10. ábra). Azt a következtetést vontuk le, hogy a γ-foszfát és a P-hurokszerű motívum közötti H-kötés kölcsönhatások elősegítik az α-foszfát körüli reakcióközpont katalitikusan kompetens konformációját, és ezzel felgyorsítják a kinetikai ciklus kémiai lépését. Emiatt a hidrolízis nagyon lassan vagy egyáltalán nem megy végbe a γ-foszfát és az V. motívum közötti kölcsönhatás hiányában, azaz dUDP, dUDP.BeFx típusú szubsztrát, vagy P-hurkot nem tartalmazó mutáns esetében.

A rendelkezésre álló ATPáz és dUTPáz kristályszerkezetek összehasonlítása során azt tapasztaljuk, hogy míg a P-hurkok és a foszfátláncok tökéletesen egymásra helyezhetők az ATPázokon belül, a dUTPáz P-hurokszerű motívuma ehhez képest eltérő konformációt vesz fel a nukleotid szubsztrát körül (11. ábra A). A két hurok egymásra illesztése azonban azt mutatja, hogy a lokális konformációik között szerkezeti hasonlóság van, még abban az egy aminosav pozícióban is, amely szekvenciális különbséget tesz a P-hurok és a dUTPáz V. motívuma között (vö. 9. ábra A és 11. ábra B). A fő különbség e konformációk között az, hogy amíg a miozinban lévő P-hurok körülöleli mind a β-, mind a γ-foszfátot, addig a dUTPáz P-hurokszerű motívuma csak a γ-foszfáttal alakít ki kölcsönhatásokat (11. ábra A). Ez a különbség, amely valószínűleg a dUTPáz hurok C-terminális helyzetéből és a feszült íves dUTP foszfátlánc konformációból adódik, szintén alátámasztja e motívum γ-foszfát diszkriminációban betöltött szerepét a dUTPázban.

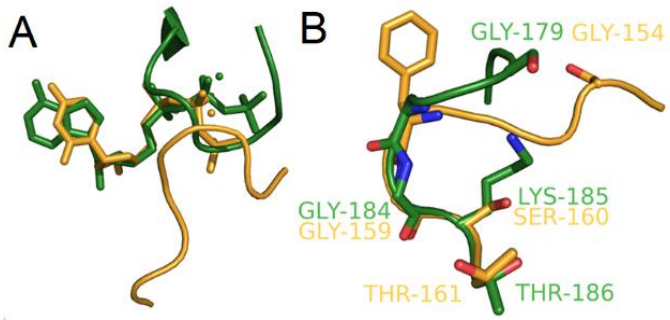

11. ábra: P-hurok konformációk összehasonlítása egy reprezentatív ATPázban (miozin) és a dUTPázban. (A) A hurok és a szubsztrát foszfátláncának relatív helyzete. (B) A két fehérjében található P-hurkok lehető legjobb egymásra illeszkedése.

A P-hurok különböző módokon hat a katalízis elősegítésére az NTPázokban, és ezért úgy gondolják, hogy több esetben egymástól függetlenül jelent meg[62]. A G-fehérjékben és a miozinokban a legvalószínűbb szerepe a katalízisben az, hogy a nukleotidot és a támadó vízmolekulát orientálja a γ-foszfát elleni hatékony nukleofil támadás, valamint a töltés stabilizálása érdekében[62,63]. A dUTPázban is szükséges a P-hurokszerű motívum γ-foszfát koordinációja a katalízisben résztvevő elemek orientálásához és az asszociatív típusú átmeneti állapot stabilizálásához – ez adja a magyarázatot arra, hogy az α-β foszfoanhidrid-kötést hidrolizáló enzim számára is szükséges a szubsztrátban a γ-foszfát jelenléte[44,48]. E hurkok teljesen eltérő topológiája és részben hasonló funkciója a foszfátkötő motívumok konvergens fejlődését jelzi a nukleotid-hidrolázok nagyobb csoportjában, beleértve a PPi -t termelő difoszfatázokat. A hasonlóságok és különbségek a dUTPáz V. motívum és az ATP- és GTPázok által gyakran használt P-hurok (vagy Walker A szekvencia) között jó példát szolgáltatnak a különböző nukleotid-hidrolízis feladatokhoz való kifinomult funkcionális adaptáció megértéséhez.

5.1.4 Csereviszony a kooperativitás és a specificitás között az uracil-mentes DNS fenntartásáért

(Szabó *et al* Sci Rep 2016[41])

A közelmúlt eredményei alapján nézetváltás következett be az allosztérikus viselkedés egy adott fehérje-architektúrán belüli megnyilvánulásának megértésében. A klasszikus nézet szerint az allosztéria különböző szerkezeti változásokon alapul, amelyek egy adott fehérje funkcionálisan eltérő konformereihez vezetnek. Mindazonáltal számos példa bizonyította, hogy az allosztérikus viselkedés nem feltétlenül igényel váltást a közvetlen konformerek között[64], hanem megmagyarázható az oldallánc[65]- vagy a főlánc-dinamika[66] megváltoztatásával vagy a meglévő fehérje konformációk eloszlásának változásával[67]. A klasszikus értelmezés mellett tehát megjelent az allosztéria finomabb, dinamikus értelmezése. Ebben a tanulmányunkban a dUTPázok szupercsaládján belül kívántuk megvizsgálni az allosztéria megnyilvánulását és ennek funkcionális következményeit. A szupercsaládba tartoznak az 1. ábrán látható dUTPáz, dCTP dezamináz (Dcd) és a bifunkciós dCTP dezamináz-dUTPáz (Dcd-dut) enzimek, amelyek a *de novo* dTTP szintézis obligát prekurzorát, a dUMP-t termelik dUTP-ből vagy dCTP-ből (1. ábra).
A dUTPáz szupercsalád tagjai fontos szerepet játszanak a pirimidin nukleotid egyensúly és a genom integritásának fenntartásában. A Dcd és Dcd-dut enzimeket a dTTP allosztérikusan szabályozza. Ezek az enzimek tehát mindhárom pirimidin nukleotidot képesek kötni (dCTP, dUTP, dTTP). Azonban az allosztérikus viselkedés megnyilvánulása a dUTPázok, a szupercsalád harmadik tagjának az előzőkkel azonos fehérje architektúráján belül évtizedekig vita tárgyát képezte.

A kérdés vizsgálatára olyan kísérleti elrendezést terveztünk, amely a dinamikus allosztéria kimutatására is alkalmas. Kovalens hibrid dUTPáz trimereket hoztunk létre, hogy meg tudjuk figyelni egy fehérjén belül az eltérő aktív hely konformációk egymásra gyakorolt hatását. A homooligomer fehérjében generált mutációk minden alegységben megjelennek, mivel az oligomer azonos monomerekből áll össze. Ahhoz, hogy a humán dUTPáz hibrid enzimeit állítsuk elő, létre kellett hoznunk egy kovalensen kapcsolt pszeudohomotrimert, amelyben minden alegység kicserélhető, hogy szelektíven tartalmazza a kívánt mutációt (12. ábra). A WWW konstrukciót a korábban is használt hDUTF158W humán dUTPáz monomerekből (W) állítottuk össze. A többi konstrukcióban a következő pszeudomonomereket alkalmaztuk a kvázi vad típusú W mellett a 13. ábrán látható elrendezésben:

- létrehoztunk egy aktív helyet, amely nem képes befogadni az uracilgyűrűt, és így sem a szubsztrátkötésben, sem az ahhoz kapcsolódó bármilyen konformációs változásban nem vesz részt (F)
- a konzervált katalitikus vizet koordináló Asp aminosavat Asn-re cseréltük az N jelű aktív helyeken. Egy ilyen kötőzseb képes a katalitikusan kompetens konformációt létrehozni, de a kötéshasítás nem történik meg detektálható mértékben
- végül az S jelű aktív helyről, praktikusan a kovalens trimer konstrukció C-terminálisáról, töröltük az előző fejezetben tárgyalt P-hurokszerű V. motívumot, így szüntetve meg a γ-foszfát koordinációt és az aromás kölcsönhatást az uracillal, ami 720-szoros aktivitáscsökkenést eredményez.

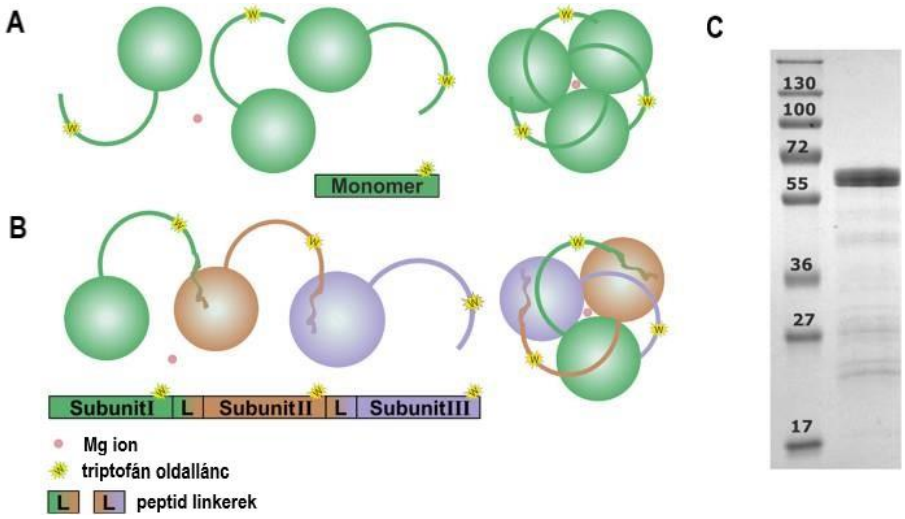

12. ábra: A kovalens trimer koncepció sematikus bemutatása. (A) Azonos monomerekből felépülő homotrimer. A zöld gömbök a hDUTF158W alegységeket jelzik. Az alegységekből kinyúló szerkezetek a dUTPáz C-terminális karját reprezentálják. A sárga csillagok jelzik a triptofánt, amely az enzimkonformációk belső fluoreszcens jele. A rózsaszín gömb Mg^{2+} iont jelez. (B) A kovalens pszeudotrimerek sematikus ábrázolása. A színátmenettel ellátott szalagok a rugalmas linkereket mutatják, amelyek az egyik dUTPáz protomer C-terminálisát összekötik egy másik N-terminálisával. A protomerek különböző színei reprezentálják a trimer belső heterogenitását, azaz minden protomer egymástól függetlenül megváltoztatható. (C) A tisztított WWW enzim SDS-PAGE analízise. A fő sáv a várt pozícióban található, amely megfelel az 58064 Da számított molekulatömegnek.

A WWN, WNN, WWS és WWF hibrideken belüli potenciális allosztérikus kölcsönhatásokat steady-state és tranziens kinetikai mérések kombinációjával vizsgáltuk. Minden konstrukció aktívnak bizonyult, jelezve, hogy az enzimciklus leállítása egy adott aktív helyen nem állítja le a szubsztrát átalakítását a többiben. Azt találtuk, hogy a maximális kezdeti sebesség (V_{max}) arányosan csökkent az inaktív helyek számával, azaz a WWN, a WWF és a WWS körülbelül 2/3 aktivitást mutatott, míg a WNN körülbelül 1/3 aktivitást a WWW-hez képest (13. ábra B). Ez azt jelzi, hogy a működő alegységre jutó aktivitás változatlan a hibrid enzimekben. Azaz megkérdőjelezhetetlen megállapítást nyert, hogy az alegységek egymástól függetlenül működnek a vizsgált dUTPázban. A dUTPáz szupercsalád enzimek összehasonlító szerkezeti elemzésével kimutattuk, hogy egy néhány aminosavból álló allosztérikus hurok és ezen enzimek központi csatornájának csekély szerkezeti különbségei drámaian eltérő allosztérikus viselkedést eredményeznek. Bemutattuk, hogy az allosztérikus szabályozás hiánya a dUTPázban a hatékonyabb dUTP-hidrolízishez való funkcionális alkalmazkodással függ össze.

Az enzimek összehasonlításakor sok esetben megfigyelhető, hogy a rugalmas aktív helyen egy hurok mutációi felelősek a megváltozott szubsztrát-specificitásért. Mivel az aktív helyek gyakran az alegységek vagy domének közötti hasadékoknál helyezkednek el, ezek a hurkok potenciálisan közvetíthetik az allosztérikus kommunikációt az aktív helyek között. Esetünkben úgy tűnik, hogy az egyetlen szubsztrátra, a dUTP-re, történő specializáció az allosztérikus kommunikáció elvesztését eredményezte. A dUTPázban azonosított, a Dcd-khez és a Dcd-dut-okhoz képest rövidebb / kevésbé mozgékony allosztérikus hurok a megnövekedett dUTP-specificitáshoz kapcsolódik. Egy másik dUTPáz „találmány" a C-terminális P-hurokszerű motívum, amely megkülönbözteti a dUDP-t a dUTP-től, és több nagyságrenddel hatékonyabbá teszi a dUTP-hidrolízist, mint a Dcd-dut-ban.

A specificitás növelése és a katalitikus teljesítmény fokozása ezen szerkezeti elemek által a dUTPázokat jelentősen hatékonyabbá teszi a dUTP-bontásban a Dcd-dut-oknál. Erre az előrelépésre szükség lehetett a DNS-ben megjelenő uracil bázis felhalmozódásának elkerülése érdekében. Az ugyanis a DNS-javító mechanizmusok aktiválódását idézi elő, ami súlyos, akár halálos következményekkel járhat a sejtre nézve[68–70].
A Dcd-k és a Dcd-dut trimerek kooperatív allosztérikus viselkedése viszont alkalmassá teszi ezeket az enzimeket a nukleotidkészlet szabályozására. Azt javasoljuk, hogy a kooperatív allosztéria és a szubsztrátspecificitás közötti csereviszony a dUTPáz szupercsaládban a dTTP-szintézishez szükséges negatív visszacsatolással szabályozható dUMP-termelés, és a DNS-beli uracil elkerüléséhez szükséges hatékony dUTP-eltávolítás szerepeihez való alkalmazkodás eseteit testesítik meg.

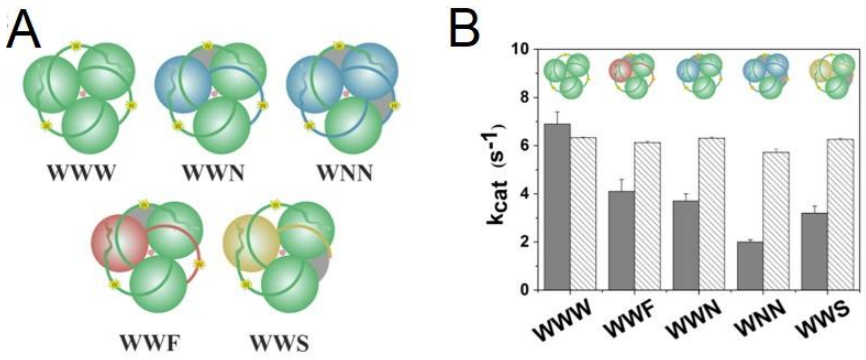

13. ábra: Az aszimmetrikus hibrid enzimek nem-kooperatív kinetikát mutatnak. Az aktív helyek egymástól független működését jelzi az aktív helyek számával egyenesen arányos enzimaktivitás.

5.1.5 A P-hurokszerű motívum mutációi szétkapcsolják a protonátvitelt és a foszfáthasítást a dUTPáz katalizálta reakcióban

(Lopata *et al*, ACS Catalysis 2015[71])

A humán dUTPáz enzimben tervezett és előállított mutációkat a *M. tuberculosis* dUTPázban is előállítottuk, mert ez a fehérje jól kristályosodik (a humán enzimmel szemben), és az erről a fehérjéről hozzáférhető nagy felbontású atomi szerkezetek további ismeretekhez juttattak bennünket. A mutációk hatása a két enzimben megegyezik egymással. Előzőleg a C-terminális kar és az aromás enzim-szubsztrát kölcsönhatás enzimkatalízisben betöltött szerepét kinetikai módszerekkel vizsgáltuk a humán dUTPázban[48,58]. Itt pedig, annak érdekében, hogy megértsük, melyek azok a kulcsfontosságú tényezők, amelyek befolyásolják a katalitikus aktivitások megfigyelt változásait, QM/MM (kvantummechanika és molekuláris mechanika kombinációja) módszertan segítségével mtdUTPáz kristályszerkezeteken tanulmányoztuk a protonátvitel és a foszfáthasítás reakciómechanizmusát a kinetikai paraméterek kísérletes meghatározása mellett. A vad típusú enzim tanulmányozását két olyan mutánséval egészítettük ki, amelyekből már készítettünk nagyfelbontású kristályszerkezet: H145A[48] és T138Stop[72]. A H145A mutáció az aromás π–π kölcsönhatást szünteti meg az enzim és a nukleobázis között (ekvivalens a humán F158A mutációval), a T138Stop pedig a teljes P-hurokszerű motívum eliminációjával jár (ekvivalens a humán T151Stop mutációval).

Az enzimkatalízis gyakran foglal magába egy vagy több protontranszfer eseményt, amelyek szorosan kapcsolódnak a katalizált kémiai reakcióhoz. Így van ez a dUTPázban is, ahol az α-foszfát hidrolízise együtt jár a nukleofil vízmolekuláról a katalitikus Asp83 oldalláncra történő protonátvitellel (14. ábra)[4,73,74]. QM/MM kísérleteinkben a csatolt protonátvitel egyetlen lépésben történt a foszfát hasítással a következő eseménysorozatban: először is, a nukleofil víz megközelítette az α-foszfátot, ezt követően a Pα – O3A kötés felszakadt (14. ábra).

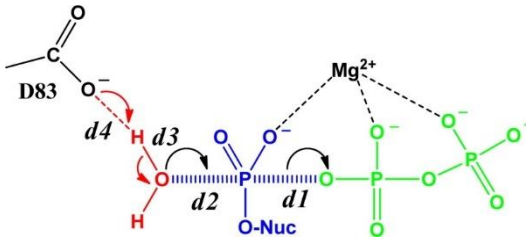

14. ábra: A QM/MM szimulációkban használt reakciókoordináta sematikus ábrázolása. A reakciókoordinátát a következőképpen definiáltuk: Q = Q_{ET} + 0,5 Q_{PT}, ahol a Q_{ET} = d1 - d2 a foszfoanhidrid kötés hasítását, vagyis a (d1) kötésbontási és a (d2) kötésképződési távolságok közötti különbséget jelöli (általánosított elektronátviteli koordináta), a Q_{PT} = d3 - d4 pedig a (d3) kötésszakadási és a (d4) képződési távolságok különbségét a vízből az Asp83-ra történő protonátvitelkor.

A vad típusú enzim átmeneti állapotában az új Pα – Owat kötés (14. ábra) a protonátvitellel egyidejűleg keletkezett. A végtermékekhez ezután a protontranszfer befejezésével jutunk el. Lényegében ugyanezt a mechanizmust figyeltük meg a mutánsokban is. A fő különbség az volt, hogy a protonátvitel függetlenedett az átmeneti állapottól a két mutánsban, és különösen későn történt a majdnem inaktív T138Stop mutáns esetében (15. ábra A). Számított reakciógátjaink jól korrelálnak a megfelelő mutánsok mért katalitikus

sebességeivel. A mutációk hatására nem észleltünk jelentős különbségeket a ligandumkötésben, a fehérje stabilitásban vagy a fehérje-ligandum komplexek szerkezetében. Számításaink azt is bizonyították, hogy a Mg^{2+} koordinációs módja kiemelkedő szerepet játszhat a katalitikus reakcióban.

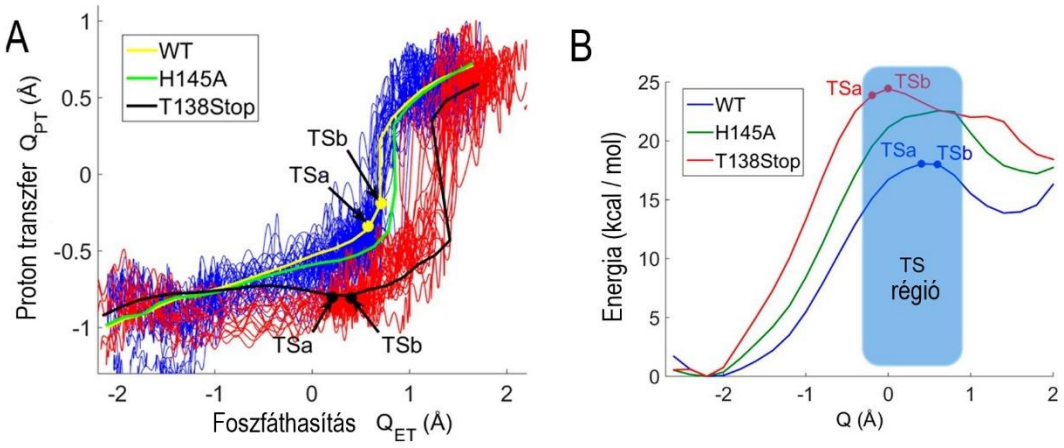

15. ábra: A mutációk következménye a reakcióútra. (A) Reakcióutak a protontranszfert és a foszfoanhidrid kötés hasadást jellemző reakciókoordináták mentén (lásd 14. ábra). A minimális energiapályákat sima vonalakkal jelöltük, vad típus (sárga), a H145A (zöld), T138Stop (fekete). A TSa és a TSb az átmeneti állapothoz legközelebb eső pontoknak felelnek meg a reaktáns és a termékoldalon a minimalizált utak mentén. (B) A katalitikus reakció energiaprofilja az átmeneti állapot (TS) régió kiemelésével.

Egy új, a Rosta csoport által fejlesztett módszer alkalmazásával a fémion körüli szimmetria mennyiségi meghatározásra nyílt lehetőség a katalitikus reakció során. A fémion koordináció folyamatos szimmetriamértékének számítása azt mutatta, hogy egy szimmetrikus, oktaéderes Mg^{2+} koordináció a vad típusban és a mutáns enzimekben is stabilizálja az átmeneti állapotot. A T138Stop mutánsban számítottuk a legszimmetrikusabb, és így a leglazább Mg^{2+} körül koordinációt a reakció során. Ezek szerint a C-terminális kar jelenléte torzítja a szimmetriát. A három rendszer töltéseloszlásának változásai az átmeneti állapotban jelentős különbségeket tártak fel a fehérjéről a szubsztrátra történő részleges töltésátvitelben. Az uracil bázis nagyobb részleges negatív töltéssel rendelkezik a mutánsok által katalizált reakció átmeneti állapotaiban, mint a vad típusú enzimében, míg a dezoxiribóz rész pozitívabban polarizált. Érdekes, hogy a γ-foszfát negatív polarizációja a legnagyobb változás az átmeneti állapot szerkezetek parciális töltései között. Az aktív hely mutációi által okozott geometriai fellazulás kulcsszerepet játszhat az átmeneti állapotok megváltoztatásában, ami a függetlenített protonátvitelhez vezethet.

Összefoglalva megmutattuk, hogy a P-hurokszerű motívum hiányának fő mechanisztikus hatása az, hogy leválasztja a foszfáthasítást az azt követő protonátviteli lépésről, ami egy magas aktiválási energiagáttal jellemezhető megváltozott reakcióutat eredményez (15. ábra).

5.1.6 A dUTPáz rejtett aktív helye a fehérje kis amplitúdójú konformációs változásain keresztül érhető el

(Lopata *et al*, JBC 2016[75])

A nukleotidot hidrolizáló enzimek interdomén hasadékokban vagy alegységek között elhelyezkedő kötőzsebei többek között a katalizált reakció oldószertől való „árnyékolását" is szolgálják. Számos ilyen jól leírt enzimben ez a kötőzseb az oldat felől részben (pl. DNS- és RNS-helikázok, citoszkeletális motorok és kis G-fehérjék) vagy teljesen nyitott (ATP-függő DNS-ligázok). Ezekben az enzimekben a nukleotidkötéshez kapcsolódó konformációs változások eredményezik az aktív hely bezárását, lehetővé téve a kötést követő reakciólépéseket[76–80]. A nukleotidkötés hatására bekövetkező konformációváltozás a rendelkezésre álló apo és ligandumot tartalmazó enzimek kristályszerkezeteinek összehasonlításával látszólag megérthető. A statikus szerkezeti adatok azonban nem helyettesítik minden esetben a dinamikus információkat. Egymolekulás optikai spektroszkópia alkalmazásával például azt mutatták ki, hogy a DNS -polimeráz I nukleotidkötő zsebe dinamikus nyitott-zárt egyensúlyt mutat, amely dNTP-kötéskor a zárt konformáció felé tolódik el[81]. Ilyen esetben a ligandum egy hosszabb időskálán zártnak tűnő zsebhez kötődhet.

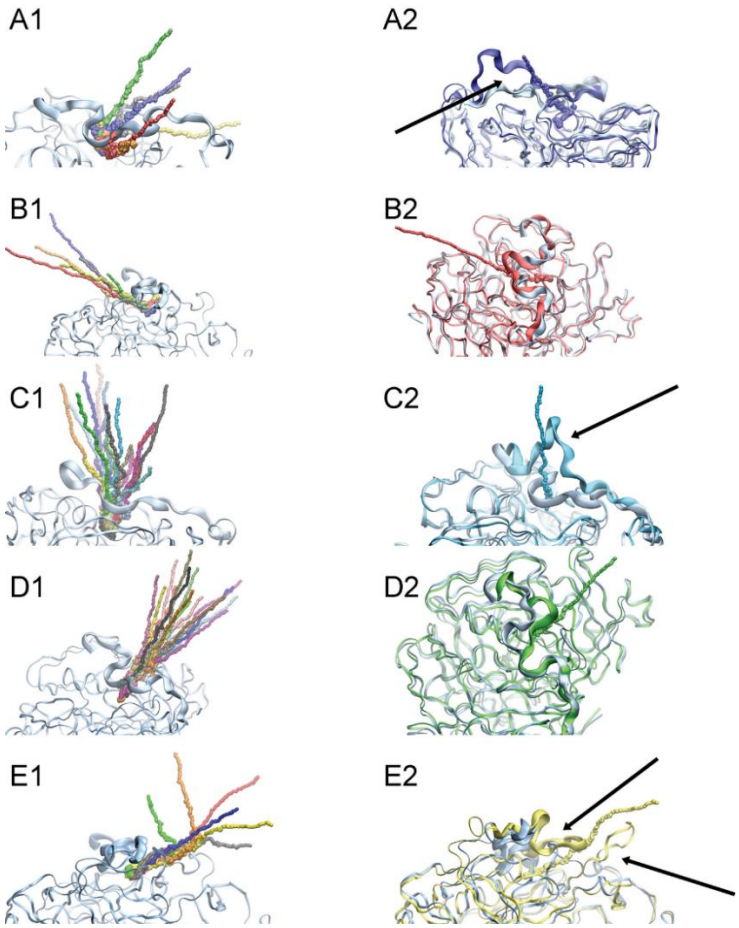

16. ábra: RAMD szimulációk. A fehérje:dUTP:Mg^{2+} komplexek kiindulási szerkezetei és reprezentatív disszociációs útvonalai (A1-E1 panelek) és a végpont fehérjeszerkezetei (A2-E2 panelek) az öt fő útvonalból (A-E). A C-terminális kar vastag szalagként van kiemelve. A futásokat ábrázoló görbéket a dUTP:Mg^{2+} komplex középpontjának gömbmodelljei rajzolják ki. A nyilak a kezdeti és a végpont szerkezetek közötti jelentősebb konformációs változásokat jelzik.

A különböző fajokból származó homotrimer dUTPázok kristályszerkezeteiben a C-terminális kar apo állapotban általában nem látszik[2,45,73]. Ezt a megfigyelést logikusan úgy értelmezték, hogy a távolabbi alegységből az aktív helyre nukleotidkötött állapotban ráhajló C-terminális kar ilyenkor nyitott állapotban van, és az előbb említett ATPázokhoz hasonló módon az aktív hely az oldat felől szabadon megközelíthető. Amikor azonban a C-terminális kar egyensúlyi konformációs állapotát a triptofán fluoreszcens érzékelővel vizsgáltuk (W158 humán dUTPázban), a különböző nukleotidokhoz kötött állapotokban mért oldószer-hozzáférhetősége alapján a kar viszonylag zárt konformációt vesz fel a reakcióciklus-idő legnagyobb részében[43].

A kristálytani és a fluoreszcencia-spektroszkópiai adatok közötti ellentmondásosnak tűnő bizonyítékok miatt nem tudtunk átfogó modellt létrehozni a szubsztrátkötésre vagy a termékfelszabadulásra. E hiány pótlására a RAMD módszert alkalmaztuk (Random Acceleration Molecular Dynamics). Fiziológiai körülmények között a ligandumkötés és disszociáció általában ezredmásodperces időskálán megy végbe, így pontos modellezése több mikroszekundum hosszú molekuláris dinamikai szimulációt és ehhez jelenleg rendelkezésre nem álló számítási kapacitást igényel. Ezért eltemetett aktív helyek esetén előnyös a folyamat felgyorsítása. A RAMD módszer a ligandumra ható mesterséges és random irányú erőt alkalmaz, amely felgyorsítja az enzimről történő disszociációs folyamatot, ezzel ésszerű időkeretet biztosítva a számítási szimulációkhoz[82]. A nagyfelbontású *M. tuberculosis* dUTPáz szerkezeteinket használtuk fel a RAMD szimulációk kivitelezésére.

A RAMD futások során egyszer sem figyeltük meg a korábban feltételezett csapóajtószerű mechanizmust, amelyben a C-terminális kar teljesen kinyílik egy konzervált prolin sarokpontjánál[83]. Ehelyett a C-terminális kar kis nyílásain keresztül hagyta el a nukleotid az aktív helyet (16. ábra). A kar, amely mindkét végén az enzim felszínéhez rögzítve maradt másodlagos kölcsönhatásai révén, csak az enzim felületéhez közel mozdult el, vagy részben és lokálisan nyílt fel. Ezek a 10–15 aminosavat érintő kis amplitúdójú mozgások (16. ábra) a többi nukleotidkötő enzimnél megfigyelhető konformációs változásokhoz képest kicsik[79,80,84]. Ez a modell konzisztens minden eddigi eredménnyel, és egyaránt magyarázza a spektroszkópiában megfigyelt predominánsan zárt, illetve a kristályszerkezetekben nem látszó, tehát dinamikus C-terminális kar konformációt. Az *in silico* adatok egy eddig le nem írt kölcsönhatást is jósoltak a C-terminális kar és a 21-es aminosav-pozíció között, amely több disszociációs útvonalban is fontosnak tűnt. Ezt a potenciális interakciót alkalmasnak találtuk a módszer validálására, ezért létrehoztunk egy új triptofán riportert (H21W) ebben a pozícióban. Szerkezetmeghatározás, tranziens kinetika, egyensúlyi ligandumkötési és oldószerhozzáférési kísérleteket kombinálva kimutattuk, hogy a W21 oldallánc valóban kölcsönhat az aktív helyet védő C-terminális karral és az aktív helyre bevitt szenzorhoz hasonlóan érzékeli a dUTP hidrolízis reakciót (17. ábra). Ezekkel az eredményekkel egyben az első direkt kísérletes bizonyítékot szolgáltattuk a RAMD módszer hatékonyságára.

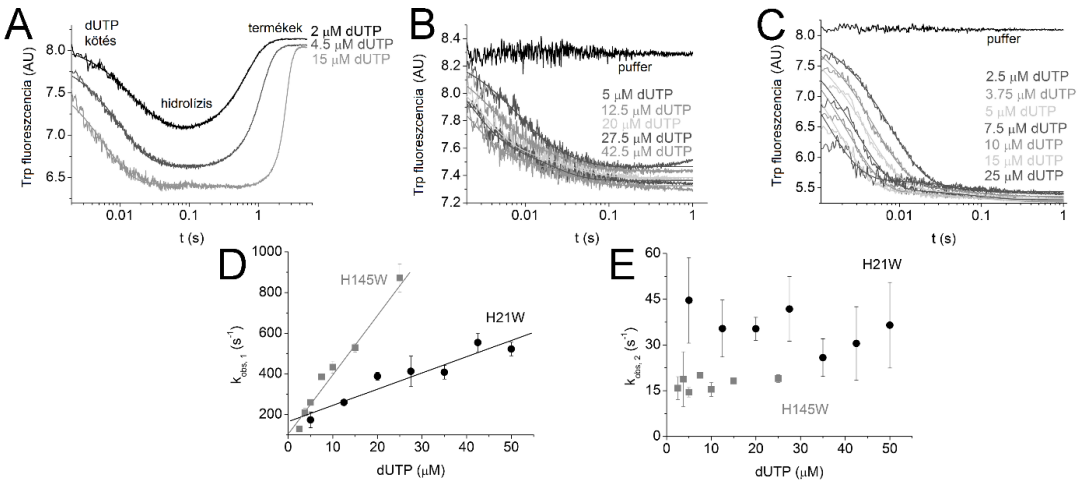

17. ábra: A RAMD predikció alapján előállított H21W mutáns a jól leírt aktív hely Trp szenzorhoz (H145W) hasonlóan érzékeli a reakciót. (A) Stopped-flow módszerrel mért egyszeri és többszöri átvitelű dUTP hidrolízis reakciók időbeli lefutása. Az exponenciális illesztésből számított sebességi állandók megfelelnek a korábban az aktív helyen lévő Trp szenzorral mért értékeknek. (B) dUTP kötés a H21W mutánshoz. (C) dUTP kötés a H145W mutánshoz. (D) A dUTP kötés gyors fázisára illesztett sebességi állandók koncentrációfüggése. Tekintettel a két enzim szerkezeti hasonlóságára, váratlan volt, hogy a ligandumkötési folyamat sokkal lassabb, ha a 21. pozícióban egy His helyett Trp oldallánc van jelen. Ez a változás azonban tovább bizonyítja, hogy ez az oldallánc részt vesz a ligandumkötésben. (E) A dUTP-kötés lassú fázisára illesztett sebességi állandók koncentrációfüggése. Úgy tűnik, hogy ez a fázis független a szubsztrát koncentrációjától, összhangban a korábbi adatokkal.

Összefoglalva, molekuladinamikai számításaink és spektroszkópiai eredményeink alátámasztják azt az elképzelést, hogy a kis hurokmozgások lehetővé teszik a nukleotidok átjárását a kötőzseb és az oldószer között anélkül, hogy a kötőzseb markáns nyitott-zárt konformációváltozáson menne át.

5.1.7 Inert kelátor? Az EDTA szorosan köti a dUTPázt, a Taq DNS polimerázt és a MutT enzimet, és gátolja a dUTPáz aktivitást

(Lopata *et al,* Biomolecules 2019[85])

A kétértékű fémionok kiemelkedő szerepet játszanak az enzimatikus katalízisben, köztük a Mg^{2+} a nukleotidok hidrolízisét katalizáló enzimekben (pl. ATPázok[86], GTPázok[87], ligázok[88], DNS és RNS polimerázok[89], Nudix-hidrolázok[90]). Számos publikáció kísérleti adatai azonban azt jelzik, hogy a dUTPáz katalitikus aktivitása csak kétszeresére csökken a Mg^{2+} kofaktor hiányában [4,45,46,91,92]. Más szerzők ugyanakkor arra a következtetésre jutottak, hogy a dUTPáz teljesen inaktív Mg^{2+} nélkül [93–95]. Az utóbbi esetekben vagy nagy koncentrációjú EDTA-t használtak a Mg^{2+} elvonására, vagy nem írták le a fémmentes körülmények biztosításának módját. A kismolekulájú szerves vegyület etilén-diamin-tetraecetsav, vagy közismert nevén EDTA, jól oldódó, optikailag inaktív, és nem reagál a legtöbb pufferben használt vegyszerrel, így előnyös választásnak tűnik a fémmentes körülmények biztosítására a biokémiai és biofizikai vizsgálatokhoz. A dUTPáz kétértékű fémionok hiányában mért aktivitása körül tapasztalt ellentmondások azonban felhívták a figyelmünket az EDTA kelátképzésen túli feltételezett egyéb hatására. Ezért kezdtük tanulmányozni az EDTA kölcsönhatását két különböző, általunk már jól ismert dUTPázzal (humán és *M. tuberculosis*) Mg^{2+}-mentes körülmények között.

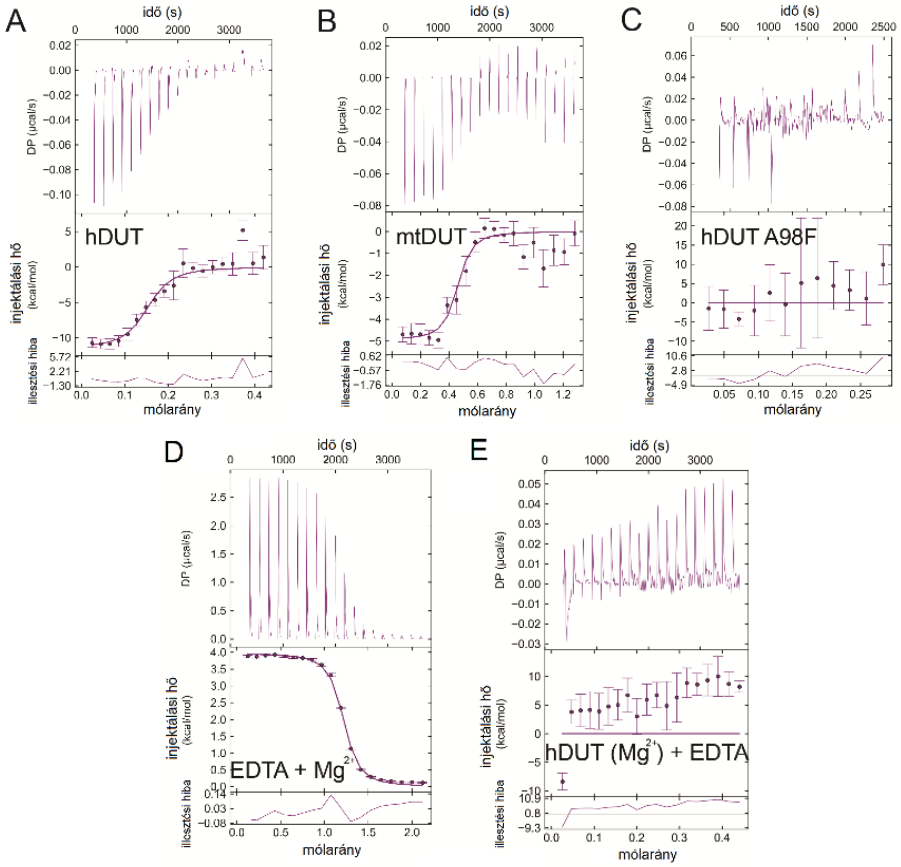

18. ábra: A dUTPázok EDTA-kötése. ITC kísérlet. (A-B) vad típusú humán és M. tuberculosis dUTPáz EDTA kötése. (C) Az A98F humán dUTPáz mutáns, amely nem tud szubsztrátot kötni, mert az aktív helyre egy nagy térigényű csoportot szerkesztettünk, EDTA-t sem köt. Ez bizonyítja, hogy az EDTA az aktív helyre kötődik. (D-E) Kontroll kísérletek, amelyek azt mutatják, hogy az (A-B)-ben megfigyelt kötési görbe nem a mintában maradt reziduális Mg^{2+}-nak köszönhető.

Korábbi eredményeinkkel egyezően ismét azt találtuk, hogy a Mg^{2+} hiánya csak felére csökkenti a katalízis sebességét. A Mg^{2+}-mentesítést extenzív dialízissel értük el, és ICP-OES (Inductively Coupled Plasma Atomic Emission Spectroscopy) módszerrel ellenőriztük. Ezután ITC-vel vizsgáltuk az EDTA kötődését a dUTPázokhoz. Mindkét enzimen nagy affinitású EDTA-kötést mértünk, amely csak abban az esetben valósult meg, ha az enzim aktív helye hozzáférhető volt a szubsztrát, és ezek szerint az EDTA, számára (18. ábra, 1. táblázat). A kötés szerkezeti alapjait *in silico* dokkolással vizsgáltuk a meglévő atomi szerkezetek segítségével, valamint az EDTA:dUTPáz komplex kristályszerkezetét is megoldottuk. Mivel azonban az EDTA az aktív helyen csak részlegesen látszik a rögzített elektronsűrűségi térképen, eltekintettünk az EDTA:dUTPáz komplex szerkezet PDB adatbázisban történő elhelyezéséről. A ligandum dokkolás megerősítette, hogy az EDTA sokféle konformációt felvehet az aktív helyhez kötött állapotban, ezért nem meglepő, hogy a kristályszerkezetben sem jól definiált. *In silico* dokkolással azt találtuk, hogy az EDTA elfoglalja az aktív helyen a szubsztrát térrészét (19. ábra), és hasonló kölcsönhatásokat képez a fehérjével, mint maga a szubsztrát. E megfigyelés nyomán feltételeztük, hogy más dNTP-kötő fehérjék aktív helyére is beköthet.

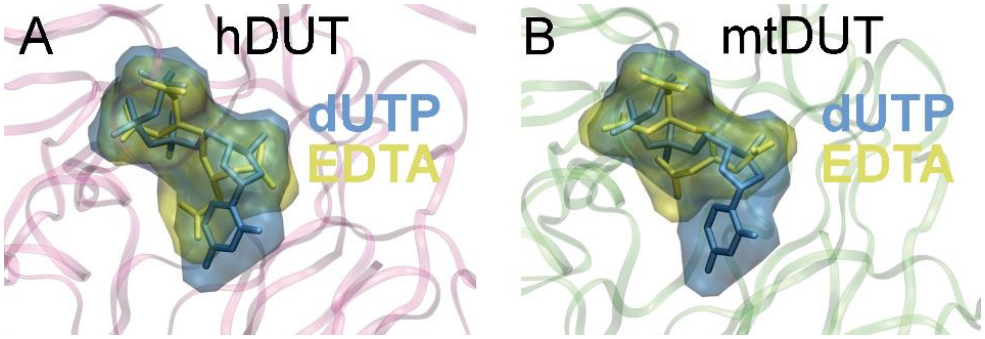

19. ábra: Az EDTA predomináns konformációja az aktív helyen részlegesen átfed a szubsztrát által elfoglalt térrésszel az in silico dokkolási kísérletekben. A kékkel jelölt térrészt a szubsztrát, míg a sárgával jelölt térrészt az EDTA tölti ki. Az EDTA kisebb térigényű, mint a szubsztrát, emiatt a dokkolási kísérletekben többféle kötött konformácót figyeltünk meg, illetve az mtDUT:EDTA kristályszerkezetben is csak részleges elektrontérképet kaptunk az EDTA-ról az aktív helyen.

Ezért két, számunkra nagy mennyiségben hozzáférhető dNTPáz, a Taq polimeráz és a MutT feltételezett EDTA kötését is megmértük ITC-vel (20. ábra A-B, 1. táblázat). Az enzim:EDTA komplexekre mért szubmikromoláris disszociációs állandó mindkét esetben jelentősen alacsonyabb, mint az enzim:szubsztrát vagy a Mg^{2+}:EDTA komplexeké. Az EDTA-kötés exotermnek bizonyult, amely főként entalpia-vezérelt (1. táblázat). A kontrollfehérjék, köztük egy ATPáz, nem léptek kölcsönhatásba az EDTA-val (20. ábra C-E). Eredményeink azt mutatják, hogy az EDTA a dNTP hidrolizáló enzimek szelektív gátlószere lehet. Ez egyrészt arra figyelmeztet, hogy az EDTA használatát újra kell gondolni az enzimreakciókat vizsgáló kísérletekben. Másrészt viszont érdemes megfontolni EDTA alapú szelektív gátlószerek kifejlesztését, mint ahogyan arra más enzimeknél már van példa[96,97].

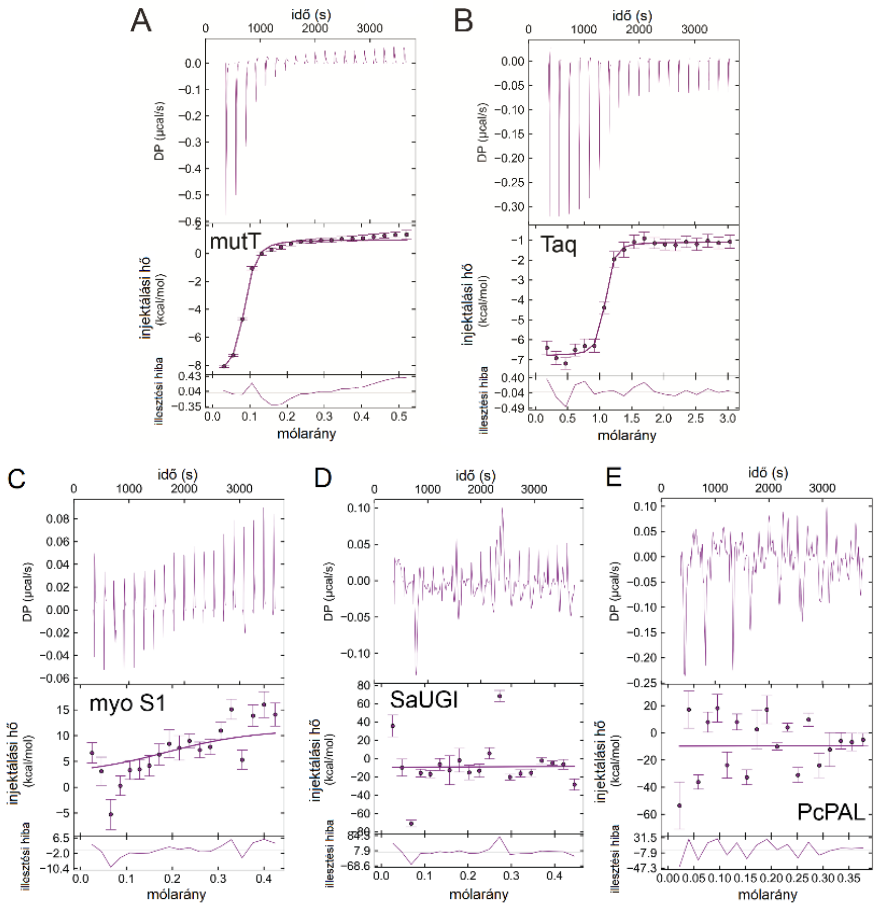

20. ábra: dNTP-t hidrolizáló és kontroll fehérjék EDTA-kötése. (A) E. coli MutT, dNTP hidrolizáló enzim és (B) Thermus aquaticus DNS polimeráz EDTA kötése. (C-E) kontroll fehérjék EDTA-val való titrálása. (C) vázizom miozin subfragmentum-1, (D) Staphylococcus aureus uracil-DNS glikoziláz inhibitor (SaUGI), (E) Petroselinum crispum fenilalanin ammónia liáz (PcPAL).

1. táblázat: Az ITC kísérletekben mért termodinamikai paraméterek 293 K hőmérsékleten és 7,5-ös pH-n.

Titrálandó	Titráns	ΔH / kcal/mol	-TΔS / kcal/mol	ΔG / kcal/mol	K_d / µM
hDUT	EDTA	-11,2 ± 0,4	2,2 ± 0,4	-9,0 ± 0,0	0,20 ± 0,009
hDUT	dUPNPP	-17,4 ± 3,6	11,5 ± 3,7	-5,9 ± 0,2	43,9 ± 14,6
mtDUT	EDTA	-4,2 ± 1,0	-5,3 ± 1,2	-9,6 ± 0,2	0,078 ± 0,023
mtDUT	dUPNPP	-4,5 ± 0,2	-2,1 ± 0,4	-6,6 ± 0,6	13,9 ± 11,7
EDTA	Mg^{2+}	4,4 ± 0,3	-12,5 ± 0,6	-8,0 ± 0,9	2,53 ± 0,18
EcMutT	EDTA	-9,7 ± 0,02	1,3 ± 0,1	-8,4 ± 0,1	0,55 ± 0,066
Taq	EDTA	-6,3 ± 0,7	-3,5 ± 0,7	-9,8 ± 0,0	0.47 0,001

5.2 A dUTPáz élettani szerepe

5.2.1 A dUTPáz fehérje és a mikobaktérium-specifikus felszíni hurok nélkülözhetetlen a *M. smegmatis* életképességéhez

(Pécsi *et al*, Plos one 2012[37])

A dUTPáz aktivitás csökkenése vagy hiánya a DNS uracil-tartalmának jelentős növekedéséhez vezethet, ami a vizsgált esetekben kromoszóma-fragmentációt és sejthalált eredményezett[98–100]. A dUTPáz aktivitás ugyanakkor a dTTP bioszintézisében is nélkülözhetetlen lehet, ha az alternatív útvonalak nem állnak rendelkezésre (1. ábra). Az összes ismert mikobaktérium faj a dUTPáz hatását feltételező, *de novo* bioszintézis útra támaszkodik (1. ábra). A jól ismert monofunkciós dUTPáz (a *dut* gén terméke) mellett egy bifunkciós dCTP-dezamináz-dUTPázt (Dcd:dut) is azonosítottak a *M. tuberculosis* genomjában[101]. Korábbi tanulmányok kimutatták az általánosan előforduló monofunkciós dUTPáz esszenciális voltát *E. coli*-ban[102] és élesztőben[68]. A *M. tuberculosis*ban végzett nagyáteresztőképességű mutagenezis vizsgálatok is azt sugallták, hogy az növekedéséhez szükség van a *dut* géntermékre, a bifunkciós enzimre azonban nem[103,104]. Miután részletesen tanulmányoztuk a mikobakteriális dUTPáz szerkezetét és enzimmechanizmusát[10,48,72], az enzim élettani hatását is elkezdtük behatóan vizsgálni. Ehhez egy új modellrendszert honosítottunk meg: a gyorsan növekvő és veszélytelen *M. smegmatis*t, a *M. tuberculosis* nem-fertőző közeli rokonát. Elsőként megvizsgáltuk, hogy a *M. smegmatis* érvényes *M. tuberculosis* modellként szolgálhat-e a timidilát bioszintézis útvonalának vizsgálatában. Miután a *M. tuberculosis* és a *M. smegmatis* dTTP bioszintézis útvonalaiban szerepet játszó enzimkészletét azonosnak találtuk, és az egymásnak megfelelő enzimek aminosav szekvencia hasonlósága is rendkívül magas volt (tipikusan 80% feletti szekvencia azonosság, a konzervált motívumokban pedig közel 100%), ezt a szervezetet választottuk a *dut* funkcionális deléciójának végrehajtására. Kétlépcsős rekombinációs génkiütéses technikával kimutattuk, hogy a monofunkciós dUTPáz elvesztése letális a *M. smegmatis* számára. A genomi dUTPáz kópiát csak abban az esetben lehetett kivágni, ha episzomálisan bevittünk egy másik dUTPázt. A letalitás azonban nem feltétlenül a dUTPáz aktivitás hiánya miatt következett be.

Bár a dUTPázt patogének elleni gyógyszercélpontnak tekintik[31,105], a szelektív gyógyszertervezést megnehezíti a humán és patogén dUTPázok közötti nagy szekvencia- és szerkezeti hasonlóság. Azonban a rendelkezésre álló dUTPáz szekvenciákat összehasonlítva egyértelműen arra a következtetésre jutottunk, hogy a mikobakteriális dUTPáz egy egyedi és szigorúan mikobaktérium-specifikus inszertet kódol a C-terminálisához közel (21. ábra A). Ez az inszert egy felszíni hurokként jelenik meg az aktív hely bejáratához közel, amint az a *M. tuberculosis* dUTPáz kristályszerkezetén[44,73,106] látható (21. ábra B). Érdekes módon a hurkot nem tartalmazó, de egyebekben érintetlen fehérje nem tudta komplementálni a letális génkiütött fenotípust. Mivel a fehérjének ez a mikobaktérium-specifikus szegmense hozzájárul a teljes enzim által közvetített élettani hatáshoz, szelektív hatóanyag-célfelületként szolgálhat.

A tisztított mikobaktérium-specifikus hurok nélküli (Δ-loop) fehérjén végzett spektroszkópiai és steady-state kinetikai méréseink arra a következtetésre vezettek, hogy az aktív hely közelében lévő öt aminosavból álló inszert nincs jelentős hatással a katalízisre (2. táblázat). A Δ-loop fehérjében megközelítőleg 67%-ra csökkent enzimaktivitás jelezte

változás jelentéktelen ahhoz képest, hogy szinte minden más, korábban általunk dUTPázba bevitt mutáció nagyságrendi aktivitáscsökkenést és K_M növekedést okozott[43,48,58]. A dUTPáz aktivitás és a mikobakteriális életképesség pontos összefüggése nem volt ismert. Azonban Guillet és mti. arról számoltak be, hogy olyan mutáns élesztőtörzsek is életképesek, amelyekben a dUTPáz enzimaktivitás a vad típusúnak kevesebb, mint 10%-ára csökkent[100]. Ez az információ arra utal, hogy a Δ-loop mutáns nem az aktivitáscsökkenés miatt nem komplementálja a letális fenotípust, hanem mert az 5 aminosav hosszú inszertre szükség van más, létfontosságú folyamatokhoz.

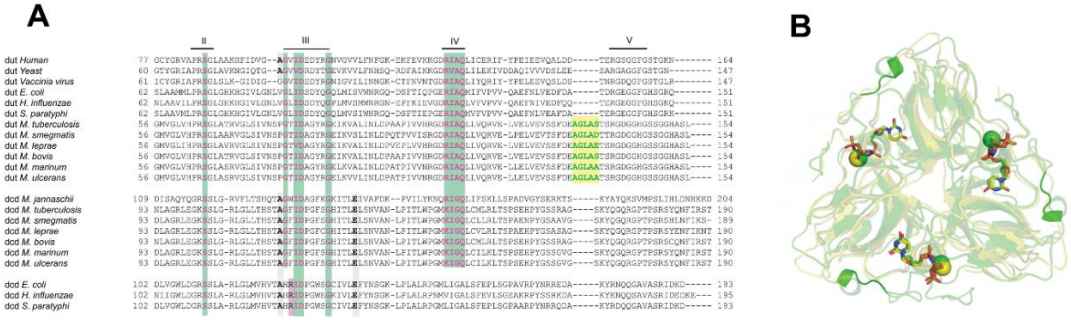

21. ábra: A mikobaktérium-specifikus felszíni hurok. (A) A konzervált motívumokat a szekvenciák felett jelöltük. Összehasonlítás céljából a legkülönbözőbb evolúciós ágakból származó reprezentatív szervezeteket választottunk. A mikobakteriális bifunkciós Dcd:dut-ok mindazokat a konzervált oldalláncokat tartalmazzák, amelyek a dUTPáz reakcióhoz szükségesek (zöld háttér). A dezaminációs reakcióhoz és a dCTP dezaminéz monofunkcionalitása szempontjából döntő fontosságú aminosavakat szürke, illetve bíbor háttérrel ábrázoltuk. A mikobakteriális dUTPáz inszertet sárgával emeltük ki. (B) A mikobakteriális inszert kihurkolódik a dUTPáz alegységek felületén (erősebb zöld szalag ábrázolás). A humán (PDB azonosító: 3EHW) és M. tuberculosis dUTPáz (PDB azonosító: 2PY4) egymásra illesztett szerkezetét sárga, illetve zöld szalagként ábrázoltuk.

Feltételezzük, hogy exponált helyzete miatt a hurok kötőfelszínt biztosíthat egy még ismeretlen fehérjepartner vagy más ligandum számára, és ennek a kölcsönhatásnak a hiánya okozhatja a vizsgálatunkban kimutatott letalitást. Úgy tűnik, hogy a mikobakteriális dUTPáz enzimaktivitáson túlmutató funkciókat is ellát, amelyeket egy egyedi szekvenciamotívum biztosít. Ennek a mikobaktérium-specifikus funkciónak a tisztázásához további vizsgálatokra van szükség.

2. táblázat: A vad típusú és a Δ-hurok deléciós mutáns M. tuberculosis dUTPáz enzimek kinetikai paraméterei és a dUTPáz-dUPNPP komplexek disszociációs állandói.

		vad típus	**Δ-loop**
Aktivitás mérés	k_{cat} (s^{-1})	1,22 ± 0,06	0,88 ± 0,02
	K_M (μM)	0,9 ± 0,5	1,1 ± 0,2
Fluoreszcencia	A_{max}	−72 ± 2	−46 ± 1
	K_d (μM)	0,3 ± 0,1	3,3 ± 0,5
CD spektrometria	K_d (μM)	0,9 ± 0,5	3,9±2,4

5.2.2 Fiziológiás funkciók szétválása a dUTPáz szupercsaládon belül: specializáció a dTTP bioszintézisére és a genomi integritás fenntartására

(Hirmondó *et al*, SciRep 2017[33])

E helyütt szeretném ismét kihangsúlyozni a dUTPáz reakció, azaz a dUTP dUMP-vé történő lebontásának kettős szerepét. Ez a kémiai átalakulás egyrészt előállítja a dTTP bioszintézis obligát prekurzorát, a dUMP-t, másrészt alacsonyan tartja a sejtbéli dUTP:dTTP arányt, és ezzel megakadályozza a dUTP beépülését a DNS-be[14]. Utóbbit preventív DNS-javításnak is nevezik, mert ezzel a megelőző lépéssel elkerülhető az uracil tömeges DNS-be való beépülése, és ezzel a genomintegritás veszélyeztetése. A dUTPáznak tulajdonított különféle szerepek, valamint a dUTPáz szupercsalád enzimeire vonatkozó génkiütéses és csendesítési adatok a különféle genetikai hátterű élőlényekben ellentmondásos képet adnak a dUTPáz hozzájárulásáról azokhoz az élettani folyamatokhoz, amelyekben részt vehet. Mivel a dNTP homeosztázis fenntartása alapvető életfolyamat és számos jelenlegi gyógyszeres terápia és gyógyszerfejlesztés fő célpontja, fontos lenne meghatározni azokat az útvonalait, amelyekhez a dUTPáz kulcsfontosságú hozzájárulással bír. A dUTPázok dTTP bioszintézishez és a DNS uraciláció megelőzéséhez való hozzájárulásának vizsgálatához a mikobaktériumot kiváló modellnek találtuk, mivel ebben az élőlénycsoportban a dTTP bioszintetikus utak a dUTPáz aktivitástól függő utakra korlátozódnak[37,107] (1. ábra).

Tanulmányunkban fokozatosan csökkentett enzimaktivitású és inaktív monofunkciós dUTPáz és inaktív bifunkciós Dcd:dut mutáns törzseket hoztunk létre a *M. smegmatis* mikobakteriális modellben, majd vizsgáltuk ezek életképességét. A mutáns fehérjék *in vitro* mért kinetikai jellemzőit a 3. táblázat foglalja össze.

3. táblázat: A WT és mutáns M. tuberculosis dUTPáz és Dcd:dut enzimek kinetikai paraméterei

Enzim	k_{cat} (s^{-1})	K_M (μM)	$K_{d,dUPNPP}$ (μM)	k_{cat}/K_M ($M^{-1}s^{-1}$)	dUTPáz hatékonyság
wt Dut	1,22 ± 0,06	1,7 ± 0,5	0,9 ± 0,5	$7,18 \cdot 10^5$	1
S148A Dut	0,43 ± 0,04	1,5 ± 0,6	1,8 ± 1,0	$2,87 \cdot 10^5$	0,4
T138stop Dut	0,0035 ± 0,0001	6,7 ± 0,4	3,9 ± 1,3	$5,22 \cdot 10^2$	0,0007
D83N Dut	0,0013 ± 0,0005	7,7 ± 6,7*	1,5 ± 0,1	$1,69 \cdot 10^2$*	0,0002
wt Dcd:dut *dUTPáz reakció*	0,033 ± 0,008	12 ± 3	-	$2,75 \cdot 10^3$	0,004
dCTP dezaminász reakció	0,022 ± 0,005	20 ± 12		$1,10 \cdot 10^3$	NA
A115F Dcd:dut	inaktív	-	-	-	0

***** bizonytalan adat az aktivitásmérés teljesítőképességének határán

Az ezeket a fehérjéket kifejező törzsekben azt találtuk, hogy akár a monofunkciós dUTPáz, akár a bifunkciós Dcd:dut aktivitása önállóan is képes támogatni a sejtnövekedést (3. B és 4. D ábra az eredeti közleményben, Függelék). A dUTPáz aktivitással nem rendelkező kettős

mutáns *M. smegmatis* törzs azonban életképtelennek bizonyult. Vizsgáltuk a különböző aktivitás-csökkenés által kiváltott élettani hatásokat, beleértve a dNTP készlet változásait, a mutációs rátát és a DNS uraciltartalmát a különböző mutáns törzsekben. Az aktivitás-csökkentett dUTPáz mutáns *M. smegmatis* törzsek megnövekedett mutációs rátát mutattak, ami a genomi uraciltartalom növekedésével járt együtt (20-150-szeres, 22. ábra). A mikobaktériumok három uracil-DNS glikoziláz enzimet is kódolnak (ung, udgB és udgX)[108–110], amelyek lehetővé teszik az uracil hatékony eltávolítását a genomból ezekben a szervezetekben[109]. Ez a kivételes funkcionális redundancia jelzi, hogy az uracil DNS-ben történő felhalmozódása nemkívánatos folyamat. Az uracil felhalmozódásának oka a mutánsaink DNS-ében ennek ellenére az lehet, hogy a DNS-polimerázok az uracil kivágása után újra beépítik a dUTP-t egy magas dUTP-koncentrációjú nukleotidkészletből (23. ábra). A dNTP-k túltermelése az endogén DNS-károsodás hatására általános stresszválasz[111–113], és valószínűleg a genotoxikus stresszel szembeni tolerancia elősegítésére szolgál. A megemelkedett dNTP-szintek viszont növelik a mutációs rátát[112,114–116], mivel a DNS polimerázok aktivitásegyensúlya átmenetileg megváltozik[115]. Ezzel az ördögi körrel megmagyarázható a különböző mutánsok mutációs rátájának hasonlóan nagy növekedése. Ennek értelmében a dNTP készlet sejtbéli koncentrációjának általános megemelkedése egy általános stresszválasz része, és nem specifikus a dUTPáz aktivitás csökkenésére. Érdekes módon, bár a dTTP:dCTP arány erősen kiegyensúlyozatlan volt a bifunkciós mutáns törzsben (23. ábra), a mutációs ráta csak kétszeresére nőtt (22. ábra), ami arra utalhat, hogy a dCTP viszonylag gyenge mutagén prekurzor.

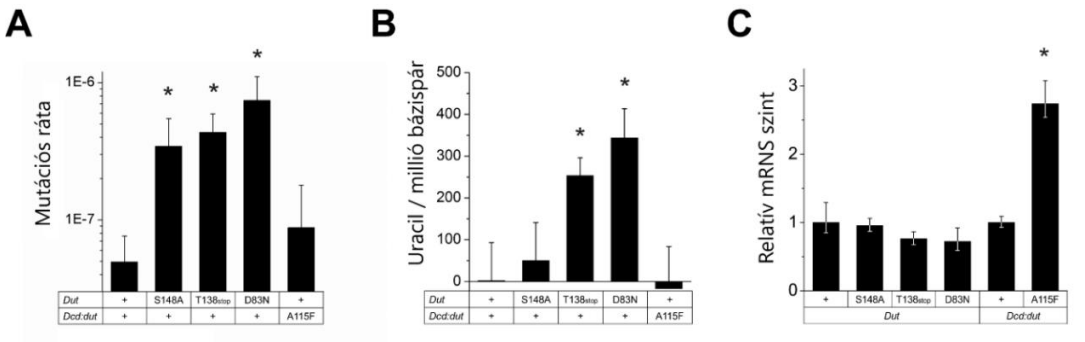

*22. ábra: A monofunkciós és bifunkciós dUTPáz mutációk hatása a M. smegmatis mutációs rátájára, a DNS uracilációra és a génexpresszióra. (A) M. smegmatis törzsek mutációs rátája. Megjegyzendő, hogy a dut mutáns törzsek mutációs rátája közvetlenül korrelál a megfelelő mutáns enzim in vitro aktivitásvesztésével. Szignifikanciaszintek: P = 0,000115 S148A esetén, P = 0,000034 T138stop és P = 0,000004 D83N esetén. A „+" a vad típusú enzimet jelöli. (B) A mutáns törzsek genomiális uraciltartalma a vad típusú törzshöz viszonyítva. A dut mutáns törzsek genomi uraciltartalma itt is korrelál a megfelelő mutáns enzim in vitro aktivitásvesztésével. Szignifikanciaszintek: P = 0,074 a T138stop esetében, P = 0,018 a D83N esetében. (C) A Dut és Dcd:dut expressziós szintek mennyiségi meghatározása a vad típusú és mutáns M. smegmatis törzsekben. Ez a kontroll annak kizárására szolgál, hogy a megfigyelt fenotípus nem a mutáció hatásával, hanem az expressziós szinttel korrelál. Szignifikanciaszint: P = 0,029 az A115F mutáns esetében. Az átlag ± SE értékek mindenütt 3 biológiai párhuzamost és 3 technikai replikátumot (3*3 mérés) reprezentálnak.*

Meglepetésünkre, a bifunkciós mutáns törzsben a csökkent dTTP-koncentráció (23. ábra) nem korlátozta a baktériumok proliferációs sebességét. Ez azt jelzi, hogy a két dUTPáz bármelyikének aktivitása elegendő a dTTP- és a DNS-szintézis támogatásához és a *M. smegmatis* hatékony szaporodásához annak ellenére, hogy a bifunkciós enzim százszor

kevésbé hatékony dUTPáz, mint a monofunkciós dUTPáz (3. táblázat és [10,107]). A 23. ábrán bemutatott további eredményeink arra utalnak, hogy a dUMP termelés és a dTTP bioszintézis főként a bifunkciós Dcd:dut enzim szabályozása alatt áll. A bifunkciós enzim képes megkötni a dTTP-t, ami gátolja annak aktivitását[117]. Ez a negatív visszacsatolás teszi lehetővé a sejtbéli dCTP:dTTP koncentrációarány általunk is megfigyelt szabályozását. A monofunkciós dUTPáz azonban csak a dUTP-t képes befogadni, és az előzőekben ismertetett munkánkban kimutattuk, hogy a nagy szerkezeti hasonlóság ellenére nincs allosztérikus szabályozása[43]. A 22-23. ábrákon látható eredményeink alapján azt javasoljuk, hogy a monofunkciós dUTPáz felelős a DNS-be való dUTP-beépülés hatékony kiküszöböléséért, míg a bifunkciós dUTPáz szerepe a megfelelő dCTP:dTTP arány fenntartása. Ennek a funkcionális szétválásnak egyértelmű előnyei vannak. A dUDP foszforilációjával és a spontán dCTP dezaminációval folyamatosan keletkező dUTP-t a dNTP készletből el kell távolítani, ezzel megakadályozva a genom uracilációját. Ehhez a funkcióhoz előnyös egy hatékony és dUTP-re specifikus enzim. A szabályozó képességek ugyanakkor egy másik, közeli rokon bifunkciós enzimbe épültek be, amely nem bizonyult hatékonynak a dUTP eltávolításában, de a DNS pirimidin építőelemeit helyes koncentrációarányba tereli (23. ábra). A bifunkciós enzim preventív vonatkozása az lehet, hogy a „veszélyes" dUTP nem szabadul fel a dCTP dezaminációs reakciót követően, hanem ugyanazon az enzimen dUMP-vé alakul[74, 108]. Örömünkre szolgált, hogy a két enzim szerkezetét és kinetikai mechanizmusát tanulmányozva a korábbi Szabó *et al.* cikkünkben levont következtetések[41] az élő szervezetben végzett, fiziológiásan releváns kísérletekben is megerősítést nyertek. Összecsengenek az itt kapott eredmények továbbá a dUTPáz-hiány letalitására vonatkozó korábbi eredményünkkel is, amely szerint az intakt monofunkciós dUTPáz fehérje jelenléte szükséges a mikobaktérium életképességéhez, nem pedig az enzimatikus aktivitása[37], amelyet a mutációs ráta emelkedése mellett a kevéssé hatékony bifunkciós enzim is képes helyettesíteni.

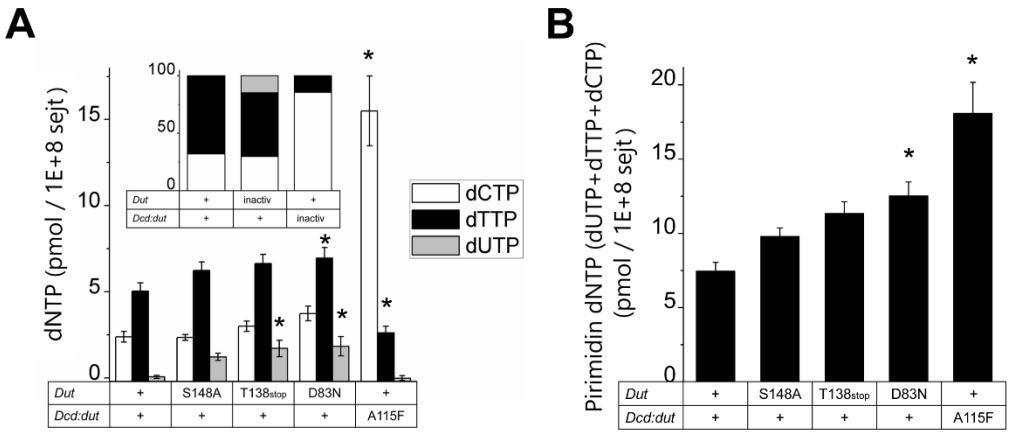

23. ábra: A Dut és a Dcd:dut mutációk hatása a pirimidin dNTP készletre. (A) A dTTP, dCTP és dUTP koncentrációkat DNS polimeráz alapú módszerrel mértük minden mutáns törzsben. A „+" a vad típusú enzimet jelöli. Az átlag ± SE 12 adatpontból származik minden esetben. A dUTP koncentrációja vad típusban és az A115F mutánsban a mérési tartományon kívül esik (<0,5 pmol / 10^8 sejt). Szignifikancia szintek: P = 0,063 a T138stop dUTP szinthez, P = 0,095 a D83N dTTP szinthez, P = 0,047 a D83N dUTP szinthez, P = 0,000012 az A115F dCTP szinthez, P = 0.066 az A115F dTTP szinthez. A betét a nukleotidok arányainak összehasonlítását mutatja a vad típusú és az inaktív mutáns törzsekben. (B) A teljes pirimidin dNTP koncentráció változása az egyes törzsek által hordozott mutációk függvényében. Szignifikanciaszintek: P = 0,05959 a D83N és P = 0,0028 az A115F esetében.

Ugyanebben a tanulmányban összegyűjtöttük a dUTPáz aktivitás-csökkenés *in vivo* hatásaival kapcsolatos szakirodalmi adatokat egy átfogó táblázatban (2. táblázat az eredeti publikációban, Függelék). Ez az akkor teljesnek mondható adatkészlet hasonló megosztást támasztott alá a dUTP-t eliminálló és a dNTP-kiegyensúlyozó szerepek között azokban a vizsgált szervezetekben is, amelyek az egyszerű mikobakteriális modellhez képes további dTTP-termelési útvonalakat is hordoznak. Mindezek az irodalmi adatok alátámasztják a monofunkciós dUTPáz fontos szerepét a dNTP készlet dUTP-mentesítésében. A sejtbéli dTTP koncentráció szabályozása azonban úgy tűnik, hogy kizárólag a dCTP-t és dCMP-t transzformáló enzimekhez kötődik, amelyek ugyan szerkezetileg nem rokonok egymással, de mindegyik allosztérikusan szabályozott[74,117–120]. E funkciók szétkapcsolásának további mélyreható vizsgálata rávilágíthat azokra az evolúciós mechanizmusokra, amelyek az információhordozó molekulák, az RNS és DNS, egyik fő különbségeként a timin megjelenését és az uracil DNS-ből való kizárását eredményezték.

5.2.3 A dUTPáz génexpresszió-szabályozásban betöltött szerepének mechanizmusa

(Szabó *et al*, NAR, 2014[40])

A mikobakteriális genetikai kísérleteinkből tudjuk, és az irodalomban is számos közvetett kísérleti bizonyíték jelzi, hogy a dUTPáznak a dNTP készlet dUTP-mentesítésén túl más esszenciális funkciója is van. Az általunk használt modellszervezetekben ennek felderítésére tett erőfeszítéseink mostanában kezdenek beérni (lásd Tervek). Olyan esetekben, amikor egy fehérje létfontosságú funkcióját közvetítő kölcsönhatás viszonylag gyenge és/vagy kinetikailag nehezen tetten érhető, a kölcsönhatás létezésének kimutatása is nagy kihívás.

A dUTPáz első rendhagyó élettani szerepének felfedezése a génexpresszió szabályozásában Nature cikként jelent meg 2010-ben[121]. A szerzők azt mutatták ki, hogy egy helper fágból származó dUTPáz szabályozza a *Staphylococcus aureus* egyik szuperantigént hordozó mobilis genetikai elemének átvitelét. Ezt a hatást úgy fejti ki, hogy a mobilis genetikai elem repressziójáért felelős Stl fehérjéhez köt, ezáltal elindítja a mobilis genetikai elem kivágási-replikációs-csomagolási ciklusát. Mivel ezek a patogenitási szigetek (*Staphylococcus aureus* Pathogenicity Islands vagy SaPI) fágfehérjéket igényelnek a csomagoláshoz, ez a stratégia biztosítja, hogy az indukált SaPI-k átvitelre kerüljenek. A különböző SaPI-represszorok és a helper-fág által kódolt antirepresszorok között rendkívül specifikus kölcsönhatások figyelhetők meg. Az Stl az első, és azóta is egyetlen irodalomban dokumentált dUTPáz kölcsönható fehérje és potens fehérje-alapú dUTPáz inhibitor (24. ábra A).

Természetesen rendkívül érdekesnek találtuk az újonnan leírt fehérje-fehérje kölcsönhatást, és azt a kérdést, hogy miért pont a dUTPáz vesz részt benne, mi lehet az összefüggés az újonnan felfedezett fiziológiás szerep és a dUTPáz aktivitás között. Mielőtt leközöltük volna eredményeinket, a kölcsönhatást elsőként leíró csoport egy, a G-fehérjék által közvetített jelátvitelre hasonlító mechanisztikus modellt jelentetett meg, amelyben a dUTPázt egy dUTP-vel szabályozott kapcsolóként jellemezték[122]. Ez a mechanizmus azonban nem összeegyeztethető a dUTPáz enzimciklus kinetikai tulajdonságaival, amely alapvetően különbözik a G-fehérjékétől[43,58,94,123–125]. Az ellentmondás feloldására a dUTPáz által kiváltott de-repressziós mechanizmus mélyreható jellemzésére volt szükség. A számos biofizikai módszerrel mért eredményeink cáfolták a korábban javasolt G-fehérje-szerű mechanizmust, és egy széles fiziológiai kontextusba is illeszkedő alternatív szabályozási modellnek adtak alapot.

A dUTPáz:Stl kölcsönhatás mechanizmusának és funkcionális következményeinek jobb megértése érdekében megvizsgáltuk az Stl kötődését az intrinszik fluoreszcens jellel ellátott dUTPázhoz a szubsztrát, a dUTP (vagy a szubsztrát analóg dUPNPP) és a termék, a dUMP jelenlétében. Mind az egyensúlyi fluoreszcencia titrálásnál (24. ábra B), mind a QCM-kísérleteknél (Suppl. 2B. ábra az eredeti publikációban, Függelék) azt találtuk, hogy a dUTP vagy dUPNPP jelenléte gátolja az Stl:dUTPáz komplex képződését. A dUTPáz:dUPNPP komplex Stl-lel végzett fluoreszcencia-titrálása a dUTPáz:Stl komplexnek megfelelő egyensúlyi fluoreszcencia-intenzitást eredményezett. Ez azt suggalja, hogy az Stl kiszorította az összes dUPNPP-t, tehát az Stl és a dUPNPP verseng a dUTPázhoz való kötődésért. A dUTPáz reakció terméke, a dUMP és az Stl nem befolyásolták egymás kötődését (24. ábra B). A dUTPáz:dUMP:Stl terner komplex képződését egy különálló

fluoreszcenciaállapot jelzi, amely alacsonyabb fluoreszcenciaintenzitású, mint a dUTPáz:Stl komplex (24. ábra B és kiegészítő 1E ábra az eredeti közleményben). A tranziens kinetikai kísérletek azt is kimutatták, hogy a dUTPáz és Stl előinkubálása teljesen megakadályozott minden enzimreakciót azon a megfigyelt időskálán, amely Stl hiányában alkalmas a reakció követésére (24. ábra C, vö. az 1. és 2. görbét). Hosszabb időskálán a fluoreszcenciaintenzitás lassú csökkenése, majd fluoreszcencianövekedés volt megfigyelhető, ami a dUTP kötődésére és a termék felszabadulására emlékeztet (vö. [43,126]).

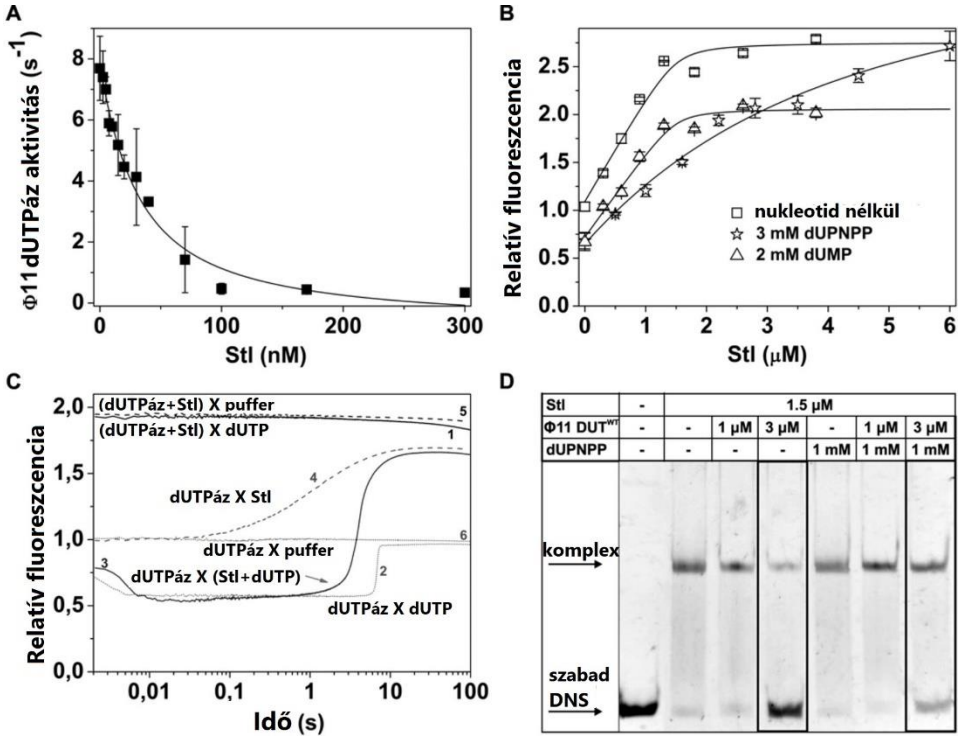

24. ábra: A dUTPáz:Stl komplex képződése megszünteti mindkét fehérje ismert funkcióját. (A) Az Stl gátló hatása a Φ11DUTWT (10 nM) katalitikus aktivitására. Három párhuzamos mérés átlagát és hibáját mutatjuk. A folytonos vonal a másodfokú kötési egyenletnek az adatokhoz való illeszkedését jelzi, és 26,64 ± 5,07 nM IC_{50} értéket eredményez. (B) A Φ11DUTF164W (1,5 μM) fluoreszcenciájának Stl-lel való titrálása dUPNPP (3 mM) vagy dUMP (2 mM) távollétében és jelenlétében. A hibasávok az SD-t jelölik n = 3 esetén. (C) Az Stl-gátlás tranziens kinetikai vizsgálata a komponensek összekeverési sorrendjének függvényében. A kísérletben 2 μM Φ11DUTF164W-t, 3 μM Stl-t és 50 μM dUTP-t kevertünk össze (keverés utáni koncentrációk); a zárójel a benne lévő komponensek előinkubációját jelzi. (D) A dUPNPP hatása a dUTPáz Stl-DNS komplex disszociációjára (EMSA kísérlet).

A kísérletekből az látszik, hogy amikor dUTP-t adunk az előinkubált Stl:dUTPáz komplexhez, a dUTP kötéséhez és hidrolíziséhez az Stl disszociációjára van szükség. Másrészt, ha a dUTP és Stl keverékét együtt adjuk a dUTPázhoz, a fluoreszcencia időbeli lefutása (24. ábra C, 3. görbe) analóg az Stl hiányában megfigyelt görbével (2. görbe), kivéve, hogy az egyensúlyi fluoreszcencia intenzitása megközelíti a dUTPáz:Stl komplexét (4. görbe). A fluoreszcencia növekedésében tükröződő Stl kötés (párhuzamosan a termék felszabadulásával, ami szintén fluoreszcencia növekedést okoz, vö. a 3. görbén lévő nyíllal) csak akkor következhet be, ha a dUTPáz:dUTP Michaelis komplex koncentrációja csökkenni kezd. Ez összhangban van a steady-state eredményekkel, és megerősíti azt a következtetést, hogy az Stl a dUTPáz kompetitív, lassú és szorosan kötődő inhibitora („slow tight-binding" inhibitor). Számos független vizsgálat közvetlen kísérleti adatai alapján azt javasoltuk, hogy

a dUTP és az StI verseng a dUTPáz kötődésért, és hogy a dUTPáz:dUTP komplex hozzáférhetetlen az StI számára. Ezért a korábban javasolt modell, amely szerint a dUTP közvetíti a dUTPáz:StI kölcsönhatást[122], megalapozatlan maradt.

Megvizsgáltuk, hogy a dUTPáz:StI komplex de-repressziós aktivitását (azaz élettani funkcióját) is modulálja-e a dUTP. Ennek érdekében EMSA-kísérleteket végeztünk (24. ábra D). Megfigyeltük, hogy a dUTPáz csak a dUTP hiányában gátolja az StI kötődését annak konszenzus DNS szekvenciájához. Ez arra utal, hogy a dUTP ellensúlyozza a de-repressziós eseményt azáltal, hogy megakadályozza a dUTPáz:StI komplex képződését. Az EMSA méréseink eredményei ismét nem támasztják alá a korábbi modellt, amelyben azt javasolták, hogy a dUTP fokozza a de-repressziót és a mobilis genetikai elemek ebből következő horizontális átvitelét. Eredményeink ehelyett azt támasztják alá, hogy a dUTP ellensúlyozza a de-repressziót. Az előző modell másik kulcsfontosságú pontja a dUTPáz C-terminális karjának szerepére vonatkozott: közvetett kísérletek alapján azt javasolták, hogy a de-represszió csak akkor következhet be, ha a dUTPáz C-terminális karja túlnyomórészt rendezett konformációt vesz fel[122], azaz dUTP-kötött formában. EMSA kísérleteink azonban egyértelműen azt mutatták, hogy a C-terminális karral csonkolt dUTPáz szintén megzavarhatja az StI DNS-hez való kötődését, nagyon hasonlóan a vad típushoz (3. ábra az eredeti közleményben).

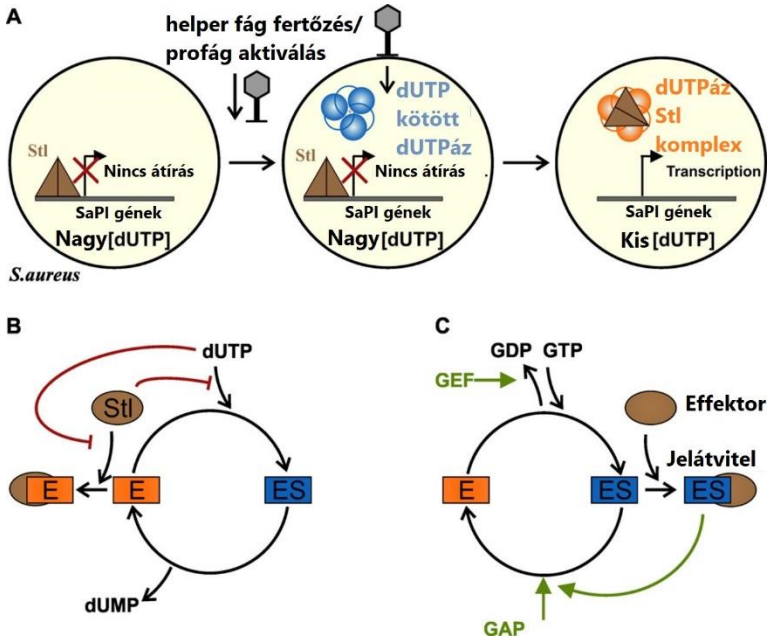

25. ábra: (A) A dUTPáz alapú SaPI aktiválás új modellje. (B) A dUTP által szabályozott dUTPáz:StI kölcsönhatás molekuláris mechanizmusa eredményeink alapján. (C) A G-fehérje kapcsolók molekuláris mechanizmusa. A B és C paneleken az ES a szubsztráthoz kötött, míg az E a szubsztrátmentes enzimet (szabad enzim vagy termékhez kötött enzim) jelenti. A piros és zöld nyilak rendre gátlást és aktiválást jelölnek.

Annak ellenére, hogy a dUTPáz jelenléte univerzálisnak tekinthető, számos *S. aureus* törzs nem kódol endogén dUTPázt, ami magas intracelluláris dUTP-szintet feltételez. Valószínű, hogy a helper fág dUTPázok felelősek a *S. aureus* dUTP-szintjének csökkentéséért. Miután a fág genomról kifejeződő dUTPáz a baktériumban lévő dUTP-t elhidrolizálta, funkciót vált, és elérhetővé válik az StI kötésére és DNS-ről való disszociáltatására, ami a SaPI horizontális transzferét elindító génexpresszióhoz vezet

(25. ábra A). A dUTP jelenlétének gátló hatása arra utal, hogy a virulenciagének aktiválása szükségszerűen a dUTP-től megtisztított nukleotidkészlet hátterében történik meg, ezzel biztosítva a mobil genetikai elem uracilmentes replikációját. Az uracil jelenléte a SaPI DNS-ben valószínűleg kedvezőtlen, mert amint azt a HIV-vel kapcsolatban is kimutatták, egy mobilis genetikai elem uraciltartalma negatívan befolyásolhatja annak integrációját az új gazdaszervezet DNS-ébe[127,128]. Ha a megfertőzött sejt aktív Ung-ot tartalmaz, az uracillall dúsított vírus-DNS elemésztődhet, mielőtt beépülne a genomba[127].

A dUTPáz-függő molekuláris kapcsolókra a dUTPáz:Stl kölcsönhatás az egyetlen eddig leírt példa. Fontos hangsúlyozni, hogy bár a dUTP által szabályozott dUTPáz:Stl kölcsönhatás modellünk ellentmond a korábban javasolt G-fehérje-szerű sémának (25. ábra B-C), mégis teljes mértékben összhangban van az ugyanabban a vizsgálatban közölt kísérleti megfigyelésekkel. Lényeges, hogy a másik csoport által generált *in vivo* eredmények is azt mutatják, hogy a SaPI aktiválásának mértéke az általunk leírt módon korrelál a dUTPáz aktivitással.

Az Stl:dUTPáz kölcsönhatás vizsgálatát szerkezeti biológiai[126,129,130] és molekuláris biológiai irányba[131] is tovább vitte kutatócsoportunk, és számos eredményt ért el a kölcsönhatás természetének felderítésében. Megemlítendő, hogy az Stl minden eddig általunk vizsgált dUTPázhoz szorosan kötődik és a legtöbb enzim aktivitását gátolja[132,133] annak ellenére, hogy élettani szerepe specifikus és az *S. aureus* profág aktivációra korlátozódik. A keresztinhibíció alapján kidolgoztunk egy nagy áteresztőképességű random mutagenezis módszert is az Stl és kölcsönható partnerei közötti kölcsönhatásban résztvevő DNS-szekvenciák és fehérjedomének, aminosavak feltárására sejtbéli környezetben[134].

5.3 A dNTP készlet mérése és összefüggései a sejt életfolyamataival

5.3.1 Felhasználóbarát, nagy áteresztőképességű módszer fejlesztése a biológiai mintákból származó dNTP pontos mennyiségi meghatározására

(Szabó et al, NAR 2020[35])

A sejtbéli dNTP koncentráció precíz mennyiségi meghatározására régóta fennálló igény ellenére a meglévő módszerek egyike sem vált rutin analitikai eljárássá. A dNTP homeosztázis szerepét egyre több folyamatban vizsgálják és tárják fel az utóbbi évtizedben: a rákos elváltozások progressziójában[135–141], az antivirális védekezésben[142], az öregedésben[143–145], a sejtciklus szabályozásában[137,138,146,147] és az antitest-hipermutációk létrejöttében[148]. Ahhoz, hogy megértsük a dNTP koncentráció változásának szerepét ezekben a folyamatokban, a legértékesebb információkat az intracelluláris dNTP-szintek közvetlen sejtben történő mérésével lehetne megszerezni. Erre irányuló projektünkről a Tervekben kaphat képet az olvasó. Mivel azonban jelenleg nem áll rendelkezésre ilyen módszer, legalább a sejtlizátumok dNTP koncentrációjának megbízható mérését szükséges megvalósítani. Erre számos nagy teljesítményű folyadékkromatográfiás (HPLC) módszert és enzimes vizsgálati eljárást fejlesztettek ki. A dNTP mennyiségi meghatározásának legnagyobb kihívása az, hogy i) más nukleotidok, elsősorban a kémiailag nagyon hasonló ribonukleozid-trifoszfátok (rNTP-k) a sejtlizátumban 100-1000-szeres feleslegben vannak jelen a dNTP-khez képest; ii) a különböző dNTP-k adott esetben csak egy metilcsoportban térnek el egymástól. A kihívás nagyságát jelzi, hogy HPLC-analízisnél az rNTP-k akár 99%-os hatékonyságú eltávolítása után fennmaradó 1% is megzavarhatja a dNTP mennyiségi meghatározását[149]. A HPLC-csatolt MS detektálás biztosítja a legnagyobb érzékenységet, de a műszer testre szabása a dNTP méréshez nem kompatibilis az egyéb, szokásos felhasználási lehetőségekkel. Emiatt összesen néhány specializált laboratóriumban születnek ezzel a módszerrel mért eredmények[149–152]. Amit a kémiai analitika nehezen tud megkülönböztetni, annak a felismerését a biológia tökélyre fejlesztette, ezért az enzim alapú módszerek elterjedtebbek[153–156].

Egy 2011-ben közölt, DNS polimerizáción alapuló fluoreszcenciás módszer (26. ábra) forradalmasítani látszott a dNTP koncentráció mérését alapvető molekuláris biológiai követelményeivel és nagy áteresztőképességével[157]. Mivel a dNTP mennyiségi meghatározásának módszerét mindennapi használatra terveztük több kutatási területen (lásd Tervek), nagyszámú mintát kívántunk nagyobb áteresztőképességgel elemezni. Együttműködésben kezdeményeztük a HPLC-MS vizsgálatokat, amelyek a már említett inkompatibilitás miatt kudarcot vallottak. A Wilson féle fluoreszcens módszer[157] tűnt az egyetlen lehetőségnek a nagy áteresztőképességű, kvantitatív dNTP mérésekhez, amelyeket qPCR készülékben, soklyukú lemezen lehet kivitelezni. Ez azonban a kezünkben nem működött, és a tanulmányra hivatkozó 29 publikáció elemzéséből az derült ki számunkra, hogy mások kezében sem. Ezért, mivel ezt tartottuk a legígéretesebb módszernek, kiderítettük, milyen akadályok nehezítik a használatát, és hogyan lehet ezeken túljutni. Három fő körülményt azonosítottuk, amely akadályozta a megbízható eredmények előállítását az eredeti módszerrel. Először is, a fluoreszcens próba Taq polimeráz általi lassú, nem specifikus hasítása miatt a dNTP beépülési reakció végpontja nem mutatható ki megbízhatóan. Másodszor, a különböző nukleotidok beépülési sebessége nagyon változó,

a dATP a leglassabb, a dCTP/dGTP pedig a leggyorsabb a dNTP-k közül. Végül a biológiai mintában lévő egyéb komponensek kiszámíthatatlan és reprodukálhatatlan módon lassítják a reakciót, ezért nem lehet végpontot mérni. Hatékonyan megoldottuk ezeket a problémákat a reakció körülményeinek optimalizálásával és a fluoreszcencia-időgörbék kinetikai elemzésével. Utóbbi lehetővé tette, hogy megkülönböztessük a dNTP beépülés folyamatát a háttérreakcióktól. Így a kinetikailag elkülönített dNTP-beépülési folyamat amplitúdója korrelál a reakcióelegyben elérhető dNTP mennyiségével (27. ábra).

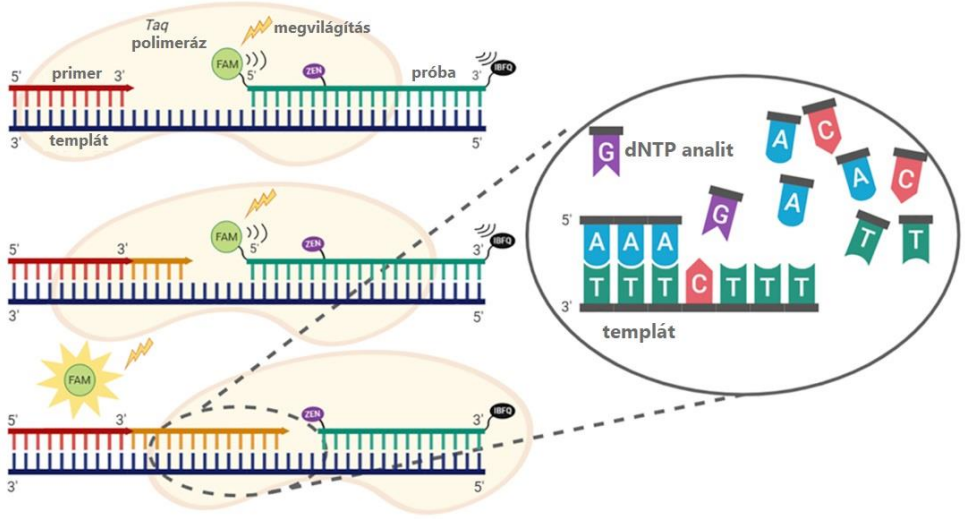

26. ábra: A fluoreszcencia-alapú dNTP mérési módszer. Ebben a példában 6 molekula dTTP-t kell beépíteni a fluoreszcens jel felszabadításához. A Taq DNS polimeráz egy primert hosszabbít meg egy általunk úgy megtervezett templát mentén, hogy abban az analit (jelen esetben a dTTP) limitált számú komplementer bázisa legyen. A dTTP-n kívül a másik három DNS építőkövet feleslegben adjuk. A dTTP csak a biológiai mintából származhat. Ha a dTTP rendelkezésre áll, a polimeráz eljut a próbáig. Amint exonukleáz aktivitásával levágja a FAM fluorofórt tartalmazó bázist a próbáról, az felszabadul addigi kioltott állapotából, és fluoreszcens jel keletkezik. A fluoreszcens jel a mérhető dinamikus tartományban egyenesen arányos a dTTP mintában lévő mennyiségével. Az ábrát az eredeti Wilson et al. közleményből adaptáltam[157].

A biológiai mintákban a dNTP beépülésének megváltozott kinetikai tulajdonságai a dNTP-k egyéb nukleotidokkal a polimeráz kötőhelyéért való versengéséből származhatnak (elsősorban rNTP, (d)NDP és (d)NMP). Bár ez a versengés csökkenti az előrehaladás sebességét, a reakció amplitúdóját ez nem befolyásolja. Eredeti közleményünk Supplementary Table I-ében tüntettük fel a módszer kimutatási határait és pontosságát egy adott kísérleti körülményhalmazban. A mérés dinamikus tartományát a DNS templát megválasztásával és a körülmények finomhangolásával lehet változtatni a mérésekben. Minden esetre úgy tapasztaltuk, hogy a pontos mennyiségi meghatározás alsó határa 1-3 pmol dNTP / minta, amelyet a sejtmérettől, a sejt dNTP-tartalmától függően körülbelül 10^6 sejtből vagy 10^8 baktériumból lehet hatékonyan nyerni.

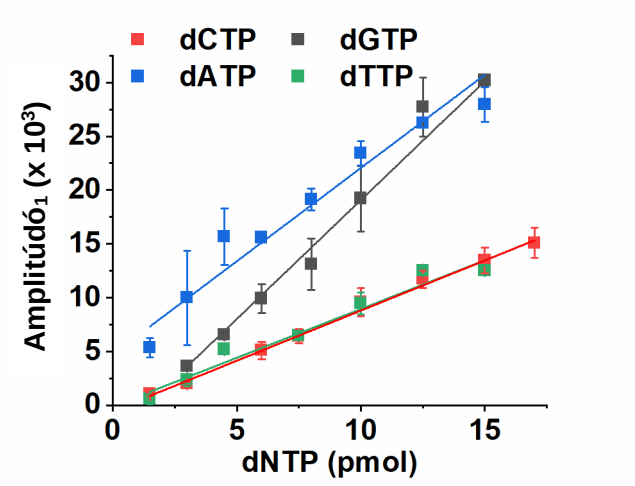

27. ábra: A specifikus dNTP-beépülési fázis (A1) amplitúdójának lineáris összefüggése a minta dNTP tartalmával pontos mennyiségi meghatározást tesz lehetővé. dCTP-dT2, dGTP-dT2, dATP-dT1 és dTTP-dT2 templátokat használtunk a TEMPase Taq polimerázzal. A görbék lineáris illesztésével a következő R^2 paramétereket kaptuk: dCTP, 0,99; dGTP, 0,999; dATP, 0,98; dTTP, 0,95.

Kifejlesztettünk egy olyan szoftvert is (http://nucleotidy.enzim.ttk.mta.hu/), amely egyszerűsített adatelemzést kínál a kinetikában tapasztalatlan kutatók számára. A nucleoTIDY szoftver használatával a teljes elemzési folyamat, beleértve a vizsgálati görbék kinetikai kezelését, a kalibrációs görbék megszerkesztését és a dNTP mennyiségének kiszámítását a tényleges biológiai mintákban, mindössze néhány percet vesz igénybe egy 96 lyukú lemez esetében (28. ábra).

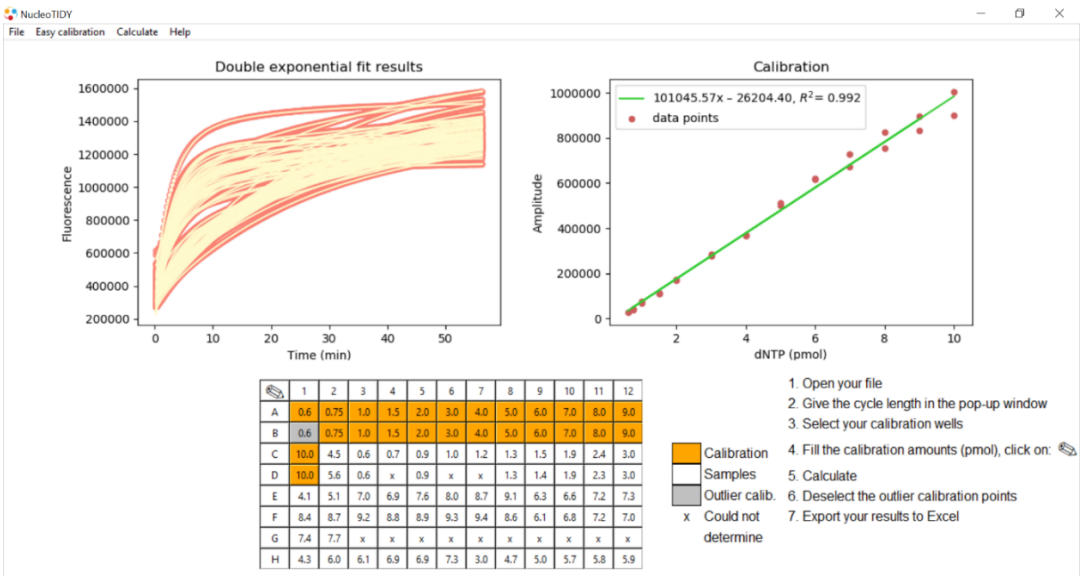

28. ábra: A NucleoTIDY szoftver működés közben. A bal felső panelen a piros ábrasereg a mért fluoreszcens időgörbéket jelzi, míg a sárga görbék mutatják a mért adatokra illesztett kettős exponenciális függvényt. A jobb felső panelen a szoftver az alul látható 96 lyukú lemezen grafikusan kijelölt kalibrációs pontokat számítja ki és tünteti fel, hogy a kalibrációs egyenes minősége ellenőrizhető legyen. A lemez mintaként definiált helyein a kalibráció alapján számított értékek láthatóak. Ezek táblázatos formában letölthetőek a szoftverből. Bemeneti fájlként a leggyakoribb forgalomban lévő qPCR gépek output fájljait közvetlenül lehet használni.

A sors fintora, hogy bár a dUTP kvantitatív kimutatására voltunk leginkább kíváncsiak, ennek megbízhatósága nagymértékben függött a dUTP:dTTP aránytól, a nukleotidok eltérő beépülési kinetikája miatt. A dUTPázzal kezelt (csak dTTP-t tartalmazó) és a nem kezelt (dTTP+dUTP-t tartalmazó) adatpontok összehasonlítása alkalmas lehet nagy mennyiségű dUTP kimutatására egy mintában. Azonban azt javasoltuk, hogy sem az eredeti, sem a jelen módszer nem alkalmazható a dUTP mennyiségi meghatározására. Ehelyett kifejlesztettünk egy másik, kimondottan a dUTP-re adaptált mérést, amely jelenleg publikálás alatt áll.

A dNTP magas koncentrációinak mérésekor az eredeti módszer teljesítménye (a dATP-t kivéve) megközelíti az általunk továbbfejlesztett módszerét. Az emlőssejtekből származó dNTP-koncentrációk meghatározása azonban vitathatatlanul megköveteli a bemutatott módszerfejlesztést (29. ábra). Ezek a fejlesztések a dNTP mennyiségi meghatározását széles körben elérhetővé teszik a tudományos közösség számára tetszőleges biológiai mintában.

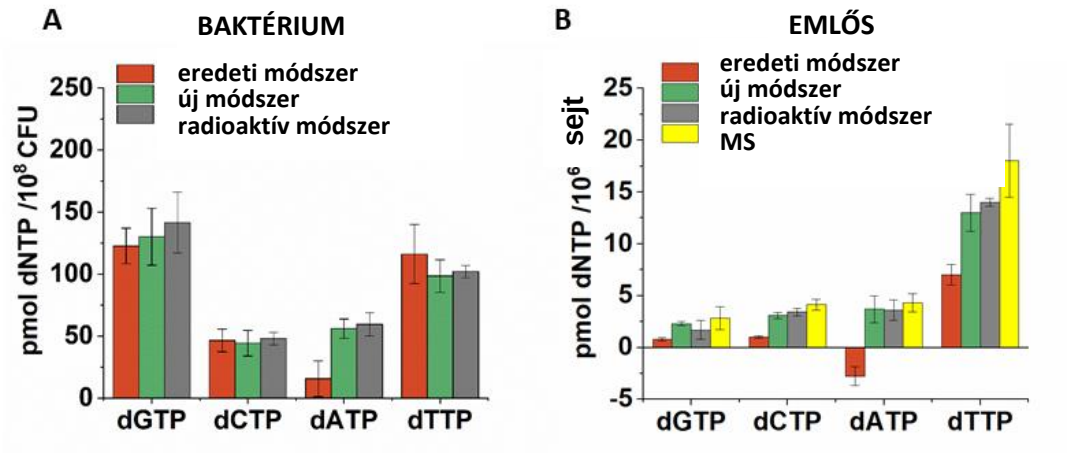

29. ábra: A továbbfejlesztett dNTP mennyiségi mérési módszer összehasonlítása az eredeti fluoreszcencia-alapú, a „gold standard" radioaktív izotóp alapú és az MS alapú módszerrel. (A) A dNTP mennyiségi meghatározása M. smegmatis mintákban. Az adatok két biológiai párhuzamos és 3 technikai ismétlés átlagát és standard hibáját reprezentálják. A bemutatott dNTP mennyiségeket ugyanarra a mintára három különböző módszerrel határoztuk meg. Ugyanazokat a nyers görbéket számszerűsítettük az eredeti és az új, továbbfejlesztett fluoreszcens módszereinkkel. (B) dNTP mennyiségi meghatározása humán MES-SA mintákban. Az adatok két biológiai párhuzamos és legalább 3 technikai ismétlés átlagát és standard hibáját jelentik. Az MS adatokat a Machon és munkatársai által publikált ábrákról olvastuk le[158].

5.3.2 A biológiai mintákban mért dNTP készletek és készletváltozások adatbázisa

(Pancsa *et al*, 2021 NAR[159])

A dNTP anyagcserét több mint 50 éve kutatják. Annak ellenére, hogy rendkívül nagy mennyiségű mért dNTP adat halmozódott fel az irodalomban, ezek nehezen átláthatóak és összehasonlíthatóak az alkalmazott módszertan, az adatminőség és a megjelenítés nagy változatossága miatt. A dNTP készlet változásainak egészséges élettani és rosszindulatú folyamatokban betöltött, az előző fejezetben referenciákkal is alátámasztott, szerepe iránti növekvő érdeklődés (30. ábra) ösztönözte azt az erőfeszítésünket, hogy az eddig mért sejtbéli dNTP mennyiségeket biokémikus szemlélettel rendszerezzük. Bioinformatikus kollégákkal együtt létrehoztuk a dNTPpoolDB nevű adatbázist, amely rendezett és egyértelműen megfeleltethető információkat biztosít a biológiai mintákban végzett dNTP-mérésekről egy felhasználóbarát webes felületen keresztül (https://dntppool.org/).

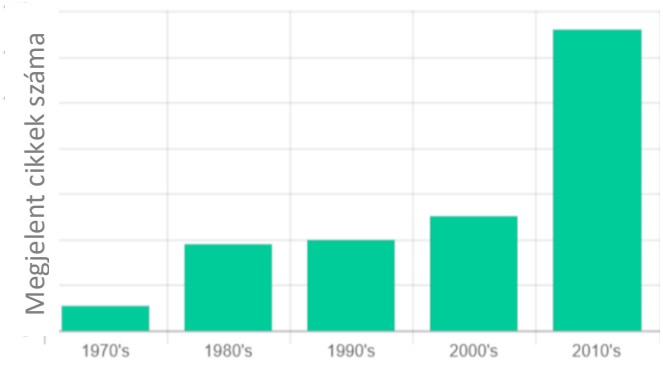

30. ábra: A dNTP mennyiségi meghatározást közlő cikkek időbeli eloszlása.

A releváns adatok megtalálása érdekében a PubMed adatbázisból kezdetben nagyszámú publikációt hívtunk le (kb. 1200), amelyekből azután manuálisan szűrtük ki azt a cikk készletet, amely valóban tartalmazott kísérletesen meghatározott dNTP-értékeket. Áttekintettük a publikációk teljes szövegét, hogy a mért dNTP adatokat a táblázatokban, ábrákon és a szövegben is azonosítsuk. Célunk az volt, hogy a mért dNTP értékekhez kapcsolódóan a lehető legtöbb, a későbbiekben használható információt strukturált módon betápláljuk az adatbázisba. Amikor csak lehetett, ismert ontológiákat és más adatbázisokra való kereszthivatkozásokat alkalmaztunk. Az adatbázis egysége a mért dNTP érték, amely vagy a DNS négy kanonikus építőkövének egyike, vagy más, egzotikus dNTP, amely képes beépülni a DNS-be. Azok a bejegyzések, amelyek csak a mért dNTP típusában különböznek egymástól, ugyanabba a készletbe tartoznak. Minden dNTP készletnek van készletazonosítója. A dNTP készletek további kapcsolatban állnak egymással a kontroll-kezelés párok definiálása révén, ahol ez lehetséges volt. A kontroll-kezelés párok automatikus összehasonlításának és grafikus ábrázolásának lehetősége mellett bármely két dNTP készlet is összehasonlítható. Az „Advanced search” és a „Pairwise comparison” funkciókkal a dNTP készlet változásait hatékonyan meg lehet találni egy kívánt paraméter függvényében. Úgy gondoljuk, hogy a különböző bejegyzések közötti kapcsolatok biztosítása nagymértékben megkönnyíti az összegyűjtött adatok bármely jövőbeni elemzését.

A legtöbb tanulmány valamilyen kezelés vagy természetesen előforduló genetikai vagy környezeti változás eredményeként létrejött dNTP készletváltozásról szól. Ezért fontos, hogy a dNTPpoolDB a releváns kísérleti körülményeket is pontosan leírja (31. ábra). Ha drogkezelésről van szó, a PubChem azonosítójára való kereszthivatkozás segítségével azonosítjuk a kezelésre használt kémiai anyagot. Ha a kezelés génmanipuláció, akkor az érintett géneket és fehérjéket az NCBI génazonosítóira, illetve az UniProt azonosítókra való kereszthivatkozások segítségével azonosítjuk, valamint megadjuk a mutációikra vonatkozó információkat (31. ábra).

Az adatok adatbázison belüli összehasonlíthatóságának növelése érdekében csökkentettük a felhasznált mértékegységek számát anélkül, hogy az adatokat szubjektív módon átalakítottuk volna. A dNTP mennyiségi meghatározására vonatkozó adatokat az irodalom gyakran relatív értékként mutatja be egy nem kezelt kontrollhoz vagy más nukleotidokhoz (jellemzően ATP, dNTP vagy NTP tartalom) viszonyítva. Ezekben az esetekben megjelöltük az összehasonlítás alapját. Különösen fontosnak tartottuk a kontroll-kezelés párok azonosítását a relatív adatok esetében az adatbázis információtartalmának növelése érdekében.

A dNTPpoolDB olyan információforrás, amely remélhetőleg a genomanyagcsere, a DNS-replikáció és -javítás, a rákkutatás, az öregedés, a vírusos és bakteriális fertőzések kutatásának területén segít megválaszolni a dNTP homeosztázis szerteágazó szerepeivel kapcsolatos alapvető kérdéseket. A dNTPpoolDB célja, hogy a tudományos közösség javát szolgálja azáltal, hogy 1) szabadon hozzáférhető, könnyen használható, szervezett és releváns adatokat biztosít a közzétett celluláris dNTP mennyiségekről és készletekről, 2) jó alapot biztosít a széles körben alkalmazott dNTP mérési módszerek objektív összehasonlításához és értékeléséhez, 3) lehetővé teszi a dNTP készletek fajspecifikus jellemzőinek azonosítását és megértését, a különböző kezelések hatására bekövetkező változásaik és a kóros állapotok kialakulásában betöltött szerepük értelmezését, 4) támpontokat ad a dNTP-k lehetséges nem-kanonikus funkcióihoz, beleértve a dNTP-k lehetséges jelátviteli és epigenetikai funkcióját.

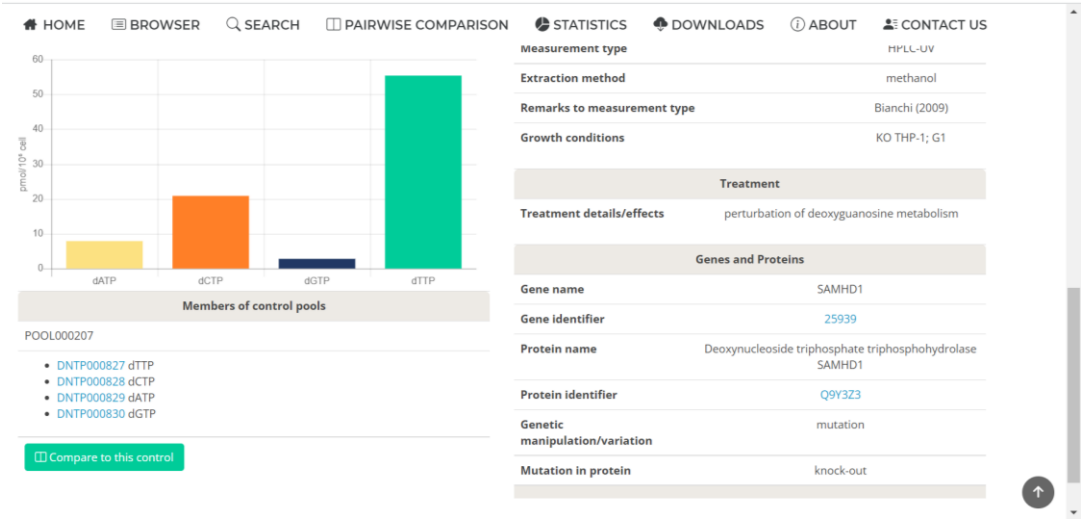

31. ábra: A dNTPpoolDB egyik entry oldalának részlete, amely mutatja a kísérleti körülményeket és az ezekhez tartozó dNTP készlet megjelenítését. Az adatbázis funkciói a felső menüszalagon láthatók.

6 Irányok és tervek

Érdeklődésünk részben a rendszerszintű vizsgálatok felé tolódott a dNTP anyagcsere és ennek élettani szerepei kapcsán. A dNTP adatbázis ötletét is az hívta életre, hogy szerettünk volna összefüggéseket találni a dNTP készlet összetétele, mérete, változásai és a faji jellemzők, egyedfejlődési stádiumok és számos egyéb paraméter között. Olyan alapvető kérdéseket vizsgálunk például, hogy van-e összefüggés a dNTP-készet összetétele és a bázisok genomi megoszlása között. Azt találtuk, hogy közvetlenül nincs. Az adott fajra jellemző ribonukleotid reduktáz enzimatikus mechanizmusa azonban elég jó prediktornak tűnik a dNTP készlet összetételére nézve. Ugyanakkor azt is tudjuk, hogy a dNTP készlet összetétele befolyásolja a DNS polimerázok hibázási mintázatát, és ezzel a mutációs spektrumot. Így közvetve összefüggés található a dNTP anyagcsere enzimek és a genom hosszútávú változásai között. A dNTP adatbázisban található adatokat folyamatosan bővítjük, a végső cél egy teljes, minden elérhető adatot tartalmazó forrás létrehozása. Párhuzamosan egy, a fenti összefüggéseket vizsgáló koncepcióismertető cikket és egy, a mérési módszerek összehasonlítását célzó tanulmányt is írunk az adatbázis alapján.

A dNTP anyagcsere modellezésére ugyanakkor egy kvantitatív kinetikai modellt is építettünk, amely alkalmas arra, hogy megjósolja akár a klinikumban használt antimetabolitok hatását az egyes anyagcsere-termékek fluxusára nézve. Az enzimek mechanizmusát változtatva a modellben a fent leírt, a dNTP adatbázisból következtetett összefüggéseket is látjuk és meg tudjuk erősíteni, pl. a ribonukletoid reduktáz mechanizmusának hatását a nukleotidkészlet összetételre. Ez a projekt Füzesi Dóra 3. éves doktorandusz doktori munkája.

A *M. smegmatisban* is végeztünk rendszerszintű vizsgálatokat. Itt arra voltunk kíváncsiak, mi állhat annak az ellentmondásnak a hátterében, hogy míg a mikobaktériumok laboratóriumban mért mutációs rátája minden esetben alacsony (10^{-10} / nemzedék), addig a tuberkulózisos betegekből izolált minták jellemzően több rezisztenciát okozó mutációt és általánosan nagy genetikai variabilitást mutatnak. Hipotézisünk az volt, hogy a gazdaszervezet által az intracelluláris kórokozóra ható sokféle stresszfaktor (oxidatív, nitrozatív, hipoxiás stb.) és a nagy mennyiségben és hosszú ideig alkalmazott antituberkulotikumok megnövelik a mutációs rátát. Ezeket a stresszfaktorokat és az összes használatban lévő tuberkulózis elleni antibiotikum hatását modelleztük sejtkultúrákon, majd az ennek következtében jelentkező mutációs mintázatot (teljes genom szekvenálás), dNTP készlet változásokat és a releváns enzimek expressziós szint változásait detektáltuk. Eredményeink alapján az irodalomban leírt mikroevolúciós modellre, amely szerint a megfertőződött egyénben kis számú mikobaktérium mikroevolúciójával alakul ki a már kezelt betegekben megfigyelt antibiotikum rezisztenciával járó genetikai diverzitás, semmilyen bizonyítékot nem találtunk. Adataink egy olyan modellt támogatnak, amelyben a betegség jelentkezését megelőzően az egyén nagyszámú, különböző genetikai háttérrel rendelkező *M. tuberculosis* baktériumot akkumulál, amelyből azután az aktív fázisban az általunk vizsgált stresszek hatására az életképesebb vonalak expandálnak. Az eredetileg a WHO által közölt, majd egy alapos metaanalízissel 2019-ben megerősített adat szerint a világ népességének negyede látensen fertőzött tuberkulózissal[160]. Ez a tuberkulózis baktériummal való tartós és a legtöbb esetben tünetmentes együttélés konzisztens az általunk javasolt akkumulációs modellel. Ez a munka Molnár Dániel 4. éves

doktorandusz doktori disszertációjának törzsét alkotja, amelynek publikációja folyamatban van.

A dNTP mérési módszer fejlesztésénél említésre került (5.3.1 fejezet), hogy a sejtbéli dNTP detektálás igazán hiánypótló lenne, jelenleg nem áll ugyanis rendelkezésre olyan módszer, amely képes valós idejű adatot szolgáltatni a dNTP-k sejten belüli mennyiségéről és eloszlásáról. Holott a dNTP-k sejtbéli eloszlását illetően alapvető kérdések várnak tisztázásra. Ilyen például az, hogy a legtöbb dNTP bioszintézisben résztvevő enzim a citoplazmában található, azonban a dUTPáz és a timidilát szintáz komplex foszforilációtól[161] vagy szumoilációtól[162] függő módon a sejtmagba helyeződik át. Miért? Ha a nukleotidok diffúziós együtthatóját tekintjük és azt, hogy a magmembrán pórusokon át tudnak jutni, nem indokolt a DNS-szintézis közvetlen közelébe helyezni a dTTP-t szintetizáló apparátust. Kutatásunk célja egy olyan dNTP-bioszenzor létrehozása, mely képes a dNTP-k szelektív *in vivo* kötésére és ennek fluoreszcens nyomjelzésére. A jelet a hozzá kovalensen kapcsolódó cirkulárisan permutált zöld fluoreszcens fehérjében (cpGFP) létrejövő konformációs változás gerjeszti. A bioszenzor prototípusát egy jól karakterizált, kivételes felépítésű monomer dUTPázból (Eppstein-Barr vírus dUTPáz) alkottuk meg, amelynek inaktív mutánsához cpGFP-t fúzionáltattunk. A szenzor *E. coli*-ban történő sikeres kifejeződését és tisztítását követően kimutattuk, hogy fluoreszcenciaváltozás következik be a szubsztrát kötése során. A bioszenzor sikeresen expresszálható emlős sejtben is. Ezek bíztató eredmények, ugyanakkor a dUTP szenzor prototípus optimalizációra szorul, és a továbbiakban az aktív hely célzott mutagenezisével dUTP szenzorból dCTP és dTTP szenzort is elő kívánunk állítani. A purin dNTP-kre készülő bioszenzorhoz egy másik fehérjét, illetve egy fehérjedomént szemeltünk ki, a ribonukleotid reduktázokban megtalálható ún. ATP cone-t, amellyel egyelőre a bakteriális expresszióig jutottunk el.

Végül, de nem utolsó sorban a mikobakteriális dUTPáz kölcsönható partnereinek kutatásáról szeretnék szót ejteni. Mivel hosszas, egyéb fehérje kölcsönható partnert kereső próbálkozásaink nem vezettek eredményre, élesztő kéthibrid kísérletből (szolgáltatás keretében) nyertünk információt a potenciális kölcsönható partnerekről. A legmegbízhatóbb találat egy, a homológ rekombinációban (HR) résztvevő DNS helikáz/nukleáz fehérje volt, az AdnA. Már ezt megelőzően bizonyítékokat gyűjtöttünk a dUTPáz nem-konvencionális funkciójáról *M. smegmatis*-ban. Megállapítottuk, hogy a defektív dUTPázt expresszáló sejtekben csökken a rekombinációs hatékonyság, és hogy megváltozott érzékenységet mutatnak kettős száltörést okozó genotoxikus gyógyszerekkel szemben. Előzetes eredményeink arra engednek következtetni, hogy a dUTPáz szerepet játszik a HR-ban az AdnA-helikázzal való kölcsönhatás révén, amelyet a mikobaktériumokra specifikus felszíni hurok (5.2.1 fejezet) közvetít részben. A DNS károsodások közül a kettős szálú DNS-törések (DSB) a legveszélyesebbek. A tuberkulózis elleni jelenleg alkalmazott leghatékonyabb fluorokinolon antibiotikumok szintén DSB-ket okoznak és így vezetnek a sejt halálához. Míg a legtöbb baktérium csak homológ rekombináció (HR) útján tudja javítani a DSB-ket, a mikobaktériumok három különböző útvonalat alkalmaznak ehhez. A DSB hibamentes javításának egyetlen módja azonban a HR, és mint ilyen, ez játssza a legfontosabb szerepet osztódó sejtekben. Az alkalmazkodás szempontjából döntő fontosságú, hogy a DSB-k a hibamentes HR, vagy a hibára hajlamos másik két útvonalon keresztül javítódnak-e. Előzetes eredményeink alapján azt javasoljuk, hogy a dUTPáz szerepet játszhat e döntés meghozatalában az AdnA helikázzal való kölcsönhatása révén.

7 Az új tudományos eredmények tézises összefoglalása

1. Feltártuk a humán és *Mycobacterium tuberculosis* dUTPáz enzimek kinetikai mechanizmusát és a nukleotidhidrolízis katalíziséhez hozzájáruló szerkezeti elemek szerepét. Meghatároztuk, hogy a szubsztrátkötés gyors és reverzibilis; a kémiai lépés, tehát az α–β-foszfátcsoportok közötti kötés felhasadása a sebességmeghatározó lépés; és a termékek gyorsan és random módon szabadulnak fel. Kimutattuk, hogy a hidrolízissel egyidejű protontranszfer következik be.
2. Kidolgoztunk egy enzimatikus eljárást a dNTP-k γ-foszfát csoportján való radioaktív jelölésére.
3. Több olyan mechanizmust javasoltunk a nukleotidhidrolízis enzimatikus katalízisével kapcsolatban, amelyek túlmutatnak a dUTPáz példáján. Megmutattuk, hogy a nukleotidhidrolízis helyétől kémiailag viszonylag távoli kölcsönhatások hogyan segíthetik elő a katalízist az átmeneti állapot komplex elektrosztatikus és/vagy geometriai stabilizálásával. Megmutattuk, hogy az enzimekben gyakran megtalálható és sokszor konzervált, az enzim és szubsztrát közötti aromás átlapolás (π-π kölcsönhatás) elektrosztatikusan hozzájárulhat a katalitikus hatáshoz.
4. Kinetikai, spektroszkópiai és szerkezeti vizsgálatok, valamint kvantumkémiai számítások kombinálásával képet alkottunk arról, hogy az ATP- és GTPázokban általánosan jelenlévő P-hurok vagy Walker A szekvencia hogyan járul hozzá a katalízisben résztvevő elemek orientálásához és az asszociatív típusú átmeneti állapot stabilizálásához egy olyan enzimben, amely a nukleotidban nem a β–γ-foszfátcsoportok közötti, hanem az α–β-foszfátcsoportok közötti hasítást katalizálja. A szerkezeti és mechanisztikus összehasonlításokkal e foszfátkötő motívum konvergens fejlődésére, és a különböző nukleotidhidrolízis feladatokhoz való kifinomult funkcionális adaptációra mutattunk példát.
5. Megmutattuk, hogy kis peptidszakaszok kis amplitúdójú mozgásai elegendőek ahhoz, hogy egy zártnak tűnő aktív helyen gyors ligandumkötés és -disszociáció menjen végbe. Ezzel a modellel az irodalomban ellentmondásosnak tűnő összes eddigi, a dUTPáz aktív hely konformációs dinamikájára vonatkozó kísérleti adatot egységes értelmezési keretbe tudtuk foglalni. Kísérletes bizonyítékot szolgáltattunk a RAMD módszer prediktív erejére.
6. Kimutattuk, hogy az EDTA szelektíven, és a fiziológiás szubsztrátnál szorosabban kötődik egyes dNTP hidrolázok (dUTPáz, Taq polimeráz, MutT) aktív helyére. Megmutattuk, hogy a dUTPáz aktivitást kompetitíven gátolja, és hogy ez a gátlás független a Mg^{2+}-ot komplexáló hatásától.
7. Meghatároztuk a dUTPáz eddigi egyetlen ismert fehérjetermészetű kölcsönható partnere, az Stl és a dUTPáz közötti kölcsönhatás kinetikai mechanizmusát. Kimutattuk, hogy az Stl a dUTPáz „slow tight-binding” inhibitora. Megdöntöttük azt a modellt, miszerint a dUTPáz egy G-fehérjeszerű kapcsoló lenne. Kidolgoztunk egy másik modellt, amelyben a dUTPáz génexpresszió-szabályozásban betöltött szerepe abban áll, hogy a *Staphylococcus aureus* virulenciagénjeinek replikációja dUTP-mentes sejtes környezetben történjen meg. Ez az uracilmentes mobilis genetikai elem hatékony horizontális transzferét szolgálja. Az uraciltartalom ugyanis negatívan befolyásolhatja a virulencia gének az új gazdaszervezet DNS-ébe történő integrációját.

8. Meghonosítottuk a mikobakteriális géntechnológiát a laboratóriumban, amely lehetővé teszi a sok szempontból speciális és gyakorlati érdeklődésre számot tartó mikobakteriális modellszervezet, a *M. smegmatis* manipulációját. Kimutattuk, hogy a dUTPáz fehérje szükséges a sejtek túléléséhez. Kiderítettük, hogy egy mikobaktérium-specifikus felszíni hurok jelenléte szükséges az életképesség fenntartásához, ugyanakkor az enzimaktivitás elrontható különösebb rövidtávú következmények nélkül. Kimutattuk, hogy a mikobaktérium két dUTPáz aktivitással rendelkező enzime közül legalább az egyik aktivitása szükséges a túléléshez, tehát a dUTPáz-aktivitás esszenciális a mikobaktériumban.
9. A dUTPáz enzimcsalád tagjainak enzimológiai, szerkezeti és a *M. smegmatis*-on belüli funkcionális vizsgálatával kimutattuk, hogy az ezen enzimek között csak apró különbségeket tartalmazó háromdimenziós fehérjeszerkezetben rejlő allosztérikus szabályozás lehetősége csak a fiziológiás funkciótól függően valósul meg. A kooperatív allosztéria és a szubsztrátspecificitás között csereviszonyt fedeztünk fel, amely összefügg a negatív visszacsatolással szabályozható dTTP bioszintézis és a hatékony dUTP elbontás funkcióinak szétválásával. Kimutattuk, hogy az intramolekuláris szabályozó képesség a katalitikus hatékonyság csökkenésével jár egy, a teljes konzervált fehérjéhez képest apró, szerkezeti elemnek köszönhetően, amely a kétféle funkció közötti váltást közvetíti. Rámutattunk a funkcionális szétválás előnyeire, és arra, hogy a rendelkezésre álló irodalmi adatokban is felfedezhető ez az addig explicit módon le nem írt jelenség.
10. Továbbfejlesztettünk egy enzimatikus analitikai eljárást a dNTP-k mennyiségi meghatározására, amely így széles körben hozzáférhetővé teszi a nagyáteresztőképességű dNTP koncentráció méréseket.
11. Létrehoztuk az irodalomban található, kísérletesen meghatározott dNTP mennyiségek és ezek különböző hatásokra történt változásainak adatbázisát. A dNTPpoolDB lehetővé teszi a dNTP készletek fajspecifikus jellemzőinek azonosítását és megértését, a különböző kezelések hatására bekövetkező változásaik és a kóros állapotok kialakulásában betöltött szerepük értelmezését, és támpontokat ad a dNTP-k lehetséges nem-kanonikus funkcióinak megismeréséhez.

8 Köszönetnyilvánítás

E disszertáció írása közben felidéztem számos felemelő, a kollégáimmal, diákjaimmal folytatott brainstrorming alkalmat, amelyeken egy-egy adathalmaz értelmet nyert és történetté formálódott. Ezek számomra a kutatás legkedvesebb pillanatai. Mindenkinek hálás vagyok, aki részt vett ezekben a pillanatokban vagy az ezekhez vezető adatgyűjtésben, koncepcióalkotásban.

Két szenior kutatót szeretnék első helyen kiemelni: Kovács Mihályt, akitől a labormunkát, az enzimkinetikát és a tudományos szemléletet tanultam, és Vértessy Beát, aki a szakmai útmutatáson és együtt gondolkodáson túl töretlen lelkesedéssel támogatta és kifogyhatatlan motivációval kövezte ki az utat ennek a dolgozatnak a megszületéséig. Mindkettőjüknek kulcsszerepet tulajdonítok a jelenlegi kutatói létem kibontakozásában. Hálával és szeretettel gondolok azokra a kiváló diákjaimra, akikkel a bemutatott munkát elvégeztük. A legtöbbet és legintenzívebben Pécsi Ildikóval, Lopata Annával, Hirmondó Ritával, Szabó Judittal, Surányi Évával, Molnár Dániellel, Füzesi Dórával és Trombitás Tamással dolgoztunk együtt (időrendben). Az ő diákjaik, Mébold Bence, Gálik Nikol, Szijjártó Péter, Horváth Ármin, Mészáros Petra, Lóczi Hanna és Kovács Szonja is hozzájárultak a projektek kivitelezéséhez. A Vértessy-csoport többi tagjának is köszönettel tartozom a közös munkálkodásért, együtt gondolkodásért, a diákok kölcsönös támogatásáért és a példátlanul jókedvű, támogató és motiváló munkahelyi légkörért. A száznál több volt és jelenlegi munkatársat nehéz lenne felsorolni, de szerzőtársaimat és közeli kollégáimat szeretném megemlíteni: az *alumni* tagok közül Takács Enikőt, Kovári Júliát, Varga Balázst, Merényi Gábort, Horváth Andrást, Róna Gergelyt, Nagy Gergelyt és Zagyva Imrét; a jelenlegiek közül pedig Békési Angélát, Leveles Ibolyát, Tankó Évát, Nyíri Kingát, Nagy Kingát, Benedek Andrást és Pálinkás Hajnalkát. Kimondottan élveztem a közös munkát a más szakterületen kiművelt kollégáimmal és szerzőtársaimmal is, akiktől mindig új szempontokat, új látásmódot lehet tanulni. Időben visszafelé haladva köszönöm a közös munkát és barátságot Pancsa Ritának, Fichó Erzsébetnek, Jójárt Balázsnak, Ozohanics Olivérnek, Mészáros Bálintnak, Dosztányi Zsuzsának, Kardos Józsefnek, Liliom Károlynak, Kovács Erikának és Málnási-Csizmadia Andrásnak.

Nemzetközi együttműködő partnereimnek, elsősorban Rosta Edinának (University College London, Anglia), James Sellers-nek (NHLBI, NIH, USA) és Tanya Parish-nek (Queen Mary University of London, Anglia) köszönöm a közös munkát.

Köszönöm továbbá a munkahelyi mentorálást és biztatást Buday Lászlónak és Nyitray Lászlónak.

A támogatást mindazon szakmai szervezeteknek köszönöm, amelyek révén a bemutatott projektek folyamatos pénzügyi támogatást élveztek (OTKA, Magyar Tudományos Akadémia, Humán Erőforrások Minisztériuma, National Institutes of Health, European Molecular Biology Organisation).

Köszönöm a családomnak és barátaimnak azt, hogy kiteljesítik az életem, és érdeklődő támogatásban részesítik a kutatási feladatokat is.

Végül, de nem utolsó sorban, köszönöm a kisgyermeket nevelő kutatónők számára létrehozott, a Magyar Tudományos Akadémia doktora cím megszerzésére irányuló támogatást, amely az anyagi támogatáson túl azzal járult hozzá nagyban e dolgozat megvalósításához, hogy határidőt szabott a benyújtására.

9 Rövidítésjegyzék

5-FU	5-fluorouracil
CFU	kolóniaképző egység, angolul „colony-forming unit”
dATP	2’-dezoxiadenozin-5’-trifoszfát
Dcd	dCTP-dezamináz
Dcd:dut	dCTP-dezamináz:dUTPáz bifunkciós enzim
dCTP	2’-dezoxicitidin-5’-trifoszfát
dGTP	2’-dezoxiguanozin-5’-trifoszfát
DNS	dezoxiribonukleinsav
dNTP	2’-dezoxiribonukleotid-5’-trifoszfát
DSB	double strand break, DNS kettősszál törés
dTMP	2’-dezoxitimidin-5’-monofoszfát
dTTP	2’-dezoxitimidin-5’-trifoszfát
dUMP	2’-dezoxiuridin-5’-monofoszfát
dUTP	2’-dezoxiuridin-5’-trifoszfát
dUTPáz	2’-dezoxiuridin-5’-trifoszfatáz enzim
Dut (*dut*)	dUTPáz (dUTPáz gén)
E. coli	*Escherichia coli*
EMSA	electrophoretic mobility shift assay
FAM	karboxifluoreszcein, fluoreszcens festék
HIV	human immunodeficiency virus (humán-immundeficienciavírus)
HPLC	nagy teljesítményű folyadékkromatográfia
HR	homológ rekombináció
ICP-OES	induktív csatolású plazma atomemissziós spektrometria
ITC	izotermális titráló kalorimetria
M. smegmatis	*Mycobacterium smegmatis*
MS	Mass Spectrometry (tömegspektrometria)
M. tuberculosis	*Mycobacterium tuberculosis*
MutT	8-oxo-dGTP difoszfatáz
NCBI	National Center for Biotechnology Information
QCM	kvarc kristály mikromérleg, angolul „quartz crystal microbalance”
qPCR	kvantitatív vagy valós idejű polimeráz láncreakció
RIF	rifampicin
RAMD	Random Acceleration Molecular Dynamics
rNDP	2’-ribonukleotid-5’-difoszfát
RNR	ribonukleotid-reduktáz
RNS	ribonukleinsav
rNTP	2’-ribonukleotid-5’-trifoszfát
Taq	*Thermus aquaticus*
TS	timidilát-szintáz enzim
Ung	uracil-DNS glikoziláz
WHO	Egészségügyi Világszervezet, angolul *„Word Health Organization”*

10 Irodalomjegyzék

10.1 A PhD fokozat megszerzése óta megjelent, az értekezés alapjául szolgáló levelező szerzős közlemények

1. Pancsa, R; Fichó, E; Molnár, D; Surányi, ÉV; Trombitás, T; Füzesi, D; Lóczi, H; Szijjártó, P; Hirmondó, R; Szabó, JE; **Tóth, J**: dNTPpoolDB: a manually curated database of experimentally determined dNTP pools and pool changes in biological samples. NUCLEIC ACIDS RESEARCH (2021), IF: 16,971
2. Szabó, JE; Suranyi, ÉV; Mébold, B; Trombitás, T; Cserepes, M; **Tóth, J**: A user-friendly, high-throughput tool for the precise fluorescent quantification of deoxyribonucleoside triphosphates from biological samples. NUCLEIC ACIDS RESEARCH 48 : 8 p. e45 , 17 p. (2020), IF: 16,971
3. Lopata, A; Jójárt, B; Surányi, ÉV; Takács, E; Bezúr, L; Leveles, I; Bendes, Á; Viskolcz, B; Vértessy, BG; **Tóth, J**: Beyond Chelation: EDTA Tightly Binds Taq DNA Polymerase, MutT and dUTPase and Directly Inhibits dNTPase Activity. BIOMOLECULES 9 : 10 Paper: 621, 19 p. (2019), IF: 4,082
4. Hirmondo, R; Lopata, A; Surányi, ÉV; Vértessy, BG; **Tóth, J**: Differential control of dNTP biosynthesis and genome integrity maintenance by the dUTPase superfamily enzymes. SCIENTIFIC REPORTS 7 : 1 Paper: 6043 , 12 p. (2017), IF: 4,122
5. Lopata, A; Leveles, I; Bendes, AA; Viskolcz, B; Vértessy, BG; Jójart, B; **Tóth, J**: A Hidden Active Site in the Potential Drug Target Mycobacterium tuberculosis dUTPase Is Accessible through Small Amplitude Protein Conformational Changes. JOURNAL OF BIOLOGICAL CHEMISTRY 291 : 51 pp. 26320-26331. , 12 p. (2016), IF: 4,125
6. Szabó, JE; Takács, E; Merényi, G; Vértessy, BG; **Tóth, J**: Trading in cooperativity for specificity to maintain uracil-free DNA. SCIENTIFIC REPORTS 6 Paper: 24219 (2016), IF: 4,259
7. Lopata, A; Jambrina, PG; Sharma, PK; Brooks, BR; **Tóth, J**; Vértessy, BG; Rosta, E: Mutations Decouple Proton Transfer from Phosphate Cleavage in the dUTPase Catalytic Reaction. ACS CATALYSIS 5 : 6 pp. 3225-3237. , 13 p. (2015), IF: 9.307
8. Szabó, JE; Németh, V; Papp-Kádár, V ; Nyíri, K; Leveles, I; Bendes, Á; Zagyva, I; Róna, G; Pálinkás, H; Besztercei, B ; Ozohanics, O; Vékey, K; Liliom, K; **Tóth, J**; Vértessy, BG: Highly potent dUTPase inhibition by a bacterial repressor protein reveals a novel mechanism for gene expression control. NUCLEIC ACIDS RESEARCH 42 : 19 pp. 11912-11920. , 9 p. (2014), IF: 9,112
9. Pécsi, I; Hirmondo, R; Brown, AC; Lopata, A; Parish, T; Vértessy, BG; **Tóth, J**: The dUTPase Enzyme Is Essential in Mycobacterium smegmatis. PLOS ONE 7 : 5 Paper: e37461 (2012), IF: 3,73
10. Pécsi, I; Szabó, JE; Adams, SD; Simon, I; Sellers, JR; Vértessy, BG; **Tóth, J**: Nucleotide pyrophosphatase employs a P-loop-like motif to enhance catalytic power and NDP/NTP discrimination. PROCEEDINGS OF THE NATIONAL ACADEMY OF SCIENCES OF THE UNITED STATES OF AMERICA 108 : 35 pp. 14437-14442. , 6 p. (2011), IF: 9,681
11. Pécsi, I; Leveles, I; Harmat, V; Vértessy, BG; **Tóth, J**: Aromatic stacking between nucleobase and enzyme promotes phosphate ester hydrolysis in dUTPase. NUCLEIC ACIDS RESEARCH 38 : 20 pp. 7179-7186. , 8 p. (2010), IF: 7,836

12. **Tóth, J**; Varga, B; Kovács, M; Málnási-Csizmadia, A; Vértessy, BG: Kinetic mechanism of human dUTPase, an essential nucleotide pyrophosphatase enzyme. JOURNAL OF BIOLOGICAL CHEMISTRY 282 : 46 pp. 33572-33582. , 11 p. (2007), IF: 5,581

10.2 A PhD fokozat megszerzése óta megjelent, az értekezéshez fel nem használt, de annak témájához kötődő saját közlemények

13. Surányi, ÉV; Hírmondó, R; Nyíri, K; Tarjányi, S; Kőhegyi, B; **Tóth, J**; Vértessy, BG: Exploiting a phage-bacterium interaction system as a molecular switch to decipher macromolecular interactions in the living cell. VIRUSES 10 : 4 Paper: 168 , 13 p. (2018), IF: 3,811
14. Nagy, GN; Suardiaz, R; Lopata, A; Ozohanics, O; Vékey, K; Brooks, BR; Leveles, I; **Tóth, J**; Vértessy, BG; Rosta, E: Structural Characterization of Arginine Fingers: Identification of an Arginine Finger for the Pyrophosphatase dUTPases. JOURNAL OF THE AMERICAN CHEMICAL SOCIETY 138 : 45 pp. 15035-15045. , 11 p. (2016), IF: 13.858
15. Hirmondó, R; Szabó, JE; Nyíri, K; Tarjányi, S; Dobrotka, P; **Tóth, J**; Vértessy, BG: Cross-species inhibition of dUTPase via the Staphylococcal Stl protein perturbs dNTP pool and colony formation in Mycobacterium. DNA REPAIR 30 pp. 21-27. , 7 p. (2015), IF: 3.929
16. Róna, G; Borsos, M; Ellis, JJ; Mehdi, AM; Christie, M; Környei, Z; Neubrandt, M; **Tóth, J**; Bozóky, Z; Buday, L; Madarász, E; Bodén, M; Kobe, B; Vértessy BG: Dynamics of re-constitution of the human nuclear proteome after cell division is regulated by NLS-adjacent phosphorylation. CELL CYCLE 13 : 22 pp. 3551-3564. , 14 p. (2014), IF: 4,565
17. Leveles, I; Németh, V; Szabó, JE; Harmat, V; Nyirí, K; Bendes, Á; Papp-Kádár, V; Zagyva, I; Róna, G; Ozohanics, O; Vékey, K; **Tóth, J**; Vértessy, BG: Structure and enzymatic mechanism of a moonlighting dUTPase: ACTA CRYSTALLOGRAPHICA SECTION D-BIOLOGICAL CRYSTALLOGRAPHY 69 : 12 pp. 2298-2308. , 11 p. (2013), IF: 7,232
18. Róna, G; Marfori, M; Borsos, M; Scheer, I; Takács, E; **Tóth, J**; Babos, F; Magyar, A; Erdei, A; Bozóky, Z; Buday, L; Kobe, B; Vértessy, BG: Phosphorylation adjacent to the nuclear localization signal of human dUTPase abolishes nuclear import: structural and mechanistic insights. ACTA CRYSTALLOGRAPHICA SECTION D-BIOLOGICAL CRYSTALLOGRAPHY 69 : 12 pp. 2495-2505. , 11 p. (2013), IF: 7,232
19. Erdélyi, P; Borsos, É; Takács-Vellai, K; Kovács, T; Kovács, AL , Sigmond, T; Hargitai, B; Pásztor, L; Sengupta, T; Dengg, M; Pécsi, I; **Tóth, J**; Nilsen, H; Vértessy, BG, Vellai T: Shared developmental roles and transcriptional control of autophagy and apoptosis in Caenorhabditis elegans. JOURNAL OF CELL SCIENCE 124 : 9 pp. 1510-1518. , 9 p. (2011), IF: 6,111
20. Merenyi, G; Kovári, J; **Tóth, J**; Takacs, E; Zagyva, I; Erdei, A; Vértessy, BG: Cellular response to efficient dUTPase RNAi silencing in stable HeLa cell lines perturbs expression levels of genes involved in thymidylate metabolism. NUCLEOSIDES NUCLEOTIDES & NUCLEIC ACIDS 30 : 6 pp. 369-390. , 22 p. (2011), IF: 0,899
21. Mészáros, B; **Tóth, J;** Vértessy, BG; Dosztányi, Zs; Simon, I: Proteins with Complex Architecture as Potential Targets for Drug Design: A Case Study of Mycobacterium tuberculosis. PLOS COMPUTATIONAL BIOLOGY 7 : 7 Paper: e1002118 , 14 p. (2011), IF: 5,215

22. Takács, E; Nagy, G; Leveles, I; Harmat, V; Lopata, A; **Tóth, J**; Vértessy, BG: Direct contacts between conserved motifs of different subunits provide major contribution to active site organization in human and mycobacterial dUTPases. FEBS LETTERS 584 : 14 pp. 3047-3054. , 8 p. (2010), IF: 3,601
23. Vértessy, BG; **Tóth, J**: Keeping uracil out of DNA: physiological role, structure and catalytic mechanism of dUTPases. ACCOUNTS OF CHEMICAL RESEARCH 42 : 1 pp. 97-106. , 10 p. (2009), IF: 18,203
24. Varga, B; Barabás, O; Kovári, J; **Tóth, J**; Hunyadi, Gulyas E; Klement, E; Medzihradszky, KF; Tölgyesi, F; Fidy, J; Vértessy, BG: Active site closure facilitates juxtaposition of reactant atoms for initiation of catalysis by human dUTPase. FEBS LETTERS 581 : 24 pp. 4783-4788. , 6 p. (2007), IF: 3,263

10.3 A PhD fokozat megszerzése óta megjelent, az értekezés témájához nem kötődő saját közlemények

25. Kovács, E; **Tóth, J**; Vertessy, BG; Liliom, K: Dissociation of calmodulin - target peptide complexes by the lipid mediator sphingosylphosphorylcholine: implications in calcium signaling. JOURNAL OF BIOLOGICAL CHEMISTRY 285 : 3 pp. 1799-1808. , 10 p. (2010), IF: 5,328
26. Kovács, E; Harmat, V; **Tóth, J**; Vértessy, BG; Módos, K; Kardos, J; Liliom, K: Structure and mechanism of calmodulin binding to a signaling sphingolipid reveal new aspects of lipid-protein interactions. FASEB JOURNAL 24 : 10 pp. 3829-3839. , 11 p. (2010) IF: 6,515
27. Forgács, E; Sakamoto, T; Cartwright, S; Belknap, B; Kovács, M; **Toth, J**; Webb, MR; Sellers, JR; White, HD: Switch 1 mutation S217A converts myosin V into a low duty ratio motor. JOURNAL OF BIOLOGICAL CHEMISTRY 284 : 4 pp. 2138-2149. , 12 p. (2009), IF: 5,328
28. Kempler, K; **Tóth, J;** Yamashita, R; Mapel, G; Robinson, K; Cardasis, H; Stevens, S; Battelle, B: Loop 2 of limulus myosin III is phosphorylated by protein kinase A. BIOCHEMISTRY 46 pp. 4280-4293. , 14 p. (2007), IF: 3,368
29. Málnási-Csizmadia, A; **Tóth, J**; Pearson, DS; Hetényi, Cs; Nyitray, L; Geeves, MA; Bagshaw, CR; Kovács, M: Selective perturbation of the Myosin recovery stroke by point mutations at the base of the lever arm affects ATP hydrolysis and phosphate release. JOURNAL OF BIOLOGICAL CHEMISTRY 282 : 24 pp. 17658-17664. , 7 p. (2007), IF: 5,581

10.4 Felhasznált irodalom

(1) Vertessy, B. G., Zalud, P., Nyman, P. O., and Zeppezauer, M. (1994) Identification of tyrosine as a functional residue in the active site of Escherichia coli dUTPase. *Biochim. Biophys. Acta 1205*, 146–50.
(2) Vertessy, B. G., Larsson, G., Persson, T., Bergman, A. C., Persson, R., and Nyman, P. O. (1998) The complete triphosphate moiety of non-hydrolyzable substrate analogues is required for a conformational shift of the flexible C-terminus in E. coli dUTP pyrophosphatase. *FEBS Lett. 421*, 83–8.
(3) Vertessy, B. G., Persson, R., Rosengren, A. M., Zeppezauer, M., and Nyman, P. O. (1996) Specific derivatization of the active site tyrosine in dUTPase perturbs ligand binding to

the active site. *Biochem. Biophys. Res. Commun. 219*, 294–300.
(4) Barabas, O., Pongracz, V., Kovari, J., Wilmanns, M., Vertessy, B. G., Barabás, O., Pongrácz, V., Kovári, J., Wilmanns, M., and Vértessy, B. G. (2004) Structural insights into the catalytic mechanism of phosphate ester hydrolysis by dUTPase. *J. Biol. Chem. 279*, 42907–15.
(5) Barabás, O., Németh, V., and Vértessy, B. G. (2006) Crystallization and preliminary X-ray studies of dUTPase from Mason–Pfizer monkey retrovirus. *Acta Crystallogr. Sect. F Struct. Biol. Cryst. Commun. 62*, 399–401.
(6) Németh-Pongrácz, V., Barabás, O., Fuxreiter, M., Simon, I., Pichová, I., Rumlová, M., Zábranská, H., Svergun, D., Petoukhov, M., Harmat, V., Klement, E., Hunyadi-Gulyás, E., Medzihradszky, K. F., Kónya, E., Vértessy, B. G., Nemeth-Pongracz, V., Barabas, O., Fuxreiter, M., Simon, I., Pichova, I., Rumlova, M., Zabranska, H., Svergun, D., Petoukhov, M., Harmat, V., Klement, E., Hunyadi-Gulyas, E., Medzihradszky, K. F., Konya, E., and Vertessy, B. G. (2007) Flexible segments modulate co-folding of dUTPase and nucleocapsid proteins. *Nucleic Acids Res. 35*, 495–505.
(7) Németh-Pongrácz, V., Snasel, J., Rumlova, M., Pichova, I., and Vértessy, B. G. (2006) Interacting Partners of M-PMV Nucleocapsid-DUTPase. *Nucleosides, Nucleotides and Nucleic Acids 25*, 1197–1200.
(8) Békési, A., Zagyva, I., Hunyadi-Gulyás, E., Pongrácz, V., Kovári, J., Nagy, A. O., Erdei, A., Medzihradszky, K. F., and Vértessy, B. G. (2004) Developmental regulation of dUTPase in Drosophila melanogaster. *J. Biol. Chem. 279*, 22362–70.
(9) Kovári, J., Barabás, O., Takács, E., Békési, A., Dubrovay, Z., Pongrácz, V., Zagyva, I., Imre, T., Szabó, P., and Vértessy, B. G. (2004) Altered active site flexibility and a structural metal-binding site in eukaryotic dUTPase: kinetic characterization, folding, and crystallographic studies of the homotrimeric Drosophila enzyme. *J. Biol. Chem. 279*, 17932–44.
(10) Varga, B., Barabás, O., Takács, E., Nagy, N., Nagy, P., and Vértessy, B. G. (2008) Active site of mycobacterial dUTPase: Structural characteristics and a built-in sensor. *Biochem. Biophys. Res. Commun. 373*, 8–13.
(11) Kerepesi, C., Szabó, J. E., Papp-Kádár, V., Dobay, O., Szabó, D., Grolmusz, V., and Vértessy, B. G. (2016) Life without dUTPase. *Front. Microbiol. 7*, 1768.
(12) Hizi, A., and Herzig, E. (2015) dUTPase: the frequently overlooked enzyme encoded by many retroviruses. *Retrovirology 12*, 70.
(13) Curtin, N. J., Harris, A. L., and Aherne, G. W. (1991) Mechanism of Cell Death following Thymidylate Synthase Inhibition: 2′-Deoxyuridine-5′-triphosphate Accumulation, DNA Damage, and Growth Inhibition following Exposure to CB3717 and Dipyridamole. *Cancer Res. 51*, 2346–2352.
(14) Vértessy, B. G., and Tóth, J. (2009) Keeping uracil out of DNA: physiological role, structure and catalytic mechanism of dUTPases. *Acc. Chem. Res. 42*, 97–106.
(15) Koehler, S. E., and Ladner, R. D. (2004) Small interfering RNA-mediated suppression of dUTPase sensitizes cancer cell lines to thymidylate synthase inhibition. *Mol. Pharmacol. 66*, 620–6.
(16) Canman, C. E., Lawrence, T. S., Shewach, D. S., Tang, H.-Y., and Maybaum, J. (1993) Resistance to Fluorodeoxyuridine-induced DNA Damage and Cytotoxicity Correlates with an Elevation of Deoxyuridine Triphosphatase Activity and Failure to Accumulate Deoxyuridine Triphosphate. *Cancer Res. 53*, 5219–5224.
(17) Canman, C. E., Radany, E. H., Parsels, L. A., Davis, M. A., Lawrence, T. S., and Maybaum, J. (1994) Induction of Resistance to Fluorodeoxyuridine Cytotoxicity and DNA Damage in Human Tumor Cells by Expression of Escherichia coli Deoxyuridinetriphosphatase. *Cancer Res. 54*, 2296–2298.
(18) Wilson, P. M., Fazzone, W., Labonte, M. J., Deng, J., Neamati, N., and Ladner, R. D.

(2008) Novel opportunities for thymidylate metabolism as a therapeutic target. *Mol. Cancer Ther. 7*, 3029–3037.

(19) Miyahara, S., Miyakoshi, H., Yokogawa, T., Chong, K. T., Taguchi, J., Muto, T., Endoh, K., Yano, W., Wakasa, T., Ueno, H., Takao, Y., Fujioka, A., Hashimoto, A., Itou, K., Yamamura, K., Nomura, M., Nagasawa, H., Shuto, S., and Fukuoka, M. (2012) Discovery of highly potent human deoxyuridine triphosphatase inhibitors based on the conformation restriction strategy. *J. Med. Chem. 55*, 5483–96.

(20) Miyakoshi, H., Miyahara, S., Yokogawa, T., Endoh, K., Muto, T., Yano, W., Wakasa, T., Ueno, H., Chong, K. T., Taguchi, J., Nomura, M., Takao, Y., Fujioka, A., Hashimoto, A., Itou, K., Yamamura, K., Shuto, S., Nagasawa, H., and Fukuoka, M. (2012) 1,2,3-Triazole-Containing Uracil Derivatives with Excellent Pharmacokinetics as a Novel Class of Potent Human Deoxyuridine Triphosphatase Inhibitors. *J. Med. Chem. 55*, 6427–6437.

(21) Miyahara, S., Miyakoshi, H., Yokogawa, T., Chong, K., Taguchi, J., Muto, T., Endoh, K., Yano, W., Wakasa, T., Ueno, H., Takao, Y., Fujioka, A., Hashimoto, A., Itou, K., Yamamura, K., Nomura, M., Nagasawa, H., Shuto, S., and Fukuoka, M. (2012) Discovery of a novel class of potent human deoxyuridine triphosphatase inhibitors remarkably enhancing the antitumor activity of thymidylate synthase inhibitors. *J. Med. Chem. 55*, 2970–2980.

(22) Yano, W., Yokogawa, T., Wakasa, T., Yamamura, K., Fujioka, A., Yoshisue, K., Matsushima, E., Miyahara, S., Miyakoshi, H., Taguchi, J., Chong, K., Takao, Y., Fukuoka, M., and Matsuo, K. (2018) TAS-114, a First-in-Class Dual dUTPase/DPD Inhibitor, Demonstrates Potential to Improve Therapeutic Efficacy of Fluoropyrimidine-Based Chemotherapy. *Mol. Cancer Ther. 17*, 1683–1693.

(23) Yokogawa, T., Yano, W., Tsukioka, S., Osada, A., Wakasa, T., Ueno, H., Hoshino, T., Yamamura, K., Fujioka, A., Fukuoka, M., Ohkubo, S., and Matsuo, K. (2021) dUTPase inhibition confers susceptibility to a thymidylate synthase inhibitor in DNA-repair-defective human cancer cells. *Cancer Sci. 112*, 422–432.

(24) Wilson, P. M., LaBonte, M. J., Lenz, H.-J., Mack, P. C., and Ladner, R. D. (2012) Inhibition of dUTPase induces synthetic lethality with thymidylate synthase-targeted therapies in non-small cell lung cancer. *Mol. Cancer Ther. 11*, 616–28.

(25) Hagenkort, A., Paulin, C. B. J., Desroses, M., Sarno, A., Wiita, E., Mortusewicz, O., Koolmeister, T., Loseva, O., Jemth, A.-S., Almlöf, I., Homan, E., Lundbäck, T., Gustavsson, A.-L., Scobie, M., Helleday, T., Hagenkort, A., Paulin, C. B. J., Desroses, M., Sarno, A., Wiita, E., Mortusewicz, O., Koolmeister, T., Loseva, O., Jemth, A.-S., Almlöf, I., Homan, E., Lundbäck, T., Gustavsson, A.-L., Scobie, M., and Helleday, T. (2017) dUTPase inhibition augments replication defects of 5-Fluorouracil. *Oncotarget 8*, 23713–23726.

(26) Davison, C., Morelli, R., Knowlson, C., McKechnie, M., Carson, R., Stachtea, X., McLaughlin, K. A., Prise, V. E., Savage, K., Wilson, R. H., Mulligan, K. A., Wilson, P. M., Ladner, R. D., and LaBonte, M. J. (2021) Targeting nucleotide metabolism enhances the efficacy of anthracyclines and anti-metabolites in triple-negative breast cancer. *npj Breast Cancer 2021 71 7*, 1–13.

(27) Chen, C., Tsao, N., Huang, L., Yen, Y., Liu, X., Lehman, C., Wang, Y., Tseng, M., Chen, Y., Ho, Y., Chen, C., and Chang, Z. (2016) The Impact of dUTPase on Ribonucleotide Reductase-Induced Genome Instability in Cancer Cells. *Cell Rep. 16*, 1287–1299.

(28) Saito, K., Nagashima, H., Noguchi, K., Yoshisue, K., Yokogawa, T., Matsushima, E., Tahara, T., and Takagi, S. (2014) First-in-human, phase I dose-escalation study of single and multiple doses of a first-in-class enhancer of fluoropyrimidines, a dUTPase inhibitor (TAS-114) in healthy male volunteers. *Cancer Chemother. Pharmacol. 73*, 577–583.

(29) Yamamoto, N., Hayashi, H., Planchard, D., Morán, T., Gregorc, V., Dowell, J., Sakai, H., Yoh, K., Nishio, M., Cortot, A., Benhadji, K., Soni, N., Huang, J., Makris, L., and Cedres,

S. (2020) A randomized, phase 2 study of deoxyuridine triphosphatase inhibitor, TAS-114, in combination with S-1 versus S-1 alone in patients with advanced non-small-cell lung cancer. *Invest. New Drugs 38*, 1588–1597.
(30) Pérez-Moreno, G., Sánchez-Carrasco, P., Ruiz-Pérez, L., Johansson, N., Müller, S., Baragaña, B., Hampton, S., Gilbert, I., Kaiser, M., Sarkar, S., Pandurangan, T., Kumar, V., and González-Pacanowska, D. (2019) Validation of Plasmodium falciparum dUTPase as the target of 5'-tritylated deoxyuridine analogues with anti-malarial activity. *Malar. J. 18*, 392.
(31) Whittingham, J. L., Leal, I., Nguyen, C., Kasinathan, G., Bell, E., Jones, A. F., Berry, C., Benito, A., Turkenburg, J. P., Dodson, E. J., Perez, L. M. R., Wilkinson, A. J., Johansson, N. G., Brun, R., Gilbert, I. H., Pacanowska, D. G., and Wilson, K. S. (2005) dUTPase as a Platform for Antimalarial Drug Design: Structural Basis for the Selectivity of a Class of Nucleoside Inhibitors. *Structure 13*, 329–338.
(32) Guda, G., Nguyen, C., Ziemkowski, P., Felczak, K., Kasinathan, G., Musso-Buendia, A., Sund, C., Zhou, X., Kaiser, M., Ruiz-Pérez, L., Brun, R., Kulikowski, T., Johansson, N., González-Pacanowska, D., and Gilbert, I. (2011) Modified 5'-trityl nucleosides as inhibitors of Plasmodium falciparum dUTPase. *ChemMedChem 6*, 309–320.
(33) Hirmondo, R., Lopata, A., Suranyi, E. V., Vertessy, B. G., and Toth, J. (2017) Differential control of dNTP biosynthesis and genome integrity maintenance by the dUTPase superfamily enzymes. *Sci. Rep. 7*, 6043.
(34) Paula A. Sherman and James A. Fyfe. (1989) Enzymatic Assay for Deoxyribonucleoside Triphosphates Using Synthetic Oligonucleotides as Template Primers. *Anal. Biochem. 226*, 222–226.
(35) Szabó, J., Surányi, É. V., Mébold, B., Trombitás, T., Cserepes, M., and Tóth, J. (2020) A user-friendly, high-throughput tool for the precise fluorescent quantification of deoxyribonucleoside triphosphates from biological samples. *Nucleic Acids Res. 48*, e45.
(36) Parish, T., Brown, A. C., Rustad, T. R., Roberts, D. M., Liao, R. P., and Sherman, D. R. (2009) Mycobacteria Protocols (Parish, T., and Brown, A. C., Eds.), pp 13–22. Humana Press, Totowa, NJ.
(37) Pecsi, I., Hirmondo, R., Brown, A. C., Lopata, A., Parish, T., Vertessy, B. G., Toth, J., and Tóth, J. (2012) The dUTPase enzyme is essential in Mycobacterium smegmatis. *PLoS One 7*, e37461.
(38) David, H. L. (1970) Probability distribution of drug-resistant mutants in unselected populations of Mycobacterium tuberculosis. *Appl. Microbiol. 20*, 810–814.
(39) Horváth, A., and Vértessy, B. G. (2010) A one-step method for quantitative determination of uracil in DNA by real-time PCR. *Nucleic Acids Res. 38*, e196.
(40) Szabó, J. E., Németh, V., Papp-Kádár, V., Nyíri, K., Leveles, I., Bendes, A. Á., Zagyva, I., Róna, G., Pálinkás, H. L., Besztercei, B., Ozohanics, O., Vékey, K., Liliom, K., Tóth, J., and Vértessy, B. G. (2014) Highly potent dUTPase inhibition by a bacterial repressor protein reveals a novel mechanism for gene expression control. *Nucleic Acids Res. 42*, 11912–20.
(41) Szabó, J. E., Takács, E., Merényi, G., Vértessy, B. G., and Tóth, J. (2016) Trading in cooperativity for specificity to maintain uracil-free DNA. *Sci. Rep. 6*, 24219.
(42) Summer, H., Grämer, R., and Dröge, P. (2009) Denaturing urea polyacrylamide gel electrophoresis (Urea PAGE). *J. Vis. Exp.* 1485.
(43) Tóth, J., Varga, B., Kovács, M., Málnási-Csizmadia, A., Vértessy, B. G., Toth, J., Varga, B., Kovacs, M., Malnasi-Csizmadia, A., and Vertessy, B. G. (2007) Kinetic mechanism of human dUTPase, an essential nucleotide pyrophosphatase enzyme. *J. Biol. Chem. 282*, 33572–82.
(44) Varga, B., Barabás, O., Kovári, J., Tóth, J., Hunyadi-Gulyás, E., Klement, E., Medzihradszky, K. F., Tölgyesi, F., Fidy, J., and Vértessy, B. G. (2007) Active site closure

facilitates juxtaposition of reactant atoms for initiation of catalysis by human dUTPase. *FEBS Lett. 581*, 4783–8.
(45) Mol, C. D., Harris, J. M., McIntosh, E. M., and Tainer, J. A. (1996) Human dUTP pyrophosphatase: uracil recognition by a β hairpin and active sites formed by three separate subunits. *Structure 4*, 1077–1092.
(46) Kovári, J., Barabás, O., Varga, B., Békési, A., Tölgyesi, F., Fidy, J., Nagy, J., and Vértessy, B. G. (2008) Methylene substitution at the alpha-beta bridging position within the phosphate chain of dUDP profoundly perturbs ligand accommodation into the dUTPase active site. *Proteins 71*, 308–19.
(47) Merényi, G., Kovári, J., Tóth, J., Takács, E., Zagyva, I., Erdei, A., and Vértessy, B. G. (2011) Cellular response to efficient dUTPase RNAi silencing in stable HeLa cell lines perturbs expression levels of genes involved in thymidylate metabolism. *Nucleosides. Nucleotides Nucleic Acids 30*, 369–90.
(48) Pecsi, I., Leveles, I., Harmat, V., Vertessy, B. G., and Toth, J. (2010) Aromatic stacking between nucleobase and enzyme promotes phosphate ester hydrolysis in dUTPase. *Nucleic Acids Res. 38*, 7179–86.
(49) Meyer, E., Castellano, R., and Diederich, F. (2003) Interactions with aromatic rings in chemical and biological recognition. *Angew. Chem. Int. Ed. Engl. 42*, 1210–1250.
(50) Hobza, P., and Sponer, J. (1999) Structure, energetics, and dynamics of the nucleic Acid base pairs: nonempirical ab initio calculations. *Chem. Rev. 99*, 3247–3276.
(51) Blakaj, D., McConnell, K., Beveridge, D., and Baranger, A. (2001) Molecular dynamics and thermodynamics of protein-RNA interactions: mutation of a conserved aromatic residue modifies stacking interactions and structural adaptation in the U1A-stem loop 2 RNA complex. *J. Am. Chem. Soc. 123*, 2548–2551.
(52) Hughes, R., and Waters, M. (2006) Model systems for beta-hairpins and beta-sheets. *Curr. Opin. Struct. Biol. 16*, 514–524.
(53) Zhou, Z., and Swenson, R. (1996) The cumulative electrostatic effect of aromatic stacking interactions and the negative electrostatic environment of the flavin mononucleotide binding site is a major determinant of the reduction potential for the flavodoxin from Desulfovibrio vulgaris [Hi. *Biochemistry 35*, 15980–15988.
(54) Versées, W., Loverix, S., Vandemeulebroucke, A., Geerlings, P., and Steyaert, J. (2004) Leaving group activation by aromatic stacking: an alternative to general acid catalysis. *J. Mol. Biol. 338*, 1–6.
(55) Guo, X., Chen, X., Weber, I., Harrison, R., and Tai, P. (2006) Molecular basis for differential nucleotide binding of the nucleotide-binding domain of ABC-transporter CvaB. *Biochemistry 45*, 14473–14480.
(56) Rickert, K., Schaber, M., Torrent, M., Neilson, L., Tasber, E., Garbaccio, R., Coleman, P., Harvey, D., Zhang, Y., Yang, Y., Marshall, G., Lee, L., Walsh, E., Hamilton, K., and Buser, C. (2008) Discovery and biochemical characterization of selective ATP competitive inhibitors of the human mitotic kinesin KSP. *Arch. Biochem. Biophys. 469*, 220–231.
(57) Boehr, D., Farley, A., Wright, G., and Cox, J. (2002) Analysis of the pi-pi stacking interactions between the aminoglycoside antibiotic kinase APH(3')-IIIa and its nucleotide ligands. *Chem. Biol. 9*, 1209–1217.
(58) Pécsi, I., Szabó, J. E., Adams, S. D., Simon, I., Sellers, J. R., Vértessy, B. G., Tóth, J., Pecsi, I., Szabo, J. E., Adams, S. D., Simon, I., Sellers, J. R., Vertessy, B. G., and Toth, J. (2011) Nucleotide pyrophosphatase employs a P-loop-like motif to enhance catalytic power and NDP/NTP discrimination. *Proc. Natl. Acad. Sci. U. S. A. 108*, 14437–42.
(59) Prasad, G. (2005) Glycine Rich P-loop Motif in Deoxyuridine Pyrophosphatase. *Curr. Protein Pept. Sci. 2*, 301–311.
(60) Chan, S., Segelke, B., Lekin, T., Krupka, H., Cho, U. S., Kim, M.-Y., So, M., Kim, C.-Y., Naranjo, C. M., Rogers, Y. C., Park, M. S., Waldo, G. S., Pashkov, I., Cascio, D., Perry, J.

L., and Sawaya, M. R. (2004) Crystal Structure of the Mycobacterium tuberculosis dUTPase: Insights into the Catalytic Mechanism. *J. Mol. Biol. 341*, 503–517.
(61) Tarbouriech, N., Buisson, M., Seigneurin, J. M., Cusack, S., and Burmeister, W. P. (2005) The monomeric dUTPase from Epstein-Barr virus mimics trimeric dUTPases. *Structure 13*, 1299–1310.
(62) Smith, C. A., and Rayment, I. (1996) Active site comparisons highlight structural similarities between myosin and other P-loop proteins. *Biophys. J. 70*, 1590.
(63) Pai, E. F., Krengel, U., Petsko, G. A., Goody, R. S., Kabsch, W., and Wittinghofer, A. (1990) Refined crystal structure of the triphosphate conformation of H-ras p21 at 1.35 A resolution: implications for the mechanism of GTP hydrolysis. *EMBO J. 9*, 2351.
(64) Motlagh, H. N., Wrabl, J. O., Li, J., and Hilser, V. J. (2014) The ensemble nature of allostery. *Nature 508*, 331–9.
(65) Petit, C. M., Zhang, J., Sapienza, P. J., Fuentes, E. J., and Lee, A. L. (2009) Hidden dynamic allostery in a PDZ domain. *Proc. Natl. Acad. Sci. 106*, 18249–18254.
(66) Tzeng, S.-R., and Kalodimos, C. G. (2009) Dynamic activation of an allosteric regulatory protein. *Nature 462*, 368–72.
(67) Gunasekaran, K., Ma, B., and Nussinov, R. (2004) Is allostery an intrinsic property of all dynamic proteins? *Proteins 57*, 433–43.
(68) Gadsden, M. H., McIntosh, E. M., Game, J. C., Wilson, P. J., and Haynes, R. H. (1993) dUTP pyrophosphatase is an essential enzyme in Saccharomyces cerevisiae. *EMBO J. 12*, 4425–31.
(69) Castillo-Acosta, V. M., Aguilar-Pereyra, F., García-Caballero, D., Vidal, A. E., Ruiz-Pérez, L. M., and González-Pacanowska, D. (2013) Pyrimidine requirements in deoxyuridine triphosphate nucleotidohydrolase deficient Trypanosoma brucei mutants. *Mol. Biochem. Parasitol. 187*, 9–13.
(70) Ting, H., Kouzminova, E. A., and Kuzminov, A. (2008) Synthetic lethality with the dut defect in Escherichia coli reveals layers of DNA damage of increasing complexity due to uracil incorporation. *J. Bacteriol. 190*, 5841–54.
(71) Lopata, A., Jambrina, P. G., Sharma, P. K., Brooks, B. R., Toth, J., Vertessy, B. G., and Rosta, E. (2015) Mutations Decouple Proton Transfer from Phosphate Cleavage in the dUTPase Catalytic Reaction. *ACS Catal. 5*, 3225–3237.
(72) Takács, E., Nagy, G., Leveles, I., Harmat, V., Lopata, A., Tóth, J., Vértessy, B. G., Takacs, E., Nagy, G., Leveles, I., Harmat, V., Lopata, A., Toth, J., and Vertessy, B. G. (2010) Direct contacts between conserved motifs of different subunits provide major contribution to active site organization in human and mycobacterial dUTPases. *FEBS Lett. 584*, 3047–54.
(73) Chan, S., Segelke, B., Lekin, T., Krupka, H., Cho, U. S., Kim, M. Y., So, M., Kim, C. Y., Naranjo, C. M., Rogers, Y. C., Park, M. S., Waldo, G. S., Pashkov, I., Cascio, D., Perry, J. L., and Sawaya, M. R. (2004) Crystal structure of the Mycobacterium tuberculosis dUTPase: insights into the catalytic mechanism. *J Mol Biol 341*, 503–517.
(74) Siggaard, J. H. B., Johansson, E., Vognsen, T., Helt, S. S., Harris, P., Larsen, S., and Willemoës, M. (2009) Concerted bifunctionality of the dCTP deaminase-dUTPase from Methanocaldococcus jannaschii: a structural and pre-steady state kinetic analysis. *Arch. Biochem. Biophys. 490*, 42–9.
(75) Lopata, A., Leveles, I., Bendes, A. A., Viskolcz, B., Vertessy, B. G., Jojart, B., and Toth, J. (2016) A hidden active site in the potential drug target Mycobacterium tuberculosis dUTPase is accessible through small-amplitude protein conformational changes. *J. Biol. Chem. 291*, jbc.M116.734012.
(76) Lee, J. Y., and Yang, W. (2006) UvrD helicase unwinds DNA one base pair at a time by a two-part power stroke. *Cell 127*, 1349–1360.
(77) Gai, D., Zhao, R., Li, D., Finkielstein, C. V, and Chen, X. S. (2004) Mechanisms of

conformational change for a replicative hexameric helicase of SV40 large tumor antigen. *Cell 119*, 47–60.
(78) Velankar, S. S., Soultanas, P., Dillingham, M. S., Subramanya, H. S., and Wigley, D. B. (1999) Crystal structures of complexes of PcrA DNA helicase with a DNA substrate indicate an inchworm mechanism. *Cell 97*, 75–84.
(79) Sablin, E. P., and Fletterick, R. J. (2001) Nucleotide switches in molecular motors: structural analysis of kinesins and myosins. *Curr Opin Struct Biol 11*, 716–724.
(80) Shuman, S., and Lima, C. D. (2004) The polynucleotide ligase and RNA capping enzyme superfamily of covalent nucleotidyltransferases. *Curr Opin Struct Biol 14*, 757–764.
(81) Santoso, Y., Joyce, C. M., Potapova, O., Le Reste, L., Hohlbein, J., Torella, J. P., Grindley, N. D., and Kapanidis, A. N. (2010) Conformational transitions in DNA polymerase I revealed by single-molecule FRET. *Proc Natl Acad Sci U S A 107*, 715–720.
(82) Ludemann, S. K., Lounnas, V., and Wade, R. C. (2000) How do substrates enter and products exit the buried active site of cytochrome P450cam? 1. Random expulsion molecular dynamics investigation of ligand access channels and mechanisms. *J Mol Biol 303*, 797–811.
(83) Takacs, E., Barabas, O., Petoukhov, M. V, Svergun, D. I., Vertessy, B. G., Takács, E., Barabás, O., Petoukhov, M. V, Svergun, D. I., and Vértessy, B. G. (2009) Molecular shape and prominent role of beta-strand swapping in organization of dUTPase oligomers. *FEBS Lett. 583*, 865–71.
(84) Yang, S.-W., Ting, H.-C., Lo, Y.-T., Wu, T.-Y., Huang, H.-W., Yang, C.-J., Chan, J.-F. R., Chuang, M.-C., and Hsu, Y.-H. H. (2016) Guanine nucleotide induced conformational change of Cdc42 revealed by hydrogen/deuterium exchange mass spectrometry. *Biochim. Biophys. Acta - Proteins Proteomics 1864*, 42–51.
(85) Lopata, A., Jójárt, B., Surányi, É. V., Takács, E., Bezúr, L., Leveles, I., Bendes, Á., Viskolcz, B., Vértessy, B. G., and Tóth, J. (2019) Beyond chelation: EDTA tightly binds taq DNA polymerase, MutT and dUTPase and directly inhibits dNTPase activity. *Biomolecules 9*.
(86) Jorgensen, P. L., Håkansson, K. O., and Karlish, S. J. D. (2003) Structure and Mechanism of Na,K-ATPase: Functional Sites and Their Interactions. *Annu. Rev. Physiol. 65*, 817–849.
(87) Sprang, S. R. (1997) G Protein Mechanisms: Insights from Structural Analysis. *Annu. Rev. Biochem. 66*, 639–678.
(88) Tomkinson, A. E., Vijayakumar, S., Pascal, J. M., and Ellenberger, T. (2006) DNA Ligases: Structure, Reaction Mechanism, and Function. *Chem. Rev. 106*, 687–699.
(89) Rothwell, P. J., and Waksman, G. (2005) Structure and mechanism of DNA polymerases. *Adv. Protein Chem. 71*, 401–40.
(90) Mildvan, A. S., Xia, Z., Azurmendi, H. F., Saraswat, V., Legler, P. M., Massiah, M. A., Gabelli, S. B., Bianchet, M. A., Kang, L.-W., and Amzel, L. M. (2005) Structures and mechanisms of Nudix hydrolases. *Arch. Biochem. Biophys. 433*, 129–143.
(91) Freeman, L., Buisson, M., Tarbouriech, N., Van der Heyden, A., Labbé, P., Burmeister, W. P., Labbe, P., Burmeister, W. P., Labbé, P., and Burmeister, W. P. (2009) The flexible motif V of Epstein-Barr virus deoxyuridine 5'-triphosphate pyrophosphatase is essential for catalysis. *J. Biol. Chem. 284*, 25280–9.
(92) Mustafi, D., Bekesi, A., Vertessy, B. G., and Makinen, M. W. (2003) Catalytic and structural role of the metal ion in dUTP pyrophosphatase. *Proc. Natl. Acad. Sci. U. S. A. 100*, 5670–5.
(93) Nord, J., Larsson, G., Kvassman, J. O., Rosengren, A. M., and Nyman, P. O. (1997) dUTPase from the retrovirus equine infectious anemia virus: specificity, turnover and inhibition. *FEBS Lett. 414*, 271–4.
(94) Larsson, G., Nyman, P. O., and Kvassman, J. O. (1996) Kinetic characterization of dUTPase from Escherichia coli. *J. Biol. Chem. 271*, 24010–6.

(95) Oliveros, M., García-Escudero, R., Alejo, A., Viñuela, E., Salas, M. L., and Salas, J. (1999) African swine fever virus dUTPase is a highly specific enzyme required for efficient replication in swine macrophages. *J. Virol. 73*, 8934–43.
(96) Fletcher, S., Keaney, E. P., Cummings, C. G., Blaskovich, M. A., Hast, M. A., Glenn, M. P., Chang, S. Y., Bucher, C. J., Floyd, R. J., Katt, W. P., Gelb, M. H., Van Voorhis, W. C., Beese, L. S., Sebti, S. M., and Hamilton, A. D. (2010) Structure-based design and synthesis of potent, ethylenediamine-based, mammalian farnesyltransferase inhibitors as anticancer agents. *J. Med. Chem. 53*, 6867–6888.
(97) Hast, M. A., Fletcher, S., Cummings, C. G., Pusateri, E. E., Blaskovich, M. A., Rivas, K., Gelb, M. H., Van Voorhis, W. C., Sebti, S. M., Hamilton, A. D., and Beese, L. S. (2009) Structural basis for binding and selectivity of antimalarial and anticancer ethylenediamine inhibitors to protein farnesyltransferase. *Chem. Biol. 16*, 181–192.
(98) Lari, S.-U., Chen, C.-Y., Vertéssy, B. G., Morré, J., and Bennett, S. E. (2006) Quantitative determination of uracil residues in Escherichia coli DNA: Contribution of ung, dug, and dut genes to uracil avoidance. *DNA Repair (Amst). 5*, 1407–20.
(99) Dubois, E., Córdoba-Cañero, D., Massot, S., Siaud, N., Gakière, B., Domenichini, S., Guérard, F., Roldan-Arjona, T., and Doutriaux, M.-P. (2011) Homologous Recombination Is Stimulated by a Decrease in dUTPase in Arabidopsis. *PLoS One 6*, e18658.
(100) Guillet, M., Van Der Kemp, P. A., and Boiteux, S. (2006) dUTPase activity is critical to maintain genetic stability in Saccharomyces cerevisiae. *Nucleic Acids Res. 34*, 2056–66.
(101) Johansson, E., Bjornberg, O., Nyman, P. O., and Larsen, S. (2003) Structure of the bifunctional dCTP deaminase-dUTPase from Methanocaldococcus jannaschii and its relation to other homotrimeric dUTPases. *J. Biol. Chem. 278*, 27916–22.
(102) el-Hajj, H. H., Zhang, H., and Weiss, B. (1988) Lethality of a dut (deoxyuridine triphosphatase) mutation in Escherichia coli. *J. Bacteriol. 170*, 1069–75.
(103) Sassetti, C. M., Boyd, D. H., and Rubin, E. J. (2003) Genes required for mycobacterial growth defined by high density mutagenesis. *Mol. Microbiol. 48*, 77–84.
(104) Griffin, J. E., Gawronski, J. D., Dejesus, M. a, Ioerger, T. R., Akerley, B. J., and Sassetti, C. M. (2011) High-resolution phenotypic profiling defines genes essential for mycobacterial growth and cholesterol catabolism. *PLoS Pathog. 7*, e1002251.
(105) Ladner, R. (2005) The Role of dUTPase and Uracil-DNA Repair in Cancer Chemotherapy. *Curr. Protein Pept. Sci. 2*, 361–370.
(106) Varga, B., Barabas, O., Takacs, E., Nagy, N., Nagy, P., and Vertessy, B. G. (2008) Active site of mycobacterial dUTPase: structural characteristics and a built-in sensor. *Biochem Biophys Res Commun 373*, 8–13.
(107) Helt, S. S., Thymark, M., Harris, P., Aagaard, C., Dietrich, J., Larsen, S., and Willemoes, M. (2008) Mechanism of dTTP inhibition of the bifunctional dCTP deaminase:dUTPase encoded by Mycobacterium tuberculosis. *J. Mol. Biol. 376*, 554–69.
(108) Kumar, P., Bharti, S. K., and Varshney, U. (2011) Uracil excision repair in Mycobacterium tuberculosis cell-free extracts. *Tuberculosis (Edinb). 91*, 212–8.
(109) Srinath, T., Bharti, S. K., and Varshney, U. (2007) Substrate specificities and functional characterization of a thermo-tolerant uracil DNA glycosylase (UdgB) from Mycobacterium tuberculosis. *DNA Repair (Amst). 6*, 1517–28.
(110) Sang, P. B., Srinath, T., Patil, A. G., Woo, E.-J., and Varshney, U. (2015) A unique uracil-DNA binding protein of the uracil DNA glycosylase superfamily. *Nucleic Acids Res. 43*, 8452–8463.
(111) Gon, S., and Beckwith, J. (2006) Ribonucleotide Reductases: Influence of Environment on Synthesis and Activity. *Antioxidants Redox Signal. 8*.
(112) Davidson, M. B., Katou, Y., Keszthelyi, A., Sing, T. L., Xia, T., Ou, J., Vaisica, J. a, Thevakumaran, N., Marjavaara, L., Myers, C. L., Chabes, A., Shirahige, K., and Brown, G.

W. (2012) Endogenous DNA replication stress results in expansion of dNTP pools and a mutator phenotype. *EMBO J. 31*, 895–907.
(113) Nordlund, P., and Reichard, P. (2006) Ribonucleotide reductases. *Annu. Rev. Biochem. 75*, 681–706.
(114) Ahluwalia, D., Bienstock, R. J., and Schaaper, R. M. (2012) Novel mutator mutants of E. coli nrdAB ribonucleotide reductase: Insight into allosteric regulation and control of mutation rates. *DNA Repair (Amst). 11*, 480–487.
(115) Gon, S., Napolitano, R., Rocha, W., Coulon, S., and Fuchs, R. P. (2011) Increase in dNTP pool size during the DNA damage response plays a key role in spontaneous and induced-mutagenesis in Escherichia coli. *Proc. Natl. Acad. Sci. 108*, 19311–19316.
(116) Kumar, D., Viberg, J., Nilsson, A. K., and Chabes, A. (2010) Highly mutagenic and severely imbalanced dNTP pools can escape detection by the S-phase checkpoint. *Nucleic Acids Res. 38*, 3975–83.
(117) Johansson, E., Thymark, M., Bynck, J. H., Fanø, M., Larsen, S., and Willemoës, M. (2007) Regulation of dCTP deaminase from Escherichia coli by nonallosteric dTTP binding to an inactive form of the enzyme. *FEBS J. 274*, 4188–98.
(118) Hou, H. F., Liang, Y. H., Li, L. F., Su, X. D., and Dong, Y. H. (2008) Crystal structures of Streptococcus mutans 2'-deoxycytidylate deaminase and its complex with substrate analog and allosteric regulator dCTP x Mg2+. *J. Mol. Biol. 377*, 220–231.
(119) Marx, A., and Alian, A. (2015) The First Crystal Structure of a dTTP-bound Deoxycytidylate Deaminase Validates and Details the Allosteric-Inhibitor Binding Site. *J. Biol. Chem. 290*, 682–90.
(120) Kadirvelraj, R., Sennett, N. C., Polizzi, S. J., Weitzel, S., and Wood, Z. A. (2011) Role of packing defects in the evolution of allostery and induced fit in human UDP-glucose dehydrogenase. *Biochemistry 50*, 5780–5789.
(121) Tormo-Mas, M. A., Mir, I., Shrestha, A., Tallent, S. M., Campoy, S., Lasa, I., Barbe, J., Novick, R. P., Christie, G. E., Penades, J. R., Tormo-Más, M. A., Mir, I., Shrestha, A., Tallent, S. M., Campoy, S., Lasa, I., Barbé, J., Novick, R. P., Christie, G. E., and Penadés, J. R. (2010) Moonlighting bacteriophage proteins derepress staphylococcal pathogenicity islands. *Nature 465*, 779–82.
(122) Tormo-Más, M. Á., Donderis, J., García-Caballer, M., Alt, A., Mir-Sanchis, I., Marina, A., and Penadés, J. R. (2013) Phage dUTPases control transfer of virulence genes by a proto-oncogenic G protein-like mechanism. *Mol. Cell 49*, 947–58.
(123) Neal, S. E., Eccleston, J. F., Hall, A., and Webb, M. R. (1988) Kinetic analysis of the hydrolysis of GTP by p21N-ras. The basal GTPase mechanism. *J. Biol. Chem. 263*, 19718–22.
(124) Vertessy, B. G. (1997) Flexible glycine rich motif of Escherichia coli deoxyuridine triphosphate nucleotidohydrolase is important for functional but not for structural integrity of the enzyme. *Proteins 28*, 568–79.
(125) Leveles, I., Németh, V., Szabó, J. E. J. E., Harmat, V., Nyíri, K., Bendes, Á. Á., Papp-Kádár, V., Zagyva, I., Róna, G., Ozohanics, O., Vékey, K., Tóth, J., Vértessy, B. G. B. G., Bendes, A. A., Papp-Kádár, V., Zagyva, I., Róna, G., Ozohanics, O., Vékey, K., Tóth, J., and Vértessy, B. G. B. G. (2013) Structure and enzymatic mechanism of a moonlighting dUTPase. *Acta Crystallogr. D. Biol. Crystallogr. 69*, 2298–308.
(126) Leveles, I., Róna, G., Zagyva, I., Bendes, Á., Harmat, V., and Vértessy, B. G. (2011) Crystallization and preliminary crystallographic analysis of dUTPase from the ϕ11 helper phage of Staphylococcus aureus. *Acta Crystallogr. Sect. F. Struct. Biol. Cryst. Commun. 67*, 1411–3.
(127) Weil, A. F., Ghosh, D., Zhou, Y., Seiple, L., McMahon, M. A., Spivak, A. M., Siliciano, R. F., and Stivers, J. T. (2013) Uracil DNA glycosylase initiates degradation of HIV-1 cDNA containing misincorporated dUTP and prevents viral integration. *Proc. Natl. Acad. Sci.*

U. S. A. 110, E448-57.
(128) Yan, N., O'Day, E., Wheeler, L. A., Engelman, A., and Lieberman, J. (2011) HIV DNA is heavily uracilated, which protects it from autointegration. *Proc. Natl. Acad. Sci. U. S. A. 108*, 9244–9.
(129) Nyíri, K., Mertens, H. D. T., Tihanyi, B., Nagy, G. N., Kohegyi, B., Matejka, J., Harris, M. J., Szabó, J. E., Papp-Kádár, V., Németh-Pongrácz, V., Ozohanics, O., Vékey, K., Svergun, D. I., Borysik, A. J., and Vértessy, B. G. (2018) Structural model of human dUTPase in complex with a novel proteinaceous inhibitor. *Sci. Rep. 8*, 4326.
(130) Nyíri, K., Harris, M. J., Matejka, J., Ozohanics, O., Vékey, K., Borysik, A. J., and Vértessy, B. G. (2019) HDX and Native Mass Spectrometry Reveals the Different Structural Basis for Interaction of the Staphylococcal Pathogenicity Island Repressor Stl with Dimeric and Trimeric Phage dUTPases. *Biomolecules 9*, 488.
(131) Hirmondó, R., Szabó, J. E., Nyíri, K., Tarjányi, S., Dobrotka, P., Tóth, J., and Vértessy, B. G. (2015) Cross-species inhibition of dUTPase via the Staphylococcal Stl protein perturbs dNTP pool and colony formation in Mycobacterium. *DNA Repair (Amst). 30*, 21–27.
(132) Benedek, A., Pölöskei, I., Ozohanics, O., and Vértessy, B. G. (2018) The Stl repressor from Staphylococcus aureus is an efficient inhibitor of the eukaryotic fruitfly dUTPase. *FEBS Open Bio 8*, 158–167.
(133) Benedek, A., Temesváry-Kis, F., Khatanbaatar, T., Leveles, I., Surányi, É. V., Szabó, J. E., Wunderlich, L., and Vértessy, B. G. (2019) The Role of a Key Amino Acid Position in Species-Specific Proteinaceous dUTPase Inhibition. *Biomolecules 9*, 221.
(134) Surányi, É., Hírmondó, R., Nyíri, K., Tarjányi, S., Kőhegyi, B., Tóth, J., and Vértessy, B. (2018) Exploiting a Phage-Bacterium Interaction System as a Molecular Switch to Decipher Macromolecular Interactions in the Living Cell. *Viruses 10*, 168.
(135) Saxena, S., Somyajit, K., and Nagaraju, G. (2018) XRCC2 Regulates Replication Fork Progression during dNTP Alterations. *Cell Rep. 25*, 3273-3282.e6.
(136) Somyajit, K., Gupta, R., Sedlackova, H., Neelsen, K. J., Ochs, F., Rask, M., Choudhary, C., and Lukas, J. (2017) Redox-sensitive alteration of replisome architecture safeguards genome integrity. *Science 358*, 797–802.
(137) Garzón, J., Rodríguez, R., Kong, Z., Chabes, A., Rodríguez-Acebes, S., Méndez, J., Moreno, S., and Garciá-Higuera, I. (2017) Shortage of dNTPs underlies altered replication dynamics and DNA breakage in the absence of the APC/C cofactor Cdh1. *Oncogene 36*, 5808–5818.
(138) Santinon, G., Brian, I., Pocaterra, A., Romani, P., Franzolin, E., Rampazzo, C., Bicciato, S., and Dupont, S. (2018) dNTP metabolism links mechanical cues and YAP/TAZ to cell growth and oncogene-induced senescence. *EMBO J. 37*, e97780.
(139) Mathews, C. K. (2014) Deoxyribonucleotides as genetic and metabolic regulators. *FASEB J.* 1–9.
(140) Pai, C., and Kearsey, S. (2017) A Critical Balance: dNTPs and the Maintenance of Genome Stability. *Genes (Basel). 8*, 57.
(141) Wang, Q., Liu, X., Zhou, J., Huang, Y., Zhang, S., Shen, J., Loera, S., Yuan, X., Chen, W., Jin, M., Shibata, S., Liu, Y., Chu, P., Wang, L., and Yen, Y. (2013) Ribonucleotide Reductase Large Subunit M1 Predicts Poor Survival Due to Modulation of Proliferative and Invasive Ability of Gastric Cancer. *PLoS One 8*, e70191.
(142) Chen, S., Bonifati, S., Qin, Z., St Gelais, C., and Wu, L. (2019) SAMHD1 Suppression of Antiviral Immune Responses. *Trends Microbiol. 27*, 254–267.
(143) Rotskaya, U. N., Rogozin, I. B., Vasyunina, E. a, Malyarchuk, B. a, Nevinsky, G. a, and Sinitsyna, O. I. (2010) High frequency of somatic mutations in rat liver mitochondrial DNA. *Mutat. Res. 685*, 97–102.
(144) Maine, I. P., Chen, S. F., and Windle, B. (1999) Effect of dGTP concentration on human

and CHO telomerase. *Biochemistry 38*, 15325–32.
(145) Gupta, A., Sharma, S., Reichenbach, P., Marjavaara, L., Nilsson, A. K., Lingner, J., Chabes, A., Rothstein, R., and Chang, M. (2013) Telomere Length Homeostasis Responds to Changes in Intracellular dNTP Pools. *Genetics 193*, 1095–1105.
(146) Ke, P. Y., Kuo, Y. Y., Hu, C. M., and Chang, Z. F. (2005) Control of dTTP pool size by anaphase promoting complex/cyclosome is essential for the maintenance of genetic stability. *Genes Dev. 19*, 1920–1933.
(147) Hu, C.-M., and Chang, Z.-F. (2007) Mitotic control of dTTP pool: a necessity or coincidence? *J. Biomed. Sci. 14*, 491–497.
(148) Thientosapol, E. S., Bosnjak, D., Durack, T., Stevanovski, I., van Geldermalsen, M., Holst, J., Jahan, Z., Shepard, C., Weninger, W., Kim, B., Brink, R., and Jolly, C. J. (2018) SAMHD1 enhances immunoglobulin hypermutation by promoting transversion mutation. *Proc. Natl. Acad. Sci. U. S. A. 115*, 4921–4926.
(149) Chen, P., Liu, Z., Liu, S., Xie, Z., Aimiuwu, J., Pang, J., Klisovic, R., Blum, W., Grever, M. R., Marcucci, G., and Chan, K. K. (2009) A LC-MS/MS method for the analysis of intracellular nucleoside triphosphate levels. *Pharm. Res. 26*, 1504–15.
(150) Mičová, K., Friedecký, D., and Adam, T. (2017) Mass Spectrometry for the Sensitive Analysis of Intracellular Nucleotides and Analogues, in *Mass Spectrometry* (Aliofkhazraei, M., Ed.). InTech, DOI: 10.5772/68073.
(151) Galashevskaya, A., Sarno, A., Vågbø, C. B., Aas, P. A., Hagen, L., Slupphaug, G., and Krokan, H. E. (2013) A robust, sensitive assay for genomic uracil determination by LC/MS/MS reveals lower levels than previously reported. *DNA Repair (Amst). 12*, 699–706.
(152) Kong, Z., Jia, S., Chabes, A. L., Appelblad, P., Lundmark, R., Moritz, T., and Chabes, A. (2018) Simultaneous determination of ribonucleoside and deoxyribonucleoside triphosphates in biological samples by hydrophilic interaction liquid chromatography coupled with tandem mass spectrometry. *Nucleic Acids Res. 46*, e66.
(153) Sherman, P. A., and Fyfe, J. A. (1989) Enzymatic assay for deoxyribonucleoside triphosphates using synthetic oligonucleotides as template primers. *Anal. Biochem. 180*, 222–226.
(154) Ferraro, P., Franzolin, E., Pontarin, G., Reichard, P., and Bianchi, V. (2010) Quantitation of cellular deoxynucleoside triphosphates. *Nucleic Acids Res. 38*, e85–e85.
(155) Diamond, T. L., Roshal, M., Jamburuthugoda, V. K., Reynolds, H. M., Merriam, A. R., Lee, K. Y., Balakrishnan, M., Bambara, R. A., Planelles, V., Dewhurst, S., and Kim, B. (2004) Macrophage tropism of HIV-1 depends on efficient cellular dNTP utilization by reverse transcriptase. *J. Biol. Chem. 279*, 51545–53.
(156) Dong, J., Wu, T., Xiao, Y., Xu, L., Fang, S., and Zhao, M. (2016) A fuel-limited isothermal DNA machine for the sensitive detection of cellular deoxyribonucleoside triphosphates. *Chem. Commun. 52*, 11923–11926.
(157) Wilson, P. M., LaBonte, M. J., Russell, J., Louie, S., Ghobrial, A. A., and Ladner, R. D. (2011) A novel fluorescence-based assay for the rapid detection and quantification of cellular deoxyribonucleoside triphosphates. *Nucleic Acids Res. 39*, e112–e112.
(158) Machon, C., Jordheim, L. P., Puy, J. Y., Lefebvre, I., Dumontet, C., and Guitton, J. (2014) Fully validated assay for the quantification of endogenous nucleoside mono- and triphosphates using online extraction coupled with liquid chromatography-tandem mass spectrometry. *Anal. Bioanal. Chem. 406*, 2925–2941.
(159) Pancsa, R., Fichó, E., Molnár, D., Surányi, É. V., Trombitás, T., Füzesi, D., Lóczi, H., Szijjártó, P., Hirmondó, R., Szabó, J. E., and Tóth, J. (2013) dNTPpoolDB: a manually curated database of experimentally determined dNTP pools and pool changes in biological samples. *Nucleic Acids Res. 1*, 13–14.
(160) Cohen, A., Mathiasen, V. D., Schön, T., and Wejse, C. (2019) The global prevalence of

latent tuberculosis: a systematic review and meta-analysis. *Eur. Respir. J. 54*.
(161) Róna, G., Marfori, M., Borsos, M., Scheer, I., Takács, E., Tóth, J., Babos, F., Magyar, A., Erdei, A., Bozóky, Z., Buday, L., Kobe, B., and Vértessy, B. G. (2013) Phosphorylation adjacent to the nuclear localization signal of human dUTPase abolishes nuclear import: structural and mechanistic insights. *Acta Crystallogr. Sect. D Biol. Crystallogr. 69*, 2495–2505.
(162) Chon, J., Stover, P. J., and Field, M. S. (2017) Targeting Nuclear Thymidylate Biosynthesis. *Mol. Aspects Med. 53*, 48.

11 Függelék

A Függelék az értekezés alapjául szolgáló 12 teljes közleményt tartalmazza a tárgyalás sorrendjében.

THE JOURNAL OF BIOLOGICAL CHEMISTRY VOL. 282, NO. 46, pp. 33572–33582, November 16, 2007
© 2007 by The American Society for Biochemistry and Molecular Biology, Inc. Printed in the U.S.A.

Kinetic Mechanism of Human dUTPase, an Essential Nucleotide Pyrophosphatase Enzyme*

Received for publication, July 30, 2007, and in revised form, September 7, 2007 Published, JBC Papers in Press, September 11, 2007, DOI 10.1074/jbc.M706230200

Judit Tóth[‡1], **Balázs Varga**[‡], **Mihály Kovács**[§], **András Málnási-Csizmadia**[§], **and Beáta G. Vértessy**[‡2]

From the [‡]*Institute of Enzymology, Biological Research Center, Hungarian Academy of Sciences, Karolina út 29, 1113 Budapest, Hungary and the* [§]*Eötvös Loránd University, Budapest, Hungary*

Human dUTPase is essential in controlling relative cellular levels of dTTP/dUTP, both of which can be incorporated into DNA. The nuclear isoform of the enzyme has been proposed as a promising novel target for anticancer chemotherapeutic strategies. The recently determined three-dimensional structure of this protein in complex with an isosteric substrate analogue allowed in-depth structural characterization of the active site. However, fundamental steps of the dUTPase enzymatic cycle have not yet been revealed. This knowledge is indispensable for a functional understanding of the molecular mechanism and can also contribute to the design of potential antagonists. Here we present detailed pre-steady-state and steady-state kinetic investigations using a single tryptophan fluorophore engineered into the active site of human dUTPase. This sensor allowed distinction of the apoenzyme, enzyme-substrate, and enzyme-product complexes. We show that the dUTP hydrolysis cycle consists of at least four distinct enzymatic steps: (i) fast substrate binding, (ii) isomerization of the enzyme-substrate complex into the catalytically competent conformation, (iii) a hydrolysis (chemical) step, and (iv) rapid, nonordered release of the products. Independent quenched-flow experiments indicate that the chemical step is the rate-limiting step of the enzymatic cycle. To follow the reaction in the quenched-flow, we devised a novel method to synthesize γ-^{32}P-labeled dUTP. We also determined by indicator-based rapid kinetic assays that proton release is concomitant with the rate-limiting hydrolysis step. Our results led to a quantitative kinetic model of the human dUTPase catalytic cycle and to direct assessment of relative flexibilities of the C-terminal arm, critical for enzyme activity, in the enzyme-ligand complexes along the reaction pathway.

dUTPase is the unique enzyme that specifically hydrolyzes the α-β pyrophosphate bond of dUTP to yield dUMP and PP_i (1). The enzyme is essential in maintaining DNA integrity in dividing cells (2, 3). Its activity is responsible for setting the physiological dUTP/dTTP concentration ratios (1:24) (4), thus preventing high rates of uracil incorporation into newly synthesized DNA. Although uracil in DNA is tolerated to a certain level by the base excision DNA repair mechanisms, higher levels of uracil in DNA trigger double-strand breaks and lead to cell death (5). Several lines of evidence show that up-regulated dUTPase is responsible for desensitizing tumors to drugs inhibiting the thymidylate synthase pathway, thus acting as an important survival factor for tumor cells (6, 7). Increased levels of the nuclear isoform of the enzyme correlate to worsened prognosis of several tumors, as revealed by detailed analysis of tissue samples (8, 9). dUTPase has therefore emerged as a high potential anticancer drug target, which possesses several additional, possibly advantageous features for drug design. Unlike most nucleotide-metabolizing enzymes, dUTPase is extremely specific to its substrate nucleotide, potentially allowing construction of substrate analogue antagonists with similarly high specificity. The nuclear isoform of the enzyme is under strict cell cycle control; its expression is mostly limited to rapidly dividing (including cancer) cells (10, 11). In addition to the fact that the enzyme is an important focus in biomedical research, dUTPase also serves as a model system for detailed analysis of enzyme-catalyzed nucleotide pyrophosphorolysis.

Current knowledge of the dUTPase mechanism is mainly based on three-dimensional structural approaches. Most dUTPases are homotrimers with a unique active site architecture, where all three monomers contribute to each of the three catalytic sites. High resolution crystal structures of the human (hDUT)[3] (12, 13) and other (14–18) dUTPases provided important mechanistic clues. The catalytic site is formed by five conserved motifs, four of which are contributed by two adjacent monomers. The fifth motif, positioned on the C-terminal arm, is usually provided by the third monomer. The C terminus, associated with an increased conformational freedom, was suggested to close upon the active site during the chemical step (12, 14, 19). Cleavage of the α-β pyrophosphate linkage is initiated by a nucleophilic attack from the catalytic water molecule coordinated by a conserved aspartate (Asp^{102} in the human enzyme) within the third motif accommodating the uracil and deoxyribose moieties of dUTP (16).

* This work was supported by Hungarian Scientific Research Fund Grant K68229, Howard Hughes Medical Institutes (HHMI) Grants 55005628 and 55000342, and a European Molecular Biology Organization (EMBO) long term postdoctoral fellowship (to J. T.); National Institutes of Health (NIH) Grant D43 TW006230 (1 R01 TW007241-01) funded by the Fogarty International Center and the NHLBI, NIH, an EMBO-HHMI startup grant, and the Bolyai Fellowship of the Hungarian Academy of Sciences (to M. K.); and grants from the Alexander von Humboldt Foundation and Varga József Foundation and Hungarian Economic Competitiveness Operative Programme Grants GVOP-3.2.1.-2004-05-0412/3.0, FP6 STREP 012127, and FP6 SPINE2c LSHG-CT-2006-031220. The costs of publication of this article were defrayed in part by the payment of page charges. This article must therefore be hereby marked "*advertisement*" in accordance with 18 U.S.C. Section 1734 solely to indicate this fact.

[1] To whom correspondence may be addressed. E-mail: tothj@enzim.hu.
[2] To whom correspondence may be addressed. E-mail: vertessy@enzim.hu.

[3] The abbreviations used are: hDUT, nuclear isoform of human dUTPase, His-tagged; dUPNPP, α,β-imido-dUTP; $hDUT^{W158}$, F158W mutant of nuclear isoform of human dUTPase, His-tagged; NATA, *N*-acetyl-L-tryptophanamide; NDPK, nucleoside triphosphate kinase.

This is an Open Access article under the CC BY license.

Modern pharmacology demands knowledge of the precise mechanism of action of target enzymes. However, structural data have not yet been complemented by detailed solution kinetic studies for any eukaryotic dUTPase, possibly due to the lack of suitable optical signals reporting enzymatic events. Relying on proton escape during nucleotide pyrophosphorolysis, pH indicator-based assays were used to continuously follow dUTP hydrolysis (20, 21), but these methods are transparent to conformational changes of the enzyme. In this study, we took advantage of an intrinsic tryptophan sensor that we had recently engineered in the C-terminal arm of hDUT (Trp^{158}) (13) to resolve the fundamental steps of the enzymatic cycle using fast kinetic methods. Trp^{158} replaces a conserved phenylalanine residue that interacts with the uracil ring of dUTP (Fig. 1*C*) (12, 13). The mutational replacement of the benzene ring with an indole moiety did not perturb the enzyme activity (13). In the present study, the active site Trp^{158} sensor also allowed assessment of the proposed structural ordering of the C-terminal arm in the distinct enzyme-ligand complexes, relevant for the reaction cycle. Furthermore, we have developed a protocol for quenched-flow analysis, which is the first to allow the direct monitoring of the hydrolysis step of a dUTPase. We unambiguously show that the chemical step is rate-limiting and that the C-terminal arm is predominantly ordered in all enzymatic states.

EXPERIMENTAL PROCEDURES

Materials—The His-tagged nuclear isoform of human dUTPase (hDUT) and its F158W mutant construct ($hDUT^{W158}$) were expressed and purified as described previously (13, 22). Protein concentration was measured using the Bio-Rad protein assay reagent and by UV absorbance (λ_{280} = 10,430 M^{-1} cm^{-1} for hDUT and λ_{280} = 15,930 M^{-1} cm^{-1} for $hDUT^{W158}$) and is given in monomers. All measurements were carried out in 20 mM HEPES, pH 7.4, buffer, also containing 40 mM NaCl, 2 mM $MgCl_2$, and 1 mM dithiothreitol (unless otherwise stated), at 20 °C. dUMP, dUDP, dUTP, and α,β-imido-dUTP (dUPNPP) were purchased from Jena Bioscience (Germany), and [γ-^{32}P]ATP was from Izinta Ltd. Myosin was purified from rabbit skeletal muscle according to Ref. 23. Other reagents were from Sigma.

Enzyme Activity—Enzyme activity was measured in steady-state pH indicator-based assays as described in Ref. 20 and was typically found to be 6 ± 2 s^{-1}. Active site titration was used to determine K_M and also to evaluate the active fraction of hDUT and $hDUT^{W158}$ preparations. In the absorbance stopped-flow setup, an assay buffer containing 100 μM phenol red indicator and 1 mM HEPES, pH 7.5, provided optimal monitoring of dUTP hydrolysis. To avoid mixing artifacts, the enzyme was dialyzed in this assay buffer prior to active site titration. Measured time courses (*cf.* Fig. 3*C*) were subjected to global fit analysis using GEPASI (24). The floated parameters were k_1, k_{-1}, k_2, and [*E*] of the Michaelis-Menten scheme,

$$E + S \underset{k_{-1}}{\overset{k_1}{\rightleftharpoons}} ES \xrightarrow{k_2} EP$$

SCHEME 1

where $K_M = (k_{-1} + k_2)/k_1$ and $k_2 = k_{cat}$.

The inactive protein fraction in the measured hDUT or $hDUT^{W158}$ preparation was only in the range of the uncertainty of protein concentration determination (5–10%).

Fluorescence Spectra and Intensity Titrations—Fluorescence spectra and intensity titrations were recorded on a Jobin Yvon Spex Fluoromax-3 spectrofluorometer with excitation at 297 nm (slit 1 nm), emission between 320 and 400 nm (slit 5 nm), or at 347 nm. Because large concentrations of nucleotides were used, care was taken to correct for any additional fluorescence or inner filter effect imposed on the measured intensities by the nucleotide stock solutions.

Acrylamide Quenching—Acrylamide quenching was carried out by the addition of minute volumes of a 5 M acrylamide solution to the enzyme, enzyme-ligand, or *N*-acetyl-L-tryptophanamide (NATA) solutions. Raw data were corrected for the fluorescence arising from the acrylamide solution itself. F_0/F *versus* [Q] curves were analyzed using a modified Stern-Volmer equation (Equation 1),

$$F_0/F = 1 + K_{SV}[Q]\exp(V[Q]) \quad \text{(Eq. 1)}$$

where F_0 is the unquenched and F is the quenched fluorescence; Q is the quencher; K_{SV} is the dynamic (bimolecular) quenching constant; and V is the static (sphere of action) component of quenching (*cf.* Ref. 25).

Fluorescence Anisotropy—Fluorescence anisotropy was measured by the single-channel method in an Edinburgh Instruments FLS920P spectrofluorometer equipped with Glan-Thompson prism polarizers. Tryptophan emission spectra (λ_{ex} = 295 nm, λ_{em} = 320–400 nm) were recorded at four different polarizer configurations (VV, VH, HV, and HH, where V and H denote vertical and horizontal polarizer configurations, respectively, the first letter being designated to the excitation, the second to the emission polarizer). After base-line correction, anisotropy was calculated for the entire spectrum using Equation 2,

$$r = (I_{VV} - GI_{VH})/(I_{VV} + 2GI_{VH}) \quad \text{(Eq. 2)}$$

where r is anisotropy, I is fluorescence intensity, and $G = I_{HV}/I_{HH}$ is a wavelength-dependent parameter of the instrument setup.

Stopped-flow Experiments—Measurements were done using either an SF-2004 (KinTek Corp., Austin, TX) or a SFM-300 (Bio-Logic SAS) stopped-flow apparatus. Tryptophan fluorescence was excited at 297 nm, and emission was selected with a band-pass filter having a peak in transmittance at 340 nm. Time courses were analyzed using the curve fitting software provided with the stopped-flow apparatus or by Origin 7.5 (OriginLab Corp., Northampton, MA).

[γ-^{32}P]dUTP Synthesis—All synthesis reactions were carried out in a buffer containing 25 mM Tris, pH 7.4, and 100 mM NaCl. Autophosphorylation of 20 μM nucleoside diphosphate kinase (NDPK; from yeast; catalog number N0379; Sigma) was carried out in 5 mM EDTA at 30 °C for 10 min in a final volume of 100 μl using 20 μM [γ-^{32}P]ATP, according to Ref. 26. To remove ADP and [γ-^{32}P]ATP from the reaction in a quick manner, we applied batch adsorption on anion exchanger

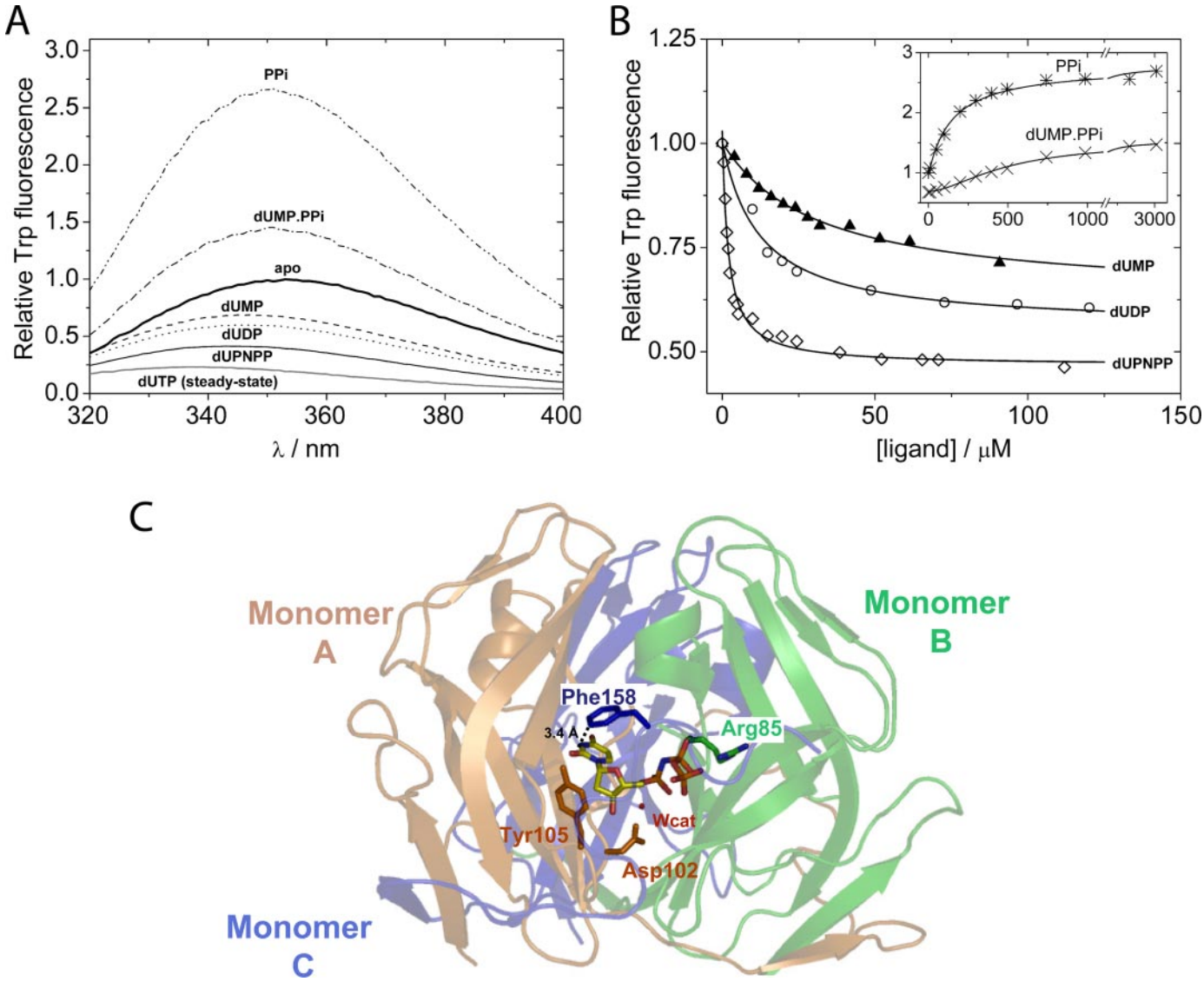

FIGURE 1. *A*, fluorescence emission spectra of hDUT^{W158} at saturating concentrations of ligands. λ_{ex} = 295 nm, data are normalized to the emission peak of the apo enzyme. [hDUTW158] = 4 μM, [dUMP] = 500 μM, [dUDP] = 300 μM, [dUPNPP] = 100 μM, [dUTP] = 2 mM, [PP_i] = 5 mM. To capture the dUTP-bound cycling steady state, a high excess of dUTP was used, and the spectrum was recorded within 30 s after dUTP was added. For analysis of fluorescence spectral parameters, see Table 1. *B*, fluorescence equilibrium titration of hDUT^{W158} with its ligands. λ_{ex} = 295 nm, λ_{em} = 347 nm; *solid lines* represent quadratic fits to the data except for the dUMP·PP_i curve, where a Hill equation with n = 1.7 provided a better fit. K_d values from the presented fits are as follows: 31 ± 4 μM for dUMP (*triangles*), 12 ± 2 μM for dUDP (*circles*), 1.9 ± 0.2 μM for dUPNPP (*diamonds*) (in the *inset*, 146 ± 15 μM for PP_i (*stars*) and 494 ± 25 μM for dUMP·PP_i (*crosses*)). The dUMP·PP_i titration was carried out by titrating dUMP-saturated enzyme (in 500 μM dUMP) with PP_i. *C*, three-dimensional structure of hDUT in complex with dUPNPP (figure produced using Protein Data Bank code 2HQU (13) and PyMOL). The three monomers (*A–C*) are represented by *color-coded schematic diagrams*. One of the three active sites is shown with the bound dUPNPP (*stick model*; *yellow* carbons and otherwise atomic *coloring*). The Phe^{158} residue (monomer C) stacks over the uracil ring. Other coordinating residues from monomers A and B and the catalytic water molecule (*red sphere*, labeled W_{cat}) are shown for orientation purposes.

resin in an expectation that the resin will only remove the negatively charged nucleotides and will not bind NDPK. The NDPK isoenzyme used in the experiment has a calculated pI of 8.65 and therefore carries a net positive charge at pH 7.4. According to the expectation, 25 μl of washed Q-Sepharose (Amersham Biosciences) added to the autophosphorylation reaction mixture immobilized all nucleotides without binding NDPK. The Q-Sepharose beads were then removed from the reaction by a 30-s centrifugation step. Subsequently, 25 μM dUDP and 10 mM Mg^{2+} were added to [^{32}P]NDPK to yield [γ-^{32}P]dUTP (incubation for 10 min at 30 °C). The enzyme was then completely removed from the [γ-^{32}P]dUTP-containing solution by phenol extraction that was carried out according to Ref. 27. For the analysis of the synthesis products (see "Results"), the radioactive nucleotide and phosphate contents were separated from each other using charcoal adsorption (as in Ref. 28). The advantage of using charcoal is that it binds all nucleotides but not P_i and PP_i. Radioactivity was counted in water in a Wallac 1409 liquid scintillation counter. We used a [γ-^{32}P]ATP stock solution of high specific activity (0.4 MBq/μl, 111 GBq/μmol) to obtain a similarly high specific activity [γ-^{32}P]dUTP sample suitable for tracing. The synthesized [γ-^{32}P]dUTP was added to a large molar excess of nonlabeled bulk dUTP in a 1:100 volume ratio. For further details of the analysis of the synthesis products, see "Results."

TABLE 1

Fluorescence properties of hDUT^{W158} apoenzyme and its ligand-bound complexes

For comparison, the respective fluorescence characteristics of NATA, representing free tryptophan, are also given. NA, not applicable.

Ligand	K_d	λ_{max}	Relative fluorescence	K_{SV}	V	Anisotropy
	μM	nm		m^{-1}		
None		353	1	6.6 ± 0.12	0.9 ± 0.06	0.077 ± 0.005
dUMP	32 ± 2	347	0.64 ± 0.03	6.1 ± 0.13	0.4 ± 0.07	0.081 ± 0.003
dUDP	12 ± 1	347	0.59 ± 0.03	5.7 ± 0.10	0.6 ± 0.05	0.085 ± 0.006
DUTP	<1	339	0.20 ± 0.06			
dUPNPP	5 ± 3	343	0.40 ± 0.04	5.0 ± 0.09	0.4 ± 0.05	0.091 ± 0.003
dUMP.PPi	479 ± 20	351	1.40 ± 0.01	6.0 ± 0.2	0.9 ± 0.10	0.106 ± 0.002
Ppi	146 ± 15	351	2.53 ± 0.02	6.8 ± 0.19	1.5 ± 0.08	0.112 ± 0.002
NATA (in the absence of protein)	NA	355	NA	17.4 ± 0.12	1.9 ± 0.02	0.0044 ± 0.0008

Quenched-flow Experiments—Quenched-flow experiments were carried out using the RQF-3 (KinTek Corp., Austin, TX) quenched-flow apparatus. 2 M HCl (⅔ M in the reaction) was used as the chemical quencher of the dUTPase reaction. Hydrolysis products were separated according to Ref. 28. The amount of the resulting $^{32}PP_i$ product was counted in water using a Wallac 1409 liquid scintillation counter (PerkinElmer Life Sciences).

Data Analysis and Numerical Simulations—Data analysis and numerical simulations were done using Origin 7.5 (OriginLab Corp., Northampton, MA) or the freely available GEPASI 3 biochemical kinetics simulation software (24), respectively.

RESULTS

Fluorescence Spectral Properties of hDUT^{W158} and Its Ligand-bound Complexes—Recently, fluorescence emission from the Trp^{158} fluorophore was shown to be significantly and characteristically quenched in dUTPase-dUPNPP and dUTPase-dUMP complexes as compared with the apoenzyme (13), in agreement with the expectation that the stacking between conserved residue Phe^{158} and the substrate uracil ring (*cf.* Fig. 1*C*) is also present in the Trp^{158} mutant enzyme. Following these observations, we quantified maximal fluorescence changes and spectral shifts of Trp^{158} upon binding to physiological ligands and to the nonhydrolyzable substrate analogue dUPNPP (Fig. 1*A* and Table 1). These data yield information on the interaction of Trp^{158} with the uracil moiety of any bound nucleotide and will allow interpreting the fluorescence-based kinetic experiments. The Trp^{158} fluorescence emission maximum of the apoenzyme was at 353 nm, a typical value for a nonburied protein tryptophan ($\lambda_{max,\ NATA}$ = 355 nm) (25) (Fig. 1*A*). Fig. 1*A* also shows that the binding of different uracil nucleotides but not that of PP_i to hDUT^{W158} quenches Trp^{158} fluorescence, probably due to aromatic stacking between the indole and uracil rings (shortest distances between atoms of the uracil moiety and those of the Phe^{158} benzene ring in hDUT are 3.4–3.7 Å, as determined in the crystal structure of the enzyme-dUPNPP complex, Protein Data Bank code 2HQU) (13) (Fig. 1*C*). The magnitude of the nucleotide-induced quench and blue shift increased in the order dUMP → dUDP → dUPNPP (Table 1). This implies that the presence of the β- and γ-phosphates causes the C-terminal arm to form more interactions with the phosphate chain of the substrate (in agreement with the structural description (13)), whereby the arm may become less flexible and may stabilize the stacking interaction between Trp^{158} and the uracil ring. Interestingly, Trp^{158} fluorescence was even more quenched during steady-state dUTPase cycling than in any of the other ligand-bound states (Fig. 1*A*). This suggests that there is at least one major steady-state intermediate that cannot be produced by the addition of the above ligands (*e.g.* the prehydrolysis mimic dUPNPP or the posthydrolysis mimic dUMP·PP_i states). A possible explanation for this finding is that a particular protein conformational change occurs in the presence of dUTP (but not in the presence of dUPNPP or other nucleotides), leading to the hydrolysis-competent state (see below).

The large fluorescence increase in the presence of PP_i indicates that the binding of this ligand also causes a conformational change in the active site. Control experiments conducted with bovine serum albumin and NATA (data not shown) ascertained that the effect of PP_i on our tryptophan sensor was specific. Interestingly, a rather similar phenomenon was observed in an earlier study in which a tryptophan engineered into the entrance of the nucleotide binding site of myosin (Trp^{129}, in close proximity to the adenine moiety of ATP) exhibited a large quench on nucleotide binding and a large fluorescence increase on PP_i binding (29). We probed the potential interaction of hDUT^{W158} with phosphate (P_i) (used at high excess), but no signal change was detected.

Fluorescence Intensity Titrations to Determine Enzyme-Ligand Dissociation Constants—Fig. 1*B* shows fluorescence intensity titrations of 4 μM hDUT^{W158} with various ligands (enzyme active site concentrations are used throughout this paper). Dissociation constants are given in Table 1. K_d values illustrate that the affinity of hDUT^{W158} increases in the order dUMP → dUDP → dUPNPP, with dUDP and dUPNPP binding being 3 and 10 times stronger than that of dUMP, respectively. dUTP binding cannot be measured using this equilibrium method, but we anticipate that its K_d value may be equal to or lower than that of dUPNPP ($K_d \sim 1$ μM). Nucleotide-free hDUT^{W158} exhibited a K_d for PP_i of 146 μM. The dissociation constant of PP_i for the ternary enzyme products complex (E·dUMP·PP_i) was about 3 times larger than that for E·PP_i. This moderate antagonistic effect between the binding of dUMP and PP_i to the enzyme is probably due to the repulsion between the negative charges of dUMP and PP_i.

Acrylamide Quenching—We have performed acrylamide quenching experiments with hDUT^{W158} to monitor the solvent accessibility of the Trp^{158} reporter (Fig. 2*A*, Table 1). For reference and control, we also measured properties of NATA, a model compound for a rotationally free and maximally solvent-

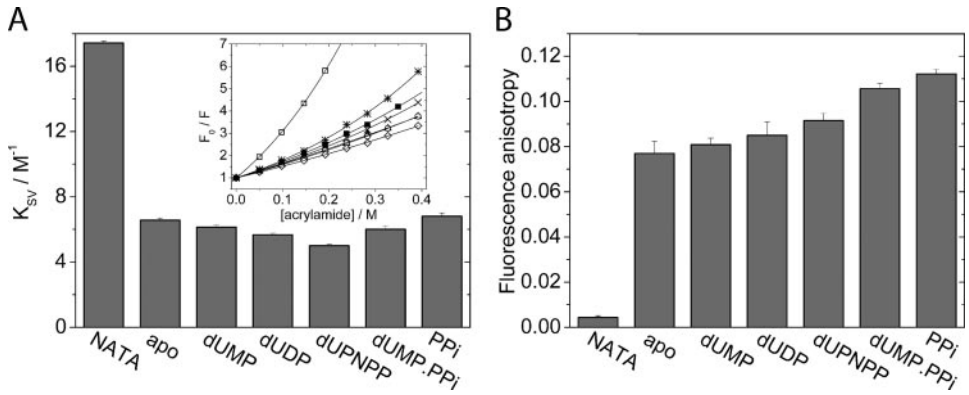

FIGURE 2. **Solvent accessibility and anisotropy of hDUT^{W158} complexed with various ligands.** *A*, 4 μM hDUT^{W158} with or without saturating concentrations of specific ligands was titrated using a 5 M acrylamide stock solution (*inset*). *Lines* on the data points are fits to the modified Stern-Volmer equation (Equation 1). The dynamic quenching components (K_{SV} values) of the fits are shown as *bars*. 1 μM NATA was used to represent a fully accessible tryptophan. *Error bars*, fitting errors. *B*, steady-state anisotropy of Trp^{158}. Concentrations are the same as in Fig. 1*A*. *Error bars*, S.D. of the data points obtained for each emission wavelength. 1 μM NATA was used to represent a tryptophan exhibiting maximal rotational diffusion.

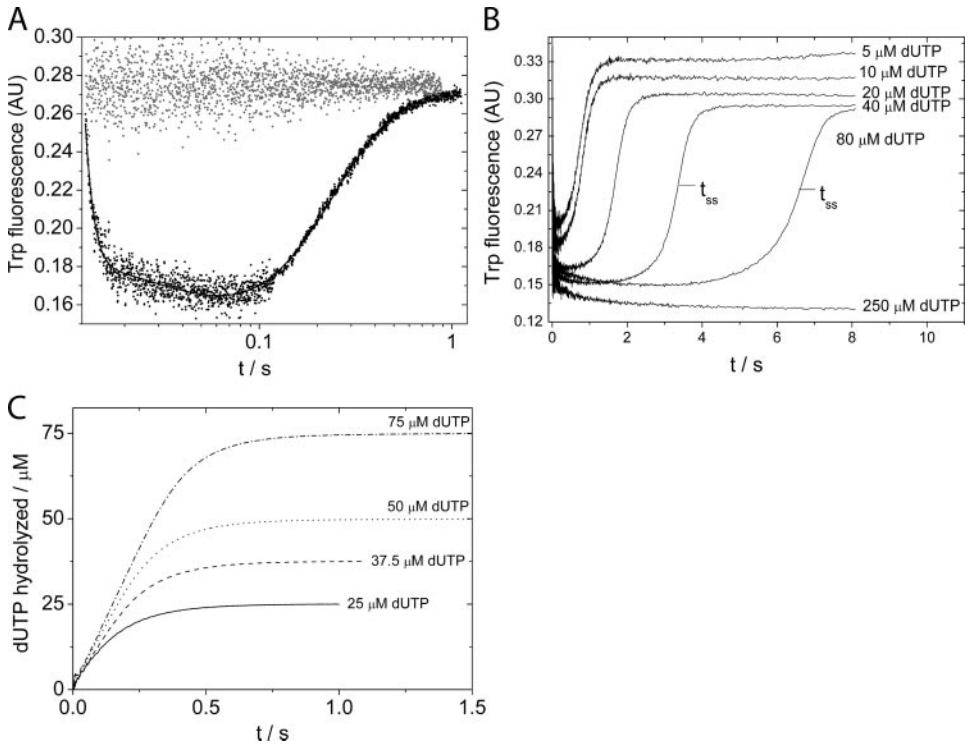

FIGURE 3. **hDUT^{W158} single turnovers as monitored using intrinsic (*A* and *B*) and extrinsic (*C*) signals.** *A*, tryptophan fluorescence stopped-flow traces of 7.5 μM hDUT^{W158} mixed with 5.25 μM dUTP (*black points*) or with buffer (*gray points*). Fluorescence was recorded at λ_{ex} = 295 nm and λ_{em} = 340 nm. *Solid line*, a triple exponential fit to the data with parameters $A_1 = 0.097$, $k_1 = 912\ s^{-1}$ for dUTP binding, $A_2 = 0.193$, $k_2 = 14\ s^{-1}$ for a first order isomerization, $A_1 = -0.269$, $k_2 = 6.7\ s^{-1}$ for the chemical step. *B*, tryptophan fluorescence stopped-flow traces of 5 μM hDUT^{W158} mixed with various concentrations of dUTP. *C*, 58 μM hDUT^{W158} mixed with 25, 37.5, 50, or 75 μM dUTP in the stopped-flow in the presence of 100 μM phenol red indicator. Absorbance was recorded at λ = 559 nm to monitor the release of protons upon dUTP hydrolysis. Curves at substoichiometric dUTP concentrations appear as single exponentials, whereas at higher dUTP concentrations, a linear steady-state phase can be observed. Global fits to all curves using the k_1, k_{-1}, and k_2 floating parameters of the Michaelis-Menten scheme (Scheme 1) yielded $K_M = 3.6 \pm 1.9\ \mu M$, $k_{cat} = 6.7 \pm 0.2\ s^{-1}$.

accessible tryptophan residue. Acrylamide titrations of the Trp^{158} fluorescence intensity are displayed as Stern-Volmer plots (Fig. 2*A*, *inset*) with a modified Stern-Volmer equation (Equation 1) fitted to the data points to separate the dynamic component (described by the K_{SV} quenching constant) from the static quenching sphere of action (V) (25). Compared with our measurement on NATA and literature data on K_{SV} values for tryptophans in short peptides (10–14 M^{-1}), Trp^{158} exhibits markedly reduced solvent accessibility (K_{SV} = 6.6 M^{-1}) even in the apoenzyme. Such a low K_{SV} was unexpected, considering that Trp^{158} is situated in the C-terminal arm of hDUT^{W158}, six residues away from the terminal amino acid. On the other hand, differences between K_{SV} values of various ligand-bound states of hDUT^{W158} are relatively small but significant (K_{SV}, ranging from 5.0 to 6.8 M^{-1}) (Fig. 2*A* and Table 1). This finding suggests that large conformational changes of the C-terminal arm upon ligand binding are unlikely to occur. The solvent accessibility of Trp^{158} decreases in the order dUMP → dUDP → dUPNPP, suggesting a gradual movement of the C-terminal arm toward the nucleotide. This observation is in line with our experiments shown in Fig. 1. Importantly, the solvent accessibilities of the *E*·dUMP·PP$_i$ and *E*·dUMP states were very similar, indicating that dUMP but not PP$_i$ induces shielding of the active site. PP$_i$ binding alone does not perturb the solvent accessibility of Trp^{158}, probably due to a relatively open active site conformation (Fig. 1).

Fluorescence Anisotropy—Fluorescence anisotropy is routinely used to describe the dynamic properties of a protein environment. Freely rotating small fluorophores are depolarized at room temperature and therefore exhibit anisotropies close to zero (*cf.* NATA in Fig. 2*B* and Table 1). We measured the steady-state anisotropies of apo-hDUT^{W158} and its ligand-bound complexes to gain further insights into the dynamic behavior of the C-terminal arm in various enzymatic states. The steady-state anisotropy of apo-hDUT^{W158} (r = 0.077) increased upon ligand binding, which reflects a steric hindrance of the fluorophore. Similarly to the previously described experiments (Figs. 1 and 2*A*), a correlation of the measured effect to the length of the phosphate chain of the nucleotide was observed (*i.e.* the value of r increased in the order apo → dUMP → dUDP → dUPNPP) (Fig. 2*B*). The largest increase in anisotropy was detected in the PP$_i$-

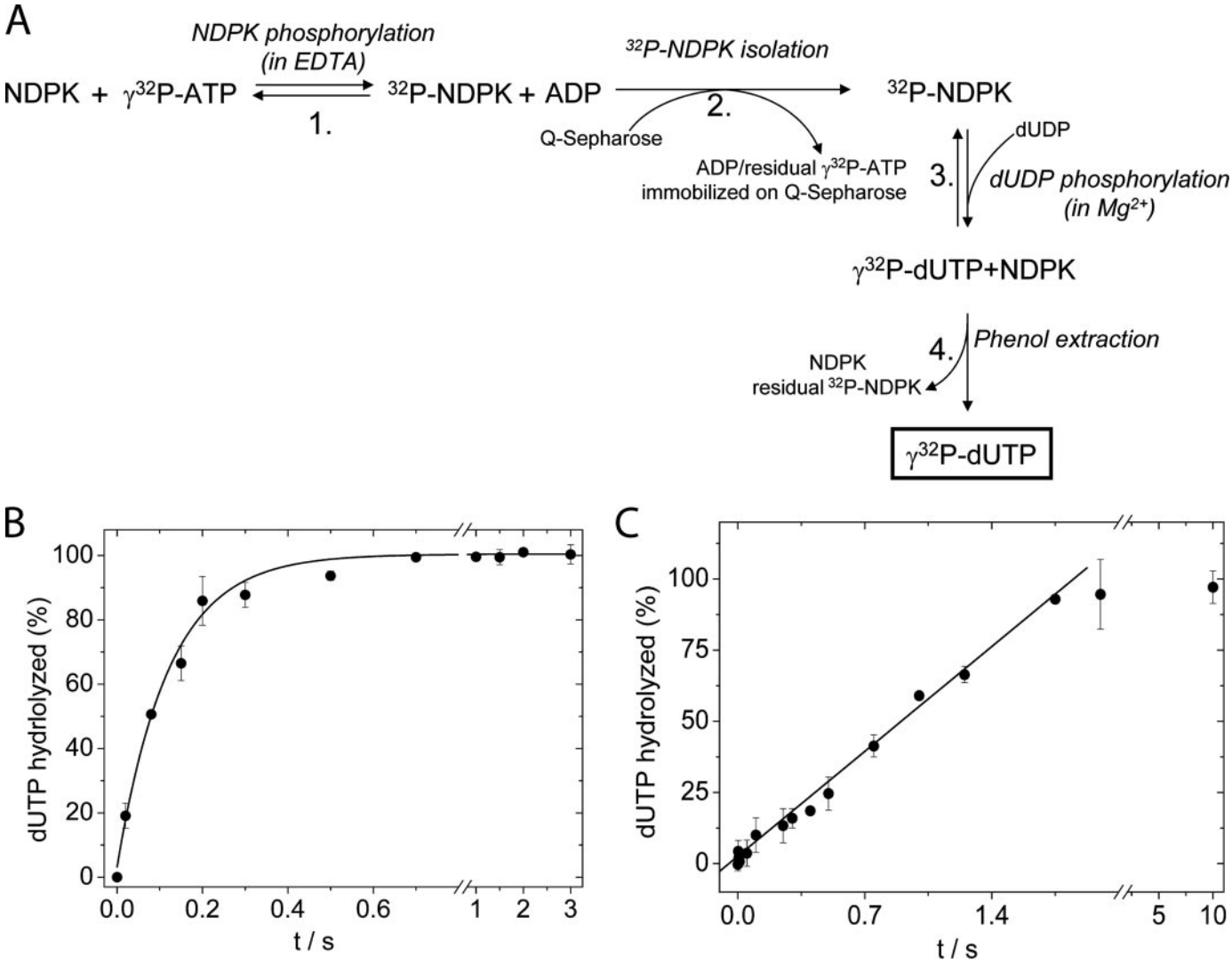

FIGURE 4. **[γ^{32}P]dUTP synthesis and quenched-flow measurements of dUTP hydrolysis.** *A*, scheme of [γ-^{32}P]dUTP synthesis. *Reactions 1* and *3* are highly reversible, while separation *steps 2* and *4* are very efficient, resulting in a [γ-^{32}P]dUTP compound that is free of contaminating radioactive nucleotides. Besides [γ-^{32}P]dUTP, the final product contains dUDP (<12.5 μM in our experiment) and $^{32}P_i$. If used as a tracer (>1:100 ratio), this preparation does not compromise the chemical purity of the bulk nucleotide solution. *B*, 100 μM hDUT and 50 μM [γ-^{32}P]dUTP were mixed (single turnover conditions), and the reaction was stopped with 1 M HCl after various incubation times. Hydrolysis was followed by measuring the relative amount of one of the hydrolysis products, the radioactive PP_i. Single exponential fits to the data (*solid line*) with $k_{obs} = 8.2 \pm 0.4\ s^{-1}$. *Error bars*, S.D. of three parallel measurements. *C*, the reaction of 18 μM hDUT^{W158} with 100 μM [γ-^{32}P]dUTP (5.6-fold excess) was followed in time. Linear fit to the data yielded a $k_{obs} = 2.9 \pm 0.04\ s^{-1}$ for the steady state. Lag or burst was not observed at the applied time resolution. *Error bars*, S.D. of three parallel measurements.

bound species ($E{\cdot}PP_i$ and $E{\cdot}dUMP{\cdot}PP_i$), although we previously showed that these are the most "open" and solvent-accessible enzyme states (Fig. 2*A*). Taken together, the anisotropy data indicate that (i) ligand binding to the polyphosphate binding site causes structural ordering of the C-terminal arm, proportionally to the length of the polyphosphate chain (without shielding Trp^{158} from the solvent); (ii) the lower anisotropy of uracil nucleotide-bound states compared with that of the $E{\cdot}PP_i$ state show that aromatic stacking to uracil slightly depolarizes Trp^{158} (Fig. 2*B* and Table 1).

Rapid Kinetics of hDUT^{W158} Followed by Intrinsic (Trp^{158}) and Extrinsic (Proton Release) Signals—In the knowledge of the fluorescence characteristics of individual enzyme-substrate (substrate analogue) and enzyme-product complexes (Fig. 1), progress curves obtained by monitoring Trp^{158} fluorescence during the interaction of hDUT^{W158} with dUTP in the stopped-flow yielded significantly more information than pH detection-based (proton release) methods. Fig. 3 shows single and multiple dUTP turnovers obtained using Trp^{158} fluorescence (*A* and *B*) or proton release (*C*) signals. Trp^{158} fluorescence traces of single dUTP turnovers ([*E*] > [S]) consisted of three exponential phases (Fig. 3*A*). A fast initial quench in fluorescence ($k_{obs} \sim 900\ s^{-1}$) was followed by an additional slower decrease ($k_{obs} \sim 20\ s^{-1}$), and then the fluorescence intensity returned to a close-to-initial value with a k_{obs} of $6.8 \pm 2.0\ s^{-1}$. In light of the steady-state fluorescence data of Fig. 1*A*, we interpret the first fast phase as the initial binding of the nucleotide in which Trp^{158} quenching occurs by stacking over the uracil ring. Considering the difference between the fluorescence intensity of the enzyme-dUPNPP complex and that during steady-state dUTPase cycling, the second slower phase can be interpreted as a dUTP-induced structural change that precedes or is concomi-

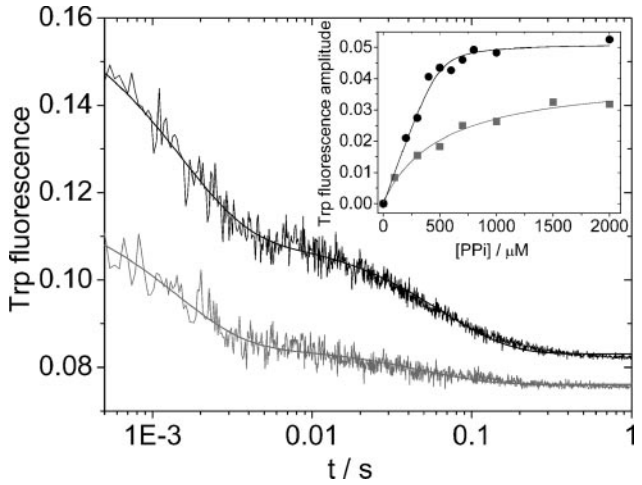

FIGURE 5. **Dissociation of PP_i measured by dUTP chasing in the stopped-flow.** Solutions of (4 μM $hDUT^{W158}$ + 2 mM PP_i) (*black trace*) or (4 μM $hDUT^{W158}$ + 300 μM dUMP + 2 mM PP_i) (*gray trace*) were mixed with 0.1 or 1 mM dUTP, respectively, in the stopped-flow. The observed fluorescence intensity change reports both the dissociation of products and the interaction with dUTP. Two exponentials fit to the data, with $A_1 = 0.053$ and $k_1 = 648\ s^{-1}$ for the fast phase and $A_2 = 0.027$ and $k_2 = 14\ s^{-1}$ for the slow phase (*black trace*) or with $A_1 = 0.032$ and $k_1 = 705\ s^{-1}$ for the fast phase and $A_2 = 0.0087$ and $k_2 = 20\ s^{-1}$ for the slow phase (*gray trace*) ($k_{obs} = 726 \pm 46, 15 \pm 0.9\ PP_i$, $684 \pm 84, 18 \pm 2.5$ dUMP·PP_i). *Inset*, PP_i concentration dependence of the fast phase amplitude (A_1). 4 μM $hDUT^{W158}$ was mixed with different concentrations of PP_i either in the absence (*black circles*) or in the presence (*gray squares*) of 300 μM dUMP. dUTP chase was accomplished by mixing with 0.1 or 1 mM dUTP (*black circles* or *gray squares*, respectively). Quadratic fits to the A_1 data of the recorded fluorescence time courses yielded an apparent K_d of 327 ± 117 μM for PP_i (*black circles*) and 532 ± 128 μM for PP_i binding to E·dUMP (*gray squares*).

tant with dUTP hydrolysis. The third phase reflects the slowest rate-limiting step of the cycle (dUTP hydrolysis or product release). (The identities of the steps associated with the second and third phases were clarified in subsequent experiments (Figs. 4 and 5).) Determination of the substrate concentration dependence of the rate constant of the first phase under pseudo-first order conditions was challenging, because either the signal/noise ratio was too low for reasonable resolution (when attempting to decrease [S] at a constant [*E*] (maintaining [S] ≪ [*E*])), or the amplitude became completely lost in the dead time of the stopped-flow apparatus (when applying a severalfold excess of [S] over the lowest detectable [*E*]). Measurements carried out using near-equimolar concentrations of enzyme and substrate indicated that the time course of this phase does depend on concentration (k_{obs} values of force-fitted exponentials were 400–1200 s^{-1} in the applied 2.5–15 μM concentration range). Numerical simulations in which this phase was assigned to a second-order binding step showed good agreement with the experimental traces, and the fundamental rate constants could be extracted (*cf.* Fig. 6*A* and Table 2). We did not observe systematic concentration dependence of the k_{obs} (termed $k_{ISO,obs}$ in Table 2) of the second exponential phase (20 ± 18 s^{-1}), which confirms the first order nature of this proposed isomerization step (Fig. 3*B*). The k_{obs} value of the third phase did not exhibit concentration dependence in the single turnover concentration regime. The k_{obs} of this phase was in good agreement with the previously determined steady-state k_{cat} of hDUT (8 ± 3 s^{-1}) (13), indicating that it represents the rate-limiting step of the dUTPase cycle. Furthermore, the duration of the steady state (t_{ss}) in multiple turnover Trp^{158} fluorescence traces (*i.e.* the time elapsed between the start of the reaction and the inflection point of the fluorescence restoration phase) (Fig. 3*B*) was consistent with the above third phase k_{obs} and steady-state k_{cat} values ($t_{ss} \approx [S]_{initial}/([E]_{total}k_{cat})$, if $[S]_{initial} \gg K_M$).

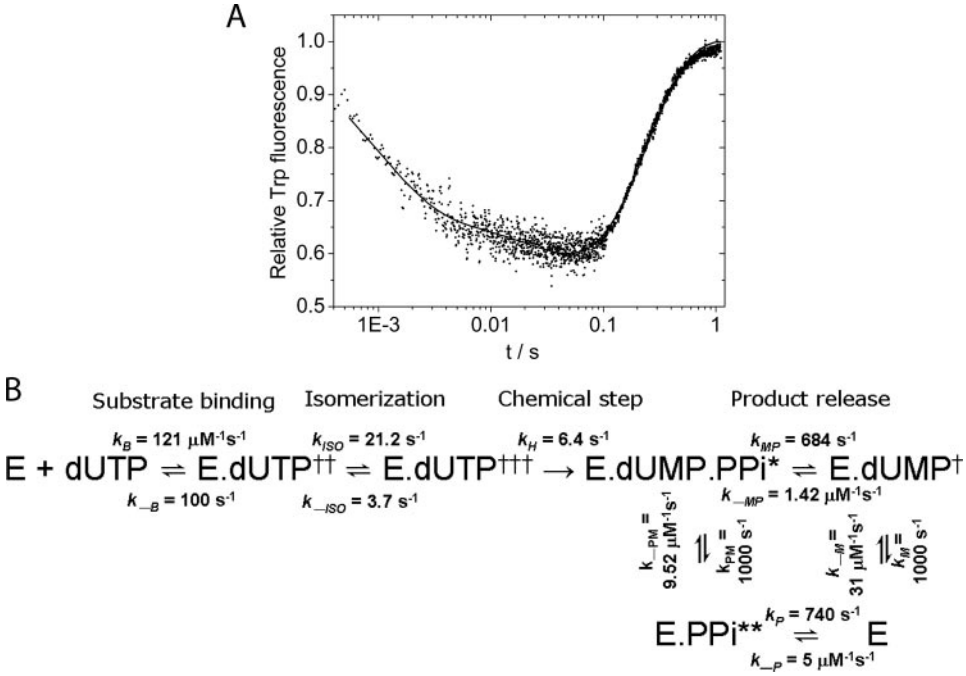

FIGURE 6. **Kinetic modeling of the human dUTPase enzymatic cycle.** *A*, taking the same example as in Fig. 3*A*, a time course upon mixing 7.5 μM $hDUT^{W158}$ with 5.25 μM dUTP is shown, prepared for global fitting (fluorescence normalized to the apoenzyme, dead time considered). The *solid line* is a global fit to the data points using the kinetic model shown in *B* and the relative fluorescence changes in Table 1. *B*, kinetic model of the hDUT enzymatic cycle. *Daggers* and *stars* indicate fluorescence decrease or increase compared with the apoenzyme, respectively. The rate constants shown in the model were used as parameters of the kinetic simulation (*A*) and are compiled in Table 2. For the k_{-PM}/k_{PM} and k_{-M}/k_M rate constant pairs, only the ratios (defined by K_d values of Tables 1 and 2) and the lower bounds for the rate constant pairs are known. These lower bounds were used in the numerical simulations as shown. Increases in the values of these rate constants (while keeping their respective ratios constant) did not cause any detectable change in the enzyme mechanism.

Fig. 3*C* shows single and multiple turnovers detected by a proton release assay in an absorbance stopped-flow setup. The amplitude of the curves was directly proportional to the initial substrate (and thus the released proton) concentration. In single turnover conditions ([*E*] > [S], lower two curves in Fig. 3*C*), the time courses corresponded to single exponentials, and k_{obs} values (6.5 ± 0.1 s^{-1}) were identical to the steady-state k_{cat} of the enzyme (Table 2). In multiple turnovers (*upper two curves* in Fig. 3*C*) a linear steady-state phase was observed without any burst of proton release. These profiles altogether imply that the enzymatic cycle is limited by a single rate-limiting step that occurs before

TABLE 2
Kinetic parameters of the hDUT enzymatic cycle

	Value	Source experiment	Figure
k_{cat} (s^{-1})	8 ± 3	Steady-state proton release assay (13)	
	6.8 ± 2.0	Fluorescence single turnovers	3, *A* and *B*
	6.5 ± 0.1	Proton release turnovers	3*C*
	6.7 ± 0.2		3*C*
K_M (μM)	3.6 ± 1.9	Michaelis-Menten global fits to proton release turnovers	3*C*
k_{cat}/K_M (M^{-1} s^{-1})	1.9×10^6		3*C*
k_B (s^{-1})	120	Global fit to fluorescence traces	6, *A* and *B*
k_{-B} (μM^{-1} s^{-1})	100		6, *A* and *B*
$k_{ISO, obs}$ (s^{-1})	20 ± 18	Fluorescence turnovers[a]	3, *A* and *B*
	24 ± 6	dUTP chasing[a]	5
k_{ISO} (s^{-1})	21.2	Global fit to fluorescence traces	6, *A* and *B*
k_{-ISO} (s^{-1})	3.7		
k_H (s^{-1})	5.5 ± 2.5	Quenched-flow single turnover	4*A*
	6.4	Global fit to fluorescence traces	6, *A* and *B*
k_{MP} (s^{-1})	684 ± 84	Fluorescence PP_i chasing from *E*·dUMP·PP_i	5
k_{-MP} (μM^{-1} s^{-1})	1.42	k_{MP}/K_d(*E*·PP_i for dUMP)[b]	5 and 6, *A* and *B*
k_{PM} (s^{-1})	>1000	Fluorescence stopped-flow[c]	6, *A* and *B*
k_{-PM} (μM^{-1} s^{-1})	> 9.5	k_{PM}/K_d (*E*·PP_i for dUMP)[d]	6, *A* and *B*
k_M (s^{-1})	>1000	Fluorescence stopped-flow[c]	6, *A* and *B*
k_{-M} (μM^{-1} s^{-1}	>31	k_M/K_d (*E* for dUMP)[b]	6, *A* and *B*
k_P (s^{-1})	740 ± 66	Fluorescence PP_i chasing from *E*·PPi	5
k_{-P} (μM^{-1} s^{-1})	5	k_P/K_d (*E* for PP_i)[b]	5 and 6, *A* and *B*

[a] $k_{ISO, obs} = k_{ISO} + k_{-ISO}$.
[b] K_d values for different ligands are listed in Table 1.
[c] The reaction was practically completed in the dead time of the stopped-flow (<1 ms).
[d] K_d (*E*·PP_i for dUMP) calculated as K_d (*E* for dUMP)K_d(*E*·dUMP for PP_i)/K_d (*E* for PP_i).

or is concomitant with proton release. We could model these proton release events with Michaelis-Menten kinetics in which a rapid equilibrium (k_1, k_{-1}) precedes the rate-limiting step ($k_2 = k_{cat}$). Global fits to the single and multiple turnover time courses using the k_1, k_{-1}, and k_2 floating parameters of Scheme 1 yielded $K_M = 3.6 \pm 1.9$ μM, $k_{cat} = 6.7 \pm 0.2$ s^{-1}, $k_{cat}/K_M \sim 1.9 \times 10^6$ M^{-1} s^{-1}, for both hDUT and hDUT^{W158} proteins.

[γ-^{32}P]dUTP Synthesis—[γ-^{32}P]dUTP is not commercially available. We therefore developed a straightforward synthesis method (Fig. 4*A*) using NDPK that converts [γ-^{32}P]ATP and dUDP into [γ-^{32}P]dUTP and ADP by a ping-pong mechanism (26, 30). We took advantage of the fact that the phosphorylated enzyme intermediate of the NDPK reaction is long lived in the absence of Mg^{2+} and thus can be separated from the phosphate donor nucleotides (26). The resulting synthesis product (after step 4 in Fig. 4*A*) contains [γ-^{32}P]dUTP, dUDP, and inorganic phosphate. To test for the presence of any non-dUTP-derived radiolabeled species that would compromise radiochemical purity, aliquots of the synthesis product were fully hydrolyzed by (i) dUTPase (extremely specific for dUTP), (ii) dUTPase + myosin (hydrolyzes NTPs (31)), or (iii) apyrase (hydrolyzes (d)NTPs and (d)NDPs (32)). All three enzyme conditions resulted in liberation of the same $^{32}P_i$ content of the total radioactive material, demonstrating that practically all hydrolyzable radioactive nucleotide species in the synthesis product was [γ-^{32}P]dUTP. The synthesis product contained 15 ± 3% non-nucleotide $^{32}P_i$ (measured in samples from which all nucleotides had been removed). Analysis showed that this fraction originated from (i) carryover from the original [γ-^{32}P]ATP solution (5%), (ii) spontaneous hydrolysis of γ-^{32}P-labeled nucleotides during the four-step procedure, and possibly (iii) slow $^{32}P_i$ release from the phosphorylated NDPK in the absence of phosphate acceptor (during step 2). The ~15% $^{32}P_i$ in the synthesis product does not reflect the P_i content of the bulk solution to be used in quenched-flow experiments, because a subsequent large dilution of the synthesis product in nonlabeled dUTP decreased the P_i/dUTP concentration ratio to less than 1:10,000 in the reagent solution used in the quenched-flow assay. The only noticeable effect of the condition that ~15% of the total radioactivity was radioactive $^{32}P_i$ was the reduction of the maximal expected signal change from 100 to 85%, which did not impede the evaluation of quenched-flow results. Similarly, the dUDP concentration of the synthesis product was drastically reduced by the dilution of [γ-^{32}P]dUTP in a large molar excess of nonlabeled dUTP (the dUDP/dUTP molar ratio was less than 1:1600 in the assay reagent). In the above described experimental conditions, the most important factor in providing chemical purity was the use of high quality nonlabeled nucleotide to be traced with a high specific activity radioactively labeled one. The total [γ-^{32}P]dUTP yield was calculated following the analysis of the radioactive constitution of the synthesis product and was found to be 25% (*i.e.* one-quarter of the [γ-^{32}P]ATP was converted specifically into [γ-^{32}P]dUTP). Considering that both reactions 1 and 3 (Fig. 4*A*) are fully reversible, this yield indicates that the procedure was highly efficient.

Direct Observation of the Chemical Step by Quenched-flow Using [γ-^{32}P]dUTP—Fig. 4*B* shows a single turnover experiment with a single exponential fit to the data points. For both wild-type hDUT and hDUT^{W158} constructs and depending on the protein preparation, the k_H of single turnovers was determined to be 5.5 ± 2.5 s^{-1}, in agreement with the k_{obs} values observed in the fluorescent and proton release turnovers (Table 2). There was no systematic difference between the k_H values of hDUT and hDUT^{W158}. When excess dUTP was mixed with hDUT (Fig. 4*C*), we observed a linear steady-state phase without any burst, clearly arguing that the rate-limiting step of the dUTPase enzymatic cycle is identical to (or precedes) the chemical step.

Product Release—The large fluorescence intensity change of Trp^{158} induced by PP_i binding allowed us to follow the dissociation of PP_i from the enzyme. We carried out dUTP chase

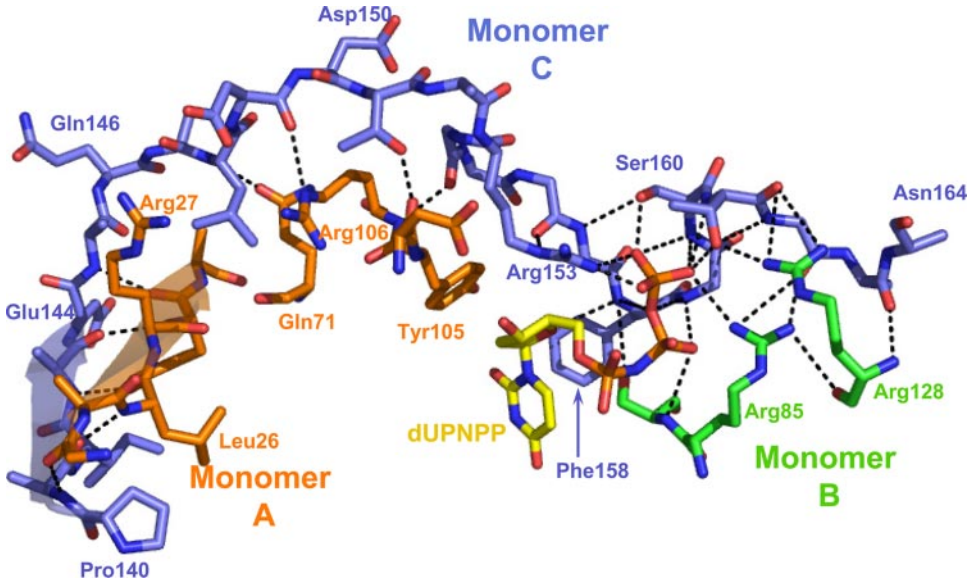

FIGURE 7. **Interactions of the C-terminal arm of hDUT with adjacent monomers and dUPNPP.** The *arrows* in the *lower left part* of the model depict β strand interactions between residues 140–144 of the C-terminal arm of monomer C (atomic *coloring* with *blue* carbons) and the N terminus of monomer A (atomic *coloring* with *orange* carbons). Residues 149–155 of monomer C are involved in contacts with side chain and main chain atoms within the conserved motif 3 of monomer A that accommodates the deoxyribose and the uracil rings of the substrate. Arm residues 155–160 contact mostly ligand atoms (*stick model*, atomic *coloring* with *yellow* carbons) and each other. The last C-terminal residues (residues 160–163) engage in extensive hydrogen bonding to the atoms of monomer B (*stick model*, atomic *coloring* with *green* carbons). Structural data are taken from Ref. 13 (Protein Data Bank code 2HQU).

experiments to avoid rebinding of the dissociated PP_i. Upon mixing the E·PP_i complex with excess dUTP in the stopped-flow, double exponential curves were recorded (Fig. 5, *upper black trace*) having a fast phase of 740 ± 66 s^{-1} and a slow phase of 24 ± 6 s^{-1}. The amplitude of the fast but not the second slow phase depended upon the concentration of PP_i (Fig. 5, *inset*). The first phase can therefore be attributed to PP_i dissociation, whereas the second phase arises from the isomerization of the ES complex occurring after the initial dUTP binding step (*cf.* Fig. 3*A*). The K_d value resulting from a one-binding site quadratic fit to the amplitude data (327 ± 117 μM) was similar to that obtained from equilibrium titrations (*cf.* Fig. 1*B* and Table 1). Product dissociation was measured also from the *E*·dUMP·PP_i complex (Fig. 5, *gray trace*). Curves exhibited k_{obs} values (684 ± 84 s^{-1}) similar to those of the *E*·PP_i curves, showing that the rate constants of PP_i dissociation from *E*·PP_i and *E*·dUMP·PP_i are similar (Table 2). In line with the lower initial fluorescence level of *E*·dUMP·PP_i compared with that of *E*·PP_i (*cf.* Fig. 1*A*), the amplitudes of the *E*·dUMP·PP_i chasing traces were lower than those of the *E*·PP_i chasing traces (Fig. 5). Binding and dissociation of dUMP was too fast to observe by stopped-flow.

Kinetic Modeling of the hDUT Enzymatic Cycle—The measured accessible parameters of the hDUT enzymatic cycle (Tables 1 and 2) allowed us to propose a model that provided good fits to our experimental data (Fig. 6*B*). Using this model, kinetic simulations of the $hDUT^{W158}$ fluorescence profile during dUTP hydrolysis yielded time courses that were very similar to the measured ones (Fig. 6*A*). Parameters for the binding (k_B, k_{-B}), isomerization (k_{ISO}, k_{-ISO}) and hydrolysis (k_H) steps were floating parameters, given that these are the events that primarily determine the fluorescence profiles during dUTP turnovers. Kinetic parameters of the product release steps were fixed so that the ratios of the dissociation and association rate constants of the individual steps yield the K_d values shown in Table 1 and thus determine the final fluorescence levels. The rate constants of product release are so fast compared with the rate-limiting step that they do not influence the turnover curves.

DISCUSSION

A central aspect of the present study is that the fluorescent signal of a single tryptophan engineered into the C-terminal arm of hDUT (Trp^{158}), which forms part of the active site, allowed precise resolution and characterization of practically all key enzymatic steps. These steps include (i) a rapid, probably diffusion-limited substrate binding, (ii) a subsequent substrate-induced structural change (isomerization) required for the formation of the catalytically competent conformation, (iii) the rate-limiting hydrolysis step, and (iv) rapid, nonordered release of the hydrolysis products (Fig. 6*B* and Table 2). The second isomerization step was not foreseen or suggested earlier due to the lack of conformationally sensitive assays to follow the reaction. Importantly, in the present work, two independent lines of evidence argue in favor of the existence of this isomerization step. First, the different extent of quenching and blue shift associated with the enzyme-dUPNPP and enzyme-dUTP (steady-state) complexes (*cf.* Fig. 1*A*) indicate the existence of at least two distinct prehydrolysis conformations of the active site. Second, the kinetic analysis of time courses in Figs. 3, *A* and *B*, and 6 clearly shows the presence of a second slower exponential component following the initial fast binding of dUTP. An intriguing feature of the mechanism is that two different dUTP-bound intermediates will be significantly populated during steady-state dUTP hydrolysis (*E*·$dUTP^{\dagger\dagger\dagger}$ will be predominant, but about 30% of the enzyme molecules will populate *E*·$dUTP^{\dagger\dagger}$). This steady-state distribution results from the k_{ISO} rate constant being in the same order of magnitude as the rate-limiting hydrolysis rate constant (k_H) (Fig. 6*B*).

We confirmed the rate-limiting nature of the chemical (hydrolysis) step by [γ-^{32}P]dUTP-based quenched-flow transient kinetic analysis (Fig. 4). To obtain the commercially unavailable [γ-^{32}P]dUTP, we developed a simple synthesis method based on the ping-pong phosphate transfer mechanism of NDPK (26). The novelty in our synthesis is that isolation of the [^{32}P]NDPK intermediate and the final γ-^{32}P-labeled nucleotide product takes place in an Eppendorf tube, requires no instrumentation, and results in a radiochemical purity that is suitable for many applications. Laborious purification of the synthesis products is not necessary, because the donor and acceptor nucleotides are spatially and temporally separated.

This straightforward method may be of great help in studying enzymes that use pyrimidine-triphosphates as substrate (*e.g.* dCTP deaminase, dTTPase, tRNA cytidyltransferase, etc.), since none of these relevant γ-labeled pyrimidine nucleotides are commercially available (or they may be purchased only as expensive custom synthesis orders). Due to the substrate promiscuity of NDPK, even base-modified nucleotide analogs may be radioactively labeled using this method for additional specific applications.

Interestingly, the estimated intracellular dUTP concentration (~0.7 μM (4)) is in the same range as the K_M of hDUT for dUTP (Tables 1 and 2). This indicates that dUTPase function is highly sensitive to cellular dUTP fluctuations around the physiological level. Our data show that product inhibition by dUMP at its estimated physiological concentration (~2.7 μM (4)) is probably not significant due to its relatively low affinity for hDUT and its rapid release from the enzyme-products complex (Tables 1 and 2).

We probed *in silico* F158W mutations in available structures and found that the replacement of Phe^{158} with a Trp residue does not cause a steric hindrance within the active site. Accordingly, we found that $hDUT^{W158}$ retains the enzymatic activity of the wild-type enzyme. The presence of an aromatic residue at this location has been suggested to be important for enzyme activity (12), and thus the fact that a Trp residue can functionally replace the native Phe^{158} implies that the fluorescence signal reports events that are highly relevant to the physiological activity of the enzyme.

Trp^{158} is sensitive to the precise nucleotide (or other ligand) content of the active site (Fig. 1*A*). The solvent shielding of Trp^{158} increases, whereas the structural flexibility of this residue decreases with increasing length of the polyphosphate chain of the nucleotide ligand (Fig. 2). PP_i binding into the binding site, however, causes a structural ordering of the arm without a solvent shielding effect. Based on our observation that $E{\cdot}PP_i$ exhibits elevated fluorescence compared with the apoenzyme (Fig. 1*A*), we speculate that PP_i binding may cause disruption of a quenching interaction of Trp^{158}, supposed to be present in the apo state. A possibility for such a quenching interaction is a cation-π type interaction (33) between Trp^{158} and the positively charged guanidino moiety of an arginine residing in its close proximity. Candidate arginines are residues 85, 128, and 135, all contributing to the binding and stabilization of the polyphosphate chain of the substrate nucleotide (Fig. 7) (13). These groups are separated by about 9–10 Å from Trp^{158} via the intercalation of the uracil group in the hDUT-dUPNPP structure. In the apo state, however, one of the candidate arginines might move closer to the phenylalanine (tryptophan) to neutralize the positive charge via cation-π stacking; hence the intermediate fluorescence level observed in the $apo\text{-}hDUT^{W158}$.

It is noteworthy that, whereas the binding of dUMP, dUDP, and dUPNPP (and even more that of dUTP) to the enzyme causes marked quenching of Trp^{158} as compared with the apo state, the posthydrolysis $E{\cdot}dUMP{\cdot}PP_i$ complex has an enhanced Trp^{158} fluorescence. We surmise that this fluorescence increase reflects a structural state in which the stacking interaction between Trp^{158} and the uracil moiety is at least partially disrupted, aiding the rapid release of products from this posthydrolytic complex.

In addition to its utility in the determination of the kinetic and thermodynamic parameters, the Trp^{158} signal also provided much information about the structural dynamics of the C-terminal arm during catalysis. Evidence is presented that this protein segment is at least partially closed upon the active site in all enzymatic states (even including the apoenzyme) (Fig. 2), and therefore its conformational freedom may be well restricted. Fig. 7 shows that the C-terminal arm of monomer A is anchored in a β-sheet with the N-terminal residues of monomer C. At its very C terminus, the arm also interacts with monomer B via strong hydrogen bonds (second anchor). Interactions of the arm with the ligand dUPNPP are mainly formed by residues situated between the monomer-monomer interacting regions. This arrangement rationalizes (i) the proposed proximity of the C terminus to the protein core even in the absence of nucleotide (in the apoenzyme) and (ii) that the C-terminal arm still conveys a significant flexibility in the apoenzyme (between the two anchor regions), as suggested in previous studies (12, 13).

We described a complex methodology to assess the fundamental steps of dUTP hydrolysis as catalyzed by human dUTPase, an important chemotherapeutic target protein. The resulting novel insights underline the importance of the dynamic behavior of the C-terminal arm during catalysis and advocate the targeting of this enzyme segment for perturbation of dUTPase function.

Acknowledgments—We thank Dr. Orsolya Barabás for useful comments on the manuscript and the Department of Immunology of Eötvös Loránd University, Budapest, for use of scintillation counter equipment.

REFERENCES

1. Shlomai, J., and Kornberg, A. (1978) *J. Biol. Chem.* **253,** 3305–3312
2. Gadsden, M. H., McIntosh, E. M., Game, J. C., Wilson, P. J., and Haynes, R. H. (1993) *EMBO J.* **12,** 4425–4431
3. el-Hajj, H. H., Zhang, H., and Weiss, B. (1988) *J. Bacteriol.* **170,** 1069–1075
4. Traut, T. W. (1994) *Mol. Cell Biochem.* **140,** 1–22
5. Pearl, L. H., and Savva, R. (1996) *Nat. Struct. Biol.* **3,** 485–487
6. Pugacheva, E. N., Ivanov, A. V., Kravchenko, J. E., Kopnin, B. P., Levine, A. J., and Chumakov, P. M. (2002) *Oncogene* **21,** 4595–4600
7. Chano, T., Mori, K., Scotlandi, K., Benini, S., Lapucci, C., Manara, M. C., Serra, M., Picci, P., Okabe, H., and Baldini, N. (2004) *Oncol. Rep.* **11,** 1257–1263
8. Ladner, R. D., Lynch, F. J., Groshen, S., Xiong, Y. P., Sherrod, A., Caradonna, S. J., Stoehlmacher, J., and Lenz, H. J. (2000) *Cancer Res.* **60,** 3493–3503
9. Romeike, B. F., Bockeler, A., Kremmer, E., Sommer, P., Krick, C., and Grasser, F. (2005) *Pathol. Res. Pract.* **201,** 727–732
10. Strahler, J. R., Zhu, X. X., Hora, N., Wang, Y. K., Andrews, P. C., Roseman, N. A., Neel, J. V., Turka, L., and Hanash, S. M. (1993) *Proc. Natl. Acad. Sci. U. S. A.* **90,** 4991–4995
11. Bekesi, A., Zagyva, I., Hunyadi-Gulyas, E., Pongracz, V., Kovari, J., Nagy, A. O., Erdei, A., Medzihradszky, K. F., and Vertessy, B. G. (2004) *J. Biol. Chem.* **279,** 22362–22370
12. Mol, C. D., Harris, J. M., McIntosh, E. M., and Tainer, J. A. (1996) *Structure* **4,** 1077–1092
13. Varga, B., Barabás, O., Kovári, J., Tóth, J., Hunyadi-Gulyás, É., Klement, É., Medzihradszky, K. F., Tölgyesi, F., Fidy, J., and Vertessy, B. G. (2007) *FEBS*

Lett. **581,** 4783–4788
14. Larsson, G., Svensson, L. A., and Nyman, P. O. (1996) *Nat. Struct. Biol.* **3,** 532–538
15. Prasad, G. S., Stura, E. A., Elder, J. H., and Stout, C. D. (2000) *Acta Crystallogr Sect. D. Biol. Crystallogr.* **56,** 1100–1109
16. Barabas, O., Pongracz, V., Kovari, J., Wilmanns, M., and Vertessy, B. G. (2004) *J. Biol. Chem.* **279,** 42907–42915
17. Nemeth-Pongracz, V., Barabas, O., Fuxreiter, M., Simon, I., Pichova, I., Rumlova, M., Zabranska, H., Svergun, D., Petoukhov, M., Harmat, V., Klement, E., Hunyadi-Gulyas, E., Medzihradszky, K. F., Konya, E., and Vertessy, B. G. (2007) *Nucleic Acids Res.* **35,** 495–505
18. Dauter, Z., Persson, R., Rosengren, A. M., Nyman, P. O., Wilson, K. S., and Cedergren-Zeppezauer, E. S. (1999) *J. Mol. Biol.* **285,** 655–673
19. Vertessy, B. G., Larsson, G., Persson, T., Bergman, A. C., Persson, R., and Nyman, P. O. (1998) *FEBS Lett.* **421,** 83–88
20. Vertessy, B. G. (1997) *Proteins* **28,** 568–579
21. Larsson, G., Nyman, P. O., and Kvassman, J. O. (1996) *J. Biol. Chem.* **271,** 24010–24016
22. Kovári, J., Barabás, O., Varga, B., Békési, A., Tölgyesi, F., Fidy, J., Nagy, J., and Vertessy, B. G. (2007) *Proteins*, in press
23. Margossian, S. S., and Lowey, S. (1982) *Methods Enzymol.* **85,** 55–71
24. Mendes, P. (1997) *Trends Biochem. Sci.* **22,** 361–363
25. Lakowicz, J. (1999) *Principles of Fluorescence Spectroscopy*, 2nd Ed., pp. 291–306 and 237–251, Springer-Verlag New York Inc., New York
26. Munoz-Dorado, J., Inouye, S., and Inouye, M. (1990) *J. Biol. Chem.* **265,** 2707–2712
27. Sambrook, J., and Russell, D. W. (2001) *Molecular Cloning: A Laboratory Manual*, Cold Spring Harbor Laboratory, Cold Spring Harbor, NY
28. Li, X. D., Rhodes, T. E., Ikebe, R., Kambara, T., White, H. D., and Ikebe, M. (1998) *J. Biol. Chem.* **273,** 27404–27411
29. Kovacs, M., Malnasi-Csizmadia, A., Woolley, R. J., and Bagshaw, C. R. (2002) *J. Biol. Chem.* **277,** 28459–28467
30. Lascu, I., and Gonin, P. (2000) *J. Bioenerg. Biomembr.* **32,** 237–246
31. White, H. D., Belknap, B., and Webb, M. R. (1997) *Biochemistry* **36,** 11828–11836
32. Molnar, J., and Lorand, L. (1961) *Arch. Biochem. Biophys.* **93,** 353–363
33. Gallivan, J. P., and Dougherty, D. A. (1999) *Proc. Natl. Acad. Sci. U. S. A.* **96,** 9459–9464

Published online 2 July 2010

Nucleic Acids Research, 2010, Vol. 38, No. 20 ***7179–7186***
doi:10.1093/nar/gkq584

Aromatic stacking between nucleobase and enzyme promotes phosphate ester hydrolysis in dUTPase

Ildiko Pecsi[1], Ibolya Leveles[1], Veronika Harmat[2], Beata G. Vertessy[1,3] and Judit Toth[1,*]

[1]Institute of Enzymology, Biological Research Center, Hungarian Academy of Sciences, Budapest, Hungary, [2]Hungarian Academy of Sciences-Eötvös Loránd University, Protein Modeling Research Group, and Eötvös Loránd University, Institute of Chemistry, Budapest, Hungary and [3]Department of Applied Biotechnology, Budapest University of Technology and Economics, Budapest, Hungary

Received April 29, 2010; Revised June 8, 2010; Accepted June 9, 2010

Downloaded from https://academic.oup.com/nar/article/38/20/7179/1309070 by guest on 04 November 2021

ABSTRACT

Aromatic interactions are well-known players in molecular recognition but their catalytic role in biological systems is less documented. Here, we report that a conserved aromatic stacking interaction between dUTPase and its nucleotide substrate largely contributes to the stabilization of the associative type transition state of the nucleotide hydrolysis reaction. The effect of the aromatic stacking on catalysis is peculiar in that uracil, the aromatic moiety influenced by the aromatic interaction is relatively distant from the site of hydrolysis at the alpha-phosphate group. Using crystallographic, kinetics, optical spectroscopy and thermodynamics calculation approaches we delineate a possible mechanism by which rate acceleration is achieved through the remote π–π interaction. The abundance of similarly positioned aromatic interactions in various nucleotide hydrolyzing enzymes (e.g. most families of ATPases) raises the possibility of the reported phenomenon being a general component of the enzymatic catalysis of phosphate ester hydrolysis.

INTRODUCTION

The prevalence of aromatic interactions in the conformation control of macromolecules is widely accepted (1) and studied in a number of biological systems [e.g. DNA double helix (2), ribonucleoproteins (3), protein folding (4)]. In the reported cases, the contribution of intra- or inter-molecular aromatic stacking (also termed as π–π interactions) to structural stabilization is comparable in strength to hydrogen bonding (3). The role of π–π interactions in enzymatic catalysis, however, receives less attention mainly restricted to studies of flavoenzymes (5) and of the N-glycosidic bond cleavage by a nucleoside hydrolase (6). These two examples are comparable in that the interacting aromatic ring is bonded (covalently or non-covalently) to the chemical reaction center. In redox reactions catalyzed by flavoenzymes, the aromatic ring of the electron acceptor flavin cofactor is the catalytic reaction center that is directly affected by a stacked aromatic amino acid residue resulting in a decreased reduction potential (7). In the second example, the investigated nucleoside hydrolase uses aromatic stacking for efficient protonation of the leaving purine base (6).

By examining the structures of nucleotide hydrolyzing enzymes in the PDB database, it appears that aromatic residues frequently reside in their active sites (8) (Figure 1A) with reported roles mostly in substrate binding [ABC transporters (9), kinesins (10), kinases (11)]. The role of these interactions in catalysis has not been addressed and may be counterintuitive given the relatively large physical and chemical distances between the site of hydrolysis and the aromatic ring of the nucleotide. We present data on the catalytic role of a π–π interaction between the enzyme dUTPase and its nucleotide substrate in a hydrolysis reaction that occurs between the α and β phosphate groups. dUTPase is a ubiquitous enzyme that hydrolyzes dUTP into the dTTP precursor dUMP and pyrophosphate, thus preventing potentially fatal uracil incorporation into DNA (12). Homotrimeric dUTPases contain a conserved aromatic residue in their active sites which is stacked over the uracil ring in all substrate-containing complete dUTPase crystal structures (12). This aromatic interaction was attributed a role in substrate binding and possibly product release purely on the basis of structural considerations (13).

To pursue this hypothesis, we created mutations at the conserved aromatic site in the human and *Mycobacterium tuberculosis* (MT) dUTPase (hDUT^{F158W}, hDUT^{F158A},

*To whom correspondence should be addressed. Tel: +36 1 2793142; Fax: +36 1 4665465; Email: tothj@enzim.hu

The authors wish it to be known that, in their opinion, the first two authors should be regarded as joint First Authors.

© The Author(s) 2010. Published by Oxford University Press.
This is an Open Access article distributed under the terms of the Creative Commons Attribution Non-Commercial License (http://creativecommons.org/licenses/by-nc/2.5), which permits unrestricted non-commercial use, distribution, and reproduction in any medium, provided the original work is properly cited.

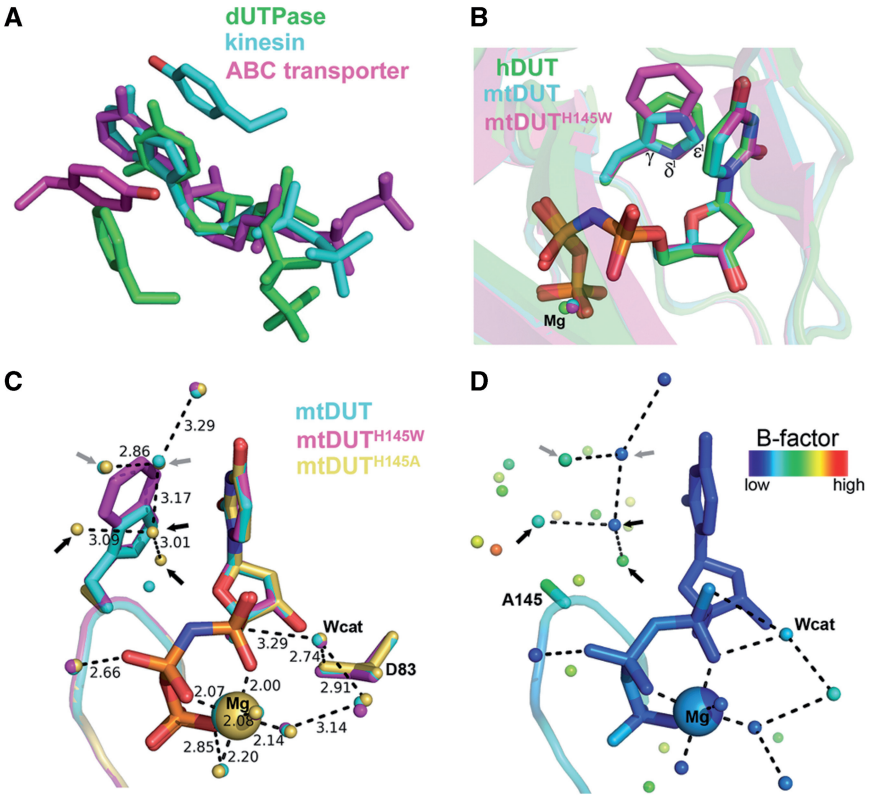

Figure 1. Structural aspects of the enzyme–substrate π−π interaction in dUTPase and in other nucleotide hydrolases. (**A**) The π−π interactions between enzyme and substrate in representatives of various nucleotide hydrolase families [PDB IDs 2HQU (13), 2NCD (29) and 1XEF (30)]. (**B**) Structural superimposition of dUTPase active sites conferring different aromatic amino acids [Phe, His, Trp in PDB IDs 2HQU (13), 2PY4 (16), 3HZA, respectively]. (**C**) Superimposition of the newly acquired mutant structures with wild-type mtDUT. Grey and black arrows point to water molecules found in both mtDUT and mtDUT^{H145A} but not in mtDUT^{H145W} or only in mtDUT^{H145A}, respectively. D83 is the catalytic residue that polarizes the nucleophile attacking water molecule (Wcat) (25). (**D**) Same view of the mtDUT^{H145A} active site colored by B factors. Note the relatively low mobility of the Trp-replacing waters.

mtDUT^{H145W}, mtDUT^{H145A}) and performed crystallographic, kinetic and spectroscopic experiments using these mutants to reveal the effect of the change/loss of the aromatic interaction on the enzymatic cycle. Contrary to the expectations, we show that elimination of the aromatic interaction only slightly affected substrate binding while it specifically decreased the rate constant of the chemical step resulting in an overall 100-fold decrease in the catalytic efficiency.

MATERIALS AND METHODS

Proteins were expressed and purified as described previously [human dUTPase (hDUT) (14), MT dUTPase (mtDUT) (15)]. Site-directed mutagenesis was performed by the QuikChange method (Stratagene) and verified by sequencing of both strands. Mutagen forward and reverse primers were 5′-ggggttcaggaggtgctggttccactgg-3′ and 5′-ccagtggaaccagcacctcctgaacccc-3′ for hDUT^{F158A} and 5′-ggcgacggtggcgcgggttcctccggc-3′ and 5′-ggcggaggaacccgcgccaccgtcgcc-3′ for mtDUT^{H145A}. Protein concentration was measured using the Bradford method (Bio-Rad Protein Assay) or by UV absorbance (λ_{280} = 10555 $M^{-1}cm^{-1}$ for hDUT and for hDUT^{F158A}, 16055 $M^{-1}cm^{-1}$ for hDUT^{F158W}, 8480 $M^{-1}cm^{-1}$ for mtDUT^{H145W} and 2980 $M^{-1}cm^{-1}$ for mtDUT^{H145A}) and is given in monomers. Proteins were dialyzed into 20 mM HEPES pH 7.5 buffer, also containing 100 mM NaCl, 5 mM $MgCl_2$ and 1 mM DTT. This dialysis buffer was used for further measurements (unless otherwise stated). Electrophoresis and chromatography reagents were from Bio-Rad and Qiagen, molecular biology products were from New England Biolabs or Fermentas. Other chemicals were from Sigma-Aldrich.

Crystallization

The mtDUT^{H145W} and mtDUT^{H145A} mutants were crystallized as described for the wild-type enzyme using the hanging drop method (16). The 3 mg ml^{-1} dUTPase and 1.25 mM α,β-imido-dUTP was mixed with the reservoir solution containing 50 mM Tris–HCl pH 7.5, 10 mM $MgCl_2$, 1.20–1.75 M ammonium sulphate and 10% glycerol in a 1:1 ratio.

Data collection and structure determination

Complete high resolution (1.2Å for mtDUT^{H145W} and 1.25Å for mtDUT^{H145A}) crystallographic data sets from well diffracting crystals were recorded at the

Downloaded from https://academic.oup.com/nar/article/38/20/7179/1309070 by guest on 04 November 2021

EMBL-beamline X12 of DESY (Hamburg) at $\lambda = 0.9786$Å or 0.9769Å wavelength. Data reduction was performed using the XDS and XSCALE (17) programs and the CCP4 program suite (18). Both structures of the mutant: α,β-imido-dUTP:Mg^{2+} complexes were determined by molecular replacement [MOLREP (19)] using the truncated wild-type mtDUT structure (PDB ID: 2PY4) as a model without ligands. Model building was carried out using the Coot program (20). For atomic resolution refinement, Shelxl from the Shelx-97 program package was used (21). A 5% random subset of the data set was computed for cross-validation throughout the refinement, resulting in Rfree-values. Ramachandran statistics (percentage of all residues): most favored/additionally allowed/generously allowed = 89.9/10.1/0 for $mtDUT^{H145W}$ and = 92.1/7.9/0 for $mtDUT^{H145A}$. Atomic coordinates and structure factor data have been deposited in the Protein Data Bank with the accession codes 3HZA and 3LOJ.

Steady-state colorimetric dUTPase assay

Protons released in the dUTPase reaction were detected by a phenol red indicator assay described in Vertessy *et al.* (22) in 1mM Hepes, pH 7.5 buffer containing 100 mM KCl, 40 μM phenol red (Merck) and 5 mM $MgCl_2$. A Specord 200 (Analytic Jena, Germany) spectrophotometer and 10-mm path length thermostatted cuvettes were used at 20°C. Absorbance was recorded at 559 nm. The Michaelis–Menten equation was fitted to the steady-state curves using Origin 7.5 (OriginLab Corp., Northampton, MA, USA).

Stopped-flow experiments

Measurements were done using an SX-20 (Applied Photophysics, UK) stopped-flow apparatus. In the absorbance stopped-flow setup, an assay buffer containing 100 μM phenol red indicator and 1 mM HEPES pH 7.5 provided optimal monitoring of dUTP hydrolysis. To avoid mixing artifacts, the enzyme was dialyzed in the assay buffer prior to the measurements. Active site titrations were carried out to assess the active protein fraction (>90% in each protein preparation). The presented single turnover (STO) curves were measured upon mixing 10 μM dUTP with 35 μM enzyme at 20°C. The measurement in the fluorescence setup was carried out exactly as described in (23). Time courses were analyzed using the curve fitting software provided with the stopped-flow apparatus or by Origin 7.5.

'Quench flow' experiments were carried out using an RQF-3 (KinTek Corp., Austin, TX, USA) quench-flow apparatus as described in Toth *et al.* (23). To obtain the presented curve, the reaction of 25-μM protein with 17.5-μM γ^{32}P-dUTP was monitored at 20°C. The resulting ^{32}PPi product was quantified in water using a Wallac 1409 Liquid Scintillation Counter (PerkinElmer, Inc.).

Circular dichroism intensity titrations

CD spectra were recorded at 20°C on a JASCO 720 spectropolarimeter using a 1-mm path length cuvette. The 50-μM protein was titrated by step-wise addition of the non-hydrolysable substrate analogue α,β-imido-dUTP (dUPNPP, purchased from Jena Bioscience, Germany) in a buffer containing 10 mM potassium-phosphate pH 7.5, and 1 mM $MgCl_2$. A spectrum between $\lambda = 250$–290 nm was recorded at each nucleotide concentration. Differential curves were obtained by subtracting the signal of dUPNPP alone from that of the corresponding complex. Differential ellipticity at $\lambda_{max} = 269$ nm was plotted against the dUPNPP concentration to obtain the binding curves. The following quadratic equation was fitted to the experimental curves:

$$y = s + \frac{A^*\left((c+x+K) - \sqrt{(c+x+K)^2 - 4^*c^*x}\right)}{2^*c}$$

$s = y$ at $c = 0$; A = amplitude; c = protein concentration; $K = K_d$.

Fluorescence spectroscopy

Maximal fluorescence quenches of the various enzyme–ligand complexes were measured in a Jobin Yvon Spex Fluoromax-3 spectrofluorometer at 20°C, with excitation at 295 nm (slit 1 nm) and emission at 347 (slit 5 nm). The saturating concentrations of ligands (4 mM dUTP, 100 μM dUPNPP, 500 μM dUMP) were added to 4 μM protein.

Statistical analysis

All measurements were carried out at least three times. Error bars represent standard deviations. In case no error bars are shown, a representative curve is displayed while the summary table (Table 1) shows the relevant standard deviations of a certain parameter obtained from several different measurements. In the stopped-flow experiments, typically 5–8 traces were collected and averaged.

RESULTS

Full conservation of the aromatic residue within the active site of dUTPases

To assess the degree of conservation of the aromatic residue located in the C-terminal segment of the dUTPase subunit, we performed a database search (p-blast) using the human enzyme as query. Following an alignment of the first 500 dUTPase sequences (Supplementary Figure S1), we analyzed the amino acid distribution in the position that engages in a non-parallel face-to-face offset stack with the uracil ring of the substrate (Figure 1B and C) in all available complete crystal structures. As a result, we counted 96.4% Phe, 1.8% His, 1.6% Tyr and 0.2% Trp. It is of interest that the most frequent Phe is non-polar and relatively small.

The crystal structure of $mtDUT^{H145W}$ suggests a high degree of conformational conservation of the stacking interaction

We chose two enzymes from two different species for our investigations for the following reasons (i) they represent

Downloaded from https://academic.oup.com/nar/article/38/20/7179/1309070 by guest on 04 November 2021

Table 1. Kinetic and substrate binding parameters of human dUTPase mutants

	k_{cat} (s^{-1})	k_H (s^{-1})	k_P (s^{-1})	K_M (μM)	$K_{d,dUPNPP}$ (μM)	k_{cat}/K_M ($M^{-1}*s^{-1}$)
$hDUT^{WT}$	5.8 ± 0.5	8.0 ± 2		1.0 ± 0.4	2.0 ± 1	$5.8*10^6$
$hDUT^{F158W}$	6.8 ± 2[a]	5.5 ± 2.5[a]	6.5 ± 0.1[a]	3.6 ± 2[a]	1.5 ± 1	$1.9*10^6$
$hDUT^{F158A}$	0.32 ± 0.1	0.13 ± 0.01	0.25 ± 0.05	5.2 ± 0.4	4.8 ± 2	$6.2*10^4$

k_H: observed rate constant of the hydrolysis step.
k_P: observed rate constant of proton release.
Errors represent standard deviations of three independent measurements. In case fitting was carried out to data points with appended standard deviations, error propagation was calculated by the fitting software.
[a]Toth *et al.* (23).

two different aromatic residues at the critical position (Phe in human and His in MT dUTPase); (ii) they share a high degree of sequence and structural similarity (Supplementary Figure S2A); (iii) a detailed enzymatic mechanism of the human enzyme is available (23); and (iv) the MT dUTPase as well as its mutants are readily crystallizable (16,24). Accordingly, we could obtain well diffracting crystals of the $mtDUT^{H145W}$ mutant in complex with the slowly hydrolysable (25) substrate analog α,β-imido-dUTP (dUPNPP). We determined its structure to 1.20 Å resolution (deposited in the PDB as 3HZA, Supplementary Table S1). Superimposition of the hDUT, mtDUT and the novel $mtDUT^{H145W}$ structures reveals that not only the aromatic residue is conserved but so is its conformation relative to the substrate (Figure 1B). Furthermore, three atoms of each aromatic ring (γ, δ^1, ε^1) can be superimposed despite the different dimensions of the rings (Figure 1B). The perfect conservation of the aromatic planes and the inter-planar angle among the three different structures implies that fine-tuning of the geometry and thus the potential energy of the π–π interaction is of significance (26).

The loss of the aromatic interaction does not perturb the overall structure and active site architecture of dUTPase

We aimed to investigate the consequences of abolishing the stacking interaction between uracil and Phe/His/Trp on the catalytic properties of dUTPase, we therefore engineered the $hDUT^{F158A}$ and $mtDUT^{H145A}$ mutants. Such a radical amino acid replacement is generally seen as the potential source of unspecific and unwanted effects on protein folding and/or activity. We therefore tried to crystallize the alanine mutants and succeeded to do so in the case of $mtDUT^{H145A}$. The collected data set allowed us to solve the structure of the mutant in complex with dUPNPP at 1.25 Å resolution (deposited in the PDB as 3LOJ, Supplementary Table S1). Superimposition of the $mtDUT^{H145A}$ with the wild-type and $mtDUT^{H145W}$ dUTPase structures indicates that loss of the aromatic residue did not perturb the overall structure or the mode of substrate binding (Supplementary Figure S2B). The considerably high resolution of our dUTPase 3D structures (mtDUT, $mtDUT^{H145W}$ and $mtDUT^{H145A}$) allowed an in-depth analysis of the water network within the active site. Figure 1C shows water molecules appearing upon loss of the aromatic elements. The replacing well-defined water network (c.f. B factors in Figure 1D) occupies approximately the space of an indole ring and integrates well into the H-bonding network observed in the wild-type crystal. The catalytic water molecule (25) as well as the rest of the conserved residues and metal cofactor are equally positioned in all mutants (Figure 1C) which suggests that any activity loss in the $mtDUT^{H145A}$ is not a result of disordering the interaction network of the catalytic site (Supplementary Figure S2). The modularity of the water network occupying the space of the aromatic rings explains the exchangeability of Phe/Trp/His/Tyr residues appearing in various dUTPase sequences (Supplementary Figure S1).

The loss of the aromatic interaction results in a decreased steady-state dUTPase activity

We have previously shown that introduction of a Trp residue to the aromatic site results in a wild-type enzymatic behavior (14,23). To evaluate the consequences of the loss of the aromatic residue to the enzymatic cycle, we measured the activity of $hDUT^{F158A}$ (Figure 2A) and $mtDUT^{H145A}$ (Figure 2B) taking advantage of the protons released in the hydrolysis reaction ('Materials and Methods' section). The maximal steady-state activity of the $hDUT^{F158A}$ mutant decreased to 0.3 s^{-1} compared to the wild-type (5.8 s^{-1}), while the Michaelis constant (K_M) increased from around 1 μM to 5 μM (Table 1). For mtDUT, we obtained a similar 20-fold decrease in k_{cat} (from 3.1 s^{-1} to 0.16 s^{-1}) and a small increase in the K_M (from 0.46 μM to 0.56 μM, Figure 2B).

A hindered chemical step is responsible for the decreased activity in the $hDUT^{F158A}$ mutant

In previous kinetic investigations of the dUTPase enzymatic cycle we established several distinguishable kinetic reaction steps of which the hydrolysis event (or chemical step) proved to be rate-limiting (23). To measure the rate constant of hydrolysis, time courses of STO dUTPase reactions were recorded using stopped-flow (Figure 3A) and quench-flow (Figure 3B) techniques. The enzyme concentration was set high ('Materials and Methods' section) so that substrate binding is not rate-limiting and is quantitative. In such conditions, single exponential fit to the proton release STO curves (black line in Figure 3A) selectively reported on the proton release and any preceding conformational event coupled to it. Curve fitting yielded $k_P = 0.25\,s^{-1}$, comparable to the maximal steady-state rate (Table 1). In order to directly observe the chemical

Downloaded from https://academic.oup.com/nar/article/38/20/7179/1309070 by guest on 04 November 2021

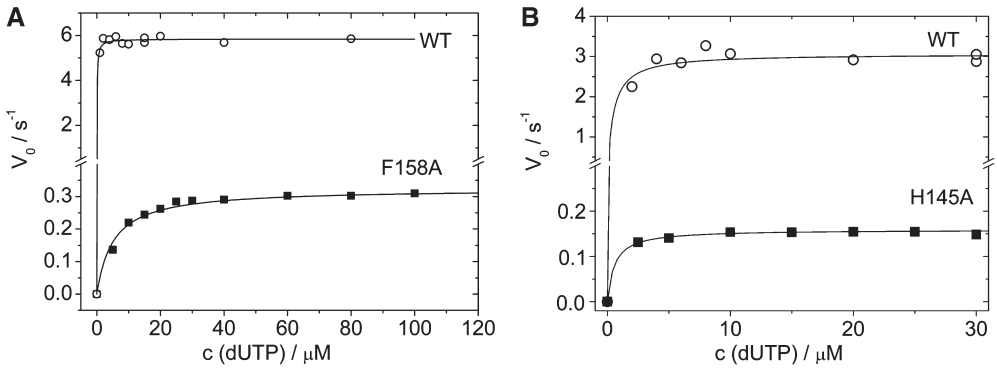

Figure 2. Loss of the aromatic interaction brings about the same reduction in k_{cat} in the mycobacterial as in the human enzyme. (**A** and **B**) Michaelis–Menten curves of hDUT versus $hDUT^{F158A}$ (steady-state parameters in Table 1) and of mtDUT versus $mtDUT^{H145A}$, respectively. (B) We evaluated the enzymatic activity of the mycobacterial dUTPase mutant in addition to the human one since our structural data was obtained using this readily crystallizable isoform. The rectangular hyperbolic fit to the Michaelis–Menten curves shown yielded $k_{cat} = 3.1 \pm 0.06$, $K_M = 0.46 \pm 0.2\,\mu M$ and $k_{cat} = 0.16 \pm 0.001$, $K_M = 0.56 \pm 0.1\,\mu M$ for mtDUT and $mtDUT^{H145A}$, respectively.

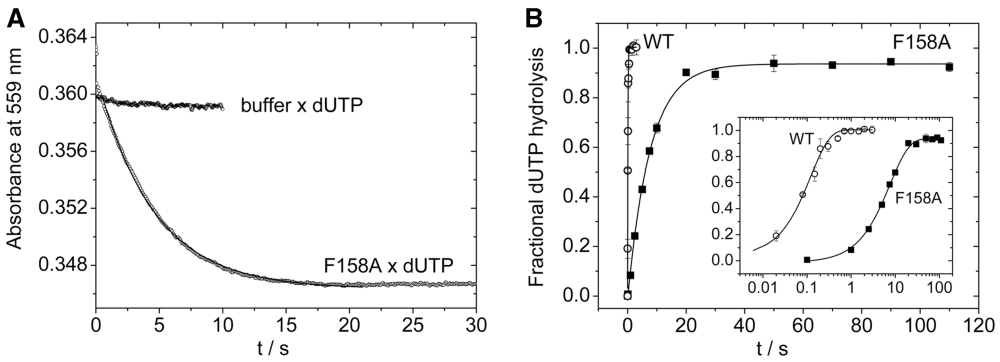

Figure 3. Proton release and hydrolysis events limit the observed steady-state rates in the $hDUT^{F158A}$ mutant. (**A**) Time courses of proton release upon mixing 15 μM $hDUT^{F158A}$ with buffer or with sub-stoichiometric (10 μM) dUTP in the stopped-flow. Single exponential fit to the curve yielded $k_{obs} = 0.23 \pm 0.007\,s^{-1}$. (**B**) Time courses of STO quench-flow experiments upon mixing hDUT or $hDUT^{F158A}$ with sub-stoichiometric radioactive dUTP. The inset shows the same on a logarithmic time scale. Calculated rate constants are summarized in Table 1.

step within the reaction cycle, we used rapid chemical quench and observed the hydrolysis of radioactively labeled dUTP. Single exponential fits to the time points (black lines in Figure 3B) yielded $k_H = 0.13\,s^{-1}$ to $hDUT^{F158A}$ and $k_H = 5.5\,s^{-1}$ to the wild-type enzyme. Compared with the steady-state rates, it is apparent that the stalled chemical step is responsible for the overall loss of enzymatic activity in the $hDUT^{F158A}$ mutant (Table 1). Also, consistently with our previous observations (23), proton release occurs concomitantly with the process observed in the chemical quench experiments as suggested by the similar rate constants obtained in the proton release and chemical quench experiments ($k_P \approx k_H$, Table 1). Based on the above observations we may argue that loss of the aromatic interaction did not alter the basic enzymatic mechanism but it directly affected the chemical step.

Substrate binding is only slightly affected by the abolition of enzyme-substrate stacking

As was mentioned previously, the most acknowledged role of aromatic interactions lies in molecular recognition and thus in modulating the affinity of interacting partners. We investigated the substrate binding equilibrium of $hDUT^{F158W}$ and $hDUT^{F158A}$ using the circular dichroism signal of the enzyme–substrate complex (Supplementary Figure S3). Saturation curves of dUPNPP binding to hDUT, $hDUT^{F158W}$ and $hDUT^{F158A}$ (Figure 4) yielded dissociation constants of 2, 1.5 and 4.8 μM for hDUT, $hDUT^{F158W}$ and $hDUT^{F158A}$, respectively (Table 1). This implies that changing one aromatic side chain to another does not affect the substrate binding affinity of dUTPase, while loss of the aromatic residue results in a 3-fold affinity decrease only. This phenomenon may be explained by earlier suggestions that the high selectivity and substrate specificity of dUTPase is provided by accommodation of the uridine moiety into a conserved β-hairpin via H-bonds (13). This binding site is apparently independent of the protein segment conferring the aromatic residue involved in the π–π interaction with the uracil ring.

DISCUSSION

As a summary of the above presented results, we found that (i) the geometry of the face-to-face offset stacking interaction between the substrate nucleotide and dUTPase is conserved; (ii) the aromatic residue involved in this interaction is interchangeable with another

Downloaded from https://academic.oup.com/nar/article/38/20/7179/1309070 by guest on 04 November 2021

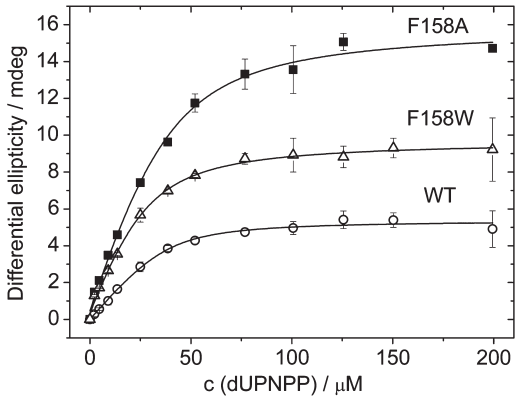

Figure 4. The effect of the loss of the aromatic interaction on substrate binding was investigated by the titration of 50 μM protein with the substrate-analog dUPNPP using the CD signal of the enzyme–substrate complex. Smooth lines represent quadratic fits to the data which yielded K_d values indicated in Table 1.

aromatic residue without structural and/or enzymatic alterations; (iii) loss of the π–π interaction does not affect the ground-state active-site conformation in the alanine mutant; and (iv) results in a significant 20–30-fold decrease in the rate constant of the chemical step. Of the known kinetic steps, the present paper focuses on the chemical step as we obtained proof of its rate-limitation by performing STO experiments in increasing concentration regimes until the rates were unchanged. As to products release, we could not measure the rate constant of dUMP dissociation from the enzyme–products complex in lack of a detectable signal in $hDUT^{F158A}$. However, even if the loss of aromatic interaction affects the otherwise fast [$\approx 1000\,s^{-1}$ (23)] dUMP dissociation, it is probably not manifested in the steady-state rate.

The relative energy states of the π−π interaction during the course of the reaction is of significance in order to understand the contribution it makes to the acceleration of the chemical event. We have three independent sets of evidences that help compiling a comprehensive picture of the behavior of the stacking interaction along the reaction trajectory.

(1) First, we have to consider the energy contribution of the aromatic interaction to the ground state enzyme–substrate complex. The small increase in $K_{d,\ dUPNPP}$ (Table 1) in the $hDUT^{F158A}$ mutant indicates that the aromatic interaction slightly stabilizes the enzyme–substrate complex. The geometry of the Phe relative to uracil would suggest a weakly repulsive interaction in a Phe–Phe model system (26) nevertheless, uracil is a heterocycle thus it may induce electrostatic polarization [dipole magnitude = 5.4 D (27)] in its interacting partner and such an effect may favor the observed geometry in the Phe–uracil interaction.

(2) A second piece of relevant information arises from the calculation of the incremental activation energy ($\Delta\Delta G^{\ddagger}$) upon loss of the aromatic interaction. Using the Eyring–Polanyi equation [Equation (1)] and the measured rate constants for the chemical step, we calculated the $\Delta\Delta G^{\ddagger}$ to be 1.9 kcal mol^{-1} for $hDUT^{F158A}$. This value corresponds to the energy of a typical aromatic interaction (11) and considering that no structural changes could be detected in the mutants, we may argue that the calculated $\Delta\Delta G^{\ddagger}$ in the largest part is specifically attributable to the loss of the aromatic interaction. If we calculate the incremental Gibbs free energy [$\Delta\Delta G_b$, Equation (2)] we obtain a higher 2.6 kcal mol^{-1} value due to the fact that K_M is also somewhat affected.

(3) The third line of evidence is yielded by the intrinsic fluorescence change observed during the course of the reaction. The aromatic stacking between the uracil ring of the ligand and the single Trp residue in $hDUT^{F158W}$ and $mtDUT^{H145W}$ reports on the ligand-bound state of the active site with a characteristic fluorescence quench [Figure 5A and (23)]. The fluorescence quench is relatively small when the product dUMP is bound while it is much larger upon binding to the slowly hydrolysable substrate analog dUPNPP (note that the extent of dUPNPP hydrolysis is negligible during such an experiment). The largest quench is observed in an actively cycling enzyme (i.e. in the presence of dUTP). Since the rate-limiting step of the enzymatic cycle is the hydrolysis step itself and the subsequent product release is fast, in the presence of large amounts of dUTP most of the enzyme population will be in a hydrolysis-competent (close-to-transition or pre-hydrolysis) state. Therefore, the signal difference between dUPNPP and dUTP may lie in the fact that dUPNPP cannot efficiently induce the hydrolysis-competent conformation. It also suggests that going through the transition state (TS) results in further fluorescence quench probably owing to an enhanced aromatic interaction between the substrate and the enzyme. In a representative STO measurement shown in Figure 5B [c.f. Toth *et al.* (23)], the rate constant of fluorescence recovery, i.e. the exit from the low fluorescence conformational state, is identical with that measured for the hydrolysis step in the chemical quench experiments (Figure 3B). This also implies that the most highly quenched fluorescence enzyme–ligand conformation is related to the hydrolysis event.

$$k = \left(\frac{k_B T}{h}\right) \exp\left(\frac{-\Delta G^{\ddagger}}{RT}\right) \quad (1)$$

$$\Delta\Delta G_b = -RT\ln\frac{(k_{cat}/K_M)_1}{(k_{cat}/K_M)_2} \quad (2)$$

k_B : Boltzman constant

h: Planks constant

R : Universal gas constant

As schematically presented in Figure 6, the hydrolysis reaction most probably occurs through an associative

Downloaded from https://academic.oup.com/nar/article/38/20/7179/1309070 by guest on 04 November 2021

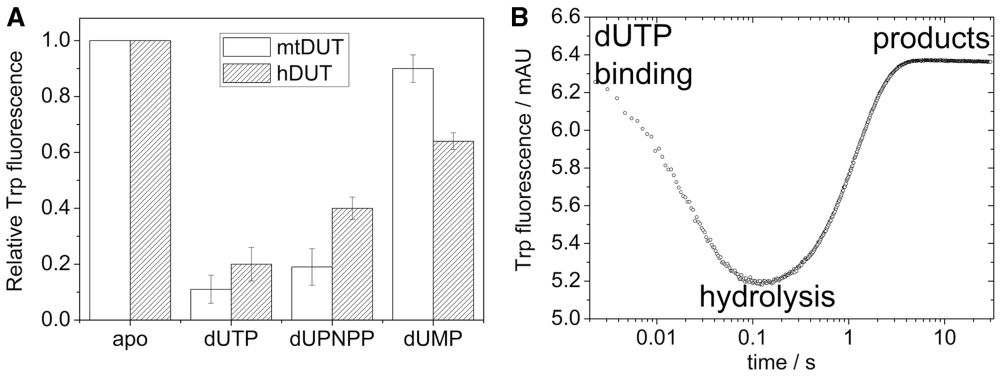

Figure 5. The Trp fluorescence of $hDUT^{F158W}$ and $mtDUT^{H145W}$ reflects the relative energy changes of the π–π interaction during the enzymatic cycle. (**A**) Maximal fluorescence changes upon substrate or product binding to the Trp-bearing active site of $mtDUT^{H145W}$ (white bars) and of $hDUT^{F158W}$ (grey bars). The aromatic stacking between the uracil ring of the ligand and the Trp residue conveys a characteristic fluorescence quench with similar ligand-dependent tendency in both enzymes [human dUTPase data from (23)]. The largest quench is observed in an actively cycling enzyme (i.e. in the presence of dUTP). (**B**) Fluorescence changes on a rapid logarithmic time base in a STO stopped-flow experiment presented above. Similar fluorescence behavior has been reported for the human dUTPase (23), hence we only show that of the $mtDUT^{H145W}$ here. Upon mixing dUTPase with dUTP, a large and rapid fluorescence quench is observed which reflect substrate binding and subsequent conformational changes of the active site. Fluorescence then recovers to its near starting level (depending on the concentration of dUMP present in the solution). The rate constant of fluorescence recovery, i.e. the exit from the low fluorescence conformational state, is identical in a STO case with that of the hydrolysis step (23).

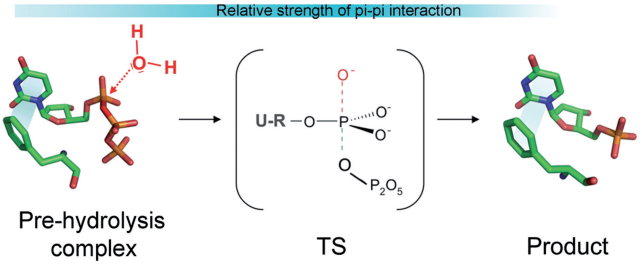

Figure 6. Schematic representation of the associative-type hydrolysis reaction catalyzed by dUTPase is shown in this figure. Stick models are based on the structures 2HQU and 1SEH conferring the ligands dUPNPP and dUMP, respectively. The TS is most probably pentacovalent and electron rich (14,25).

mechanism (25) in which the TS complex is electron rich, particularly in the proximity of the α-phosphate. Based upon the above supports, weak stabilization of the reactants complex and increased stabilization of the TS seems to offer a plausible explanation for the rate acceleration brought about by the aromatic stacking interaction. As dUTPase does not go through large conformational changes during its enzymatic cycle, its catalytic effect is likely due to long-range electrostatic stabilization and/or by geometry optimization of the TS. This report shows that one of the important contributions to this electrostatic effect comes from the investigated aromatic interaction.

Our results are in good agreement with a paper by Kaukinen *et al.* (28) that investigated the effect of stacking on self-catalyzed phosphodiester bond hydrolysis in linear single-stranded nucleic acid polymers. Their associative-type reaction mechanism and the TS geometry are comparable to the one we investigated. They found that enhancement of base stacking during the course of the reaction was an important rate accelerating and TS stabilizing factor. The stabilization energy was calculated to be 0.72–2.8 kcal mol^{-1}. Importantly, they also found that strong base–base interactions in the initial state considerably retarded the reaction due to ground state stabilization. The slightly unfavorable geometry of the Phe–uracil interaction in the initial substrate-bound state of our system may efficiently be tuned up by increasing the lateral offset of the two aromatic rings (26). This can be brought about by movement of the aromatic residue in its plane to the direction of the δ^1 atom (c.f. Figure 1B) without steric hindrance. The concept of stacking enhancement during the course of the dUTPase reaction is consistent with all of our results and calculations. This could, in fact, be a rather general mode of rate acceleration by electrostatic TS stabilization.

ACCESSION NUMBERS

3HZA, 3LOJ.

SUPPLEMENTARY DATA

Supplementary Data are available at NAR Online.

ACKNOWLEDGEMENTS

We thank Anna Lopata and Imre Zagyva for protein production and crystallization. We appreciate the support from Paul Tucker and Santosh Panjikar beamline scientists at the synchrotron beamline X12 at DESY/EMBL-Hamburg during diffraction data collection.

FUNDING

US National Institutes of Health (grant number 1R01TW008130-01); Howard Hughes Medical Institutes (grant number 55000342); Hungarian Scientific Research Funds (grant numbers PD72008, CK-78646, K68229,

Downloaded from https://academic.oup.com/nar/article/38/20/7179/1309070 by guest on 04 November 2021

K72973, NI68466); National Office for Research and Technology, Hungary (grant number JÁP_TSZ_071128_TB_INTER); EU FP6 (grant numbers: SPINE2c LSHG-CT-2006-031220, TEACH-SG LSSG-CT-2007-037198). Funding for open access charge: National Institutes of Health (grant number 1R01TW008130-01).

Conflict of interest statement. None declared.

REFERENCES

1. Meyer,E.A., Castellano,R.K. and Diederich,F. (2003) Interactions with aromatic rings in chemical and biological recognition. *Angew. Chem. Int. Ed. Engl.*, **42**, 1210–1250.
2. Hobza,P. and Sponer,J. (1999) Structure, energetics, and dynamics of the nucleic Acid base pairs: nonempirical ab initio calculations. *Chem. Rev.*, **99**, 3247–3276.
3. Blakaj,D.M., McConnell,K.J., Beveridge,D.L. and Baranger,A.M. (2001) Molecular dynamics and thermodynamics of protein-RNA interactions: mutation of a conserved aromatic residue modifies stacking interactions and structural adaptation in the U1A-stem loop 2 RNA complex. *J. Am. Chem. Soc.*, **123**, 2548–2551.
4. Hughes,R.M. and Waters,M.L. (2006) Model systems for beta-hairpins and beta-sheets. *Curr. Opin. Struct. Biol.*, **16**, 514–524.
5. Zhou,Z. and Swenson,R.P. (1996) The cumulative electrostatic effect of aromatic stacking interactions and the negative electrostatic environment of the flavin mononucleotide binding site is a major determinant of the reduction potential for the flavodoxin from Desulfovibrio vulgaris [Hildenborough]. *Biochemistry*, **35**, 15980–15988.
6. Versees,W., Loverix,S., Vandemeulebroucke,A., Geerlings,P. and Steyaert,J. (2004) Leaving group activation by aromatic stacking: an alternative to general acid catalysis. *J. Mol. Biol.*, **338**, 1–6.
7. Swenson,R.P. and Krey,G.D. (1994) Site-directed mutagenesis of tyrosine-98 in the flavodoxin from Desulfovibrio vulgaris (Hildenborough): regulation of oxidation-reduction properties of the bound FMN cofactor by aromatic, solvent, and electrostatic interactions. *Biochemistry*, **33**, 8505–8514.
8. Mao,L., Wang,Y., Liu,Y. and Hu,X. (2004) Molecular determinants for ATP-binding in proteins: a data mining and quantum chemical analysis. *J. Mol. Biol.*, **336**, 787–807.
9. Guo,X., Chen,X., Weber,I.T., Harrison,R.W. and Tai,P.C. (2006) Molecular basis for differential nucleotide binding of the nucleotide-binding domain of ABC-transporter CvaB. *Biochemistry*, **45**, 14473–14480.
10. Rickert,K.W., Schaber,M., Torrent,M., Neilson,L.A., Tasber,E.S., Garbaccio,R., Coleman,P.J., Harvey,D., Zhang,Y., Yang,Y. *et al.* (2008) Discovery and biochemical characterization of selective ATP competitive inhibitors of the human mitotic kinesin KSP. *Arch. Biochem. Biophys.*, **469**, 220–231.
11. Boehr,D.D., Farley,A.R., Wright,G.D. and Cox,J.R. (2002) Analysis of the pi-pi stacking interactions between the aminoglycoside antibiotic kinase APH(3′)-IIIa and its nucleotide ligands. *Chem. Biol.*, **9**, 1209–1217.
12. Vertessy,B.G. and Toth,J. (2009) Keeping uracil out of DNA: physiological role, structure and catalytic mechanism of dUTPases. *Acc. Chem. Res.*, **42**, 97–106.
13. Mol,C.D., Harris,J.M., McIntosh,E.M. and Tainer,J.A. (1996) Human dUTP pyrophosphatase: uracil recognition by a beta hairpin and active sites formed by three separate subunits. *Structure*, **4**, 1077–1092.
14. Varga,B., Barabas,O., Kovari,J., Toth,J., Hunyadi-Gulyas,E., Klement,E., Medzihradszky,K.F., Tolgyesi,F., Fidy,J. and Vertessy,B.G. (2007) Active site closure facilitates juxtaposition of reactant atoms for initiation of catalysis by human dUTPase. *FEBS Lett.*, **581**, 4783–4788.
15. Varga,B., Migliardo,F., Takacs,E., Vertessy,B. and Magazù,S. (2008) Experimental study on dUTPase-inhibitor candidate and dUTPase/disaccharide mixtures by PCS and ENS. *J. Mol. Struct.*, **886**, 128–135.
16. Varga,B., Barabas,O., Takacs,E., Nagy,N., Nagy,P. and Vertessy,B.G. (2008) Active site of mycobacterial dUTPase: structural characteristics and a built-in sensor. *Biochem. Biophys. Res. Commun.*, **373**, 8–13.
17. Kabsch,W. (1993) Automatic processing of rotation diffraction data from crystals of initially unknown symmetry and cell constants. *J. Appl. Cryst.*, **26**, 795–800.
18. CCP4. (1994) The CCP4 suite. Programs for protein crystallography. *Acta. Crystallogr. D Biol. Crystallogr.*, **50**, 760–763.
19. Vagin,A. and Teplyakov,A. (1997) MOLREP: an automated program for molecular replacement. *J. Appl. Crystallogr.*, **30**, 1022–1025.
20. Emsley,P. and Cowtan,K. (2004) Coot: model-building tools for molecular graphics. *Acta. Crystallogr. D Biol. Crystallogr.*, **60**, 2126–2132.
21. Sheldrick,G.M. (2008) A short history of SHELX. *Acta. Crystallogr. A*, **64**, 112–122.
22. Vertessy,B.G., Persson,R., Rosengren,A.M., Zeppezauer,M. and Nyman,P.O. (1996) Specific derivatization of the active site tyrosine in dUTPase perturbs ligand binding to the active site. *Biochem. Biophys. Res. Commun.*, **219**, 294–300.
23. Toth,J., Varga,B., Kovacs,M., Malnasi-Csizmadia,A. and Vertessy,B.G. (2007) Kinetic mechanism of human dUTPase, an essential nucleotide pyrophosphatase enzyme. *J. Biol. Chem.*, **282**, 33572–33582.
24. Chan,S., Segelke,B., Lekin,T., Krupka,H., Cho,U.S., Kim,M.Y., So,M., Kim,C.Y., Naranjo,C.M., Rogers,Y.C. *et al.* (2004) Crystal structure of the Mycobacterium tuberculosis dUTPase: insights into the catalytic mechanism. *J. Mol. Biol.*, **341**, 503–517.
25. Barabas,O., Pongracz,V., Kovari,J., Wilmanns,M. and Vertessy,B.G. (2004) Structural insights into the catalytic mechanism of phosphate ester hydrolysis by dUTPase. *J. Biol. Chem.*, **279**, 42907–42915.
26. Hunter,C.A., Singh,J. and Thornton,J.M. (1991) Pi-pi interactions: the geometry and energetics of phenylalanine-phenylalanine interactions in proteins. *J. Mol. Biol.*, **218**, 837–846.
27. Kulakowska,I., Geller,M., Lesyng,B. and Wierzchowski,K.L. (1974) Dipole moments of 2,4-diketopyrimidines. II. Uracil, thymine and their derivatives. *Biochim. Biophys. Acta.*, **361**, 119–130.
28. Kaukinen,U., Lonnberg,H. and Perakyla,M. (2004) Stabilisation of the transition state of phosphodiester bond cleavage within linear single-stranded oligoribonucleotides. *Org. Biomol. Chem.*, **2**, 66–73.
29. Sablin,E.P., Case,R.B., Dai,S.C., Hart,C.L., Ruby,A., Vale,R.D. and Fletterick,R.J. (1998) Direction determination in the minus-end-directed kinesin motor ncd. *Nature*, **395**, 813–816.
30. Zaitseva,J., Jenewein,S., Jumpertz,T., Holland,I.B. and Schmitt,L. (2005) H662 is the linchpin of ATP hydrolysis in the nucleotide-binding domain of the ABC transporter HlyB. *EMBO J.*, **24**, 1901–1910.

Downloaded from https://academic.oup.com/nar/article/38/20/7179/1309070 by guest on 04 November 2021

Aromatic stacking between nucleobase and enzyme promotes phosphate ester hydrolysis in dUTPase

Ildiko Pecsi[a,1], Ibolya Leveles[a,1], Veronika Harmat[b], Beata G. Vertessy[a,c] and Judit Toth[a]

[a]Institute of Enzymology, Biological Research Center, Hungarian Academy of Sciences, Budapest, Hungary
[b]Hungarian Academy of Sciences-Eötvös Loránd University, Protein Modeling Research Group, and Eötvös Loránd University, Institute of Chemistry, Budapest, Hungary
[c]Department of Applied Biotechnology, Budapest University of Technology and Economics, Budapest, Hungary

[1] These authors contributed equally to this work.

Corresponding author:

Judit Toth
Institute of Enzymology
Karolina út 29, H-1113, Budapest, Hungary
Phone: +36 1 2793142
fax: +36 1 4665465
e-mail: tothj@enzim.hu

Supplementary Contents:

Figures (3 figures)	2
References	6
Table	7

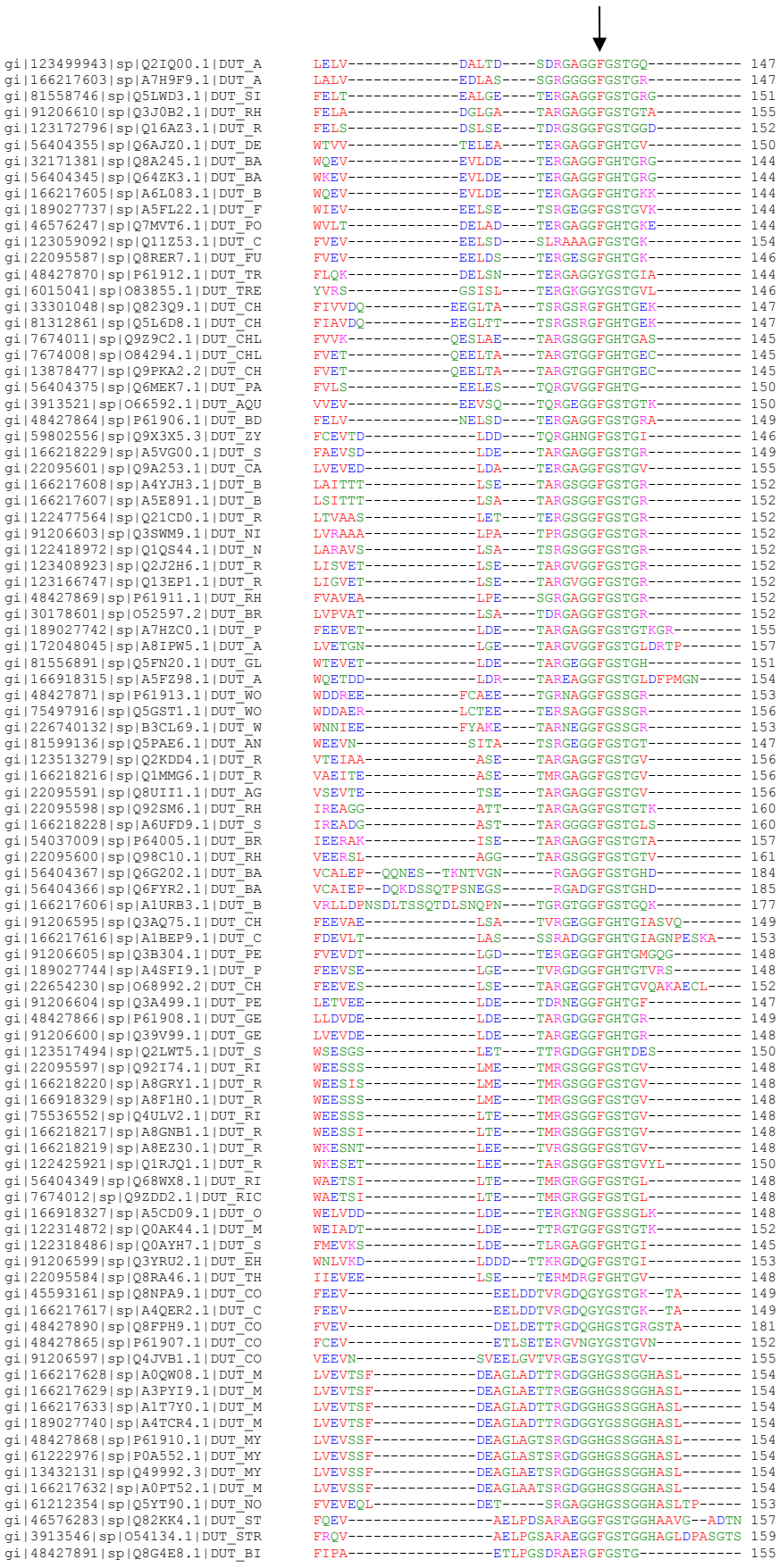
gi|123499943|sp|Q2IQ00.1|DUT_A LELV----------DALTD----SDRGAGGFGSTGQ---------- 147
gi|166217603|sp|A7H9F9.1|DUT_A LALV----------EDLAS----SGRGGGGFGSTGR---------- 147
gi|81558746|sp|Q5LWD3.1|DUT_SI FELT----------EALGE----TERGAGGFGSTGRG--------- 151
gi|91206610|sp|Q3J0B2.1|DUT_RH FELA----------DGLGA----TARGAGGFGSTGTA--------- 155
gi|123172796|sp|Q16AZ3.1|DUT_R FELS----------DSLSE----TDRGSGGFGSTGGD--------- 152
gi|56404355|sp|Q6AJZ0.1|DUT_DE WTVV----------TELEA----TERGAGGFGHTGV---------- 150
gi|32171381|sp|Q8A245.1|DUT_BA WQEV----------EVLDE----TERGAGGFGHTGRG--------- 144
gi|56404345|sp|Q64ZK3.1|DUT_BA WKEV----------EVLDE----TERGAGGFGHTGRG--------- 144
gi|166217605|sp|A6L083.1|DUT_B WQEV----------EVLDE----TERGAGGFGHTGKK--------- 144
gi|189027737|sp|A5FL22.1|DUT_F WIEV----------EELSE----TSRGEGGFGSTGVK--------- 144
gi|46576247|sp|Q7MVT6.1|DUT_PO WVLT----------DELAD----TERGAGGFGHTGKE--------- 144
gi|123059092|sp|Q11Z53.1|DUT_C FVEV----------EELSD----SLRAAAGFGSTGK---------- 154
gi|22095587|sp|Q8RER7.1|DUT_FU FVEV----------EELDS----TERGESGFGHTGK---------- 146
gi|48427870|sp|P61912.1|DUT_TR FLQK----------DELSN----TERGAGGYGSTGIA--------- 144
gi|6015041|sp|O83855.1|DUT_TRE YVRS----------GSISL----TERGKGGYGSTGVL--------- 146
gi|33301048|sp|Q823Q9.1|DUT_CH FIVVDQ----------EEGLTA----TSRGSRGFGHTGEK--------- 147
gi|81312861|sp|Q5L6D8.1|DUT_CH FIAVDQ----------EEGLTT----TSRGSRGFGHTGEK--------- 147
gi|7674011|sp|Q9Z9C2.1|DUT_CHL FVVK----------QESLAE----TARGSGGFGHTGAS--------- 145
gi|7674008|sp|O84294.1|DUT_CHL FVET----------QEELTA----TARGTGGFGHTGEC--------- 145
gi|13878477|sp|Q9PKA2.2|DUT_CH FVET----------QEELTA----TARGTGGFGHTGEC--------- 145
gi|56404375|sp|Q6MEK7.1|DUT_PA FVLS----------EELES----TQRGVGGFGHTG---------- 150
gi|3913521|sp|O66592.1|DUT_AQU VVEV----------EEVSQ----TQRGEGGFGSTGTK--------- 150
gi|48427864|sp|P61906.1|DUT_BD FELV----------NELSD----TERGAGGFGSTGRA--------- 149
gi|59802556|sp|Q9X3X5.3|DUT_ZY FCEVTD----------LDD----TQRGHNGFGSTGI---------- 146
gi|166218229|sp|A5VG00.1|DUT_S FAEVSD----------LDE----TARGAGGFGSTGR---------- 149
gi|22095601|sp|Q9A253.1|DUT_CA LVEVED----------LDA----TERGAGGFGSTGV---------- 155
gi|166217608|sp|A4YJH3.1|DUT_B LAITTT----------LSE----TARGSGGFGSTGR---------- 152
gi|166217607|sp|A5E891.1|DUT_B LSITTT----------LSA----TARGSGGFGSTGR---------- 152
gi|122477564|sp|Q21CD0.1|DUT_R LTVAAS----------LET----TERGSGGFGSTGR---------- 152
gi|91206603|sp|Q3SWM9.1|DUT_NI LVRAAA----------LPA----TPRGSGGFGSTGR---------- 152
gi|122418972|sp|Q1QS44.1|DUT_N LARAVS----------LSA----TSRGSGGFGSTGR---------- 152
gi|123408923|sp|Q2J2H6.1|DUT_R LISVET----------LSE----TARGVGGFGSTGR---------- 152
gi|123166747|sp|Q13EP1.1|DUT_R LIGVET----------LSE----TARGVGGFGSTGR---------- 152
gi|48427869|sp|P61911.1|DUT_RH FVAVEA----------LPE----SGRGAGGFGSTGR---------- 152
gi|30178601|sp|O52597.2|DUT_BR LVPVAT----------LSA----TDRGAGGFGSTGR---------- 152
gi|189027742|sp|A7HZC0.1|DUT_P FEEVET----------LDE----TARGAGGFGSTGTKGR-------- 155
gi|172048045|sp|A8IPW5.1|DUT_A LVETGN----------LGE----TARGVGGFGSTGLDRTP------- 157
gi|81556891|sp|Q5FN20.1|DUT_GL WTEVET----------LDE----TARGEGGFGSTGH---------- 151
gi|166918315|sp|A5FZ98.1|DUT_A WQETDD----------LDR----TAREAGGFGSTGLDFPMGN----- 154
gi|48427871|sp|P61913.1|DUT_WO WDDREE----------FCAEE----TGRNAGGFGSSGR---------- 153
gi|75497916|sp|Q5GST1.1|DUT_WO WDDAER----------LCTEE----TERSAGGFGSSGR---------- 156
gi|226740132|sp|B3CL69.1|DUT_W WNNIEE----------FYAKE----TARNEGGFGSSGR---------- 153
gi|81599136|sp|Q5PAE6.1|DUT_AN WEEVN----------SITA----TSRGEGGFGSTGT---------- 147
gi|123513279|sp|Q2KDD4.1|DUT_R VTEIAA----------ASE----TARGAGGFGSTGV---------- 156
gi|166218216|sp|Q1MMG6.1|DUT_R VAEITE----------ASE----TMRGAGGFGSTGV---------- 156
gi|22095591|sp|Q8UII1.1|DUT_AG VSEVTE----------TSE----TARGAGGFGSTGV---------- 156
gi|22095598|sp|Q92SM6.1|DUT_RH IREAGG----------ATT----TARGAGGFGSTGTK--------- 160
gi|166218228|sp|A6UFD9.1|DUT_S IREADG----------AST----TARGGGGFGSTGLS--------- 160
gi|54037009|sp|P64005.1|DUT_BR IEERAK----------ISE----TARGAGGFGSTGTA--------- 157
gi|22095600|sp|Q98C10.1|DUT_RH VEERSL----------AGG----TARGSGGFGSTGTV--------- 161
gi|56404367|sp|Q6G202.1|DUT_BA VCALEP--QQNES--TKNTVGN------RGAGGFGSTGHD--------- 184
gi|56404366|sp|Q6FYR2.1|DUT_BA VCAIEP--DQKDSSQTPSNEGS------RGADGFGSTGHD--------- 185
gi|166217606|sp|A1URB3.1|DUT_B VRLLDPNSDLTSSQTDLSNQPN----TGRGTGGFGSTGQK--------- 177
gi|91206595|sp|Q3AQ75.1|DUT_CH FEEVAE----------LSA----TVRGEGGFGHTGIASVQ------- 149
gi|166217616|sp|A1BEP9.1|DUT_C FDEVLT----------LAS----SSRADGGFGHTGIAGNPESKA--- 153
gi|91206605|sp|Q3B304.1|DUT_PE FVEVDT----------LGD----TERGEGGFGHTGMGQG-------- 148
gi|189027744|sp|A4SFI9.1|DUT_P FEEVSE----------LGE----TVRGDGGFGHTGTVRS-------- 148
gi|22654230|sp|O68992.2|DUT_CH FEEVES----------LSE----TARGEGGFGHTGVQAKAECL---- 152
gi|91206604|sp|Q3A499.1|DUT_PE LETVEE----------LDE----TDRNEGGFGHTGF---------- 147
gi|48427866|sp|P61908.1|DUT_GE LLDVDE----------LDE----TARGDGGFGHTGR---------- 149
gi|91206600|sp|Q39V99.1|DUT_GE LVEVDE----------LDE----TARGEGGFGHTGR---------- 148
gi|123517494|sp|Q2LWT5.1|DUT_S WSESGS----------LET----TTRGDGGFGHTDES--------- 150
gi|22095597|sp|Q92I74.1|DUT_RI WEESSS----------LME----TMRGSGGFGSTGV---------- 148
gi|166218220|sp|A8GRY1.1|DUT_R WEESIS----------LME----TMRGSGGFGSTGV---------- 148
gi|166918329|sp|A8F1H0.1|DUT_R WEESSS----------LME----TMRGSGGFGSTGV---------- 148
gi|75536552|sp|Q4ULV2.1|DUT_RI WEESSS----------LTE----TMRGSGGFGSTGV---------- 148
gi|166218217|sp|A8GNB1.1|DUT_R WEESSI----------LTE----TMRGSGGFGSTGV---------- 148
gi|166218219|sp|A8EZ30.1|DUT_R WKESNT----------LEE----TVRGSGGFGSTGV---------- 148
gi|122425921|sp|Q1RJQ1.1|DUT_R WKESET----------LEE----TARGSGGFGSTGVYL--------- 150
gi|56404349|sp|Q68WX8.1|DUT_RI WAETSI----------LTE----TMRGRGGFGSTGL---------- 148
gi|7674012|sp|Q9ZDD2.1|DUT_RIC WAETSI----------LTE----TMRGRGGFGSTGL---------- 148
gi|166918327|sp|A5CD09.1|DUT_O WELVDD----------LDE----TERGKNGFGSSGLK--------- 148
gi|122314872|sp|Q0AK44.1|DUT_M WEIADT----------LDE----TTRGTGGFGSTGTK--------- 152
gi|122318486|sp|Q0AYH7.1|DUT_S FMEVKS----------LDE----TLRGAGGFGHTGI---------- 145
gi|91206599|sp|Q3YRU2.1|DUT_EH WNLVKD----------LDDD--TTKRGDQGFGSTGI---------- 153
gi|22095584|sp|Q8RA46.1|DUT_TH IIEVEE----------LSE----TERMDRGFGHTGV---------- 148
gi|45593161|sp|Q8NPA9.1|DUT_CO FEEV----------EELDDTVRGDQGYGSTGK--TA------- 149
gi|166217617|sp|A4QER2.1|DUT_C FEEV----------EELDDTVRGDQGYGSTGK--TA------- 149
gi|48427890|sp|Q8FPH9.1|DUT_CO FVEV----------DELDETTRGDQGHGSTGRGSTA------- 181
gi|48427865|sp|P61907.1|DUT_CO FCEV----------ETLSETERGVNGYGSTGVN---------- 152
gi|91206597|sp|Q4JVB1.1|DUT_CO VEEVN----------SVEELGVTVRGESGYGSTGV---------- 155
gi|166217628|sp|A0QW08.1|DUT_M LVEVTSF----------DEAGLADTTRGDGGHGSSGGHASL------- 154
gi|166217629|sp|A3PYI9.1|DUT_M LVEVTSF----------DEAGLAETTRGEGGHGSSGGHASL------- 154
gi|166217633|sp|A1T7Y0.1|DUT_M LVEVTSF----------DEAGLADTTRGDGGHGSSGGHASL------- 154
gi|189027740|sp|A4TCR4.1|DUT_M LVEVTSF----------DEAGLADTTRGDGGYGSSGGHASL------- 154
gi|48427868|sp|P61910.1|DUT_MY LVEVSSF----------DEAGLAGTSRGDGGHGSSGGHASL------- 154
gi|61222976|sp|P0A552.1|DUT_MY LVEVSSF----------DEAGLASTSRGDGGHGSSGGHASL------- 154
gi|13432131|sp|Q49992.3|DUT_MY LVEVSSF----------DEAGLAETSRGDGGHGSSGGHASL------- 154
gi|166217632|sp|A0PT52.1|DUT_M LVEVSSF----------DEAGLAATSRGDGGHGSSGGHASL------- 154
gi|61212354|sp|Q5YT90.1|DUT_NO FVEVEQL----------DET-----SRGAGGHGSSGGHASLTP----- 153
gi|46576283|sp|Q82KK4.1|DUT_ST FQEV----------AELPDSARAEGGFGSTGGHAAVG--ADTN 157
gi|3913546|sp|O54134.1|DUT_STR FRQV----------AELPGSARAEGGFGSTGGHAGLDPASGTS 159
gi|48427891|sp|Q8G4E8.1|DUT_BI FIPA----------ETLPGSDRAERGFGSTG---------- 155

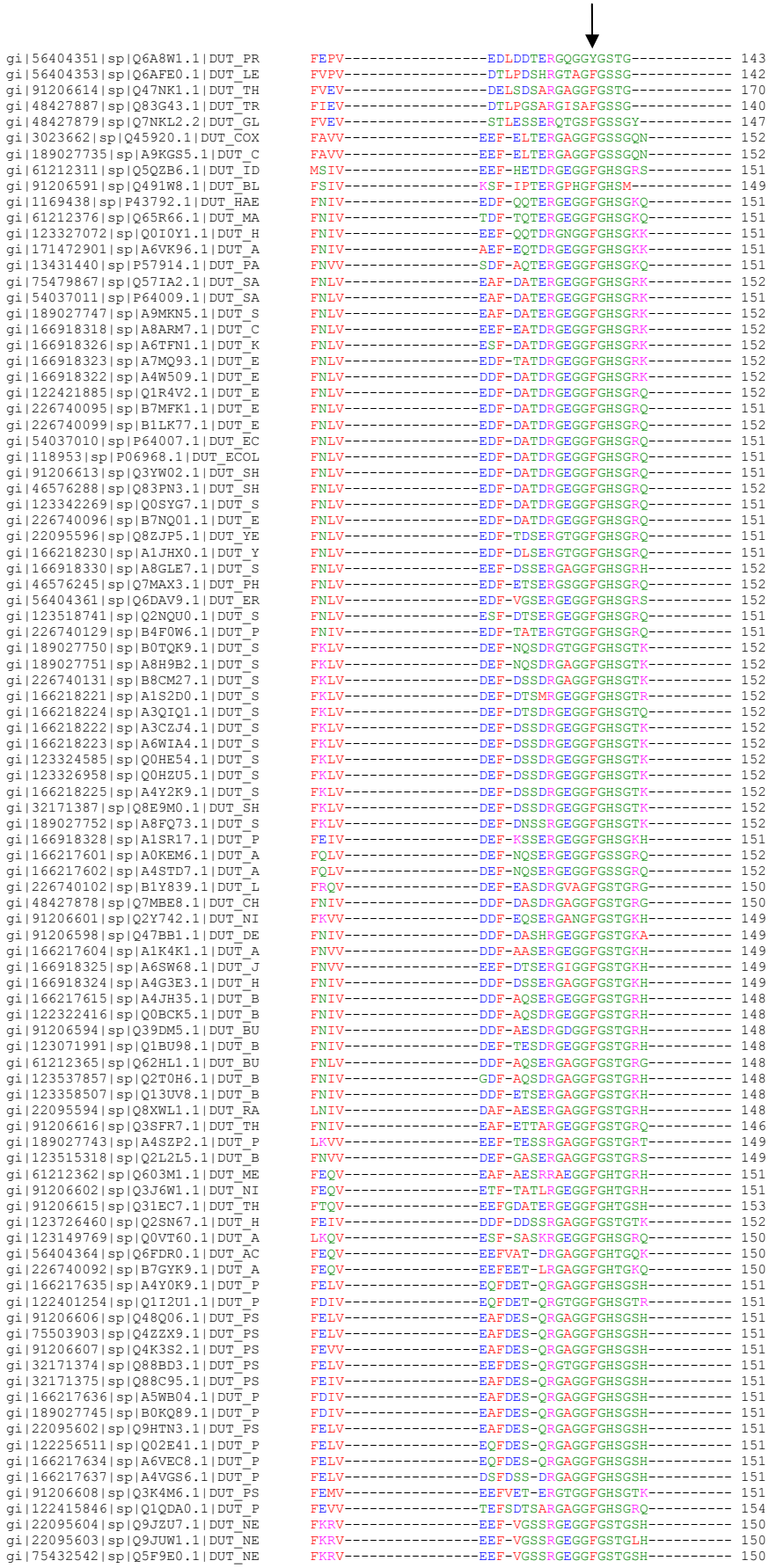
gi|56404351|sp|Q6A8W1.1|DUT_PR FEPV----------EDLDDTERGQGGYGSTG---------- 143
gi|56404353|sp|Q6AFE0.1|DUT_LE FVPV----------DTLPDSHRGTAGFGSSG---------- 142
gi|91206614|sp|Q47NK1.1|DUT_TH FVEV----------DELSDSARGAGGFGSTG---------- 170
gi|48427887|sp|Q83G43.1|DUT_TR FIEV----------DTLPGSARGISAFGSSG---------- 140
gi|48427879|sp|Q7NKL2.2|DUT_GL FVEV----------STLESSERQTGSFGSSGY---------- 147
gi|3023662|sp|Q45920.1|DUT_COX FAVV----------EEF-ELTERGAGGFGSSGQN---------- 152
gi|189027735|sp|A9KGS5.1|DUT_C FAVV----------EEF-ELTERGAGGFGSSGQN---------- 152
gi|61212311|sp|Q5QZB6.1|DUT_ID MSIV----------EEF-HETDRGEGGFGHSGRS---------- 151
gi|91206591|sp|Q491W8.1|DUT_BL FSIV----------KSF-IPTERGPHGFGHSM---------- 149
gi|1169438|sp|P43792.1|DUT_HAE FNIV----------EDF-QQTERGEGGFGHSGKQ---------- 151
gi|61212376|sp|Q65R66.1|DUT_MA FNIV----------TDF-TQTERGEGGFGHSGKQ---------- 151
gi|123327072|sp|Q0I0Y1.1|DUT_H FNIV----------EEF-QQTDRGNGGFGHSGKK---------- 151
gi|171472901|sp|A6VK96.1|DUT_A FNIV----------AEF-EQTDRGEGGFGHSGKK---------- 151
gi|13431440|sp|P57914.1|DUT_PA FNVV----------SDF-AQTERGEGGFGHSGKQ---------- 151
gi|75479867|sp|Q57IA2.1|DUT_SA FNLV----------EAF-DATERGEGGFGHSGRK---------- 152
gi|54037011|sp|P64009.1|DUT_SA FNLV----------EAF-DATERGEGGFGHSGRK---------- 151
gi|189027747|sp|A9MKN5.1|DUT_S FNLV----------EAF-DATERGEGGFGHSGRK---------- 152
gi|166918318|sp|A8ARM7.1|DUT_C FNLV----------EEF-EATDRGEGGFGHSGRK---------- 152
gi|166918326|sp|A6TFN1.1|DUT_K FNLV----------ESF-DATDRGEGGFGHSGRK---------- 152
gi|166918323|sp|A7MQ93.1|DUT_E FNLV----------EDF-TATDRGEGGFGHSGRK---------- 152
gi|166918322|sp|A4W509.1|DUT_E FNLV----------DDF-DATDRGEGGFGHSGRK---------- 152
gi|122421885|sp|Q1R4V2.1|DUT_E FNLV----------EDF-DATDRGEGGFGHSGRQ---------- 152
gi|226740095|sp|B7MFK1.1|DUT_E FNLV----------EDF-DATDRGEGGFGHSGRQ---------- 151
gi|226740099|sp|B1LK77.1|DUT_E FNLV----------EDF-DATDRGEGGFGHSGRQ---------- 152
gi|54037010|sp|P64007.1|DUT_EC FNLV----------EDF-DATDRGEGGFGHSGRQ---------- 151
gi|118953|sp|P06968.1|DUT_ECOL FNLV----------EDF-DATDRGEGGFGHSGRQ---------- 151
gi|91206613|sp|Q3YW02.1|DUT_SH FNLV----------EDF-DATDRGEGGFGHSGRQ---------- 151
gi|46576288|sp|Q83PN3.1|DUT_SH FNLV----------EDF-DATDRGEGGFGHSGRQ---------- 152
gi|123342269|sp|Q0SYG7.1|DUT_S FNLV----------EDF-DATDRGEGGFGHSGRQ---------- 151
gi|226740096|sp|B7NQ01.1|DUT_E FNLV----------EDF-DATDRGEGGFGHSGRQ---------- 151
gi|22095596|sp|Q8ZJP5.1|DUT_YE FNLV----------EDF-TDSERGTGGFGHSGRQ---------- 151
gi|166218230|sp|A1JHX0.1|DUT_Y FNLV----------EDF-DLSERGTGGFGHSGRQ---------- 151
gi|166918330|sp|A8GLE7.1|DUT_S FNLV----------EEF-DSSERGAGGFGHSGRH---------- 152
gi|46576245|sp|Q7MAX3.1|DUT_PH FNLV----------EDF-ETSERGSGGFGHSGRQ---------- 152
gi|56404361|sp|Q6DAV9.1|DUT_ER FNLV----------EDF-VGSERGEGGFGHSGRS---------- 152
gi|123518741|sp|Q2NQU0.1|DUT_S FNLV----------ESF-DTSERGEGGFGHSGRQ---------- 151
gi|226740129|sp|B4F0W6.1|DUT_P FNIV----------EDF-TATERGTGGFGHSGRQ---------- 151
gi|189027750|sp|B0TQK9.1|DUT_S FKLV----------DEF-NQSDRGTGGFGHSGTK---------- 152
gi|189027751|sp|A8H9B2.1|DUT_S FKLV----------DEF-NQSDRGAGGFGHSGTK---------- 152
gi|226740131|sp|B8CM27.1|DUT_S FKLV----------DEF-DSSDRGAGGFGHSGTK---------- 152
gi|166218221|sp|A1S2D0.1|DUT_S FKLV----------DEF-DTSMRGEGGFGHSGTR---------- 152
gi|166218224|sp|A3QIQ1.1|DUT_S FKLV----------DEF-DTSDRGEGGFGHSGTQ---------- 152
gi|166218222|sp|A3CZJ4.1|DUT_S FKLV----------DEF-DSSDRGEGGFGHSGTK---------- 152
gi|166218223|sp|A6WIA4.1|DUT_S FKLV----------DEF-DSSDRGEGGFGHSGTK---------- 152
gi|123324585|sp|Q0HE54.1|DUT_S FKLV----------DEF-DSSDRGEGGFGHSGTK---------- 152
gi|123326958|sp|Q0HZU5.1|DUT_S FKLV----------DEF-DSSDRGEGGFGHSGTK---------- 152
gi|166218225|sp|A4Y2K9.1|DUT_S FKLV----------DEF-DSSDRGEGGFGHSGTK---------- 152
gi|32171387|sp|Q8E9M0.1|DUT_SH FKLV----------DEF-DSSDRGEGGFGHSGTK---------- 152
gi|189027752|sp|A8FQ73.1|DUT_S FKLV----------DEF-DNSSRGEGGFGHSGTK---------- 152
gi|166918328|sp|A1SR17.1|DUT_P FEIV----------DEF-KSSERGEGGFGHSGKH---------- 151
gi|166217601|sp|A0KEM6.1|DUT_A FQLV----------DEF-NQSERGEGGFGSSGRQ---------- 152
gi|166217602|sp|A4STD7.1|DUT_A FQLV----------DEF-NQSERGEGGFGSSGRQ---------- 152
gi|226740102|sp|B1Y839.1|DUT_L FRQV----------DEF-EASDRGVAGFGSTGRG---------- 150
gi|48427878|sp|Q7MBE8.1|DUT_CH FNIV----------DDF-DASDRGAGGFGSTGRG---------- 150
gi|91206601|sp|Q2Y742.1|DUT_NI FKVV----------DDF-EQSERGANGFGSTGKH---------- 149
gi|91206598|sp|Q47BB1.1|DUT_DE FNIV----------DDF-DASHRGEGGFGSTGKA---------- 149
gi|166217604|sp|A1K4K1.1|DUT_A FNVV----------DDF-AASERGEGGFGSTGKH---------- 149
gi|166918325|sp|A6SW68.1|DUT_J FNVV----------EEF-DTSERGIGGFGSTGKH---------- 149
gi|166918324|sp|A4G3E3.1|DUT_H FNIV----------DDF-DSSERGAGGFGSTGKH---------- 149
gi|166217615|sp|A4JH35.1|DUT_B FNIV----------DDF-AQSERGEGGFGSTGRH---------- 148
gi|122322416|sp|Q0BCK5.1|DUT_B FNIV----------DDF-AQSDRGEGGFGSTGRH---------- 148
gi|91206594|sp|Q39DM5.1|DUT_BU FNIV----------DDF-AESDRGDGGFGSTGRH---------- 148
gi|123071991|sp|Q1BU98.1|DUT_B FNIV----------DEF-TESDRGEGGFGSTGRH---------- 148
gi|61212365|sp|Q62HL1.1|DUT_BU FNLV----------DDF-AQSERGAGGFGSTGRG---------- 148
gi|123537857|sp|Q2T0H6.1|DUT_B FNIV----------GDF-AQSDRGAGGFGSTGRH---------- 148
gi|123358507|sp|Q13UV8.1|DUT_B FNIV----------DDF-ETSERGAGGFGSTGKH---------- 148
gi|22095594|sp|Q8XWL1.1|DUT_RA LNIV----------DAF-AESERGAGGFGSTGRH---------- 148
gi|91206616|sp|Q3SFR7.1|DUT_TH FNIV----------EAF-ETTARGEGGFGSTGRQ---------- 146
gi|189027743|sp|A4SZP2.1|DUT_P LKVV----------EEF-TESSRGAGGFGSTGRT---------- 149
gi|123515318|sp|Q2L2L5.1|DUT_B FNVV----------DEF-GASERGAGGFGSTGRS---------- 149
gi|61212362|sp|Q603M1.1|DUT_ME FEQV----------EAF-AESRRAEGGFGHTGRH---------- 151
gi|91206602|sp|Q3J6W1.1|DUT_NI FEQV----------ETF-TATLRGEGGFGHTGRH---------- 151
gi|91206615|sp|Q31EC7.1|DUT_TH FTQV----------EEFGDATERGEGGFGHTGSH---------- 153
gi|123726460|sp|Q2SN67.1|DUT_H FEIV----------DDF-DDSSRGAGGFGSTGTK---------- 152
gi|123149769|sp|Q0VT60.1|DUT_A LKQV----------ESF-SASKRGEGGFGHSGRQ---------- 150
gi|56404364|sp|Q6FDR0.1|DUT_AC FEQV----------EEFVAT-DRGAGGFGHTGQK---------- 150
gi|226740092|sp|B7GYK9.1|DUT_A FEQV----------EEFEET-LRGAGGFGHTGKQ---------- 150
gi|166217635|sp|A4Y0K9.1|DUT_P FELV----------EQFDET-QRGAGGFGHSGSH---------- 151
gi|122401254|sp|Q1I2U1.1|DUT_P FDIV----------EQFDET-QRGTGGFGHSGTR---------- 151
gi|91206606|sp|Q48Q06.1|DUT_PS FELV----------EAFDES-QRGAGGFGHSGSH---------- 151
gi|75503903|sp|Q4ZZX9.1|DUT_PS FELV----------EAFDES-QRGAGGFGHSGSH---------- 151
gi|91206607|sp|Q4K3S2.1|DUT_PS FEVV----------EAFDES-QRGAGGFGHSGSH---------- 151
gi|32171374|sp|Q88BD3.1|DUT_PS FELV----------EEFDES-QRGTGGFGHSGSH---------- 151
gi|32171375|sp|Q88C95.1|DUT_PS FEIV----------EAFDES-QRGAGGFGHSGSH---------- 151
gi|166217636|sp|A5WB04.1|DUT_P FDIV----------EAFDES-QRGAGGFGHSGSH---------- 151
gi|189027745|sp|B0KQ89.1|DUT_P FDIV----------EAFDES-QRGAGGFGHSGSH---------- 151
gi|22095602|sp|Q9HTN3.1|DUT_PS FELV----------EAFDES-QRGAGGFGHSGSH---------- 151
gi|122256511|sp|Q02E41.1|DUT_P FELV----------EQFDES-QRGAGGFGHSGSH---------- 151
gi|166217634|sp|A6VEC8.1|DUT_P FELV----------EQFDES-QRGAGGFGHSGSH---------- 151
gi|166217637|sp|A4VGS6.1|DUT_P FELV----------DSFDSS-DRGAGGFGHSGSH---------- 151
gi|91206608|sp|Q3K4M6.1|DUT_PS FEMV----------EEFVET-ERGTGGFGHSGTK---------- 151
gi|122415846|sp|Q1QDA0.1|DUT_P FEVV----------TEFSDTSARGAGGFGHSGRQ---------- 154
gi|22095604|sp|Q9JZU7.1|DUT_NE FKRV----------EEF-VGSSRGEGGFGSTGSH---------- 150
gi|22095603|sp|Q9JUW1.1|DUT_NE FKRV----------EEF-VGSSRGEGGFGSTGLH---------- 150
gi|75432542|sp|Q5F9E0.1|DUT_NE FKRV----------EEF-VGSSRGEGGFGSTGSH---------- 150

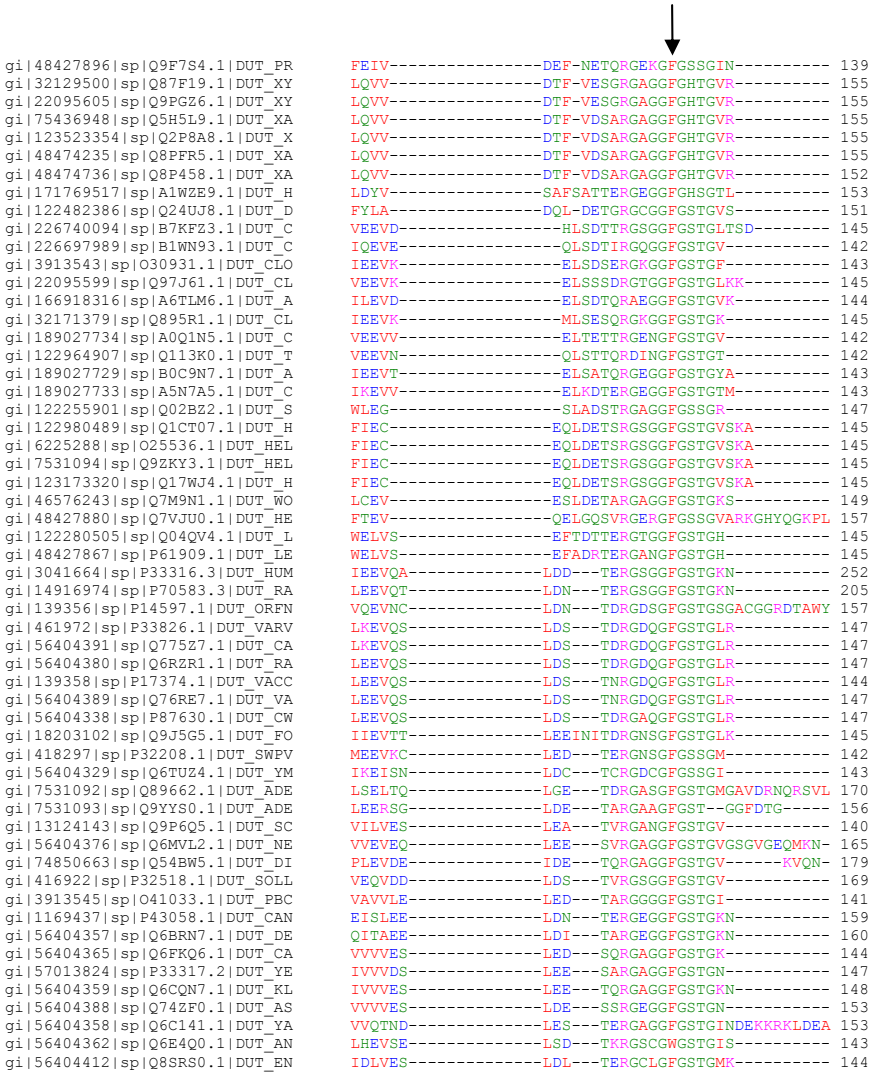

Figure S1. Amino acid sequence alignment shows the conservation of the aromatic residue in dUTPases

Trimeric dUTPases share a high sequence and structural similarity across species. We searched for homologues of the nuclear isoform of hDUT in the Non-redundant protein sequences (nr) database using the blastp tool of NCBI. The sequences of the first 500 hits were used to create an alignment using ClustalW2 (EMBL-EBI). The figure shows a portion of this alignment conferring the conserved aromatic side chain (shown by the arrow). Note, that within the current list, eukaryotes only contain Phe, while all mycobacterial species confer a His in the critical position. Color coding is as follows: red, small and hydrophobic residues; blue, acidic residues; magenta, basic residues; green, polar non-charged residues.

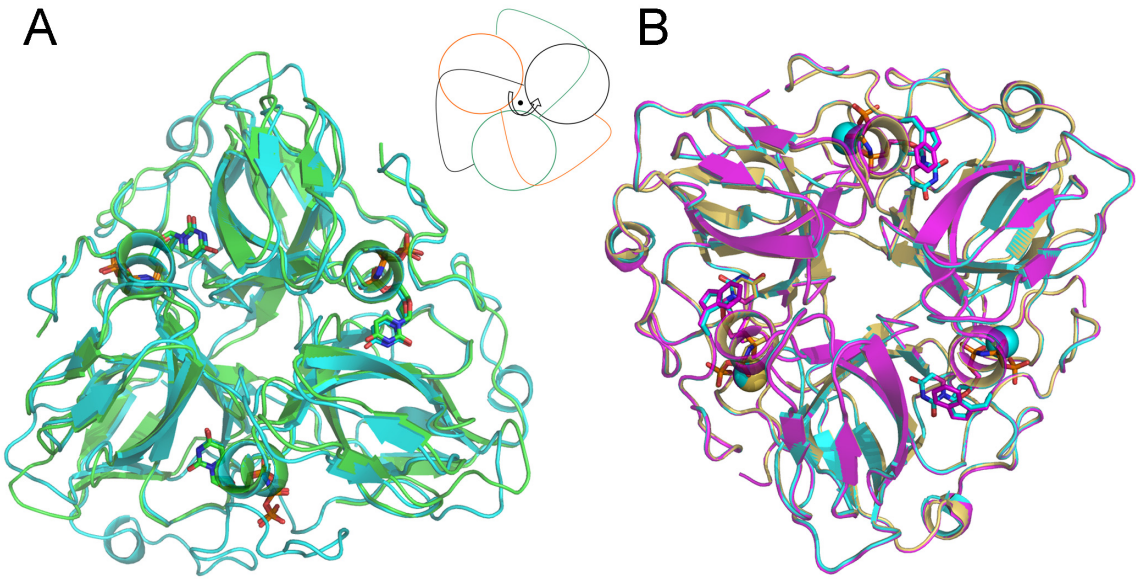

Figure S2. Structural superimposition of the wild-type and the newly crystallized mutant dUTPases

Panel **A** shows a structural superimposition of the wild-type human (green, PDB ID: 2HQU (1)) and *Mycobacterium tuberculosis* (MT) (cyan, PDB ID: 2PY4 (2)) dUTPases in complex with the slowly hydrolysable substrate analog dUPNPP (3) (shown as a stick model) to demonstrate the high structural similarity between dUTPases. In panel **B**, we superimposed the wild-type MT dUTPase with the two newly acquired mutants (mtDUT^{H145W}, magenta, PDB ID: 3HZA; mtDUT^{H145A}, gold, PDB ID: 3LOJ) in order to provide evidence for that the mutations of the aromatic residue did not perturb the overall structure. Note the intricate quaternary structure (also depicted by the pictograms) in which the three equivalent active sites of the homotrimer are composed of polypeptide fragments from each subunit.

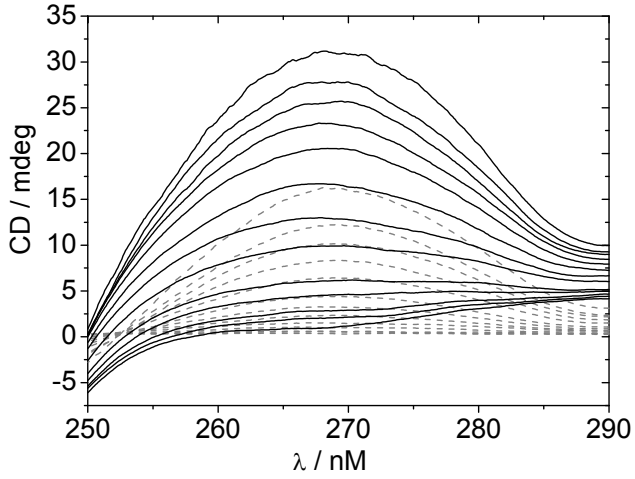

Figure S3. Complex formation between hDUT^{F158A} and dUPNPP as reported by circular dichroism

The dissociation constants (K_d) of various dUTPase – substrate-analog complexes were determined using the change in the circular dichroism (CD) signal of the nucleotide upon binding to the enzyme. 50 μM enzyme was titrated by stepwise addition of 0-200 μM dUPNPP to the cuvette (solid lines) and the CD spectrum series of the same concentrations of dUPNPP were recorded separately as reference (dashed line). The data points of the hyperbolic binding curves in Fig. 2D represent the difference of the reference and protein curves at the absorption maximum of the nucleotide, 269 nm.

References

1. Mol, C.D., Harris, J.M., McIntosh, E.M. and Tainer, J.A. (1996) Human dUTP pyrophosphatase: uracil recognition by a beta hairpin and active sites formed by three separate subunits. *Structure*, **4**, 1077-1092.
2. Varga, B., Barabas, O., Takacs, E., Nagy, N., Nagy, P. and Vertessy, B.G. (2008) Active site of mycobacterial dUTPase: structural characteristics and a built-in sensor. *Biochem Biophys Res Commun*, **373**, 8-13.
3. Barabas, O., Pongracz, V., Kovari, J., Wilmanns, M. and Vertessy, B.G. (2004) Structural insights into the catalytic mechanism of phosphate ester hydrolysis by dUTPase. *J Biol Chem*, **279**, 42907-42915.

Table S1. **Data collection and refinement statistics**

	$mtDUT^{H145W}$ (PDB ID: 3HZA)	$mtDUT^{H145A}$ (PDB ID: 3LOJ)
Data collection		
Space group	P 6_3	P 6_3
Cell dimensions		
a, *b*, *c* (Å)	55.06, 55.06, 83.79	54.59, 54.59, 83.05
α, β, γ (°)	90, 90, 120	90, 90, 120
Resolution (Å)	20-1.20 (1.23-1.20)	30-1.25 (1.30-1.25)
R_{merge}	0.039 (0.472)	0.041 (0.631)
$I / \sigma I$	18.4 (2.02)	24.7 (3.87)
Completeness (%)	94.2 (69.9)	97.9 (95.7)
Redundancy	3.73 (1.46)	9.00 (8.67)
Refinement		
Resolution (Å)	1.20	1.25
No. reflections: work/free	40085/2252	37154/2075
R_{work} / R_{free}	0.1167/0.1593	0.1276/0.1770
No. atoms		
Protein	1245	1203
Ligand/cofactor/solvent	45	46
Water	184	202
B-factors		
Protein	17.499	18.075
Ligand/cofactor/solvent	29.322	23.463
Water	32.713	36.177
R.m.s. deviations		
Bond lengths (Å)	0.012	0.016
Bond angles (°)	0.029	0.035

Values in parentheses are for highest-resolution shell.

Nucleotide pyrophosphatase employs a P-loop-like motif to enhance catalytic power and NDP/NTP discrimination

Ildikó Pécsi[a,1], Judit E. Szabó[a,1], Scott D. Adams[a,b], István Simon[a], James R. Sellers[c], Beáta G. Vértessy[a,d,2], and Judit Tóth[a,c,2]

[a]Institute of Enzymology, Biological Research Center, Hungarian Academy of Sciences, H-1113, Budapest, Karolina út 29., Hungary; [b]Feinberg School of Medicine, Northwestern University, Chicago, IL 60611; [c]Laboratory of Molecular Physiology, National Heart, Lung, and Blood Institute, National Institutes of Health, Bethesda, MD 20892; and [d]Department of Applied Biotechnology, Budapest University of Technology and Economics, H-1111, Budapest, Budafoki út 6-8., Hungary

Edited* by Edwin W. Taylor, Northwestern University Feinberg School of Medicine, Chicago, IL, and approved July 5, 2011 (received for review September 15, 2010)

We investigated the potential (d)NDP/(d)NTP discrimination mechanisms in nucleotide pyrophosphatases. Here, we report that dUTPase, an essential nucleotide pyrophosphatase, uses a C-terminal P-loop-like sequence in a unique mechanism for substrate discrimination and efficient hydrolysis. Our spectroscopy and transient kinetics results on human dUTPase mutants combined with previous structural studies indicate that (*i*) H-bond interactions between the γ-phosphate and the P-loop-like motif V promote the catalytically competent conformation of the reaction center at the α-phosphate group; (*ii*) these interactions accelerate the chemical step of the kinetic cycle and that (*iii*) hydrolysis occurs very slowly or not at all in the absence of the γ-phosphate—motif V interactions, i.e., in dUDP, dUDP.BeFx, or in the motif V-deleted mutant. The physiological role of dUTPase is to set cellular dUTP : dTTP ratios and prevent injurious uracil incorporation into DNA. Based upon comparison with related pyrophosphate generating (d)NTPases, we propose that the unusual use of a P-loop-like motif enables dUTPases to achieve efficient catalysis of dUTP hydrolysis and efficient discrimination against dUDP at the same time. These specifics might have been advantageous on the appearance of uracil-DNA repair. The similarities and differences between dUTPase motif V and the P-loop (or Walker A sequence) commonly featured by ATP- and GTPases offer insight into functional adaptation to various nucleotide hydrolysis tasks.

NTP hydrolysis | nucleotide discrimination | dUTP pyrophosphatase | Walker A motif | evolutionary adaptation

It is an intriguing question how pyrophosphate generating nucleotide hydrolases distinguish between (d)NDP and (d)NTP both containing the α-β phosphoanhydride bond to be hydrolyzed. In the present paper, we investigate two fundamental questions related to the nucleotide pyrophosphatase enzymatic activity exhibited by the enzyme dUTPase and by other pyrophosphatases: (*i*) the mechanism of discrimination between nucleoside di- and triphosphate ligands; (*ii*) the potential contribution of a P-loop-like motif to such discrimination. The enzyme dUTPase naturally evoked these questions as it specifically performs the hydrolysis of dUTP between the α-β phosphates with no further coupled reactions and it contains a P-loop-like motif (Fig. 1*A*). In addition, the structural comparison between Mg:dUDP- and Mg:dUTP analog-bound enzymes does not offer a straightforward explanation to why dUDP is not hydrolyzed because the scissile bond and the nucleophile adopt the same conformation in both (Fig. 1*B* and in stereo in Fig. S1*A*, the sole Mg:dUDP-complexed structure is superposed with a human Mg:dUPNPP complex).

dUTPase hydrolyzes dUTP to yield dUMP (a precursor for dTTP biosynthesis) and pyrophosphate (PP_i). The action of dUTPase is the only known direct mechanism to minimize uracil incorporation into DNA (1). Most dUTPases are homotrimers and confer three active sites. The substrate in each active site is bound by conserved sequence motifs from all three subunits. Therefore, although each subunit contains all necessary residues for substrate binding, trimer formation is indispensable to bring these residues in proximity for the cognate binding site (1, 2). dUTPase, similar to many other nucleotide binding proteins, contains a conserved loop motif (motif V) to coordinate the phosphate chain of the protein. The C terminus conferring this loop is not part of the globular enzyme core, it reaches far from its protomer to isolate a remote active site from the solvent (Fig. S2). The sequence of the C-terminal motif V shares a limited number of features with those of the P-loop motifs (Fig. 1*A*) (3, 4) present in a large number of ATPase and GTPase enzyme families known as P-loop NTPases including kinases, cytoskeleton and DNA motors, membrane pumps, and transporters.

It has been shown that the C terminus of dUTPase is necessary for dUTP hydrolysis but not for nucleotide binding or structural integrity (3, 5–7). Surprisingly, the active site architecture with bound substrate in the crystal structure of the C-terminally truncated inactive enzyme is identical to that of the wild-type (WT) (7). On the basis of activity measurements on full length and enzymatically truncated *Escherichia coli* enzymes, it was concluded that ordering of the flexible C terminus upon the active site, which occurs only in the presence of the gamma phosphate (γ-P) containing substrate analog dUPNPP is responsible for dUDP/dUTP discrimination (3, 5). There seems to be a clear difference, however, between the conformational freedom of the C terminus of *E. coli* and several other investigated dUTPases as evidenced by structural data in the crystal (8–11) and in solution (3, 5, 6, 12). Our previous results in human dUTPase suggest that the C-terminal motif V remains close to the active site even in apo state (13) whereas the *E. coli* motif V becomes loose without the substrate (12).

It was earlier proposed that closing of the C-terminal motif V upon the active site forces an unfavorable eclipsed conformation on the nucleotide substrate which may be responsible for catalysis (4). However, the dUPNPP substrate analog maintains its eclipsed [either *gauche* or *trans*, (14)] conformation in several crystal structures in which the C-terminal arm is disordered

Author contributions: B.G.V. and J.T. designed research; I.P., J.E.S., S.D.A., and J.T. performed research; I.S. and J.R.S. contributed new reagents/analytic tools; I.P., J.E.S., S.D.A., and J.T. analyzed data; and I.P., J.E.S., I.S., J.R.S., B.G.V., and J.T. wrote the paper.

The authors declare no conflict of interest.

*This Direct Submission article had a prearranged editor.

[1]I.P. and J.E.S. contributed equally to this work.

[2]To whom correspondence may be addressed. E-mail: tothj@enzim.hu or vertessy@enzim.hu.

This article contains supporting information online at www.pnas.org/lookup/suppl/doi:10.1073/pnas.1013872108/-/DCSupplemental.

Downloaded at MTA TTKKUTATOKOZPONTI KONYVTAR on November 4, 2021

(i.e., flexible) (8–10, 15, 16). The peculiar eclipsed conformation thus seems to be independent of the flexibility of the C-terminal motif V. It remained therefore an open question as to how this P-loop-like sequence contributes to the hydrolytic event which occurs via nucleophilic attack on the α-phosphate (15).

To gain insight into the mechanism of discrimination potentially related to the P-loop-like sequence (as earlier proposed in ref. 5), we designed mutants which fully or partially lost contact between the γ-P of the substrate nucleotide and the P-loop-like sequence. The coordination of the γ-P of the nucleotide and the amino acid sites which were mutated are depicted in Fig. 1*C* (and in stereo in Fig. S1*B*). The mutations were intended to partially (Ser160Ala/Thr161Ala termed hDUT$^{ST/AA}$, and Arg153Lys termed hDUT$^{R/K}$) or completely (Thr151Stop termed hDUT^{armless}) disrupt the secondary interaction network between the γ-P and the protein as also shown in an earlier work by Freeman et al. (7). These mutant enzymes were then subjected to kinetic and ligand binding analysis. Fortunately, the P-loop-like sequence of dUTPase is situated at the very C terminus of the polypeptide chain (Fig. S2) and therefore, its mutation or deletion does not endanger the overall fold and conformation of the full protein (Fig. S3) (3, 5, 10, 12). We also analyzed the available structural and kinetics data on the structurally and/or functionally related bifunctional dUDP/dUTPase, dCTP deaminase (DCD), and bifunctional dCTP deaminase/dUTPase (DCD-DUT) enzymes and compared them to our results.

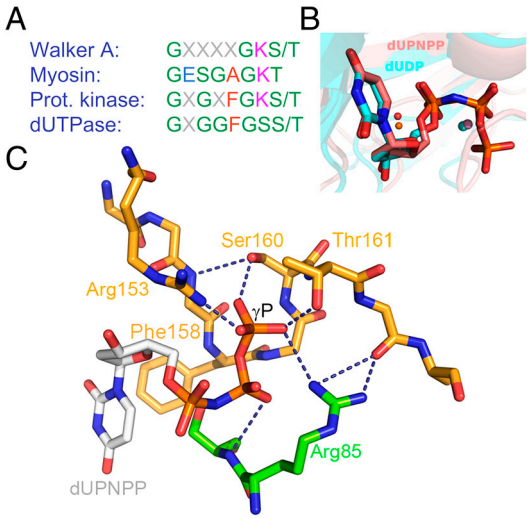

Fig. 1. The P-loop-like C-terminal motif V and its interactions with the substrate, (*A*), Consensus P-loop motifs from well known P-loop NTPases compared with the P-loop-like sequence of dUTPases. Coloring is as follows, polar residues, green; apolar r., red; negatively charged r., blue; and positively charged r., magenta (*B*), Alignment of two dUTPase active sites containing uridine di- and triphosphate ligands [atomic coloring with cyan and pink carbons, PDB IDs 1SLH (9) and 2HQU (8) from *M. tuberculosis* and *Homo sapiens*, respectively]. The positions of the α-β phosphates are identical and the catalytic water (orange for the tri- and magenta for the diphosphate structure) and Mg^{2+} ions (spheres in colors corresponding to the related nucleosides) are in place for putative hydrolysis of the α-β phosphate bond in both structures. (*C*), Coordination of the γ-P of the substrate by amino acids subjected to mutation in this study. The homotrimeric protein (2, PDB ID: 2HQU) is colored by subunits (subunit C, atomic coloring with orange carbons; subunit B atomic coloring with green carbons). dUPNPP is depicted as atomic colored sticks with gray carbons. Dashed lines depict hydrogen bonds partially abolished by the mutations thus hampering the coordination of the γ-P. Arg85 of subunit B is shown to complete the H-bonding network around the γ-P. Phe158, which engages in an aromatic stacking with uracil, is exchanged to a Trp to yield the specific fluorescence signal throughout this study. For better viewing, these structural images are also shown in stereo mode in Fig. S1.

Here we present a mechanism by which the P-loop-like motif of dUTPase promotes catalysis and discriminates against dUDP at the same time. We demonstrate that the unique use of a P-loop-like nucleotide binding sequence in dUTPase among nucleotide pyrophosphatases is functional adaptation to high dUTP specificity likely related to the development of uracil-DNA repair. The structural and functional similarity to P-loops is also discussed.

Results and Discussion

Mutations in the P-Loop-Like Sequence Disable dUTPase's Ability to Effectively Discriminate Between the Nucleoside Di- and Triphosphate Ligands. We took advantage of the discriminative power of the tryptophan (Trp) sensor built into the active site in place of F158 (shown in Fig. 1 and ref. 17) to investigate the interaction of dUTPase C-terminal motif V mutants with physiological ligands. The fluorescence of W158 is characteristically quenched in the dUTPase-ligand complexes compared with the apoenzyme (13) due to an aromatic stacking interaction between the uracil ring and the conserved aromatic side chain of the C-terminal motif V (18). The effect of the Trp substitution on the enzymatic and ligand binding properties of dUTPase is minor [$k_{cat} = 5.8 \pm 0.5$ and $6.8 \pm 2\ s^{-1}$, $K_{d,dUPNPP} = 1.5 \pm 1$ and $2.0 \pm 1\ \mu M$ for the WT and Trp mutant, respectively when measured for direct comparison (18)]. In the apoenzyme, the C-terminal motif V displays increased flexibility in solution (5, 6) and is disordered in the crystal structure [PDB ID: 1Q5U (8)] but the C-terminal arm stays in proximity to the active site through nucleotide-independent intersubunit interactions according to our previous spectroscopy

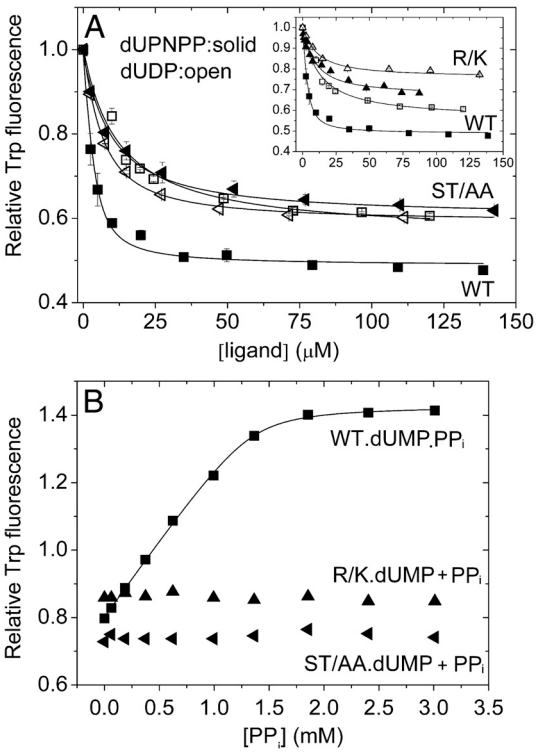

Fig. 2. Effect of mutations in the P-loop-like sequence on nucleotide and PPi binding. Fluorescence intensity titration of the loop Trp is shown upon dUTPase binding to (*A*), dUPNPP (solid symbols) and dUDP (open symbols) (hDUT$^{R/K}$ data shown in the inset separately for clarity) or (*B*), upon dUMP saturated dUTPase binding to PP_i. Signal intensities are normalized to the nucleotide-free state. Smooth lines through the data are hyperbolic fits yielding K_d values listed in Table 1. WT (squares), hDUT$^{R/K}$ (triangles), and hDUT$^{ST/AA}$ (left-pointing triangles) were used at 4 μM concentration. Error bars indicate SD for $n = 3$. Further evidences on nucleotide binding properties of the mutants are shown in the *SI Results and Discussion*.

Downloaded at MTA TTKKUTATOKOZPONTI KONYVTAR on November 4, 2021

results (13). Fig. 2*A* shows fluorescence intensity titrations upon dUTPase binding to dUDP or to the nonhydrolysable substrate analog α-β-imidodUTP (dUPNPP). Both dUDP and dUPNPP binding curves of the hDUT$^{ST/AA}$ mutant run close to the dUDP binding curve of the WT enzyme indicating that the binding mode of dUPNPP in this mutant is similar to the dUDP-bound conformation of the WT. The hDUT$^{R/K}$ mutant also displays a reduction in the fluorescence quench brought about by ligand binding (Fig. 2*A* inset). We also applied circular dichroism (CD) spectroscopy to measure ligand binding as the hDUT^{armless} mutant lacks the fluorescence signal (Fig. S4). The CD measurements are in line with the fluorescence-based ones in cases where both techniques were applied (Table 1). Dissociation constants obtained from data fitting are collected in Table 1 and show that while the WT binds dUPNPP stronger than dUDP, the complexes of the mutants with dUPNPP or dUDP are almost equally strong. The hDUT^{armless} mutant exhibits smaller binding constants than the other enzyme constructs in agreement with the fewest contacts it has with the ligands. Binding of the product dUMP to the mutants is not significantly affected as compared to the WT (Fig. S5, Table 1) and is one order of magnitude weaker than that of the substrate.

A strong proof of compromised γ-P binding by the C-terminal motif V mutants is shown in Fig. 2*B*. We could not observe any sign of ternary product complex (enzyme.dUMP.PPi) formation even at high PPi concentrations in contrast to results obtained with the WT. The lack of a binding curve here may indicate a highly elevated K_d or an altered binding mode that is not followed by the characteristic fluorescence signal change (13).

In summary, the similar degree of fluorescence quench and similar dissociation constants for the dUDP- and dUPNPP-mutant complexes together with an undetectable PPi binding to the mutant enzymes indicate that the P-loop-like nucleotide binding motif is the γ-P "detector" of dUTPase.

Mutations of the P-Loop-Like Sequence Result in a Large Decrease in the Enzymatic Activity and Specifically in the Hydrolysis Rate Constant. The catalytic activity and efficiency of dUTPase is severely affected in these mutants in the order of hDUT^{armless} > hDUT$^{R/K}$ > hDUT$^{ST/AA}$ ≫ WT (Fig. S6, Table 2). These results are in line with the expectations as only some H-bonds are disrupted in the hDUT$^{ST/AA}$ and hDUT$^{R/K}$ mutants, while in the hDUT^{armless}, the entire γ-P coordination is abolished. Our results also agree with earlier data showing the near inactivity of armless mutants (5, 7, 10, 19) and of *R/K* mutants (7, 10, 20).

To determine the mechanism underlying the steady-state behavior of the mutant enzymes, transient kinetics experiments investigating the previously described kinetic steps (13) were performed on all or selected mutants. The kinetic parameters of dUTP binding to and dissociating from the hDUT$^{ST/AA}$ were determined via stopped-flow using the Trp signal. Fig. 3*A* shows the time courses upon mixing hDUT$^{ST/AA}$ with increasing concentrations of dUTP. The curves were fitted with double exponential functions. As in the case of the WT, a concentration dependent fast and a first-order slow phase (representing 5–8% of the total amplitude) could be distinguished. The concentration dependence of the fast process (Fig. 3*B*) yielded $k_{dUTP,on} = 84\ \mu M^{-1}\ s^{-1}$ and $k_{dUTP,off} = 250\ s^{-1}$. These rate constants report somewhat faster dUTP binding than to the WT enzyme [(13), Table 2], while the rate constants of the second, isomerization, process are similar in both enzymes ($k_{ISO} = 29\ s^{-1}$ vs. $24\ s^{-1}$ in the WT).

Table 1. Dissociation constants of WT and P-loop mutant hDUT complexes with deoxyuridin mono-, di- and triphosphate ligands determined by Trp fluorescence or by CD

	K_d (μM)		
Enzyme	dUMP	dUDP	dUPNPP
WT	78 ± 4	12 ± 1	5.0 ± 3 3.4 ± 1*
hDUT$^{R/K}$	96 ± 14	12 ± 1	11 ± 4 10 ± 4 *
hDUT$^{ST/AA}$	74 ± 6	5.6 ± 0.6	6.5 ± 1 6.8 ± 3 *
hDUT^{armless}	ND	9.5 ± 3 *	14 ± 0.4 *

*determined by differential CD spectroscopy
ND: not determined

We took the next kinetic step, hydrolysis, under investigation by using the quenched-flow method. As shown in Fig. 3*C* (note the logarithmic time scale) the single turnover hydrolysis curves of the mutants report a large decrease in the hydrolysis rate constants compared to the WT. Single exponential functions fitted well to the curves and yielded rate constants (k_H) comparable to those of the steady-state rate (Table 2).

Our fluorescence (Fig. 2*A*) and quenched-flow (Fig. 3*C*) data together indicate that perturbation of the secondary interactions between the C-terminal motif V and the γ-P results in a reduced ability of the enzyme-substrate complex to adopt a catalytically competent conformation. Hydrolysis still occurs at a reduced rate, the reduction being proportional to the expected severity of the perturbation (WT ≫ hDUT$^{ST/AA}$ > hDUT$^{R/K}$ > hDUT^{armless}, Table 2). The C-terminal motif V is the major but not the only structural element of the enzyme that coordinates the γ-P. Arg85 of another conserved motif is also important for activity probably via the coordination and charge neutralization of the β- and γ-P (Fig. 1*C*, Fig. S1*B*). This interaction may explain the residual activity of the mutant enzyme lacking the P-loop-like sequence (hDUT^{armless}).

We attempted to measure the kinetics of product release from the enzyme-product(s) complex by dUTP chasing (Fig. 3*D*). The WT enzyme exhibited slower apparent dUTP binding when mixed with the enzyme.PPi complex as dissociation of PPi from the enzyme limited the dUTP binding process (13). Conversely, we observed no such effect when repeating the experiment using the hDUT$^{ST/AA}$ mutant. The reason PPi dissociation was not observed may be that (*i*) PPi dissociation is as fast as, or faster than dUTP binding at the applied dUTP concentration, or (*ii*) no quantitative enzyme.PPi complex was formed. Both possibilities imply that the PPi off-rate from the P-loop mutant is probably higher than that from the WT ($k_p = 740\ s^{-1}$ in ref. 13) and thus does not alter the steady-state rate.

This transient kinetic analysis indicates that the only kinetic step that affects the observed steady-state rate in the mutants is hydrolysis itself (i.e., hydrolysis or an indistinguishable conformational transition coupled to it). Other changes in the substrate binding and product release kinetics are not manifested in the steady-state rate because these processes remained orders of magnitude faster. We may conclude that the interaction of the γ-P with the C-terminal P-loop-like sequence in dUTPase promotes the entry into a hydrolysis competent state and therefore the frequency of the hydrolytic events. This phenomenon may be brought about by optimization of the geometry of the pre-hydrolysis enzyme.substrate complex or by electrostatics, i.e., partially distributing the excess negative charges through secondary interactions.

It is important to point out that the conserved aromatic residue within the P-loop-like sequence (Fig. 1*A*) makes a significant contribution to rate acceleration in dUTPase via its stacking interaction with the uracil ring of the substrate as we reported recently in the *Mycobacterium tuberculosis* and human enzymes (18). The lack of this interaction in the hDUT^{armless} mutant acts together with the lack of γ-P coordination. Interestingly, the P-loop-like motif in dUTPase forms catalytically important interactions with two distinct parts of the nucleotide substrate at both sides of the scissile bond.

The Presence of γ-P Is Required for Hydrolysis of the α-β Phosphoanhydride Bond by dUTPase. As dUTPase removes PPi instead of only the terminal phosphate group of the nucleotide, it is possible to

Downloaded at MTA TTKKUTATOKOZPONTI KONYVTAR on November 4, 2021

Table 2. Kinetic parameters of WT and P-loop mutant dUTPases

Enzyme	V_{max} (s^{-1})	K_M (μM)	k_{cat}/K_M (M^{-1} s^{-1})	k_H (s^{-1})	$k_{dUTP,on}$ (μM^{-1} s^{-1})	$k_{dUTP,off}$ (s^{-1})	k_{ISO} (s^{-1})
WT	6.5 ± 0.2	1.3 ± 0.5	5.0×10^6	5.5 ± 3 *	120 *	100 *	24 ± 6
$hDUT^{R/K}$	0.078 ± 0.002	6.1 ± 1.7	1.3×10^4	0.048 ± 0.001	ND	ND	ND
$hDUT^{ST/AA}$	0.26 ± 0.1	12 ± 2	2.2×10^5	0.16 ± 0.01	84 ± 8	250 ± 40	29 ± 5
$hDUT^{armless}$	0.010 ± 0.0007	ND	7.1×10^3 †	0.014 ± 0.0004	NA	NA	NA

*data from Toth and coworkers (1)
†K_d for the $hDUT^{armless}$.dUPNPP complex was used instead of K_M
ND: not determined
NA: not applicable

investigate the effect of γ-P substitution using nucleotide analogs. The ADP.BeF_x complex has been reported to act as ATP analog (21, 22), we therefore assayed the binding (Fig. S7*A*) and hydrolysis (Fig. S7*B*) of the dUDP.BeF_x complex by the WT enzyme. Using fluorescence spectroscopy we detected binding of BeF_x to the enzyme.dUDP complex characterized by a fluorescence quench similar to that of dUPNPP binding. Hydrolysis, nevertheless, did not occur in the enzyme.dUDP.BeF_x complex (see *SI Results and Discussion*). If dUDP.BeF_x is truly a nucleoside triphosphate analog in dUTPase as indicated by our spectroscopy result, then it suggests that the γ-P specifically is required for hydrolysis of the α-β phosphoanhydride bond.

The hydrolysis of dUDP by the WT and motif V mutant enzymes was also investigated using thin layer chromatography (TLC). Although this method allowed the use of high enzyme and dUDP concentrations, dUDP hydrolysis was not detected in agreement with previous reports (Fig. S8) (23).

Because the presence of an intact C-terminal motif V enhances the catalytic efficiency of dUTPase 720-fold (k_{cat}/K_M values in Table 2), the γ-P—motif V interaction probably is the major factor in discriminating the nonsubstrate dUDP from the substrate dUTP in accordance with previous suggestions from *E. coli* (3, 5).

Comparison to Functionally Related Enzymes Suggests That the P-Loop-Like Motif in dUTPase Is Evolutionary Adaptation to High dUTP Specificity and dUDP Discrimination. The use of a P-loop-like sequence to promote nucleotide pyrophosphatase activity and NDP/NTP discrimination is unique in dUTPase (for details see *SI Results and Discussion*). The most relevant structural and functional comparison to make is therefore with the homologous dUTPase superfamily enzymes dCTP deaminase (DCD) and dCTP deaminase/dUTPase (DCD-DUT), as well as with the nonhomologous but functionally comparable bifunctional dUDP/dUTPase. dUTPase, DCD, and DCD-DUT share a common fold and the first four motifs responsible for nucleotide and Mg^{2+} binding (Fig. 4*A* and in stereo in Fig. S9*A*). Importantly, however, only dUTPase possesses a P-loop-like sequence as its motif V. The C terminus of the other members of the superfamily also

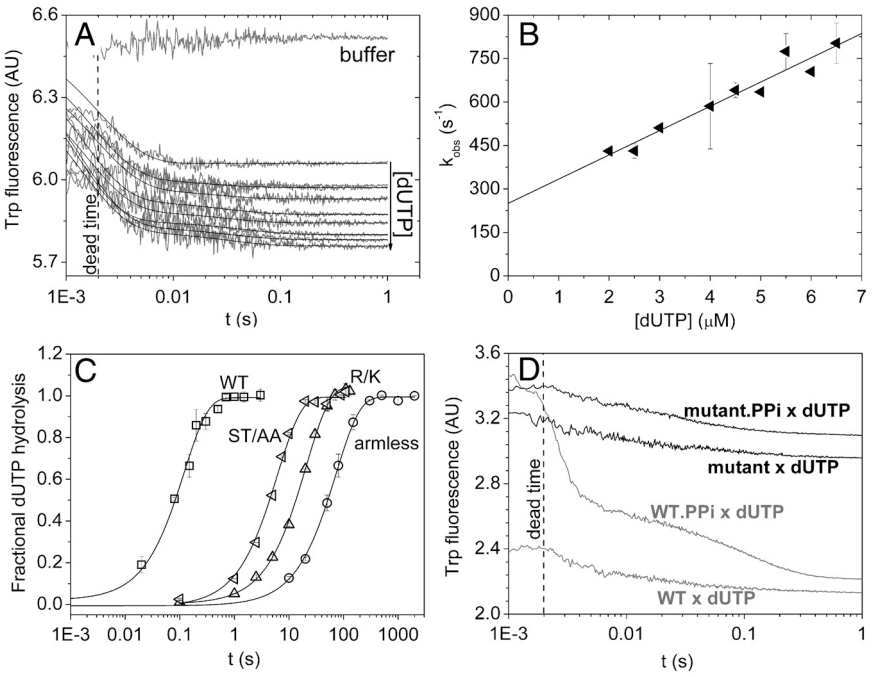

Fig. 3. Transient kinetic analysis of the mutants, (*A* and *B*) show stopped-flow experiments of $hDUTA^{ST/AA}$ binding to dUTP. (*A*), Fluorescence time courses recorded upon the initial binding phase of the reaction of various concentrations of dUTP with 0.8 μM $hDUT^{ST/AA}$. Smooth lines are the best double exponential fits to the experimental curves. The first exponential (fast phase with 95–98% of the total amplitude) is analyzed in (*B*). The second exponential of small amplitude did not depend on concentration and yielded $k_{ISO} = 29 \pm 5$ s^{-1} (SD for $n = 10$). (*B*), Concentration dependence of the observed rate constant of the fast phase. The linear fit yielded a second-order binding rate constant of 84 ± 8 μM^{-1} s^{-1} and a dissociation rate constant of 250 ± 36 s^{-1}. Errors represent SD for $n = 20$. (*C*), Single turnover γ^{32}P-dUTP hydrolysis by the WT and mutant dUTPases measured using the quench-flow technique. 25 μM protein was mixed with 12.5 μM γ^{32}P-dUTP and the reaction was followed till completion. Each curve was fitted with single exponentials yielding hydrolysis rate constants of 5.5 ± 2.5 s^{-1} for WT (squares), 0.16 ± 0.01 s^{-1} for $hDUT^{ST/AA}$ (left-pointing triangles), 0.048 ± 0.001 s^{-1} for $hDUT^{R/K}$ (triangles), and 0.01 ± 0.001 s^{-1} for $hDUT^{armless}$ (circles). Errors represent SD for $n = 3$. (*D*), Time courses of PP_i dissociation from the WT and $hDUT^{ST/AA}$ was measured by dUTP chasing in the stopped-flow. 4 μM enzyme or its preequilibrated complex with 2 mM PP_i was mixed with 1 mM dUTP. The fast phase of the dUTP binding reaction is lost in the dead-time as expected (13). In the chasing reaction, PP_i dissociation limits the rate of dUTP binding which can be followed in case of the WT enzyme (gray lines) while no PP_i dissociation can be observed in the mutant (black lines). WT and $hDUT^{ST/AA}$ curves are shifted on the *y*-axis compared to each other for better viewing.

Downloaded at MTA TTKKUTATOKOZPONTI KONYVTAR on November 4, 2021

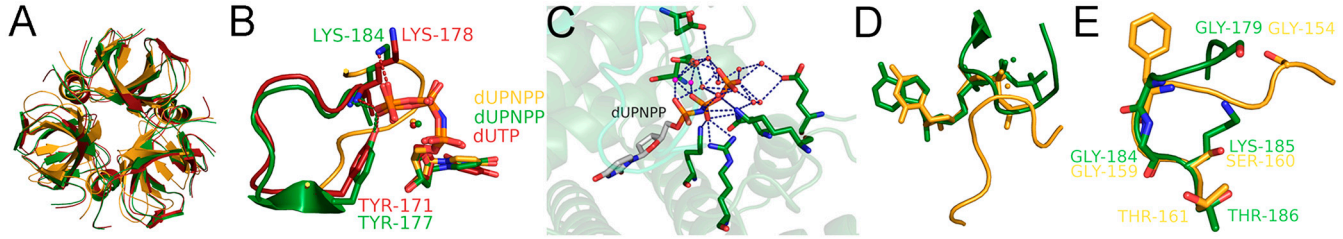

Fig. 4. γ-P-protein interactions in dUTPase-related and in P-loop enzymes, (*A*), Identical fold of protein cores of *M. tuberculosis* dUTPase (PDB ID: 2PY4, orange), *M. tuberculosis* DCD-DUT (PDB ID: 2QPL, green), and *E. coli* DCD (PDB ID: 1XS1, red). The enzymes were superimposed with UCSF Chimera. (*B*), Superimposition of the actives sites of the above structures. The nucleotides and the C terminus contacting the phosphate chain are highlighted. Amino acids contacting the γ-P in DCD and DCD-DUT, and nucleotides are presented as sticks with atomic coloring. Mg^{2+} ions are presented as spheres. The γ-P interactions in dUTPase already shown in Fig. 1*C* are omitted here for clarity. (*C*), The active site of *Campylobacter jejuni* dUDP/dUTPase [PDB ID: 2CIC (30)]. β- and γ-P coordinating groups and their contacts to dUPNPP (atomic coloring with gray carbons) are highlighted. While the β-P has many contacts to the protein, the γ-P is only coordinated by water molecules (red spheres). Dashed blue lines depict hydrogen bonds. The protein is colored by subunits, Mg^{2+} ions as purple spheres. (*D*), Comparison of the relative positions of the C-terminal motif V in dUTPase (PDB ID: 2HQU, orange) and the P-loop in *Dictyostelium discoideum* myosin II [PDB ID: 1MMN (34), green]. dUPNPP and ATP are presented as sticks, Mg^{2+} ions as spheres. (*E*), Superimposition of the two loops presented in (*D*), aligned for the loop and not for the nucleotide. Walker A amino acids are highlighted by stick representation (atomic coloring). These structural images are also shown in stereo mode in Fig. S9.

goes through a disordered-to-ordered transition upon substrate binding (24). This transition, however, results in relatively few interactions with the γ-P (Fig. 4*B* and in stereo in Fig. S9*B*) (25). These enzymes are significantly worse catalysts of dUTP hydrolysis than dUTPase ($k_{cat}/K_M = 4.5 \times 10^3$ s^{-1} M^{-1}) for DCD-DUT from *M. tuberculosis* at 37 °C (26) and 3.5×10^4 s^{-1} M^{-1} from *Methanococcus jannaschii* at 60 °C (27) to be compared to 5×10^6 s^{-1} M^{-1} at 25 °C for hDUT) even though their active site architecture including the position of the catalytic Asp and water molecule are similar. This observation implies that it is probably the presence of the C-terminal P-loop-like sequence that makes dUTPase the most efficient dUTP hydrolase within the superfamily. We therefore propose that the use of a P-loop-like sequence is an evolutionary adaptation of current dUTPases that allows for efficient catalysis of dUTP hydrolysis. The uracil world being more ancient than that including the methylated uracil, thymine, the action of dUTPase in preventing uracil incorporation into DNA must have gained importance only with the appearance of thymine and the uracil-specific DNA repair systems.

The bifunctional dUDP/dUTPase enzymes generate dUMP from both dUDP and dUTP with comparable k_{cat}/K_M values in the order of 10^6 s^{-1} M^{-1} by a mechanism similar to that of DNA polymerases (28, 29). We analyzed the available structures of these enzymes and discovered that the γ-P of bound dUTP is only coordinated by water molecules and is largely exposed to the bulk solvent (Fig. 4*C* and in stereo in Fig. S9*C*). In the bifunctional enzyme, it is the β-P that makes extensive contacts with the enzyme residues and Mg^{2+} also necessary for catalysis (compare to Fig. 5*A* in ref. 30, Fig. 4*C*). The bifunctional dUDP/dUTPase activity in this case coincides with the lack of a P-loop-like sequence or other γ-P coordinating structural element. This phenomenon further supports our suggestion that a P-loop-like motif may be responsible for structural discrimination between (d)NDP and (d)NTP when no downstream coupled reaction occurs.

Discrimination against dUDP hydrolysis is probably not a major force of selection in the functional adaptation of trimeric dUTPases. It is more likely an incidental phenomenon that accompanies the increased catalytic efficiency dUTPases gained with the presence of a P-loop-like sequence.

Structural and Functional Comparison of the P-Loop-Like Motif V in dUTPase and the P-Loop in NTPases Indicates Convergent Evolution. Comparing ATPases and dUTPase, we observe that while the P-loops and the phosphate chains can be perfectly superimposed within ATPases (shown in Fig. 5 in ref. 31), the P-loop-like motif in dUTPase adopts a different conformation relative to the nucleotide substrate (Fig. 4*D*). The superposition of the two loops, however, shows that there is structural similarity between their local conformation particularly around the single amino acid that makes the sequential difference between P-loop and dUTPase motif V (Fig. 4*E* and in stereo in Fig. S9*D*). The main difference between these conformations is that the P-loop in myosin (example for ATPase) surrounds both the β- and the γ-P, whereas the P-loop-like motif in dUTPase only contacts the γ-P (Fig. 1*C* and 4*D*). This difference, likely arising from the C-terminal position of the dUTPase loop and an eclipsed dUTP conformation, also supports the role of this motif in γ-P discrimination in dUTPase. The discriminatory role of the P-loop has also been shown in GTPases, in which most of the P-loop interactions target the β-P. Consequently, P-loop mutations may cause decreased dUDP affinity and preference for GTP binding finally resulting in overstimulation of certain signaling pathways (32).

The P-loop acts in different ways to achieve catalysis in NTPases and is therefore thought to have independently evolved in multiple instances (31). In G-proteins and myosins, its most likely role in catalysis is to orient the nucleotide and the attacking water molecule for efficient nucleophilic attack on the γ-P as well as charge stabilization (31, 33). In dUTPase, the γ-P coordination of the P-loop-like motif is also necessary for orientation of the catalytic apparatus and stabilization of the associative type transition state (17, 18). The completely different topology and the partly similar function of these loops indicates convergent evolution of phosphate binding motifs in a larger group of nucleotide hydrolases including PPi generating diphosphatases.

Methods

Proteins were expressed and purified as described previously (17). Site-directed mutagenesis was performed by the QuikChange method (Stratagene) and verified by sequencing of both strands. The following mutants where created: Ser160 and Thr161 to Ala ($hDUT^{ST/AA}$), Arg153 to Lys ($hDUT^{R/K}$) while the truncated mutant missing the entire P-loop was created by generating a stop codon in place of the Thr151 residue ($hDUT^{armless}$). The enzyme conferring a single Trp in the active site ($hDUT^{F158W}$) was used as WT (cf. ref. 13) thus all mutations were created within this construct. Protein concentration was measured using the Bradford method (Bio-Rad Protein Assay) and by UV absorbance ($\lambda_{280} = 10{,}555$ M^{-1} cm^{-1} for WT and $hDUT^{armless}$, $\lambda_{280} = 16{,}055$ M^{-1} cm^{-1} for $hDUT^{F158W}$, $hDUTA^{R/K}$, and $hDUT^{ST/AA}$) and is given in monomers. dUMP, dUDP, dUTP, and α,β-imido-dUTP (dUPNPP) where purchased from Jena Bioscience, other chemicals where from Sigma Aldrich. All measurements were carried out in a buffer comprising 20 mM Hepes pH 7.5, 100 mM NaCl, 2 mM $MgCl_2$ and 1 mM DTT if not stated otherwise.

Stopped-Flow Experiments. Measurements were made using an SX-20 (Applied Photophysics) stopped-flow apparatus. Measurement was carried out exactly as described in ref. 13. Time courses were analyzed using the curve fitting software provided with the stopped-flow apparatus or by Origin 7.5.

Downloaded at MTA TTKKUTATOKOZPONTI KONYVTAR on November 4, 2021

Quench flow experiments were carried out in an RQF-3 (KinTek Corp.) quench-flow apparatus using [γ-^{32}P]dUTP as described earlier (13).

Fluorescence Intensity Titrations. Fluorescence was measured in a Jobin Yvon Spex Fluoromax-3 spectrofluorometer at 20 °C, with excitation at 295 nm (slit 1 nm) and emission between 320–400 nm (slit 5 nm), or at 347 nm. 4 μM protein was titrated by addition of 1–2 μL aliquots from concentrated nucleotide solutions. Because large concentrations of nucleotides were used, care was taken to correct for any additional fluorescence or inner filter effect imposed on the measured intensities by the nucleotide stock solutions.

Statistical Analysis. All measurements were carried out at least three times. Error bars represent standard deviations. Where no error bars are shown, a representative curve is displayed while the summary table shows the relevant standard deviations of a certain parameter obtained from several different measurements. In the stopped-flow experiments, typically 5–8 traces were collected and averaged.

ACKNOWLEDGMENTS. This work was supported by the US National Institutes of Health (Grant number 1R01TW008130-01); the János Bolyai Research Scholarship of the Hungarian Academy of Sciences, the Howard Hughes Medical Institutes (Grant number 55000342); the Hungarian Scientific Research Funds (Grant numbers PD72008, CK-78646, K68229, K72973, and NI68466); the National Office for Research and Technology, Hungary (Grant number JÁP_TSZ_071128_TB_INTER) and the EU FP6 (Grant numbers SPINE2c LSHG-CT-2006-031220, TEACH-SG LSSG-CT-2007-037198) and the Alexander von Humboldt Foundation.

1. Vertessy BG, Toth J (2009) Keeping uracil out of DNA: physiological role, structure and catalytic mechanism of dUTPases. *Acc Chem Res* 42:97–106.
2. Persson R, Cedergren-Zeppezauer ES, Wilson KS (2001) Homotrimeric dUTPases; structural solutions for specific recognition and hydrolysis of dUTP. *Curr Protein Pept Sc* 2:287–300.
3. Vertessy BG (1997) Flexible glycine rich motif of *Escherichia coli* deoxyuridine triphosphate nucleotidohydrolase is important for functional but not for structural integrity of the enzyme. *Proteins* 28:568–579.
4. Prasad GS (2001) Glycine rich P-loop motif in deoxyuridine pyrophosphatase. *Curr Protein Pept Sc* 2:301–311.
5. Vertessy BG, et al. (1998) The complete triphosphate moiety of non-hydrolyzable substrate analogues is required for a conformational shift of the flexible C-terminus in *E. coli* dUTP pyrophosphatase. *FEBS Lett* 421:83–88.
6. Nord J, Nyman P, Larsson G, Drakenberg T (2001) The C-terminus of dUTPase: observation on flexibility using NMR. *FEBS Lett* 492:228–232.
7. Freeman L, et al. (2009) The flexible motif V of Epstein-Barr virus deoxyuridine 5′-triphosphate pyrophosphatase is essential for catalysis. *J Biol Chem* 284:25280–25289.
8. Mol CD, Harris JM, McIntosh EM, Tainer JA (1996) Human dUTP pyrophosphatase: uracil recognition by a beta hairpin and active sites formed by three separate subunits. *Structure* 4:1077–1092.
9. Chan S, et al. (2004) Crystal structure of the Mycobacterium tuberculosis dUTPase: insights into the catalytic mechanism. *J Mol Biol* 341:503–517.
10. Nemeth-Pongracz V, et al. (2007) Flexible segments modulate co-folding of dUTPase and nucleocapsid proteins. *Nucleic Acids Res* 35:495–505.
11. Varga B, et al. (2008) Active site of mycobacterial dUTPase: structural characteristics and a built-in sensor. *Biochem Biophys Res Commun* 373:8–13.
12. Takacs E, Barabas O, Petoukhov MV, Svergun DI, Vertessy BG (2009) Molecular shape and prominent role of beta-strand swapping in organization of dUTPase oligomers. *FEBS Lett* 583:865–871.
13. Toth J, Varga B, Kovacs M, Malnasi-Csizmadia A, Vertessy BG (2007) Kinetic mechanism of human dUTPase, an essential nucleotide pyrophosphatase enzyme. *J Biol Chem* 282:33572–33582.
14. Kovari J, et al. (2008) Methylene substitution at the alpha-beta bridging position within the phosphate chain of dUDP profoundly perturbs ligand accommodation into the dUTPase active site. *Proteins* 71:308–319.
15. Barabas O, Pongracz V, Kovari J, Wilmanns M, Vertessy BG (2004) Structural insights into the catalytic mechanism of phosphate ester hydrolysis by dUT ase. *J Biol Chem* 279:42907–42915.
16. Tarbouriech N, Buisson M, Seigneurin JM, Cusack S, Burmeister WP (2005) The monomeric dUTPase from Epstein-Barr virus mimics trimeric dUTPases. *Structure* 13:1299–1310.
17. Varga B, et al. (2007) Active site closure facilitates juxtaposition of reactant atoms for initiation of catalysis by human dUTPase. *FEBS Lett* 581:4783–4788.
18. Pecsi I, Leveles I, Harmat V, Vertessy BG, Toth J (2010) Aromatic stacking between nucleobase and enzyme promotes phosphate ester hydrolysis in dUTPase. *Nucleic Acids Res* 38:7179–7186.
19. Nord J, Kiefer M, Adolph HW, Zeppezauer MM, Nyman PO (2000) Transient kinetics of ligand binding and role of the C-terminus in the dUTPase from equine infectious anemia virus. *FEBS Lett* 472:312–316.
20. Shao H, et al. (1997) Characterization and mutational studies of equine infectious anemia virus dUTPase. *Biochim Biophys Acta* 1339:181–191.
21. Ponomarev MA, Timofeev VP, Levitsky DI (1995) The difference between ADP-beryllium fluoride and ADP-aluminum fluoride complexes of the spin-labeled myosin subfragment 1. *FEBS Lett* 371:261–263.
22. Fisher AJ, et al. (1995) X-ray structures of the myosin motor domain of Dictyostelium discoideum complexed with MgADP.BeFx and MgADP.AlF4. *Biochemistry* 34:8960–8972.
23. Larsson G, Nyman PO, Kvassman JO (1996) Kinetic characterization of dUTPase from *Escherichia coli*. *J Biol Chem* 271:24010–24016.
24. Huffman JL, Li H, White RH, Tainer JA (2003) Structural basis for recognition and catalysis by the bifunctional dCTP deaminase and dUTPase from Methanococcus jannaschii. *J Mol Biol* 331:885–896.
25. Johansson E, et al. (2005) Structures of dCTP deaminase from *Escherichia coli* with bound substrate and product: reaction mechanism and determinants of mono- and bifunctionality for a family of enzymes. *J Biol Chem* 280:3051–3059.
26. Helt SS, et al. (2008) Mechanism of dTTP inhibition of the bifunctional dCTP deaminase:dUTPase encoded by Mycobacterium tuberculosis. *J Mol Biol* 376:554–569.
27. Li H, Xu H, Graham DE, White RH (2003) The Methanococcus jannaschii dCTP deaminase is a bifunctional deaminase and diphosphatase. *J Biol Chem* 278:11100–11106.
28. Hidalgo-Zarco F, et al. (2001) Kinetic properties and inhibition of the dimeric dUTPase-dUDPase from Leishmania major. *Protein Sci* 10:1426–1433.
29. Musso-Buendia JA, et al. (2009) Kinetic properties and inhibition of the dimeric dUTPase-dUDPase from Campylobacter jejuni. *J Enzym Inhib Med Ch* 24:111–116.
30. Moroz OV, et al. (2004) The crystal structure of a complex of Campylobacter jejuni dUTPase with substrate analogue sheds light on the mechanism and suggests the "basic module" for dimeric d(C/U)TPases. *J Mol Biol* 342:1583–1597.
31. Smith CA, Rayment I (1996) Active site comparisons highlight structural similarities between myosin and other P-loop proteins. *Biophys J* 70:1590–1602.
32. Klockow B, Ahmadian MR, Block C, Wittinghofer A (2000) Oncogenic insertional mutations in the P-loop of Ras are overactive in MAP kinase signaling. *Oncogene* 19:5367–5376.
33. Pai EF, et al. (1990) Refined crystal structure of the triphosphate conformation of H-ras p21 at 1.35 A resolution: implications for the mechanism of GTP hydrolysis. *Embo J* 9:2351–2359.
34. Gulick AM, Bauer CB, Thoden JB, Rayment I (1997) X-ray structures of the MgADP, MgATPgammaS, and MgAMPPNP complexes of the Dictyostelium discoideum myosin motor domain. *Biochemistry* 36:11619–11628.

Downloaded at MTA TTKKUTATOKOZPONTI KONYVTAR on November 4, 2021

Supporting Information

Pécsi et al. 10.1073/pnas.1013872108

SI Results and Discussion

The hDUT^{armless} Mutant Preserves Its Trimeric Structure. The C-terminal arm of dUTPase conferring the P-loop-like sequence leaves its protomer and spans another protomer to reach the active site of the third one (Fig. S2). We designed the armless mutation such that the sequence likely responsible for keeping the trimer together remains unaffected (1). We performed gel filtration chromatography with both the wild-type (WT) and the mutant (Fig. S3) and experimentally proved the intact nature of the expressed hDUT^{armless} protein (cf. ref. 2).

dUTPase Does Not Hydrolyze the dUDP.BeF$_x$ Complex. We investigated the mechanism of dUTP binding and hydrolysis by C-terminal motif V mutants, in which some or all of the secondary interactions between the γ-P and the enzyme are compromised. When using dUDP.BeF$_x$, however, we changed the properties of the γ-P and not of the protein. The bond between the β-P and the beryllium atom is thought to exhibit covalent features (3) while the fluoride is able to form H-bonds thus potentially mimicking a nucleoside triphosphate. Our efforts to crystallize the enzyme.dUDP.BeF$_x$ complex remained fruitless. However, we used fluorescence spectroscopy to gain insight into the binding mode of BeF$_x$. As shown in Fig. S7*A*, addition of Be^{2+} and F^- to the hDUT.dUDP complex results in a high quench of the Trp fluorescence ($F_{rel} = 0.35$) spectroscopically identical to that induced by dUPNPP. Such high fluorescence reduction is usually observed in hDUT.dUPNPP and hDUT.dUTP complexes (4, 5). Therefore, it is likely that BeF$_x$ binds to the γ-P site within the active site and induces similar conformation to that of the prehydrolysis analog dUPNPP.

The fluorescence measurements had already indicated that hydrolysis between the α- and β-phosphates probably does not occur as no fluorescence change could be observed within several hours of complex formation (the enzyme.dUMP complex is characterized by a fluorescence level close to the apo state). To confirm this result, we carried out additional experiments in single turnover conditions which also included an enzyme denaturation step so that even the enzyme-bound hydrolysis product would be freed into the solution. Fig. S7*B* displays the result of such an experiment using ion-exchange chromatography for the detection of the nucleoside released from the denatured enzyme. Compared to the control dUMP and dUDP chromatograms, no hydrolysis is apparent in the enzyme.dUDP.BeF$_x$ complex. We obtained similar results when samples were subjected to thin layer chromatography.

The enzyme.ADP.BeF$_x$ complex was shown to mimic the ATP-bound prehydrolysis conformations in myosin (6, 7) and other enzymes. It was also shown the ADP.BeF$_x$ analog is able to adopt the eclipsed conformation observed for dUPNPP in dUTPase (PDB ID: 2BEF) (8). We show that the complex is spectroscopically identical to the prehydrolysis complex formed with dUPNPP. It is therefore expected that the dUDP.BeF$_x$ analog is capable of forming adequate contacts with the P-loop-like motif V and transmitting conformational changes to the rest of the nucleotide analog. Surprisingly, however, it seems that the presence of γ-P in particular is necessary for hydrolysis to occur on the α-P suggesting that quantum chemical calculations are necessary to gain more insight into this phenomenon.

The Use of a P-Loop-Like Sequence to Promote Nucleotide Pyrophosphatase Activity and NDP/NTP Discrimination Is Unique in dUTPase. We carried out an extensive search in the literature to learn how other nucleotide pyrophosphatases achieve discrimination between nucleoside di- and triphophates. In nucleic acid polymerases, analyses of high resolution structures may simply explain that some structural elements essential for catalysis are missing when (d)NDP is bound into the active site [e.g., catalytic Mg^{2+} missing in Pol IV, (9)]. Other enzymes are suggested to work with large domain movements which promote an extensive interaction network between the γ-P and the enzyme necessary to achieve the hydrolysis-competent conformation [mRNA capping enzyme, ATP dependent DNA ligase (10, 11)]. In many cases, however, no mechanism of discrimination is proposed or inferred from the available data. The PDB database contains few structures with nucleotide pyrophosphatases liganded with (d)NDP. In the absence of structural data the function may help illuminate the mechanism of (d)NDP/(d)NTP discrimination. Most of these enzymes not only possess nucleotide pyrophosphatase activity but also possess phosphoryl transfer activity as well, thus coupling hydrolysis to a second reaction. In this case, the energy balance of (d)NTP hydrolysis may cover the cost of the secondary reaction while that of (d)NDP hydrolysis may not [$\Delta G^{\circ}_{ATP\rightarrow AMP} = -45.6$ kJ/mol vs. $\Delta G^{\circ}_{ADP\rightarrow AMP} = -32.6$ kJ/mol (12)].

Interestingly, we have not found any other example amongst the nucleotide pyrophosphatase enzymes which contains a P-loop-like sequence or P-loop to promote hydrolysis. It seems that dUTPase uniquely uses this widespread nucleotide binding motif for the hydrolysis of the α-β phosphate bond.

SI Methods

Circular Dichroism Intensity Titrations. CD spectra were recorded at 20 °C on a JASCO 720 spectropolarimeter using a 1 mm path length cuvette. 50 μM protein was titrated by stepwise addition of the nonhydrolysable substrate analog dUPNPP in a buffer containing 10 mM potassium-phosphate pH 7.5 and 1 mM $MgCl_2$. A spectrum between $\lambda = 250$–290 nm was recorded at each nucleotide concentration. Differential curves were obtained by subtracting the signal of dUPNPP alone from that of the corresponding complex. Differential ellipticity at $\lambda_{max} = 269$ nm was plotted against the dUPNPP concentration to obtain the binding curves. The following quadratic equation was fitted to the experimental curves:

$$y = s + A^*((c + x + K) - \sqrt{(c + x + K)^2 - 4^*c^*x})/2^*c$$

$s = y$ at $x = 0$; A = amplitude; c = protein concentration; $K = K_d$

Gelfiltration chromatography was carried out using a Superdex 200 10/30 GL column in an AKTA Purifier (GE Healthcare) chromatography system. Proteins were loaded in equal amounts and were subjected to isocratic elution in a buffer comprising 20 mM Hepes pH 7.5, 100 mM NaCl, 2 mM $MgCl_2$ and 1 mM DTT.

Steady-State Colorimetric dUTPase Assay. Protons released in the dUTPase reaction were detected by phenol red pH indicator in 1 mM Hepes pH 7.5 buffer also containing 100 mM KCl, 40 μM phenol red (Merck) and 5 mM $MgCl_2$. A Specord 200 (Analytic Jena, Germany) spectrophotometer and 10 mm path length thermostatted cuvettes were used at 20 °C. Absorbance was recorded at 559 nm. The Michaelis-Menten equation was fitted to the steady-state curves using Origin 7.5 (OriginLab Corp., Northampton, MA).

Ion-exchange chromatography was carried out using a BioScale Q2 (BioRad) column in an AKTA Purifier (GE Healthcare) chromatography system. 25 nmol dUMP/dUDP was loaded in a buffer containing 20 mM Hepes pH 7.5, 2 mM $MgCl_2$, 50 mM NaCl and 1 mM DTT followed by isocratic elution. The hDUT.dUDP.BeF_x complex was composed of 10 μM hDUT, 50 μM dUDP, 50 μM $BeCl_2$ and 2 mM NaF. The protein was removed from the solution before loading onto the column by heating followed by centrifugation.

Thin Layer Chromatography. 2.5 × 7.5 cm TLC Baker-flex plates coated with silica gel IB2-F (layer thickness, 0.2 mm) containing an UV254 fluorescence indicator were used (J. T. Baker, Germany, product number 4449-02). The following reaction solutions were prepaired: 85 μM WT dUTPase and $hDUT^{armless}$ mutant enzyme were mixed separately with 1 mM dUDP and incubated for 3 h at room temperature. To stop the reaction, 3 μL from the reaction mixture was incubated at 80 °C for 20 s after each hour. For control 1 mM dUMP was applied. 3 × 1 μL sample was loaded manually using a finely tapered micropipette tip, dried and run in a humidified glass beaker containing isopropanol/ammonium/water (v/v/v) 6:3:1 solution. When the solvent front has reached 1 cm from the top of the plate, the plates were dried completely with a hair dryer and exposed to UV light for evaluation.

1. Takacs E, Barabas O, Petoukhov MV, Svergun DI, Vertessy BG (2009) Molecular shape and prominent role of beta-strand swapping in organization of dUTPase oligomers. *FEBS Lett* 583:865–871.
2. Vertessy BG (1997) Flexible glycine rich motif of *Escherichia coli* deoxyuridine triphosphate nucleotidohydrolase is important for functional but not for structural integrity of the enzyme. *Proteins* 28:568–579.
3. Petsko GA (2000) Chemistry and biology. *Proc Natl Acad Sci USA* 97:538–540.
4. Toth J, Varga B, Kovacs M, Malnasi-Csizmadia A, Vertessy BG (2007) Kinetic mechanism of human dUTPase, an essential nucleotide pyrophosphatase enzyme. *J Biol Chem* 282:33572–33582.
5. Varga B, et al. (2007) Active site closure facilitates juxtaposition of reactant atoms for initiation of catalysis by human dUTPase. *FEBS Lett* 581:4783–4788.
6. Ponomarev MA, Timofeev VP, Levitsky DI (1995) The difference between ADP-beryllium fluoride and ADP-aluminum fluoride complexes of the spin-labeled myosin subfragment 1. *FEBS Lett* 371:261–263.
7. Fisher AJ, Smith CA, Thoden JB, Smith R, Sutoh K, Holden HM, Rayment I (1995) X-ray structures of the myosin motor domain of Dictyostelium discoideum complexed with MgADP.BeFx and MgADP.AlF4. *Biochemistry* 34:8960–8972.
8. Xu YW, Morera S, Janin J, Cherfils J (1997) AlF3 mimics the transition state of protein phosphorylation in the crystal structure of nucleoside diphosphate kinase and MgADP. *Proc Natl Acad Sci USA* 94:3579–3583.
9. Ling H, Boudsocq F, Woodgate R, Yang W (2001) Crystal structure of a Y-family DNA polymerase in action: a mechanism for error-prone and lesion-bypass replication. *Cell* 107:91–102.
10. Hakansson K, Doherty AJ, Shuman S, Wigley DB (1997) X-ray crystallography reveals a large conformational change during guanyl transfer by mRNA capping enzymes. *Cell* 89:545–553.
11. Sriskanda V, Shuman S (1998) Mutational analysis of Chlorella virus DNA ligase: catalytic roles of domain I and motif VI. *Nucleic Acids Res* 26:4618–4625.
12. Frey PA, Arabshahi A (1995) Standard free energy change for the hydrolysis of the alpha, beta-phosphoanhydride bridge in ATP. *Biochemistry* 34:11307–11310.

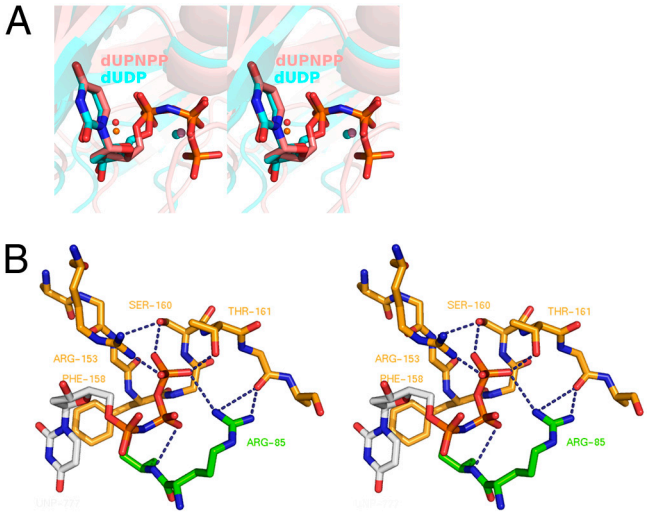

Fig. S1. Stereo representation of the structures displayed in (*A*), Fig. 1*B*; (*B*), Fig. 1*C*

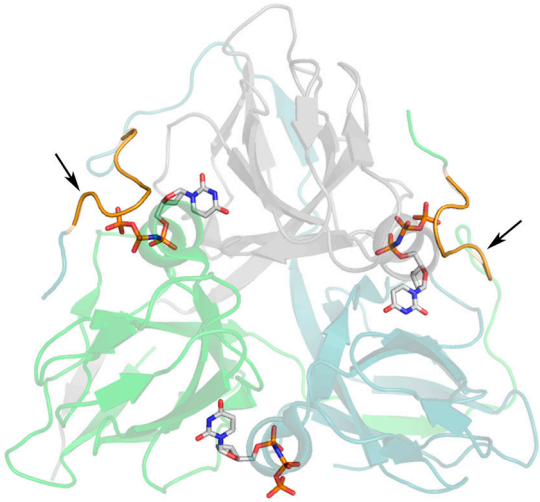

Fig. S2. The position of the P-loop-like motif in the trimeric structure of dUTPase. The structure of human dUTPase (PDB ID: 2HQU) is shown as a cartoon representation colored by subunits. The substrate analog dUPNPP is shown as a stick model (atomic coloring with gray carbons). The P-loop-like motives are highlighted in orange and pointed out by the arrows. Note that the C-terminal sequence of the gray subunit is missing from the refined structure and is therefore not shown. Also note that the loop isolates the bound nucleotide from the bulk solvent and surrounds the γ phosphate group.

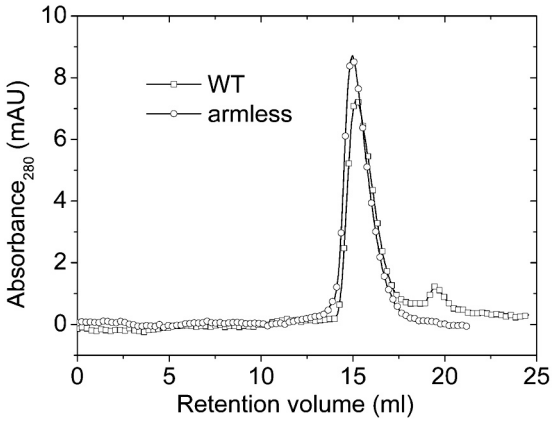

Fig. S3. Preservation of the trimeric quaternary structure in the hDUT^{armless} mutant demonstrated by gelfiltration. Purified WT (squares) and hDUT^{armless} (circles) proteins were subjected to gelfiltration chromatography in subsequent runs using the AKTA system equipped with a Superdex 200 10/300 column. The trimeric recombinant WT protein has a calculated molecular mass of 60 kDa. A trimeric hDUT^{armless} is calculated to be 55 kDa while its monomeric form would be 19 kDa- well separatable on a Superdex 200 column. A difference of 5 kDa, however, is not expected to be resolved. The retention volume was 15 mL for both proteins which indicated that deletion of the C terminus did not disturb the oligomerization of the hDUT^{armless} mutant. Consequently, the severe activity loss observed in this mutant is not due to an aberrant quaternary structure.

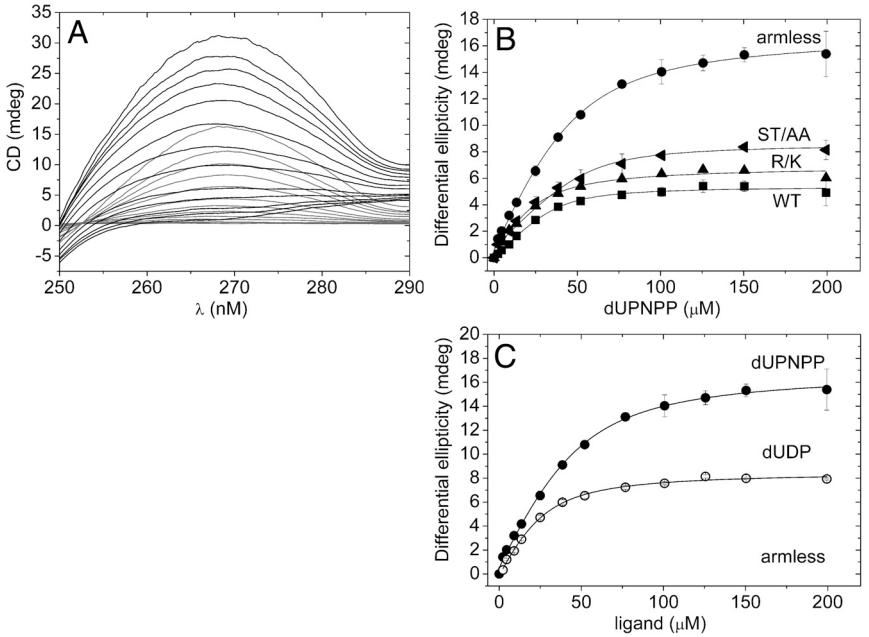

Fig. S4. Effect of mutations in the P-loop-like sequence on nucleotide binding as reported by CD. Fig. S4 shows CD equilibrium titrations of WT and mutant dUTPases by stepwise addition of the ligand (dUPNPP or dUDP). (*A*), CD spectra of 0–200 μM dUPNPP (gray lines) and its complex with 50 μM hDUT$^{R/K}$ (black lines). Such spectra were used to extract the maximal signal change at 269 nm in function of the ligand concentration to yield the binding curves shown in boxes (*B* and *C*). (*B*), Comparison of dUPNPP binding to the WT and mutant dUTPases. Solid lines represent hyperbolic fits to the data yielding the following K_d values: 3.4 ± 1.4 μM for WT (squares), 6.8 ± 2.9 μM for hDUT$^{ST/AA}$ (left-pointing triangles), 10 ± 4.1 μM for hDUT$^{R/K}$ (triangles), and 14 ± 0.43 μM for hDUT^{armless} (circles). (*C*) shows dUPNPP and dUDP binding to the hDUT^{armless} mutant. Hyperbolic fit to the data yielded a K_d of 9.5 ± 2.5 μM for dUDP (open circles) while the dUPNPP titration (solid circles) presented is identical with that seen in (*B*). Error bars represent SD for three or more independent measurements.

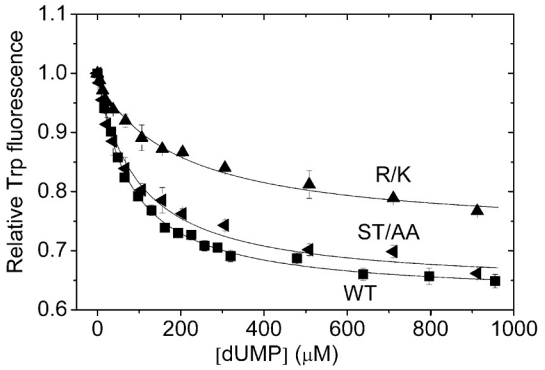

Fig. S5. Effect of mutations in the P-loop-like sequence on dUMP binding. Fluorescence intensity titration of the active site Trp is shown upon dUMP binding to WT (squares), hDUT$^{ST/AA}$ (left-pointing triangles), or hDUT$^{R/K}$ (triangles) dUTPase. Signal intensities are normalized to the nucleotide-free state. Smooth lines through the data are hyperbolic fits yielding K_d values of 78 ± 3.8 μM for the WT, 74 ± 5.6 μM for hDUT$^{ST/AA}$, and 96 ± 14 μM for hDUT$^{R/K}$. Error bars represent SD for three or more independent measurements. As the loop does not participate in dUMP binding, a significant change in the K_d or the maximal fluorescence quench of the protein.dUMP complex was not expected in the mutants.

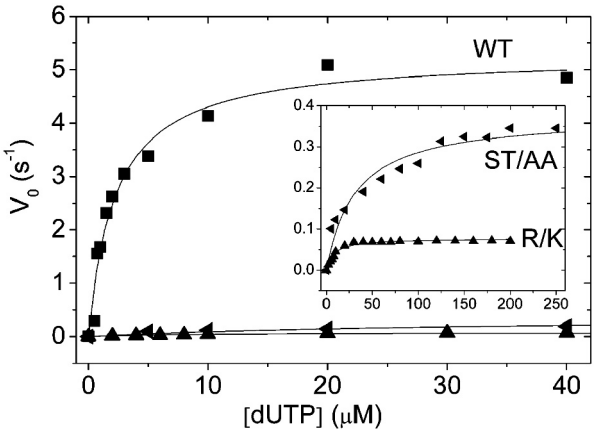

Fig. S6. Effect of mutations in the P-loop-like sequence on steady-state dUTPase activity. Michaelis-Menten curves for WT (squares), hDUT$^{R/K}$ (triangles), and hDUT$^{ST/AA}$ (left-pointing triangles) measured using the phenol red pH indicator assay. The inset shows the hDUT$^{R/K}$ and hDUT$^{ST/AA}$ curves enlarged. Fitting the Michaelis-Menten equation to the curves yielded the following V_{max} and K_M values: 5 s^{-1} and 2.3 μM for WT, 11.6 ± 1.74 μM for hDUT$^{ST/AA}$, and 6.1 ± 1.7 μM for hDUT$^{R/K}$. Similar curve for the hDUT^{armless} mutant could not be determined due to its largely diminished activity. Errors represent SD for $n = 3$.

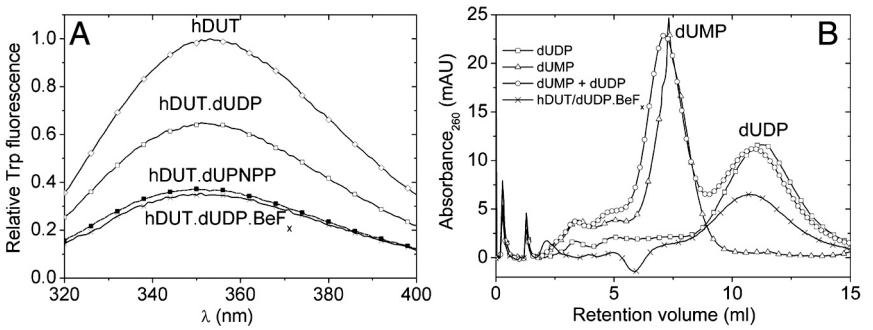

Fig. S7. Interaction of dUTPase with dUDP.BeF$_x$. (*A*), Trp fluorescence spectra of 10 μM WT ($F_{max} = 1$), its complex with 50 μM dUDP ($F_{max} = 0.64$), with 50 μM of the substrate analog dUPNPP ($F_{max} = 0.36$) and with 50 μM dUDP.BeF$_x$ ($F_{max} = 0.35$). The enzyme.dUDP.BeF$_x$ complex is composed of 10 μM WT, 50 μM dUDP, 50 μM $BeCl_2$, and 2 mM NaF. (*B*), Separation of dUDP and dUMP by ion-exchange chromatography on BioScale Q2 column to detect the end-product of dUTPase reaction with dUDP.BeF$_x$. dUMP (triangles) and dUDP (squares) were run separately or mixed together (circles) for reference. The enzyme.dUDP.BeF$_x$ complex (crosses) was incubated for several hours before chromatography. Only dUDP could be detected indicating that hydrolysis between the α-β phosphates did not occur.

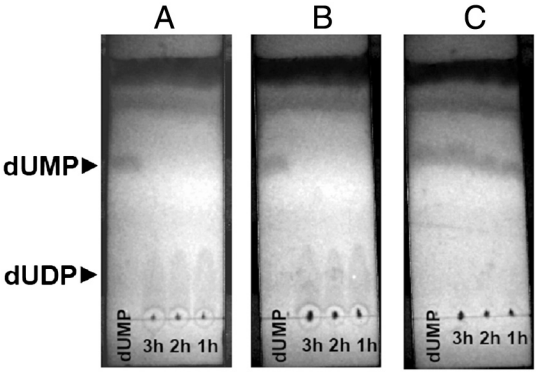

Fig. S8. dUDP is not hydrolyzed by either the WT or the C-terminally truncated enzyme. (*A*), 85 μM hDUT^{armless} was incubated with 1 mM dUDP for 1, 2, or 3 h at room temperature. The lack of any signal at the dUMP position indicates that hydrolysis did not occur. (*B*), 85 μM WT hDUT incubated with 1 mM dUDP. Hydrolysis is not detected. (*C*), Control dUTP hydrolysis by the WT hDUT shows the hydrolysed dUMP product. 1 mM dUMP was applied on each TLC plate for control.

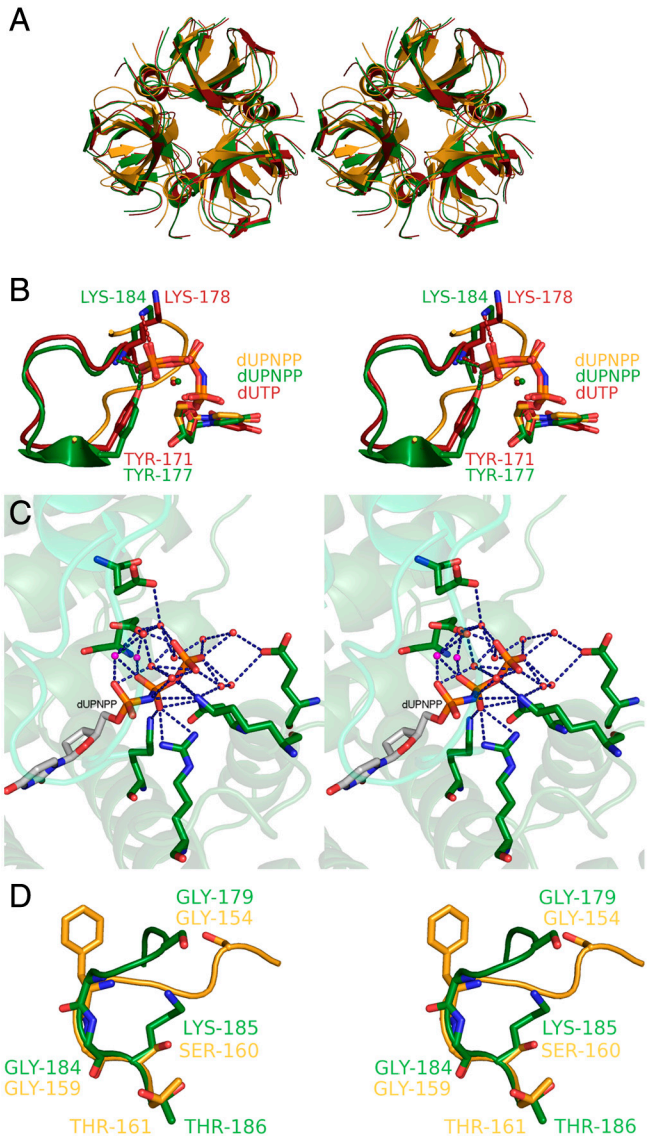

Fig. S9. Stereo representation of the structures displayed in (*A*), Fig. 4*A*; (*B*), Fig. 4*B*; (*C*), Fig. 4*C*; and (*D*), Fig. 4*E*

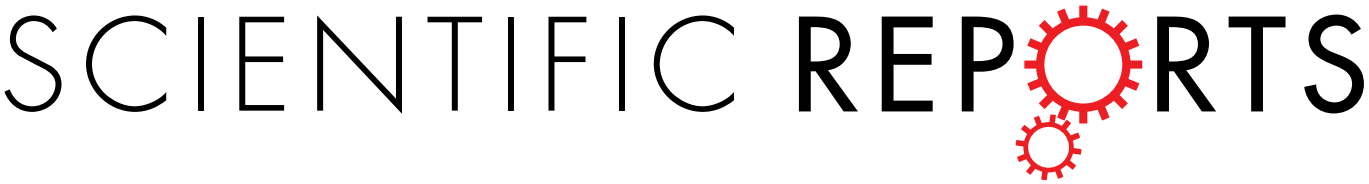

OPEN

Trading in cooperativity for specificity to maintain uracil-free DNA

Received: 15 February 2016
Accepted: 22 March 2016
Published: 11 April 2016

Judit E. Szabó[1], Enikő Takács[1], Gábor Merényi[1,†], Beáta G. Vértessy[1,2] & Judit Tóth[1]

Members of the dUTPase superfamily play an important role in the maintenance of the pyrimidine nucleotide balance and of genome integrity. dCTP deaminases and the bifunctional dCTP deaminase-dUTPases are cooperatively regulated by dTTP. However, the manifestation of allosteric behavior within the same trimeric protein architecture of dUTPases, the third member of the superfamily, has been a question of debate for decades. Therefore, we designed hybrid dUTPase trimers to access conformational states potentially mimicking the ones observed in the cooperative relatives. We studied how the interruption of different steps of the enzyme cycle affects the active site cross talk. We found that subunits work independently in dUTPase. The experimental results combined with a comparative structural analysis of dUTPase superfamily enzymes revealed that subtile structural differences within the allosteric loop and the central channel in these enzymes give rise to their dramatically different cooperative behavior. We demonstrate that the lack of allosteric regulation in dUTPase is related to the functional adaptation to more efficient dUTP hydrolysis which is advantageous in uracil-DNA prevention.

Allosteric characteristics of protein-ligand interactions present a research field with great traditions but also with key current interest[1,2]. Recent developments in the understanding of the manifestation of allosteric behavior within a given protein architecture lead to a shift from the classical view to a more subtle dynamic view of allostery. According to the classical view, allostery is based on a series of distinct structural changes leading to functionally different conformers of a given protein. However, several examples demonstrated that the allosteric behavior does not necessarily require switches between direct conformers[3] but can be explained by alterations of side chain[4] or main chain dynamics[5] or by a shift in the distribution of preexisting protein conformations[6]. In the present study, we set out to investigate the manifestation of allostery within the superfamily of dUTPases. The superfamily comprises the dUTPase, dCTP deaminase (DCD) and the bifunctional dCTP deaminase-dUTPase (DCD-DUT) enzymes that produce dUMP, the obligatory *de novo* dTTP synthesis precursor from either dUTP or dCTP, respectively (Fig. 1).

The removal of dUTP from the cellular dNTP pool is also a vital function of dUTPases. These enzymes thus play an important role in the maintenance of the pyrimidine nucleotide balance and genome integrity[7–12]. dUTPase and DCD(-DUT) share a common homotrimeric structural core[13–16] (Fig. 2a). The three subunits form a central channel and three equivalent active sites at the intersubunit clefts (Fig. 2a). This intricate quaternary structure intuitively suggests the possibility for allosteric control within the enzyme. In effect, the allosteric communication between the active sites of DCD family enzymes has been investigated in several species[15,17–19] and was found to operate through the central channel[15,19]. The cooperative conformational change in these enzymes occurs in a loop (referred to as allosteric loop from now on) located at the interface of the nucleotide binding site and the central channel (Fig. 2b). The allosteric loop can adopt the mutually exclusive active and inactive conformations. The conformational change of one loop facilitates the same conformational change in the other two loops of the trimer due to steric hindrance within the central channel[15,19]. This mechanism thus conforms to the classical view of allostery.

[1]Institute of Enzymology, Research Centre for Natural sciences, Hungarian Academy of sciences, Budapest, Hungary. [2]Department of Applied Biotechnology and Food Science, Budapest University of Technology and Economics, Budapest, Hungary. [†]Present address: Gábor Merényi, Department of Molecular Biosciences, The Wenner-Gren Institute, Stockholm University, Sweden. Correspondence and requests for materials should be addressed to J.T. (email: toth.judit@ttk.mta.hu)

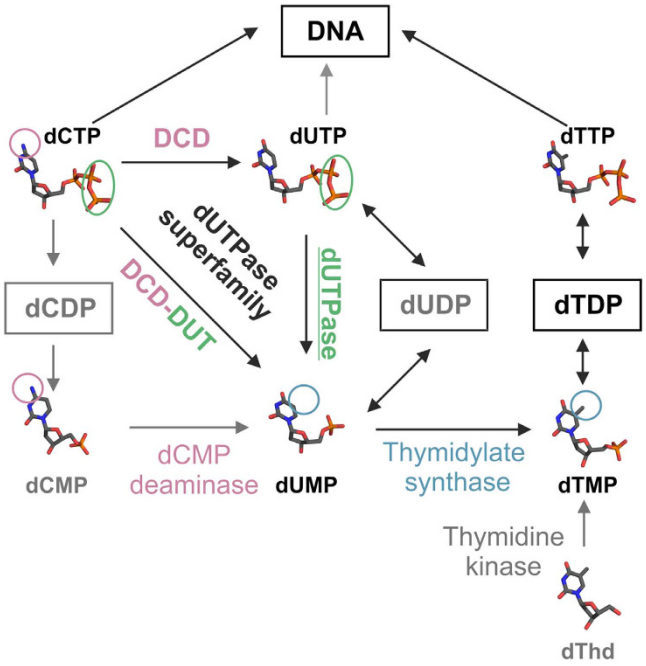

Figure 1. Overview of the dTTP biosynthesis pathways. The three dimensional structures of the nucleotides were extracted from pdb files (dCTP: 1XS4; dUTP: 2V9X; dUMP: 1SNF; dTMP: 1TMK; dTTP: 2QXX; dCMP: 1B5E; dThd: 2V9X) and are shown as atomic colored sticks (C: grey, O: red; N: blue; P: orange). Circled chemical groups call attention to the differences relevant to the enzymatic reactions that transform pyrimidine nucleotides into each other.

dUTPases, the other family that belongs to the dUTPase superfamily, display an even more intricate interaction pattern between their subunits than DCDs do. The C-terminal arm of dUTPases in almost all cases reaches across the trimer to the remote active site and therefore, all three subunits provide conserved residues to each active site[16]. This structure inspired the proposition that allosteric communication between the active sites of dUTPases should also exist[20–22]. Crystallographic observations in the human dUTPase suggested that some allosteric effect must help the release of the dUMP product[20]. Another study investigating the nature of the central channel of dUTPases found considerable difference in hydropathy between eukaryotic and prokaryotic dUTPases[21]. It was proposed that allostery can emerge through the hydrophilic central channel in eukaryotic dUTPases. A later NMR study suggested that the *Drosophila* enzyme exhibits cooperativity in both substrate and product binding based on signal intensity titrations well above the K_d of the respective complexes[22]. In the EIAV (Equine Infections Anemia Virus) enzyme, a Trp at the central channel senses the nucleotide-bound states of the active site[23] corroborating the potential of active site communication through the central channel. On the other hand, detailed kinetic analyses of dUTPases from various species (human[24], *E. coli*[25], EIAV[23], *Plasmodium falciparum*[26]) failed to directly detect any cooperative behavior in the enzymatic mechanism.

The cooperativity in DCD is best observed when dTTP, its feedback inhibitor binds to the active site. As the accommodation of the additional metal group on the thymine ring is possible only in the inactive conformation[15,19], the shift in the equilibrium between the active and inactive conformational states and the cooperative behavior is more pronounced in the presence of dTTP[15,19,27]. The substrate binding pocket of dUTPases, however, does not accommodate other bases than uracil with considerable affinity[20,25,28]. This property of dUTPases may make it difficult to recognize any allosteric behavior. The inherent allosteric potential in proteins may only appear by mutations that shift the distribution of the various conformational states[6,29]. Therefore, we designed mutations to access inactive conformational states in dUTPase potentially mimicking the ones observed in DCD and DCD-DUT. To this end, we created covalently linked human dUTPase pseudoheterotrimers (called hybrids henceforth) in which the active sites could be turned off selectively (Fig. 2c). We studied how the interruption of different steps of the enzyme cycle in one active site of the hybrid affects the activity of the non-mutated active sites using various enzymatic and structural biology approaches. Our experimental results combined with the comparative analysis of the structural features of dUTPase superfamily enzymes reveals an intriguing trade-off between regulation and efficiency, two ways of functional adaptation to distinct metabolic functions.

Results

Establishment and enzyme activity of asymmetric dUTPase hybrids. Mutations introduced to a homooligomeric protein appear in each subunit as the oligomer is assembled from identical monomers (Fig. 3a). To generate hybrid enzymes of the human dUTPase (hDUT), we therefore needed to create a covalently linked pseudohomotrimer (termed WWW) in which each subunit could be exchanged to selectively contain the desired mutation (Fig. 3b). The WWW construct was assembled from the previously described sensor-bearing

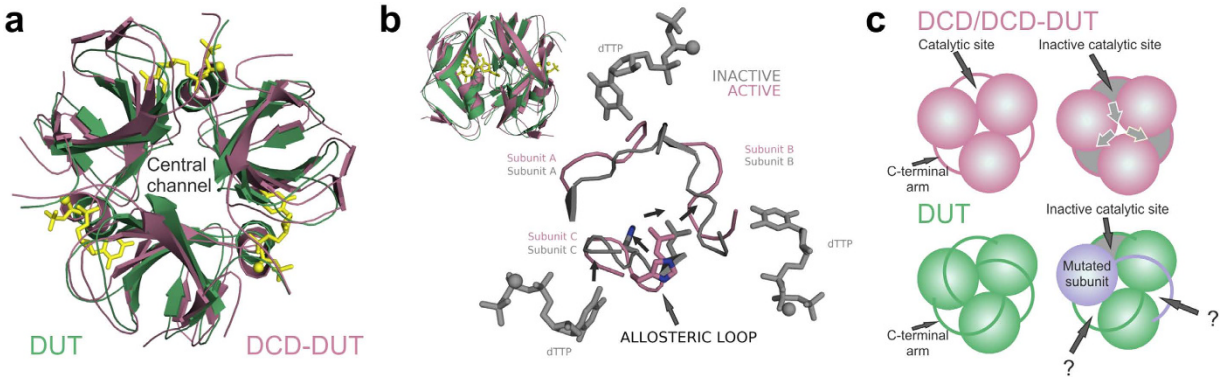

Figure 2. Structure and communication in the homotrimers of the dUTPase superfamily. (**a**) "Topview" of the superpositioned core structures of a dUTPase (from *Mycobacterium tuberculosis*, PDB: 2PY4) and a bifunctional DCD-DUT (also from *Mycobacterium tuberculosis*, PDB: 2QLP). The substrate analog dUPNPP (yellow sticks) in complex with Mg^{2+} ions (yellow spheres) is also shown within the dUTPase structure to highlight the active sites. (**b**) Upper left corner: "side" view of the superpositioned enzyme cores from panel (**a**). The position of the enlarged cross-section plane is indicated by the yellow sticks. Concerted conformational switch within the central channel of DCD-DUT is shown by superposing the apo enzyme in active conformation (PDB: 2QLP) with the dTTP bound enzyme in inactive conformation (PDB: 2QXX). Arrows highlight the most important conformational changes. Note, that only the inactive conformation can accommodate the methyl group of dTTP (grey sticks, Mg^{2+} ions: grey spheres). (**c**) Schematic representation of active site communication within the dUTPase superfamily. Grey color at the active sites represents enzymatic inactivity. In DCD (-DUT), arrows in the central channel indicate that the inactive conformation is spread through the central channel in a concerted way.

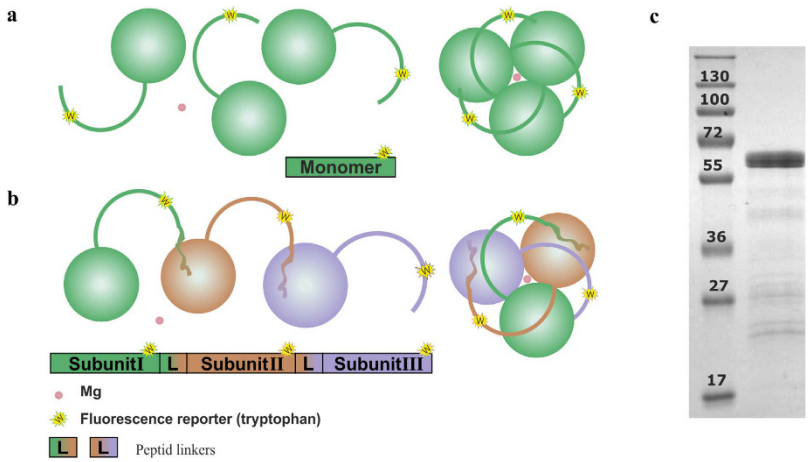

Figure 3. Schematic representation of the covalent trimer concept. (**a**) Schematic representation of the assembly of the $hDUT^{F158W}$ dUTPase. Green spheres represent the sensor-bearing $hDUT^{F158W}$ subunits. The structures reaching out from the subunits represent the swapping C-terminal arm of dUTPase. Yellow stars mark the tryptophan serving as intrinsic fluorescence signal of the enzyme conformations. The pink sphere indicates a Mg^{2+} ion. (**b**) Schematic representation of the covalent pseudotrimers. The projection of the swapping arms with color transition represents the flexible linkers connecting the C-terminus of one dUTPase protomer to the N-terminus of another one. Different colors of the protomers represent the possible heterogeneity within the trimer, i.e. every protomer can be changed independently from each other. (**c**) SDS-PAGE analysis of the purified WWW enzyme. The main band is located at the expected position which corresponds to the calculated molecular weight of 58064 Da.

$hDUT^{F158W}$ human dUTPase[24,30] monomers (W) connected with flexible peptide linkers[31] (see Online Methods and Supplementary Table 1). We previously used the F158W substitution to follow the enzymatic reaction steps using the intrinsic fluorescent signal of tryptophan 158[24,32,33]. In this position, a conserved aromatic residue overlaps with the uracil ring of the substrate in every dUTPase[33]. The electrostatic interaction between the tryptophan and uracil modifies the fluorescence properties of the tryptophan residue in a conformation-sensitive manner allowing the monitoring of the enzymatic cycle. The WWW enzyme could be expressed and purified (Fig. 3c) with similarly high yield as the homotrimer. We introduced each further mutation into the WWW scaffold by exchanging one or more of the W cassettes.

	k_{cat} (s^{-1})##	k_{sto} (s^{-1})##	K_M (μM)#	$K_{d,dUTP}$ (μM)#
$hDUT^{F158W}$	8 ± 3*	6.4*	3.6 ± 1.9*	0.83*
WWW	6.9 ± 0.5	6.33 ± 0.03	1.7 ± 0.5	0.29 ± 0.02
WWF	4.1 ± 0.5	6.13 ± 0.05	0.4 ± 0.3	0.29 ± 0.10
WWN	3.7 ± 0.3	6.31 ± 0.05	0.4 ± 0.3	0.59 ± 0.08
WNN	2.0 ± 0.1	5.72 ± 0.13	2.1 ± 0.5	0.29 ± 0.03
WWS	3.2 ± 0.3	6.26 ± 0.04	2.5 ± 1.2	0.70 ± 0.02

Table 1. Kinetic parameters. *Data from Toth *et al.* JBC[24]. #Errors represent the fitting error. ##Errors represent the standard error (SE).

The sequence of the linker (ASGAGGSEGGGSEGGTSGATG/SL/Q) was borrowed from a study in which it was used for the same purpose: genetic manipulation of individual subunits. The visible N- and C-terminal amino acids of hDUT can be found 28.62 Å apart in the 2HQU structure. The 22 amino acid linker spans 77 Å when maximally streched. The flexible N-terminal 23 amino acids add another 80.5 Å streched length to the linker. Therefore, we anticipated that this linker does not restrict the wild-type dynamics of the hDUT structure. To test whether the linkers influence the enzymatic properties of the WWW enzyme, we applied transient kinetic analysis using the fluorescent signal of W158. The kinetic parameters of substrate binding and hydrolysis as well as the characteristic fluorescence changes during the course of the reaction remained similar in WWW to that measured in $hDUT^{F158W}$ (Supplementary Fig. 1, Table 1). We also performed limited tryptic digestion of the covalent enzyme to cleave the linkages between the subunits. The cleaved enzyme displayed basically identical steady-state and transient kinetic properties to that of the covalently linked one (Supplementary Fig. 2). We concluded that the linkers do not influence the enzymatic mechanism and thus the covalent enzyme is suitable for further investigations.

Four different hybrid enzymes were subsequently created to investigate the possible allosteric effects of conformational changes upon substrate binding, hydrolysis or product release (Fig. 4a).

To investigate the allosteric effect of a possible global conformational change upon substrate binding, we created an active site that is unable to accommodate the uracil ring (Supplementary Fig. 3a) and is thus defective in substrate binding and any conformational change coupled to it. Control experiments with the homotrimeric form of the A98F mutant ($hDUT^{F158W, A98F}$) confirmed that it could not bind the substrate and was entirely inactive (Supplementary Fig. 3b–f). We introduced this mutation to the covalent construct to obtain WWF.

The following constructs were designed to investigate whether conformational changes occurring upon hydrolysis or product release are necessary to be transmitted to neighboring active sites for the global activity of the trimer.

In the WWN and WNN constructs, the conserved catalytic Asp from the third conserved motif was changed to Asn (Supplementary Fig. 3g) in one or two active sites, respectively. This Asp/Asn substitution has been described to reduce the catalytic activity close to zero while the substrate binding properties do not change[34]. We also tested the enzymatic properties of $hDUT^{D102N,F158W}$ and found that the catalytic activity decreased below the detectable level ($<0.002\,s^{-1}$) both under steady-state and single turnover conditions while the substrate binding properties remained unaffected compared to $hDUT^{F158W}$ (Supplementary Fig. 3h).

In the WWS enzyme, we removed the C-terminal P-loop-like motif of the last subunit of the pseudoheterotrimer. This conserved motif interacts with the γ-phosphate of dUTP and stacks over the uracil ring to orient the catalytic apparatus and stabilize the transition state[30,32,33,35]. The P-loop-like motif is only present in dUTPases and is missing from DCDs or DCD-DUTs. Its removal results in major decrease (~720 fold) of the catalytic constant and minor (~3 fold) increase in the dissociation constant of the enzyme-substrate complex[30].

dUTPase active sites work independently from each other. Potential allosteric interactions within the hybrids WWN, WNN, WWS and WWF were analyzed using the combination of steady state and transient kinetic measurements. All constructs proved to be active indicating that the arrest of the enzyme cycle in a given active site does not compromise the enzymatic turnover in the others. Steady-state activity titrations of all hybrid enzymes exhibited Michaelis-Menten kinetics (Fig. 4b). The maximal initial velocities (V_{max}) decreased proportionally with the number of inactivated sites, i.e. WWN, WWF and WWS displayed about 2/3, while WNN displayed approximately 1/3 activity compared to WWW (Fig. 4c, Table 1). This indicates that the activity per working subunit is unaltered in the hybrid enzymes. The Michaelis constants did not change considerably compared to the WT (Table 1). Single turnover stopped-flow measurements showed that the kinetic mechanism of the asymmetric hybrids is identical with that of the control WWW (Supplementary Fig. 4). The k_{obs} for substrate binding and the single turnover rate constants (k_{STO}) remained unaltered (Table 1, Fig. 4c). This implies that the observed decrease in the steady-state activity is only due to the decreased active site concentration.

The kinetics of substrate binding to the hybrid enzymes was also investigated under pseudo first order conditions. A large part of the time courses got lost in the dead-time of the instrument which hindered the determination of the rate constants. The total signal change, however, could be used to determine the dissociation constants (K_d) of the enzyme-dUTP complexes (Fig. 4d). The obtained K_d-s were similar to that of the WWW-dUTP complex (Table 1).

In summary, a global active to inactive conformational transition observable in DCDs could not be identified in dUTPase even in conditions potentially mimicking the asymmetry in a partially dTTP-saturated DCD enzyme

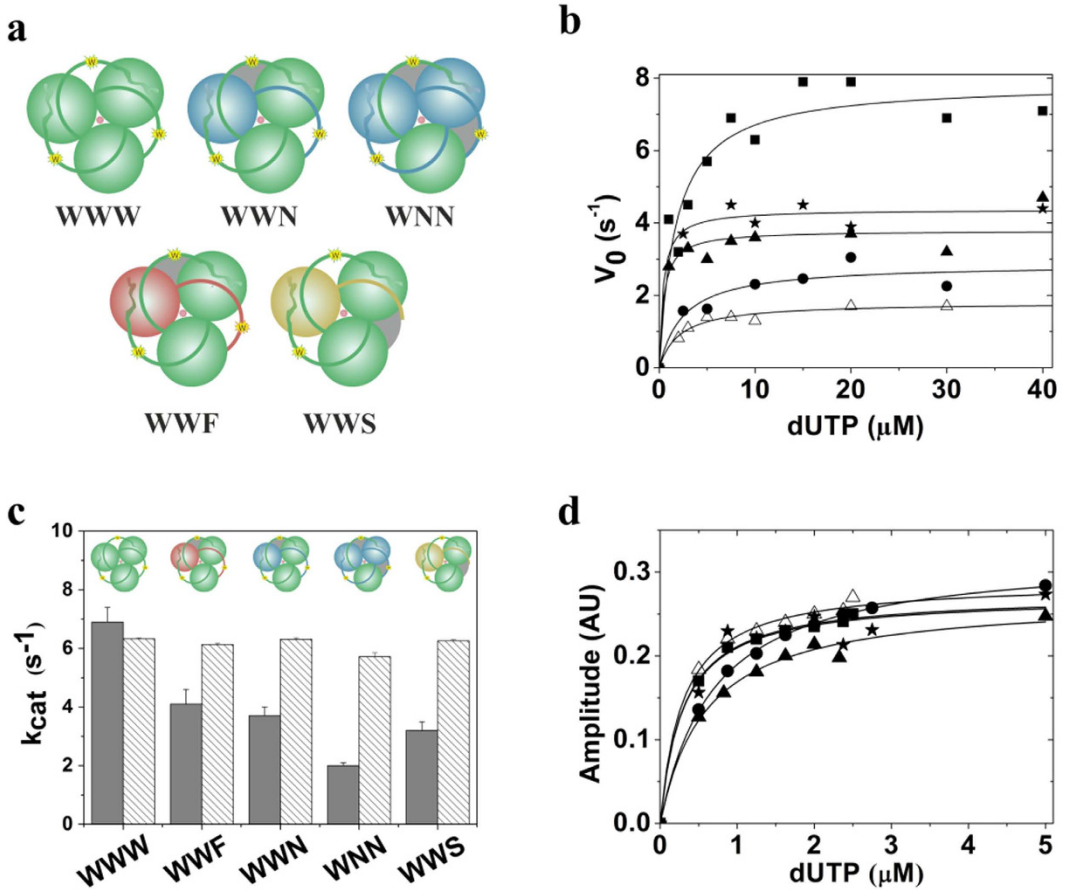

Figure 4. Asymmetric hybrid enzymes exhibit non-cooperative kinetics in the different reaction steps. (**a**) Schematic representation of the created hybrids (covalent heterotrimers). Blue, red and yellow spheres represent dUTPase protomers containing the D102N, A98F and T148STOP mutations, respectively. Note, that all protomers contain the F158W mutation as well, except for the T148STOP mutant. Grey areas indicate enzymatic inactivity. (**b**) Steady-state kinetics of human dUTPase constructs: WWW (solid square), WWN (solid triangles), WNN (open triangles), WWF (solid stars), WWS (solid circle). Smooth lines through the data are hyperbolic fits yielding $V_{max} = 7.9 \pm 0.5\,s^{-1}$ for WWW, $V_{max} = 4.4 \pm 0.2\,s^{-1}$ for WWF, $V_{max} = 3.8 \pm 0.2\,s^{-1}$ for WWN, $V_{max} = 1.8 \pm 0.1\,s^{-1}$ for WNN, $V_{max} = 2.9 \pm 0.3\,s^{-1}$ for WWS. K_M values are listed in Table 1. (**c**) Comparison of the catalytic constants (striped bar) and apparent catalytic constants (grey bar) for determined by single turnover (transient kinetics) and steady-state experiments, respectively. See also Table 1 for the data. (**d**) Fluorescence intensity titrations upon dUTP binding to the various dUTPase constructs measured by stopped-flow (the symbol code is identical to that in panel (**b**). Smooth lines through data are hyperbolic fits yielding K_d values summarized in Table 1.

(Fig. 2c). On the contrary, Fig. 4c clearly indicates that the active sites turn over independently from each other. In case of a cooperative transition to a global inactive state we would expect inactivity following the first turnover or non-proportional activity decrease in the hybrid enzymes containing one or two defective active sites.

The conformational flexibility of human dUTPase is restricted by Mg^{2+} binding to the central channel. The conformational changes resulting in the observed cooperative behavior is transmitted through the central channel in DCD family enzymes. We therefore investigated the structural features of the channel possibly responsible for the lack of conformational transmission in dUTPase. The site of cooperative conformational change of DCD(-DUT) enzymes corresponds to one of the two suggested Mg^{2+} binding sites in the human dUTPase[20,36] (Asp95, Fig. 5a). In contrast, no metal binding to DCD(-DUT) enzymes has been reported.

To evaluate the role of Mg^{2+} binding to the central channel of $hDUT^{F158W}$, we conducted in solution structural investigations in the presence and absence of Mg^{2+}. The near-UV CD spectra showed considerable changes upon the addition of Mg^{2+} to the apo $hDUT^{F158W}$ indicating that the metal ion binds to the enzyme and modifies its structure (Fig. 5b). The largest signal change was observable at 285 nm probably yielded by the rearrangement of Tyr residues (Fig. 5a). The far-UV CD spectra, on the other hand, showed only minor changes upon Mg^{2+} addition (Fig. 5b inset) implying that metal binding may not induce major changes in the secondary structure. The WWW enzyme showed similar spectral changes to $hDUT^{F158W}$ upon the addition of Mg^{2+} (Supplementary Fig. 5a,b).

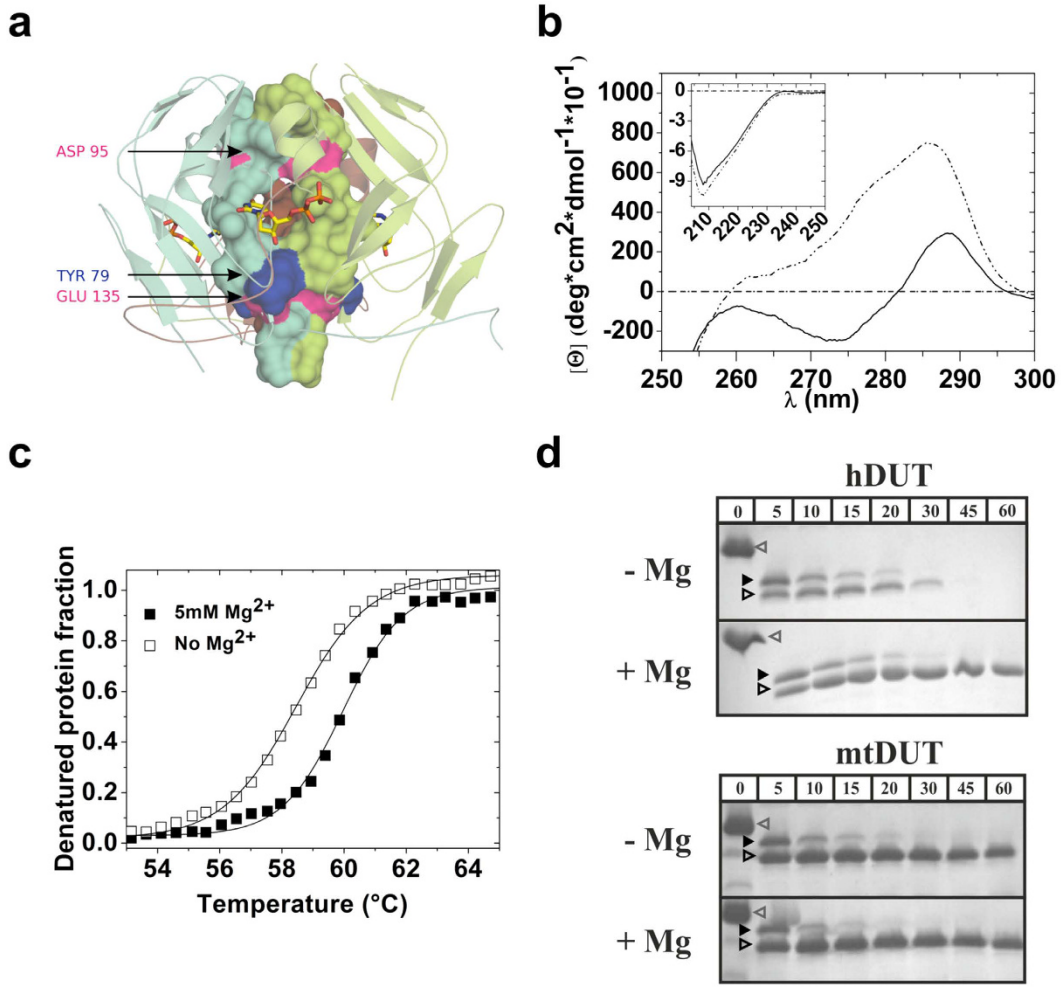

Figure 5. Mg^{2+} binding to the central channel reduces the flexibility of the dUTPase trimer. (**a**) Predicted Mg^{2+} binding sites (pink) within the central channel of human dUTPase (PDB: 1Q5H, colored by subunits). The residues constituting the channel wall are shown as surface while the rest of the molecule is shown as cartoon representation. The Tyr residues possibly responsible for the change in the near UV spectra upon Mg^{2+} binding are shown in blue. Active sites are highlighted by the bound dUDP (shown as sticks with atomic coloring). (**b**) Near UV and Far UV (inset) spectra of $hDUT^{F158W}$ in the presence (dash-dot-dot) and in the absence (solid line) of 5 mM $MgCl_2$. The spectrum of the buffer is marked by dash-dot line. (**c**) Thermal unfolding of $hDUT^{F158W}$ in the presence and in the absence of 5 mM Mg^{2+}. Smooth lines through the data are Boltzmann fits (Equation (4)). The melting temperatures (transition midpoints) are $Tm = 59.8 \pm 0.2$ °C in the presence of $MgCl_2$ and $Tm = 58.4 \pm 0.2$ °C in the absence of $MgCl_2$ ($n = 3$). Errors represent SD. (**d**) Limited trypsinolysis of $hDUT^{F158W}$ and $mtDUT^{H145W}$ performed in the presence and in the absence of 5 mM $MgCl_2$. The open gray arrow head, the black arrow head and the open black arrow head indicate the intact, the N-terminal cleaved and the N- and C-terminal cleaved enzymes, respectively. The densitometric analysis of the relative amount of the core enzyme (intact enzyme + N-terminal cleaved enzyme + N- and C-terminal cleaved enzyme) is shown in Supplementary Fig. 5d.

The thermal denaturation of $hDUT^{F158W}$ could be described with a two-state equilibrium model indicating that the heat-induced unfolding of the trimer happens in one step, without a significantly populated intermediate state of dissociated and folded monomers[37] (Fig. 5c). In the absence of Mg^{2+}, we observed a slight but reproducible decrease in the melting temperature (T_m) (Fig. 5c) suggesting that the stability of the enzyme is slightly decreased in the absence of Mg^{2+} similarly to what was found in the *D. melanogaster* dUTPase[38]. The covalent WWW enzyme produced a more complicated melting curve (Supplementary Fig. 5c). However, the stabilization effect of Mg^{2+} could also be observed.

To test the potentially increased flexibility of $hDUT^{F158W}$ in the absence of Mg^{2+}, we performed limited trypsinolysis. $hDUT^{F158W}$ was highly sensitive to tryptic digestion in the absence of Mg^{2+} (Fig. 5d and Supplementary Fig. 6) whereas the control *Mycobacterium tuberculosis* dUTPase (mtDUT) that does not contain Mg^{2+} binding sites in its central channel (Fig. 6f) was not (Fig. 5d and Supplementary Fig. 6). Following the expected cleavage of the flexible N- and C-termini[32], the remaining enzyme core – which is otherwise stable for long time – disappeared within an hour (Fig. 5d). In case of the mtDUT, the enzyme core remained stable during the one our

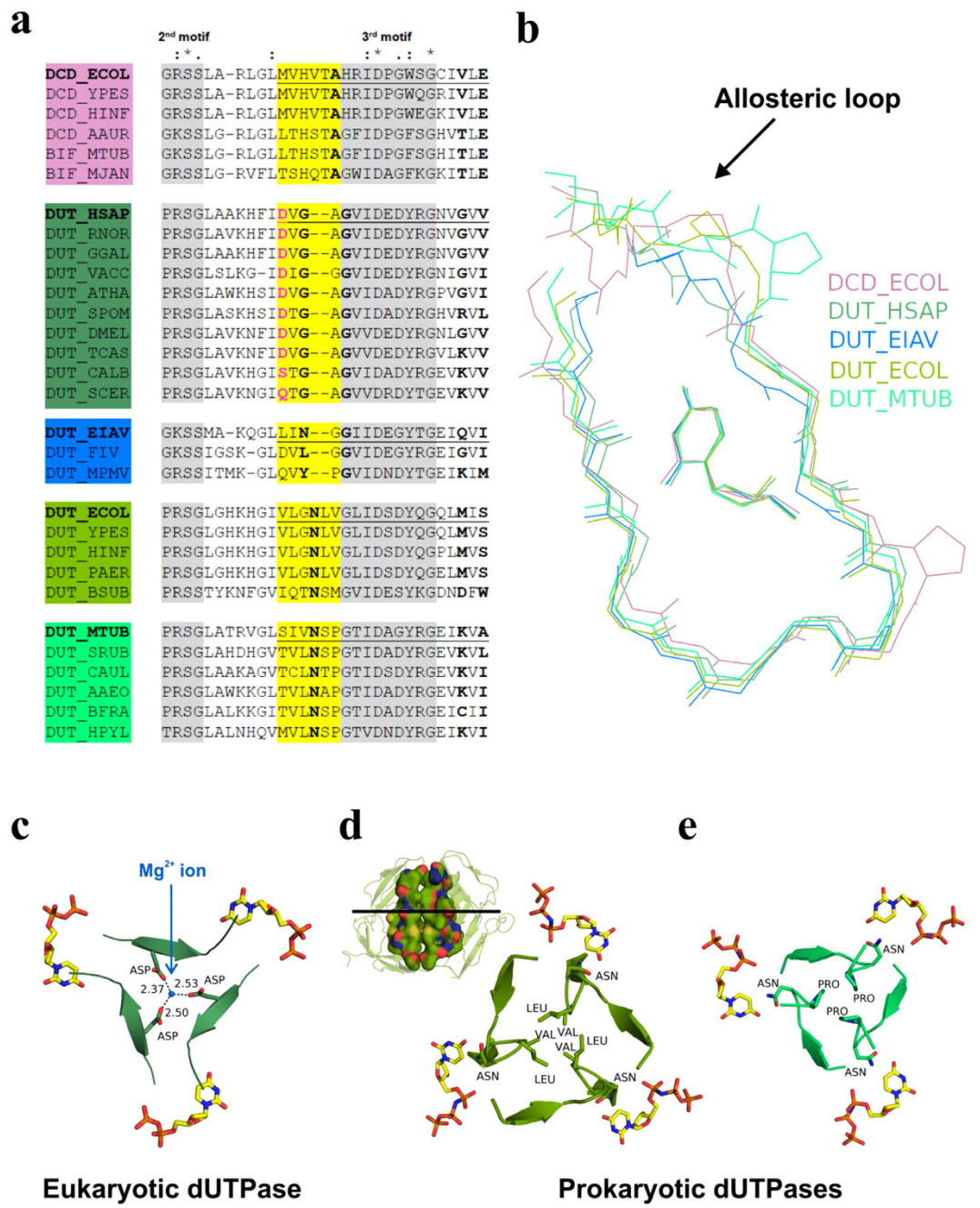

Figure 6. Stabilization of the central channel hinders conformational coupling with the active sites in dUTPases. (**a**) Sequence comparison of the allosteric loop region within the dUTPase superfamily. The alignment was created by clustalW with minimal manual editing. Allosteric loop, yellow highlight; the uracil binding cleft, underlined; conserved motifs, grey highlight; uracil ring coordination, bold. Amino acid conservation is distinguished by: identity (*), strong similarity (:) and weak similarity (.). (**b**) Superposition of the 3D structures of representative dUTPase superfamily enzymes from panel (**a**) (PDB: *E. coli* DCD – 1XS1, hDUT – 2HQU, EIAV DUT – 1DUC, *E. coli* DUT – 1RN8, MTB DUT – 3HZA). The superposition was performed by the alignment of the bound nucleotides using PyMol. Only the main chain atoms of the proteins and the nucleoside part of the ligands are shown for clarity. The color code refers to the proteins in panel (**a**). Note the structural variance in the allosteric loop. (**c–e**) Cross section of the central channel of hDUT (1Q5H), *E. coli* DUT and MTB DUT at the level of the uracil binding pocket. The side chains within the central channel and the bound ligands are shown as sticks with atomic coloring. The Mg^{2+} ion is represented as blue non-bound sphere. In panel **(d)** the longitudinal view of the threefold trimer interface (two subunits are shown) of the *E. coli* DUT is also shown using surface representation with atomic coloring to highlight the hydrophobic character of the central channel.

experiment. This phenomenon indicates that the quaternary structure of $hDUT^{F158W}$ is significantly more flexible in the absence than in the presence of Mg^{2+}.

Structural comparison of dUTPase superfamily enzymes reveals trade-off in conformational flexibility and active site specificity. To understand the structural basis of the mechanistic differences within the dUTPase superfamily, we compared the central channel, the region of the allosteric loop and the nucleobase binding region in DCDs and dUTPases (Fig. 6).

The amino acids responsible for the binding of the nucleobase are located around motif 3 (Fig. 6a) at the N- and C-terminal parts of the β-hairpin accommodating the nucleoside (Fig. 6b). The N-terminal few amino acids of the β-hairpin overlap with the allosteric loop in the DCD family. We found that this region is highly diverse in size and amino acid composition within the superfamily (Fig. 6a,b).

In eukaryotic dUTPases, the loop is shorter by 2 or 3 amino acids than in DCDs resulting in a tighter uracil binding cleft. In these enzymes, mostly main chain atoms establish hydrogen bonding interactions with the nucleobase, which was proposed to contribute to their specificity for uracil[20]. The very same loop confers the Mg^{2+} binding site facing the central channel (Fig. 6c, Fig. 5a).

In retroviral dUTPases (EIAV shown as the representative), the loop is even shorter than that of the Mg^{2+} binding site-bearing eukaryotic dUTPases (Fig. 6a,b).

The allosteric loop of prokaryotic dUTPases is of the same length as that of DCDs. However, its amino acid composition is different (Fig. 6a) resulting in a tighter central channel mainly due to the LV/SM/SP/AP peptides protruding in it (Fig. 6a,b). The conformational flexibility of the channel is restricted by the hydrophobic interactions of the modified allosteric loop (Fig. 6d) or by a conserved Pro (Fig. 6e). In DCDs, the conserved Ala of the allosteric loop engages in H-bonding with the oxo group of the substrate uracil. If thymine is bound to the active site, the HVTA peptide containing this Ala moves into the channel (cf. Fig. 2b). In contrast, a conserved Asn plays the same H-bonding role in prokaryotic dUTPases but it resides in a conformationally restricted peptide (Fig. 6a,d,e).

The sequence and structural comparison with DCD enzymes reveals that the various evolutionary branches of dUTPases possess an altered or shortened allosteric loop which coincides with the conformational stabilization of the central channel. Interestingly, most of the observed alterations contribute to the specificity for dUTP at the same time. We propose that the central channel of dUTPases features increased stability at the cost of lacking the potential for mediating cooperativity as observed in DCDs. Apparently, the same structural element of the active site is responsible for substrate specificity and for the communication through the central channel.

Discussion

Allosteric enzyme regulation is one of the general means of controlling biochemical processes. The appropriate concentration and balance of dNTPs for DNA synthesis and repair is commonly regulated by both homotrop and heterotop allosteric mechanisms[39,40]. Feedback inhibition by dTTP in two of the three dUTPase superfamilies, DCDs and the bifunctional DCD-DUTs (Fig. 1), seems to be important to maintain the appropriate dCTP/dTTP ratio[15,19]. The feedback inhibitor dTTP binds to the active sites which communicate with each other within the homotrimer resulting in an all-or-none inhibition pattern. This is a more complicated and more efficient inhibition mechanism than simple competitive inhibition due to the fact that 1 dTTP molecule elicits the complete inhibition of 3 active sites. Interestingly, the activity of the non-homologous dCMP deaminases is also modified by dCTP and dTTP with intricate regulation pattern involving cooperativity[41–43]. Probably, this kind of regulation is important in maintaining the correct dCTP/dTTP ratio[44].

We attempted to detect allosteric behavior in dUTPases by engineering hybrid enzymes to restrict putative allosteric transmission between active sites at various stages of the enzymatic cycle. Interestingly, however, the enforced asymmetry in the dUTPase trimer did not elicit any instance of cooperative behavior despite the fact that dUTPases have the most intertwined trimeric structure of all within the dUTPase superfamily. We determined that i) the active sites work independently from each other; ii) Mg^{2+} binding in the central channel reduces the flexibility and increases the thermal stability of the quaternary structure; iii) the allosteric loop that connects the active site to the central channel is conformationally restricted in dUTPases compared to DCD family enzymes. This phenomenon is interrelated with structural solutions for increased dUTP specificity in every case.

It is common in enzyme evolution that mutations in flexible active site loops are responsible for altered substrate specificity[45]. Since active sites are often located at intersubunit/interdomain clefts, these flexible loops have a potential to mediate allosteric communication between the active sites. In our case, it seems that the specialization for a single substrate results in the loss of allosteric communication. The shorter/less flexible allosteric loop compared to that of DCDs and DCD-DUTs is related to increased dUTP specificity (Fig. 6). Another dUTPase "invention" is the C-terminal P-loop-like motif that discriminates against dUDP and makes dUTP hydrolysis more efficient by several orders of magnitude than DCD-DUTs[30]. The gain of specificity together with the enhancement of the catalytic power represent features that make dUTPases significantly more powerful in dUTP breakdown as compared to DCD-DUTs. This advance may be necessary to avoid the appearance of the non-canonical uracil base in DNA that induces the activation of DNA repair mechanisms upon non-physiological uracil accumulation leading to severe to fatal consequences for the cell[46–48]. The cooperative allosteric behavior in DCDs and DCD-DUTs, on the other hand, make these enzymes suitable for the regulation of the nucleotide pool. We propose that the trade-off between cooperativity and specificity in the dUTPase superfamily represents instances of adaptation to the distinct roles of dUMP production for dTTP synthesis and dUTP elimination for uracil-DNA avoidance, respectively.

Methods

Reagents. Molecular biology products were from New England Biolabs (US) and Fermentas (Canada), electrophoresis and chromatography reagents were from Bio-Rad (US) and Qiagen (Netherland). Phenol red was

from Merck (Germany). dUMP, dUDP and α,β-imido-dUTP (dUPNPP) was from Jena Bioscience (Germany), dUTP and other chemicals were from Sigma–Aldrich (US).

Cloning and mutagenesis. Site-directed mutagenesis was performed by the QuikChange method (Stratagene) and was verified by sequencing. The enzyme conferring a tryptophan sensor in the active site ($hDUT^{F158W}$) was used as wild-type[24,32,33]. The following mutants were created within this construct: Asp102 to Asn ($hDUT^{F158W,D102N}$) and Ala98 to Phe ($hDUT^{F158W,A98F}$). Mutagen forward and reverse primers are presented in Supplementary Table 1. The covalent wild type enzyme (WWW) was created by genetic engineering. $hDUT^{F158W}$ was amplified with primers encoding linkers and various restriction sites (Supplementary Table 1) to create the three subunits of WWW. The subunits were cloned to pET45b plasmid as individual restriction cassettes. Covalent pseudoheterotrimers (hybrids) were then created by changing one or two of the wild type cassettes in WWW to mutant one(s).

Protein expression and purification. Expression and purification of noncovalent human dUTPase proteins were done as described previously in Varga *et al.* FEBS Letters[32]. Covalent dUTPase pseudotrimers were expressed and purified similarly, except that BL21 Rosetta (pLysS) cells (Novagen) were used instead of BL21. The expression and purification of the His-tagged *Mycobacterium tuberculosis* dUTPase (mtDUT) was done based on Varga *et al.* BBRC[49]. The protein concentration was measured using the Bradford method (Bio-Rad Protein Assay) and by UV absorbance. Extinction coefficients were calculated based on the amino acid sequence using the ProtParam tool (http://web.expasy.org/protparam/). Extinction coefficients for the proteins were: $\lambda_{280} = 16055\,M^{-1}cm^{-1}$ for the $hDUT^{F158W}$, $hDUT^{F158W,D102N}$ and $hDUT^{F158W,A98F}$; $\lambda_{280} = 48290\,M^{-1}\,cm^{-1}$ for the WWW, WWF, WWN and WNN and $\lambda_{280} = 42790\,M^{-1}\,cm^{-1}$ for the WWS construct. Protein concentration is given in monomer/subunit concentration in every case. All measurements were carried out in a buffer comprising 20 mM HEPES pH 7.5, 100 mM NaCl, 2 mM $MgCl_2$ and 2 mM ß-mercaptoethanol ("assay buffer") if not stated otherwise.

Steady-state colorimetric dUTPase assay was performed as described in Varga *et al.* BBRC[49]. This phenol red indicator assay was used to detect the protons released in the dUTPase reaction. 0.01–1 μM protein was used for the dUTPase assay in a buffer containing 1 mM HEPES pH 7.5, 100 mM KCl, 40 μM phenol red and 5 mM $MgCl_2$. A Specord 200 spectrophotometer (Analytic Jena, Germany) and 10 mm path length thermostatted cuvettes were used at 20 °C and absorbance was recorded at 559 nm. The initial velocity was determined from the first 10% of the progress curves. Initial velocities were plotted against substrate concentration and the results were fitted with the Michaelis–Menten equation.

Fluorescence measurements. Fluorescence spectra and intensity titrations were recorded on a Jobin Yvon Spex Fluoromax-3 spectrofluorometer in the assay buffer at 20 °C. Trp fluorescence was excited at 297 nm, emission spectra were recorded between 320–400 nm while the fluorescence intensity titrations were detected at 345 nm. Additional fluorescence or inner filter effect imposed on the measured intensities during the titration experiments were corrected by subtracting the corresponding buffer spectra. Titration data were fitted with the equation describing 1:1 stoichiometry for the dissociation equilibrium assuming no cooperativity:

$$y = s + A * \frac{(c + x + K) \pm \sqrt{(c + x + K)^2 - 4cx}}{2c} \quad (1)$$

where x is the ligand concentration and y is the fluorescence intensity, $s = y$ at $x = 0$, A is the amplitude of the fluorescence intensity change, c is the enzyme concentration and K is the dissociation constant of the ligand complex.

Thermofluor assay. Thermal shift assays were carried out on an Mx3000P® QPCR System (Agilent Technologies Company). Thermal shift reactions were performed in a 96-well thin-wall microplate in a total volume of 25 μl containing 500× diluted Sypro® Orange dye. Samples were heated from 25.0 to 80.0 °C. The speed of heating was 1 °C/minute. The protein concentration of $hDUT^{F158W}$ was 0.8 mg/ml in the measurements, while the WWW enzyme was used at 2 mg/ml concentration. To compensate for the difference in the ionic strength between the samples with and without $MgCl_2$, NaCl was added according to Equation 2:

$$I = 0.5 * \sum(c_i * z_i^2) \quad (2)$$

where I is the ionic strength, c_i is the concentration, z_i is the charge of the particular ion and i is the index of summation.

The raw data of the heat-induced unfolding monitored by fluorescence emission were converted to the apparent fraction of native protein F_N, according to Equation (3):

$$F_N = \frac{(\theta_U + m_U * T) - \theta}{(\theta_U + m_U * T) - (\theta_N + m_N * T)} \quad (3)$$

where θ is the observed spectroscopic signal at temperature T, θ_N and θ_U are the intercepts and m_N and m_U are the slopes of the pre- and post-transitional base lines of the raw data, respectively. The F_N vs. T plot was converted to the F_U vs. T plot by using the $F_N + F_U = 1$ equation, where F_U is the fraction of unfolded protein. The F_U vs. T plot was then fitted with the Boltzmann (Equations (4)) the midpoint of the transition

$$y = \frac{A_1 + A_2}{1 + e^{\frac{x - x_0}{dx}}} + A_2 \quad (4)$$

where *A1* and *A2* are the pre- and post-transitional base lines and x_0 is the transition midpoint.

Circular dichroism measurements. CD spectra recording was carried out in a JASCO 720 spectropolarimeter at 20 °C using a quartz cuvette with 1 mm (far UV) or 10 mm (near UV) path length. Far UV and near UV spectra were recorded at 200–250 nm or 250–300 nm, respectively. All protein containing spectra were corrected by subtracting the corresponding buffer spectra.

Fast kinetics experiments. Fluorescence stopped-flow measurements were carried out at 20 °C using an SX-20 stopped-flow apparatus (Applied Photophysics, UK) as described previously[24]. Equal volumes (50 μl) of dUTPase enzyme and dUTP solutions were mixed and 8 traces were recorded and averaged for each time course. Under single turnover conditions, a triple exponential equation was fitted to the averaged traces to determine the catalytic constants based on Tóth *et al.* JBC[24]. For the determination of binding rate constants, the ligand titration was performed under pseudo-first order conditions. The observed rate constants for the two binding steps described previously (collision complex formation and isomerisation[24]) were determined by fitting double exponential equations. Where exponential equation for the first part of the time course could not been fitted due to the large signal loss in the dead time, the K_d was estimated by plotting the amplitudes of the fluorescence decrease against ligand concentration followed by fitting a hyperbole.

Limited trypsinolysis. The limited tryptic digestion of dUTPases was performed at 37 °C using 0.5 mg/ml protein concentration and 1:20 trypsin: dUTPase ratio in assay buffer also containing either 0.1 mM EDTA or 5 mM $MgCl_2$. The tryptic digestion was terminated by the addition of 1 mM PMSF to the samples taken at different time points. The time dependence of the trypsinolysis was analyzed on SDS-PAGE. Limited trypsinolysis in the presence of 1 mM α,β-imido-dUTP was performed likewise in the same buffer either with or without Mg^{2+}. SDS-PAGE gels were analyzed by densitometry with the UVIdoc software.

The cleavage of the linkers of the WWN covalent enzymes was performed at 25 °C using 0.8 mg/ml protein concentration and 1:500 trypsin: dUTPase ratio in the assay buffer also containing 1 mM α,β-imido-dUTP for the protection of the C-terminus[32] and 5 mM $MgCl_2$. The digestion was terminated by the addition of 1 mM benzamidine hydrochloride after 5 minutes. The sample was dialyzed against assay buffer containing 1mM benzamidine and 5 mM $MgCl_2$ to remove α,β-imido-dUTP. The control sample was treated similarly without the addition of trypsin. The trypsinolysis product, the W/W/N heterotrimer, was analysed on SDS-PAGE and by enzymatic assays.

Data fitting and statistical analysis. Data fitting was performed using Origin 7.5 (OriginLab Corp., Northampton, MA) or the stopped-flow software. Error bars represent the standard deviation of the mean of several measurements depending on the type of assay (detailed at each Method section and in the legends of the Figures and Tables).

References

1. Changeux, J.-P. Allostery and the Monod-Wyman-Changeux model after 50 years. *Annu. Rev. Biophys.* **41,** 103–33 (2012).
2. Changeux, J.-P. 50 Years of Allosteric Interactions: the Twists and Turns of the Models. *Nat. Rev. Mol. Cell Biol.* **14,** 819–29 (2013).
3. Motlagh, H. N., Wrabl, J. O., Li, J. & Hilser, V. J. The ensemble nature of allostery. *Nature* **508,** 331–9 (2014).
4. Petit, C. M., Zhang, J., Sapienza, P. J., Fuentes, E. J. & Lee, A. L. Hidden dynamic allostery in a PDZ domain. *Proc. Natl. Acad. Sci. USA* **106,** 18249–54 (2009).
5. Tzeng, S.-R. & Kalodimos, C. G. Dynamic activation of an allosteric regulatory protein. *Nature* **462,** 368–72 (2009).
6. Gunasekaran, K., Ma, B. & Nussinov, R. Is allostery an intrinsic property of all dynamic proteins? *Proteins* **57,** 433–43 (2004).
7. Warner, H. R., Duncan, B. K., Garrett, C. & Neuhard, J. Synthesis and metabolism of uracil-containing deoxyribonucleic acid in Escherichia coli. *J. Bacteriol.* **145,** 687–95 (1981).
8. Studebaker, a W., Lafuse, W. P., Kloesel, R. & Williams, M. V. Modulation of human dUTPase using small interfering RNA. *Biochem. Biophys. Res. Commun.* **327,** 306–10 (2005).
9. Merényi, G. *et al.* Cellular response to efficient dUTPase RNAi silencing in stable HeLa cell lines perturbs expression levels of genes involved in thymidylate metabolism. *Nucleosides. Nucleotides Nucleic Acids* **30,** 369–90 (2011).
10. Castillo-Acosta, V. M., Estévez, A. M., Vidal, A. E., Ruiz-Perez, L. M. & González-Pacanowska, D. Depletion of dimeric all-alpha dUTPase induces DNA strand breaks and impairs cell cycle progression in Trypanosoma brucei. *Int. J. Biochem. Cell Biol.* **40,** 2901–13 (2008).
11. Castillo-Acosta, V. M. *et al.* Increased uracil insertion in DNA is cytotoxic and increases the frequency of mutation, double strand break formation and VSG switching in Trypanosoma brucei. *DNA Repair (Amst).* **11,** 986–95 (2012).
12. Békési, A. *et al.* Developmental regulation of dUTPase in Drosophila melanogaster. *J. Biol. Chem.* **279,** 22362–70 (2004).
13. Johansson, E., Bjornberg, O., Nyman, P. O. & Larsen, S. Structure of the bifunctional dCTP deaminase-dUTPase from Methanocaldococcus jannaschii and its relation to other homotrimeric dUTPases. *J. Biol. Chem.* **278,** 27916–22 (2003).
14. Johansson, E. *et al.* Structures of dCTP deaminase from Escherichia coli with bound substrate and product: reaction mechanism and determinants of mono- and bifunctionality for a family of enzymes. *J. Biol. Chem.* **280,** 3051–9 (2005).
15. Helt, S. S. *et al.* Mechanism of dTTP inhibition of the bifunctional dCTP deaminase:dUTPase encoded by Mycobacterium tuberculosis. *J. Mol. Biol.* **376,** 554–69 (2008).
16. Vértessy, B. G. & Tóth, J. Keeping uracil out of DNA: physiological role, structure and catalytic mechanism of dUTPases. *Acc. Chem. Res.* **42,** 97–106 (2009).
17. Price, a R. Bacteriophage PBS2-induced deoxycytidine triphosphate deaminase in Bacillus subtilis. *J. Virol.* **14,** 1314–7 (1974).
18. Björnberg, O., Neuhard, J. & Nyman, P. O. A bifunctional dCTP deaminase-dUTP nucleotidohydrolase from the hyperthermophilic archaeon Methanocaldococcus jannaschii. *J. Biol. Chem.* **278,** 20667–72 (2003).
19. Johansson, E. *et al.* Regulation of dCTP deaminase from Escherichia coli by nonallosteric dTTP binding to an inactive form of the enzyme. *FEBS J.* **274,** 4188–98 (2007).

20. Mol, C. D., Harris, J. M., McIntosh, E. M. & Tainer, J. A. Human dUTP pyrophosphatase: uracil recognition by a beta hairpin and active sites formed by three separate subunits. *Structure* **4,** 1077–92 (1996).
21. Fiser, A. & Vértessy, B. G. Altered subunit communication in subfamilies of trimeric dUTPases. *Biochem. Biophys. Res. Commun.* **279,** 534–42 (2000).
22. Dubrovay, Z. *et al.* Multidimensional NMR identifies the conformational shift essential for catalytic competence in the 60-kDa Drosophila melanogaster dUTPase trimer. *J. Biol. Chem.* **279,** 17945–50 (2004).
23. Nord, J., Kiefer, M., Adolph, H. W., Zeppezauer, M. M. & Nyman, P. O. Transient kinetics of ligand binding and role of the C-terminus in the dUTPase from equine infectious anemia virus. *FEBS Lett.* **472,** 312–6 (2000).
24. Tóth, J., Varga, B., Kovács, M., Málnási-Csizmadia, A. & Vértessy, B. G. Kinetic mechanism of human dUTPase, an essential nucleotide pyrophosphatase enzyme. *J. Biol. Chem.* **282,** 33572–82 (2007).
25. Larsson, G., Nyman, P. O. & Kvassman, J. O. Kinetic characterization of dUTPase from Escherichia coli. *J. Biol. Chem.* **271,** 24010–6 (1996).
26. Quesada-Soriano, I. *et al.* Kinetic properties and specificity of trimeric Plasmodium falciparum and human dUTPases. *Biochimie* **92,** 178–86 (2010).
27. Thymark, M., Johansson, E., Larsen, S. & Willemoës, M. Mutational analysis of the nucleotide binding site of Escherichia coli dCTP deaminase. *Arch. Biochem. Biophys.* **470,** 20–6 (2008).
28. Nord, J., Larsson, G., Kvassman, J. O., Rosengren, a M. & Nyman, P. O. dUTPase from the retrovirus equine infectious anemia virus: specificity, turnover and inhibition. *FEBS Lett.* **414,** 271–4 (1997).
29. Laine, E., Auclair, C. & Tchertanov, L. Allosteric communication across the native and mutated KIT receptor tyrosine kinase. *PLoS Comput. Biol.* **8,** e1002661 (2012).
30. Pécsi, I. *et al.* Nucleotide pyrophosphatase employs a P-loop-like motif to enhance catalytic power and NDP/NTP discrimination. *Proc. Natl. Acad. Sci. USA* **108,** 14437–42 (2011).
31. Martin, A., Baker, T. a & Sauer, R. T. Rebuilt AAA+motors reveal operating principles for ATP-fuelled machines. *Nature* **437,** 1115–20 (2005).
32. Varga, B. *et al.* Active site closure facilitates juxtaposition of reactant atoms for initiation of catalysis by human dUTPase. *FEBS Lett.* **581,** 4783–8 (2007).
33. Pécsi, I., Leveles, I., Harmat, V., Vértessy, B. G. & Tóth, J. Aromatic stacking between nucleobase and enzyme promotes phosphate ester hydrolysis in dUTPase. *Nucleic Acids Res.* **38,** 7179–7186 (2010).
34. Barabás, O., Pongrácz, V., Kovári, J., Wilmanns, M. & Vértessy, B. G. Structural insights into the catalytic mechanism of phosphate ester hydrolysis by dUTPase. *J. Biol. Chem.* **279,** 42907–15 (2004).
35. Lopata, A. *et al.* Mutations Decouple Proton Transfer from Phosphate Cleavage in the dUTPase Catalytic Reaction. *ACS Catal.* **5,** 3225–3237 (2015).
36. Miyahara, S. *et al.* Discovery of highly potent human deoxyuridine triphosphatase inhibitors based on the conformation restriction strategy. *J. Med. Chem.* **55,** 5483–96 (2012).
37. Takács, E., Grolmusz, V. K. & Vértessy, B. G. A tradeoff between protein stability and conformational mobility in homotrimeric dUTPases. *FEBS Lett.* **566,** 48–54 (2004).
38. Kovári, J. *et al.* Altered active site flexibility and a structural metal-binding site in eukaryotic dUTPase: kinetic characterization, folding, and crystallographic studies of the homotrimeric Drosophila enzyme. *J. Biol. Chem.* **279,** 17932–44 (2004).
39. Hofer, A., Crona, M., Logan, D. T. & Sjöberg, B.-M. DNA building blocks: keeping control of manufacture. *Crit. Rev. Biochem. Mol. Biol.* **47,** 50–63 (2012).
40. Mathews, C. K. Deoxyribonucleotides as genetic and metabolic regulators. *FASEB J.* **28,** 3832–40 (2014).
41. Marx, A. & Alian, A. The first crystal structure of a dTTP-bound deoxycytidylate deaminase validates and details the allosteric-inhibitor binding site. *J. Biol. Chem.* **290,** 682–90 (2015).
42. Ellims, P. H., Kao, A. Y. & Chabner, B. A. Kinetic behaviour and allosteric regulation of human deoxycytidylate deaminase derived from leukemic cells. *Mol. Cell. Biochem.* **57,** 185–190 (1983).
43. Møllgaard, H., Neuhard, J., Mollgaard, H. & Neuhard, J. Deoxycytidylate deaminase from bacillus subtilis. Purification, characterization, and physiological function. *J. Biol. Chem.* **253,** 3536–42 (1978).
44. Sánchez, A. *et al.* Replication fork collapse and genome instability in a deoxycytidylate deaminase mutant. *Mol. Cell. Biol.* **32,** 4445–54 (2012).
45. Glasner, M. E., Gerlt, J. A. & Babbitt, P. C. Evolution of enzyme superfamilies. *Current Opinion in Chemical Biology* **10,** 492–497 (2006).
46. Gadsden, M. H., McIntosh, E. M., Game, J. C., Wilson, P. J. & Haynes, R. H. dUTP pyrophosphatase is an essential enzyme in Saccharomyces cerevisiae. *EMBO J.* **12,** 4425–31 (1993).
47. Castillo-Acosta, V. M. *et al.* Pyrimidine requirements in deoxyuridine triphosphate nucleotidohydrolase deficient Trypanosoma brucei mutants. *Mol. Biochem. Parasitol.* **187,** 9–13 (2013).
48. Kouzminova, E. A. & Kuzminov, A. Chromosomal fragmentation in dUTPase-deficient mutants of Escherichia coli and its recombinational repair. *Mol. Microbiol.* **51,** 1279–95 (2004).
49. Varga, B. *et al.* Active site of mycobacterial dUTPase: structural characteristics and a built-in sensor. *Biochem. Biophys. Res. Commun.* **373,** 8–13 (2008).

Acknowledgements

This work was supported by the Hungarian Scientific Research Fund [OTKA K115993, NK 84008, K109486]; the MedinProt program of the Hungarian Academy of Sciences; the International Centre for Genetic Engineering and Biotechnology [ICGEB CRP/HUN14-01] and the European Commission FP7 Biostruct-X project [contract No. 283570]. Funding for open access charge: Hungarian Scientific Research Fund.

Author Contributions

J.E.S., E.T., G.M., B.G.V. and J.T. designed research; J.E.S., E.T., G.M. and J.T. performed research; J.E.S., E.T. and J.T. analyzed data; and J.E.S., E.T., G.M., B.G.V. and J.T. wrote the paper.

Additional Information

Supplementary information accompanies this paper at http://www.nature.com/srep

Competing financial interests: The authors declare no competing financial interests.

How to cite this article: Szabó, J. E. *et al.* Trading in cooperativity for specificity to maintain uracil-free DNA. *Sci. Rep.* **6**, 24219; doi: 10.1038/srep24219 (2016).


This work is licensed under a Creative Commons Attribution 4.0 International License. The images or other third party material in this article are included in the article's Creative Commons license, unless indicated otherwise in the credit line; if the material is not included under the Creative Commons license, users will need to obtain permission from the license holder to reproduce the material. To view a copy of this license, visit http://creativecommons.org/licenses/by/4.0/

Trading in cooperativity for specificity to maintain uracil-free DNA

Judit E. Szabó[1], Enikő Takács[1], Gábor Merényi[1#], Beáta G. Vértessy[1,2], Judit Tóth[1 *]

[1]Institute of Enzymology, Research Centre for Natural sciences, Hungarian Academy of sciences, Budapest, Hungary
[2]Department of Applied Biotechnology and Food Science, Budapest University of Technology and Economics, Budapest, Hungary

* To whom correspondence should be addressed. Tel: +36-1-3826-707; Email: toth.judit@ttk.mta.hu

Present Address: Gábor Merényi, Department of Molecular Biosciences, The Wenner-Gren Institute, Stockholm University

Supplementary Results

The linkers in WWW do not influence the dUTPase enzymatic cycle

The WWW construct showed similar enzymatic properties to those of hDUT^{F158W} under steady state conditions (V_{max} = 6.9 ± 1.2 s^{-1}, K_M = 1.3 ± 0.34 μM, Figure 4, Table 1). To confirm that the covalent linkage of the dUTPase monomers does not alter the enzymatic mechanism, we performed transient kinetic analysis as well. We determined the single turnover catalytic rate constant of the WWW enzyme (k_{STO} = 6.2 ± 0.2 s^{-}) and found it almost identical to the one reported for hDUT^{F158W} (k_{STO} = 6.4 ± 0.2 s^{-1} (1)) (Supplementary Figure 1A, Table 1). The substrate binding properties of WWW also proved to be similar to those of hDUT^{F158W} (Supplementary Figure 1B-C). WWW also binds dUTP in two steps. However, the observed rate constants for the collision complex formation were found to be higher than in the case of hDUT^{F158W} indicating that that dUTP binds somewhat faster to the covalently linked enzyme. The observed rate constant of the second binding phase (proposed to be the isomerization of the enzyme-substrate complex (1)) did not depend on the dUTP concentration in the investigated concentration range (high above the K_M). In this concentration range, the observed rate constants for an isomerization step approximate the sum of the forward and the backward rates of the suspected conformational change. In the kinetic model for the hDUT^{F158W}, the rate constants for the isomerization step are k_{iso}= 21.2 s^{-1} and k_{-iso}= 3.7 s^{-1} (1). Therefore, the obtained k_{obs2} = 30.4 ± 9.13 $s^{-1}$for dUTP binding to WWW corresponds well to the isomerization observed rate constants of a wild type enzyme. This indicates that this step of the enzyme reaction remains unaltered by the linkage of dUTPase monomers. The concentration dependence of the total fluorescence intensity change of the stopped flow time courses was used to determine the K_d of the enzyme.dUTP complexes (Figure 4D). All these parameters determined for WWW and previously for hDUT^{F158W} can be compared in Table 1.

In summary, the only notable change in the enzymatic mechanism was detected in the kinetics of the collision complex formation with the substrate. We propose that the increase in the rate constant of the first dUTP binding step may be due to the altered flexibility of the swapping arm due to the inserted peptide linker. The swapping arm confers the P-loop-like motif that participates in dUTP binding and hydrolysis (2).

Characterization of the mutations applied to create the asymmetric hybrid enzymes

We designed a mutation to impair dUTP binding to the active site of dUTPase. We introduced an aromatic ring into the tight ß hairpin of the uracil binding pocket of the active site by the replacement of Ala98 with the bulky Phe. The Phe was expected to prevent ligand binding by excluding its uracil moiety from its cognate binding site (Supplementary Figure 3B). To characterize the mutation, we first created a homotrimer containing the A98F change in each of the three active sites. As expected, the hDUT$^{F158W,\ A98F}$ homotrimer did not exhibit any dUTPase activity (Supplementary Figure 3A). To exclude that the lack of enzymatic activity resulted from a compromised protein structure, we

measured the thermal unfolding properties of the hDUT$^{F158W, A98F}$ protein. The thermal unfolding curve of hDUT$^{F158W, A98F}$ was cooperative and yielded identical melting temperature (T_m) to that of hDUT^{F158W} (Supplementary Figure 3C-D). As the binding of a cognate ligand to the enzyme stabilizes its structure and thus shifts the T_m of the complex higher, we performed the experiment in the presence of saturating deoxyuracil nucleotides as well (dUMP and dUTP). While a large increase in T_m was observed in the wild type enzyme-nucleotide complexes, the unfolding curve of the hDUT$^{F158W, A98F}$ protein remained unaffected by the nucleotides (Supplementary Figure 3C-D). To further test the stability and nucleotide binding ability of the hDUT$^{F158W, A98F}$ protein, we performed limited trypsinolysis experiments in the presence and absence of nucleotides as well. It was shown earlier that the flexible N- and C-termini become readily cleaved in the apo enzyme while the substrate analog dUPNPP protects the C-terminus against tryptic cleavage (3). The resulting protein core remains stable for long time(3). In case of the apo enzyme, the limited trypsinolysis resulted in similar digestion patterns in both hDUT^{F158W} and hDUT$^{F158W, A98F}$ (Supplementary Figure 3E). The protection effect of dUPNPP was well observable in hDUT^{F158W} but was absent in hDUT$^{F158W, A98F}$ (Supplementary Figure 3E). Both the thermal unfolding and the limited trypsinolysis results confirm that the hDUT$^{F158W, A98F}$ protein is well folded but is not able to bind dUTP or dUMP.

The effect of Mg^{2+} binding to WWW

To reinforce the effect of Mg^{2+} binding to the central channel on the global structure of dUTPase, we repeated the CD experiments carried out with hDUT^{F158W} (Figure 5B-C) using the WWW construct as well. The near-UV CD spectrum of WWW (Supplementary Figure 5A) showed some differences in the Phe region (250-270 nm) compared with that of hDUT^{F158W}. The hDUT^{F158W} protein contains a Phe (F48) in the flexible N-terminal part. The presence of the linker in WWW probably changes the conformational properties of the linked N-terminus in the second and third subunits. The N-terminal part of the human dUTPase is involved in nuclear import (4) but not in the catalytic reaction (3, 4). The addition of $MgCl_2$ resulted in the same characteristic spectral changes as in hDUT^{F158W}. The far-UV CD spectrum showed no changes upon the addition of $MgCl_2$, similarly to what was observed in hDUT^{F158W} (Supplementary Figure 5B).

Altogether, these results reinforce that Mg^{2+} binds to the unliganded dUTPase structure and evokes a stabilization effect.

Supplementary References

1. Tóth,J., Varga,B., Kovács,M., Málnási-Csizmadia,A. and Vértessy,B.G. (2007) Kinetic mechanism of human dUTPase, an essential nucleotide pyrophosphatase enzyme. *J. Biol. Chem.*, **282**, 33572–82.

2. Pécsi,I., Szabó,J.E., Adams,S.D., Simon,I., Sellers,J.R., Vértessy,B.G. and Tóth,J. (2011) Nucleotide pyrophosphatase employs a P-loop-like motif to enhance catalytic power and NDP/NTP discrimination. *Proc. Natl. Acad. Sci. U. S. A.*, **108**, 14437–42.

3. Varga,B., Barabás,O., Kovári,J., Tóth,J., Hunyadi-Gulyás,E., Klement,E., Medzihradszky,K.F., Tölgyesi,F., Fidy,J. and Vértessy,B.G. (2007) Active site closure facilitates juxtaposition of reactant atoms for initiation of catalysis by human dUTPase. *FEBS Lett.*, **581**, 4783–8.

4. Bozóky,Z., Róna,G., Klement,É., Medzihradszky,K.F., Merényi,G., Vértessy,B.G. and Friedrich,P. (2011) Calpain-catalyzed proteolysis of human dutpase specifically removes the nuclear localization signal peptide. *PLoS One*, **6**, e19546.

5. Kovári,J., Barabás,O., Takács,E., Békési,A., Dubrovay,Z., Pongrácz,V., Zagyva,I., Imre,T., Szabó,P. and Vértessy,B.G. (2004) Altered active site flexibility and a structural metal-binding site in eukaryotic dUTPase: kinetic characterization, folding, and crystallographic studies of the homotrimeric Drosophila enzyme. *J. Biol. Chem.*, **279**, 17932–44.

6. Barabás,O., Pongrácz,V., Kovári,J., Wilmanns,M. and Vértessy,B.G. (2004) Structural insights into the catalytic mechanism of phosphate ester hydrolysis by dUTPase. *J. Biol. Chem.*, **279**, 42907–15.

Supplementary Table 1

Name	For/Rev	R. site	Sequence	Goal
D102N	for	-	GGAGCTGGTGTCATAAATGAAGATTATAGAGGAAATGTTGG	Mutagenesis
	rev	-	CCAACATTTCCTCTATAATCTTCATTTATGACACCAGCTCC	
A98F	for	-	GATGTAGGATTTGGTGTCATAGATG	Mutagenesis
	rev	-	CATCTATGACACCAAATCCTACATC	
Subunit I.	for	Kpn1	GGGGTACCATGCCCTGCTCTGAAGAG	Assembly of WWW with linkers
	rev	BamH 1	CGGGATCCGGTCGCGCCGCTGGTGCCGCCTTCGCTGCCGCCGCCTTCGCTGCCGCCCGCGCCGCTCGCATTCTTTCCAGTGGAACC	
Subunit II.	for	BamH 1	CGGGATCCATGCCCTGCTCTGAAGAG	
	rev	Pst1	AACTGCAGGGTCGCGCCGCTGGTGCCGCCTTCGCTGCCGCCGCCTTCGCTGCCGCCCGCGCCGCTCGCATTCTTTCCAGTGGAACC	
Subunit III.	for	Pst1	AACTGCAGATGCCCTGCTCTGAAGAG	
	rev	Hind3	CCCAAGCTTTTAATTCTTTCCAGTGGAACC	
Subunit III. change	for	Pst1	CTACGCGGCTGCAGATGCCCTGCTCTGAAGAGACAC	Subunit III. exchange
	rev	Xho1	GCGCCAGCTCGAGTTAATTCTTTCCAGTGGAACC	
Linker1:			ASGAGGSEGGGSEGGTSGATGS	
Linker2:			ASGAGGSEGGGSEGGTSGATLQ	

Supplementary Figures

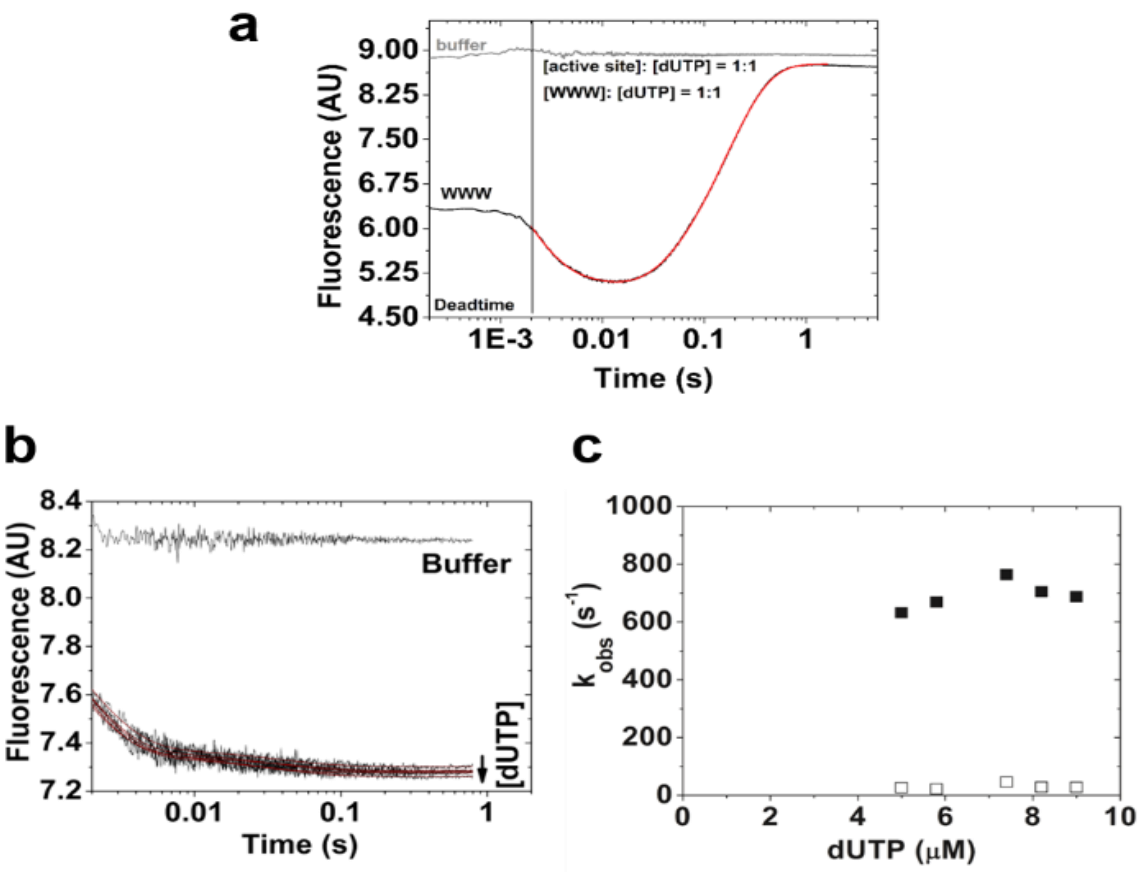

Supplementary Figure 1

Transient kinetic analysis of dUTP binding and hydrolysis by the WWW enzyme

A, Fluorescence time courses recorded upon mixing 20 μM WWW with substoichiometric dUTP or with buffer. The single turnover trace was fitted with triple exponential function (red curve) that yielded 6.24 s^{-1} for the single turnover rate constant (k_{STO}). Both the value of the k_{STO} and the characteristic fluorescence changes of the time course denote wild type enzymatic behavior(1). ***B,*** Fluorescence time courses recorded upon mixing various concentrations of dUTP with 0.5 μM WWW (postmixing concentration). Smooth lines are double exponential fits to the curves. A large fraction of the amplitude is lost in the dead time of the stopped flow instrument. ***C***, Analysis of the rate constants of the dUTP binding time courses in panel B. The solid squares denote $k_{obs,1}$ for the fast phase of the fitted double exponential. Since a large portion of the amplitude is missing, the concentration dependence of $k_{obs,1}$ did not yield exact association and dissociation constants. Open squares denote $k_{obs,2}$ of the second phase. $k_{obs,2}$ is independent of the dUTP concentration and its mean value is 30.4 ± 9.13 s^{-1}. Based on these results, the WWW enzyme is indistinguishable from the $hDUT^{F158W}$ wild type enzyme (1).

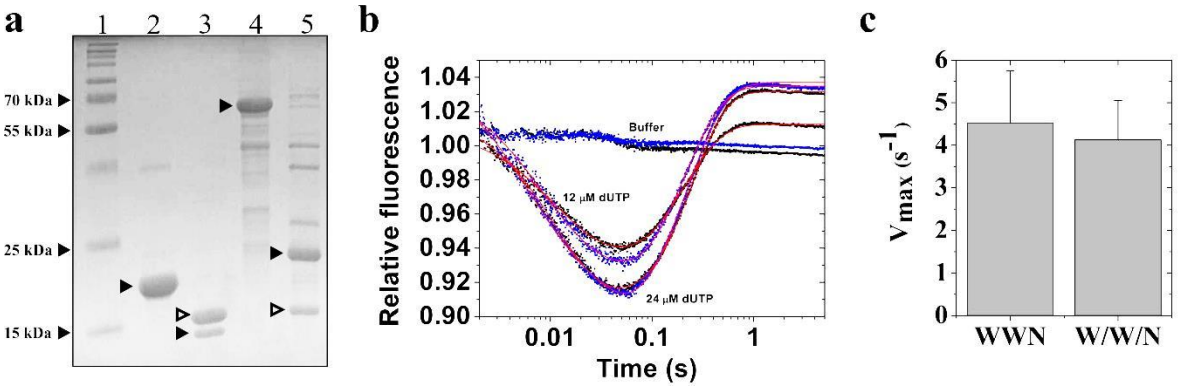

Supplementary Figure 2

Covalent coupling of the dUTPase monomers does not disturb the enzymatic properties of the functional trimers

A, PAGE analysis of the products of limited trypsinolysis. Lane 1: marker; lane 2: hDUT; Lane 3: hDUT treated with tryspin (empty arrow head: N-terminal cleaved protein fragment, black arrowhead: N- and C-terminal cleaved protein fragment); Lane 4: WWN covalent heterotrimer; Lane 5: WWN heterotrimer treated with tryspin. dUPNPP was present to give protection against the cleavage of the C-terminus (contains the catalytically important conserved motif V). The black arrowhead and the empty arrowhead points to monomers with linkers (2 monomers / trimer) and without linker (one monomer / trimer), respectively. Note that an N- and C-terminally cleaved fragment is not present thanks to the protective effect of the bound dUPNPP. ***B,*** Single turnover analysis of intact (WWN) and cleaved (W/W/N) heterotrimers measured by stopped flow. k_{STO} values derived from triple exponential fits (red curves) to the time courses were 5.5 ± 0.1 s^{-1} (12 μM dUTP) and 5.9 ± 0.1 s^{-1} (24 μM dUTP) for WWN; 5.6 ± 0.1 s^{-1} (12 μM dUTP) and 5.3 ± 0.1 s^{-1} (24 μM dUTP) for W/W/N. Errors represent fitting errors. ***C,*** Steady state activity of the WWN (4.5 ± 1.2 s^{-1}, n = 3) and of the W/W/N (4.1 ± 0.9 s^{-1}, n = 2) enzymes.

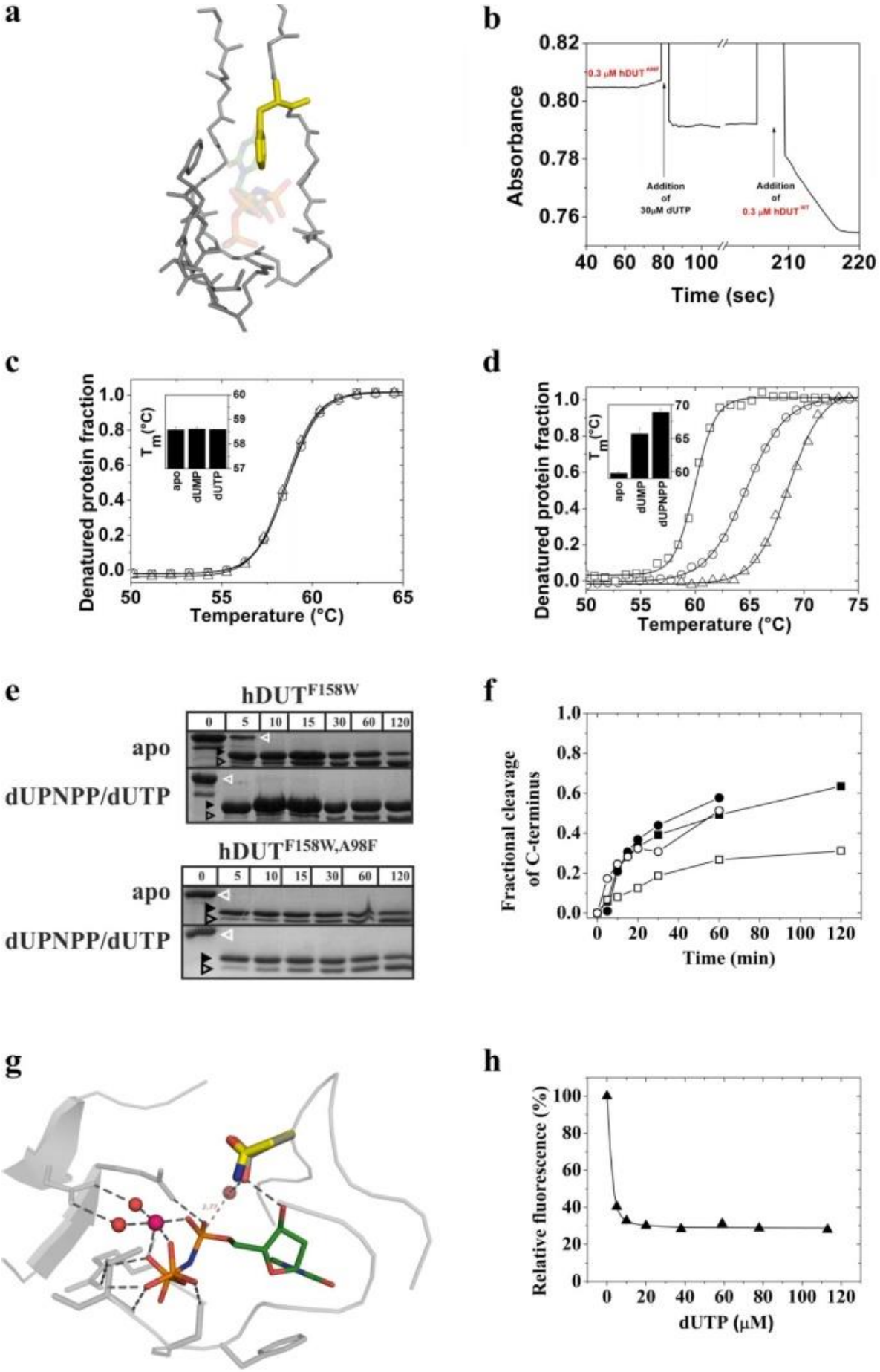
a
b
0.82
0.80
0.78
0.76
Absorbance
0.3 μM hDUT^A98F
Addition of 30μM dUTP
Addition of 0.3 μM hDUT^WT
40 60 80 100 210 220
Time (sec)
c
Denatured protein fraction
1.0 0.8 0.6 0.4 0.2 0.0
50 55 60 65
Temperature (°C)
T_m (°C)
60 59 58 57
apo dUMP dUTP
d
Denatured protein fraction
1.0 0.8 0.6 0.4 0.2 0.0
50 55 60 65 70 75
Temperature (°C)
T_m (°C)
70 65 60
apo dUMP dUPNPP
e
hDUT^F158W
0 5 10 15 30 60 120
apo
dUPNPP/dUTP
hDUT^F158W,A98F
0 5 10 15 30 60 120
apo
dUPNPP/dUTP
f
Fractional cleavage of C-terminus
1.0 0.8 0.6 0.4 0.2 0.0
0 20 40 60 80 100 120
Time (min)
g
h
Relative fluorescence (%)
100 80 60 40 20 0
0 20 40 60 80 100 120
dUTP (μM)

Supplementary Figure 3

Characterization of the A98F and the D102 mutations

A, Structural model of the active site of the A98F mutant hDUT (PyMol). The uracil-binding ß hairpin and the 5th motif from the swapping arm of human dUTPase are shown as grey stick backbone. dUTP is shown as transparent sticks with atomic coloring. The single allowed conformation of Phe98 in this structure is highlighted by yellow coloring. This structural representation shows that the aromatic ring of Phe98 occupies the binding site of the uracil moiety of the substrate. ***B***, Enzyme activity assay. The A98F protein is premixed in the assay buffer, the dUTPase reaction is initiated by the addition of dUTP. No enzyme activity is detected until the addition of the wild type enzyme that hydrolyzes the intact dUTP. ***C-D***, Thermal unfolding of the A98F mutant (***C***) and of the wild type dUTPase (***D***), respectively, in the absence of nucleotides (square), in the presence of 5 mM dUMP (circle) or 1 mM dUTP (triangle). Smooth lines through the data are Boltzmann fits (Equation (4))yielding the melting temperatures presented as bar graph in the inset. ***E***, Limited trypsinolysis of the wild type ($hDUT^{F158W}$) and the A98F mutant ($hDUTF^{158W,\ A98F}$) in the absence and in the presence of 1 mM dUPNPP. Numbers denote the duration of the tryptic treatment in minutes. The open white arrow head, the solid black arrow head and the open black arrow head shows the intact, the N-terminally cleaved and the N- and C-terminally cleaved enzyme, respectively. ***F,*** Densitometric analysis of the limited trypsinolysis experiment. The graph shows the relative amount of the N- and C-terminally cleaved protein compared to the total amount of protein. It has previously been established that trypsin readily cleaves the flexible N-terminus of dUTPases in a nucleotide-independent manner, while the binding of dUTP or dUPNPP to the enzyme protects the also flexible C-terminus from tryptic digestion (5). We observe this protection in the wild type enzyme but not in the A98F mutant (see apo vs. dUPNPP/dUTP samples on the gel at 120 min). These data together demonstrate that the A98F substitution hinders the binding of dUTP to the active site while it does not perturb the overall structure (folding, stability) of the protein. ***G***, Structural representation of the D102N mutation in the active site of hDUT (generated by Pymol). The active site building amino acids are shown as grey cartoon and stick backbone. dUTP and residue 102 are shown as sticks with atomic coloring. The Mg^{2+} ion is shown as a magenta sphere, the water molecules are shown as red spheres. D102 coordinates the nucleophile catalytic water molecule while the mutant D102N is not expected to efficiently coordinate this water molecule (6). ***H,*** Fluorescence intensity titration is shown upon dUTP binding to $hDUT^{F158W,\ D102N}$. The smooth line through the data is a quadratic fit (Equation (1)) yielding K_d = 0.7 μM. The quasi wild type relative fluorescence change and K_d (cf. data from the literature (1)) indicate that the substrate binding properties of the $hDUT^{F158W,\ D102N}$ mutant remained unaffected by the D102N mutation.

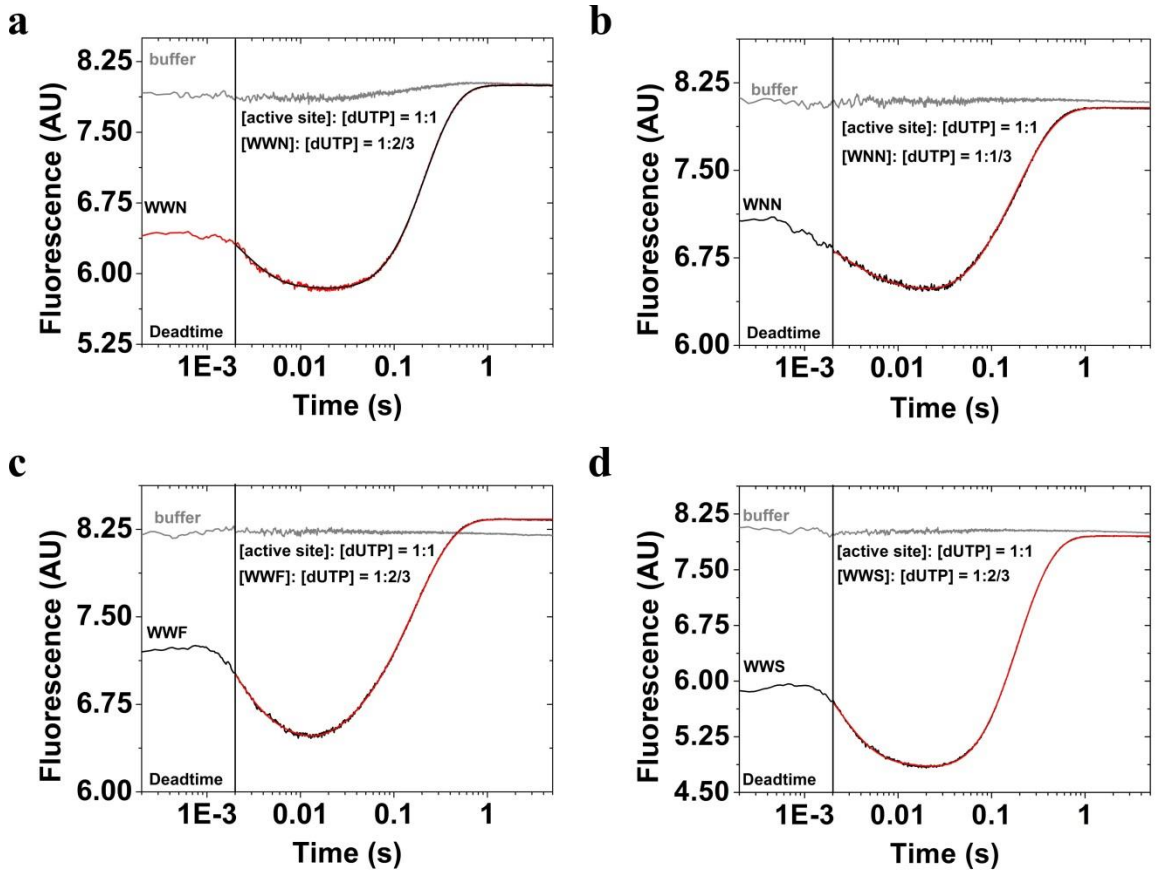

Supplementary Figure 4

Single turnover dUTP hydrolysis time courses of the hybrid enzymes

Fluorescence time courses were recorded upon mixing substoichiometric dUTP with 20μM WWN (***A***), WNN (***B***), WWF (***C***) or WWS (***D***). Single turnover traces were fitted with triple exponential function yielding the following k_{STO} values: 6.43 s^{-1} for WWN, 5.4 s^{-1} for WNN, 5.99 s^{-1} for WWF and 6.26 s^{-1} for WWS. Each measurement was repeated several times, the mean values and errors are shown in Figure 4C and in Table 1. Note that the signal changes are not comparable dues to the optimization of the detector sensitivity in each measurement.

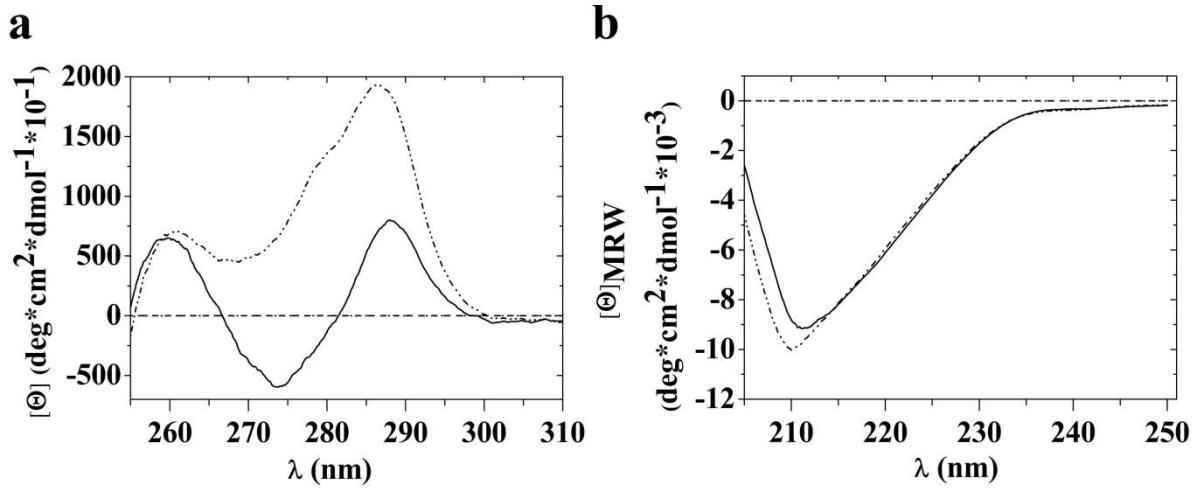

Supplementary Figure 5

The Mg^{2+} binding properties of WWW are similar to those of $hDUT^{F158W}$ (cf. Figure 5)

A, Near UV and ***B,*** far UV CD spectra of WWW in the presence (dash-dot-dot) and in the absence (solid line) of Mg^{2+}. The buffer signal is shown as dash-dash-dot lines.

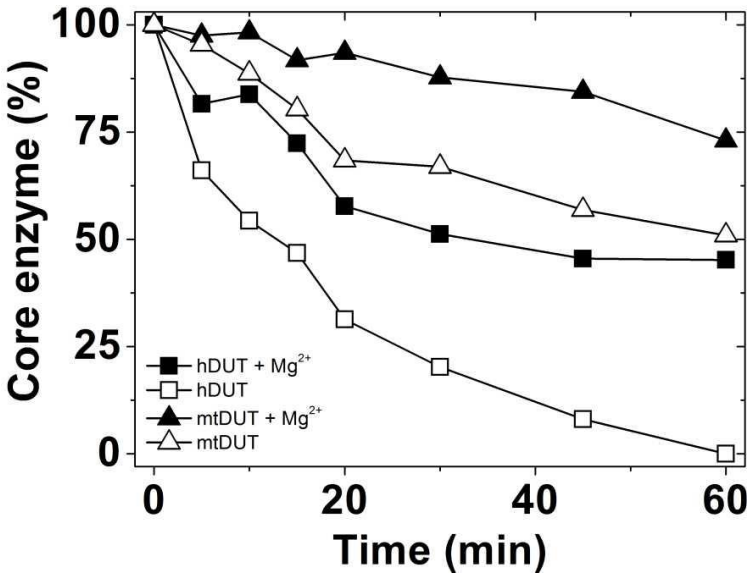

Supplementary Figure 6

Densitometric analysis of the limited trypsinolysis experiment shown in Figure 5D

The relative amount of core enzyme is plotted against time. Core enzyme = intact enzyme + N-terminal cleaved enzyme + N- and C-terminal cleaved enzyme

ACS Catalysis

Research Article

pubs.acs.org/acscatalysis

Mutations Decouple Proton Transfer from Phosphate Cleavage in the dUTPase Catalytic Reaction

Anna Lopata,[†,¶] Pablo G. Jambrina,[‡] Pankaz K. Sharma,[§,#] Bernard R. Brooks,[∥] Judit Toth,[*,†] Beata G. Vertessy,[*,†,⊥] and Edina Rosta[*,‡]

[†]Institute of Enzymology, Research Centre for Natural Sciences, Hungarian Academy of Sciences, Budapest H1113, Hungary

[‡]Department of Chemistry, King's College London, London SE1 1DB, United Kingdom

[§]College of Pharmacy, Graduate School of Pharmaceutical Sciences, Ewha Womans University, Seoul 120-750, Korea

[∥]Laboratory of Computational Biology, National Heart, Lung, and Blood Institute, National Institutes of Health, Rockville, Maryland 20892-9314, United States

[⊥]Department of Applied Biotechnology and Food Science, Budapest University of Technology and Economics, Budapest H1111, Hungary

Supporting Information

ABSTRACT: Most enzymes present a catalytic mechanism where one or more proton transfer events occur coupled tightly together with the enzymatic chemical reaction. We show here that inactivating mutations decouple this proton transfer step from the phosphate cleavage reaction in dUTPase. Homotrimeric dUTPase enzymes catalyze the hydrolysis of dUTP to dUMP and pyrophosphate, using largely similar structural and functional groups as most AAA+ enzymes. dUTPases typically use a single Mg^{2+} ion as a cofactor in the active site that is formed by direct protein−protein contacts including all three protomers. Here we focus on the C-terminal arm structural motif, which has sequence and functional similarities to P-loop motifs and is required for catalysis. In this work, we have studied the functional roles of the C-terminal arm in ligand binding and catalysis by using QM/MM (quantum mechanics/molecular mechanics) calculations in conjunction with site-directed mutagenesis experiments. We also present a new method to assess the metal ion coordination symmetry during the catalytic reaction. Using this new implementation, we identified that the coordination symmetry follows a consistent pattern in the three systems studied, reaching the most symmetrical state near the transition states. We found that the phosphate cleavage proceeds with a concerted bimolecular (A_ND_N) mechanism with a loose dissociative transition state and that it is coupled with a proton transfer step involving a unanimously conserved Asp residue. We show that the main mechanistic effect of the lack of the C-terminal arm is to decouple the phosphate cleavage from the subsequent proton transfer step, resulting in a high-barrier altered reaction pathway.

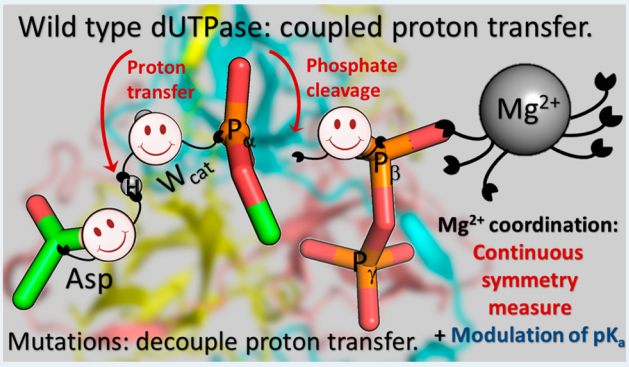

KEYWORDS: *QM/MM (quantum mechanics/molecular mechanics), dUTPase, continuous symmetry measure, one-metal ion catalytic mechanism, ab initio, DFT (density functional theory), coupled proton transfer*

INTRODUCTION

The dUTPase (deoxyuridine triphosphate nucleotidohydrolase) enzymes catalyze the hydrolysis of dUTP (deoxyuridine triphosphate) to dUMP (deoxyuridine monophosphate) and pyrophosphate to avoid incorporation of uracil into the DNA instead of thymine and to provide the dUMP precursor for *de novo* dTTP (deoxythymidine triphosphate) biosynthesis.[1] An additional enzymatic activity, deamination of dCTP (deoxycytidine triphosphate) to dUTP, may also be carried out by bifunctional dUTPases in *Archaea*[2−5] and also in *Mycobacterium tuberculosis* (*M. tuberculosis*), which also has a monofunctional dUTPase.[6] The dUTPases comprise two structurally different classes:[7] first, the β sheet-type dUTPases, possessed by most organisms, employ a one-metal ion catalytic mechanism,[8,9] and usually form a homotrimer[10] or a monomer,[11] while the second class, the α helical-type dUTPases, possessed by kinetoplastids,[12] form dimers and employ a two-metal ion catalytic mechanism.[13,14]

In β sheet-type trimeric dUTPases, each active site is constituted from motifs of all three protomers, which are all required to interact for achieving proper enzymatic activity.[15,16] These dUTPases have a C-terminal arm structural motif that has sequence similarity to P-loop motifs[17] also present in triphosphate hydrolysis catalyzing enzymes including kinases,

Received: December 24, 2014
Revised: March 3, 2015
Published: April 8, 2015

Downloaded via RESEARCH CTR NATURAL SCIENCES (HAS) on November 4, 2021 at 10:39:48 (UTC).
See https://pubs.acs.org/sharingguidelines for options on how to legitimately share published articles.

© 2015 American Chemical Society

DOI: 10.1021/cs502087f
ACS Catal. 2015, 5, 3225−3237

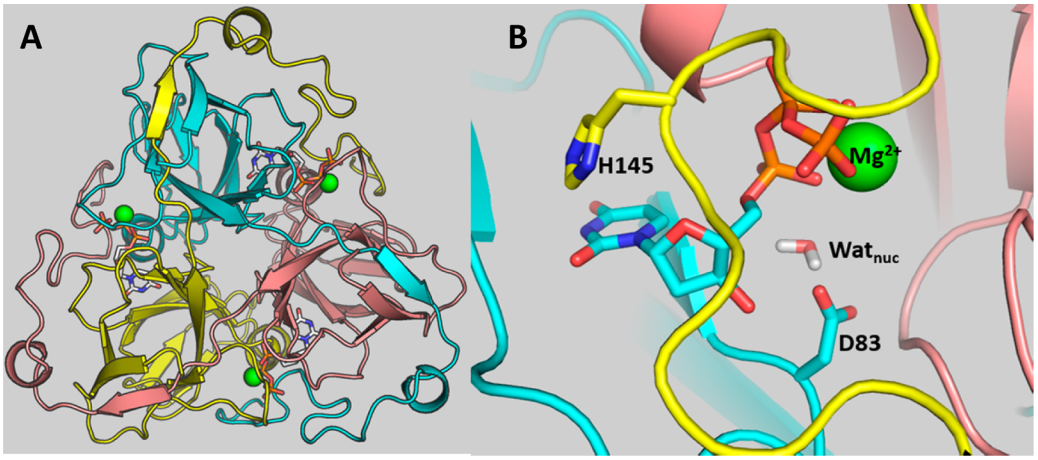

Figure 1. (A) Homotrimeric structure of the biological *M. tuberculosis* dUTPase assembly. Each active site consists of all the three protomers (yellow, cyan, and salmon cartoon), a dUTP molecule (sticks with atomic coloring), and a single Mg^{2+} ion cofactor (green sphere). (B) Active site of *M. tuberculosis* dUTPase from the WT simulation system. H145 (sticks) forms $\pi-\pi$ interactions with the uracil base of the substrate dUTP (sticks) at the interface of the three protomers, interacting with all the three chains (yellow, cyan, and salmon cartoon).

motor proteins, and membrane pumps.[18−20] In addition to the key C-terminal arm, the requirement of divalent metal ion cofactors for efficient catalysis is also shared by AAA+ (ATPases associated with diverse cellular activities) enzymes in general, commonly a single Mg^{2+} coordinating the phosphate groups of the substrate. Substitution of this Mg^{2+} with Ca^{2+} generally results in substantial loss of activity,[21,22] with only a few exceptions reported (e.g., for human endogenous retrovirus (HERV-K) dUTPases).[23] The P-loop-like C-terminal arms, the Mg^{2+} ion bound triphosphate nucleotides, and the binding interface of the remaining two protomers all contribute to the resulting three active sites of the native dUTPase complex.

Here, we focus on the role of the C-terminal arm of *M. tuberculosis* dUTPase (Figure 1A) in the catalytic activity and in ligand-binding properties. We use both computationally intensive, accurate mixed quantum mechanics/molecular mechanics (QM/MM) calculations[24] and site-directed mutagenesis experiments. We study the wild-type (WT) dUTPase, a mutant lacking the entire C-terminal arm (denoted by T138Stop), and a second mutant including only a H145A mutation. The C-terminal arm structural motif has several conserved residues (Figure 2), one of which, His145, has well-conserved aromatic $\pi-\pi$ interactions with the nucleobase of the substrate.[17,25,26] His145 has a prominent location in the dUTPase active site: it interacts simultaneously with both the other two protomers and the substrate (Figure 1B). Deletion of the full C-terminal arm results in major activity loss for the T138Stop enzyme. The His to Ala mutation H145A preserves substrate binding; however, the catalytic rate decreases by a factor of 10. The measured binding affinities and catalytic rates of the T138Stop and H145A enzymes are consistent with the essential role of the C-terminal arm in other dUTPase proteins investigated.[17,25,27−32]

To better understand the underlying energetic and structural causes determining the catalytic activity, we carried out QM/MM calculations of the reaction mechanism for proton transfer and phosphate cleavage in the WT and the two mutant (H145A and T138Stop) enzyme complexes. We recently identified a one-step associative A_ND_N catalytic mechanism for the hydrolysis at the α-phosphate, involving also a coupled proton transfer step from the nucleophilic water to the catalytic Asp83 residue.[33] Here we show that essentially the same

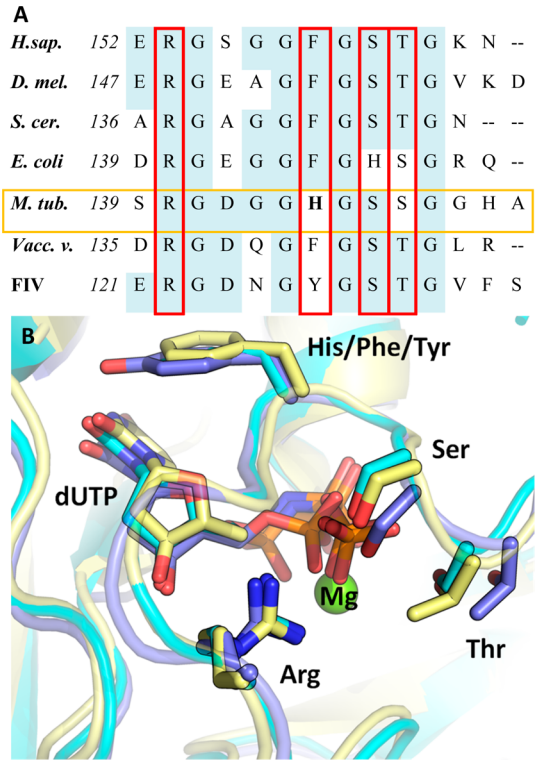

Figure 2. (A) Clustal W alignment of the C-termini of dUTPases from widely different species: human (*Homo sapiens, H. sap.*), *Drosophila melanogaster* (*D. mel.*), *Saccharomyces cerevisiae* (*S. cer.*), *E. coli*, *M. tuberculosis*, *Vaccinia virus* (*Vacc. v.*), and feline immunodeficiency virus (FIV). The conserved residues coordinating the dUTP are shown within a red frame. (B) Superimposed structures of the active sites of human, mycobacterial and FIV dUTPases (PDB IDs: 3EHW (unpublished), 2PY4,[26] and 1F7R,[36] respectively). The conserved residues coordinating the dUPNPP molecule, which is a slowly hydrolyzable dUTP analogue, are shown as sticks, protein shown as cartoon (yellow, cyan, and dark blue, respectively). Note that the presented FIV dUTPase structure contains dUDP with trans conformation instead of dUPNPP, and there is no Mg^{2+} ion coordinated to the phosphate chain of the substrate analogue.

mechanism takes place in all three dUTPase systems investigated. The coupled proton transfer and the phosphate

DOI: 10.1021/cs502087f
ACS Catal. 2015, 5, 3225−3237

cleavage occur in a single step that has a loose dissociative transition state (TS) structure. The proton transfer directly follows the phosphate bond breaking, and it is coupled together with the new phosphorus−oxygen bond formation at the TS for the WT. For the H145A and T138Stop enzymes, the proton transfer is decoupled from the phosphorus−oxygen bond formation at the TS, in particular for the nearly inactive T138Stop dUTPase. In addition, we also found evidence that the specific metal ion coordination mode may play a prominent role. We analyzed the metal ion coordination during the reaction by calculating a continuous symmetry measure for the Mg^{2+}-ion coordination.[34] Changes in charge distributions of the three systems for the TS structures also reveal relevant differences in the partial charge transfer from the protein to the substrate due to the missing native protein−protein and protein−substrate interactions.

Our QM/MM calculations offer unique insights into the structural and electronic changes taking place along the catalytic reaction and, in conjunction with the experimental data, provide evidence on the crucial role of the dUTPase C-terminal arm in modulating ligand binding geometry and catalytic activity.[35]

MATERIALS AND METHODS

Experimental Methods. *Reagents.* Molecular biology products were obtained from New England Biolabs (U.S.A.) and Fermentas (Canada), electrophoresis and chromatography reagents were from Bio-Rad (U.S.A.) and Qiagen (Netherland). Phenol red was from Merck (Germany), dUDP and dUPNPP (α,β-imido-dUTP) was from Jena Bioscience (Germany); dUTP and other chemicals were from Sigma-Aldrich (U.S.A.).

Mutations on the C-Terminal Arm. C-terminal arm mutants have been generated to elucidate the roles of protein−protein and protein−substrate interactions of this conserved arm motif on dUTPase function. Two mutants were generated (H145A and T138Stop) focusing on the conserved residue of His145 (Figures 1 and 2) and a mutant lacking the last 17 residues of the C-terminal arm. Site-directed mutagenesis was performed by Stratagene's QuikChange method and was verified by sequencing. Mutagen forward and reverse primers were the following:

H145A 5′-GGCGACGGTGGCGCGGGTTCCTCCGGC-3′
5′-GCCGGAGGAACCCGCGCCACCGTCGCC-3′
T138Stop 5′-GGGCTGGCCTCGTGATCCCGCGGCGACGG-3′
5′-CCGTCGCCGCGGGATCACGAGGCCAGCCC-3′

Cloning, Protein Expression, and Purification. Cloning, protein expression, and purification were performed as described previously in Varga et al.[26] and as follows. Recombinant dUTPase with an N-terminal 6xHis-tag was expressed in *E. coli* strain BL21(DE3)pLysS. The final supernatant after cell extraction was loaded on a Ni-NTA column (Novagen) and purified according to the Novagen protocol. His-tag purification allows for specific purification of the recombinant proteins from the endogenous one. Protein concentration was measured using the Bradford method (Bio-Rad Protein Assay) and is given in monomers. Proteins were dialyzed against a buffer pH 7.5, containing 20 mM HEPES, 100 mM NaCl, 2 mM $MgCl_2$ and 1 mM DTT.

Steady-State Colorimetric dUTPase Assay. Steady-state colorimetric dUTPase assay was performed as described in Pecsi et al.[25] Phenol red indicator assay was used to detect protons released in the dUTPase reaction. 0.1−2 μM protein in a buffer pH 7.5 was used containing 1 mM HEPES, 100 mM KCl, 40 μM phenol red, and 5 mM $MgCl_2$. A Specord 200 (Analytic Jena, Germany) spectrophotometer and 10 mm path length thermostated cuvettes were used at 20 °C and absorbance was recorded at 559 nm. Initial velocity was determined from the first 10% of the progress curve. The Michaelis−Menten equation was fitted to the steady-state curves.

Enzyme−Ligand Dissociation Constant Measurements. Enzyme−ligand dissociation constant measurements were carried out as circular dichroism intensity titrations. CD spectra were recorded at 20 °C on a JASCO 720 spectropolarimeter using a 10 mm path length cuvette. Protein concentration was 50 μM in a buffer pH 7.5, containing 20 mM HEPES, 50 mM NaCl and 2 mM $MgCl_2$. A spectrum between 250 and 290 nm was recorded at each nucleotide concentration, as described in Pecsi et al.[25] Differential curves were obtained by subtracting the signal of the ligand alone from that of the corresponding complex. Differential ellipticity at 269 nm was plotted against the ligand concentration to obtain the binding curves.

Protein solution was titrated with dUPNPP or dUDP using minute aliquots from a concentrated stock solution. Titration data were fit to the equation describing 1:1 stoichiometry for the dissociation equilibrium with no cooperativity:

$$y = s + \frac{A[(c + x + K) - \sqrt{(c + x + K)^2 - 4cx}]}{2c}$$

where x is the nucleotide concentration and y is the circular dichroism intensity, $s = y$ at $x = 0$, A is the amplitude of the circular dichroism intensity change, c is the enzyme concentration, and K is the dissociation constant (K_d).

Thermal Stability. Thermal stability measurements were carried out with a JASCO 720 spectropolarimeter using a 1 mm path length cuvette. Wild type and mutants enzymes (25 μM) were measured in a buffer pH 7.5, containing 100 mM NaH_2PO_4 and 2 mM $MgCl_2$. The solution was heated from 20 to 80 °C, and differential ellipticity was recorded by every 0.5 °C at 210 nm. The obtained values were plotted against temperature, and the following Boltzmann curve was fitted:

$$y = A2 + \frac{A1 - A2}{1 + e^{x - x0/\mathrm{dx}}}$$

where $A1$ is the initial value and $A2$ is the final value of the differential ellipticity, dx is the time constant, and $x0$ is the inflection point of the curve which is the melting point.

Data Fitting and Statistical Analysis. All experimental measurements were carried out at least three times. Error bars represent standard deviations of the mean of the measurements. Data fitting was performed using Origin 7.5 (OriginLab Corp., Northampton, MA).

Computational Methods. *Structural Model.* The calculations were initiated from the X-ray crystal structures of the wild type and mutant *M. tuberculosis* dUTPase enzymes (Table S1). The original dUPNPP ligand in the crystal structures was manually modified to dUTP. There is a lack of the catalytic water in the T138Stop crystal structure; however, a distinct electron density with a high temperature factor can be seen at the usual position of the attacking water molecule, and this information was used to position a catalytic water molecule into the structure of the T138Stop mutant (Figure S2B). Coordinates of the hydrogen atoms were generated with

DOI: 10.1021/cs502087f
ACS Catal. 2015, 5, 3225−3237

CHARMM[37] using standard protonation states of all ionizable residues (also see SI text about potential protonation states of H145). Crystallographic water molecules in the vicinity of the protein and the substrate were preserved while the system has been placed in a cube of TIP3P water to cover at least 10 Å radius in all directions from the protein. Several water molecules were then replaced with a Monte Carlo procedure by ions to account for a 0.10 M NaCl solution, and further Na^+ ions were added for neutralization.[38] CHARMM27 extended atom force field was used for the molecular mechanics interactions, with periodic boundary conditions, Ewald summation, and a 12 Å cutoff for the evaluation of the nonbonded interactions. After an initial equilibration for 10 ns, with constraints to the initial PDB structure, the final structure was taken as the starting point for subsequent MM and QM/MM minimizations.

QM/MM Setup and Minimizations. The equilibrated classical system was trimmed to a sphere of 21 Å radius centered at the position of the P_α atom of the dUTP, and all residues further than 15 Å were kept fixed. Q-Chem program[39] version 3.1 was used to perform QM calculations, at the B3LYP[40]/6-31+G(d) density functional theory (DFT) level of theory. The quantum mechanical system was coupled with the CHARMM program[37] using full electrostatic embedding.[41] Standard link atom treatment was used to bisect bonds between the QM and MM region, adding hydrogen atoms for the missing ligands. For the QM/MM minimizations, a complex reaction coordinate (Q, Figure 3) was defined as the difference between the forming and breaking bond distances in which both phosphate transfer (ET, in analogy with generalized electron transfer) and proton transfer (PT) are incorporated.[42,43] Using this reaction coordinate, the geometries were minimized starting with the initial enzyme−substrate structures and following the reaction through the transition state to the product state. Minimizations were performed using the adopted basis Newton−Raphson scheme as implemented by D. J. States[44] in CHARMM, both in the forward and backward directions to obtain hysteresis-free results.[42]

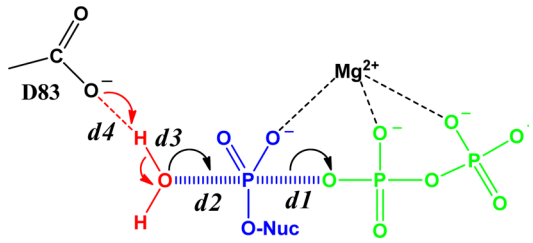

Figure 3. Schematic representation of the reaction coordinate used in the QM/MM simulations. We defined $Q = Q_{ET} + 0.5\ Q_{PT}$, where $Q_{ET} = d1 - d2$ denotes the difference between the bond breaking ($d1$) and bond forming ($d2$) distances for the phosphate cleavage (generalized electron transfer coordinate), and $Q_{PT} = d3 - d4$ is the difference between the bond breaking ($d3$) and forming ($d4$) distances for the proton transfer from the water to the Asp83.

The quantum region contained the Thr81 and Ile82 backbones, the amide group of Gln113, the side chains of Asp83, Ser65, Thr69 (only in the T138Stop mutant), Ser147 and Ser148 (in the WT and H145A mutant), the side chain of residue 145 (His in the WT, Ala in the H145A mutant), the guanidino group of Arg140 (in the WT and H145A mutant) and Arg64 (only in the T138Stop mutant), the Mg^{2+} ion with its full coordination shell, nearby crystallographic water molecules, and the dUTP molecule (Figure S1). Thus, the WT, H145A, and T138Stop systems contained 132, 137, and 108 atoms, respectively, in the minimizations with the largest QM region.

After the full QM/MM minimization of the corresponding structures, the charge distribution was analyzed with the Gaussian program package[45] using the CHELPG charge evaluation[46] based on fitting the atomic charges to reproduce the electrostatic potential.[47] In these calculations, the same QM region was used at the same level of theory with an identical polarization scheme as done in the QM/MM minimizations, including the same protein environment in the calculations as external point charges.

QM/MM Dynamics. Short downhill QM/MM dynamics trajectories were generated starting from the minimized WT system near the transition state. The quantum region contained the Thr81 and Ile82 backbones, the amide group of Gln113, the side chains of Asp83, Ser65, His145, Ser147, and Ser148, the guanidino group of Arg140 the Mg^{2+} ion with its full coordination shell, nearby crystallographic water molecules, and the dUTP molecule (121 atoms in total, Figure S1A). We used Langevin dynamics with a friction coefficient of 8 ps^{-1}[48] and an integration time step of 1 fs. During the trajectories, the outer simulation shell was kept fixed as described above. Keeping also the QM region fixed initially, 10 ps long classical MD simulations were carried out first for each downhill trajectory to obtain an ensemble of TS structures with respect to the classical region. These simulations were then followed by unconstrained dynamics using QM/MM calculations with no atoms fixed except for residues further than 15 Å from the P_α atom.

Downhill trajectories were also generated for the T138Stop mutant as described above. The quantum region contained the Thr81 and Ile82 backbones, the amide group of Gln113, the side chains of Asp83, Ser65, Thr69, the Mg^{2+} ion with its full coordination shell, nearby crystallographic water molecules, and the dUTP molecule (95 atoms in total, Figure S1C).

Symmetry Measure Calculations. To analyze the coordination shell of the Mg^{2+} ion, we introduce a continuous, dimensionless symmetry parameter S, similarly to the parameter introduced in Zabrodsky et al.[34] for general geometric structures. Our symmetry measure (S) is defined as

$$S = \min_{\{r,\mathbf{M}\}}\left(\frac{1}{6}\sum_{i=1}^{6}\left|\mathbf{e}_i - \mathbf{M}\left(\frac{\mathbf{x}_i}{r}\right)\right|^2\right) \quad (1)$$

Here, $\mathbf{x}_i$ are the oxygen position vectors (i = 1,...,6) for a given structure, and $\mathbf{e}_i$ are the 6 unit vectors corresponding to the ideal symmetrical octahedral geometry ($\mathbf{e}_1$ = (1,0,0), $\mathbf{e}_2$ = (0,1,0), $\mathbf{e}_3$ = (0,0,1), $\mathbf{e}_4$ = (−1,0,0), $\mathbf{e}_5$ = (0,−1,0), and $\mathbf{e}_6$ = (0,0,−1)). For each optimized structure along the reaction profile, we determined S as the minimum distance to an ideal octahedron. This was done by simultaneous optimization of four parameters: (i) the scaling distance r and (ii) the three Euler angles corresponding to the independent elements of the 3D rotation matrix, $\mathbf{M}$. For each optimized structure along the path, we minimized the average distance between the ideal fully symmetric octahedron ($\mathbf{e}_i$) and the rotated, distance scaled, adimensional/dimensionless, octahedron with edges composed of the actual oxygen atom positions of the Mg^{2+} ligands.

DOI: 10.1021/cs502087f
ACS Catal. 2015, 5, 3225−3237

RESULTS AND DISCUSSION

Steady-State Activities. Steady-state activities of the WT, T138Stop, and H145A mutants were determined by fitting Michaelis–Menten curves to the measured data points (Figure 4). The activity of the H145A mutant decreased by 1 order of magnitude, whereas the T138Stop mutant shows 3 orders of magnitude activity decrease. Both values are in agreement with the homologous mutations in the human dUTPase enzyme.[17,25]

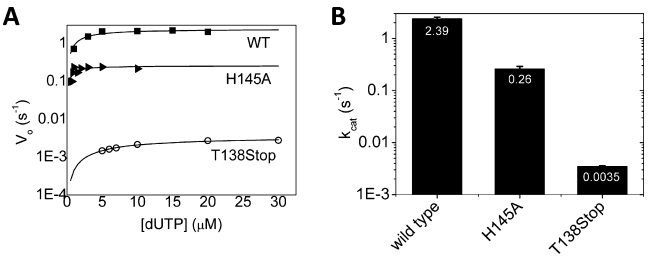

Figure 4. (A) Michaelis–Menten enzymatic activity curves of the wild type and the mutants. (B) Steady-state activity of the dUTPase mutants. Note that both the initial velocity (V_0) and the catalytic rate constant (k_{cat}) values of the mutants are shown on a logarithmic scale.

Ligand Binding. Ligand binding experiments show that the mutants bind the dUTP analogue α,β-imido-dUTP (dUPNPP) only ~2–4 times weaker than it does the wild type (Table 1).

Table 1. Measured Kinetic and Ligand Binding Parameters of the Mutants

mutant	WT	H145A	T138Stop
k_{cat} (s^{-1})	3.1 ± 0.06	0.26 ± 0.03	0.0035 ± 0.0001
K_M (μM)	0.46 ± 0.2	0.6 ± 0.2	6.7 ± 0.4
$K_{d\ dUPNPP}$ (μM)	0.9 ± 0.5	2.1 ± 1.0	3.9 ± 1.3
$K_{d\ dUDP}$ (μM)	12.7 ± 3.6	13.6 ± 2.9	13.7 ± 2.3
T_m (°C)	61.2 ± 0.1	58.0 ± 0.4	62.4 ± 0.1

This small change in ligand binding is consistent with the observed structural similarity of the H145A and T138Stop mutants compared to the wild type (see below). We also measured the dUDP binding in the mutant proteins and found no difference compared to the wild type. Because the mutations had some effect on the binding of dUPNPP, but not on the binding of dUDP, the mutated residues thus may promote the selectivity between dUTP and dUDP, as described previously.[17]

No Large-Scale Structural Changes. Thermal stability of the mutants and the wild type has been measured to ensure that the observed differences are not the results of changes in the entire enzyme structure. The measured melting temperatures are similar for both the mutants and the wild type, confirming that the mutations did not induce significant changes in the global protein structure (Table 1).

Crystal Structures. Crystal structures were previously obtained for the H145A[25] and for the T138Stop[15] mutants. These structures demonstrated that the substrate binding is not significantly affected by the mutations and that the overall protein assemblies and substrate binding remained largely similar. The RMSD of the common amino acid atoms with respect to the wild type is 0.12 Å for H145A and 0.20 Å for T138Stop mutant. A smaller but potentially important change in the substrate position was observed for the T138Stop mutant. The substrate gamma phosphate orientation changed compared to the coordinating Mg^{2+} that is not observed for the H145A (Figure S2A). All other residues remained within 0.5 Å compared to the wild type for both the T138Stop and the H145A mutants.

Structural Changes Compared to the Crystal Structures. There are no significant changes between our structures obtained after minimization and the original crystallographic structures. The overall RMSD of the optimized reactant state (RS) structures and the crystallographic structures are 0.252 Å for the WT, 0.477 Å for the H145A, and 0.336 Å for the T138Stop mutant. The largest deviations are 1.77 Å for the Asp28 O in the case of the H145A mutant and 1.37 Å for the Ser65 O in the case of the T138Stop mutant. These changes are relatively small compared to the crystal structure resolution (1.80 and 1.25 Å for the H145A and T138Stop mutant, respectively), and may also be affected by the presence of the dUPNPP instead of the native dUTP substrate. It is worthwhile to note that both the Asp28 and Ser65 residues are well conserved and found to be important for efficient catalysis.[15,49] An analogous residue to Ser65 has also been found in an alternative conformation in *Bacillus subtilis* dUTPase.[50]

Reaction Mechanism. To investigate the detailed reaction mechanism and the effects of the mutations on the catalytic activity, we performed hybrid QM/MM calculations on the wild type, H145A and T138Stop mutants. Our preliminary minimizations, in which only the phosphate bond forming and breaking coordinates were constrained, confirmed that the proton transfers from the nucleophilic water molecule to the oxygen of the Asp83 carboxylic group. We observed that, when no bias was used on the proton transfer process (i.e., only the Q_{ET} coordinate is biased), as the product was approached, the proton spontaneously transferred to the Asp83. Asp83 is a strictly conserved residue, essential for catalytic activity of trimeric dUTPases. Accordingly, it has been identified in numerous dUTPases as being the universal proton acceptor in the catalytic mechanism.[10,23,51,52] We therefore performed subsequent minimizations along the reaction pathway using the complete reaction coordinate, defined as $Q = d1 - d2 + 0.5(d3 - d4)$ (Figures 3 and 5). Q accounts for all bond breaking and forming processes involved in the rate-limiting catalytic step, including the proton transfer from the nucleophilic water molecule to the acceptor Asp83 residue. For all three obtained pathways, the reaction follows a one-step A_ND_N mechanism regarding the phosphate hydrolysis (Figure S3). The proton transfer from the nucleophilic water to the Asp83 immediately follows the phosphorus bond-forming and bond-breaking steps in a concerted mechanism (Figure 5). The reaction is initiated by the attack of the nucleophilic water, leading to an associative pathway for the phosphate cleavage that has been identified in solution and in several enzymes that carry out phosphate cleavage or transfer (see e.g., Florián et al.[53,54] and Klahn et al.[55]).

This mechanism is also consistent with the experimentally observed pH change that is used to directly follow the reaction kinetics[56] and with the lack of observed intermediates for the phosphate hydrolysis.[33] It is found in *E. coli* dUTPase that two protons transfer to the reaction medium in a concerted mode, immediately following the rate-limiting step.[56] These proton transfer events were also found dependent on two ionizable groups in the protein substrate complex with pK_a values of 5.8 and 10.3.[56] Although the WT and H145A reaction pathways are closely similar to each other, with the H145A pathway being somewhat less concerted (Figures 5 and 6B), a striking

DOI: 10.1021/cs502087f
ACS Catal. 2015, 5, 3225–3237

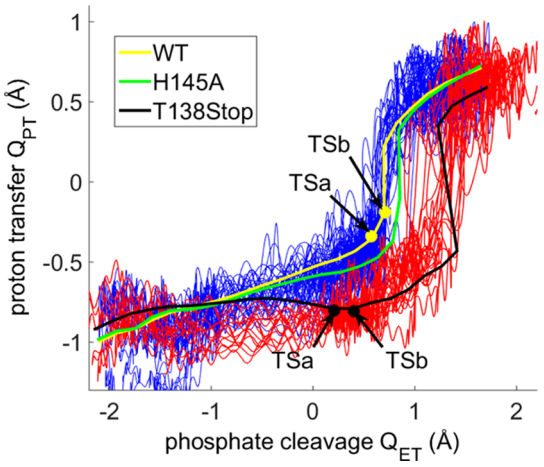

Figure 5. Reaction pathways along the Q_{PT} and Q_{ET} reaction coordinates. Minimum energy pathways are shown for the WT (yellow), H145A (green), and T138Stop (black) systems. Unbiased downhill QM/MM MD trajectories are also shown for the WT (blue) enzyme and for the T138Stop (red) mutant. The downhill trajectories (thin lines) were initiated from near the corresponding transition state (TS) positions for each system (arrows and symbols). TSa and TSb correspond to the nearest points to the transition state on the reactant and on the product side along the minimized pathways, respectively (see the Downhill Trajectories section for further details).

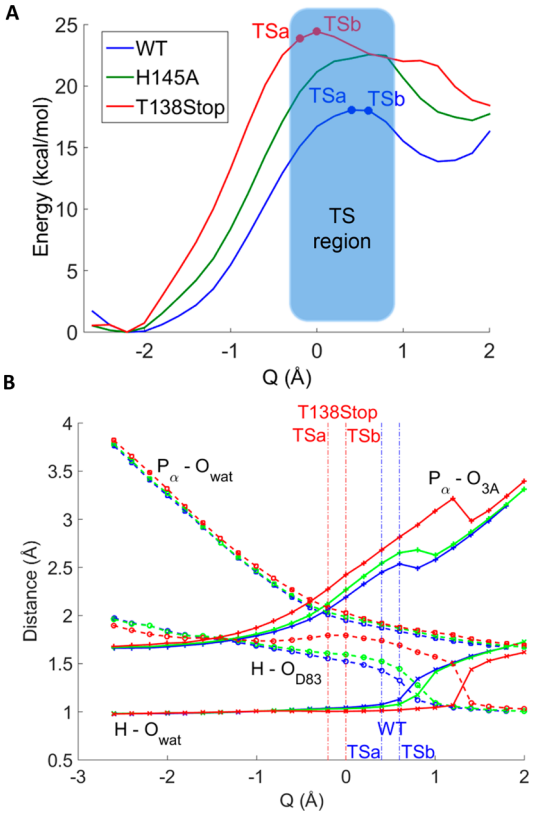

Figure 6. (A) Energy profiles for the catalytic reaction and (B) distances of the forming (P_α–O_{wat}, dashed lines and squares), breaking (P_α–O_{3A}, solid lines and + symbols), forming H–O_{D83} (dashed lines and circles), and breaking open H–O_{wat} (solid lines and x symbols) bonds along the reaction coordinate Q. WT, H145A and T138Stop systems are shown with blue, green and red, respectively. TS region is highlighted for WT and T138Stop. TSa and TSb (vertical dash-dot lines) correspond to adjacent points at the TS along the optimized pathways, at the reactant and product side, respectively (see the Downhill Trajectories section for further details).

difference is observed for the T138Stop mutant. For this enzyme, which lacks the C-terminal arm, we observed a much more stepwise reaction profile (Figures 5 and 6), with the proton transfer being decoupled from the phosphate cleavage. A comparison of the bond-forming and -breaking distances (Figure 6B) reveals that the crossing points of equal P–O distances happen the earliest for the T138Stop mutant, followed by the H145A and the WT enzymes along the reaction coordinate Q. Accordingly, the crossing point for the O–H distances is located along Q first for the WT enzyme, followed closely by the H145A, and finally it takes place at the largest Q value for the T138Stop system. We find consistently that the extent of concertedness of the proton transfer (PT) correlates with the calculated energy barrier, and the experimental activity (cf. also Tables 1, 2).

The reaction energies (Table 2 and Figure 6A) are in very good qualitative agreement with the experimental catalytic rates, particularly the observed trend of decreased catalytic activities of T138Stop with respect to WT and H145A. The calculated activation energies are shown in Table 2, together with the activation Gibbs free energies which were obtained from the measured catalytic rate constants using a 6.1×10^{12} s^{-1} prefactor. The energy barrier for the WT enzyme is in excellent quantitative agreement with the derived experimental activation free energy. The order of activities among the three enzymes is also properly predicted. The calculated barriers are higher for the H145A and T138Stop mutants than the experimentally observed ones; however, their relative activities are recovered consistently. In the future, more computationally demanding free-energy calculations with extensive sampling could be used to account quantitatively for the energy profiles evidenced in this study.

Transition States Geometries and Electronic Structure. To characterize the transition states, we have analyzed the geometrical parameters corresponding to the bonds breaking and forming during the phosphate cleavage and the proton

Table 2. Measured Activation Free Energies and Calculated Activation Energies (kcal/mol)

	measured $\Delta G^{\ddagger}$	calcd $\Delta E^{\ddagger}$
wild type	16.6	18.0
H145A	17.9	22.6
T138Stop	20.4	24.4

transfer processes (Table S2). In all three systems, the transition state corresponds to long P_α–O_{3A} leaving group distances, viz., in the range of 2.3–2.6 Å, where the P_α–O_{3A} bond is already broken. These late-transition-state structures thus have a dissociative character and fit well into the loose transition states extensively described in previous experimental studies, based on oxygen kinetic isotope effect data and the slopes of Brønsted plots in linear free energy relationships for analogous phosphate cleavage reactions in enzymes and in solution.[57−60] Interestingly, the O_{wat}–P_α bond length shows greater variations at the TS for the three enzymes; it is the shortest for the WT and the longest for the T138Stop mutant. Overall, the WT enzyme presents the most "loose" transition state geometry, whereas the almost inactive T138Stop enzyme has the most compact transition state.

To further compare the bonding patterns at the transition states of the three different systems, we also performed Natural

DOI: 10.1021/cs502087f
ACS Catal. 2015, 5, 3225−3237

Bond Orbital (NBO) analysis at the respective transition state geometries. Consistent with the coupled proton transfer pathway (Figure 5), the bonding analysis reveals simultaneous occurrence of the following events: bond forming between the O_{wat}–P_{α} atoms, bond breaking at the O_{wat}–H_{wat} bond, and formation of the new O_{D83}–H_{wat} bond (Figure 7, top). The two

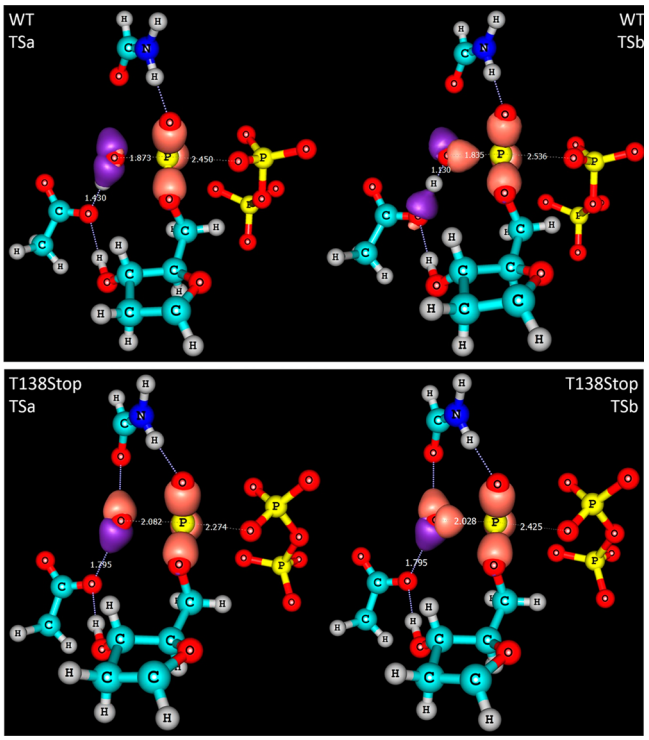

Figure 7. NBO analysis of the transition state structures in the WT and T138Stop enzymes. The molecular orbitals at the 0.2 au electron density level are shown for all natural bonds of only the H_{wat}, O_{wat}, and P_{α} atoms. For clarity, only part of the QM region corresponding to the deoxyribose triphosphate, the nucleophilic water, the proton accepting Asp83 side chain and the Thr81 and Ile82 backbones are shown.

structures at the barrier top correspond to the changing bonding pattern with respect to these three bonds, highlighting all the bonds formed by the H_{wat}, O_{wat}, and P_{α} atoms in each case. The H145A enzyme has a more flat transition state region, with already formed O_{wat}–P_{α} bond at the Q = 0.2 Å and Q = 0.8 Å regions (Figure S4). The energy then finally drops corresponding to the deprotonation of the water at larger reaction coordinate values (Figure 6A). The proton transfer and the phosphate cleavage are the most decoupled for the T138Stop enzyme, where the transition state corresponds only to the formation of the O_{wat}–P_{α} bond (Figure 7, bottom). The NBO analysis provides a consistent picture clarifying the nature of the chemical bonding at the transition states in all three systems. We find that the P_{α}–O_{3A} bond between the leaving group and the phosphorus is broken in all three cases, presenting a concerted mechanism with a loose dissociative TS. The NBO analysis also confirms the simultaneous bond formation of the new O_{wat}–P_{α} bond and the proton transfer from the water to the Asp83 for the WT system, whereas the transition state corresponds to the formation of the new O_{wat}–P_{α} bond only in the T138Stop enzyme, and the proton transfer follows subsequently.

Solvent Kinetic Isotope Effects. To determine the involvement of the proton transfer in the catalytic reactions, we carried out frequency calculations at the reactant and transition states using the QM/MM optimized geometries of the reaction pathways. The MM atoms were considered as point charges only, and therefore, the additional imaginary frequencies corresponding to the approximate Hessian were excluded.[61] These frequencies were consistently the same both for the RS and TS geometries, whereas additional imaginary frequencies with the larger intensity peaks were present in the TS structures only. The vibrational motion of these TS frequencies corresponded to the bond breaking and forming coordinates. We estimated the solvent kinetic isotope effects (solvent KIEs) by performing calculations using standard proton mass as well as using deuterated water molecules. On the basis of the estimated free energy difference ($\Delta\Delta G^{\ddagger}$) between the calculated zero-point vibrational energies for the D_2O/H_2O systems at the TS/RS, we obtained the solvent kinetic isotope effects of about 1.8 to 3.2 for the WT (corresponding to the TSa: Q = 0.4 Å and TSb: Q = 0.6 Å structures, respectively), 1.4 to 2.2 for the H145A (corresponding to the optimized structures within the range of Q = 0.2 to 0.8 Å), and 1.01−1.02 for the T138Stop systems (corresponding to TSb: Q = 0.0 Å and TSa: Q = −0.2 Å structures, respectively). The results suggest the loss of solvent KIEs for the nearly inactive T138Stop mutant.

Downhill Trajectories. As an additional test of the mechanistic reaction pathway found with QM/MM minimizations, we ran sets of downhill QM/MM trajectories. Geometry optimizations in proteins are well-known to suffer from being trapped in some of the myriads of local minima, and free energy calculations are necessary for more quantitative results.[62,63] Here we tested whether our minimized pathways correspond to the ones obtained by dynamical trajectories. We initiated random downhill trajectories from near the transition states for the WT enzyme and the T138Stop mutant, starting from different thermally equilibrated classical regions. The obtained trajectories initiated at conformations close to the transition state (Figure 6) indeed terminated both at the reactant side and the product side, confirming that the starting structures were part of the TS ensemble.

For the WT system, a total of 86 simulations were initiated from the QM/MM optimized structures at the Q = 0.4 Å (66 trajectories, all 100 fs long), and Q = 0.6 Å (20 trajectories of length between 317 and 584 fs) values of the reaction coordinate (Figure 5, TSa and TSb, respectively). Out of the 66 trajectories initiated at Q = 0.4 Å (closer to the reactants, TSa), 4 remained near the transition state, 14 reached the product state, and 48 the reactant state. Out of the 20 trajectories, initiated at Q = 0.6 Å (closer to product, TSb), 12 reached the product state, and 8 the reactant state.

For the T138Stop system, 20 trajectories were initiated both at Q = −0.2 Å (Figure 5, TSa), and also at Q = 0.0 Å, at the free energy barrier maximum (Figure 5, TSb). Trajectories were run between 70 and 1000 fs long, each dynamics reaching reaction coordinate values either below Q = −1.47 Å (RS) or above Q = 1.61 Å (PS). Fourteen out of the 20 trajectories reached the product state, and 6 the reactant state starting from Q = 0.0 Å, and 12 reached the reactant state, 8 the product state starting at Q = −0.2 Å. Note that we have carried out both forward and backward minimizations using our complex reaction coordinate to avoid hysteresis as much as possible.[42]

DOI: 10.1021/cs502087f
ACS Catal. 2015, 5, 3225−3237

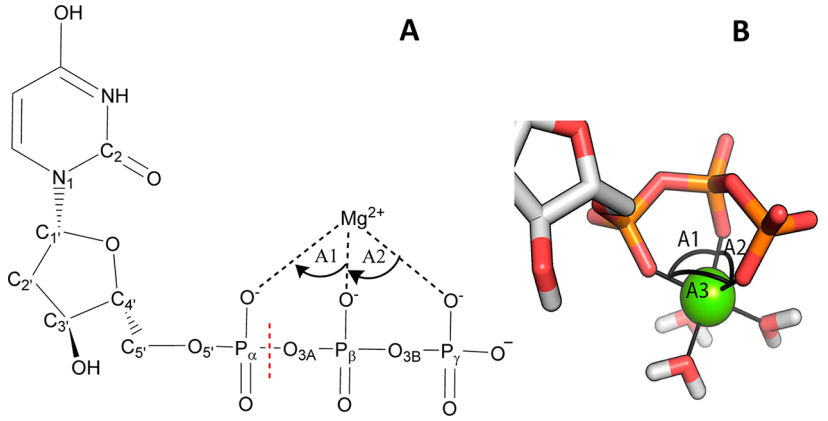

Figure 8. (A) Schematic view of the dUTP molecule coordinated to the Mg^{2+} ion. (B) The hexacoordinated Mg^{2+} ion, as bound in the active site. Definition of the three angles, A1, A2, and A3, are also shown.

Note also that the downhill reaction pathways for WT and T138Stop are initiated near the maxima of the corresponding energy profiles. These positions, do not necessarily have to coincide with the actual TS locations (i.e., having a splitting probability of 0.5) along the reaction coordinate Q[64] though in this case they are clearly very close.

We obtained a very good correlation between the reaction pathway calculated by QM/MM minimizations and the ensemble of pathways obtained via downhill trajectories (Figure 5). We could also confirm the distinct difference between the reaction pathways for the WT and T138Stop enzymes, with the latter being much more stepwise.

Mg^{2+}-Ion Coordination. Mg^{2+} is an essential cofactor in most phosphoryl transfer and hydrolysis catalyzing enzymes. Its role in modulating the catalytic reaction, however, is not yet well understood. We investigated the Mg^{2+} coordination, in particular, focusing on the O−Mg−O angles during the reaction (Figures 8 and S5). Three angles, labeled A1, A2, and A3 (Figure 8B), are most relevant to characterizing the phosphate−magnesium binding geometry: (i) A1, between the α- and β-phosphates and the Mg^{2+} (O1A−Mg−O1B); (ii) A2, between the β- and γ-phosphates and the Mg^{2+} (O1B−Mg−O2G); and (iii) A3, between the α- and γ-phosphates and the Mg^{2+} (O1A−Mg−O2G). The increase in A1 and A2 (Figure S5) correlates strongly with the changes in the reaction coordinate, whereas A3 changes only in case of the T138Stop mutant. A1 and A2 reach the ideal 90° angle−required for the symmetric octahedral Mg^{2+} coordination−right before the transition state region of the reaction pathway. A3, on the other hand, remains at around 100° throughout the reaction profile for the WT and H145A enzymes (Figure S5), thus causing a small distortion from an ideal octahedral Mg-coordination. The γ-phosphate in the T138Stop mutant is not coordinated by key protein residues observed in the WT, due to the lack of the C-terminal arm. Accordingly, as compared with the wild type, the Mg^{2+} coordination in this mutant leads to the largest differences in the values of A3 (Figure S5), an angle involving the γ-phosphate.

Continuous Symmetry Measure. To provide a generic, quantitative analysis tool measuring the changes in the Mg^{2+} coordination (i.e., the symmetry) along the reaction profile, we implemented a simple algorithm to calculate a continuous symmetry measure[34] around the Mg^{2+}. We use this symmetry measure S (see eq 1) to follow the changes along catalytic reactions. Previously, symmetry measures have been applied to a variety of systems, such as studies of interconversion paths in transition metal chemistry.[65−67] We determined the overall coordination symmetry in the three different systems using the continuous symmetry measure S (Figure 9). Interestingly, all

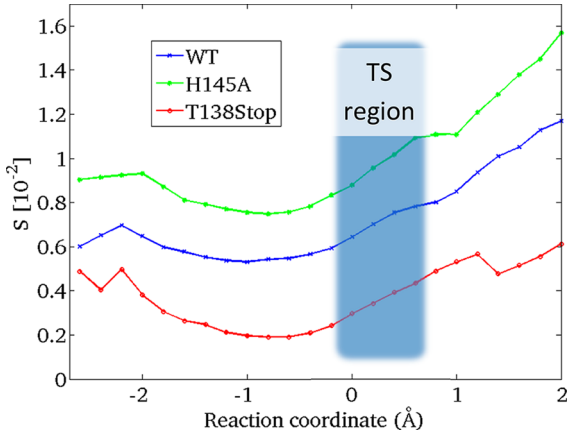

Figure 9. Symmetry parameter (S) along the reaction profile. Mg^{2+} coordination becomes most symmetric (i.e., smaller S values) before the transition state region (TS, blue area) is reached. A more symmetrical Mg^{2+}-coordination could drive the reaction toward the TS region. S is defined according to eq 1.

systems display the same general trend: the coordination becomes gradually more symmetrical as the reaction progresses, and a minimum in S is reached before the transition state. After this point, the symmetry measure S increases again, as the product state is reached. Interestingly, the T138Stop mutant has the most relaxed and symmetrical Mg^{2+} coordination compared with the WT and H145A, due to the lack of the C-terminal arm, which would coordinate the phosphate chain of dUTP (Figure 9). Reaching more symmetrical coordination around the Mg^{2+} should energetically stabilize the TS compared with the reactant state (RS), and the lack of this difference in the stabilization between RS and TS may lead to decreased activity. In general, however, it is hard to quantify the energetic contribution arising due only to the changes in the Mg^{2+}-coordination. Based on thorough gas-phase and solution studies by the Florián group,[68] analyzing the energetics of distortions in metal ion coordination, the energetic stabilization may be estimated on the order of 2 kcal/mol. To sum up, the Mg^{2+}-coordination symmetry varies along the reaction coordinate

DOI: 10.1021/cs502087f
ACS Catal. 2015, 5, 3225−3237

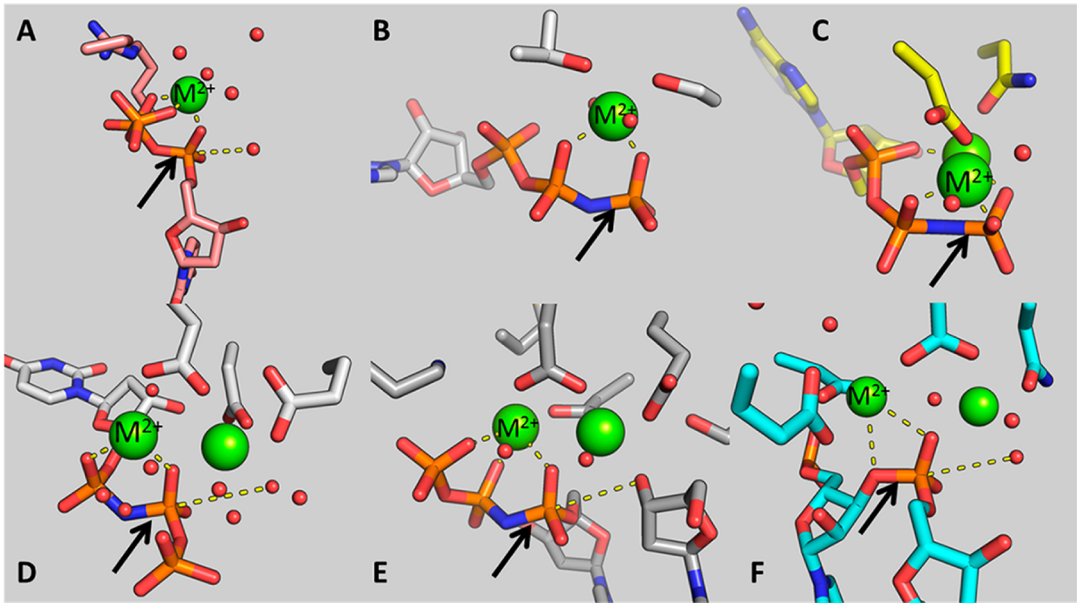

Figure 10. Equivalent active-site metal ion (M^{2+}) positions in various phosphate processing enzymes. The residues within 4 Å around the metal ions (green spheres) are shown as sticks. Prototype Mg^{2+} coordination geometries are presented for trimeric dUTPases (A, PDB ID: 2PY4), ATPases (B, PDB ID: 3ZFD), Ser/Thr kinases (C, PDB ID: 4DFX), dimeric dUTPases (D, PDB ID: 2CIC), polymerases (E, PDB ID: 4Q8E), and RNases H (F, PDB ID: 1ZBL). The scissile P−O bonds (or its nonhydrolyzable equivalents) are highlighted by arrows.

consistently in all our three systems, and thus, the metal coordination symmetry emerges as a possible contributing factor to the catalytic mechanism.

Role of the C-Terminal Arm in Substrate Specificity. Interestingly, the particularly important role of the A2 and A3 angles involving the γ-phosphate (Figure 8B) could contribute to the dUDP/dUTP specificity via the C-terminal arm, preventing the dUDP hydrolysis while allowing it for dUTP. For *E. coli* enzymes, it was found that the flexible C-terminal arm takes up an ordered structure only in the presence of the γ-phosphate,[29,30] whereas other organisms such as the human dUTPase may have a C-terminal arm located in the vicinity of the active site, even when a bound substrate is absent.[69] A recent mutational study demonstrated that the C-terminal arm P-loop-like motif is required for catalytic activity and it also helps to discriminate against dUDP substrates.[17] The differences we observed in angles A2 and A3 along the catalytic reaction (Figure S5) with the C-terminal arm present (WT and H145A) and absent (T138Stop) are also consistent with distinct changes in the dihedral angles of the triphosphate chain. Three relevant dihedral angles of the triphosphate backbone, $O_{5'}-P_\alpha-O_{3A}-P_\beta$ (A), $P_\alpha-O_{3A}-P_\beta-O_{3B}$ (B), and $O_{3A}-P_\beta-O_{3B}-P_\gamma$ (C) (Figure S6), show a distinctly different orientation of the chain for the T138Stop mutant as compared to the WT and H145A. The same trend is also observed in the original crystallographic structures with nonhydrolyzable ligands (Table S1 and Figure S2A). This may offer new mechanistic insights about the role of the C-terminal arm structural motif in the dUDP/dUTP specificity.

Analogy with Two-Metal Ion Catalysis. In many enzymes that carry out phosphoryl transfer and hydrolysis, the reacting phosphate groups are coordinated via divalent metal ions, in the active site, mainly Mg^{2+} (Figure 10). A common ubiquitous two-metal ion catalytic mechanism was proposed for polymerases and nucleases by Steitz and Steitz.[70] In this mechanism, metal ion A coordinates the nucleophile, whereas metal ion B coordinates the leaving group. Similar to dUTPases, only a single metal ion is involved in the catalytic reaction of several enzymes, such as nucleases with the ββα-Me structural motifs,[71,72] or HUH motifs (where H's denote two histidine residues separated by a hydrophobic residue, U).[69,73,74] An analogous role of the single metal ion in one-metal ion catalysis has been proposed to metal ion B in two-metal ion catalysis based on structural data.[8] An additional emerging role for metal ion B is to take on a more symmetrical coordination near the transition state region and thereby to facilitate catalysis.[8,43] These roles show great similarities to the roles of metal ion B in two-metal ion catalysis.[43]

An analogous metal ion is also present in most AAA+ ATPases coordinating the ATP at the β- and γ-phosphates, but not the α-phosphates (Figure 10B). Related phosphate transfer reactions are carried out by kinases cleaving ATP and transferring the γ-phosphate to an alcohol group of an amino acid side chain (typically Ser, Thr, or Tyr). In this important family of enzymes, two Mg^{2+} ions are commonly observed in high-resolution crystal structures, with a consensus structure for Ser/Thr kinases where one of the metal ions coordinates α-, β-, and the γ-phosphates, whereas the second metal ion coordinates β- and γ-phosphates, as in for example cyclic AMP-dependent protein kinase (PKA, Figure 10C).[75] Intriguingly, both metal ions coordinate the cleaved γ-phosphate of the ATP for these catalytic reactions, whereas none coordinate the attacking oxygen nucleophile in these highly specific enzymes, just as in dUTPases. The role of the two metal ions in these kinases therefore resembles the role of metal ion B in two-metal ion catalysis, and the single metal ion observed in one-metal ion catalysis in ATPases and dUTPase. Interestingly, the Mg^{2+} to Ca^{2+} substitution effects are typically also similarly inhibitory[76] for two-metal ion catalysis as well as for the one-metal ion catalysis in dUTPase[21,22] and in several ATPases[77−81] and kinases,[78,82,83] with some notable exceptions.[84,85]

This key metal ion often coordinates the cleaved phosphate. This helps the catalysis by lowering the pK_a of the phosphate group. As the overall effect of this Mg^{2+} coordination, the α-

DOI: 10.1021/cs502087f
ACS Catal. 2015, 5, 3225−3237

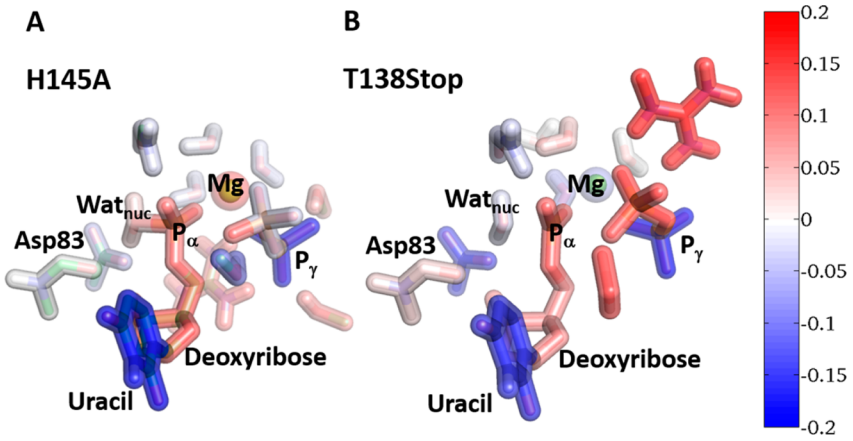

Figure 11. Charge distribution difference for the QM region of (A) H145A and (B) T138Stop mutants compared with the WT enzyme, using the CHELPG atomic charge scheme as implemented in Gaussian09. The atoms are displayed in solid sticks using a color scheme based on the elements and with wider transparent sticks using a blue-white-red color scheme, in the range of −0.2 *e* to +0.2 *e* (scale bar in atomic units), based on the charge difference for the group of atoms between the (A) H145A or (B) T138Stop simulation and the WT. For definition of the atomic groups and the numerical values for the charge differences, see Table S3.

phosphate oxygen atoms are more acidic, and thus their protonation is significantly less favorable. Accordingly, the single most likely proton transfer pathway corresponds to the protonation of the Asp83, and protonation of the α-phosphate is unfavorable.

The prominent role of the Mg^{2+} ion in lowering of the pK_a of its ligands is also important for the second ion in two-metal ion catalysis. In this case, the second Mg^{2+} ion typically coordinates the nucleophilic water (or the attacking group, in general). This was observed to lead to a mechanism with early proton transfer, preceding the coupled phosphate cleavage in the RNase H catalytic reaction.[43,76] Likewise, early proton transfer was found to take place in the two-metal ion-catalyzed reactions of DNA polymerases[86] and adenylyl cyclases.[87] In one-metal ion catalysis, the unligated nucleophilic water has a higher pK_a, which explains the difference in the mechanism leading to the late proton transfer observed in this study as well.

A key consensus role thus emerges for a functional Mg^{2+} ion that coordinates the cleaved phosphate. The specific active site geometry and fine-tuning of the pK_a-s of the catalytic groups by the metal ion leads to a reaction mechanism that is very different from the corresponding slow, uncatalyzed reaction in water.[88,89] Thus, the Mg^{2+} ion appears to have an essential contribution for the highly specific catalytic reactions, by (i) lowering the pK_a of the leaving group, and by (ii) imposing a specific constrained geometry for the triphosphate chain, which drives the reaction toward its transition state and products.

Conserved $\pi-\pi$ Stacking Interaction with the NTP Nucleobase. Despite the relatively large (∼7 Å) distance of the H145 residue from the P_α cleavage site, this residue has a significant contribution to the catalytic activity. It establishes a $\pi-\pi$ stacking interaction with the uracil ring (Figure 1B),[25] taking up a T-shaped orientation of the rings.[90] This well-conserved interaction is also observed in many other trinucleotide-binding enzymes, including ABC transporters,[91] kinesins,[92] or kinases.[93] The general importance of aromatic residues corresponding to the H145 amino acid across many dUTPases was established in a study of 500 dUTPase sequences.[25] Among these 500 structures, the most conserved residue is Phe (96.4% of cases), whereas His accounted for 1.8% of the structures. Based on our measurements and on the kinetic measurements reported,[25] the catalytic rate was affected when the aromatic residue was mutated to an Ala, whereas the substrate binding remained relatively intact as compared to the wild type. The loss of catalytic activity was about 10 to 20-fold,[25] both in the human and in the *M. tuberculosis* enzymes. There is thus an outstanding puzzling question as to how the conserved $\pi-\pi$ stacking interaction affects the catalytic reaction, from such a remote distance to the cleavage site.

Charge Distribution of the QM Regions at the TS. T-shaped $\pi-\pi$ stacking interactions are thought to have more electrostatic character compared with sandwich-shaped orientations.[94] To better understand whether the $\pi-\pi$ stacking interactions with the nucleobase may produce additional charge transfer that in turn would promote catalysis, we calculated the partial charges for the minimized structures. We compared the charge distribution in the WT with the mutants, in their respective TS conformations. It is important to emphasize that the charge distribution of the high energy TS is the main determining factor of the catalytic barrier, whereas the charge distribution at the RS is less relevant for predicting reactivity. For both mutants, we calculated the difference in the distribution of partial charges, as illustrated in Figure 11 using a color coding where blue means that the group is more negative than the WT, red means that the group is more positive, and white means no change in overall charge. The color code ranges between −0.2 and 0.2 *e*. The numerical values are also given in Table S3.

We observed that the uracil ring has a significantly altered polarization due to the missing $\pi-\pi$ stacking interaction, and this also affects the sugar moiety (Figure 11 and Table S3). However, the geometric differences corresponding to the H145A mutation are likely the main reason for the decreased activity of the H145A mutant (SI text).

Intriguingly, both mutants have similar changes in the polarization of the active site at the TS geometries. We find that the largest change is observed in the polarization of the relatively distant γ-phosphate, interestingly, which becomes more negative at the H145A and T138Stop enzymes compared to the WT TS. Likewise, the uracil group also becomes more negative at the TS in the H145A and T138Stop mutants compared with the WT, whereas the deoxyribose and the α-phosphate groups have a more positive partial charge in the mutant enzymes.

DOI: 10.1021/cs502087f
ACS Catal. 2015, 5, 3225−3237

CONCLUSIONS

Phosphate cleavage and transfer reactions are universal in all biological processes of all living organisms. Furthermore, phosphate-based reaction mechanisms have many common aspects shared among the majority of enzymes that carry out the corresponding catalytic reactions, such as the use of divalent Mg^{2+} ions.[35]

We investigated here the phosphate cleavage reaction in the WT and two mutant forms (H145A and T138Stop) of dUTPase enzyme complexes. Our analysis of steady-state activities of the WT and T138Stop and H145A mutants showed that the activity of the H145A mutant is lower by 1 order of magnitude, while that of the T138Stop mutant is lower by 3 orders of magnitude, as compared to the WT, in agreement with the homologous mutation in the human dUTPase enzyme.[17] To understand what the key factors are that might control the observed changes in the catalytic activities, we studied the reaction mechanism of proton transfer and phosphate cleavage using QM/MM methodology. We found a one-step associative A_ND_N pathway for the catalytic mechanism with a loose dissociative TS in all three systems. The dUTPase hydrolysis of the α-phosphate also involves a coupled proton transfer from the nucleophilic water to the catalytic Asp83 residue. The coupled proton transfer occurred in a single step with the phosphate cleavage in the following sequence of events. First, the nucleophilic water approached the phosphate. Subsequently, the $P_\alpha-O_{3A}$ bond broke. At the TS in the WT enzyme, the new $P_\alpha-O_{wat}$ bond formed at the same time as the proton transfer from the water to the Asp83 was initiated. The final products were then reached by completing the proton transfer. Essentially, we observed the same mechanism taking place in all the three systems. The main difference was that the proton transfer was decoupled from the TS in the two mutants as confirmed by NBO analysis, and it happened particularly late in the nearly inactive T138Stop mutant. We did not observe major differences in the ligand binding, protein stability, or in the structures of the assembled complexes. However, the degree of concertedness of the proton transfer and the phosphate bond formation at the TS were correlated strongly with the known catalytic activities. We observed less concerted proton transfer in case of the H145A mutant and further significantly decreased concertedness for the T138Stop mutant. Our calculations also suggest the loss of solvent KIEs for the T138Stop mutant. Our calculated reaction barriers are also in agreement with the catalytic rates measured in our corresponding site-directed mutagenesis experiments. The observed concerted coupled proton transfer appears to be a general mechanism in enzymes that catalyzes phosphate transfer and cleavage reactions.[43,76,95−98]

Our calculations also provided evidence that the specific metal ion coordination mode may play a prominent role in the catalytic reaction. We developed a new implementation to quantitatively determine the symmetry around the metal ion during the catalytic reaction. Based on our analysis using the calculated continuous symmetry measure[34] of the metal ion coordination throughout the reaction, a symmetric, octahedral Mg^{2+} coordination was shown to stabilize the TS for all cases. All three systems displayed the same trend for the change in the metal-coordination symmetry along the reaction pathway. The T138Stop mutant had the most symmetrical and thus the most relaxed coordination around the Mg^{2+} throughout the reaction, due to the lack of the C-terminal arm. Changes in the charge distributions of the three systems in their respective TS, also revealed significant differences in the partial charge transfer from the protein to the substrate, due to the missing native protein−protein and protein−substrate interactions in the mutants. The uracil group has a larger partial negative charge in the mutant structures at the TS compared to the WT, whereas deoxyribose is more positively polarized. Interestingly, the negative polarization of the γ-phosphate is the largest change between the partial charges of the TS structures. Geometrical relaxation of the active site due to mutations could play a key role in altering the TS-s, leading to a more decoupled proton transfer. The key emerging roles for a functional Mg^{2+} ion that coordinates the phosphate leaving group are (i) to lower the pK_a of the cleaved phosphate groups and (ii) to impose constrained coordination geometry on the Mg^{2+}, which drives the reaction toward the transition state and product.

The structural and electronic changes involved in the dUTPase catalytic reaction evidenced here, in conjunction with the experimental data, shed new light on the crucial role of the dUTPase C-terminal arm in modulating ligand binding geometry and catalytic activity and of the essential roles of the Mg^{2+} ion cofactor. Detailed understanding of the reaction process provided by this study could lead to the design of new drugs and new approaches to rationally control the activity of dUTPase and other (e.g., ATPase, kinase or polymerase) enzymes.

ASSOCIATED CONTENT

Supporting Information

The following file is available free of charge on the ACS Publications website at DOI: 10.1021/cs502087f.

Supporting Information consists of six additional figures (Figures S1−S6), three tables of data (Tables S1−S3), and two paragraphs on the protonation state of H145 and on the structural and polarization effect of the H145A mutation (PDF)

AUTHOR INFORMATION

Corresponding Authors

*E-mail: tothj@enzim.hu.
*E-mail: Vertessy.Beata@ttk.mta.hu.
*E-mail: Edina.Rosta@kcl.ac.uk.

Present Addresses

[¶](A.L.) Laboratory of Molecular Physiology, National Heart, Lung, and Blood Institute, National Institutes of Health, Bethesda, MD 20892, U.S.A. and Astbury Centre for Structural Molecular Biology, Faculty of Biological Sciences, University of Leeds, Leeds, LS2 9JT, U.K.
[#](P.K.S.) Department of Chemistry, Cotton College State University, Guwahati 781001, India.

Notes

The authors declare no competing financial interest.

ACKNOWLEDGMENTS

This work was supported by the Intramural Research Program of the National Institutes of Health, the Hungarian Scientific Research Fund (OTKA NK 84008, K109486), the Baross program of the New Hungary Development Plan (3DSTRUCT, OMFB-00266/2010 REG-KM-09-1-2009-0050), the Hungarian Academy of Sciences (TTK IF-28/2012), and the European Commission FP7 Biostruct-X project (contract no. 283570). This work used the computational

DOI: 10.1021/cs502087f
ACS Catal. 2015, 5, 3225−3237

resources of the NIH biowulf cluster, and the CCPBioSim via the ARCHER U.K. National Supercomputing Service. A.L. was awarded the student travel grant of the Budapest University of Technology and Economics. P.K.S. thanks Prof. Sun Choi at Ewha Womans University for laboratory facilities and the Korean Federation of Science and Technology Societies (KOFST) for a research fellowship under the Brain Pool program.

REFERENCES

(1) McIntosh, E. M.; Ager, D. D.; Gadsden, M. H.; Haynes, R. H. *Proc. Natl. Acad. Sci. U. S. A.* **1992**, *89*, 8020−8024.
(2) Björnberg, O.; Neuhard, J.; Nyman, P. O. *J. Biol. Chem.* **2003**, *278*, 20667−20672.
(3) Johansson, E.; Björnberg, O.; Nyman, P. O.; Larsen, S. *J. Biol. Chem.* **2003**, *278*, 27916−27922.
(4) Huffman, J. L.; Li, H.; White, R. H.; Tainer, J. A. *J. Mol. Biol.* **2003**, *331*, 885−896.
(5) Li, H.; Xu, H.; Graham, D. E.; White, R. H. *J. Biol. Chem.* **2003**, *278*, 11100−11106.
(6) Helt, S. S.; Thymark, M.; Harris, P.; Aagaard, C.; Dietrich, J.; Larsen, S.; Willemoes, M. *J. Mol. Biol.* **2008**, *376*, 554−569.
(7) Vertessy, B. G.; Toth, J. *Acc. Chem. Res.* **2009**, *42*, 97−106.
(8) Yang, W. *Nat. Struct. Mol. Biol.* **2008**, *15*, 1228−1231.
(9) Mustafi, D.; Bekesi, A.; Vertessy, B. G.; Makinen, M. W. *Proc. Natl. Acad. Sci. U. S. A.* **2003**, *100*, 5670−5.
(10) Chan, S.; Segelke, B.; Lekin, T.; Krupka, H.; Cho, U. S.; Kim, M.-y.; So, M.; Kim, C.-Y.; Naranjo, C. M.; Rogers, Y. C.; Park, M. S.; Waldo, G. S.; Pashkov, I.; Cascio, D.; Perry, J. L.; Sawaya, M. R. *J. Mol. Biol.* **2004**, *341*, 503−517.
(11) Tarbouriech, N.; Buisson, M.; Seigneurin, J.-M.; Cusack, S.; Burmeister, W. P. *Structure* **2005**, *13*, 1299−1310.
(12) Camacho, A.; Arrebola, R.; Pena-Diaz, J.; Ruiz-Perez, L. M.; Gonzalez-Pacanowska, D. *Biochem. J.* **1997**, *325* (Pt 2), 441−447.
(13) Moroz, O. V.; Harkiolaki, M.; Galperin, M. Y.; Vagin, A. A.; Gonzalez-Pacanowska, D.; Wilson, K. S. *J. Mol. Biol.* **2004**, *342*, 1583−97.
(14) Hemsworth, G. R.; Moroz, O. V.; Fogg, M. J.; Scott, B.; Bosch-Navarrete, C.; Gonzalez-Pacanowska, D.; Wilson, K. S. *J. Biol. Chem.* **2011**, *286*, 16470−81.
(15) Takacs, E.; Nagy, G.; Leveles, I.; Harmat, V.; Lopata, A.; Toth, J.; Vertessy, B. G. *FEBS Lett.* **2010**, *584*, 3047−54.
(16) Fiser, A.; Vertessy, B. G. *Biochem. Biophys. Res. Commun.* **2000**, *279*, 534−42.
(17) Pécsi, I.; Szabó, J. E.; Adams, S. D.; Simon, I.; Sellers, J. R.; Vértessy, B. G.; Tóth, J. *Proc. Natl. Acad. Sci. U. S. A.* **2011**, *108*, 14437−14442.
(18) Walker, J. E.; Saraste, M.; Runswick, M. J.; Gay, N. J. *EMBO J.* **1982**, *1*, 945−951.
(19) Ogura, T.; Wilkinson, A. J. *Genes Cells* **2001**, *6*, 575−597.
(20) Hanson, P. I.; Whiteheart, S. W. *Nat. Rev. Mol. Cell Biol.* **2005**, *6*, 519−529.
(21) Hidalgo-Zarco, F.; Camacho, A. G.; Bernier-Villamor, V.; Nord, J.; Ruiz-Perez, L. M.; Gonzalez-Pacanowska, D. *Protein Sci.* **2001**, *10*, 1426−33.
(22) Persson, R.; McGeehan, J.; Wilson, K. S. *Protein Expression Purif.* **2005**, *42*, 92−9.
(23) Harris, J. M.; McIntosh, E. M.; Muscat, G. E. O. *J. Mol. Biol.* **1999**, *288*, 275−287.
(24) Warshel, A.; Levitt, M. *J. Mol. Biol.* **1976**, *103*, 227−249.
(25) Pecsi, I.; Leveles, I.; Harmat, V.; Vertessy, B. G.; Toth, J. *Nucleic Acids Res.* **2010**, *38*, 7179−86.
(26) Varga, B.; Barabas, O.; Takacs, E.; Nagy, N.; Nagy, P.; Vertessy, B. G. *Biochem. Biophys. Res. Commun.* **2008**, *373*, 8−13.
(27) Mol, C. D.; Harris, J. M.; McIntosh, E. M.; Tainer, J. A. *Structure* **1996**, *4*, 1077−92.
(28) Shao, H.; Robek, M. D.; Threadgill, D. S.; Mankowski, L. S.; Cameron, C. E.; Fuller, F. J.; Payne, S. L. *Biochim. Biophys. Acta, Protein Struct. Mol. Enzymol.* **1997**, *1339*, 181−91.
(29) Vertessy, B. G. *Proteins: Struct., Funct., Genet.* **1997**, *28*, 568−79.
(30) Vertessy, B. G.; Larsson, G.; Persson, T.; Bergman, A. C.; Persson, R.; Nyman, P. O. *FEBS Lett.* **1998**, *421*, 83−8.
(31) Nord, J.; Kiefer, M.; Adolph, H. W.; Zeppezauer, M. M.; Nyman, P. O. *FEBS Lett.* **2000**, *472*, 312−6.
(32) Freeman, L.; Buisson, M.; Tarbouriech, N.; Van der Heyden, A.; Labbe, P.; Burmeister, W. P. *J. Biol. Chem.* **2009**, *284*, 25280−9.
(33) Barabás, O.; Németh, V.; Bodor, A.; Perczel, A.; Rosta, E.; Kele, Z.; Zagyva, I.; Szabadka, Z.; Grolmusz, V. I.; Wilmanns, M.; Vértessy, B. G. *Nucleic Acids Res.* **2013**, *41*, 10542−10555.
(34) Zabrodsky, H.; Peleg, S.; Avnir, D. *J. Am. Chem. Soc.* **1992**, *114*, 7843−7851.
(35) Palermo, G.; Cavalli, A.; Klein, M. L.; Alfonso-Prieto, M.; Dal Peraro, M.; De Vivo, M. *Acc. Chem. Res.* **2015**, 220−228.
(36) Prasad, G. S.; Stura, E. A.; Elder, J. H.; Stout, C. D. *Acta Crystallogr., Sect. D: Biol. Crystallogr.* **2000**, *56*, 1100−9.
(37) Brooks, B. R.; Bruccoleri, R. E.; Olafson, B. D.; States, D. J.; Swaminathan, S.; Karplus, M. *J. Comput. Chem.* **1983**, *4*, 187−217.
(38) Jo, S.; Kim, T.; Iyer, V. G.; Im, W. *J. Comput. Chem.* **2008**, *29*, 1859−1865.
(39) Shao, Y.; Molnar, L. F.; Jung, Y.; Kussmann, J.; Ochsenfeld, C.; Brown, S. T.; Gilbert, A. T.; Slipchenko, L. V.; Levchenko, S. V.; O'Neill, D. P.; DiStasio, R. A., Jr.; Lochan, R. C.; Wang, T.; Beran, G. J.; Besley, N. A.; Herbert, J. M.; Lin, C. Y.; Van Voorhis, T.; Chien, S. H.; Sodt, A.; Steele, R. P.; Rassolov, V. A.; Maslen, P. E.; Korambath, P. P.; Adamson, R. D.; Austin, B.; Baker, J.; Byrd, E. F.; Dachsel, H.; Doerksen, R. J.; Dreuw, A.; Dunietz, B. D.; Dutoi, A. D.; Furlani, T. R.; Gwaltney, S. R.; Heyden, A.; Hirata, S.; Hsu, C. P.; Kedziora, G.; Khalliulin, R. Z.; Klunzinger, P.; Lee, A. M.; Lee, M. S.; Liang, W.; Lotan, I.; Nair, N.; Peters, B.; Proynov, E. I.; Pieniazek, P. A.; Rhee, Y. M.; Ritchie, J.; Rosta, E.; Sherrill, C. D.; Simmonett, A. C.; Subotnik, J. E.; Woodcock, H. L., 3rd; Zhang, W.; Bell, A. T.; Chakraborty, A. K.; Chipman, D. M.; Keil, F. J.; Warshel, A.; Hehre, W. J.; Schaefer, H. F., 3rd; Kong, J.; Krylov, A. I.; Gill, P. M.; Head-Gordon, M. *Phys. Chem. Chem. Phys.* **2006**, *8*, 3172−91.
(40) Becke, A. *J. Chem. Phys.* **1993**, *98*, 5648−5652.
(41) Woodcock, H. L., 3rd; Hodoscek, M.; Gilbert, A. T.; Gill, P. M.; Schaefer, H. F., 3rd; Brooks, B. R. *J. Comput. Chem.* **2007**, *28*, 1485−502.
(42) Rosta, E.; Woodcock, H. L.; Brooks, B. R.; Hummer, G. *J. Comput. Chem.* **2009**, *30*, 1634−41.
(43) Rosta, E.; Nowotny, M.; Yang, W.; Hummer, G. *J. Am. Chem. Soc.* **2011**, *133*, 8934−41.
(44) Chu, J.-W.; Trout, B. L.; Brooks, B. R. *J. Chem. Phys.* **2003**, *119*, 12708−12717.
(45) Frisch, M. J.; Trucks, G. W.; Schlegel, H. B.; Scuseria, G. E.; Robb, M. A.; Cheeseman, J. R.; Scalmani, G.; Barone, V.; Mennucci, B.; Petersson, G. A.; Nakatsuji, H.; Caricato, M.; Li, X.; Hratchian, H. P.; Izmaylov, A. F.; Bloino, J.; Zheng, G.; Sonnenberg, J. L.; Hada, M.; Ehara, M.; Toyota, K.; Fukuda, R.; Hasegawa, J.; Ishida, M.; Nakajima, T.; Honda, Y.; Kitao, O.; Nakai, H.; Vreven, T.; Montgomery, J. A.; Peralta, J. E.; Ogliaro, F.; Bearpark, M.; Heyd, J. J.; Brothers, E.; Kudin, K. N.; Staroverov, V. N.; Kobayashi, R.; Normand, J.; Raghavachari, K.; Rendell, A.; Burant, J. C.; Iyengar, S. S.; Tomasi, J.; Cossi, M.; Rega, N.; Millam, J. M.; Klene, M.; Knox, J. E.; Cross, J. B.; Bakken, V.; Adamo, C.; Jaramillo, J.; Gomperts, R.; Stratmann, R. E.; Yazyev, O.; Austin, A. J.; Cammi, R.; Pomelli, C.; Ochterski, J. W.; Martin, R. L.; Morokuma, K.; Zakrzewski, V. G.; Voth, G. A.; Salvador, P.; Dannenberg, J. J.; Dapprich, S.; Daniels, A. D.; Farkas; Foresman, J. B.; Ortiz, J. V.; Cioslowski, J.; Fox, D. J. *Gaussian 09*, revision B.01; Gaussian, Inc.: Wallingford, CT, 2009.
(46) Breneman, C. M.; Wiberg, K. B. *J. Comput. Chem.* **1990**, *11*, 361−373.
(47) Singh, U. C.; Kollman, P. A. *J. Comput. Chem.* **1984**, *5*, 129−145.

DOI: 10.1021/cs502087f
ACS Catal. 2015, 5, 3225−3237

(48) Pastor, R. W.; Brooks, B. R.; Szabo, A. *Mol. Phys.* **1988**, *65*, 1409−1419.
(49) Palmen, L. G.; Becker, K.; Bulow, L.; Kvassman, J. O. *Biochemistry* **2008**, *47*, 7863−74.
(50) Garcia-Nafria, J.; Timm, J.; Harrison, C.; Turkenburg, J. P.; Wilson, K. S. *Acta Crystallogr., Sect. D: Biol. Crystallogr.* **2013**, *69*, 1367−1380.
(51) Barabas, O.; Pongracz, V.; Kovari, J.; Wilmanns, M.; Vertessy, B. G. *J. Biol. Chem.* **2004**, *279*, 42907−15.
(52) Siggaard, J. H.; Johansson, E.; Vognsen, T.; Helt, S. S.; Harris, P.; Larsen, S.; Willemoes, M. *Arch. Biochem. Biophys.* **2009**, *490*, 42−9.
(53) Florián, J.; Warshel, A. *J. Phys. Chem. B* **1998**, *102*, 719−734.
(54) Zhang, Z.; Eloge, J.; Florián, J. *Biochemistry* **2014**, *53*, 4180−4191.
(55) Klahn, M.; Rosta, E.; Warshel, A. *J. Am. Chem. Soc.* **2006**, *128*, 15310−15323.
(56) Larsson, G.; Nyman, P. O.; Kvassman, J. O. *J. Biol. Chem.* **1996**, *271*, 24010−6.
(57) Lassila, J. K.; Zalatan, J. G.; Herschlag, D. *Annu. Rev. Biochem.* **2011**, *80*, 669−702.
(58) Di Sabato, G.; Jencks, W. P. *J. Am. Chem. Soc.* **1961**, *83*, 4400−4405.
(59) Kirby, A. J.; Varvoglis, A. G. *J. Am. Chem. Soc.* **1967**, *89*, 415−423.
(60) Gorenstein, D. G.; Lee, Y. G.; Kar, D. *J. Am. Chem. Soc.* **1977**, *99*, 2264−2267.
(61) Ghysels, A.; Woodcock, H. L.; Larkin, J. D.; Miller, B. T.; Shao, Y.; Kong, J.; Neck, D. V.; Speybroeck, V. V.; Waroquier, M.; Brooks, B. R. *J. Chem. Theory Comput.* **2011**, *7*, 496−514.
(62) Klahn, M.; Braun-Sand, S.; Rosta, E.; Warshel, A. *J. Phys. Chem. B* **2005**, *109*, 15645−15650.
(63) Oláh, J.; Mulholland, A. J.; Harvey, J. N. *Proc. Natl. Acad. Sci. U. S. A.* **2011**, *108*, 6050−6055.
(64) Berezhkovskii, A. M.; Tofoleanu, F.; Buchete, N.-V. *J. Chem. Theory Comput.* **2011**, *7*, 2370−2375.
(65) Casanova, D.; Cirera, J.; Llunell, M.; Alemany, P.; Avnir, D.; Alvarez, S. *J. Am. Chem. Soc.* **2004**, *126*, 1755−1763.
(66) Alvarez, S.; Alemany, P.; Casanova, D.; Cirera, J.; Llunell, M.; Avnir, D. *Coord. Chem. Rev.* **2005**, *249*, 1693−1708.
(67) Tuvi-Arad, I.; Rozgonyi, T.; Stirling, A. *J. Phys. Chem. A* **2013**, *117*, 12726−12733.
(68) Pontikis, G.; Borden, J.; Martínek, V. c.; Florián, J. *J. Phys. Chem. A* **2009**, *113*, 3588−3593.
(69) Tóth, J.; Varga, B.; Kovács, M.; Málnási-Csizmadia, A.; Vértessy, B. G. *J. Biol. Chem.* **2007**, *282*, 33572−33582.
(70) Steitz, T. A.; Steitz, J. A. *Proc. Natl. Acad. Sci. U. S. A.* **1993**, *90*, 6498.
(71) Friedhoff, P.; Franke, I.; Meiss, G.; Wende, W.; Krause, K. L.; Pingoud, A. *Nat. Struct. Mol. Biol.* **1999**, *6*, 112−113.
(72) Kühlmann, U. C.; Moore, G. R.; James, R.; Kleanthous, C.; Hemmings, A. M. *FEBS Lett.* **1999**, *463*, 1−2.
(73) Ton-Hoang, B.; Guynet, C.; Ronning, D. R.; Cointin-Marty, B.; Dyda, F.; Chandler, M. *EMBO J.* **2005**, *24*, 3325−3338.
(74) Barabas, O.; Ronning, D. R.; Guynet, C.; Hickman, A. B.; Ton-Hoang, B.; Chandler, M.; Dyda, F. *Cell* **2008**, *132*, 208−220.
(75) Bastidas, A. C.; Deal, M. S.; Steichen, J. M.; Keshwani, M. M.; Guo, Y.; Taylor, S. S. *J. Mol. Biol.* **2012**, *422*, 215−229.
(76) Rosta, E.; Yang, W.; Hummer, G. *J. Am. Chem. Soc.* **2014**, *136*, 3137−3144.
(77) Beauge, L.; Campos, M. A. *Biochim. Biophys. Acta, Biomembr.* **1983**, *729*, 137−149.
(78) Skou, J. C. *Biochim. Biophys. Acta* **1957**, *23*, 394−401.
(79) Fukushima, Y.; Post, R. L. *J. Biol. Chem.* **1978**, *253*, 6853−6862.
(80) Knauf, P. A.; Proverbio, F.; Hoffman, J. F. *J. Gen. Physiol.* **1974**, *63*, 324−336.
(81) Collins, K.; Sellers, J. R.; Matsudaira, P. *J. Cell Biol.* **1990**, *110*, 1137−47.
(82) Ryves, W. J.; Dajani, R.; Pearl, L.; Harwood, A. J. *Biochem. Biophys. Res. Commun.* **2002**, *290*, 967−972.
(83) Lu, S.-Y.; Huang, Z.-M.; Huang, W.-K.; Liu, X.-Y.; Chen, Y.-Y.; Shi, T.; Zhang, J. *Proteins: Struct., Funct., Genet.* **2013**, *81*, 740−753.
(84) Deweese, J. E.; Osheroff, N. *Metallomics* **2010**, *2*, 450−459.
(85) Gerlits, O.; Waltman, M. J.; Taylor, S.; Langan, P.; Kovalevsky, A. *Biochemistry* **2013**, *52*, 3721−3727.
(86) Florian, J.; Goodman, M. F.; Warshel, A. *J. Am. Chem. Soc.* **2003**, *125*, 8163−77.
(87) Mones, L.; Tang, W. J.; Florian, J. *Biochemistry* **2013**, *52*, 2672−82.
(88) Duarte, F.; Aqvist, J.; Williams, N. H.; Kamerlin, S. C. *J. Am. Chem. Soc.* **2015**, *137*, 1081−93.
(89) Guthrie, J. P. *J. Am. Chem. Soc.* **1977**, *99*, 3991−4001.
(90) Meyer, E. A.; Castellano, R. K.; Diederich, F. *Angew. Chem., Int. Ed.* **2003**, *42*, 1210−1250.
(91) Guo, X.; Chen, X.; Weber, I. T.; Harrison, R. W.; Tai, P. C. *Biochemistry* **2006**, *45*, 14473−80.
(92) Rickert, K. W.; Schaber, M.; Torrent, M.; Neilson, L. A.; Tasber, E. S.; Garbaccio, R.; Coleman, P. J.; Harvey, D.; Zhang, Y.; Yang, Y.; Marshall, G.; Lee, L.; Walsh, E. S.; Hamilton, K.; Buser, C. A. *Arch. Biochem. Biophys.* **2008**, *469*, 220−31.
(93) Boehr, D. D.; Farley, A. R.; Wright, G. D.; Cox, J. R. *Chem. Biol.* **2002**, *9*, 1209−17.
(94) Sinnokrot, M. O.; Sherrill, C. D. *J. Am. Chem. Soc.* **2004**, *126*, 7690−7.
(95) Lans, I.; Medina, M.; Rosta, E.; Hummer, G.; Garcia-Viloca, M.; Lluch, J. M.; González-Lafont, À. *J. Am. Chem. Soc.* **2012**, *134*, 20544−20553.
(96) Castro, C.; Smidansky, E.; Maksimchuk, K. R.; Arnold, J. J.; Korneeva, V. S.; Gotte, M.; Konigsberg, W.; Cameron, C. E. *Proc. Natl. Acad. Sci. U. S. A.* **2007**, *104*, 4267−4272.
(97) Ganguly, A.; Thaplyal, P.; Rosta, E.; Bevilacqua, P. C.; Hammes-Schiffer, S. *J. Am. Chem. Soc.* **2014**, *136*, 1483−1496.
(98) Wang, J.; Yang, W. *J. Phys. Chem. B* **2013**, *117*, 9354−9361.

DOI: 10.1021/cs502087f
ACS Catal. 2015, 5, 3225−3237

Supporting Information: Mutations decouple proton transfer from phosphate cleavage in the dUTPase catalytic reaction

Anna Lopata[a,†], Pablo G. Jambrina[b], Pankaz K. Sharma[c,ǂ], Bernard R. Brooks[d], Judit Toth[a*], Beata G. Vertessy[a,e*] and Edina Rosta[b*]

[a]*Institute of Enzymology, Research Centre for Natural Sciences, Hungarian Academy of Sciences, Budapest,H1113, Hungary*

[b]*Department of Chemistry, King's College London, London, SE1 1DB, United Kingdom*

[c]*College of Pharmacy, Graduate School of Pharmaceutical Sciences, Ewha Womans University, Seoul 120-750 Korea*

[d]*Laboratory of Computational Biology, National Heart, Lung, and Blood Institute, National Institutes of Health, Rockville, Maryland 20892-9314, United States*

[e]*Department of Applied Biotechnology and Food Science, Budapest University of Technology and Economics, H1111 Hungary*

[†]*Present Address: Anna Lopata, Laboratory of Molecular Physiology, National Heart, Lung, and Blood Institute, National Institutes of Health, Bethesda, MD, 20892, USA and Astbury Centre for Structural Molecular Biology, Faculty of Biological Sciences, University of Leeds, Leeds, LS2 9JT, UK*

[ǂ]*Present Address: Pankaz K. Sharma, Department of Chemistry, Cotton College State University, Guwahati 781001, India*

[*]*tothj@enzim.hu, Vertessy.Beata@ttk.mta.hu, Edina.Rosta@kcl.ac.uk*

Protonation state of H145. We considered the possibility that H145 may be protonated when the substrate is bound. In the catalytic active site, negatively charged groups dominate despite the presence of two conserved Arg residues and the Mg^{2+} ion. The dUTP has a formal charge of -4 *e*, and the catalytic Asp83 is also deprotonated. Accordingly, preliminary pK_a calculations using the H++ server (5) predicted an upshift of the His pK_a when the substrate is bound. We have also obtained a lower catalytic barrier (11 kcal/mol) from minimizations with protonated H145 in the WT enzyme, compared to the same system with a neutral H145. However, we cannot conclude whether this residue may be charged or not, because we do not know the free energy difference corresponding to protonating the H145. Further pK_a calculations and free energy calculations are needed to shed light on this question. Nevertheless, we expect that a potential protonation of the His residue is not part of a conserved mechanism, because (i) a H145W mutation does not significantly change the catalytic rate (1) and (ii) most dUTPases (over 96%) have a neutral Phe residue in place of the His.

Structural and polarization effects of the H145A mutation. We aimed to elucidate whether the changes in partial charges were due to (i) the differences in the geometry of the TS structures, or (ii) the missing interaction with the imidazole ring of the His, and if these changes would influence the reaction energy barriers significantly. To this end, we calculated the partial charges in a system that is identical to the WT at the TS, but where the QM atoms representing the His residue were deleted. The differences in the partial charges are now entirely due to the missing interactions, since all the other coordinates are identical. We consequently observed that the uracil group became more negatively charged whereas the deoxyribose more positively charged (Table S3). We also observed that the α-P phosphate was slightly more positively charged; however, the extent of charge transfer was less, and no other significant additional polarization effects were observed. We also calculated the energy barrier of the catalytic reaction for the WT reaction pathway where we removed the His residue from the protein by omitting it from the QM region, and kept all the other coordinates otherwise identical along the pathway. We found similar barrier height as in the WT pathway. Therefore, the lack of the His residue implies subtle structural changes in the TS, which contribute to the elevated energy barrier. To separate polarization effects from geometrical relaxations, we optimized the WT reaction pathway with the His residue in the MM region, thus eliminating the charge transfer from the H145 to the uracil. We found that the barrier remained about the same, only slightly smaller (17.6 kcal/mol, data not shown). Thus,

geometric differences are likely the main reason for the decreased activity of the H145A mutant.

Intriguingly, we observe further major differences if we consider the geometric relaxation and analyze the changes in the polarization of the key groups involved in the catalytic reaction at the respective TS structures. Surprisingly, the largest change is observed in the polarization of the γ-phosphate, which becomes more negative for the mutants compared to the WT. This additional negative charge is the largest difference in the partial charges amongst all the groups for both the T138Stop and the H145A mutants (Table S3). In addition, for both mutants, the polarization of the uracil group becomes even more prominent once the mutant TS geometries are used to calculate the charges. Consistent with the results, where only the His was removed from the active site (Table S3, column 3), the deoxyribose is also more positive, and the α- and β-phosphates are slightly more positive or their charges do not significantly change (Figure 11, Table S3). Considering the geometric relaxations as well in the reaction pathways of the mutants, we obtained significantly increased barrier height as shown in Table 2 and Figure 6A, consistently with the experimental trend in reactivity.

The Asp83 residue also becomes more negative when the TS geometry of the mutants is considered, and this charge shift is more pronounced for the T138Stop than for the H145A mutant. This negative shift in the charge of the proton-accepting carboxylic group can be explained by the fact that the proton transfer is more decoupled, and has proceeded to a lesser extent at the TS of the mutants compared with the TS of the WT, where the proton from the nucleophilic water has already partly transferred. These changes in the charge distribution are in good agreement with the observed reaction mechanism, where PT is most decoupled for T138Stop and it also happens later along this pathway (Figure 5).

Table S1. High-resolution crystal structures used for QM/MM simulations. Dihedral angles $O_{5'}$–P_α–O_{3A}–P_β (A) P_α–O_{3A}–P_β–O_{3B} (B) and O_{3A}–P_β–O_{3B}–P_γ (C) are also given in deg.

Protein	PDB ID	Resolution	Dihedral A	Dihedral B	Dihedral C
wild type[1]	2PY4	1.49 Å	109.8	-78.0	122.2
H145A[2]	3LOJ	1.80 Å	115.3	-82.0	121.4
T138Stop[3]	3I93	1.25 Å	131.3	-100.6	101.6

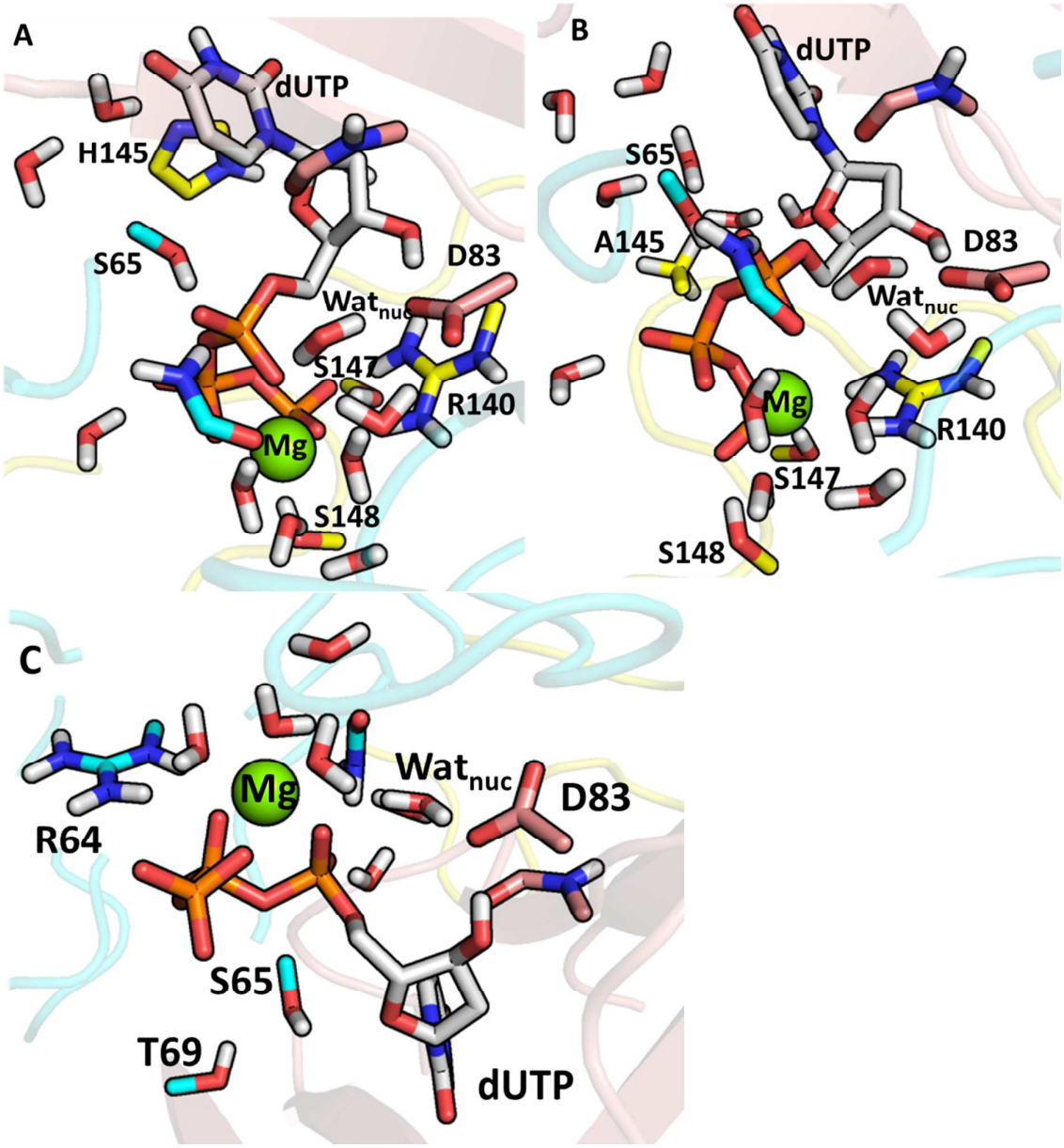

Figure S1. Active site of dUTPase (A) WT, B) H145A, C) T138Stop). Atoms included in the QM region for QM/MM minimizations are shown as sticks. For clarity, nonpolar hydrogens are omitted, except for the Ala145 sidechain in panel B. The three protomers are denoted with yellow, cyan and salmon cartoons with their C-atoms also colored accordingly in the stick representations, dUTP carbons are colored white.

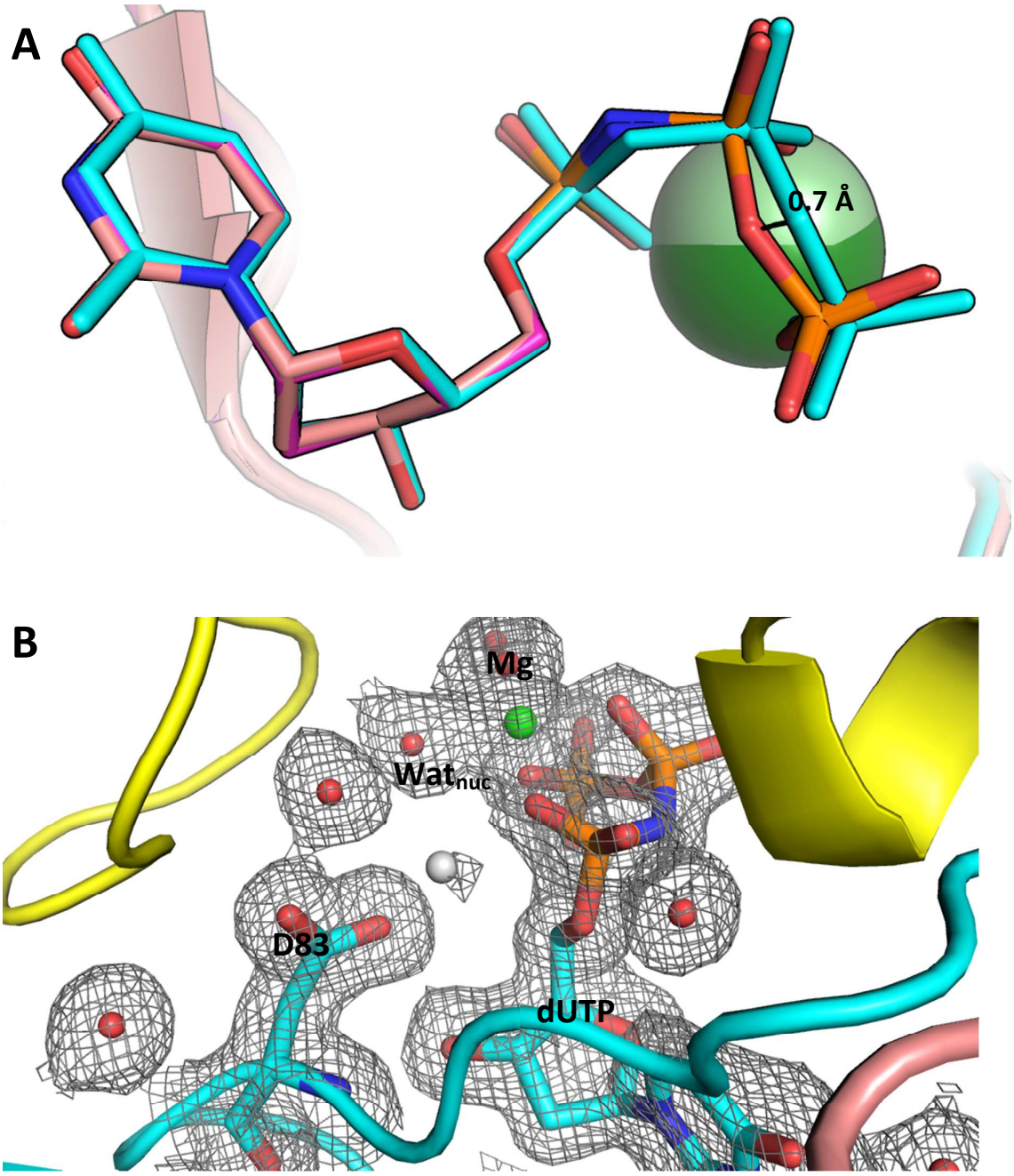

Figure S2. A) Comparison of the substrate orientation in the WT (with the carbon atoms colored salmon, PDB ID: 2PY4), H145A (with the carbon atoms colored pink, PDB ID: 3LOJ), and T138Stop (light blue, PDB ID: 3I93) *M. tuberculosis* dUTPase structures. A 0.7 Å shift is observed for the location of the O3B atom in the T138Stop structure compared with WT and H145A. **B)** Electron-density map of the active site region of T138Stop (PDB ID: 3I93, cartoon representation) shows the unassigned nucleophilic water molecule added in our simulations (grey sphere). Assigned atoms are shown as sticks with atomic coloring, and the 2Fo-Fc electron-density map contoured at 0.5 σ is shown as a gray mesh.

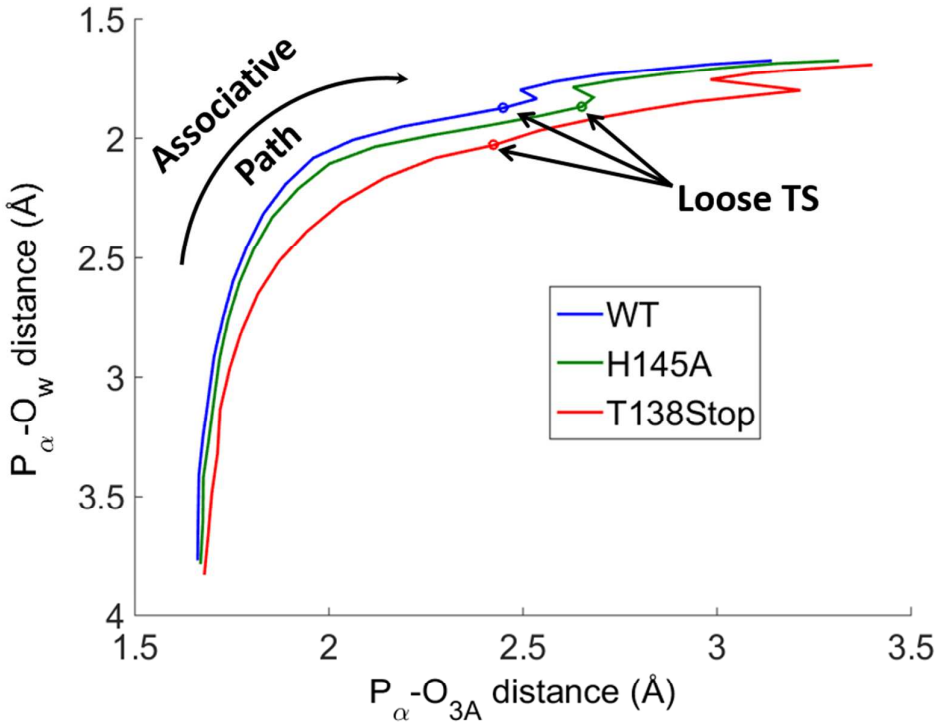

Figure S3: More O'Ferrall Jencks diagram of the dUTPase reaction pathway, using the □-phosphate bond breaking (abscissa) and bond forming (ordinate) coordinates for the WT (blue), H145A (green), and T138Stop (red) systems, which shows an associative mechanism (A_ND_N).

Table S2. Geometric parameters of the transition state species. Distances are given in Å.

Enzyme Structure		*P-O$_{3A}$*	*P-O$_{wat}$*	*O$_{wat}$-H$_{wat}$*	*H$_{wat}$-O$_{Asp83}$*
WT	TSa	2.45	1.87	1.08	1.43
	TSb	2.54	1.84	1.13	1.33
T138Stop	TSa	2.27	2.08	0.99	1.91
	TSb	2.43	2.03	0.99	1.87
H145A	Q=0.2	2.27	1.99	1.03	1.60
	Q=0.8	2.65	1.87	1.08	1.45

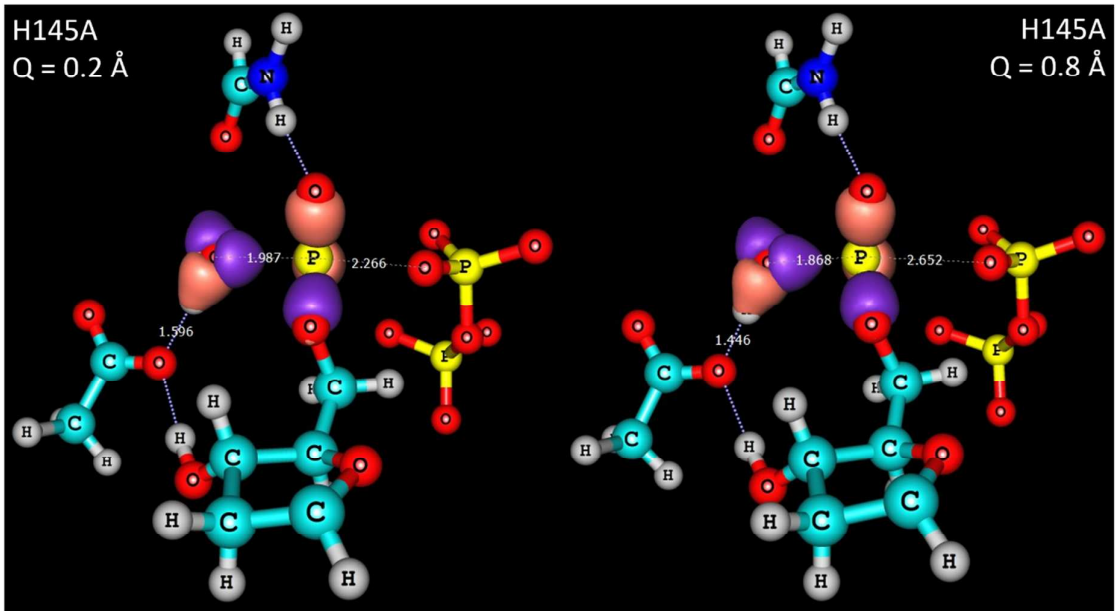

Figure S4. NBO analysis of the structures at the transition state region in the H145A enzyme corresponding to Q = 0.2 Å and Q = 0.8 Å. The molecular orbitals at the 0.2 au electron density level are shown for all natural bonds of the H_{wat}, O_{wat}, and P_{α} atoms only. For clarity, only parts of the QM region corresponding to the deoxyribose triphosphate, the nucleophilic water, the proton accepting Asp83 sidechain, and the Thr81 and Ile82 backbones are shown.

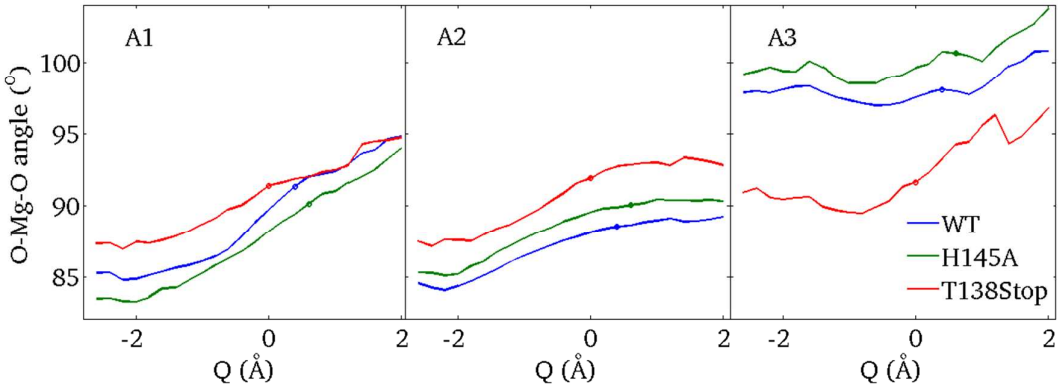

Figure S5. Mg^{2+}-coordination angles (O–Mg–O) between the (i) α- and β-phosphate (A1), (ii) β- and γ-phosphate (A2), and (iii) α- and γ-phosphate (A3) along the reaction coordinate Q for the WT (blue), H145A (green), and T138Stop (red) systems. Dots denote the TS locations.

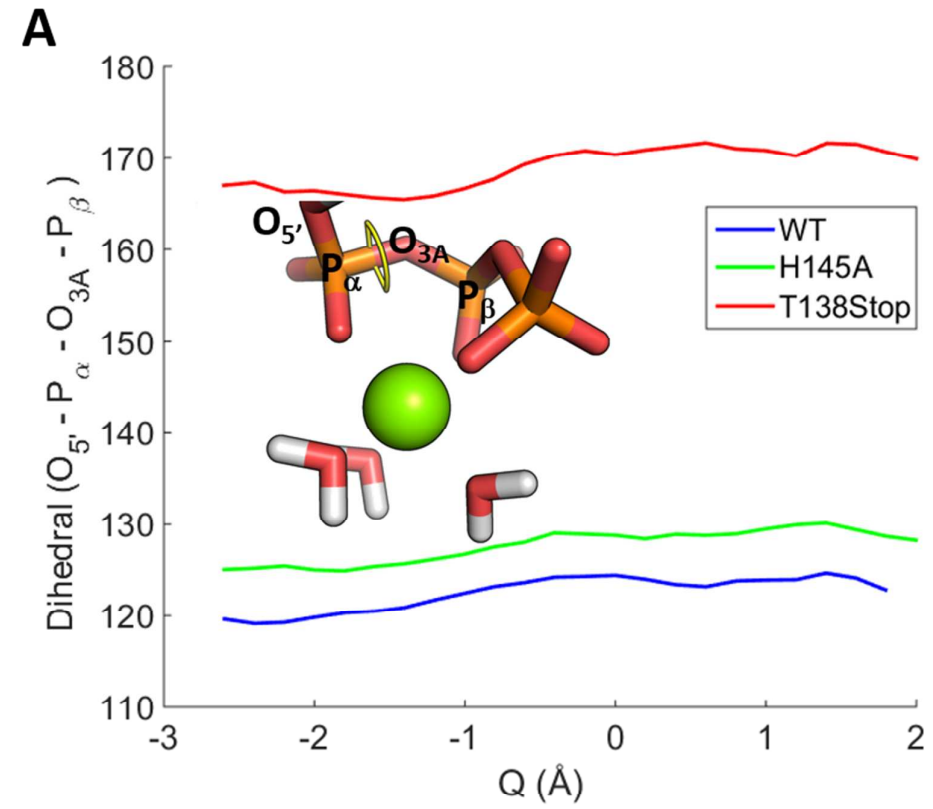
A
180
170
160
150
140
130
120
110
-3
-2
-1
0
1
2
Q (Å)
Dihedral ($O_{5'}$ - P_α - O_{3A} - P_β)
$O_{5'}$
O_{3A}
P_α
P_β
WT
H145A
T138Stop

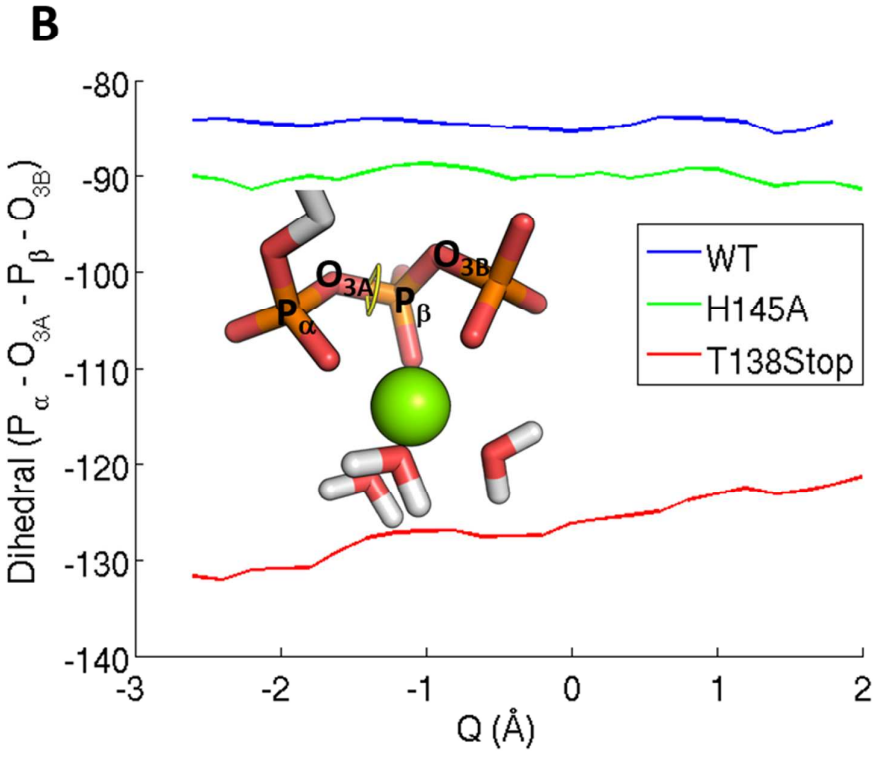
B
-80
-90
-100
-110
-120
-130
-140
-3
-2
-1
0
1
2
Q (Å)
Dihedral (P_α - O_{3A} - P_β - O_{3B})
O_{3A}
O_{3B}
P_α
P_β
WT
H145A
T138Stop

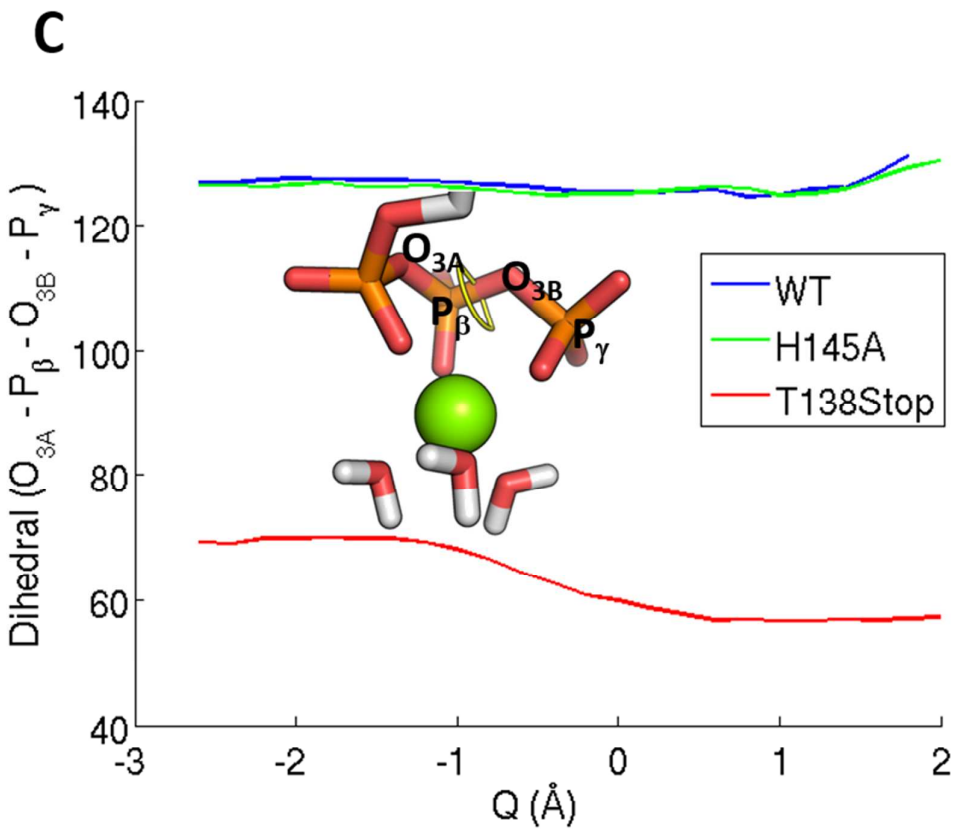

Figure S6. Dihedral angles of the phosphate chain along the reaction coordinate. Dihedral angles $O_{5'}$–P_α–O_{3A}–P_β (A) P_α–O_{3A}–P_β–O_{3B} (B) and O_{3A}–P_β–O_{3B}–P_γ (C) along the reaction coordinate *Q* for the WT (blue), H145A (green), and T138Stop (red) systems.

Table S3. Change in the total charge of selected groups in the QM region (in atomic units). The difference was calculated at the TS of the H145A and the T138Stop mutants compared with the TS of the WT enzyme. The CHELPG charge scheme was used to obtain the atomic charges of each respective system. The third column (WT, no His145) shows charge differences for a complex, where the WT TS structure was used, but the atoms corresponding to the His145 were deleted from the QM region during the QM calculation (with all other MM point charges otherwise included). This calculation evaluates the polarization effects of His145, separating any additional effects due to geometric relaxation in lack of His145. The dUTP was divided into 5 different groups: uracil, deoxyribose, P_α, P_β, and P_γ. The assignment of the oxygen atoms to P_α, P_β, or P_γ was based on their atom names as in the PDB. Additionally, the O5' (the oxygen which is bound to P_α and the deoxyribose ring) was also assigned to the P_α group.

Group	H145A	T138Stop	WT, no His145
Uracil	**-0.17**	**-0.14**	**-0.06**
Deoxyibose	**0.10**	**0.06**	**0.06**
P_α	**0.07**	**0.09**	**0.02**
P_β	**-0.02**	**0.11**	**-0.01**
P_γ	**-0.17**	**-0.37**	**0.01**
Mg^{2+}	**0.13**	**-0.07**	**0.00**
D83	**-0.04**	**-0.14**	**0.00**
W_{cat}	**0.02**	**-0.02**	**-0.01**
R140	**0.07**		**0.00**

References

1. Varga, B., Barabas, O., Takacs, E., Nagy, N., Nagy, P. and Vertessy, B.G. (2008) Active site of mycobacterial dUTPase: structural characteristics and a built-in sensor. *Biochem Biophys Res Commun*, **373**, 8-13.
2. Prasad, G.S., Stura, E.A., Elder, J.H. and Stout, C.D. (2000) Structures of feline immunodeficiency virus dUTP pyrophosphatase and its nucleotide complexes in three crystal forms. *Acta Crystallogr D Biol Crystallogr*, **56**, 1100-1109.
3. Pecsi, I., Leveles, I., Harmat, V., Vertessy, B.G. and Toth, J. (2010) Aromatic stacking between nucleobase and enzyme promotes phosphate ester hydrolysis in dUTPase. *Nucleic acids research*, **38**, 7179-7186.
4. Takacs, E., Nagy, G., Leveles, I., Harmat, V., Lopata, A., Toth, J. and Vertessy, B.G. (2010) Direct contacts between conserved motifs of different subunits provide major contribution to active site organization in human and mycobacterial dUTPases. *FEBS Lett*, **584**, 3047-3054.
5. Anandakrishnan, R., Aguilar, B. and Onufriev, A.V. (2012) H++ 3.0: automating pK prediction and the preparation of biomolecular structures for atomistic molecular modeling and simulations. *Nucleic Acids Res*, **40**, W537-541.

THE JOURNAL OF BIOLOGICAL CHEMISTRY VOL. 291, NO. 51, pp. 26320–26331, December 16, 2016
© 2016 by The American Society for Biochemistry and Molecular Biology, Inc. Published in the U.S.A.

A Hidden Active Site in the Potential Drug Target *Mycobacterium tuberculosis* dUTPase Is Accessible through Small Amplitude Protein Conformational Changes*[S]

Received for publication, May 5, 2016, and in revised form, November 4, 2016 Published, JBC Papers in Press, November 4, 2016, DOI 10.1074/jbc.M116.734012

Anna Lopata[‡1], Ibolya Leveles[‡], Ábris Ádám Bendes[‡2], Béla Viskolcz[§], Beáta G. Vértessy[‡¶], Balázs Jójárt[‖], and Judit Tóth[‡3]

From the [‡]Institute of Enzymology, Research Centre for Natural Sciences, Hungarian Academy of Sciences, Budapest, Hungary H1117, the [§]Institute of Chemistry, University of Miskolc, Miskolc, Hungary H3529, the [¶]Department of Applied Biotechnology, Budapest University of Technology and Economics, Budapest, Hungary H1111, and [‖]Department of Chemical Informatics, University of Szeged, Szeged, Hungary H6725

Edited by Norma Allewell

dUTPases catalyze the hydrolysis of dUTP into dUMP and pyrophosphate to maintain the proper nucleotide pool for DNA metabolism. Recent evidence suggests that dUTPases may also represent a selective drug target in mycobacteria because of the crucial role of these enzymes in maintaining DNA integrity. Nucleotide-hydrolyzing enzymes typically harbor a buried ligand-binding pocket at interdomain or intersubunit clefts, facilitating proper solvent shielding for the catalyzed reaction. The mechanism by which substrate binds this hidden pocket and product is released in dUTPases is unresolved because of conflicting crystallographic and spectroscopic data. We sought to resolve this conflict by using a combination of random acceleration molecular dynamics (RAMD) methodology and structural and biochemical methods to study the dUTPase from *Mycobacterium tuberculosis*. In particular, the RAMD approach used in this study provided invaluable insights into the nucleotide dissociation process that reconciles all previous experimental observations. Specifically, our data suggest that nucleotide binding takes place as a small stretch of amino acids transiently slides away and partially uncovers the active site. The *in silico* data further revealed a new dUTPase conformation on the pathway to a relatively open active site. To probe this model, we developed the Trp^{21} reporter and collected crystallographic, spectroscopic, and kinetic data that confirmed the interaction of Trp^{21} with the active site shielding C-terminal arm, suggesting that the RAMD method is effective. In summary, our computational simulations and spectroscopic results support the idea that small loop movements in dUTPase allow the shuttling of the nucleotides between the binding pocket and the solvent.

Commonly, nucleotide-hydrolyzing enzymes harbor a binding pocket for their cognate ligand at interdomain or intersubunit clefts. This arrangement facilitates proper solvent shielding for the catalyzed reaction. Many well described enzymes bind nucleotides in a relatively open (*e.g.* DNA and RNA helicases, molecular motors, and small G-proteins) or completely open (ATP-dependent DNA ligases) binding pocket. Conformational changes associated with nucleotide binding result in the closure of the active site, enabling the subsequent reaction steps (1–5). The conformational change of the enzyme upon nucleotide binding can be understood by comparing the available apo and ligand-containing crystal structures. However, using single molecule optical spectroscopy in addition to the static structural data, the nucleotide binding pocket of DNA polymerase I was shown to exhibit dynamic open-closed equilibrium in the binary complex with DNA that is shifted toward the closed conformation upon dNTP binding (6). In such a case, the ligand may bind to a pocket that appears relatively closed on a millisecond-second time scale.

Homotrimeric dUTPases have three equivalent active sites in the clefts constituted by two neighboring subunits (Fig. 1) (7, 8). The C-terminal arm of the third subunit folds over the active site and shields the substrate from the solvent (Fig. 1*A*). This segment of the polypeptide is only visible in protein crystals that contain substrate analogues. In the apo state, the C-terminal arm is undefined in the crystal structures of dUTPases from widely different species (9–11). This observation has been interpreted as an open-closed transition of the C-terminal arm and the active site. The steady-state conformational states of the C-terminal arm were probed by a fluorescent sensor (Trp^{158} in human dUTPase). The measured solvent accessibility of this sensor in various nucleotide-bound states suggested that the

* This work was supported by National Institutes of Health Grant 1R01TW008130; National Research, Development and Innovation Office Hungarian Scientific Research Fund Grants OTKA K109486, K115993, and K119493; the Hungarian Academy of Sciences MedInProt Program; International Centre for Genetic Engineering and Biotechnology (ICGEB) Research Grant CRP/HUN14-01; and Hungarian Scientific Research Funds. The authors declare that they have no conflicts of interest with the contents of this article. The content is solely the responsibility of the authors and does not necessarily represent the official views of the National Institutes of Health.

[S] This article contains supplemental Movies S1–S5.

[1] Present address: Laboratory of Molecular Physiology, NHLBI, National Institutes of Health, Bethesda, MD 20892; and School of Molecular and Cellular Biology, Faculty of Biological Sciences, University of Leeds, Leeds, UK, LS2 9JT.

[2] Present address: Faculty of Biochemistry and Molecular Medicine, University of Oulu, Oulu, Finland, 90014; and Biocenter Oulu, University of Oulu, Oulu, Finland, 90014.

[3] Recipient of the János Bolyai Research Scholarship of the Hungarian Academy of Sciences. To whom correspondence should be addressed: Institute of Enzymology, Research Centre for Natural Sciences, Hungarian Academy of Sciences, Magyar tudósok körútja 2, Budapest, Hungary, H1117. Tel.: 36-1-3826707; Fax: 36-1-4631401; E-mail: toth.judit@ttk.mta.hu.

This is an Open Access article under the CC BY license.

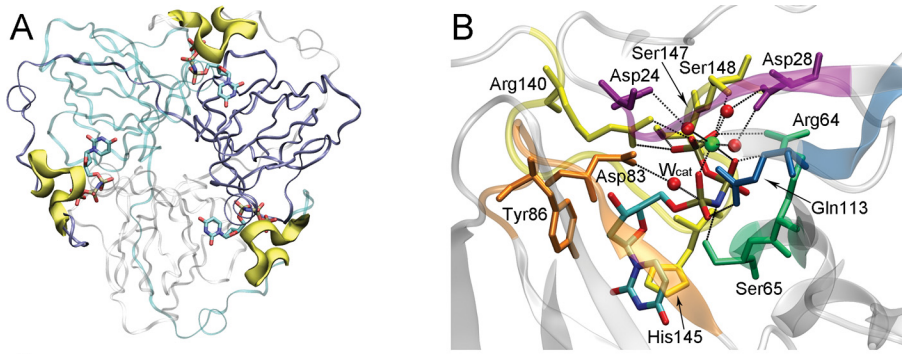

C

MSTTLAIVRL DPGLPLPSRA HDGDAGVDLY SAEDVELAPG RRALVRTGVA
VAVPFGMVGL VHPRSGLATR VGLSIVNSPG TIDAGYRGEI KVALINLDPA
APIVVHRGDR IAQLLVQRVE LVELVEVSSF DEAGLASTSR GDGGHGSSGG
HASL

FIGURE 1. **Three-dimensional structure and conserved motifs of the *M. tuberculosis* dUTPase.** *A*, three-dimensional structure of the *M. tuberculosis* dUTPase enzyme complexed with dUPNPP (PDB code 2PY4 (33)). The subunits are shown as *white*, *cyan*, and *blue ribbons*, whereas the fifth conserved motif located on the C-terminal arm is highlighted as *thick yellow ribbon* in all subunits. *B*, three-dimensional structure of the active site of *M. tuberculosis* dUTPase enzyme complexed with dUPNPP (PDB code 2PY4 (33)). The protein backbone is shown as *white ribbon*, and the conserved motifs are highlighted with stick representation of different colors (*violet*, *green*, *orange*, *blue*, and *yellow* for first, second, third, fourth, and fifth conserved motif, respectively). dUTP is visualized by atomic colored stick representation. Mg^{2+} ion, the water molecules of the Mg^{2+} ion coordination sphere, and the catalytic water molecule are shown as *green* and *red spheres*, respectively. *C*, amino acid sequence of the *M. tuberculosis* dUTPase. The conserved motifs are color-coded according to *B*.

arm resides in a relatively closed conformation during the largest fraction of the reaction cycle time (12). A presumed open-closed conformational transition upon ligand binding could not be observed. Because of the seeming contradictory evidence between the crystallographic and fluorescence spectroscopy data, we could not establish a comprehensive model of substrate binding or product release. To fill this gap, we implemented the random acceleration molecular dynamics (RAMD)[4] method for its ability to gain high resolution information on the enzyme-nucleotide interaction. Under physiological conditions, ligand binding and dissociation usually takes place on a microsecond-millisecond time scale and requires several microsecond long molecular dynamics simulation for accurate modeling (13–16). Therefore, in case of buried active sites, guided or biased molecular dynamics simulations such as steered molecular dynamics (17, 18), RAMD (19), and metadynamics (20, 21) are preferably used to accelerate the process of ligand binding or dissociation. The RAMD method (19) applies an artificial random oriented force that acts on the ligand and accelerates the dissociation process, offering a reasonable time scale for computational simulations. Because of the reduced simulation time scale and the randomly oriented force, a larger sample size of ligand dissociation pathways are explored at atomic resolution. Considering that ligand binding is a reversible process, this method can be used to explore substrate dissociation and binding pathways as well (19). The RAMD method has been successfully employed to study ligand dissociation paths in cytochrome P450 (19), rhodopsin (22), haloalkane dehalogenase (23), histone deacetylase (24), heme oxygenase (25), thyroid hormone receptor (26), P-glycoprotein (27), and B-RAF kinase (28), among many others.

High resolution crystal structures (10, 29–35), a detailed kinetic mechanism (12, 36, 37) and additional regulatory functions (38–40) have already been revealed for dUTPases in a wide variety of species. Previously, we have investigated the detailed mechanism of substrate binding, hydrolysis, and product release in dUTPase using a combination of structural and transient kinetics methods (12, 41). These results obtained from crystal structures and from spectroscopic measurements on the millisecond time scale movements did not allow insights into the possible substrate binding pathways to the hidden active site of dUTPase. This process may have pharmacological significance because we have recently shown that the dUTPase enzyme may be a selective drug target in mycobacteria (42). This enzyme plays a crucial role in DNA integrity by catalyzing the hydrolysis of dUTP into dUMP and pyrophosphate, producing the precursor for dTTP biosynthesis. At the same time, the dUTPase reaction is also responsible for balancing a low intracellular dUTP:dTTP ratio required in most organisms to avoid DNA uracilation that may have serious consequences (8, 43).

In this study, we determine the putative ligand shuttling pathway of dUTP between the solvent and the active site of the *Mycobacterium tuberculosis* dUTPase using RAMD simulations in combination with experimental methods including X-ray crystallography, fast kinetics, ligand binding, and solvent accessibility experiments. The results suggested that active site residues are predominately in the closed conformation over the entire reaction cycle and during the nucleotide binding process. We observe a small stretch of amino acids that slides transiently away with small amplitude movements to partially uncover the active site. In addition,

[4] The abbreviations used are: RAMD, random acceleration molecular dynamics; PDB, Protein Data Bank; RMSD, root mean square deviation; dUPNPP, 2′-deoxyuridine 5′-α,β-imido-triphosphate; NATA, *N*-acetyl-L-tryptophanamide.

this is the first study that demonstrates direct experimental validation of the powerful RAMD method.

Results

RAMD Simulations Reveal the High Spatiotemporal Resolution Movements of the Active Site upon Substrate Unbinding—Of 72 individual RAMD simulations performed, 55 led to productive dissociation of the ligand from the active site. In the remaining 17 runs, the ligand did not exit the active site during the entire 300-ps length of the simulations. A representative of unproductive simulations can be seen in Fig. 2.

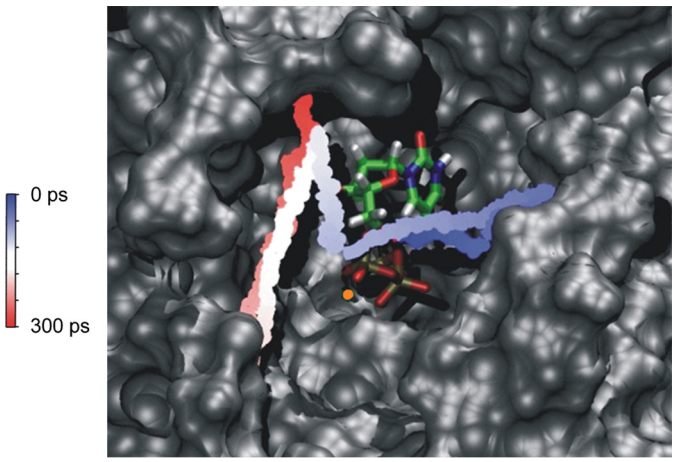

FIGURE 2. **A representative of the 17 unproductive RAMD runs.** The enzyme can be seen with *gray surface* representation. For clarity, the C-terminal arm is omitted from this picture. dUTP is visualized as atomic coloring stick model, and Mg^{2+} is an *orange sphere*. The path of the center of mass of the dUTP-Mg^{2+} complex is visualized as a *blue*, *white*, and *red line*.

Based on the order of dissociation of the substrate from the various interaction points within the protein listed below, the 55 productive RAMD runs could be classified into five major unbinding pathways A–E (Fig. 3). The difference between these paths can be best appreciated visually by watching supplemental Movies S1–S5. To understand the classification criteria in the text format analysis in Table 1, it is crucial to describe the interactions of the substrate within the active site. The first conserved motif (*violet* in Fig. 1, *B* and *C*) coordinates the Mg^{2+} of the physiological substrate-Mg^{2+} complex through water molecules. The second and fourth motifs (*green* and *blue*, respectively in Fig. 1, *B* and *C*) coordinate the phosphate chain of the substrate, whereas the third motif (*orange* in Fig. 1, *B* and *C*) maintains interactions with the uracil and deoxyribose moieties of the nucleotide (35). The fifth motif (*yellow* in Fig. 1, *B* and *C*) located on the C terminus coordinates the γ-phosphate and the uracil ring of the substrate and is responsible for diphosphate/triphosphate ligand discrimination mainly by promoting hydrolysis of the triphosphate nucleotide (41). In agreement with this, it has been shown in a wide variety of dUTPases that the enzymatic activity of C-terminally truncated mutants is drastically lower (practically 0) than that of the WT (11, 34, 37, 41, 44, 45).

The structural element in the focus of the present study is the fifth motif as it shields the nucleotide binding cavity and restricts nucleotide shuttling. Fig. 4 highlights the position of this motif relative to the observed exit routes and also shows its overall conformational change between the initial and final time points of the RAMD runs. In pathway A, the N-terminal part of the C-terminal arm transiently moves away from the enzyme core as the substrate leaves the active site, whereas the

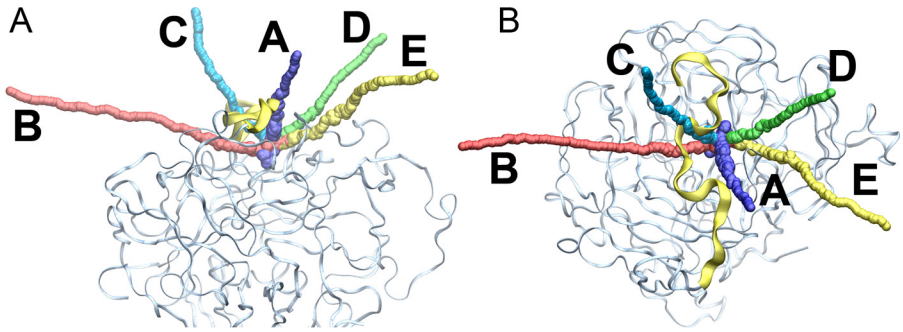

FIGURE 3. **Exit routes of five representative simulations from the five major ligand unbinding pathways.** *A*, the enzyme is shown with *light blue ribbon model*, and the C-terminal arm is highlighted as *flat yellow ribbon*. The *curves*, representing the five major pathways, are the sphere models of the center of mass of the dUTP-Mg^{2+} complex during the course of simulations. *B*, the same structures upon rotating the protein by 90°.

TABLE 1

Analysis of the five ligand binding pathways

In the RMSD calculation, 305 atoms (residues 130–154) were superposed.

Pathway name	A	B	C	D	E
Number of runs	6	6	18	19	6
Substrate dissociation from indicated protein segments in the order of interaction break-up (M stands for conserved motif)	M4 M2 M1 M3 M5	M1 M4 M3 M2 Leu^{44} Lys^{91} M5	M3 M1 M2 M4 M5	M3 M2 M1 M4 M5	M3 M2 M4 Phe^{55} Val^{119}–Glu^{123} M1 M5
Maintenance of octahedral coordination between Mg^{2+} and the phosphate oxygens of dUTP	No	Yes	No	Yes	Yes
RMSD of the C-terminal arm (Å)	5.6 ± 1.4	3.4 ± 0.5	6.7 ± 2.2	4.6 ± 0.8	6.3 ± 1.3

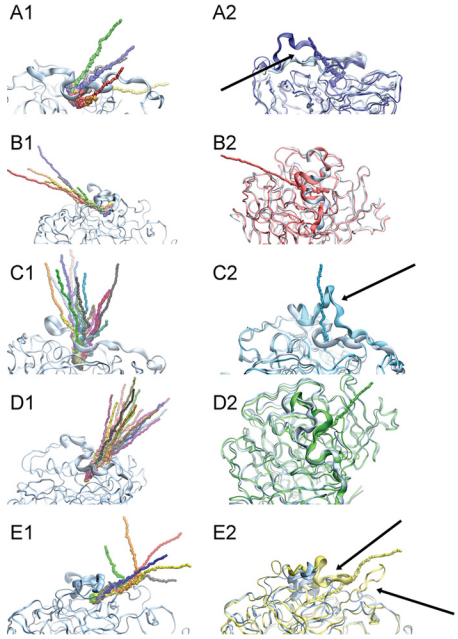

FIGURE 4. **Initial structures and exit routes of the dUTP-Mg^{2+} complex of all simulations (*panels A1–E1*) and end point protein structures of representative runs (*panels A2–E2*) from the five major pathways (*A–E*).** The enzyme is shown as *light blue ribbon model*, and the C-terminal arm is highlighted as *flat ribbon*. The *curves* representing the runs are the *sphere models* of the center of the dUTP-Mg^{2+} complex during the course of simulations. *Arrows* indicate the notable conformational changes between the start and end point structures.

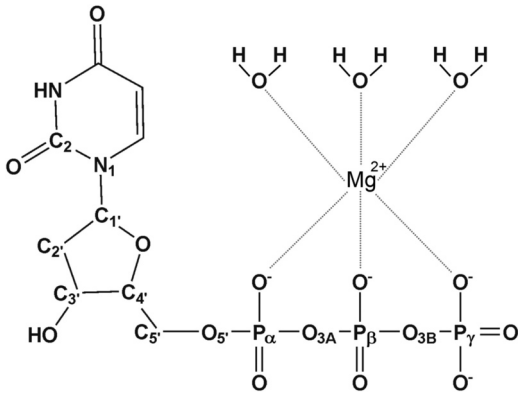

FIGURE 5. **Schematic representation of the dUTP-Mg^{2+} complex.** The coordination sphere of the Mg^{2+} ion is constituted from the phosphate chain of dUTP and three water molecules.

rest of the C-terminal arm keeps its position (Fig. 4*A* and supplemental Movie S1). In pathway C, partial unfolding of the C-terminal arm can be observed, whereas all intermolecular contacts are broken between the C-terminal arm and the protein core (Fig. 4*C* and supplemental Movie S3). In contrast, the C-terminal arm moves on the surface of the protein without losing its interactions with the rest of the protein in pathways B, D, and E (Fig. 4, *B*, *D*, and *E*, and supplemental Movies S2, S4, and S5). In three of the runs (shown in *green*, *orange*, and *gray* in Fig. 4*E*), the route of ligand exit changes its direction after its initial progress, which is due to a steric clash with the first conserved motif forcing the ligand to exit at different directions.

Another subtle difference that was observed during the analysis of the RAMD runs was that in pathways A and C, but not in pathways B, D, or E, the coordination geometry between Mg^{2+}

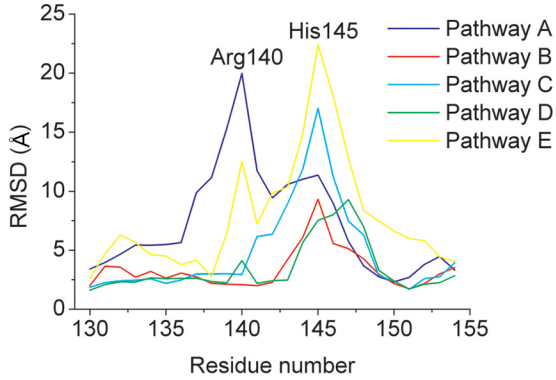

FIGURE 6. **Maximal RMSD values of single amino acids in the C-terminal arm during the five representative RAMD runs.**

and the phosphate chain of dUTP (Fig. 5) becomes distorted as the ligand exits the active site (Table 1). This distortion coincides with a larger conformational change of the C-terminal arm as also reflected by the root mean square deviation (RMSD) for the C-terminal arm between the initial and final conformations (Table 1).

Importantly, the C-terminal arm remains close to the enzyme core in each RAMD simulation as opposed to opening up completely and exposing the active site to the solvent (supplemental Movies S1–S5). A quantitative analysis of the displacement of amino acids within the C-terminal arm can be viewed in Fig. 6. The small RMSD values characteristic to amino acids 130–135 and 150–155 indicate that the proximal and distal regions of the arm stay in contact with the enzyme core. The fifth conserved motif is situated in between these sequences and takes active part in the ligand exit process as reported by the elevated RMSD values. His^{145} acts as the aromatic lid over the active site present in all dUTPases by engaging in a π-π stacking interaction with uracil (Fig. 1*B*) (35, 46). This interaction was earlier exploited to study the enzymatic cycle as it reports on ligand binding and product unbinding using various spectroscopic methods (12). The high RMSD values of His^{145} explain the observed spectroscopic changes and reinforce the importance of π-π stacking interactions in directing ligand exit (47). Arg^{140}, responsible for γ-phosphate coordination, also displays relatively high RMSD values in pathways A and E. This phenomenon will be discussed in the subsequent sections.

These RAMD results provide the first body of evidence that reconciles all the previous ensemble spectroscopic measurements and crystallographic data concerning the movements and role of the C-terminal arm during substrate binding. Upon substrate binding or product release, the nucleotide moves through small and transient spaces available as a stretch of the C-terminal polypeptide chain moves away from the shielding position. Such a mechanism involves relatively small conformational changes (12) of a yet dynamic C-terminal arm (37, 48) and a relatively closed active site even without bound substrate (12).

New Substrate-dependent Interaction Point Detected in the RAMD Runs—During detailed analysis of the pathways, some less conserved residues in the neighborhood of the conserved motifs appeared to take active part in the substrate unbinding

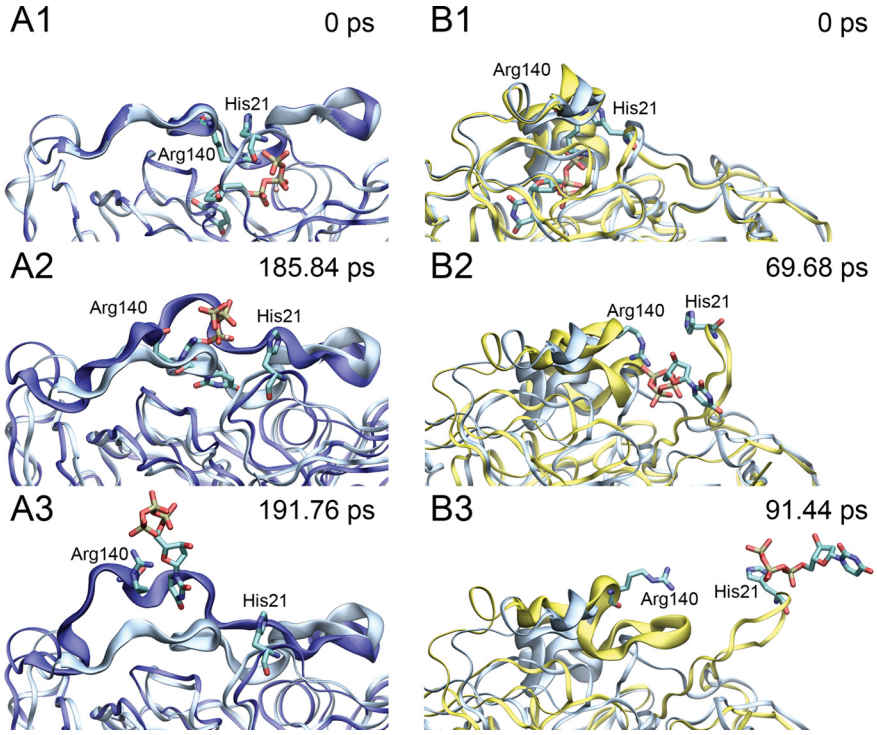

FIGURE 7. **Snapshots from pathways A and E showing the His^{21}–Arg^{140} interaction.** The initial enzyme structure is shown as *light blue ribbon* model, whereas the actual structure during the course of the simulation is shown as a *blue* and *yellow ribbon* model for pathways A (*panels A1–A3*) and E (*panels B1–B3*), respectively. The C-terminal arm is highlighted as *thick ribbon* in all cases. The dUTP-Mg^{2+} complex and the His^{21} and Arg^{140} residues are visualized as *stick models* with atomic coloring, and the hydrogen atoms are omitted for clarity.

TABLE 2
Data collection and refinement statistics of PDB code 4GCY

Space group	P 6_3
Unit cell	
a, *b*, *c* (Å)	54.94, 54.94, 83.86
α, β, γ (°)	90, 90, 120
Resolution (Å)	27.95–1.50 (1.58–1.50)[a]
Total no. of reflections	173,193
No. of unique reflections	23,022
Redundancy	7.5 (4.8)
Completeness (%)	100 (100)
$<I>/<\sigma(I)>$	11.8 (2.1)
R_{meas} (%)[b]	0.085 (0.578)
Refinement	
No. of protein atoms	1216
Ligand atoms/water/Mg^{2+} ions	28/156/1
R_{cryst}/R_{free} (%)[c,d]	12.35/15.62
Overall B-factors (Å^2)[e]	25.862/21.482/27.401/22.047
Deviations from ideal stereochemistry	
RMSD bonds (Å)	0.015
RMSD angles (°)	1.555
Ramachandran plot analysis[f]	
Most favored (%)	99.30
Additionally allowed (%)	0.70
Disallowed (%)	0.00

[a] The values in parentheses are for the highest resolution shell.
[b] $R_{meas} = \Sigma[n/(n-1)]^{1/2}(|I_i - <I>|)/\Sigma(<I>)$, where the sum is calculated over all observations of a measured reflection (I_i), and $<I>$ is the mean intensity of all the measured observations (I_i).
[c] $R_{cryst} = \Sigma(|F_{obs} - F_{calc}|)/\Sigma(F_{obs})$, where F_{obs} is the observed structure factor amplitude, and F_{calc} is that calculated from the model.
[d] R_{free} is equivalent to R_{cryst} but where 5% of the measured reflections have been excluded from refinement in thin shells and set aside for cross-validation purposes.
[e] Average *B* values for all atoms/ ligand atoms/water/Mg^{2+} ions.
[f] Ramachandran plot analysis was from MolProbity.

process. Particularly, a yet undescribed stacking interaction between the imidazole ring of His^{21} (N-terminal of the first conserved motif) and the guanidino group of Arg^{140} (fifth conserved motif) residues displayed characteristic changes. This interaction in pathways A and E seems to break up as the ligand exits the active site (Fig. 7 and supplemental Movies S1 and S5), also explaining the large displacement of Arg^{140} indicated in Fig. 6. In the other three pathways, this interaction persists during the entire simulation. We found this phenomenon interesting because it directly involves the opening of the active site and the anchoring of the C-terminal arm (Arg^{140}) to the enzyme core (His^{21}). We carried out the further detailed biochemical and structural biology experiments to validate this *in silico* observation and to learn more about the substrate binding process.

Implementation of a Reporter to Study the His^{21}-Arg^{140} Interaction—To continuously monitor the interaction between His^{21} and Arg^{140} during the reaction cycle, we introduced a single Trp fluorescent sensor into position 21. We already had experience with His to Trp changes in this protein that left the protein fold and activity unaffected and provided useful signals (33, 42, 49). Position 21 is conserved in the bacterial phylum Actinobacteria. Tyr may replace His in some sequences (Atopobium, Olsonella, and Actinoplanes), which also suggests that the aromatic nature of the amino acid in this position is important. The H21W point mutant *M. tuberculosis* dUTPase was thus generated to study the dynamic behavior of the interaction between the protein core and the C-terminal arm of the protein.

Crystal Structure of the H21W Mutant—The crystal structure of the H21W mutant has been solved to 1.5 Å resolution and deposited to the PDB database under code 4GCY (for crystallographic data see Table 2). The global structure of the mutant enzyme is highly similar to the WT (PDB code 2PY4

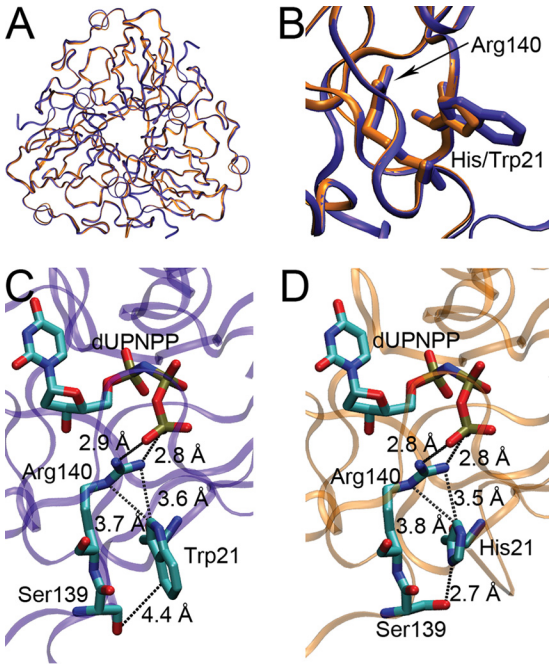

FIGURE 8. **Crystal structure of the H21W mutant.** *A*, superimposition of the WT *M. tuberculosis* dUTPase (PDB code 2PY4 (33), *orange*) and the H21W mutant (PDB code 4GCY, *violet*). The proteins are visualized as colored ribbon model, and dUPNPP can be seen as atomic colored sticks. The global structures of the two proteins are highly similar, which is supported by the 0.2 Å RMSD of the protein backbone atoms. *B*, enlarged view of *A*, where the side chains of the mutated residues are shown as stick models. The indole ring of the Trp residue and the imidazole ring of the His residue are in the same position. *C* and *D*, possible interacting points of the Trp^{21} residue (*C*) or the His^{21} residue (*D*) are Ser^{139} and Arg^{140} from the crystal structure of the H21W mutant (*C*) or the WT *M. tuberculosis* dUTPase (*D*). Arg^{140} is coordinating the γ-phosphate oxygen of the substrate. The protein backbone is shown as *violet* (*C*) or *orange* (*D*) ribbon model, and the residues and the non-hydrolyzable substrate analogue dUPNPP can be seen as atomic colored sticks.

(33)), which is clearly demonstrated by the 0.2 Å RMSD of the protein backbone atoms (Fig. 8*A*). It should be mentioned that parts of the flexible termini of the structure are affected by slight model bias and are flagged as real space *R* value *Z* score outliers. This, however, does not affect the accurate interpretation of the protein core and the discussed residues of interest. Thus, the active site can be considered as equivalent to that of the WT. The RMSD of the non-hydrolyzable substrate analogue dUPNPP-Mg^{2+} complexes in the reference and new structure is 0.1 Å. The mutant Trp side chain is in the same position as the His side chain in the WT (Fig. 8*B*), despite the fact that the indole ring of the Trp residue is larger and more hydrophobic than the imidazole ring of the His. The indole ring establishes similar interactions with the backbone atoms of Ser^{139} and Arg^{140} and with the side chain of Arg^{140} (Fig. 8*C*) to those of the imidazole ring (Fig. 8*D*). The hydrogen bond with the side chain of Ser^{139} vanished upon the substitution. Arg^{140} is the first residue of the fifth conserved motif. It has a crucial role in the coordination of the γ-phosphate of the substrate by a bifurcated hydrogen bond (10) and hence in the enzymatic catalysis (41, 50). These structural similarities suggest a WT behavior for the H21W mutant similar to a previously described H145W mutant, where the mutated aromatic residue stacks against the uracil ring of the substrate establishing a π-π stacking interaction (35).

TABLE 3

Kinetic and thermodynamic parameters measured for the H145W and H12W *M. tuberculosis* dUTPase mutants

k_{cat}, catalytic rate constant obtained from steady-state measurements; $k_{1\ on}$, second order dUTP binding rate constant obtained from stopped flow measurements; $k_{1\ off}$, dUTP dissociation rate constant obtained from stopped flow measurements; $k_{2\ obs}$, observed isomerization rate constant for dUTP binding; $K_{d,dUPNPP}$, dissociation constant for the enzyme-dUPNPP complex obtained from equilibrium fluorescence titration; $K_{d,dUDP}$, dissociation constant for the enzyme-dUDP complex obtained from equilibrium circular dichroism titration.

	H145W	H21W
k_{cat} (s^{-1})	3.1 ± 0.06 (35)	2.9 ± 0.3
$k_{1\ on}$ ($s^{-1}\ \mu M^{-1}$)	29.2 ± 1.7	8.0 ± 0.7
$k_{1\ off}$ (s^{-1})	104 ± 20	165 ± 13
$k_{2\ obs}$ (s^{-1})	13.2 ± 2.4	36.2 ± 12.4
$K_{d,dUPNPP}$ (μM)	0.32 ± 0.1	2.9 ± 0.6
$K_{d,dUDP}$ (μM)	22.5 ± 9.4	1.9 ± 1.0

Enzymatic Mechanism Probed by Transient Kinetics—The k_{cat} of the H21W mutant was measured to be 2.9 s^{-1} (Table 3) which is comparable with that of the WT (3.1 s^{-1} according to Pecsi *et al.* (35)). Next, we assayed whether the fluorescence of the Trp^{21} residue reports any events of the reaction cycle. Surprisingly, the H21W mutant displays similar fluorescent signal change during the enzymatic cycle as previously reported for the H145W active site Trp mutant (Fig. 9*A*) (35, 49). In the H21W mutant, however, the Trp residue is outside of the active site, presumably far from the substrate during the chemical reaction. It is only connected to the active site through the interaction with Arg^{140} pointed out in our RAMD runs. This suggests that the movements of the C-terminal arm during the reaction are efficiently transmitted to the Trp^{21} residue. As a result, the fluorescence intensity of the Trp^{21} residue decreases upon substrate binding and remains quenched in the steady-state hydrolysis phase to recover upon products dissociation (Fig. 9*A*).

Using the large fluorescent signal, we recorded time courses in substoichiometric dUTP concentrations in the stopped flow apparatus to obtain the true single turnover rate constant (k_{sto}) of the dUTPase reaction (Fig. 9*A*). The exponential fit to the fluorescence recovery phase yielded k_{sto} = 3.1 s^{-1}. The observation that k_{cat} equals k_{sto} with a fluorescent reaction profile similar to that of the H145W dUTPase implies the same enzymatic mechanism in which dUTP hydrolysis is rate-limiting (12).

The kinetics of dUTP binding was also measured using stopped flow (Fig. 9*B*). For comparison, the yet undescribed substrate binding kinetics of H145W was measured as well (Fig. 9*C*) (our previous kinetic investigation (12) was carried out using the human enzyme). The observed ligand binding rate constants are plotted against the ligand concentration and fitted with linear functions to obtain the microscopic association and dissociation rate constants (k_{on} and k_{off}, respectively; Fig. 9, *D* and *E*, and Table 3). Compared with the human enzyme, the *M. tuberculosis* H145W enzyme displays similarly high k_{off} value and somewhat lower k_{on} value. Rate constants of the H21W mutant are in the same range as those for the H145W; however, there is a 3.5-fold decrease in the k_{on} value and a 50% increase in the k_{off} value. The apparent dissociation constants of the enzyme-dUTP complexes could not be determined from the amplitudes of the fluorescence change caused by saturating conditions. In view of the structural similarity between the two

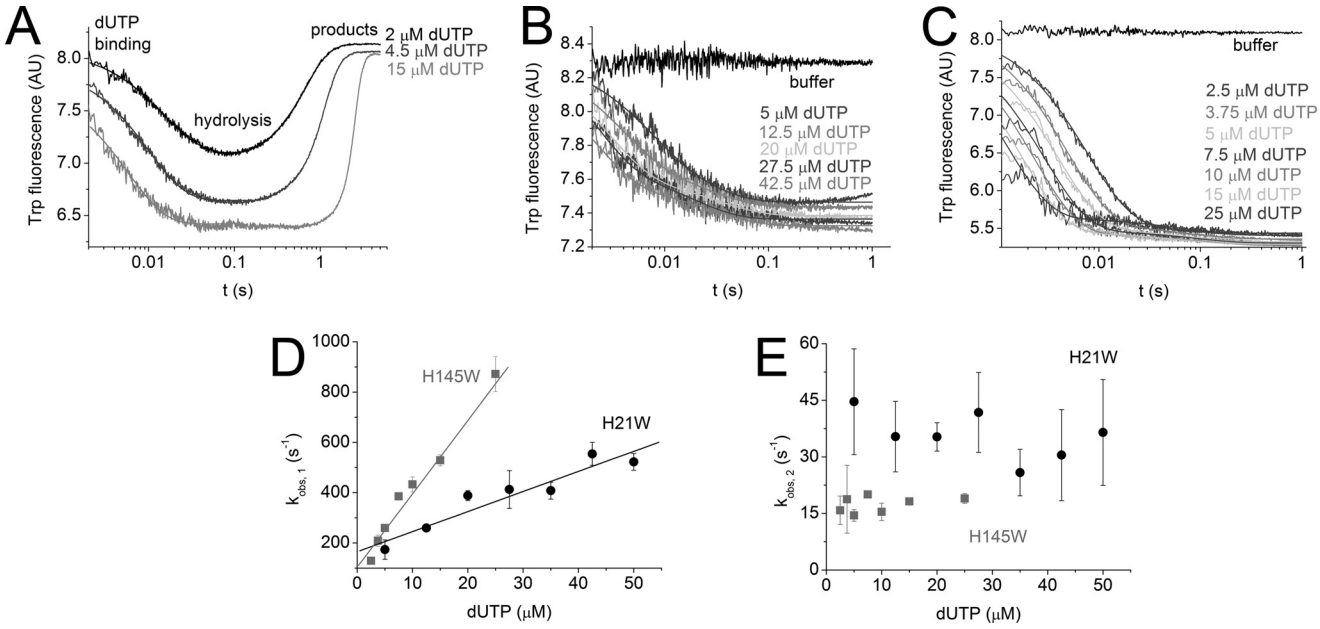

FIGURE 9. **Fast kinetics of the H21W and H145W mutants.** The latter was described earlier to display WT behavior (35). *A*, the fluorescence time courses of the H21W mutant hydrolyzing sub- and superstoichiometric amounts of substrate show similar progression to those reported for the H145W mutant. 3 μM enzyme was mixed with various concentrations of dUTP (post-mix concentrations). Triple exponential function was fitted to the single turnover curve obtained for the lowest, substoichiometric dUTP concentration which yielded 3.1 s^{-1} for the third phase ($k_{1,obs} = 69\ s^{-1}$, $k_{2,obs} = 3.6\ s^{-1}$). In earlier works, this rate constant was identified as the single turnover rate constant (k_{STO}) (12). *B* and *C*, dUTP binding to the H21W (*B*) or to the H145W (*C*) mutant. 1 μM enzyme was mixed with buffer or with various concentrations of dUTP in pseudo first order conditions. Double exponential function was fitted to the data. *D*, concentration dependence of the observed catalytic rate constants of the fast phase of dUTP binding ($k_{obs,1}$). *E*, concentration dependence of the observed catalytic rate constants of the slow phase of dUTP binding ($k_{obs,2}$). This phase seems to be independent of the substrate concentration in agreement with previous data.

enzymes (Fig. 8), it was not expected that the ligand binding process would be much slower when a Trp residue is present instead of a His in position 21. This change, however, further proves that this residue is involved in the ligand binding pathway.

Ligand Binding—To reveal more mechanistic details of the involvement of residue 21 in the ligand binding/dissociation pathways, we carried out comparative fluorescence and circular dichroism studies. The fluorescent spectra of the apo H21W mutant enzyme and its complexes with dUMP, dUDP, and the dUTP-mimicking, practically non-hydrolyzable dUPNPP were recorded (Fig. 10*A*). The relative fluorescence quench induced by these ligands differs considerably from that observed previously in the H145W mutant (Fig. 10*B*). Only dUPNPP induced a significant fluorescence intensity decrease, whereas the dUDP and dUMP complexes of the H21W mutant remained fluorescently silent. In contrast, all ligand-enzyme complexes of H145W show a decrease in fluorescence intensity (49) according to the extent of C-terminal arm rigidity, which stabilizes the stacking interaction between the indole ring of Trp and uracil (12). The Trp incorporated in the H21W mutant thus only reports the binding of the triphosphate nucleotides. This phenomenon is consistent with the RAMD results, suggesting that the Trp^{21} residue is in interaction with Arg^{140} responsible for coordinating the γ-phosphate of the ligand exclusively (Fig. 8*C*). The dissociation constant of the enzyme-dUPNPP complex was determined using fluorescence intensity titrations and was found to be 1 order of magnitude larger than that of the H145W-dUPNPP complex (Fig. 10*C*).

Binding of dUDP could not be measured using fluorescent titration in a lack of a detectable signal (Fig. 10*A*). However, to ensure that dUDP indeed binds to the H21W mutant, circular dichroism titration measurements were performed. Determination of the K_d of the enzyme-dUDP complex using this method is only possible with relatively high error because the concentrations applied in the measurements are necessarily far above the K_d. Nevertheless, it is clear from the data that the H21W mutant binds dUDP significantly tighter than the H145W ($p = 0.046$) (Fig. 10*D*).

The results of the nucleoside mono-, di-, and triphosphate binding experiments together with the RAMD data suggest that Trp^{21} senses the nucleotide-bound state of the active site through its interaction with Arg^{140}. Arg^{140} probably remains in the apo state conformation when only monophosphate or diphosphate nucleotides bind to the active site (Fig. 10*A*). Because the C-terminal arm (including Arg^{140}) is usually only visible in crystal structures that contain the triphosphate ligand, the apo state conformation of Arg^{140} has never been reported before. However, the dUDP-complexed structure of the *M. tuberculosis* dUTPase is available for comparison for the position and mobility of Arg^{140} in two different nucleotide-bound states (Fig. 11). By comparing the relative B-factors of Arg^{140} within the same structure in Fig. 11 (*A* and *B*), it is clear that with a lack of the γ-phosphate, the mobility of the Arg residue is much higher. This phenomenon suggests that only a relatively static Arg^{140} is able to change the fluorescence properties of Trp^{21}, probably through cation-π interaction, and thus yields a specific sensor for nucleoside triphosphate binding. It is interesting that modification of the electrostatic properties of the aromatic interacting partner (*i.e.* His to Trp change) perturbed the nucleotide affinities to the enzyme (Table 3). A possible explanation to this phenomenon may be that the Arg^{140}–

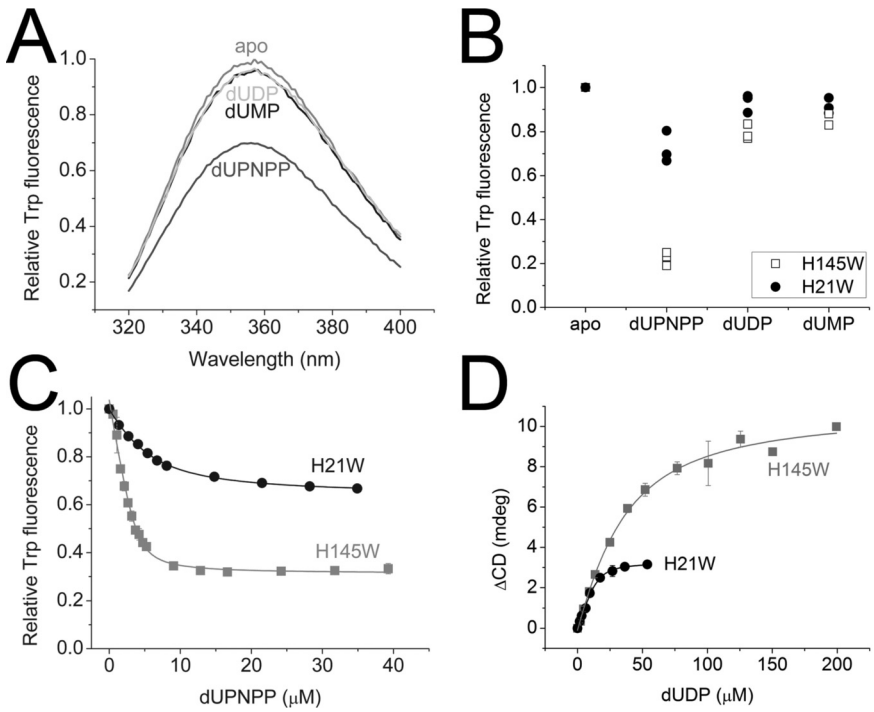

FIGURE 10. **Fluorescence and circular dichroism studies of ligand binding to the H145W and H21W mutants.** *A*, fluorescence spectra of the H21W mutant enzyme with and without nucleoside mono-, di-, and triphosphate ligands. *B*, fluorescence intensities of the H145W (49) and H21W mutant enzymes with saturating ligand concentrations. *C*, fluorescence titration of H145W and H21W with the dUPNPP substrate analogue; quadratic fit to the data yielded dissociation constants ($K_{d,\mathrm{dUPNPP}}$) shown in Table 3. *D*, circular dichroism titration of H145W and H21W with dUDP; quadratic fit to the data yielded dissociation constants ($K_{d,\mathrm{dUDP}}$) shown in Table 3.

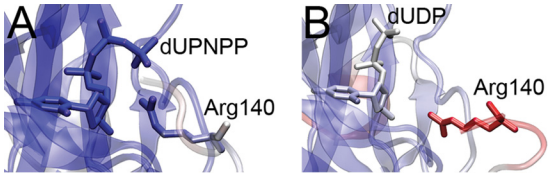

FIGURE 11. **Thermal mobility of the Arg^{140} residue in various ligand bound complexes.** The enzyme is shown as *thick transparent ribbon*, whereas the ligand and Arg^{140} are visualized as sticks. Coloring represents the relative crystallographic B factor for each atom (*blue*, less mobility; *red*, more mobility). *A*, the structure of *M. tuberculosis* dUTPase complexed with dUPNPP (PDB code 1SIX (10)). *B*, the structure of *M. tuberculosis* dUTPase complexed with dUDP (PDB code 1SLH (10)). Note that Arg^{140} is in different conformation and that Arg^{140} has much more mobility compared with the dUPNPP-complexed structure.

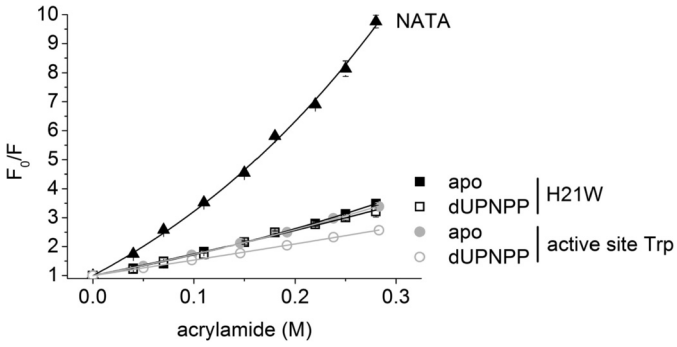

FIGURE 12. **Solvent accessibility of Trp^{21} with and without ligand bound to the protein.** Acrylamide titration curves are shown. The modified Stern-Volmer equation was fitted to the data yielding quenching constants 18.8, 6.4, 7.1, 6.7, and 5.3 M^{-1} for NATA, apo H21W, dUPNPP-bound H21W, apo active site Trp, and dUPNPP-bound active site Trp, respectively.

Trp^{21} interaction is more stable than the Arg^{140}–His^{21} interaction in the WT. This in turn results in less frequent dislocation of the C-terminal arm (Fig. 7) and finally in the slower kinetics observed for dUTP binding (Table 3).

Solvent Accessibility—The solvent accessibility of the incorporated Trp^{21} residue was measured by acrylamide quenching to obtain further dynamic information about the vicinity of the studied interaction. The acrylamide quenching of *N*-acetyl-L-tryptophanamide (NATA) was measured as reference and control for a rotationally free and maximally solvent-accessible Trp residue. The quenching constants (K_{SV}) for the apo and the dUPNPP-bound enzymes were similar and significantly reduced compared with NATA (Fig. 12). The solvent accessibility of the active site Trp in the apo state and in the dUPNPP-bound complex are also shown for comparison (12). The comparative data indicate that the Trp^{21} residue is buried similarly to the active site Trp. This suggests that part of the C-terminal arm shielding Trp^{21} from the solvent is associated to the protein core in equilibrium even in the apo enzyme. Consistently in all of the RAMD runs, we also observed that the C-terminal arm remains associated with the enzyme core following dUTP dissociation.

Discussion

This study combined computational, biochemical, and biophysical methods to gain insights into the nucleotide binding of a nucleotide-hydrolyzing enzyme at exceptionally high time and structural resolution. The RAMD method provided the high time and structural resolution, whereas the numerous experimental data served to validate the results of the computational simulation. In terms of mechanistic detail, the RAMD runs can be regarded as fast transient kinetics experiments on a

single molecule level. It appears that the assembly of the phenomena observed in single RAMD runs agrees well with the ensemble solution kinetics results presented earlier. The RAMD models reveal how the substrate can leave/enter the active site without completely opening the C-terminal arm. A previously hypothesized mechanism like a "hinge door" in which the C-terminal arm completely opens up at the hinge of a conserved Pro (51) was not observed in the RAMD simulations. Instead, we observed the nucleotide shuttling between the active site and the solvent through small openings of the C-terminal arm. The arm, fixed at both ends to the enzyme core via secondary interactions, moves only by sliding away close to the enzyme surface or by opening partially and locally. These movements involving 10–15 residues are small compared to the conformational changes observed for other nucleotide binding enzymes (4, 5, 52). In DNA helicases and polymerases, substrate binding involves displacement of whole domains (1–3, 6). It should be mentioned that the RAMD method may not be capable of modeling large loop motions because relevant reports are missing. However, our computational simulations and spectroscopic results together unequivocally support the finding that small loop movements allow the shuttling of the nucleotides between the binding pocket and the solvent in dUTPase, whereas larger scale movements may not be excluded.

There may be an apparent contradiction between the C-terminal arm not being visible in the crystal structures and the RAMD simulations showing only small amplitude movements of the C-terminal arm. These phenomena, however, are complementary. The electron density maps represent the average conformation of all atoms in a protein crystal. The inability to localize an entity may be due to movements on a small amplitude scale just exceeding the atomic distance. Molecular dynamics simulations, on the other hand, investigate single molecules rather than a population average and commonly reveal small amplitude movements. The example of dUTPase demonstrates that the comparison of crystal structures in various nucleotide-bound states alone is not fully informative of the nucleotide binding mechanism.

This study yielded novel insights regarding the dynamics and other properties of the interaction between dUTP and Mg^{2+} as well. The RAMD method offered a unique opportunity to observe that this interaction is maintained during the whole ligand binding/unbinding process, although the octahedral coordination between Mg^{2+} and dUTP became distorted in some of the pathways.

As proof of principle, we chose the His^{21} residue *de novo* predicted by the RAMD simulations to be involved in substrate dissociation to validate our data. It turned out that the replacement of this residue with a Trp yielded a sensitive fluorescence reporter specific to triphosphate nucleotide binding. As such, Trp^{21} reported the hydrolysis reaction similarly to the active site nucleotide sensor, Trp^{145}. Using the combination of structural and optical spectroscopic methods, we proposed a possible molecular mechanism for nucleotide sensing by Trp^{21} relatively far from the active site. This phenomenon also shines light onto the possibility to exploit this specific interaction in target-based drug design against actinobacterial pathogens.

Experimental Procedures

System Preparation for Molecular Dynamics Simulation—The initial structure for the simulations was the crystal structure of the *M. tuberculosis* dUTPase complexed with dUPNPP (PDB code 2PY4 (33)). The original dUPNPP ligand in the crystal structure was manually modified to dUTP. The protonation states of the titratable groups were determined by means of the ProPka algorithm (53, 54) at pH 7.4, and the optimization of hydrogen bonding interactions was performed using the PDB2PQR program package (55). The structure obtained was solvated using the TIP3P water model (56), and a minimum distance of 14 Å was used between any atom of the protein and the wall of the periodic box. The number of Na^+ cations and Cl^- anions was 49 and 34, respectively, to neutralize the system and mimic the physiological ionic strength (0.15 M NaCl). For description of the protein and dUTP, the CHARMM27 parameters (57) including the CMAP correction term for proteins (58) were applied, whereas the ions were described by the parameters of Beglov and Roux (59).

Molecular Dynamics Simulations—Molecular dynamics simulations were performed with the NAMD2.7 software (60) applying the following protocol: (i) 1600 steps minimization with restrained protein atoms using a 10 kcal mol^{-1} $Å^{-2}$ force constant; (ii) 3200 steps minimization; (iii) 32-ps NVT dynamics, where number of atoms (N), volume (V), and temperature (T) are fixed (T = 310 K, Langevin dynamics (61)) with restrained protein atoms using a 10 kcal mol^{-1} $Å^{-2}$ force constant; and (iv) NPT dynamics, where number of atoms (N), pressure (P), and temperature (T) are fixed (p = 1 atm, T = 310 K) with the Noosé-Hoover Langevin piston method (61, 62). The time step was set to 1 fs, a cutoff value of 10 Å was applied (using a smoothing function from 8 Å), and the long range electrostatic interactions were calculated with the Particle Mesh Ewald (PME) method (63). Two independent, 2-ns-long simulations with different initial velocities were conducted to relax the system, and the structures of the last frames were used in the subsequent RAMD simulations. During the 300-ps-long RAMD simulations, the acceleration was set to 0.066 kcal mol^{-1} $Å^{-1}$ (atomic mass unit)$^{-1}$, and the successful exit event was accepted if the distance between the center of mass of protein and that of dUTP was larger than 50 Å. Every 80 fs, new orientation was generated if the distance traveled by the ligand was less than 0.1 Å, and the trajectory was saved every 80 fs. No restraints were applied when conducting the RAMD simulations. From both starting structures and every binding cavity, 12 RAMD simulations were started resulting in 72 calculations. Once the ligand escapes into the solvent, the dissociation pathway becomes smooth because of the constant force acting on the substrate. This linearity of the ligand trajectories within the bulk solvent is irrelevant for the ligand finding the possible paths out of the active site.

Analysis of the Trajectories—Analysis of the trajectories was performed with the Visual Molecular Dynamics (64) package, which was used to generate Figs. 1–4, 7, 8, and 11 and supplemental Movies S1–S5.

Reagents—Molecular biology products were from New England Biolabs and Fermentas, electrophoresis and chromatogra-

phy reagents were from Bio-Rad and Qiagen. Phenol red was from Merck, dUDP and dUPNPP was from Jena Bioscience, and dUTP and other chemicals were from Sigma-Aldrich.

Mutagenesis—To generate the *M. tuberculosis* H21W mutant dUTPase, site-directed mutagenesis was performed by Stratagene's QuikChange method and was verified by sequencing. The mutagenic forward and reverse primers were 5′-GCCCAGCCGCGCTTGGGACGGCGACGCCGGCG-3′ and 5′-CGCCGGCGTCGCCGTCCCAAGCGCGGCTGGGC-3′.

Cloning, Protein Expression, and Purification—were performed as described previously in Ref. 33. Recombinant dUTPase with an N-terminal His_6 tag was transformed into *Escherichia coli* strain Rosetta(DE3)pLysS, which was used for protein expression. The final supernatant after cell extraction was loaded on a nickel-nitrilotriacetic acid column (Novagen) and purified according to the Novagen protocol. Because wild type lacks a useful tryptophan to monitor ligand binding, we have used the H145W mutant for kinetic studies. This tryptophan substitution in the active site has been previously shown to not affect catalytic activity (33). Protein concentration was measured using the Bradford method (Bio-Rad protein assay) and is given in subunits. Protein was dialyzed against buffer pH 7.5, containing 20 mM HEPES, 100 mM NaCl, 2 mM $MgCl_2$, and 1 mM DTT, and measurements were carried out in this buffer if not stated otherwise.

Crystallization—The H21W mutant was crystallized as described for the WT enzyme using the hanging drop diffusion method (33). 250 μM dUTPase and 1.25 mM dUPNPP were mixed with the reservoir solution containing 50 mM Tris-HCl, pH 7.5, 10 mM $MgCl_2$, 1.20–1.75 M ammonium sulfate, and 10% glycerol in a 1:1 ratio.

Data Collection and Structure Determination—High resolution complete crystallographic data set from a single flash frozen crystal was collected at Eötvös University using RIGAKU RU-H2R rotating anode home source at $\lambda = 1.5418$ Å on 100 K temperature. Reflection data were recorded on RIGAKU R-AXIS IV++ image plate detector.

Data reduction was performed using iMosflm and Scala programs and the CCP4 program suite (65). The structure of the H21W mutant in complex with dUPNPP and Mg^{2+} was determined by molecular replacement using MolRep, where the model was the WT dUTPase structure (PDB code 2PY4 (33)). $R_{merge} = \sum(|I_i - <I>|)/\sum(<I>)$, where the sum is calculated over all observations of a measured reflection (I_i), and $<I>$ is the mean intensity of all the measured observations (I_i).

Manual model building was carried out running the WinCoot program (66). Refmac5 software from CCP4 program package (65) was used for high resolution refinement. R_{free} values were computed from cross-validation throughout the refinement, using 5% random subset of the data set. Ramachandran statistics were as follows: 99.3% favored, 0.7% additionally allowed, and 0% generously allowed. The coordinates and structure factor data have been deposited in the Protein Data Bank under PDB code 4GCY.

Steady-state Colorimetric dUTPase Assay—Steady-state colorimetric dUTPase assay was performed as described in Ref. 35. Phenol red indicator assay was used to detect protons released in the dUTPase reaction. 0.1 μM protein was used in a buffer containing 1 mM HEPES, pH 7.5, 100 mM KCl, 40 μM phenol red, and 5 mM $MgCl_2$. A Specord 200 (Analytic, Jena, Germany) spectrophotometer and 10-mm-path length cuvettes were used at 20 °C, and absorbance was recorded at 559 nm. Initial velocity was determined from the first 10% of the progress curve.

Stopped Flow Experiments—Measurements were done using an SX-20 (Applied Photophysics) stopped flow apparatus as described in Refs. 12 and 35. Trp fluorescence was excited at 297 nm, and emission was selected with a 320-nm long pass filter. Time courses were recorded upon mixing sub- and superstoichiometric concentrations of dUTP with 1 or 3 μM enzyme at 20 °C (post-mix concentrations). Single turnover curves could be fitted with three exponentials (12). The two fast phases represent ligand binding, whereas the third, fluorescence recovery phase represents the hydrolysis-limited product release event and yields the single turnover rate constant (12). The fluorescence decrease of the time courses resulted from mixing excess dUTP over active sites and was fitted with double exponential function. Each time course shown is the mean of five measurements recorded sequentially in the same experiment. The k_{obs} *versus* dUTP concentration plots show the mean and standard error of three independent measurements. Time courses were analyzed using the curve fitting software provided with the stopped flow apparatus or by Origin 7.5. (OriginLab Corp., Northampton, MA).

Determination of the Enzyme-Ligand Dissociation Constants—Determination of the enzyme-ligand dissociation constants was done by fluorescence intensity titrations and circular dichroism intensity titrations. Fluorescence intensity titrations were recorded at 20 °C on a Jobin Yvon Spex Fluoromax-3 spectrofluorometer with excitation at 295 nm (slit, 1 nm), emission at 347 nm (slit 5 nm) using proteins at 4 μM concentration as described in Ref. 49. CD spectra were recorded at 20 °C on a JASCO 720 spectropolarimeter using a 10-mm-path length cuvette. Protein concentration was 50 μM in a buffer containing 20 mM HEPES, pH 7.5, 50 mM NaCl, and 2 mM $MgCl_2$. A spectrum between 250 and 290 nm was recorded at each nucleotide concentration as described in Ref. 35. Differential curves were obtained by subtracting the signal of the ligand alone from that of the corresponding complex. Differential ellipticity at 269 nm was plotted against the ligand concentration to obtain the binding curves.

In both types of measurement, protein solution was titrated with dUPNPP or dUDP using small volumes from a concentrated stock solution. The following equation describing 1:1 stoichiometry for the dissociation equilibrium was fitted to the titration data,

$$y = s + \frac{A[(c + x + K) - \sqrt{(c + x + K)^2 - 4cx}]}{2c} \quad \text{(Eq. 1)}$$

where x is the nucleotide concentration, y is the fluorescence or circular dichroism intensity, $s = y$ at $x = 0$, A is the amplitude of the fluorescence or circular dichroism intensity change, c is the enzyme concentration, and K is the dissociation constant (K_d).

Acrylamide Quenching—Acrylamide quenching was carried out by the addition of small volumes of a 5 M acrylamide solution to the enzyme, enzyme-dUPNPP, or NATA solutions as described in Ref. 12. Raw data were corrected for the fluorescence arising from the acrylamide solution itself. F_0/F *versus* [Q] curves were analyzed using a modified Stern-Volmer equation,

$$F_0/F = 1 + K_{SV}[Q]e^{V[Q]} \quad \text{(Eq. 2)}$$

where F_0 is the unquenched, F is the quenched fluorescence, [Q] is the quencher, K_{SV} is the dynamic (bimolecular) quenching constant, and V is the static (sphere of action) component of quenching.

Author Contributions—A. L. and B. J. conceived the idea for the project and carried out the simulations. A. L. conducted the *in vitro* experiments under J. T.'s supervision. I. L. and Á. Á. B. carried out structure determination. A. L., J. T., and B. J. analyzed the results. A. L., J. T., B. J., B. V., and B. G. V. wrote the paper.

Acknowledgments—We thank M. Lábadi for technical support at the High Performance Computing (HPC) Centre of the University of Szeged, Veronika Harmat for crystallography help, and Judit E. Szabó for useful comments on the manuscript.

References

1. Lee, J. Y., and Yang, W. (2006) UvrD helicase unwinds DNA one base pair at a time by a two-part power stroke. *Cell* **127,** 1349–1360
2. Gai, D., Zhao, R., Li, D., Finkielstein, C. V., and Chen, X. S. (2004) Mechanisms of conformational change for a replicative hexameric helicase of SV40 large tumor antigen. *Cell* **119,** 47–60
3. Velankar, S. S., Soultanas, P., Dillingham, M. S., Subramanya, H. S., and Wigley, D. B. (1999) Crystal structures of complexes of PcrA DNA helicase with a DNA substrate indicate an inchworm mechanism. *Cell* **97,** 75–84
4. Sablin, E. P., and Fletterick, R. J. (2001) Nucleotide switches in molecular motors: structural analysis of kinesins and myosins. *Curr. Opin Struct. Biol.* **11,** 716–724
5. Shuman, S., and Lima, C. D. (2004) The polynucleotide ligase and RNA capping enzyme superfamily of covalent nucleotidyltransferases. *Curr. Opin Struct. Biol.* **14,** 757–764
6. Santoso, Y., Joyce, C. M., Potapova, O., Le Reste, L., Hohlbein, J., Torella, J. P., Grindley, N. D., and Kapanidis, A. N. (2010) Conformational transitions in DNA polymerase I revealed by single-molecule FRET. *Proc. Natl. Acad. Sci. U.S.A.* **107,** 715–720
7. Fiser, A., and Vértessy, B. G. (2000) Altered subunit communication in subfamilies of trimeric dUTPases. *Biochem. Biophys. Res. Commun.* **279,** 534–542
8. Vértessy, B. G., and Tóth, J. (2009) Keeping uracil out of DNA: physiological role, structure and catalytic mechanism of dUTPases. *Acc. Chem. Res.* **42,** 97–106
9. Mol, C. D., Harris, J. M., McIntosh, E. M., and Tainer, J. A. (1996) Human dUTP pyrophosphatase: uracil recognition by a β hairpin and active sites formed by three separate subunits. *Structure* **4,** 1077–1092
10. Chan, S., Segelke, B., Lekin, T., Krupka, H., Cho, U. S., Kim, M. Y., So, M., Kim, C. Y., Naranjo, C. M., Rogers, Y. C., Park, M. S., Waldo, G. S., Pashkov, I., Cascio, D., Perry, J. L., *et al.* (2004) Crystal structure of the *Mycobacterium tuberculosis* dUTPase: insights into the catalytic mechanism. *J. Mol. Biol.* **341,** 503–517
11. Vertessy, B. G., Larsson, G., Persson, T., Bergman, A. C., Persson, R., and Nyman, P. O. (1998) The complete triphosphate moiety of non-hydrolyzable substrate analogues is required for a conformational shift of the flexible C-terminus in *E. coli* dUTP pyrophosphatase. *FEBS Lett.* **421,** 83–88
12. Tóth, J., Varga, B., Kovács, M., Málnási-Csizmadia, A., and Vértessy, B. G. (2007) Kinetic mechanism of human dUTPase, an essential nucleotide pyrophosphatase enzyme. *J. Biol. Chem.* **282,** 33572–33582
13. Shan, Y., Kim, E. T., Eastwood, M. P., Dror, R. O., Seeliger, M. A., and Shaw, D. E. (2011) How does a drug molecule find its target binding site? *J. Am. Chem. Soc.* **133,** 9181–9183
14. Dror, R. O., Pan, A. C., Arlow, D. H., Borhani, D. W., Maragakis, P., Shan, Y., Xu, H., and Shaw, D. E. (2011) Pathway and mechanism of drug binding to G-protein-coupled receptors. *Proc. Natl. Acad. Sci. U.S.A.* **108,** 13118–13123
15. Dror, R. O., Green, H. F., Valant, C., Borhani, D. W., Valcourt, J. R., Pan, A. C., Arlow, D. H., Canals, M., Lane, J. R., Rahmani, R., Baell, J. B., Sexton, P. M., Christopoulos, A., and Shaw, D. E. (2013) Structural basis for modulation of a G-protein-coupled receptor by allosteric drugs. *Nature* **503,** 295–299
16. Thomas, T., Fang, Y., Yuriev, E., and Chalmers, D. K. (2016) Ligand binding pathways of clozapine and haloperidol in the dopamine D_2 and D_3 receptors. *J. Chem. Inf. Model.* **56,** 308–321
17. Gao, M., Craig, D., Vogel, V., and Schulten, K. (2002) Identifying unfolding intermediates of FN-III(10) by steered molecular dynamics. *J. Mol. Biol.* **323,** 939–950
18. Lüdemann, S. K., Lounnas, V., and Wade, R. C. (2000) How do substrates enter and products exit the buried active site of cytochrome P450cam?: 2. Steered molecular dynamics and adiabatic mapping of substrate pathways. *J. Mol. Biol.* **303,** 813–830
19. Lüdemann, S. K., Lounnas, V., and Wade, R. C. (2000) How do substrates enter and products exit the buried active site of cytochrome P450cam?: 1. Random expulsion molecular dynamics investigation of ligand access channels and mechanisms. *J. Mol. Biol.* **303,** 797–811
20. Gervasio, F. L., Parrinello, M., Ceccarelli, M., and Klein, M. L. (2006) Exploring the gating mechanism in the ClC chloride channel via metadynamics. *J. Mol. Biol.* **361,** 390–398
21. Grazioso, G., Limongelli, V., Branduardi, D., Novellino, E., De Micheli, C., Cavalli, A., and Parrinello, M. (2012) Investigating the mechanism of substrate uptake and release in the glutamate transporter homologue Glt(Ph) through metadynamics simulations. *J. Am. Chem. Soc.* **134,** 453–463
22. Wang, T., and Duan, Y. (2007) Chromophore channeling in the G-protein coupled receptor rhodopsin. *J. Am. Chem. Soc.* **129,** 6970–6971
23. Klvana, M., Pavlova, M., Koudelakova, T., Chaloupkova, R., Dvorak, P., Prokop, Z., Stsiapanava, A., Kuty, M., Kuta-Smatanova, I., Dohnalek, J., Kulhanek, P., Wade, R. C., and Damborsky, J. (2009) Pathways and mechanisms for product release in the engineered haloalkane dehalogenases explored using classical and random acceleration molecular dynamics simulations. *J. Mol. Biol.* **392,** 1339–1356
24. Kalyaanamoorthy, S., and Chen, Y.-P. (2012) Exploring inhibitor release pathways in histone deacetylases using random acceleration molecular dynamics simulations. *J. Chem. Inf. Model.* **52,** 589–603
25. Pietra, F. (2013) On the pathways of biologically relevant diatomic gases through proteins: dioxygen and heme oxygenase from the perspective of molecular dynamics. *Chem. Biodivers.* **10,** 556–568
26. Zhuang, S., Bao, L., Linhananta, A., and Liu, W. (2013) Molecular modeling revealed that ligand dissociation from thyroid hormone receptors is affected by receptor heterodimerization. *J. Mol. Graph. Model.* **44,** 155–160
27. Zhang, J., Li, D., Sun, T., Liang, L., and Wang, Q. (2015) Interaction of P-glycoprotein with anti-tumor drugs: the site, gate and pathway. *Soft Matter* **11,** 6633–6641
28. Niu, Y., Li, S., Pan, D., Liu, H., and Yao, X. (2016) Computational study on the unbinding pathways of B-RAF inhibitors and its implication for the difference of residence time: insight from random acceleration and steered molecular dynamics simulations. *Phys. Chem. Chem. Phys.* **18,** 5622–5629
29. Prasad, G. S., Stura, E. A., Elder, J. H., and Stout, C. D. (2000) Structures of feline immunodeficiency virus dUTP pyrophosphatase and its nucleotide complexes in three crystal forms. *Acta Crystallogr. D Biol. Crystallogr.* **56,** 1100–1109

30. González, A., Larsson, G., Persson, R., and Cedergren-Zeppezauer, E. (2001) Atomic resolution structure of *Escherichia coli* dUTPase determined ab initio. *Acta Crystallogr. D Biol. Crystallogr.* **57,** 767–774
31. Barabás, O., Pongrácz, V., Kovári, J., Wilmanns, M., and Vértessy, B. G. (2004) Structural insights into the catalytic mechanism of phosphate ester hydrolysis by dUTPase. *J. Biol. Chem.* **279,** 42907–42915
32. Tarbouriech, N., Buisson, M., Seigneurin, J. M., Cusack, S., and Burmeister, W. P. (2005) The monomeric dUTPase from Epstein-Barr virus mimics trimeric dUTPases. *Structure* **13,** 1299–1310
33. Varga, B., Barabás, O., Takács, E., Nagy, N., Nagy, P., and Vértessy, B. G. (2008) Active site of mycobacterial dUTPase: structural characteristics and a built-in sensor. *Biochem. Biophys. Res. Commun.* **373,** 8–13
34. Freeman, L., Buisson, M., Tarbouriech, N., Van der Heyden, A., Labbé, P., and Burmeister, W. P. (2009) The flexible motif V of Epstein-Barr virus deoxyuridine 5′-triphosphate pyrophosphatase is essential for catalysis. *J. Biol. Chem.* **284,** 25280–25289
35. Pecsi, I., Leveles, I., Harmat, V., Vertessy, B. G., and Toth, J. (2010) Aromatic stacking between nucleobase and enzyme promotes phosphate ester hydrolysis in dUTPase. *Nucleic Acids Res.* **38,** 7179–7186
36. Larsson, G., Nyman, P. O., and Kvassman, J. O. (1996) Kinetic characterization of dUTPase from *Escherichia coli*. *J. Biol. Chem.* **271,** 24010–24016
37. Nord, J., Kiefer, M., Adolph, H. W., Zeppezauer, M. M., and Nyman, P. O. (2000) Transient kinetics of ligand binding and role of the C-terminus in the dUTPase from equine infectious anemia virus. *FEBS Lett.* **472,** 312–316
38. Tormo-Más, M. A., Mir, I., Shrestha, A., Tallent, S. M., Campoy, S., Lasa, I., Barbé, J., Novick, R. P., Christie, G. E., and Penadés, J. R. (2010) Moonlighting bacteriophage proteins derepress staphylococcal pathogenicity islands. *Nature* **465,** 779–782
39. Szabó, J. E., Németh, V., Papp-Kádár, V., Nyíri, K., Leveles, I., Bendes, A. Á., Zagyva, I., Róna, G., Pálinkás, H. L., Besztercei, B., Ozohanics, O., Vékey, K., Liliom, K., Tóth, J., and Vértessy, B. G. (2014) Highly potent dUTPase inhibition by a bacterial repressor protein reveals a novel mechanism for gene expression control. *Nucleic Acids Res.* **42,** 11912–11920
40. Hill, R. L, and Dokland, T. (2016) The type 2 dUTPase of bacteriophage ϕNM1 initiates mobilization of *Staphylococcus aureus* bovine pathogenicity island 1. *J. Mol. Biol.* **428,** 142–152
41. Pécsi, I., Szabó, J. E., Adams, S. D., Simon, I., Sellers, J. R., Vértessy, B. G., and Tóth, J. (2011) Nucleotide pyrophosphatase employs a P-loop-like motif to enhance catalytic power and NDP/NTP discrimination. *Proc. Natl. Acad. Sci. U.S.A.* **108,** 14437–14442
42. Pecsi, I., Hirmondo, R., Brown, A. C., Lopata, A., Parish, T., Vertessy, B. G., and Tóth, J. (2012) The dUTPase enzyme is essential in Mycobacterium smegmatis. *PLoS One* **7,** e37461
43. Muha, V., Horváth, A., Békési, A., Pukáncsik, M., Hodoscsek, B., Merényi, G., Róna, G., Batki, J., Kiss, I., Jankovics, F., Vilmos, P., Erdélyi, M., and Vértessy, B. G. (2012) Uracil-containing DNA in Drosophila: stability, stage-specific accumulation, and developmental involvement. *PLoS Genet.* **8,** e1002738
44. Vertessy, B. G. (1997) Flexible glycine rich motif of *Escherichia coli* deoxyuridine triphosphate nucleotidohydrolase is important for functional but not for structural integrity of the enzyme. *Proteins* **28,** 568–579
45. Németh-Pongrácz, V., Barabás, O., Fuxreiter, M., Simon, I., Pichová, I., Rumlová, M., Zábranská, H., Svergun, D., Petoukhov, M., Harmat, V., Klement, E., Hunyadi-Gulyás, E., Medzihradszky, K. F., Kónya, E., and Vértessy, B. G. (2007) Flexible segments modulate co-folding of dUTPase and nucleocapsid proteins. *Nucleic Acids Res.* **35,** 495–505
46. García-Nafría, J., Burchell, L., Takezawa, M., Rzechorzek, N. J., Fogg, M. J., and Wilson, K. S. (2010) The structure of the genomic *Bacillus subtilis* dUTPase: novel features in the Phe-lid. *Acta Crystallogr. D Biol. Crystallogr.* **66,** 953–961
47. Cojocaru, V., Winn, P. J., and Wade, R. C. (2012) Multiple, ligand-dependent routes from the active site of cytochrome P450 2C9. *Curr. Drug Metab.* **13,** 143–154
48. Nord, J., Nyman, P., Larsson, G., and Drakenberg, T. (2001) The C-terminus of dUTPase: observation on flexibility using NMR. *FEBS Lett.* **492,** 228–232
49. Takács, E., Nagy, G., Leveles, I., Harmat, V., Lopata, A., Tóth, J., and Vértessy, B. G. (2010) Direct contacts between conserved motifs of different subunits provide major contribution to active site organization in human and mycobacterial dUTPases. *FEBS Lett.* **584,** 3047–3054
50. Shao, H., Robek, M. D., Threadgill, D. S., Mankowski, L. S., Cameron, C. E., Fuller, F. J., and Payne, S. L. (1997) Characterization and mutational studies of equine infectious anemia virus dUTPase. *Biochim. Biophys. Acta* **1339,** 181–191
51. Takács, E., Barabás, O., Petoukhov, M. V., Svergun, D. I., and Vértessy, B. G. (2009) Molecular shape and prominent role of beta-strand swapping in organization of dUTPase oligomers. *FEBS Lett.* **583,** 865–871
52. Yang, S.-W., Ting, H.-C., Lo, Y.-T., Wu, T.-Y., Huang, H.-W., Yang, C.-J., Chan, J.-F. R., Chuang, M.-C., and Hsu, Y.-H. (2016) Guanine nucleotide induced conformational change of Cdc42 revealed by hydrogen/deuterium exchange mass spectrometry. *Biochim. Biophys. Acta* **1864,** 42–51
53. Li, H., Robertson, A. D., and Jensen, J. H. (2005) Very fast empirical prediction and rationalization of protein pKa values. *Proteins* **61,** 704–721
54. Bas, D. C., Rogers, D. M., and Jensen, J. H. (2008) Very fast prediction and rationalization of pKa values for protein-ligand complexes. *Proteins* **73,** 765–783
55. Dolinsky, T. J., Nielsen, J. E., McCammon, J. A., and Baker, N. A. (2004) PDB2PQR: an automated pipeline for the setup of Poisson-Boltzmann electrostatics calculations. *Nucleic Acids Res.* **32,** W665–7
56. Jorgensen, W. L., Chandrasekhar, J., Madura, J. D., Impey, R. W., and Klein, M. L. (1983) Comparison of simple potential functions for simulating liquid water. *J. Chem. Phys.* **79,** 926–935
57. MacKerell, A. D., Bashford, D., Bellott, M., Dunbrack, R. L., Evanseck, J. D., Field, M. J., Fischer, S., Gao, J., Guo, H., Ha, S., Joseph-McCarthy, D., Kuchnir, L., Kuczera, K., Lau, F. T., Mattos, C., *et al.* (1998) All-atom empirical potential for molecular modeling and dynamics studies of proteins. *J. Phys. Chem. B.* **102,** 3586–3616
58. Mackerell, A. D., Jr., Feig, M., and Brooks, C. L., 3rd (2004) Extending the treatment of backbone energetics in protein force fields: Limitations of gas-phase quantum mechanics in reproducing protein conformational distributions in molecular dynamics simulations. *J. Comput. Chem.* **25,** 1400–1415
59. Beglov, D., and Roux, B. (1994) Finite representation of an infinite bulk system: solvent boundary potential for computer-simulations. *J. Chem. Phys.* **100,** 9050–9063
60. Phillips, J. C., Braun, R., Wang, W., Gumbart, J., Tajkhorshid, E., Villa, E., Chipot, C., Skeel, R. D., Kalé, L., and Schulten, K. (2005) Scalable molecular dynamics with NAMD. *J. Comput. Chem.* **26,** 1781–1802
61. Feller, S. E., Zhang, Y. H., Pastor, R. W., and Brooks, B. R. (1995) Constant-pressure molecular-dynamics simulation: the Langevin piston method. *J. Chem. Phys.* **103,** 4613–4621
62. Martyna, G. J., Tobias, D. J., and Klein, M. L. (1994) Constant-pressure molecular-dynamics algorithms. *J. Chem. Phys.* **101,** 4177–4189
63. Darden, T., York, D., and Pedersen, L. (1993) Particle mesh Ewald: an N. Log(N) method for Ewald sums in large systems. *J. Chem. Phys.* **98,** 10089–10092
64. Humphrey, W., Dalke, A., and Schulten, K. (1996) VMD: Visual molecular dynamics. *J. Mol. Graph.* **14,** 33–38
65. Winn, M. D., Ballard, C. C., Cowtan, K. D., Dodson, E. J., Emsley, P., Evans, P. R., Keegan, R. M., Krissinel, E. B., Leslie, A. G., McCoy, A., McNicholas, S. J., Murshudov, G. N., Pannu, N. S., Potterton, E. A., Powell, H. R., *et al.* (2011) Overview of the CCP4 suite and current developments. *Acta Crystallogr. D Biol. Crystallogr.* **67,** 235–242
66. Emsley, P., and Cowtan, K. (2004) Coot: model-building tools for molecular graphics. *Acta Crystallogr. D Biol. Crystallogr.* **60,** 2126–2132

biomolecules

MDPI

Article

Beyond Chelation: EDTA Tightly Binds Taq DNA Polymerase, MutT and dUTPase and Directly Inhibits dNTPase Activity

Anna Lopata [1,2,3], Balázs Jójárt [4], Éva V. Surányi [1,2], Enikő Takács [1], László Bezúr [5], Ibolya Leveles [1,2], Ábris Á. Bendes [1,6], Béla Viskolcz [7], Beáta G. Vértessy [1,2] and Judit Tóth [1,*]

1 Institute of Enzymology, Research Centre for Natural Sciences, Hungarian Academy of Sciences, 1113 Budapest, Hungary; lopata.anna@gmail.com (A.L.); suranyi.eva@ttk.mta.hu (É.V.S.); enikot@gmail.com (E.T.); leveles.ibolya@ttk.mta.hu (I.L.); abris.bendes@oulu.fi (Á.Á.B.); vertessy@kutatok.org (B.G.V.)
2 Department of Applied Biotechnology, Budapest University of Technology and Economics, 1111 Budapest, Hungary
3 Institute of Biophysical Chemistry, Goethe University, 60438 Frankfurt am Main, Germany
4 Institute of Food Engineering, Faculty of Engineering, University of Szeged, 6724 Szeged, Hungary; jojartb@gmail.com
5 Department of Inorganic and Analytical Chemistry, Budapest University of Technology and Economics, 1111 Budapest, Hungary; bezur@mail.bme.hu
6 Faculty of Biochemistry and Molecular Medicine, University of Oulu, 90220 Oulu, Finland
7 Institute of Chemistry, University of Miskolc, 3515 Miskolc, Hungary; bela.viskolcz@uni-miskolc.hu
* Correspondence: toth.judit@ttk.mta.hu; Tel.: +36-1382-67-93

Received: 11 September 2019; Accepted: 15 October 2019; Published: 17 October 2019

Abstract: EDTA is commonly used as an efficient chelator of metal ion enzyme cofactors. It is highly soluble, optically inactive and does not interfere with most chemicals used in standard buffers making EDTA a common choice to generate metal-free conditions for biochemical and biophysical investigations. However, the controversy in the literature on metal-free enzyme activities achieved using EDTA or by other means called our attention to a putative effect of EDTA beyond chelation. Here, we show that EDTA competes for the nucleotide binding site of the nucleotide hydrolase dUTPase by developing an interaction network within the active site similar to that of the substrate. To achieve these findings, we applied kinetics and molecular docking techniques using two different dUTPases. Furthermore, we directly measured the binding of EDTA to dUTPases and to two other dNTPases, the Taq polymerase and MutT using isothermal titration calorimetry. EDTA binding proved to be exothermic and mainly enthalpy driven with a submicromolar dissociation constant considerably lower than that of the enzyme:substrate or the Mg:EDTA complexes. Control proteins, including an ATPase, did not interact with EDTA. Our findings indicate that EDTA may act as a selective inhibitor against dNTP hydrolyzing enzymes and urge the rethinking of the utilization of EDTA in enzymatic experiments.

Keywords: dNTP hydrolysis; EDTA; dNTP pool sanitizing enzymes; dNTPase inhibitor

1. Introduction

Divalent metal ions including Mg^{2+}, Cu^{2+}, Fe^{2+}, Mn^{2+}, Ni^{2+}, and Zn^{2+} play prominent roles in enzymatic catalysis. The small organic compound ethylene diamine tetraacetic acid or commonly known as EDTA is frequently used to chelate these metal ions to investigate enzyme function in the absence of metal co-factors. This molecule comprises four carboxylic acid groups, thus have an

overall negative charge. Its structure is flexible when unbound and adopts a rigid conformation while complexed with a single divalent metal ion (Me^{2+}). All four carboxylic acid groups and two amines are involved in the hexacoordinated EDTA:Me^{2+} complex. It is highly soluble, optically inactive, and does not interfere with most chemicals used in standard buffers. Thus, EDTA seems to be a beneficial and safe choice to generate metal-free conditions for biochemical and biophysical investigations.

For enzymes catalyzing the hydrolysis of nucleotides to yield (d)NDP and P_i (inorganic phosphate) (e.g., ATPases [1], GTPases [2]) or (d)NMP + PP_i (e.g., ligases [3], DNA and RNA polymerases [4], Nudix hydrolases [5], and dUTPases) metal ions, notably Mg^{2+}, are usually considered to be of high functional importance. In most cases, k_{cat} (steady-state catalytic activity) values are reported to decrease by several orders of magnitude in lack of these metal ions. Nucleotide hydrolyzing enzymes can operate with either one or two Mg^{2+} ions bound. The enzyme dUTPase is a preventive DNA repair protein that hydrolyses dUTP into dUMP and pyrophosphate, performing a dNTP pool sanitizing role. Thereby it prevents uracil incorporation into DNA that would eventually lead to hyperactive DNA repair cycles and cell death [6]. In most species, it forms a homotrimer with three active sites that are built up from five conserved motifs [6]. The substrate dUTP-Mg^{2+} complex binds to the active site and is coordinated by multiple H-bonds and a π-π stacking interaction [7]. Numerous publications provided experimental data indicating that the lack of the Mg^{2+} co-factor decreases the k_{cat} of dUTPase only by a factor of two [8–12]. Some publications, however, concluded the total inactivity of dUTPase without Mg^{2+} [13–15]. In the latter cases, high concentration of EDTA was used, or the method of providing metal-free conditions was not described.

To investigate the underlying cause of this controversy, we studied the effect of EDTA on dUTP hydrolysis catalysed by two different dUTPases (from *Homo sapiens*, hDUT, UniProt ID: P33316); and from *Mycobacterium tuberculosis*, mtDUT, UniProt ID: P9WNS5) in Mg^{2+}-free conditions. We observed kinetic inhibition by EDTA in the absence of Mg^{2+}. We then measured direct binding of EDTA to dUTPases and 5 other enzymes (including another dNTP pool sanitizing enzyme [16,17] and a DNA polymerase) using isothermal titration calorimetry. Our results show that EDTA binds selectively to the nucleotide binding pocket of dNTP processing enzymes. To understand the structural basis of this specific binding, we took a computational approach and explored the interactions of EDTA within the active site of dUTPases. We found that EDTA develops similar interactions with the protein to those of the cognate substrate.

2. Materials and Methods

2.1. Reagents

We used our previously cloned N-terminally His-tagged dUTPases of human (hDUT and A98F hDUT) and of *Mycobacterium tuberculosis* origin (mtDUT). The *Escherichia coli* MutT (EcMutT) plasmid was a kind gift of Umesh Varshney, Indian Institute of Science, Bangalore, India. These proteins were expressed and purified as described previously [17–20]. We also used TEMpase Hot Start DNA polymerase from VWR (Radnor, PA, USA), a modified *Thermus aquaticus* originating DNA polymerase (Taq polymerase). This protein was heat activated for 15 min at 95 °C before the ITC measurement. Furthermore, we used our previously cloned *N*-terminally His-tagged *Staphylococcus aureus* uracil glycosylase inhibitor (SaUGI) [21] and *Petroselinum crispum* phenylalanine ammonia-lyase (PcPAL) [22] proteins. The rabbit skeletal myosin subfragment-S1 was a kind gift of Máté Gyimesi, Eötvös University, Budapest, Hungary. These proteins were expressed and purified as described previously [23–25]. The proteins were dialyzed against a buffer pH 7.5 comprising 20 mM HEPES, 100 mM NaCl and 1 mM TCEP. Protein concentration was determined by UV absorbance (ε_{280} = 10430 $M^{-1}cm^{-1}$ for hDUT, ε_{280} = 15930 $M^{-1}cm^{-1}$ for A98F hDUT, ε_{280} = 2980 $M^{-1}cm^{-1}$ for mtDUT, ε_{280} = 28990 $M^{-1}cm^{-1}$ for EcMutT, ε_{280} = 112760 $M^{-1}cm^{-1}$ for Taq polymerase, ε_{280} = 21890 $M^{-1}cm^{-1}$ for SaUGI and ε_{280} = 45,840 $M^{-1}cm^{-1}$ for PcPAL) or using the Bradford assay and is given in monomers. Other reagents were from Sigma-Aldrich (St. Louis, MO, USA).

2.2. ICP-OES

The Mg content of the solutions used in our experiments was determined by inductively coupled plasma optical emission spectrometry. Instrument settings were Labtest Plasmalab ICP spectrometer with 40 element vacuum polychromator, wavelength: 279.553 nm, 27 MHz Ar-Ar plasma, forward power: 1.3 kW, sample introduction with V-groove nebulizer at 2.8 mL/min sample flow rate. Limit of quantitation for Mg was 0.001 mg/L (0.04 µM).

2.3. Photometric Enzyme Activity Measurement

Continuous pH indicator-based assays were performed to measure enzyme activity at 20 °C as described in [26]. Briefly, 1 µM protein was used in a buffer pH 7.5 containing 1 mM HEPES, 100 mM KCl and 40 µM phenol red. A Specord 200 (Analytic, Jena, Germany) spectrophotometer and 10-mm-path length cuvettes were used, and absorbance was recorded at 559 nm. Initial velocity was determined from the first 10% of the progress curve. To explore the inhibitory effect of EDTA on both enzymes, we added this compound to the reaction mixtures at 30 and 100 µM concentration for hDUT and at 300 µM concentration for mtDUT. Data fitting was accomplished using OriginPro 7.5 (OriginLab Corp, Northampton, MA, USA).

2.4. Thermofluor Stability Assay

Solutions of 40 µM (0.8 mg/mL) protein in 20 mM HEPES pH 7.5, 100 mM NaCl, 10 mM ß-ME also containing 1000x dilution of Sypro® Orange supplemented either with 5 mM $MgCl_2$ or 100 µM EDTA were added to the wells of a 96-well thin-wall ABgene® PCR plate (Thermo Fisher Scientific, Waltham, MA, USA). Apo enzyme, dUPNPP-complexed and dUMP-complexed enzymes were tested with the addition of saturating concentration of the ligand (100 µM dUPNPP or 1 mM dUMP) where applicable. The plates were sealed with ABgene® Adhesive PCR Plate Sealing Tape (Thermo Fisher Scientific, Waltham, MA, USA) and heated in a Mx3000Pro QPCR System (Agilent Technologies, Santa Clara, CA, USA) from 25 to 90 °C. Fluorescence changes in the wells of the plate were monitored simultaneously with a photomultiplier tube (PMT). The wavelengths for excitation and emission were 492 and 516 nm, respectively.

2.5. Protein and Ligand Preparation Procedure for Molecular Docking

The protonation states of the titratable groups were determined by means of the ProPka algorithm [27,28] at pH 7.4, and the optimization of H-bonding interactions was performed using the PDB2PQR program package version 2.1.1 [29]. The original dUPNPP ligand in both human and *Mycobacterium tuberculosis* dUTPase crystal structures (PDB IDs: 3EHW, under publication in a separate paper and 2PY4 [20], respectively) was manually modified to dUTP.

The structure of the ligand (both EDTA and EDTA-Mg^{2+} complex) was taken from that of 1ZLQ [30]. The Fe^{3+} ion was replaced by a Mg^{2+} ion, and the coordination complex with EDTA was prepared manually using the Molecular Operating Environment 2007.09 program package (Chemical Computing Group, Montreal, Canada) [31]. Subsequent minimization was performed using the MMFF94x force field [32–36]. Gasteiger charges [37] were assigned to the enzyme and to the ligand using the same software.

2.6. Molecular Docking

Docking calculations were performed by means of the AutoDock version 4.2.3 software [38] using default settings and parameters as follows. The protein was kept rigid in the calculations and the ligand was allowed to be flexible. Lennard-Jones parameters 12–10 and 12–6 were used for modelling H-bonds and van der Waals interactions, respectively. To calculate the electrostatic grid map, the distance-dependent dielectric constant of Mehler and Solmayer was utilized. The Lamarckian Genetic Algorithm [39] with the pseudo-Solis and Wets method was used in the docking procedure,

with 300 individuals in the population. The stopping criterion was defined by setting the total number of energy evaluations to 2.0×10^7. The translation step was set to 5 Å/step, and in both quaternion and torsion steps 5.0 degrees/step was applied. The docking procedure was performed 25 × 16 (400) times for each enzyme-ligand complex.

Both blind docking [40,41] and active site docking calculations were performed. In blind docking, the grid box was centered on the whole protein and the number of grid points was set to 176 × 144 × 176 for both hDUT and mtDUT. In active site docking, the grid box was centered on the geometric center of dUTP and was large enough to accommodate the dUTP. The number of grid points was set to 42 × 34 × 46 and 46 × 34 × 38 for hDUT and mtDUT, respectively. The lattice point distance was set to 0.375 Å for every docking calculation.

2.7. Determination of the Enzyme-Ligand Interaction Network

The 'Ligand interactions' module [42] of MOE 2007.09 (Chemical Computing Group, Montreal, Canada) [31] was used for the 2D depiction of enzyme ligand interactions. The algorithm to determine the interaction sites in the 'Ligand interactions' module includes the following considerations: (1) Only heavy atom distances are considered; (2) first those residues are determined as interaction sites which are in a 4.5 Å proximity of any ligand atoms; (3) thereafter the distance limit is increased by 0.1 Å, and a new residue is determined as possible site if at least 2 atoms of that residue are within the new distance criteria; (4) increasing the distance by 0.1 Å and the number of the interacting atom by 1, this step is repeated 10 times. The possible H-bond interactions are determined by applying a scoring function. The strength of the H-bond is expressed as percentage probability. We applied a 10% cut-off in identifying possible H-bond interactions.

2.8. Isothermal Titration Calorimetry (ITC) Measurement

ITC experiments were carried out at 293 K on a Microcal ITC_{200} instrument (Malvern Instruments, Malvern, UK), following previously described experimental design [43]. The proteins were dialysed against a buffer pH 7.5 comprising 20 mM HEPES, 100 mM NaCl and 1 mM TCEP. We used 10–250 μM enzyme (hDUT, A98F hDUT, mtDUT, EcMutT, Taq polymerase) in the cell and 70–500 μM EDTA or 500–1500 μM dUPNPP in the syringe. For SaUGI, PcPAL and rabbit myosin S1, 20–80 μM enzyme was used in the cell and 40–120 μM EDTA in the syringe. Next, 5 mM $MgCl_2$ was used in the syringe to titrate 500 μM EDTA in the cell. Protein concentrations correspond to subunits. Enzymes were also titrated with buffer to consider mixing and dilution heat effects. The titrations were performed with the injection syringe rotating at 750× *rpm* (and at 200× *rpm* for mtDUT). A series of 20 injections spaced 180 s apart from each other was performed with injection volumes 0.5 μL for the first and 2 μL for the subsequent 19 injections. All measurements were carried out in duplicates.

The integration of the obtained isotherms was performed using NITPIC v1.2.5 [44] and the global analysis was performed using SEDPHAT v12p1b [45,46]. The fitting model in SEDPHAT was A + B to AB heteroassociation (1:1 binding model), thereby obtaining stoichiometry (*n*), apparent binding affinity (K_a) and enthalpy change (ΔH) parameters. The fitting was followed by export to GUSSI v1.3.2 to plot the processed data for publication-quality figure preparation [47].

2.9. Figures

Kinetic and thermostability graphs were prepared using OriginPro 7.5 (OriginLab Corp., Northampton, MA, USA). ITC graphs were prepared by GUSSI v1.3.2 [47]. Ligand interaction network images were prepared by MOE 2007.09 [31]. Structural images were prepared using the Visual Molecular Dynamics package [48] or the PyMOL Molecular Graphics System, Version 2.0 Schrödinger, LLC (New York, NY, USA) [49].

3. Results

3.1. Assessment of the Mg^{2+} Content of the Assay Solutions

To be able to measure the specific effects of EDTA, we needed to establish Mg^{2+}-free or low Mg^{2+} concentration conditions without the use of EDTA. Therefore, we used high purity reagents and measured the exact Mg content of our buffers with atomic spectroscopy. The high sensitivity inductively coupled plasma optical emission spectrometry yields a quantitation limit of 0.001 mg/L for any oxidation state of Mg. The Mg content of our dH_2O, dialysis buffer and dUTP nucleotide stock fell under the quantitation limit. The concentration of other divalent or trivalent metals (Mn, Ni, Co, Cr, Sr) that could potentially complement the function of Mg^{2+} fell under the quantitation limit, as well. However, the Mg content of our activity assay buffer was measured to be 0.007 ± 0.00014 mg/L (0.3 μM) despite the fact that we purchased the finest chemicals available. The smallest reported dissociation constant for the ATP:Mg^{2+} complex is 46.3 μM [50]. We considered this value to calculate the equilibrium concentration of the dUTP:Mg^{2+} complex possibly present in our reaction mixtures. As we used a range of 2–90 μM dUTP in our kinetics measurements, the calculated concentrations of the dUTP:Mg^{2+} complex were 0.02–0.4 μM in the solutions, i.e., at most 1% of the total dUTP was complexed with Mg^{2+} in our assays.

3.2. EDTA Decreases Enzyme Activity

We measured the dUTP hydrolysing activity of hDUT and mtDUT in the presence of Mg^{2+} (reported previously [20,51]) or EDTA and in the absence of both compounds (Figure 1, Table 1). In the absence of Mg^{2+}, the activity decreased to 70% and 33%, while the K_M increased with 10% (within experimental uncertainty) and 50% for hDUT and mtDUT, respectively. The relatively modest change in the kinetic parameters upon lowering the Mg^{2+} concentration close to zero was not unexpected. We previously investigated the reaction mechanism of these enzymes using transient kinetics and QM/MM methods and found that the primary role of the Mg^{2+} in this system is to enforce a coordination constraint upon the enzyme–substrate complex which drives the reaction towards the transition state [51,52]. The rate-limiting proton-transfer reaction during hydrolysis is not directly dependent on the Mg^{2+} ion and therefore, a complete abolishment of the reaction is not expected in the absence of Mg^{2+} [52]. What was unexpected, however, is that the addition of EDTA further perturbed the enzyme kinetic parameters (Figure 1, Table 1). hDUT was inhibited even by as low as 30 μM EDTA so that the K_M increased 2.7-fold. 100 μM EDTA practically abolished the activity decreasing the k_{cat} to 6%. mtDUT was adversely affected by only higher concentrations of EDTA (300 μM) increasing the K_M 3.7-fold compared to that measured in the absence of Mg^{2+} and EDTA (Table 1).

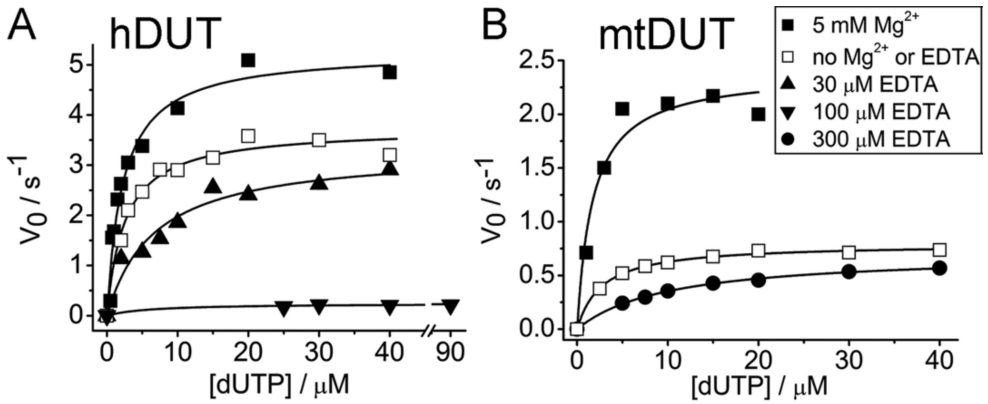

Figure 1. EDTA inhibits the enzyme activity of dUTPase. Figure shows Michaelis-Menten curves of hDUT (**A**) and mtDUT (**B**) in Mg^{2+}-saturated condition (solid square), without Mg^{2+} or EDTA (open square) and in the presence of EDTA (solid triangles and circle). K_M and k_{cat} values of the fitted datasets can be found in Table 1.

Table 1. Kinetic parameters of hDUT and mtDUT in the presence of Mg^{2+} or EDTA or in the absence of both.

	hDUT			mtDUT	
	k_{cat}/s^{-1}	$K_M/\mu M$		k_{cat}/s^{-1}	$K_M/\mu M$
5 mM Mg^{2+}, no EDTA	5.27 ± 0.24	2.26 ± 0.33	5 mM Mg^{2+}, no EDTA	2.39 ± 0.16	1.72 ± 0.51
No Mg^{2+}, no EDTA	3.71 ± 0.12	2.49 ± 0.37	No Mg^{2+}, no EDTA	0.79 ± 0.01	2.70 ± 0.18
30 μM EDTA, no Mg^{2+}	3.30 ± 0.26	6.72 ± 1.69	300 μM EDTA, no Mg^{2+}	0.71 ± 0.01	10.04 ± 0.50
100 μM EDTA, no Mg^{2+}	0.24 ± 0.03	6.16 ± 5.34			

The increase in K_M suggests competitive inhibition, meaning that EDTA competes with the ligand for the same binding site. Decreasing k_{cat} indicates non-competitive inhibition, i.e., the inhibitor binds to somewhere else other than the active site. Our results suggest that EDTA binds to the active site of both hDUT and mtDUT and it may additionally bind to other binding site(s), as well. The calculated 1–0.44% dUTP:Mg^{2+} content of the total dUTP present throughout the measured concentration range clearly does not account for the relatively high, 70% and 33% residual activity obtained for hDUT and mtDUT, respectively. Thus, these results strengthen the observations reported in [8–11] that Mg^{2+} or other divalent metal ions only increase, not enable, the hydrolytic activity of dUTPase roughly by a factor of two.

3.3. EDTA Does Not Destabilize the Enzyme

To exclude possible detrimental effects of EDTA on the structural stability of dUTPases, we measured the melting temperatures of hDUT in the presence of 5 mM $MgCl_2$, of 100 μM EDTA or in the absence of both (Figure 2, Table 2). We chose hDUT as the steady state kinetic experiments showed that EDTA has a greater effect on hDUT than on mtDUT. The thermofluor data revealed that the thermostability of the enzyme is similar in the presence and absence of EDTA (Table 2). In the presence of Mg^{2+}, the melting temperatures of the apo, dUMP and dUPNPP complexed enzymes increase with 0.9, 2.6 and 3.8 °C, respectively (Table 2). These results suggest that Mg^{2+} stabilizes the protein, especially when complexed with the substrate analogue or with the product. The results also suggest that EDTA does not have an effect on enzyme stability that could account for the largely decreased activity.

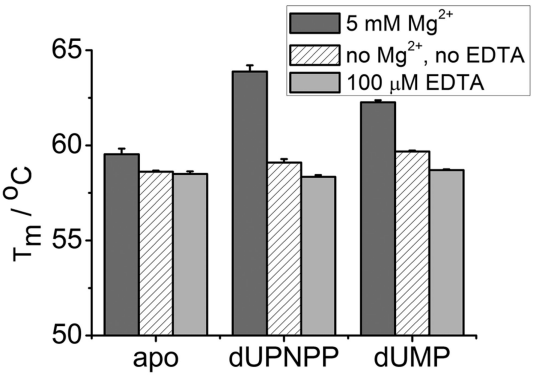

Figure 2. Melting temperatures of hDUT in the presence and absence of Mg^{2+} and EDTA. The apo enzyme and both complexes with the substrate analogue dUPNPP and the product dUMP were measured in Mg^{2+}-saturated condition (dark gray), without Mg^{2+} or EDTA (white with stripes) and in the presence of EDTA (light gray). Calculated melting temperatures can be found in Table 2.

Table 2. Melting temperatures of hDUT obtained by thermofluor assay.

	T_m (5 mM Mg^{2+})/°C	T_m (No Mg^{2+}, no EDTA)/°C	T_m (100 μM EDTA)/°C
apo	59.5 ± 0.3	58.6 ± 0.1	58.5 ± 0.1
dUPNPP	63.9 ± 0.3	59.1 ± 0.2	58.3 ± 0.1
dUMP	62.3 ± 0.1	59.7 ± 0.1	58.7 ± 0.1

3.4. Blind Docking Indicates EDTA Binding to the Surface and the Active Site of Both dUTPases

To identify potential binding sites of EDTA on the dUTPase enzyme, we chose to apply blind docking to both hDUT (PDB ID: 3EHW) and mtDUT (PDB ID: 2PY4 [20]) using the AutoDock 4.2.3 program package [38]. In these calculations, the whole protein structure is considered as potential binding surface, thus the ligand can explore distinct binding cavities and modes, as well. The blind docking calculations were performed 400 times for both EDTA and dUTP ligands. Among these runs, EDTA recognized the orthosteric binding site in hDUT and mtDUT 1 and 18 times, respectively. In the remaining cases, the surface of the protein was identified as EDTA recognition site (Figure 3). For comparison, the physiological substrate dUTP bound to the orthosteric cavity 5 and 22 times in hDUT and mtDUT, respectively. Thus, the obtained small numbers of orthosteric cavity exploration by EDTA could still represent effective binding to the active site. The difference in the number of active site bound ligands in hDUT and mtDUT might originate from the difference in their surface polarity. 16.3% and 10.1% of the protein surface is positively charged (arginine or lysine residues) in hDUT and in mtDUT, respectively. In effect, the larger basic surface in hDUT can result in more frequent binding on the surface of the protein by the negatively charged EDTA and dUTP. These results suggest that EDTA binds both to the surface and the active site of the dUTPase enzyme.

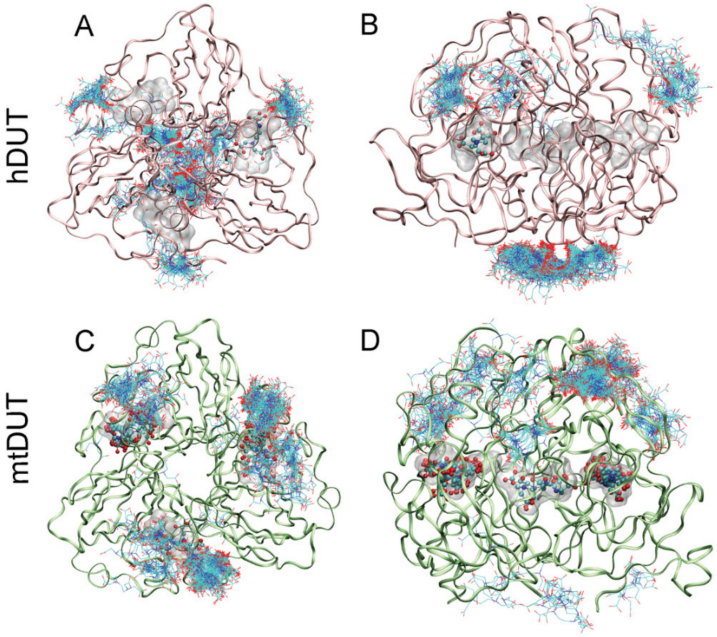

Figure 3. Blind docking of EDTA to dUTPase enzymes. Figures show all 400 docked EDTA molecules to hDUT (**A**,**B**) and mtDUT (**C**,**D**). Panels B and D show the same structure as A and C, respectively, upon rotating the protein by 90°. The active sites of dUTPases contain bound dUTP represented with the transparent space filling method (Maximal Speed Molecular Surfaces [53]). EDTA molecules bound to the active site are shown with ball and stick representation, whereas EDTA molecules bound to the surface of the enzyme are shown as only stick representation. Protein backbone is shown as pink and green ribbon for hDUT and mtDUT, respectively.

3.5. Molecular Docking Suggests That Nucleotide and EDTA Share Common Interaction Points Within the Active Site

To investigate the binding conformation of EDTA in the active site of dUTPase, we performed active site docking. For comparison, docking with the cognate ligand, dUTP, was also performed to the same protein structures. The accuracy and reliability of the docking simulation is confirmed by the low RMSD values (0.001 Å for both mtDUT and hDUT) comparing the docked dUTP to the dUPNPP within the crystal structure. The low RMSD value implies that the docking process reproduced the location and the conformation of the physiological ligand in the crystal structures. Figure 4 shows that the physiological ligand, dUTP, and EDTA explore the same space within the active site. In particular, EDTA overlaps with the phosphate chain and the sugar in both structures and in hDUT, EDTA also overlaps with the uracil ring of the physiological ligand. We also performed docking of the EDTA:Mg^{2+} complex to the dUTPase active sites and obtained ΔG_{bind} values close to zero. This implies that this complex is unlikely to productively bind to the active site and emphasizes the role of the free negative charges and/or the flexibility of EDTA in its interaction with the assayed proteins.

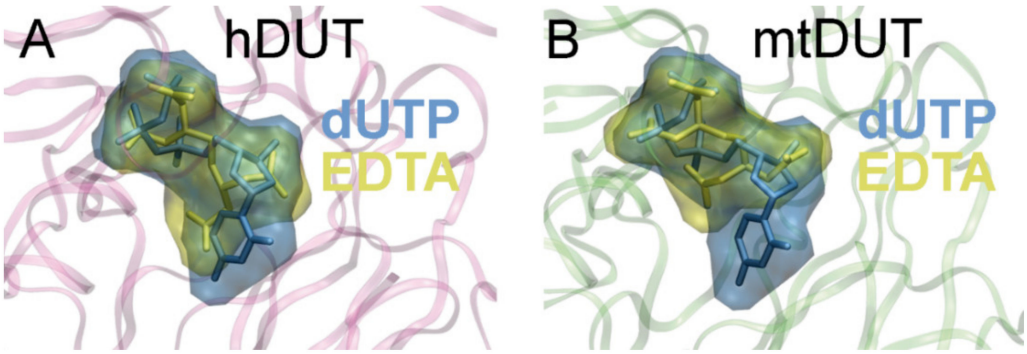

Figure 4. Molecular docking shows that EDTA occupies the same binding site in the dUTPase active site as the cognate ligand, dUTP. The Maximal Speed Molecular Surfaces [53] of dUTP (blue) and EDTA (yellow) largely overlap in both (**A**) hDUT and (**B**) mtDUT. Both ligands are also shown as stick representation besides the transparent surface representation. Protein backbone is shown as pink and green ribbon for hDUT and mtDUT, respectively.

We also mapped the secondary interactions within the enzyme-EDTA complexes and compared this interaction network to that of the enzyme:dUTP complexes (Figure 5.). The H-bonding interactions in particular are compiled in Table 3. All of the residues predicted to interact with EDTA are found in one of the five conserved motifs present in all dUTPases [6]. Arg85/64 (amino acid numbering in hDUT and mtDUT, respectively), Asp102/83 and Arg153/140 are key and conserved amino acids in the binding site and were predicted as anchor points in EDTA binding, too. These residues are responsible for the coordination of the catalytic water (Asp102/83) and of the phosphate chain [54–56]. Two important residues in binding the γ-phosphate of the nucleotide substrate, Ser160/147 and Thr161/Ser148 [56,57] were determined to be key participants in the enzyme–EDTA interaction as well. These shared anchor points suggest that EDTA binds to the same site within the enzyme active site as the physiological substrate dUTP.

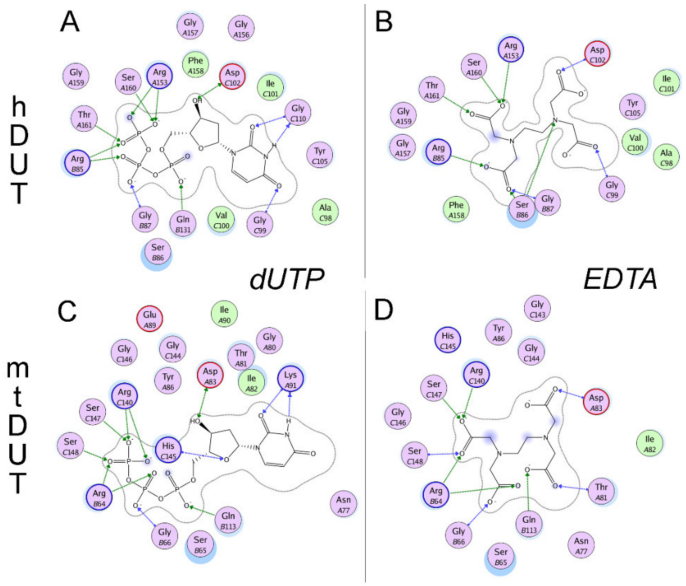

Figure 5. Comparison of the interaction networks between dUTPase:dUTP and dUTPase:EDTA complexes obtained by docking. (**A**) hDUT:dUTP complex, (**B**) hDUT:EDTA complex representing the most populated structure from active site docking, (**C**) mtDUT:dUTP complex, (**D**) mtDUT:EDTA complex representing the most populated structure from active site docking. Residues shown are within 5.4 Å from the ligand potentially interacting with it as determined by the 'Ligand interactions' algorithm [42] of MOE 2007.09 [31]. Color coding is as follows: Lilac background, polar residue; green background, apolar residue; blue border, basic residue; red border, acidic residue; blue halo, solvent accessible residues; blue smudge, solvent accessible atoms of the ligand; green arrow, H-bonds with residue side chain; blue arrow, H-bonds with residue backbone. No Mg^{2+} ions were present in this docking simulation. Ionic interactions between arginine sidechains and the phosphate chain of dUTP or the acetate part of EDTA were treated as H-bonds by the algorithm.

Table 3. H-bonding interaction points between dUTPase enzymes and EDTA or dUTP according to the active site dockings.

hDUT		**mtDUT**	
EDTA	**dUTP**	**EDTA**	**dUTP**
Arg85 (II)	Arg85 (II)	Arg64 (II)	Arg64 (II)
Ser86 (II)			
Gly87 (II)	Gly87 (II)	Gly66 (II)	Gly66 (II)
Gly99 (III)	Gly99 (III)		
		Thr81 (III)	
Asp102 (III)	Asp102 (III)	Asp83 (III)	Asp83 (III)
	Gly110 (III)		Lys91 (III)
	Gln131 (IV)	Gln113 (IV)	Gln113 (IV)
Arg153 (V)	Arg153 (V)	Arg140 (V)	Arg140 (V)
			His145 (V)
Ser160 (V)	Ser160 (V)	Ser147 (V)	Ser147 (V)
Thr161 (V)	Thr161 (V)	Ser148 (V)	Ser148 (V)

Roman numerals in parenthesis represent the adequate conserved motifs, rows represent identical positions in the 3D structure [6].

3.6. Isothermal Titration Calorimetry Data Directly Prove EDTA Binding to the Nucleotide Binding Pocket of dUTPase

We used isothermal titration calorimetry (ITC) to obtain direct proof of EDTA binding to dUTPases. Figure 6 shows titrations of the human and mycobacterial dUTPases (panels A and B, respectively) with EDTA. The titration curves indicate exothermic binding between dUTPases and EDTA in the absence of Mg^{2+} ion. The thermodynamic parameters indicate strong binding with the K_d in the nanomolar range (199 nM for hDUT, and 78 nM for mtDUT) (Table 4). As our *in silico* results indicated that EDTA binds to the active site of dUTPases, we aimed to investigate this hypothesis *in vitro*. Thus, we performed the ITC measurement using an active site mutant of dUTPase. The previously described A98F hDUT mutant excludes dUTP from its active site as the phenyl ring of the F98 residue occupies the space of the uracil ring of dUTP [19]. As shown by the docking of EDTA to hDUT in Figure 4A, the binding site of EDTA overlaps with that of the uracil ring. Therefore, we expected that EDTA binding to the A98F hDUT mutant would be compromised if EDTA binding occurs in the dUTP binding pocket. The ITC titration of A98F hDUT with EDTA clearly shows that the active site mutant hDUT lost its EDTA binding capacity (Figure 6C). Thus, we concluded that EDTA binding to dUTPase primarily occurs in the nucleotide binding pocket.

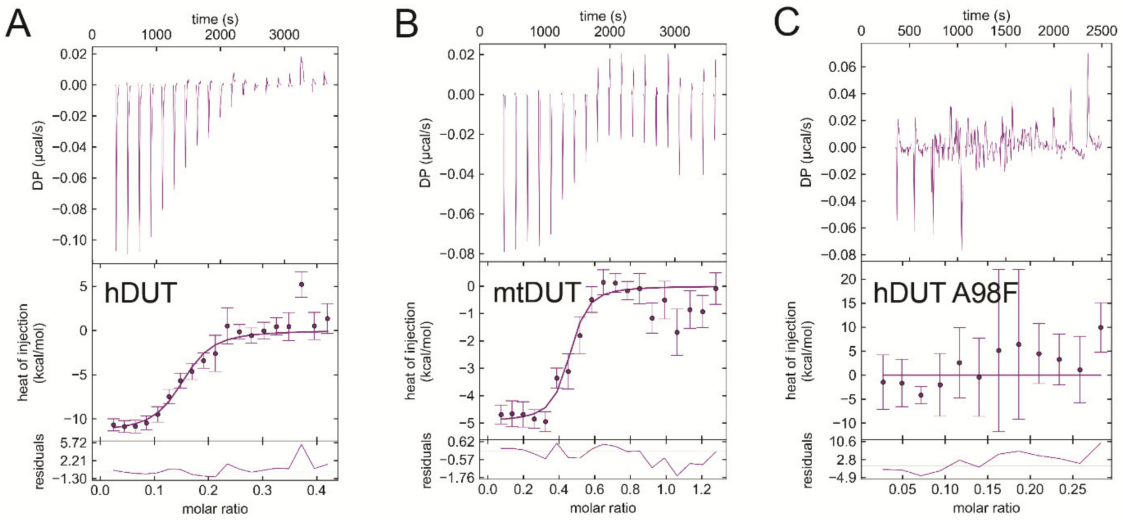

Figure 6. Isothermal titration calorimetry (ITC) titrations of wild-type and active-site mutant dUTPases with EDTA prove strong and direct EDTA binding to the active site. (**A**) hDUT titrated with EDTA. (**B**) mtDUT titrated with EDTA. (**C**) Titration of the A98F hDUT mutant with EDTA shows no binding between the molecules. Titrations were carried out at pH 7.5 and at 293 K.

Table 4. Thermodynamic parameters yielded by the analysis of the ITC measurements. K_d values are apparent dissociation constants at pH 7.5 and at 293 K. Values shown are averages and standard deviations.

Titrand	Titrant	ΔH/kcal/mol	−TΔS/kcal/mol	ΔG/kcal/mol	K_d/µM
hDUT	EDTA	−11.2 ± 0.4	2.2 ± 0.4	−9.0 ± 0.0	0.20 ± 0.009
hDUT	dUPNPP	−17.4 ± 3.6	11.5 ± 3.7	−5.9 ± 0.2	43.9 ± 14.6
mtDUT	EDTA	−4.2 ± 1.0	−5.3 ± 1.2	−9.6 ± 0.2	0.078 ± 0.023
mtDUT	dUPNPP	−4.5 ± 0.2	−2.1 ± 0.4	−6.6 ± 0.6	13.9 ± 11.7
EDTA	Mg^{2+}	4.4 ± 0.3	−12.5 ± 0.6	−8.0 ± 0.9	2.53 ± 0.18
EcMutT	EDTA	−9.7 ± 0.02	1.3 ± 0.1	−8.4 ± 0.1	0.55 ± 0.066
Taq polymerase	EDTA	-6.3 ± 0.7	−3.5 ± 0.7	−9.8 ± 0.0	0.047 ± 0.001

As a control, we titrated the dUTPases with their practically non-hydrolysable substrate analogue dUPNPP in the absence of Mg^{2+} ion. Both hDUT and mtDUT exhibited exothermic dUPNPP binding (Supplementary Figure S1A,B, respectively). The obtained K_d value for the hDUT:dUPNPP complex is 44 μM. The same titration in the presence of Mg^{2+} has previously been done yielding K_d values between 2–7 μM [7,18,51]. Taking into consideration that Mg^{2+} supports a more favorable charge distribution within the substrate-bound active site [52], the obtained one order of magnitude increase in the K_d values without Mg^{2+} is reasonable.

We also performed EDTA titrations with Mg^{2+} as a control (Figure 7A). Mg^{2+} binding to EDTA proved to be an endothermic reaction well separable from EDTA binding to dUTPases. The dissociation constant of the complex is around 3 μM confirming literature data [58]. We performed a further control measurement, where we added extra Mg^{2+} into the buffer of hDUT and then titrated with EDTA (Figure 7B). Here we observed a mixed binding curve, suggesting that the exothermic binding of EDTA to the enzyme and the endothermic binding of EDTA to Mg^{2+} take place at the same time. As this curve is much different from the EDTA-hDUT or EDTA-mtDUT binding curves (Figure 6A,B), we could rule out the possibility of measuring the binding of potential residual Mg^{2+}.

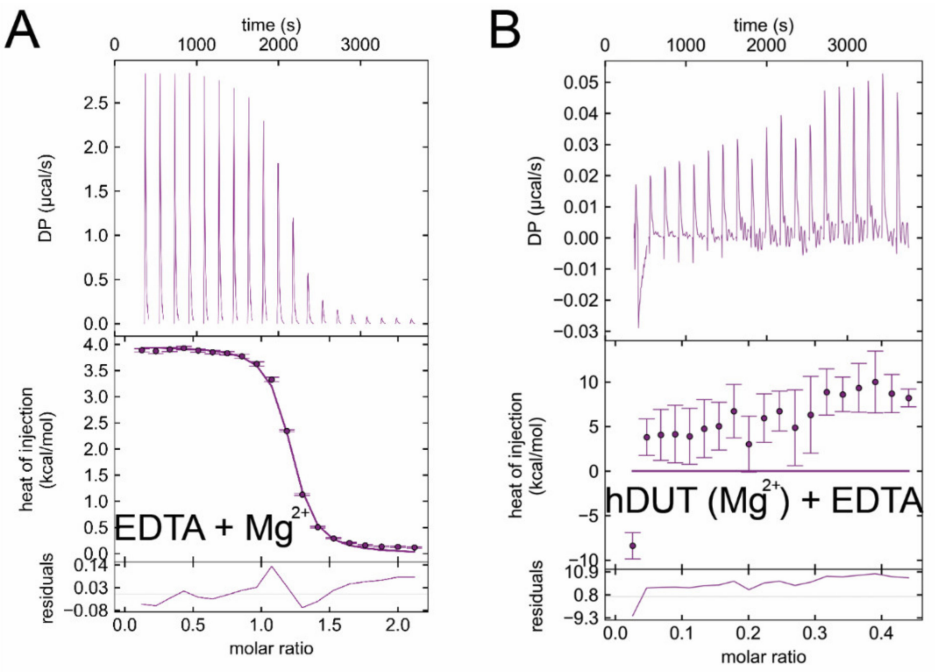

Figure 7. Control ITC measurements. (**A**) ITC titration of EDTA with $MgCl_2$. (**B**) ITC titration of hDUT with additional 5 mM $MgCl_2$ in the buffer with EDTA. Titrations were carried out at pH 7.5 and at 293 K.

3.7. EDTA Binds to Taq Polymerase and MutT, Two Additional dNTP Processing Enzymes

As EDTA occupied the dNTP binding site in both dUTPases investigated, we hypothesized that EDTA could bind other dNTP processing enzymes, as well. We selected two more enzymes, the *Escherichia coli* MutT (EcMutT) exhibiting 8-oxo-dGTPase activity [17] and the *Thermus aquaticus* DNA polymerase (Taq polymerase) [59] to test their ability to bind EDTA. Figure 8A shows the ITC curve of EcMutT and EDTA binding in the absence of Mg^{2+}. Interestingly, the interaction of EDTA with EcMutT shows similar characteristics to that with dUTPases (Table 4). It is worth mentioning that EcMutT is a promiscuous enzyme which hydrolyses other dNTPs including dGTP, dCTP, dTTP, and dUTP beside 8-oxo-dGTP [60]. The Taq polymerase exhibits the strongest measured exothermic binding to EDTA in the absence of Mg^{2+} (K_d = 47 nM, Figure 8B, Table 4). This enzyme promiscuously processes all dNTPs.

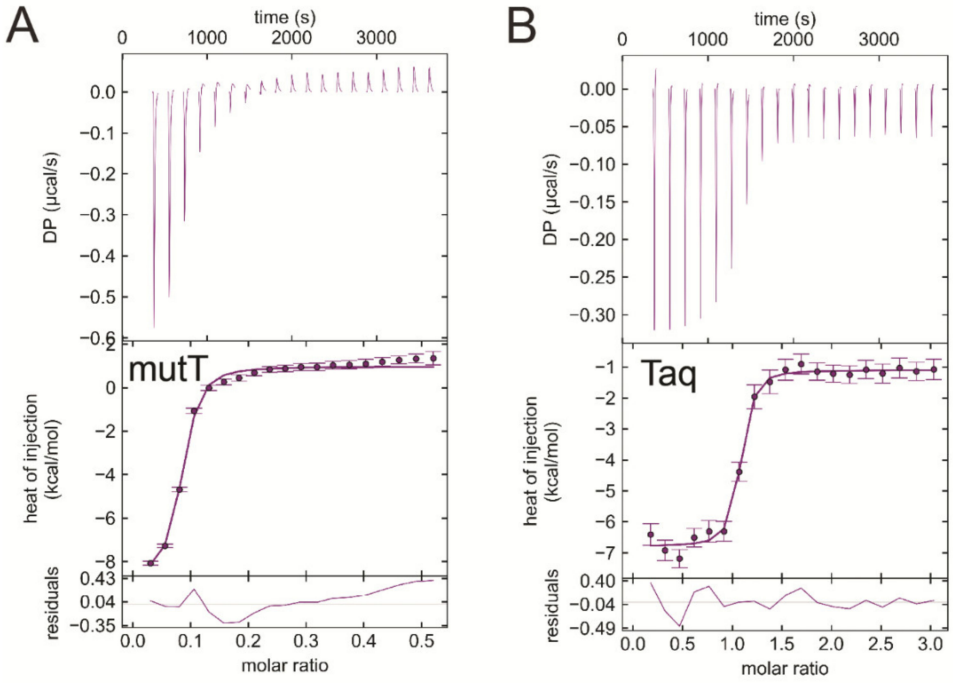

Figure 8. ITC titration of various dNTP hydrolyzing proteins with EDTA (**A**) EcMutT titration with EDTA. (**B**) *Thermus aquaticus* DNA polymerase titration with EDTA represents strong binding between the reactants. Titrations were carried out at pH 7.5 and at 293 K.

We also tested enzymes that either have an ATP binding site (skeletal myosin S1) or have no nucleotide binding site at all (uracil glycosylase inhibitor and phenylalanine ammonia-lyase). As Supplementary Figure S2 shows, these proteins not having a dNTP binding pocket do not interact with EDTA in the ITC measurements.

4. Discussion

The controversy in the literature about dUTPase activity in the absence of metal(II) ions brought our attention to a putative, novel effect of EDTA on hydrolytic activity. We show, in effect, that EDTA competes with dUTP for the active site. EDTA is commonly used in biochemical experiments to establish metal-free conditions. However, EDTA has previously been reported to exhibit inhibitory effect on various types of enzymes via partially known (competitive inhibition of human liver arginase [61], electron donor in the reactions catalyzed by veratryl alcohol oxidase [62], and horseradish peroxidase [63,64]) or unknown mechanisms (prenyltransferase MaPT [65], peptidase activity of the angiotensin-converting enzyme [66]). Furthermore, a series of ethylenediamine-based farnesyltransferase inhibitors has been developed and evaluated as antimalarial and anticancer agents [67,68]. Nevertheless, the multifactorial effect of EDTA on enzymes has not penetrated the scientific community. Now that we show potent interaction with enzymes playing key cellular roles including a DNA polymerase and DNA repair enzymes, the view of EDTA being an inert biochemical reagent will hopefully be shifted.

EDTA inhibited the Mg^{2+}-free dUTP hydrolysis activity of both dUTPases with similar mechanism but to a different degree (cf. Table 1). This observation is consistent with the results of the docking simulations and of the ITC measurements. We found that the inhibition comprises of a competitive and a non-competitive element in both dUTPases. The ITC experiments and the docking simulations showed that EDTA binds to the active site of dUTPase directly competing with the physiological substrate dUTP (Figures 4–6). EDTA assumes somewhat different conformations though in the two different active sites despite the fact that the conformations of the dUTP ligand in the two structures are identical. The analysis of the interaction network within the EDTA bound active sites of hDUT and

mtDUT also shows some differences (Table 3, Figure 5). However, the fact that EDTA exhibited strong interaction with four different dNTP hydrolyzing enzymes and no interaction with an ATPase calls our attention to enzyme residues that are responsible for the specificity of the nucleotide sugar (i.e., ribose (NTP) or 2′ deoxyribose (dNTP)). Taking a closer look at the protein environment of the C2′ atom of the bound nucleotide in all five of these enzymes (Figure 9), it is visible that the dNTP-specific enzymes (i.e., dUTPases, Taq, and MutT) sterically ensure the exclusion of the 2′OH while the NTP-specific enzyme, myosin does not. The residues shown in Figure 9 are responsible for the discrimination of the nucleotide sugars and are conserved in dUTPases [6] and in DNA polymerase I enzymes [69] and at least partially conserved in MutT (Figure S3). In the two dUTPases investigated, the same residues are involved in the interaction with EDTA (Figure 5, Ile101/82 and Tyr105/86).

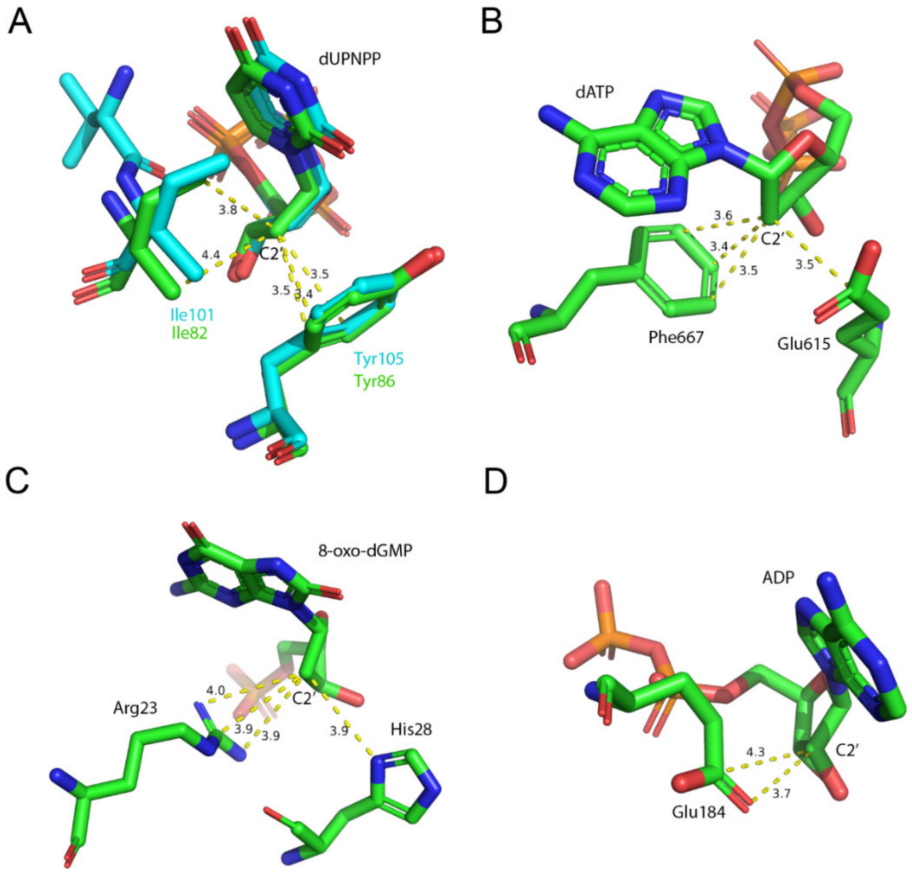

Figure 9. Molecular environment of the C2′ atom of the nucleotide within the active sites of the investigated (d)NTP hydrolyzing enzymes. Residues within 4 Å of C2′ are shown. (**A**) mtDUT (green, PDB ID: 2PY4 [20]) aligned with hDUT (cyan, PDB ID: 3EHW) both in complex with the non-hydrolysable dUTP analogue, dUPNPP. The conserved Ile and Tyr residues exclude a potential hydroxyl group on 2C′ atom. (**B**) The C2′ atom of the nucleotide within the Taq polymerse (PDB ID: 6Q4V [70]) fits in a sterically restricted environment. (**C**) *E. coli* MutT in complex with the hydrolysis product 8-oxo-dGMP (PDB ID: 3A6T [71]). A potential hydroxyl group on C2′ atom is similarly excluded as in the previous two enzymes. (**D**) Squid myosin S1 in complex with ADP (PDB ID: 3I5F [72]). The C2′ atom is sterically restricted from only one direction. The opposite side of the sugar plane faces the solvent.

The striking results showing that EDTA occupies the active site in a manner similar to the nucleotide ligand urged us to obtain EDTA complexed dUTPase crystal structures. We put much effort in crystallization trials and collected several data sets from co-crystallized and soaked crystals as well. However, we could only observe potential molecular details of the acetate groups of EDTA within the

active site of the mtDUT. After several trials, we concluded that EDTA, especially the ethylenediamine moiety might be too flexible to be observed in the crystal phase.

The interaction of EDTA with Mg^{2+} is endothermic while the interaction of EDTA with proteins proved to be exothermic. Thus, the two processes can be clearly separated from each other and any residual Mg^{2+} did not disturb the evaluation of EDTA binding to the proteins. While the EDTA:Mg^{2+} interaction is clearly driven by entropy predominantly due to the metal ion dehydration [73], EDTA binding to the proteins is more enthalpy-driven (Table 4). The relatively small entropy and larger enthalpy contribution to EDTA binding to the enzyme active sites is in accordance with our hypothesis that EDTA remains highly flexible within the active site while engaging in a significant number of secondary interactions with active site residues (Figure 5). Interestingly, the K_d vaIues of the enzyme:EDTA complexes are in the submicromolar range, 1–3 orders of magnitude lower than those of the Mg^{2+}:EDTA or the enzyme:substrate complexes (Table 4) even in the presence of Mg^{2+} (K_d of the (Mg^{2+}dNTP):enzyme complex being in the tens of micromolar range in Taq [59] and MutT [17], and in the low micromolar range in dUTPases [18,51]).

The blind docking simulations suggested that EDTA may also bind to the surface of the enzyme potentially contributing the observed non-competitive type inhibition. The most populated EDTA binding surface areas differ in hDUT and mtDUT (Figure 3). EDTA seems to preferably bind to one of the entrances of the polar central channel of hDUT (Figure 3 A–B) while it only weakly populates the corresponding apolar area in mtDUT in the docking runs (Figure 3 C–D). Considering the enzymatic mechanism, EDTA binding to the outer central channel may not have great or any effect on the enzymatic activity as this part have not shown significant conformational changes in previous studies [55,74]. On the other hand, EDTA may perturb the interaction of the C-terminal arm with the protein core as this contact surface is the first and second most populated EDTA binding site in mtDUT and hDUT, respectively, in the docking simulations (Figure 3). The intact C-terminal arm–protein core interaction is necessary for the hydrolysis to occur as this interaction provides the shielding of the active site from the solvent [52,57,74]. The differences in the predicted EDTA-protein interactions, especially at the C-terminal arm can explain the observed differences in EDTA-inhibited dUTPase activities between hDUT and mtDUT. Using wild type and active site mutant dUTPases, we have conclusively identified the binding site to be the active site in the ITC measurements (Figure 6) and could not differentiate additional binding sites. The rather non-specific binding predicted on the molecular surface is not expected to be accompanied by a large thermal effect and therefore, the docking and the ITC results do not challenge each other.

The presented results call attention to the possibility that EDTA may be a binding partner/inhibitor of many more dNTP hydrolyzing enzymes. In addition, previous studies have shown that removal of EDTA from buffers might not be straightforward. EDTA is often retained in the dialysis bag even though the pore size is over hundred times larger than the molecule itself and buffer changing does not improve removal efficiency either [75]. Moreover, EDTA was reported to bind to both strong and weak anion exchange resins and to be only eluted at 240 mM NaCl, leading to 10-200 fold enrichment of EDTA in the elute compared to the initial solution [76,77]. Therefore, the common unsuspecting use of EDTA as a metal chelator during enzyme preparation procedures may introduce unwanted effects and misinterpretation of enzyme activity results.

5. Conclusions

In conclusion, we found that EDTA is able to occupy the conserved dNTP binding sites in two dUTPases and potently binds to Taq polymerase and MutT, as well, while not interacting with the myosin ATPase. Our results together with the cited literature call attention to the fact that EDTA has multifactorial effects on several enzymes and therefore, the rethinking of the use of EDTA in enzymatic experiments is necessary. Considering that the chemical synthesis of substituted ethylenediamines is relatively straightforward, we propose that ethylenediamine-based inhibitors could be developed

against DNA polymerases, various DNA repair and other nucleotide hydrolyzing enzymes for use in molecular biology experiments.

Supplementary Materials: The following are available online at http://www.mdpi.com/2218-273X/9/10/621/s1, Figure S1: ITC titrations with dUTPases and dUPNPP confirm the functionality of the enzyme, Figure S2: ITC titrations show the lack of binding between EDTA and *Staphylococcus aureus* uracil glycosylase inhibitor, *Petroselinum crispum* phenylalanine ammonia-lyase and rabbit myosin subfragment 1, Figure S3: The alignment of MutT protein sequences indicate that the residues involved in 2′ deoxyribose exclusion from the active site are conserved amongst the above species.

Author Contributions: A.L. and E.T. performed the biochemical assays. A.L. and B.J. carried out the docking simulations. É.V.S. performed the ITC measurements. L.B. performed the ICP-OES measurement. I.L. and Á.Á.B. performed crystallography. B.V., B.G.V. and J.T supervised the experiments. A.L., B.J., É.V.S., and J.T. wrote the manuscript. All authors read and commented on the paper.

Funding: This work was supported by the National Research, Development and Innovation Office [K115993, FK124527, K119493, NVKP_16-1-2016-0020, 2017-1.3.1-VKE-2017-00002, 2017-1.3.1-VKE-2017-00013, VEKOP-2.3.2-16-2017-00013 to BGV, NKP-2018-1.2.1-NKP-2018-00005] and by the BME-Biotechnology FIKP grant (BME FIKP-BIO) of the Ministry of Human Capacities. AL was awarded the 'Students for science' grant of the Sándor Wekerle Foundation. BV thanks for the financial support for the European Union and the Hungarian State, co-financed by the European Regional Development Fund in the framework of the GINOP-2.3.4-15-2016-00004 project, aimed to promote the cooperation between the higher education and the industry. JT is the recipient of the János Bolyai Research Scholarship of the Hungarian Academy of Sciences. Funding for open access charge: Hungarian Scientific Research Funds.

Acknowledgments: The authors thank M. Lábadi for technical support at the HPC Centre of the University of Szeged and Daumantas Matulis for the advice on the melting temperature measurement.

Conflicts of Interest: The authors declare no conflict of interest. The funders had no role in the design of the study; in the collection, analyses, or interpretation of data; in the writing of the manuscript, or in the decision to publish the results.

References

1. Jorgensen, P.L.; Håkansson, K.O.; Karlish, S.J.D. Structure and Mechanism of Na, K-ATPase: Functional Sites and Their Interactions. *Annu. Rev. Physiol.* **2003**, *65*, 817–849. [CrossRef] [PubMed]
2. Sprang, S.R. G Protein Mechanisms: Insights from Structural Analysis. *Annu. Rev. Biochem.* **1997**, *66*, 639–678. [CrossRef] [PubMed]
3. Tomkinson, A.E.; Vijayakumar, S.; Pascal, J.M.; Ellenberger, T. DNA Ligases: Structure, Reaction Mechanism, and Function. *Chem. Rev.* **2006**, *106*, 687–699. [CrossRef] [PubMed]
4. Rothwell, P.J.; Waksman, G. Structure and mechanism of DNA polymerases. *Advances Protein Chem.* **2005**, *71*, 401–440. [PubMed]
5. Mildvan, A.S.; Xia, Z.; Azurmendi, H.F.; Saraswat, V.; Legler, P.M.; Massiah, M.A.; Gabelli, S.B.; Bianchet, M.A.; Kang, L.-W.; Amzel, L.M. Structures and mechanisms of Nudix hydrolases. *Arch. Biochem. Biophys.* **2005**, *433*, 129–143. [CrossRef] [PubMed]
6. Vértessy, B.G.; Tóth, J. Keeping uracil out of DNA: physiological role, structure and catalytic mechanism of dUTPases. *Acc. Chem. Res.* **2009**, *42*, 97–106. [CrossRef]
7. Pecsi, I.; Leveles, I.; Harmat, V.; Vertessy, B.G.; Toth, J. Aromatic stacking between nucleobase and enzyme promotes phosphate ester hydrolysis in dUTPase. *Nucleic Acids Res.* **2010**, *38*, 7179–7186. [CrossRef]
8. Mol, C.D.; Harris, J.M.; McIntosh, E.M.; Tainer, J.A. Human dUTP pyrophosphatase: uracil recognition by a beta hairpin and active sites formed by three separate subunits. *Structure* **1996**, *4*, 1077–1092. [CrossRef]
9. Kovári, J.; Barabás, O.; Takács, E.; Békési, A.; Dubrovay, Z.; Pongrácz, V.; Zagyva, I.; Imre, T.; Szabó, P.; Vértessy, B.G. Altered Active Site Flexibility and a Structural Metal-binding Site in Eukaryotic dUTPase. *J. Biol. Chem.* **2004**, *279*, 17932–17944. [CrossRef]
10. Freeman, L.; Buisson, M.; Tarbouriech, N.; Van der Heyden, A.; Labbé, P.; Burmeister, W.P. The Flexible Motif V of Epstein-Barr Virus Deoxyuridine 5′-Triphosphate Pyrophosphatase Is Essential for Catalysis. *J. Biol. Chem.* **2009**, *284*, 25280–25289. [CrossRef]
11. Mustafi, D.; Bekesi, A.; Vertessy, B.G.; Makinen, M.W. Catalytic and structural role of the metal ion in dUTP pyrophosphatase. *Proc. Natl. Acad. Sci. USA* **2003**, *100*, 5670–5675. [CrossRef]

12. Kovári, J.; Barabás, O.; Varga, B.; Békési, A.; Tölgyesi, F.; Fidy, J.; Nagy, J.; Vértessy, B.G. Methylene substitution at the α–β bridging position within the phosphate chain of dUDP profoundly perturbs ligand accommodation into the dUTPase active site. *Proteins Struct. Funct. Bioinforma.* **2008**, *71*, 308–319. [CrossRef] [PubMed]
13. Nord, J.; Larsson, G.; Kvassman, J.O.; Rosengren, A.M.; Nyman, P.O. dUTPase from the retrovirus equine infectious anemia virus: specificity, turnover and inhibition. *FEBS Lett.* **1997**, *414*, 271–274. [PubMed]
14. Larsson, G.; Nyman, P.O.; Kvassman, J.O. Kinetic characterization of dUTPase from Escherichia coli. *J. Biol. Chem.* **1996**, *271*, 24010–24016. [CrossRef] [PubMed]
15. Oliveros, M.; García-Escudero, R.; Alejo, A.; Viñuela, E.; Salas, M.L.; Salas, J. African swine fever virus dUTPase is a highly specific enzyme required for efficient replication in swine macrophages. *J. Virol.* **1999**, *73*, 8934–8943. [PubMed]
16. Nagy, G.N.; Leveles, I.; Vértessy, B.G. Preventive DNA repair by sanitizing the cellular (deoxy)nucleoside triphosphate pool. *FEBS J.* **2014**, *281*, 4207–4223. [CrossRef] [PubMed]
17. Sang, P.B.; Varshney, U. Biochemical Properties of MutT2 Proteins from Mycobacterium tuberculosis and M. smegmatis and Their Contrasting Antimutator Roles in Escherichia coli. *J. Bacteriol.* **2013**, *195*, 1552–1560. [CrossRef] [PubMed]
18. Varga, B.; Barabás, O.; Kovári, J.; Tóth, J.; Hunyadi-Gulyás, E.; Klement, E.; Medzihradszky, K.F.; Tölgyesi, F.; Fidy, J.; Vértessy, B.G. Active site closure facilitates juxtaposition of reactant atoms for initiation of catalysis by human dUTPase. *FEBS Lett.* **2007**, *581*, 4783–4788. [CrossRef]
19. Szabó, J.E.; Takács, E.; Merényi, G.; Vértessy, B.G.; Tóth, J. Trading in cooperativity for specificity to maintain uracil-free DNA. *Sci. Rep.* **2016**, *6*, 24219. [CrossRef]
20. Varga, B.; Barabás, O.; Takács, E.; Nagy, N.; Nagy, P.; Vértessy, B.G. Active site of mycobacterial dUTPase: structural characteristics and a built-in sensor. *Biochem. Biophys. Res. Commun.* **2008**, *373*, 8–13. [CrossRef]
21. Papp-Kádár, V.; Balázs, Z.; Vékey, K.; Ozohanics, O.; Vértessy, B.G. Mass spectrometry-based analysis of macromolecular complexes of Staphylococcus aureus uracil-DNA glycosylase and its inhibitor reveals specific variations due to naturally occurring mutations. *FEBS Open Bio* **2019**, *9*, 420–427. [PubMed]
22. Bartha-Vári, J.H.; Toşa, M.I.; Irimie, F.-D.; Weiser, D.; Boros, Z.; Vértessy, B.G.; Paizs, C.; Poppe, L. Immobilization of Phenylalanine Ammonia-Lyase on Single-Walled Carbon Nanotubes for Stereoselective Biotransformations in Batch and Continuous-Flow Modes. *ChemCatChem* **2015**, *7*, 1122–1128. [CrossRef] [PubMed]
23. Papp-Kádár, V.; Balázs, Z.; Nagy, G.N.; Juhász, T.; Liliom, K.; Vértessy, B.G. Functional analysis on a naturally occurring variant of the Staphylococcus Aureus uracil DNA Glycosylase inhibitor. *Period. Polytech. Chem. Eng.* **2018**, *62*, 51–56. [CrossRef]
24. Bata, Z.; Qian, R.; Roller, A.; Horak, J.; Bencze, L.C.; Paizs, C.; Hammerschmidt, F.; Vértessy, B.G.; Poppe, L. A Methylidene Group in the Phosphonic Acid Analogue of Phenylalanine Reverses the Enantiopreference of Binding to Phenylalanine Ammonia-Lyases. *Adv. Synth. Catal.* **2017**, *359*, 2109–2120. [CrossRef]
25. Takács, B.; Billington, N.; Gyimesi, M.; Kintses, B.; Málnási-Csizmadia, A.; Knight, P.J.; Kovács, M. Myosin complexed with ADP and blebbistatin reversibly adopts a conformation resembling the start point of the working stroke. *Proc. Natl. Acad. Sci. USA* **2010**, *107*, 6799–6804. [CrossRef]
26. Szabó, J.E.; Németh, V.; Papp-Kádár, V.; Nyíri, K.; Leveles, I.; Bendes, A.Á.; Zagyva, I.; Róna, G.; Pálinkás, H.L.; Besztercei, B.; et al. Highly potent dUTPase inhibition by a bacterial repressor protein reveals a novel mechanism for gene expression control. *Nucleic Acids Res.* **2014**, *42*, 11912–11920. [CrossRef]
27. Li, H.; Robertson, A.D.; Jensen, J.H. Very fast empirical prediction and rationalization of protein pKa values. *Proteins Struct. Funct. Bioinforma.* **2005**, *61*, 704–721. [CrossRef]
28. Bas, D.C.; Rogers, D.M.; Jensen, J.H. Very fast prediction and rationalization of pKa values for protein-ligand complexes. *Proteins* **2008**, *73*, 765–783. [CrossRef]
29. Dolinsky, T.J.; Nielsen, J.E.; McCammon, J.A.; Baker, N.A. PDB2PQR: an automated pipeline for the setup of Poisson-Boltzmann electrostatics calculations. *Nucleic Acids Res.* **2004**, *32*, W665–W667. [CrossRef]
30. Cherrier, M.V.; Martin, L.; Cavazza, C.; Jacquamet, L.; Lemaire, D.; Gaillard, J.; Fontecilla-Camps, J.C. Crystallographic and spectroscopic evidence for high affinity binding of FeEDTA(H2O)- to the periplasmic nickel transporter NikA. *J. Am. Chem. Soc.* **2005**, *127*, 10075–10082. [CrossRef]

31. Chemical Computing Group Inc. MOE (The Molecular Operating Environment) Version 2007.09, software available from Chemical Computing Group Inc., 1010 Sherbrooke Street West, Suite 910, Montreal, Canada H3A 2R7. 2007. Available online: http://www.chemcomp.com (accessed on 1 May 2013).
32. Halgren, T.A. Merck molecular force field. I. Basis, form, scope, parameterization, and performance of MMFF94. *J. Comput. Chem.* **1996**, *17*, 490–519. [CrossRef]
33. Halgren, T.A. Merck molecular force field. II. MMFF94 van der Waals and electrostatic parameters for intermolecular interactions. *J. Comput. Chem.* **1996**, *17*, 520–552. [CrossRef]
34. Halgren, T.A. Merck molecular force field. III. Molecular geometries and vibrational frequencies for MMFF94. *J. Comput. Chem.* **1996**, *17*, 553–586. [CrossRef]
35. Halgren, T.A.; Nachbar, R.B. Merck molecular force field. IV. conformational energies and geometries for MMFF94. *J. Comput. Chem.* **1996**, *17*, 587–615. [CrossRef]
36. Halgren, T.A. Merck molecular force field. V. Extension of MMFF94 using experimental data, additional computational data, and empirical rules. *J. Comput. Chem.* **1996**, *17*, 616–641. [CrossRef]
37. Gasteiger, J.; Marsili, M. Iterative partial equalization of orbital electronegativity—a rapid access to atomic charges. *Tetrahedron* **1980**, *36*, 3219–3228. [CrossRef]
38. Morris, G.M.; Huey, R.; Lindstrom, W.; Sanner, M.F.; Belew, R.K.; Goodsell, D.S.; Olson, A.J. AutoDock4 and AutoDockTools4: Automated docking with selective receptor flexibility. *J. Comput. Chem.* **2009**, *30*, 2785–2791. [CrossRef] [PubMed]
39. Morris, G.M.; Goodsell, D.S.; Halliday, R.S.; Huey, R.; Hart, W.E.; Belew, R.K.; Olson, A.J. Automated docking using a Lamarckian genetic algorithm and an empirical binding free energy function. *J. Comput. Chem.* **1998**, *19*, 1639–1662. [CrossRef]
40. Hetényi, C.; van der Spoel, D. Efficient docking of peptides to proteins without prior knowledge of the binding site. *Protein Sci.* **2002**, *11*, 1729–1737. [CrossRef]
41. Hetényi, C.; van der Spoel, D. Blind docking of drug-sized compounds to proteins with up to a thousand residues. *FEBS Lett.* **2006**, *580*, 1447–1450. [CrossRef]
42. Clark, A.M.; Labute, P. 2D depiction of protein-ligand complexes. *J. Chem. Inf. Model.* **2007**, *47*, 1933–1944. [CrossRef] [PubMed]
43. Róna, G.; Marfori, M.; Borsos, M.; Scheer, I.; Takács, E.; Tóth, J.; Babos, F.; Magyar, A.; Erdei, A.; Bozóky, Z.; et al. Phosphorylation adjacent to the nuclear localization signal of human dUTPase abolishes nuclear import: structural and mechanistic insights. *Acta Crystallogr. D. Biol. Crystallogr.* **2013**, *69*, 2495–2505. [CrossRef] [PubMed]
44. Keller, S.; Vargas, C.; Zhao, H.; Piszczek, G.; Brautigam, C.A.; Schuck, P. High-precision isothermal titration calorimetry with automated peak-shape analysis. *Anal. Chem.* **2012**, *84*, 5066–5073. [CrossRef] [PubMed]
45. Zhao, H.; Piszczek, G.; Schuck, P. SEDPHAT—A platform for global ITC analysis and global multi-method analysis of molecular interactions. *Methods* **2015**, *76*, 137–148. [CrossRef] [PubMed]
46. Brautigam, C.A.; Zhao, H.; Vargas, C.; Keller, S.; Schuck, P. Integration and global analysis of isothermal titration calorimetry data for studying macromolecular interactions. *Nat. Protoc.* **2016**, *11*, 882–894. [CrossRef] [PubMed]
47. Brautigam, C.A. Calculations and Publication-Quality Illustrations for Analytical Ultracentrifugation Data. *Methods Enzymol.* **2015**, *562*, 109–133. [PubMed]
48. Humphrey, W.; Dalke, A.; Schulten, K. VMD: visual molecular dynamics. *J. Mol. Graph.* **1996**, *14*, 33–38. [CrossRef]
49. Schrödinger LLC. The PyMOL Molecular Graphics System, Version 1.2r3pre. Available online: http://www.schrodinger.com/pymol (accessed on 19 October 2018).
50. Zhang, W.; Truttmann, A.C.; Lüthi, D.; McGuigan, J.A. Apparent Mg2+-adenosine 5-triphosphate dissociation constant measured with Mg2+ macroelectrodes under conditions pertinent to 31P NMR ionized magnesium determinations. *Anal. Biochem.* **1997**, *251*, 246–250. [CrossRef]
51. Tóth, J.; Varga, B.; Kovács, M.; Málnási-Csizmadia, A.; Vértessy, B.G. Kinetic Mechanism of Human dUTPase, an Essential Nucleotide Pyrophosphatase Enzyme. *J. Biol. Chem.* **2007**, *282*, 33572–33582. [CrossRef]
52. Lopata, A.; Jambrina, P.G.; Sharma, P.K.; Brooks, B.R.; Toth, J.; Vertessy, B.G.; Rosta, E. Mutations Decouple Proton Transfer from Phosphate Cleavage in the dUTPase Catalytic Reaction. *ACS Catal.* **2015**, *5*, 3225–3237. [CrossRef]

53. Sanner, M.F.; Olson, A.J.; Spehner, J.C. Reduced surface: An efficient way to compute molecular surfaces. *Biopolymers* **1996**, *38*, 305–320. [CrossRef]
54. Barabás, O.; Pongrácz, V.; Kovári, J.; Wilmanns, M.; Vértessy, B.G. Structural insights into the catalytic mechanism of phosphate ester hydrolysis by dUTPase. *J. Biol. Chem.* **2004**, *279*, 42907–42915. [CrossRef] [PubMed]
55. Barabás, O.; Németh, V.; Bodor, A.; Perczel, A.; Rosta, E.; Kele, Z.; Zagyva, I.; Szabadka, Z.; Grolmusz, V.I.; Wilmanns, M.; et al. Catalytic mechanism of α-phosphate attack in dUTPase is revealed by X-ray crystallographic snapshots of distinct intermediates, 31P-NMR spectroscopy and reaction path modelling. *Nucleic Acids Res.* **2013**, *41*, 10542–10555. [CrossRef] [PubMed]
56. Hirmondo, R.; Lopata, A.; Suranyi, E.V.; Vertessy, B.G.; Toth, J. Differential control of dNTP biosynthesis and genome integrity maintenance by the dUTPase superfamily enzymes. *Sci. Rep.* **2017**, *7*, 6043. [CrossRef] [PubMed]
57. Pecsi, I.; Szabo, J.E.; Adams, S.D.; Simon, I.; Sellers, J.R.; Vertessy, B.G.; Toth, J. Nucleotide pyrophosphatase employs a P-loop-like motif to enhance catalytic power and NDP/NTP discrimination. *Proc. Natl. Acad. Sci.* **2011**, *108*, 14437–14442. [CrossRef] [PubMed]
58. O'Brien, L.C.; Root, H.B.; Wei, C.-C.; Jensen, D.; Shabestary, N.; De Meo, C.; Eder, D.J. M2+ •EDTA Binding Affinities: A Modern Experiment in Thermodynamics for the Physical Chemistry Laboratory. *J. Chem. Educ.* **2015**, *92*, 1547–1551. [CrossRef]
59. Brandis, J.W.; Edwards, S.G.; Johnson, K.A. Slow rate of phosphodiester bond formation accounts for the strong bias that Taq DNA polymerase shows against 2',3'-dideoxynucleotide terminators. *Biochemistry* **1996**, *35*, 2189–2200. [CrossRef] [PubMed]
60. Maki, H.; Sekiguchi, M. MutT protein specifically hydrolyses a potent mutagenic substrate for DNA synthesis. *Lett. Nat.* **1992**, *355*, 273–275. [CrossRef]
61. Carvajal, N.; Orellana, M.S.; Bórquez, J.; Uribe, E.; López, V.; Salas, M. Non-chelating inhibition of the H101N variant of human liver arginase by EDTA. *J. Inorg. Biochem.* **2004**, *98*, 1465–1469. [CrossRef]
62. Shah, M.; Grover, T.; Barr, D.; Aust, S. On the mechanism of inhibition of the veratryl alcohol oxidase activity of lignin peroxidase H2 by EDTA. *J. Biol. Chem.* **1992**, *267*, 21564–21569.
63. Banerjee, R.K. EDTA inhibits peroxidase-catalyzed iodide oxidation through interaction at the iodide binding site. *Biochim. Biophys. Acta - Gen. Subj.* **1989**, *992*, 393–396. [CrossRef]
64. Bhattacharyya, D.K.; Adak, S.; Bandyopadhyay, U.; Banerjee, R.K. Mechanism of inhibition of horseradish peroxidase-catalysed iodide oxidation by EDTA. *Biochem. J.* **1994**, *298 (Pt 2*, 281–288. [CrossRef]
65. Ding, Y.; Williams, R.M.; Sherman, D.H. Molecular analysis of a 4-dimethylallyltryptophan synthase from Malbranchea aurantiaca. *J. Biol. Chem.* **2008**, *283*, 16068–16076. [CrossRef]
66. Kondoh, G.; Tojo, H.; Nakatani, Y.; Komazawa, N.; Murata, C.; Yamagata, K.; Maeda, Y.; Kinoshita, T.; Okabe, M.; Taguchi, R.; et al. Angiotensin-converting enzyme is a GPI-anchored protein releasing factor crucial for fertilization. *Nat. Med.* **2005**, *11*, 160–166. [CrossRef] [PubMed]
67. Hast, M.A.; Fletcher, S.; Cummings, C.G.; Pusateri, E.E.; Blaskovich, M.A.; Rivas, K.; Gelb, M.H.; Van Voorhis, W.C.; Sebti, S.M.; Hamilton, A.D.; et al. Structural basis for binding and selectivity of antimalarial and anticancer ethylenediamine inhibitors to protein farnesyltransferase. *Chem. Biol.* **2009**, *16*, 181–192. [CrossRef] [PubMed]
68. Fletcher, S.; Keaney, E.P.; Cummings, C.G.; Blaskovich, M.A.; Hast, M.A.; Glenn, M.P.; Chang, S.-Y.; Bucher, C.J.; Floyd, R.J.; Katt, W.P.; et al. Structure-based design and synthesis of potent, ethylenediamine-based, mammalian farnesyltransferase inhibitors as anticancer agents. *J. Med. Chem.* **2010**, *53*, 6867–6888. [CrossRef] [PubMed]
69. Delarue, M.; Poch, O.; Tordo, N.; Moras, D.; Argos, P. An attempt to unify the structure of polymerases. *Protein Eng.* **1990**, *3*, 461–467. [CrossRef] [PubMed]
70. Kropp, H.M.; Diederichs, K.; Marx, A. The Structure of an Archaeal B-Family DNA Polymerase in Complex with a Chemically Modified Nucleotide. *Angew. Chem. Int. Ed. Engl.* **2019**, *58*, 5457–5461. [CrossRef] [PubMed]
71. Nakamura, T.; Meshitsuka, S.; Kitagawa, S.; Abe, N.; Yamada, J.; Ishino, T.; Nakano, H.; Tsuzuki, T.; Doi, T.; Kobayashi, Y.; et al. Structural and dynamic features of the MutT protein in the recognition of nucleotides with the mutagenic 8-oxoguanine base. *J. Biol. Chem.* **2010**, *285*, 444–452. [CrossRef]

72. Yang, Y.; Gourinath, S.; Kovács, M.; Nyitray, L.; Reutzel, R.; Himmel, D.M.; O'Neall-Hennessey, E.; Reshetnikova, L.; Szent-Györgyi, A.G.; Brown, J.H.; et al. Rigor-like structures from muscle myosins reveal key mechanical elements in the transduction pathways of this allosteric motor. *Structure* **2007**, *15*, 553–564. [CrossRef]
73. Moeschler, H.J.; Schaer, J.J.; Cox, J.A. A thermodynamic analysis of the binding of calcium and magnesium ions to parvalbumin. *Eur. J. Biochem.* **1980**, *111*, 73–78. [CrossRef] [PubMed]
74. Lopata, A.; Leveles, I.; Bendes, Á.Á.; Viskolcz, B.; Vértessy, B.G.; Jójárt, B.; Tóth, J. A Hidden Active Site in the Potential Drug Target Mycobacterium tuberculosis dUTPase Is Accessible through Small Amplitude Protein Conformational Changes. *J. Biol. Chem.* **2016**, *291*, 26320–26331. [CrossRef] [PubMed]
75. Mónico, A.; Martínez-Senra, E.; Cañada, F.J.; Zorrilla, S.; Pérez-Sala, D. Drawbacks of Dialysis Procedures for Removal of EDTA. *PLoS ONE* **2017**, *12*, e0169843. [CrossRef] [PubMed]
76. Sharpe, J.C.; London, E. Inadvertent Concentrating of EDTA by Ion Exchange Chromatography: Avoiding Artifacts That Can Interfere with Protein Purification. *Anal. Biochem.* **1997**, *250*, 124–125. [CrossRef]
77. Chumanov, R.S.; Burgess, R.R. Artifact-inducing enrichment of ethylenediaminetetraacetic acid and ethyleneglycoltetraacetic acid on anion exchange resins. *Anal. Biochem.* **2011**, *412*, 34–39. [CrossRef]

© 2019 by the authors. Licensee MDPI, Basel, Switzerland. This article is an open access article distributed under the terms and conditions of the Creative Commons Attribution (CC BY) license (http://creativecommons.org/licenses/by/4.0/).

Supplementary data to

Beyond chelation: EDTA tightly binds Taq DNA polymerase, MutT and dUTPase and directly inhibits dNTPase activity

Anna Lopata[1,2], Balázs Jójárt[3], Éva V. Surányi[1,2], Enikő Takács[1], László Bezúr[4], Ibolya Leveles[1,2], Ábris Á. Bendes[1], Béla Viskolcz[5], Beáta G. Vértessy[1,2] and Judit Tóth[1,*]

[1] Institute of Enzymology, Research Centre for Natural Sciences, Hungarian Academy of Sciences, Budapest, 1113, Hungary
[2] Department of Applied Biotechnology, Budapest University of Technology and Economics, Budapest, 1111, Hungary
[3] Institute of Food Engineering, Faculty of Engineering, University of Szeged, Szeged, 6724, Hungary
[4] Department of Inorganic and Analytical Chemistry, Budapest University of Technology and Economics, Budapest, 1111, Hungary
[5] Institute of Chemistry, University of Miskolc, Miskolc, 3515, Hungary

* To whom correspondence should be addressed. toth.judit@ttk.mta.hu, Tel: +36 1 3826793

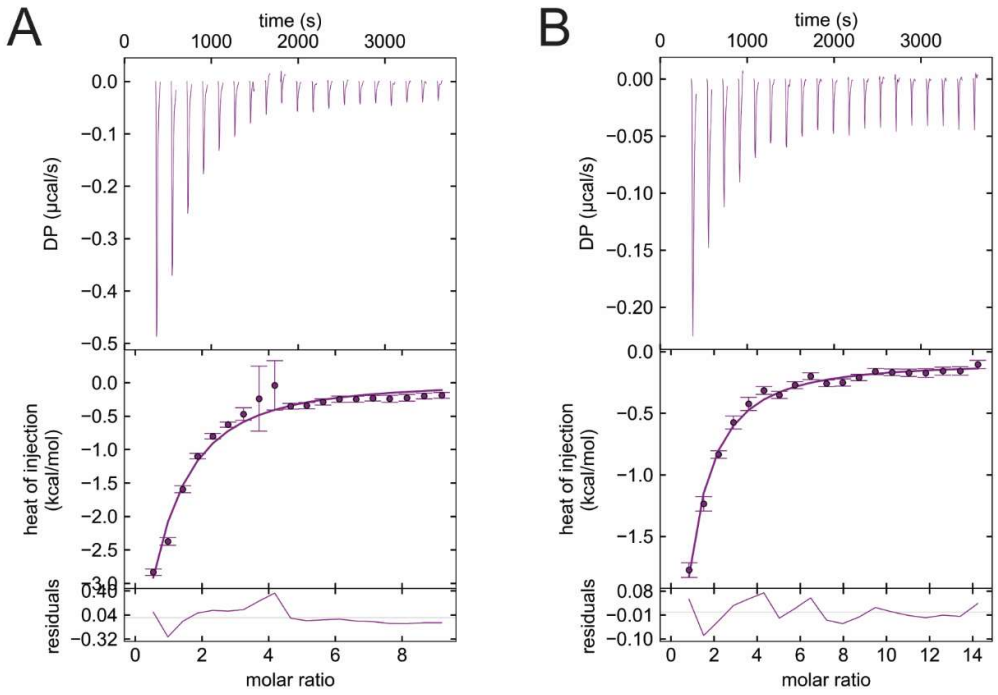

Figure S1 ITC titrations with dUTPases and dUPNPP confirm the functionality of the enzyme. A) hDUT and dUPNPP titration B) mtDUT and dUPNPP titration represent the binding between the components. Parameters of the fitting are the following: A) ΔH = –19.9 kcal/mol, $-T\Delta S$ = 14.1 kcal/mol, ΔG = –5.7 kcal/mol, K_d = 54 µM, n = 0.41; B) ΔH = –4.4 kcal/mol,
$-T\Delta S$ = –1.8 kcal/mol, ΔG = –6.2 kcal/mol, K_d = 22 µM, n = 1.

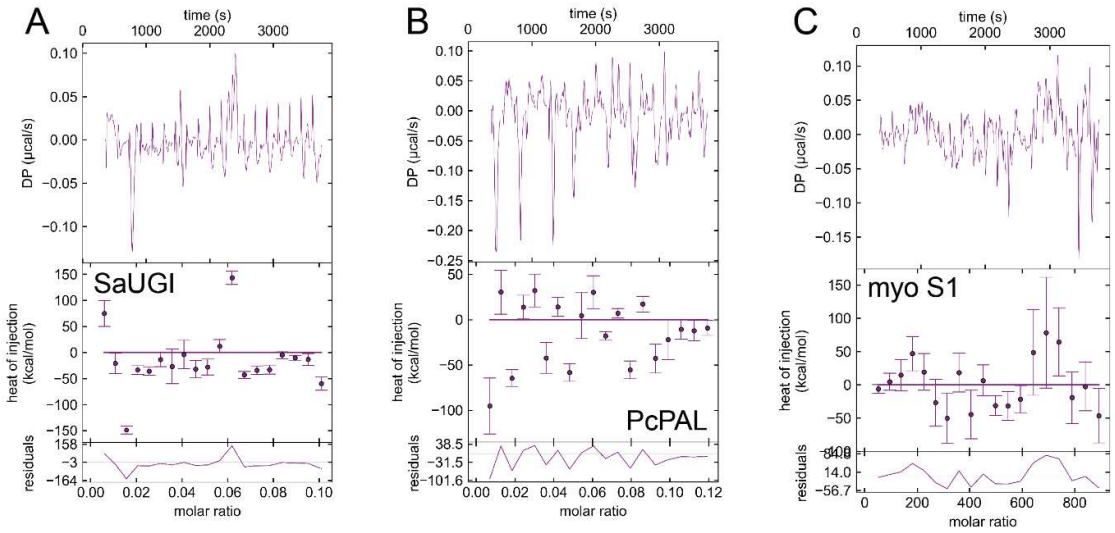

Figure S2 ITC titrations show the lack of binding between EDTA and A) *Staphylococcus aureus* uracil glycosylase inhibitor (SaUGI), B) *Petroselinum crispum* phenylalanine ammonia-lyase (PcPAL) and C) rabbit myosin subfragment 1 (myo S1).

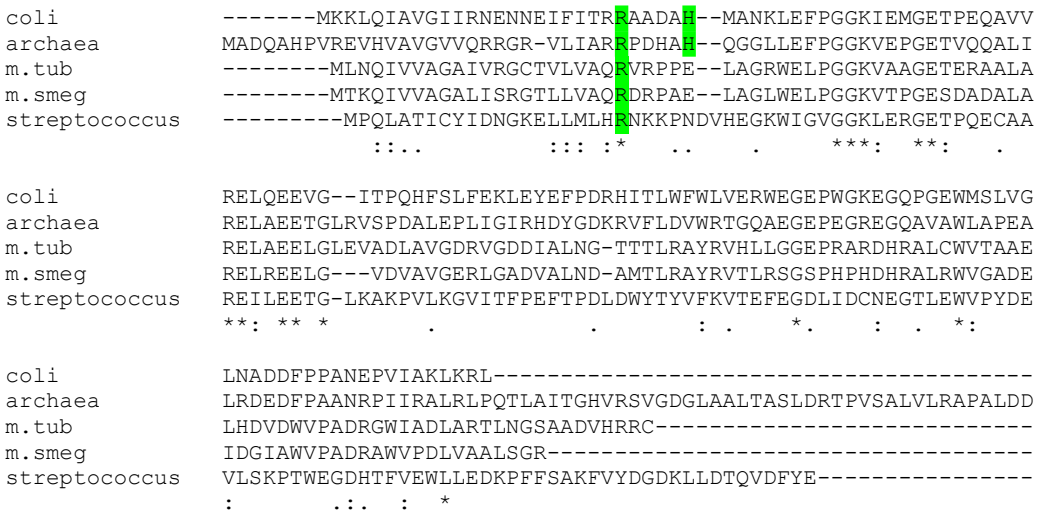

Figure S3 The alignment of MutT protein sequences indicate that the residues involved in 2' deoxyribose exclusion from the active site (green) are conserved amongst the above species. Arg23 can be found in *Escherichia coli*, *Streptococcus pneumoniae*, *Mycobacterium tuberculosis*, *Mycobacterium smegmatis* and in *Euryarchaeota archaeon*. His28 is additionally conserved in *Escherichia coli* and in *Euryarchaeota archaeon*. However no homologue residues were found in MutT proteins from *Bacillus subtilis*, *Haemophilus influenzae*, *Arabidopsis thaliana* and *Homo sapiens*. This region is not part of the conserved motif identified by Koonin 1993 NAR.

Aligned proteins:

>sp|P08337|MUTT_ECOLI 8-oxo-dGTP diphosphatase OS=Escherichia coli (strain K12) OX=83333 GN=mutT PE=1 SV=1

>sp|P41354|MUTX_STRPN 8-oxo-dGTP diphosphatase OS=Streptococcus pneumoniae serotype 4 (strain ATCC BAA-334 / TIGR4) OX=170187 GN=mutX PE=1 SV=2

>tr|A0A2E4GCL2|A0A2E4GCL2_9EURY DNA mismatch repair protein MutT OS=Euryarchaeota archaeon OX=2026739 GN=CL958_03010 PE=4 SV=1

>sp|P9WIY1|MUTT2_MYCTU Putative 8-oxo-dGTP diphosphatase 2 OS=Mycobacterium tuberculosis (strain ATCC 25618 / H37Rv) OX=83332 GN=mutT2 PE=1 SV=1

>tr|A0A0D6IWC3|A0A0D6IWC3_MYCSM Mutator protein MutT2/NUDIX hydrolase OS=Mycobacterium smegmatis OX=1772 GN=mutT2 PE=3 SV=1

OPEN ACCESS Freely available online

PLoS one

The dUTPase Enzyme Is Essential in *Mycobacterium smegmatis*

Ildiko Pecsi[1,2], Rita Hirmondo[1], Amanda C. Brown[2], Anna Lopata[1], Tanya Parish[2], Beata G. Vertessy[1,3]*, Judit Tóth[1]*

1 Institute of Enzymology, RCNS, Hungarian Academy of Sciences, Budapest, Hungary, **2** Queen Mary University of London, Barts and the London School of Medicine and Dentistry, London, United Kingdom, **3** Department of Applied Biotechnology and Food Sciences, Budapest University of Technology and Economics, Budapest, Hungary

Abstract

Thymidine biosynthesis is essential in all cells. Inhibitors of the enzymes involved in this pathway (e.g. methotrexate) are thus frequently used as cytostatics. Due to its pivotal role in mycobacterial thymidylate synthesis dUTPase, which hydrolyzes dUTP into the dTTP precursor dUMP, has been suggested as a target for new antitubercular agents. All mycobacterial genomes encode dUTPase with a mycobacteria-specific surface loop absent in the human dUTPase. Using *Mycobacterium smegmatis* as a fast growing model for *Mycobacterium tuberculosis*, we demonstrate that dUTPase knock-out results in lethality that can be reverted by complementation with wild-type dUTPase. Interestingly, a mutant dUTPase gene lacking the genus-specific loop was unable to complement the knock-out phenotype. We also show that deletion of the mycobacteria-specific loop has no major effect on dUTPase enzymatic properties *in vitro* and thus a yet to be identified loop-specific function seems to be essential within the bacterial cell context. In addition, here we demonstrated that *Mycobacterium tuberculosis* dUTPase is fully functional in *Mycobacterium smegmatis* as it rescues the lethal knock-out phenotype. Our results indicate the potential of dUTPase as a target for antitubercular drugs and identify a genus-specific surface loop on the enzyme as a selective target.

Citation: Pecsi I, Hirmondo R, Brown AC, Lopata A, Parish T, et al. (2012) The dUTPase Enzyme Is Essential in *Mycobacterium smegmatis*. PLoS ONE 7(5): e37461. doi:10.1371/journal.pone.0037461

Editor: Olivier Neyrolles, Institut de Pharmacologie et de Biologie Structurale, France

Received December 8, 2011; **Accepted** April 20, 2012; **Published** May 24, 2012

Copyright: © 2012 Pecsi et al. This is an open-access article distributed under the terms of the Creative Commons Attribution License, which permits unrestricted use, distribution, and reproduction in any medium, provided the original author and source are credited.

Funding: This work was supported by the US National Institutes of Health [grant number 1R01TW008130];, the Howard Hughes Medical Institutes [grant number 55000342]; the Hungarian Scientific Research Funds [grant numbers PD72008, CK-78646, K68229, K72973, NI68466]; the National Office for Research and Technology, Hungary [grant number JÁP_TSZ_071128_TB_INTER] and the EU FP6 [grant numbers SPINE2c LSHG-CT-2006-031220, TEACH-SG LSSG-CT-2007-037198]. JT is the recipient of the János Bolyai Research Scholarship of the Hungarian Academy of Sciences. IP is the recipient of an EMBO Short Term Fellowship and the Postgraduate Research Fellowship of Gedeon Richter Plc. Hungary. The funders had no role in study design, data collection and analysis, decision to publish, or preparation of the manuscript.

Competing Interests: The authors declare that the first author received funding from a commercial source (Gedeon Richter Plc). This does not alter the authors' adherence to all the PLoS ONE policies on sharing data and materials.

* E-mail: vertessy@enzim.hu (BGV); or tothj@enzim.hu(JT)

Introduction

Despite over a century of extensive research, tuberculosis (TB), the infectious disease caused by *Mycobacterium tuberculosis (M. tuberculosis)*, still remains a public health problem worldwide. It has been estimated that more than two billion people are latently infected with *M. tuberculosis* and a total of around eight million new cases [1,2] and 1.6 million deaths occurred in 2010 as reported by the WHO [3]. The emergence of multidrug resistant strains of *M. tuberculosis* [4] as well as the existence of extensively drug resistant TB in more than 40 countries [5] and the global spread of HIV are among the factors underlying the resurgence of TB research [6]. New drugs and second generation vaccines are required to control this deadly human pathogen [7].

An in-depth understanding of the physiological role of enzymes involved in the metabolic pathways of mycobacteria is crucial to identify good targets for rational drug design. Enzymes of the essential thymidylate metabolic pathway are frequently used as targets in anticancer and antimicrobial treatments [8]. The dUTPase enzyme has recently been proposed as a useful target in mycobacteria [9,10,11,12] and in other diseases including cancer and malaria [13,14,15,16]. dUTP is a natural intermediate in the dTTP biosynthetic pathway and is being continuously synthesized in all dividing cells (Figure 1). The enzyme dUTPase is responsible for i) keeping the cellular dUTP/dTTP ratio at a low level to restrict availability of dUTP as a DNA building block and for ii) providing the dTTP precursor dUMP [17,18,19,20].

Decrease in or lack of dUTPase activity may lead to major increase in the uracil content of DNA which resulted in chromosome fragmentation and cell death in the studied cases [21,22,23]. Importantly, in all known mycobacterium species, thymidylate biosynthesis necessarily relies on two *de novo* biosynthetic pathways both involving dUTPase action (Figure 1). In addition to the well-known monofunctional dUTPase (Rv2697c), a bifunctional dCTP deaminase/dUTPase (Rv0321) (earlier suggested to exist only in Archea [24,25]) is also encoded within the *M. tuberculosis* genome [26]. This bifunctional enzyme catalyses both the dCTP deamination reaction and the triphosphate hydrolysis of the resulting dUTP directly producing dUMP from dCTP [27] (Figure 1). Curiously, this bifunctional enzyme has only been reported in *M. tuberculosis* of all mycobacterium species so far. In contrast to mycobacteria, humans encode the dCMP deaminase and the thymidine kinase genes thus providing two alternatives for the dUTPase-mediated [9] pathway.

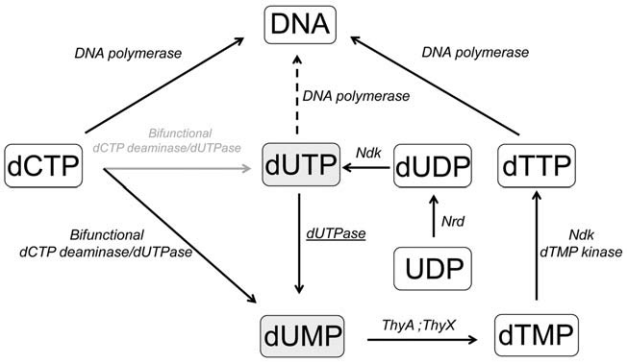

Figure 1. Key enzymes of the *de novo* thymidylate biosynthesis pathway in mycobacteria. Various enzymes present in this pathway are as follows: bifunctional deoxycytidine triphosphate deaminase/ deoxyuridine triphosphate nucleotidohydrolase (bifunctional dCTPdeaminase/ dUTPase), deoxyuridine 5′-triphosphate nucleotidohydrolase (dUTPase), nucleoside diphosphate kinase (Ndk), thymidylate kinase (dTMP kinase), thymidylate synthase (ThyA, ThyX) and ribonucleoside diphosphate reductase (Nrd). The dUTPase enzyme (underlined) converts dUTP (grey highlighted box) into dUMP (grey highlighted box) thereby provides input into dTTP synthesis and eliminates dUTP. An abnormally elevated dUTP/dTTP ratio will lead to uracil incorporation into DNA, as indicated by the dashed arrow. DNA synthesis is provided by several different polymerases (for simplicity no specific polymerases are named here).
doi:10.1371/journal.pone.0037461.g001

Previous studies have demonstrated the essentiality of the generally occurring monofunctional dUTPase (product of the *dut* gene) in *E. coli* [28] and in yeast [29,30]. High density mutagenesis studies suggested that *M. tuberculosis* requires the product of *dut* but not the bifunctional enzyme for growth [31,32]. In contrast to the thorough biochemical characterization of the *M. tuberculosis* dUTPase enzyme [10,11,12,33], no detailed information has yet been published about the physiological effect of *dut* deletion mutants in mycobacteria. We therefore directed our efforts to obtain formal genetic proof of the essentiality of dUTPase in *Mycobacterium smegmatis* (*M. smegmatis*). We assessed whether the fast growing and non-hazardous *M. smegmatis* can serve as a valid model for *M. tuberculosis* in the investigation of the thymidylate synthesis pathway and chose this organism to carry out the functional deletion of *dut*.

Although dUTPase is often proposed as a drug target [13,14], a potential problem in selective drug design against this enzyme is the high sequence and structure similarity between the human and pathogen dUTPases. Therefore, we specifically investigated a mycobacteria-specific insert both in enzymatic and phenotypic studies.

Results

M. smegmatis and M. tuberculosis share a similar set of enzymes for thymidylate metabolism as revealed by a comparative genomic approach

Comparison of the amino-acid sequences of enzymes involved in thymidylate biosynthesis (shown in Figure 1) revealed that *M. smegmatis* encodes the same enzymes as *M. tuberculosis* does (Table 1), while no homologs of human dCMP deaminase (Uniprot: P32321) or human thymidine kinase (Uniprot: P04183) were identified in these genomes. The role of dCMP deaminase and thymidine kinase in other organisms is to provide the major flux of dUMP production and thymidine salvage, respectively. Such alternative pathways do not seem to exist in mycobacteria, reinforcing the emphasis on dUTPase. In addition, a ClustalW sequence alignment of the C-termini of dUTPases from widely different species exposes a five amino acid long insert that distinguishes mycobacterial dUTPases from the human and other homologs (Figure 2A, B).

Similar Blast search and sequence comparison in the *Mycobacterium leprae*, *Mycobacterium ulcerans*, and *Mycobacterium bovis* pathogens indicated that these species also encode all known enzymes of thymidylate metabolism in mycobacteria sharing above 84% identity. Thymidylate kinase is an exception; its amino acid sequence is more variable between different species (around 66% identity).

In conclusion, we postulate that the thymidine metabolism enzymes of *M. smegmatis* are highly similar not exclusively to *M. tuberculosis*, but also to other mycobacterial pathogens.

The dCTP deaminase of M. smegmatis is presumably a bifunctional dCTP deaminase/dUTPase

A previous study demonstrated that the enzyme annotated as "dCTP deaminase" in *M. tuberculosis* functions also as a dUTPase [26]. It is most relevant for our study to examine whether *M. smegmatis* and *M. tuberculosis* encodes an identical enzyme set for dUMP production. Therefore, we carried out multiple sequence-alignments for dUTPases, putative and confirmed bifunctional dCTP deaminase/dUTPases and dCTP deaminases from various species. These sequence comparisons show that the mycobacterial enzymes annotated for dCTP deaminases contain conserved amino acid residues that are indispensable for dUTPase activity (Figure 2A). According to Helt *et al.* these residues are: Ser102, Asp119 and Gln148 (*M. tuberculosis* numbering, [26]) All of these residues are conserved in mycobacterial dCTP deaminases, dUTPases and the confirmed bifunctional dCTP deaminase/ dUTPase enzymes from *M. tuberculosis* and *Methanocaldococcus jannaschii* (Figure 2A). One of the residues indispensable for dUTP hydrolysis is Asp119, which coordinates the catalytic water molecule and interacts with the 3′-OH of the bound nucleotide in dUTPases [34]. As seen in Figure 2A, this residue is conserved in the whole superfamily. The monofunctional dCTP deaminases, however, contain a conserved Arg (Arg126 in *E. coli*) residue (outlined by pink in Figure 2A) which occupies the position of the nucleophile water molecule and forms a salt bridge with the Asp in the catalytic position (Asp128 in *E. coli* [35]). That is why dUTP hydrolysis in monofunctional dCTP deaminases cannot occur. The position of this Arg is occupied by an aromatic residue (Phe, Trp) in dUTP hydrolyzing bifunctional enzymes (Figure 2A), similarly to the putative mycobacterial bifunctional dCTP deaminase/dUTPases.

In the next step, we built the 3D structure of the *M. smegmatis* dCTP deaminase by homology modeling using the *M. tuberculosis* bifunctional dCTP deaminase/dUTPase as template (87% sequence identity). The Ramachandran plot of the homology model shows that nearly 90% of the residues are in the most favored regions and less than 1% of the residues can be found in the disallowed regions which indicate the excellent reliability of the model (data not shown). The overall 3D structures of the *M. tuberculosis* and *M. smegmatis* enzymes are highly similar as seen in Figure 2C which is also supported by the 0.33 Å RMSD value comparing all atoms of the proteins. Importantly, the residues characteristic to bifunctional dCTP deaminase/dUTPase enzymes [26,35] are in identical positions in *M. smegmatis* and *M. tuberculosis* (Figure 2D). In summary, data presented in Figure 2 indicates that *M. smegmatis* and other mycobacteria likely possess a bifunctional dCTP deaminase/dUTPase enzyme.

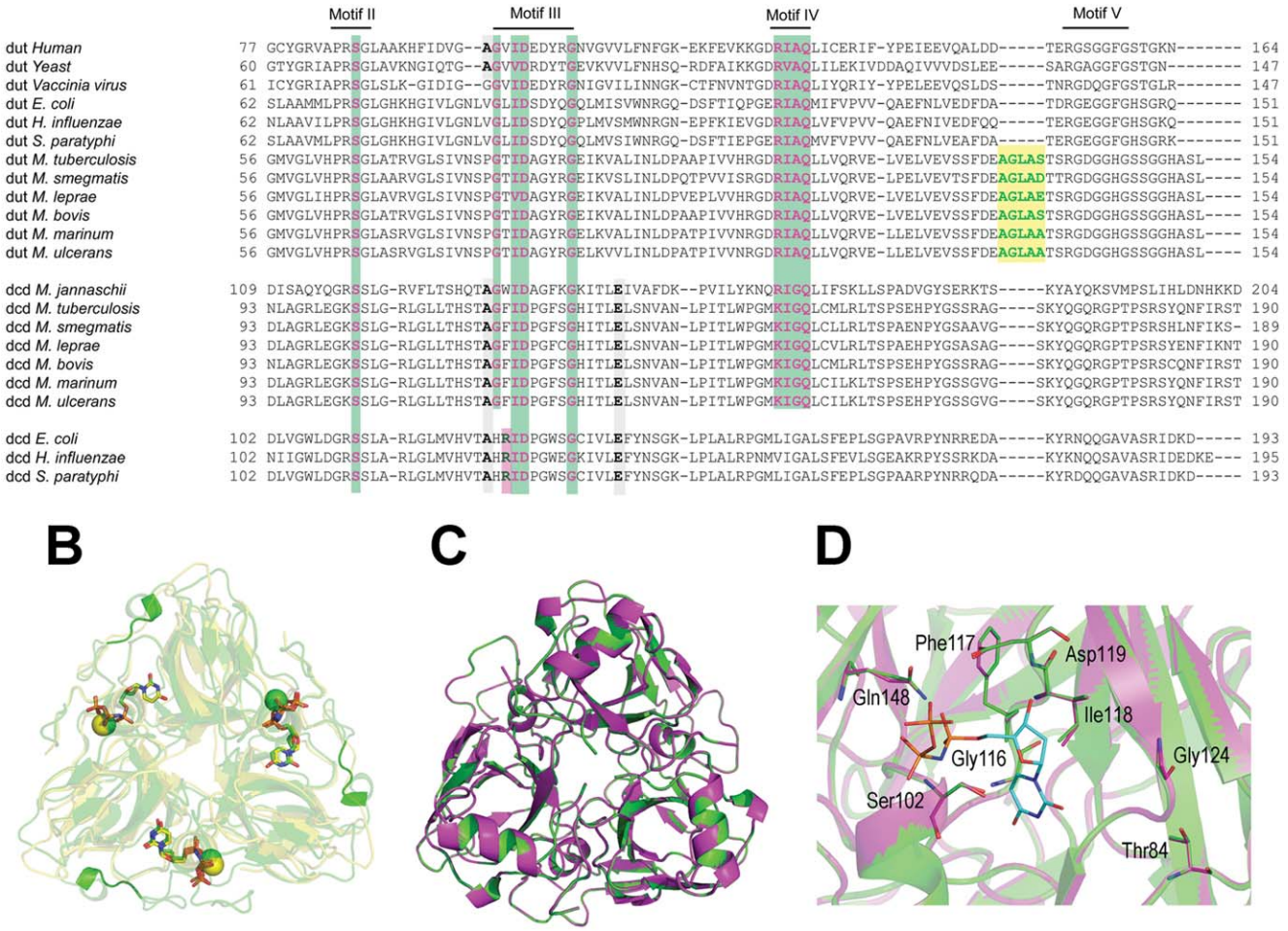

Figure 2. Sequence and structural comparison of selected members of the dUTPase superfamily. (**A**) Conserved motifs are indicated above the sequences as lines. Representative organisms from widely different evolutionary branches are also included for comparison. Mycobacterial dCTP deaminases contain all those conserved residues that are indispensable for dUTPase reaction. Residues conserved between dUTPases and bifunctional dCTP deaminase/dUTPases are important for the dephosphorylation reaction and indicated with green boxes. Residues important for the deamination reaction and crucial for dCTP deaminase monofunctionality are depicted as gray and magenta boxes, respectively. Mycobacterial dUTPases contain an insert present solely in the mycobacterial *dut*, this insert is shown as a yellow box. The alignment was performed with ClustalW. (**B**) The mycobacterial insert induces a loop structure on the surface of the dUTPase monomer. The superimposed structure of hDUT (PDB ID: 3EHW, under publication in a separate paper) and mtDUT (PDB ID: 2PY4) are depicted as yellow and green cartoon representation, respectively. The mycobacterial insert can be seen as cartoon tube representation. In the active sites the bound ligands, dUPNPP and Mg^{2+} can be seen, whereby the Mg^{2+} is visualized as a yellow (hDUT) or green (mtDUT) sphere while dUPNPP is represented as sticks with atomic coloring (carbons in yellow and green). Structures were prepared using PyMol. (**C**) Superimposed overall structure of the *M. tuberculosis* bifunctional dCTP deaminase/dUTPase and the *M. smegmatis* dCTP deaminase enzymes in green and magenta cartoon representation, respectively. (**D**) Enlarged view from **C** showing the conserved residues and the non-hydrolysable substrate analog α-β-imido-dUTP (dUPNPP) as modeled to the active site. Residues and the dUPNPP molecule are in stick representation with atomic coloring (green, magenta and cyan carbons for *M. tuberculosis*, *M. smegmatis* enzymes and dUPNPP, respectively). Note the closely identical organization of both the overall structure and the active site in *M. tuberculosis* and *M. smegmatis* dUTPases.
doi:10.1371/journal.pone.0037461.g002

The dut gene is essential for growth in M. smegmatis

Previous high density mutagenesis study provided the prediction that *M. tuberculosis* requires dUTPase for viability [31] and this finding was further corroborated in a recent genome wide study [32]. In order to address this question directly we used an efficient, reliable two-step deletion strategy [36] to knock out the functional *dut* gene from the chromosome of *M. smegmatis*. Figure 3 shows the chromosomal location and environment of *dut* and the regions used to construct the vectors applied in this study. A schematic representation of the workflow is shown in Figure 4, while the results of the experiments are displayed in Figure 5. We first attempted to construct a marked disrupted deletion mutant of the *dut* gene in the wild-type (WT) background (Figure 4A). A non-replicating delivery vector termed p2Nbk-*dut*h (Figure S1A) was introduced into *M. smegmatis* and single crossover recombinants (SCOs) were selected (see Figure 4B for work-flow and Figure 5A for results). In the next step, double crossovers (DCOs) were generated from the SCOs (Figure 4C) and screened by PCR to determine if the WT or the disrupted *dut* deletion mutant allele was present (Figure 4D). Of the 59 potential DCOs screened 49 were found to be WT DCOs while the other 10 proved to be spontaneous sucrose-resistant (suc^R) SCO strains (sucrose was used

Table 1. Homology of *M. tuberculosis* and *M. smegmatis* proteins present in the thymidylate synthesis pathway.

Enzyme	Identities[1] (%)	Similarities[2] (%)	Gene name in Mtb	Gene name in Msm
Bifunctional dCTP deaminase/dUTPase	87	95	Rv0321	MSMEG_0678
dUTPase	85	94	Rv2697c	MSMEG_2765
Nucleoside diphosphate kinase Ndk	80	88	Rv2445c	MSMEG_4627
Thymidylate (dTMP) kinase	64	71	Rv3247c	MSMEG_1873
Thymidylate synthase ThyA	87	92	Rv2764c	MSMEG_2670
Thymidylate synthase ThyX	86	92	Rv2754c	MSMEG_2683
Ribonucleoside diphosphate reductase NrdE	92	97	Rv3051c	MSMEG_1019, MSMEG_2299
Ribonucleoside diphosphate reductase NrdF2	92	95	Rv3048c	MSMEG_1033, MSMEG_2313

1 = % identical amino-acids;
2 = classified on the basis of chemical properties (e.g. polar vs. non-polar) of the respective amino-acids side chains.
doi:10.1371/journal.pone.0037461.t001

for negative selection). The fact that we could not isolate disrupted deletion mutants in the WT background indicated that the deletion mutant phenotype is probably lethal.

The dUTPase gene, *dut*, is in a predicted operon (http://operondb.cbcb.umd.edu/cgi-bin/operondb/homol_pairs.cgi?gene1_id = 219933082&gene2_id = 219933083) with an unannotated protein downstream of *dut* (*M. SMEGMATIS_2766*) (Figure 3). Therefore, the inability to isolate deletion mutants in the WT background may have been due to the disruption of the downstream gene of unknown function. To unequivocally confirm that *dut* alone is essential we constructed a merodiploid strain carrying an additional copy of *dut* expressed from its native promoter using a mycobacteriophage L5-based integrating vector (Figure S1B). After confirming the integration of the complementing vector into the SCO strains, DCOs were generated in this background and screened by PCR (Figures 4, 5). Of the 19 potential DCOs screened, 13 were WT while 6 contained the *dut* disrupted allele (Figure 5B). Consequently, *dut* can be disrupted at its native locus if a functional copy of the same gene is supplied elsewhere. The expected genotype of the disrupted deletion mutant strains was confirmed by Southern blot analysis (Figure 5C). These results prove the essentiality of *dut* in *M. smegmatis* as we could only obtain deletion mutants at the native *dut* locus in a merodiploid strain ($p<0.00025$, using Fisher's exact test).

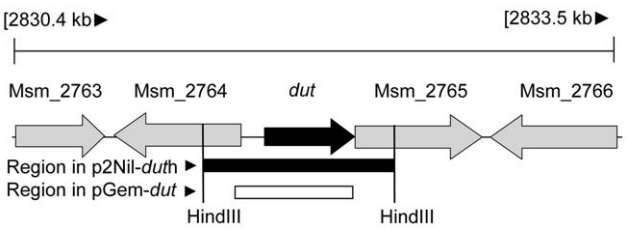

Figure 3. Genomic environment of the *dut* gene. Arrangement of the neighboring genes on the chromosome of the mc^2 -155 *M. smegmatis* strain is shown together with the regions amplified for the construction of p2Nbk-*dut*h and pGem-*dut*. Relevant restriction sites are also shown. The chromosomal location of the *dut* gene is represented by black arrow, the region cloned into the delivery vector (p2Nbk-*dut*h) is indicated with a black rectangle, and the region cloned in the complementing vector (pGem-*dut*) is shown by a white rectangle.
doi:10.1371/journal.pone.0037461.g003

M. tuberculosis and M. smegmatis dUTPases are functionally equivalent

We previously showed that thymidylate metabolism enzymes share high sequence similarity within the *Mycobacterium* genus (Table 1). To demonstrate functional similarity experimentally, we tried to rescue the lethal phenotype of *dut* disruption with the expression of *M. tuberculosis* dUTPase in the mutant DCO strain. A complement vector carrying the *M. tuberculosis dut* gene was constructed and electroporated into SCO cells. After confirmation of the plasmid integration event, the resulting strains were screened for DCO events. Out of 20 potential DCOs screened, 10 genomic *dut* disrupted mutant cell lines carrying the *M. tuberculosis* protein could be isolated (Figure 6A). We also obtained 9 WT and 1 sucrose-resistant SCO strains. The expected genotype of the disrupted deletion mutant strains were confirmed by Southern blot analysis (Figure 6B). To check if normal protein expression is driven from the complementing plasmids in *M. smegmatis*, we carried out a Western-blot analysis using the FLAG-tag epitopes engineered on the proteins. Our results show that the expression of the dUTPase protein from *M. tuberculosis* and *M. smegmatis* are comparable (Figure 6C). The fact that the *M. tuberculosis dut* could revert lethality in our *M. smegmatis* system suggests that *M. tuberculosis* and *M. smegmatis* dUTPases are functionally equivalent.

The mycobacteria-specific surface loop is essential for viability

The mycobacteria-specific C-terminal insert in dUTPase presents itself as a unique opportunity to selectively target the mycobacterial protein in a human background. Nevertheless, the functional and the physiological role of this five-aminoacid-insert, although well conserved in mycobacteria, is still unknown. In order to address this intriguing question, we attempted to complement the lethal deletion mutant phenotype with the *dut* gene lacking the mycobacteria-specific insert. For this, a complement vector carrying the *dut* mutation termed Δ-loop was constructed and electroporated into SCO cells. Following the confirmation of the plasmid integration event, the resulting strains were subjected to an extensive DCO screen (Figure 7A). Out of 88 potential DCOs screened no deletion mutant cell line could be isolated. We also compared the protein expression levels in merodiploid strains carrying the WT or the Δ-loop mutant dUTPase complementing copies besides the intact endogenous *dut* gene. The Western-blot on FLAG-tagged dUTPase constructs showed that the expression efficiencies of WT and Δ-loop

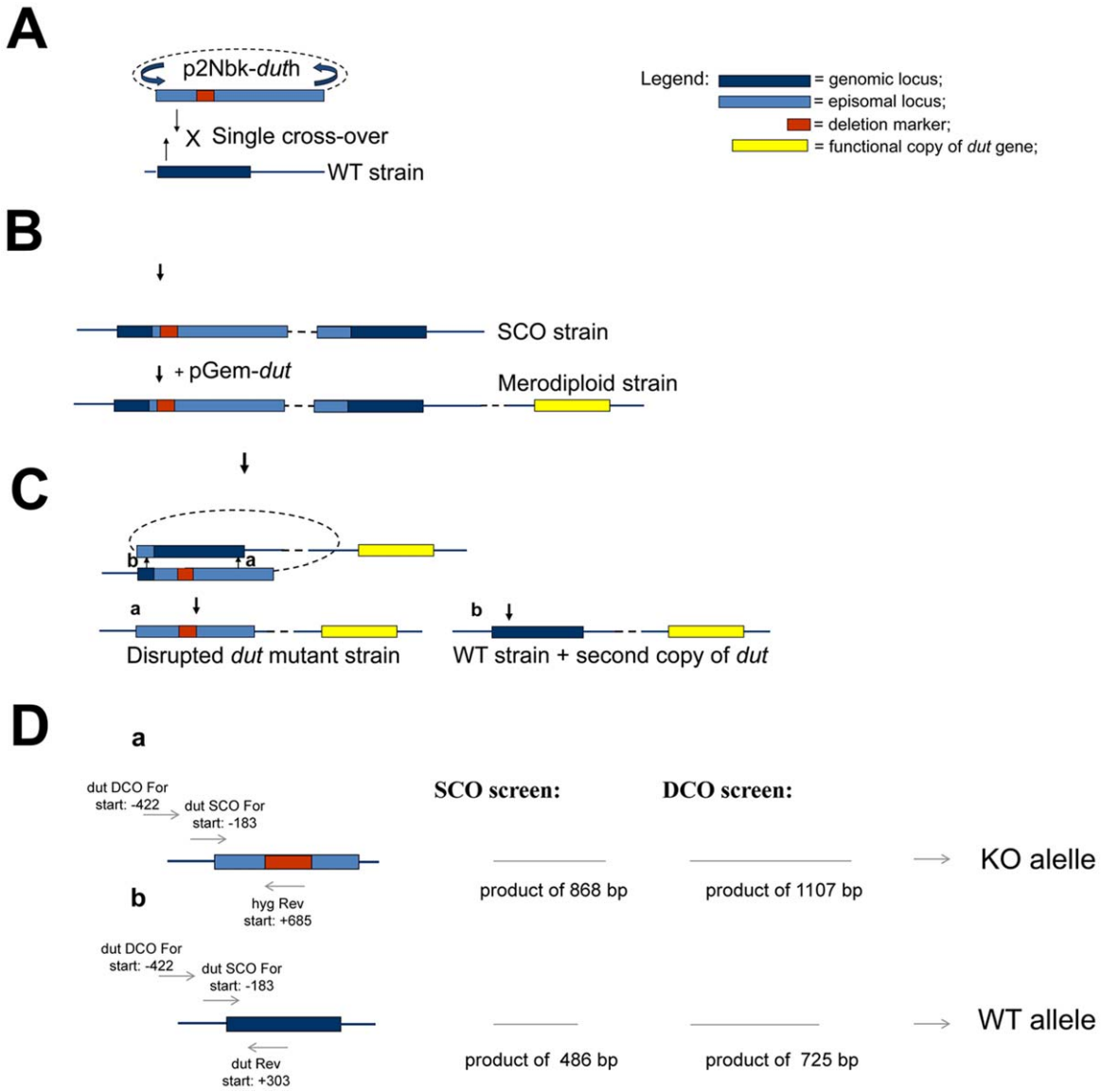

Figure 4. Schematic representation of allelic replacement by homologous recombination. (**A**) Generation of SCO strains. p2Nbk-*dut*h was electroporated into WT competent *M. smegmatis*, and single-crossover (SCO) transformants were selected. (**B**) Merodiploid strains were constructed by electroporating the complementing plasmid (pGem-*dut*) into the SCO strains. (**C**) Generation of disrupted *dut* deletion mutant strain. The double crossover event may result either a disrupted *dut* deletion mutant strain (a), or a wild type strain (b). (**D**) Strategy for SCO and DCO screening. a) shows primers and expected PCR products for the knock-out (KO) allele while b) shows the same for the WT allele. Abbreviations: WT; wild type; SCO; single crossover; DCO; double cross over.
doi:10.1371/journal.pone.0037461.g004

dUTPases are indistinguishable (Figure 7B). The fact that we could not isolate any viable *dut* deletion mutant in a Δ-loop background strongly suggests that the mycobacteria-specific segment is essential for the growth of *M. smegmatis*.

The lack of the mycobacteria-specific surface loop results in minor changes in the enzymatic properties of M. tuberculosis dUTPase

Upon obtaining the above striking result with the Δ-loop strain we were interested to reveal the enzymatic behavior of the Δ-loop enzyme (mtDUT$^{\Delta\text{-loop}}$) *in vitro*. Because the Δ-loop strain was not viable, one might presume that the enzymatic activity of mtDUT$^{\Delta\text{-loop}}$ would be compromised. To investigate the enzymatic efficiency of the mtDUT$^{\Delta\text{-loop}}$, we expressed and purified the mutant protein (Figure 8A) which proved to be as stable as the WT *in vitro*.

To evaluate the consequences of the loss of the specific insert to the enzymatic cycle, we measured the activity of mtDUT$^{\Delta\text{-loop}}$ and compared it to that of mtDUT^{H145W} [11] used as WT. As shown in Figure 8B, the maximal steady-state activity of the mtDUT$^{\Delta\text{-loop}}$ deletion mutant decreased to 0.8 s^{-1} compared to the WT (1.2 s^{-1}) while the Michaelis constant (K_M) was found to fall between 0.9–1.1 μM for both enzymes (Table 2). The observed 1.2-fold decrease in V_{max} and the similar K_M values indicate that the catalytic efficiency of dUTPase is little affected by this mutation. The surface loop is relatively close to the active site of the enzyme and it was therefore possible that the lack of it disturbs substrate binding. We investigated this possibility by determining

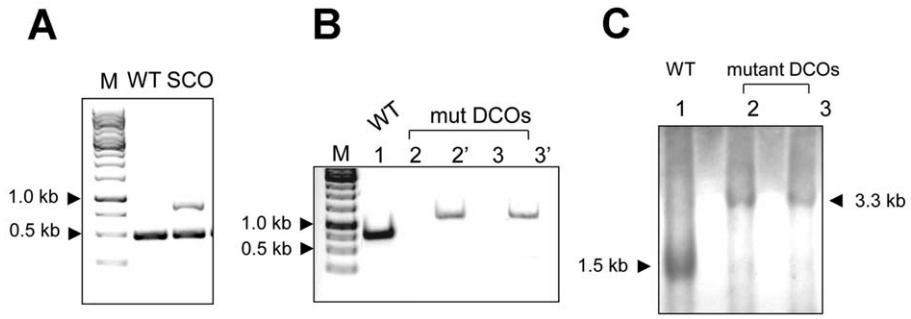

Figure 5. The *dut* gene is essential in *M. smegmatis*. M stands for the 1 kb DNA marker from Fermentas. (**A**) Identification of SCO strain by colony PCR. SCO strains were generated by homolog recombination of p2Nbk-*dut*h with chromosomal copy of *dut*. Chromosomal DNA from *M. smegmatis* mc ^{2}-155 was used as a positive control yielding the 486 bp fragment (lane WT); the suicide vector integration due to single-crossover event yielded the 860 bp fragment. (lane SCO). (**B**) Colony PCR analysis of the generated double crossover (DCO) strains. For demonstration, only a subset of 19 samples are shown here. The identical numbers represent samples from the same cell line. The potential DCO cell lines were screened for both the WT copy (indicated as 2, 3) and for the disrupted deletion mutant *dut* gene (labeled as 2′ 3′). The lengths of the expected PCR product for the wild type (WT) *dut* gene and for the disrupted *dut* mutant were 0.7 and 1.1 kb, respectively. (**C**) Southern blot analysis of DCOs. The probe used to perform the hybridization corresponds to the 1.5 kb WT (lane 1) and the 3.3 kb disrupted *dut* deletion mutant (lane 2 and 3) restriction fragment, respectively.
doi:10.1371/journal.pone.0037461.g005

the dissociation constant (K_d) of the WT and deletion mutant dUTPase complexed with the non-hydrolysable substrate analog α-β-imido-dUTP (dUPNPP) using fluorescence and circular dichroism (CD) titration. We took advantage of the discriminative power of a Trp sensor built in the active site [10,37] to measure the binding by fluorescence titration. This Trp residue substitutes a conserved histidine residue which overlaps with the uracil ring of the substrate dUTP forming a Π – Π aromatic stacking interaction. It was shown that introduction of a Trp residue to the aromatic site results in WT enzymatic behavior [37]. According to Toth *et al.*, the fluorescence signal of the Trp residue changes upon substrate binding which allows for the measurement of the dissociation constant of the enzyme-substrate complex [37]. Figure 8C shows fluorescence intensity titrations upon dUPNPP binding to dUTPase. The $mtDUT^{\Delta\text{-loop}}$ mutant displays a reduction in the observed fluorescence quench upon ligand binding compared to the WT and yielded about ten times higher K_d (Table 2). Titration of the differential CD signal of the enzyme-substrate complex upon dUPNPP binding to $mtDUT^{H145W}$ and $mtDUT^{\Delta\text{-loop}}$ yielded dissociation constants of 0.9 and 3.9 μM for the WT and for $mtDUT^{\Delta\text{-loop}}$, respectively (Figure 8D and Table 2). The CD measurements are in line with the fluorescence-based ones in that the mutation slightly affects the substrate binding affinity of dUTPase (4.3–11 fold decrease). It must be noted that the binding affinity of dUPNPP and the cognate substrate dUTP to the enzyme may be different from each other to a small extent. Nevertheless, relative changes tend to be the same regardless of the substrateanalog.

In summary, deletion of the mycobacterium-specific insert had no major effects on dUTPase enzymatic properties *in vitro* despite its essentiality in the living cell.

Discussion

In the present paper, we investigated the physiological effect of dUTPase gene disruption in *M. smegmatis*. Lethality of dUTPase

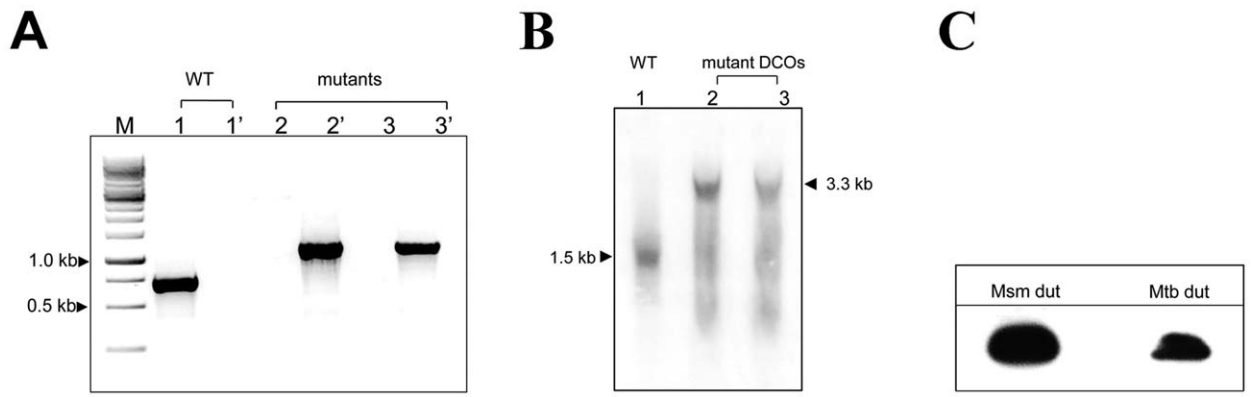

Figure 6. The *M. tuberculosis* dUTPase is able to complement the lethal phenotype in *M. smegmatis*. (**A**) Colony PCR analysis of the generated DCO strains. For demonstration, only a subset of 20 samples are shown here. M stands for the 1 kb DNA marker from Fermentas. The identical numbers represent samples from the same cell line. Every cell line was screened for both the WT copy (indicated as 1, 2, 3) and for the disrupted deletion mutant *dut* gene (labeled as 1′ 2′ 3′). The lengths of the expected PCR product for the wild type (WT) *dut* gene and for the disrupted *dut* mutant were 0.7 and 1.1 kb, respectively. (**B**) Southern-blot analysis of *dut* disrupted, *M. tuberculosis dut* coding mutants. WT was used for control. The probe used to perform the hybridization corresponds to the 1.5 kb WT (lane 1) and the 3.3 kb *dut* disrupted mutant (lane 2 and 3) restriction fragment, respectively. (**C**) Western-blot analysis of FLAG-tagged *M. tuberculosis* dUTPase expression in *M. smegmatis*.
doi:10.1371/journal.pone.0037461.g006

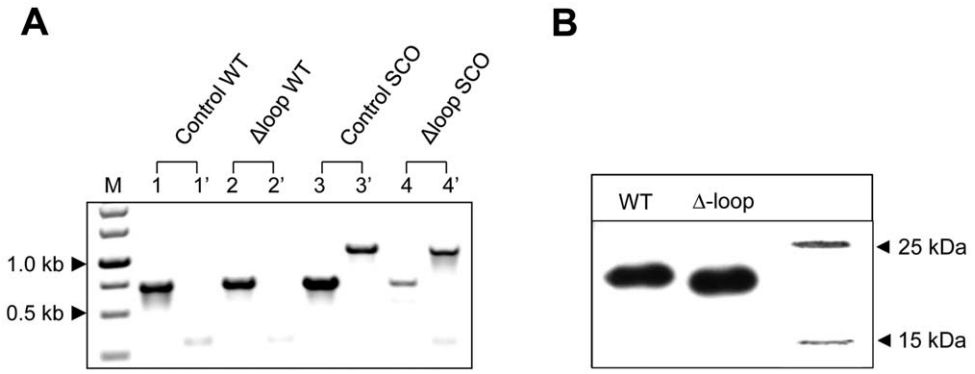

Figure 7. The Δ-loop mutant dUTPase is unable to rescue the lethal phenotype despite its normal expression level. (**A**) Colony PCR analysis of the generated double crossover (DCO) strains. 88 strains were screened and no mutant cell line could be isolated. For demonstration, only a subset of the samples are shown here. M stands for the 1 kb DNA marker from Fermentas. The identical numbers represent samples from the same cell line. Every cell line was screened for both the WT copy (indicated as 1, 2, 3, 4) and for the disrupted mutant *dut* gene (labeled as 1′ 2′ 3′ 4′). The lengths of the expected PCR product for the wild type (WT) *dut* gene and for the disrupted *dut* mutant were 0.7 and 1.1 kb, respectively. (**B**) Western-blot analysis of FLAG-tagged WT and Δ-loop dUTPase expression in *M. smegmatis* transformed with the appropriate construct.
doi:10.1371/journal.pone.0037461.g007

deletion mutants has been reported before only in *E. coli* [28] and yeast [29,30]. Current understanding of the mycobacterial DNA repair system is still poor compared with that of other bacterial (e.g. *E. coli*) organisms [38,39]. It is known, however, that the *M. tuberculosis* and *M. smegmatis* genomes lack several of the DNA repair genes and that *M. tuberculosis* polymerases are highly error-prone [40]. We had thus considered that in case of mycobacteria the importance of preventive DNA repair measures, as e.g. exerted by dUTPase is remarkably high. The results presented here corroborate this assumption. In order to demonstrate the

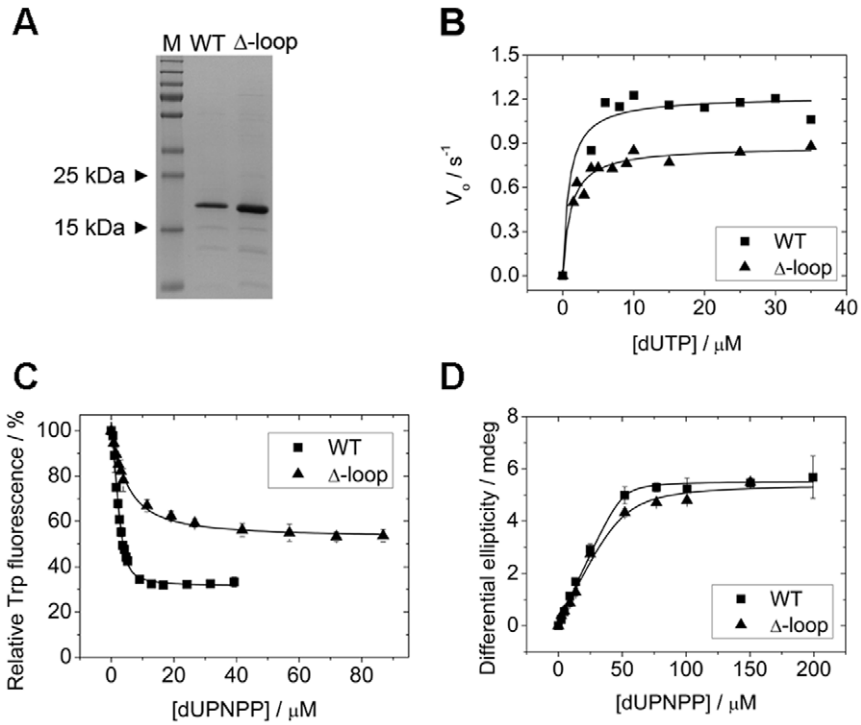

Figure 8. Effect of the Δ-loop mutation on the substrate hydrolysis and binding of *M. tuberculosis* dUTPase. (**A**) SDS-PAGE analysis of the purified proteins used in this study. M stands for the PageRuler Plus Prestained Protein Ladder (Fermentas). The WT and Δ-loop mutant dUTPases have calculated molecular weights of 18.0 kDa and 17.6 kDa, respectively. (**B**) The steady-state activity of WT and Δ-loop mutant dUTPase is shown. Michaelis-Menten curves for the WT (squares) and the Δ-loop mutant (triangle) were measured using the phenol red pH indicator assay. Fitting the Michaelis-Menten equation to the curves yielded the following V_{max} and K_M values: 1.22±0.06 s^{-1} and 0.9±0.5 μM for WT, 0.88±0.02 s^{-1} and 1.1±0.2 μM for Δ-loop. (**C**) Fluorescence intensity titration of the WT and the Δ-loop mutant using the single Trp signal is shown upon dUPNPP binding. Smooth lines through the data are quadratic fits yielding the K_d values listed in Table 2. Errors represent S.D. for n = 3. For more parameters see Table 2. (**D**) CD equilibrium titrations. Comparison of ligand (dUPNPP) binding to the WT and to the Δ-loop mutant dUTPase. Smooth lines represent quadratic fits to the data yielding the following K_d values: 0.9±0.5 μM for WT and 3.9±2.4 μM for Δ-loop.
doi:10.1371/journal.pone.0037461.g008

Table 2. Kinetic parameters of WT and Δ-loop deletion mutant *M. tuberculosis* dUTPase enzymes and dissociation constants of dUTPase-dUPNPP complexes.

		WT	Δ−loop
Activity measurement	k_{cat} (s^{-1})	1.22±0.06	0.88±0.02
	K_M (μ M)	0.9±0.5	1.1±0.2
Fluorescence intensity titrations	A_{max} (%)	−72±2	−46±1
	K_d (μ M)	0.3±0.1	3.3±0.5
Circular dichroism measurement	K_d (μ M)	0.9±0.5	3.9±2.4

doi:10.1371/journal.pone.0037461.t002

importance of the enzyme dUTPase in mycobacterial viability, we applied a two-step homologous recombination based strategy. We could isolate disrupted deletion mutants solely when a second, functional copy of *dut* was provided, which proves that this enzyme is essential in *M. smegmatis*.

The sequence analysis and homology modeling experiments demonstrated that thymidylate biosynthesis is homologous in all known mycobacteria and therefore, our findings probably apply to all of them. We showed that the mycobacterial dCTP deaminases are well conserved and most likely exert the dCTP deaminase/dUTPase function so far only studied in *M. tuberculosis*. High density mutagenesis reports [31,32] suggested that the bifunctional dCTP deaminase/dUTPase enzyme is dispensable for viability. Our current study demonstrates that the loss of monofunctional dUTPase is lethal to *M. smegmatis*, nevertheless, lethality may not be due to the lack of dUTPase activity. It is yet to be systematically investigated how dUTP hydrolysis activity exerted by the mono- and bifunctional dUTPases affects viability in mycobacteria.

Comparison of the available dUTPase sequences unambiguously led to the conclusion that mycobacterial dUTPase confer a unique and strictly mycobacteria-specific insert close to the C-terminus of the polypeptide chain (Figure 2A). This insert induces the formation of a surface loop close to the entrance of the active site as can be seen in the crystal structure of *M. tuberculosis* dUTPase (Figure 2B) [10,12,41]. We demonstrated that the mycobacteria-specific loop is essential for viability. As this segment of the protein contributes to the physiological effect conveyed by the whole enzyme, it could serve as a powerful selective target surface on the molecule.

Our spectroscopic and steady-state kinetics measurements on the purified $mtDUT^{\Delta\text{-loop}}$ protein led to the conclusion that the five-aminoacid-insert near the active site does not have a major impact on catalysis itself (Figure 8B, C, D). The enzymatic activity reduced to approximately 67% in $mtDUT^{\Delta\text{-loop}}$ is not significant compared to the orders of magnitude decrease in activity and increase in K_M caused by almost any other mutation we previously introduced to homologous dUTPases [33,37,42]. The exact correlation of dUTPase activity with mycobacterial viability is not known. However, Guillet *et al.* reported that mutant yeast strains are viable with dUTPase enzymatic activity reduced to less than 10% of the wild-type one [30]. This finding suggests that $mtDUT^{\Delta\text{-loop}}$ could probably complement the lethal phenotype if the five-aminoacid-long insert would not be required for other processes.

There are several studies in the literature mapping essential domains to determine protein function in mycobacteria (e.g. the WhiB-like proteins [43] or the UvrD1protein [44]). The majority of the residues investigated in these papers were strictly required for enzyme activity. This is not the case with the mycobacterium-specific dUTPase loop. We speculate that due to its exposed position, it might provide a binding surface for a yet unknown protein partner or another ligand and this interaction might mediate the essential function detected in our assay. A recently published study demonstrated that some bacteriophage dUTPases have two different and genetically distinct activities [45]. It seems that mycobacterial dUTPase may also have functions beyond their enzymatic activity provided by a unique and essential sequence motif. To elucidate the specific function of this short sequence extensive further studies are required.

Key enzymes of the *de novo* thymidine biosynthesis pathway (Figure 1) are attractive targets in the search for novel antitubercular therapeutics. The currently used target enzymes are the essential thymidylate synthase ThyX in *M. tuberculosis* [46,47,48] and ThyA in general [8,49]. Here we provide formal genetic proof of dUTPase essentiality in a mycobacterium for the first time and propose dUTPase as a potential drug target. Based on high sequence similarities and on the functional equivalence of the *M. tuberculosis* and *M. smegmatis* dUTPases, we suggest that the dUTPase enzyme and its mycobacteria-specific loop might bear similar key physiological roles in other, pathogenic mycobacterial species. The pathogens *Mycobacterium leprae*, and *Mycobacterium ulcerans*, the causative agents of leprosy and Buruli ulcers, respectively, still remain a serious problem. Incidences of Buruli ulcers are increasing in certain areas of the tropics such as West Africa [50]. In addition, *Mycobacterium bovis* has a broad host range, producing tuberculosis in several mammals including humans and cattle, having a considerable economic and public health importance in its own right [51].

In summary, we showed that disruption of the *dut* gene results in lethality in *M. smegmatis* and that the mycobacteria-specific insert is required for effective complementation of the lethal phenotype. We also showed that the mycobacteria-specific insert has only subtle contribution to the enzymatic activity of dUTPase and is therefore presumed to mediate an important non-enzymatic function within the bacterium. Finally, an inventory of the mycobacterial enzymes of thymidylate synthesis indicates that mycobacteria share a common dTTP biosynthetic route and that our findings in *M. smegmatis* may be applied to other, pathogenic mycobacterial species.

Materials and Methods

Protein sequence analysis and homology modeling

To determine the degree of identity between the enzymes involved in the thymidylate metabolism of *M. tuberculosis* and *M. smegmatis*, we carried out amino acid sequence search and comparisons using the http://blast.ncbi.nlm.nih.gov/Blast.cgi web server and the protein-protein BLAST algorithm. Default parameter settings were applied. Multiple sequence alignments were performed using the ClustalW software. The prediction of the 3D structure of the dCTP deaminase of *M. smegmatis* (Uniprot: A0QQ98) was performed by comparative homology modeling using the SWISS-MODEL Server and Workspace http://swissmodel.expasy.org/ [52]. For template, the apo crystal structure of the *M. tuberculosis* bifunctional dCTP deaminase: dUTPase (PDB: 2QLP) was used (87% sequence identity with the *M. smegmatis* enzyme) [26]. The quality of the generated model was evaluated by the ANOLEA [53], QMEAN [54] and PROCHECK [55] programs.

Bacterial strains, media and growth conditions

M. smegmatis mc^2155 [56] was grown in Lemco medium (broth) or with the addition of 15 g L^{-1} Bacto agar (solid) as described

previously [57]. Kanamycin was added at g/ml, hygromycin B at 100 μg/ml, gentamicin at 10 μg/ml, and streptomycin at 20 μg/ml concentration. For sucrose selection, 5% (wt/v) sucrose was included. X-Gal (5-bromo-4-chloro-3-indolyl-β- D- galactopyranoside) was used at 40 μg/ml.

Construction of the suicide delivery vector

The suicide delivery vector was constructed to generate the *dut* deletion mutant using a rapid cloning system [36]. First, a 2.1 kb fragment containing the *dut* gene together with its flanking region was amplified by polymerase chain reaction (PCR) from the *M. smegmatis* genome (region indicated in Figure 3). The 2.1 kb fragment was subsequently cloned into p2NIL [36] using the *Hind*III restriction site. The hygromycin marker gene (*hyg*) was PCR amplified from the pGOAL19 plasmid [36] using primers that carry the AgeI restriction sites. The marked disrupted allele was subsequently constructed by inserting the 1.8 kb *hyg* gene into the single AgeI site in the middle of the *dut* gene, resulting in a disrupted, non-functional dUTPase. The 6.1 kb PacI cassette carrying the *lacZ* and *sacB* selection markers from pGOAL17 [36] was cloned into the sole PacI site of p2NIL to yield p2Nbk-*dut*h. Primers used for cloning, mutagenesis and screening are compiled in Table S1.

Construction of the complementing vectors

To make the complementing construct for the *M. smegmatis* WT *dut*, PCR was used to amplify the complete gene together with the native promoter 337 bp upstream of dut. Thereafter the 0.8 kb PCR product was A-tailed and cloned into pGEM T-Easy (Promega). The Gm-Int *Hind*III cassette from the pUC-Gm-Int plasmid [58] was introduced into the resulting construct to yield the integrating vector pGem-*dut*. The Δ-loop deletion mutant *dut* complementing vector was made by the QuikChange method (Stratagene) using the pGem-*dut* as template. The *M. tuberculosis dut* coding complementing vector was made by exchanging the *M. smegmatis dut* coding sequence for the *M. tuberculosis dut* coding sequence. A FLAG-tag was cloned into all vectors subsequently. All sequences were verified by restriction digestion and sequencing.

Generation of SCO, DCO and merodiploid strains

5 μg of UV pretreated plasmid DNA [59] was electroporated into competent *M. smegmatis* [60], then single-crossover (SCO) transformants were selected on medium containing kanamycin, hygromycin and X-Gal. Merodiploid strains were constructed by electroporating the SCO strains with the appropriate complementing plasmids followed by isolation of kanamycin-, hygromycin-, and gentamicin-resistant transformants. Double crossovers (DCOs) were generated in the wild-type and merodiploid background by streaking cells onto plates lacking antibiotics. DCO selection was performed on medium containing sucrose, X-Gal, and gentamicin as required [36]. Colony PCR screening was carried out using gene-specific screening primers (Table S1) and Red-Taq polymerase (Sigma Aldrich) to determine whether the wild-type or the deletion mutant allele was present in the targeted chromosomal location.

Genomic DNA isolation was carried out as follows

10 mL liquid culture of *M. smegmatis* was harvested, and the cells were resuspended in 1 mL 10 mM Tris pH 7.5. Thereafter 0.1 mm glass beads were added to 2 mL volume, the cells were disrupted by vortex and ice incubation by turn. After centrifugation the supernatant was manipulated routinely to purify DNA by phenol:chloroform:IAA (25:24:1) extraction followed by isopropanol precipitation [61].

Southern blot analysis was carried out using the DecaLabel™ DNA Labeling Kit (Fermentas) according to the manufacturer's instructions

Restriction digestion of the genomic DNA was performed using NcoI and PstI resulting in 1.5 kb and 3.3 kb fragments in the case of WT and *dut*-disrupted mutant strains, respectively. The probe was a 0.7 kb fragment encompassing the *dut* gene (for primers see Table S1).

Verification of protein expression from the complement vector

1 μg FLAG-tagged pGEM vector carrying the WT or the Δ-loop *M. smegmatis*, or the WT *M. tuberculosis dut* was electroporated into competent *M. smegmatis* cells. Gentamycin-resistant transformants were isolated and the integration of the complementing vector was confirmed by PCR reaction. FLAG-tagged *dut* coding strains were grown until the OD_{600} reached 0.4–0.5 then the cells were harvested by centrifugation. Pellets were resuspended in lysis-buffer (50 mM Tris-HCl, pH = 7.5; 140 mM NaCl; 1 mM EDTA; 0.5% SDS; 1% Triton X-100; 0.5 mM PMSF; 2 mM BA; 15 mM β-mercaptoethanol; 0,1 mg/ml DNase) and sonicated (Elma, S30H ElmaSonic, D78224) for 4 times 5 minutes. Concentrations of the final supernatants of the cell extraction were measured using Nanodrop ND-1000 and equalized by dilution before Western-blot analysis. Protein lysates were heated at 95°C for 5 min, separated by SDS-PAGE, and transferred to PVDF membrane for immunoblotting with the specific antibody against FLAG-tag (Sigma, Monoclonal ANTI-FLAG® M2 antibody). Immune-complexes were visualized using enhanced chemiluminescence. The blotted polyacrylamide gel stained with Comassie Brilliant Blue and the PVDF membrane stained with Ponceau were used as loading controls.

Mutagenesis, cloning and dut gene expression

Site-directed mutagenesis was carried out according to the Stratagene QuikChange site-directed mutagenesis instructions and verified by sequencing of both strands. The Δ-loop deletion mutant ($mtDUT^{\Delta\text{-loop}}$) was created by deletion of the five (Ala133-Ser137) loop-specific amino acids (for mutagenic primers see Table S1). The recombinant dUTPase carrying an N-terminal hexa-His tag was cloned into pET19-b vector and expressed in *Escherichia coli* BL21(DE3) (pLysS) cells. For protein overexpression, the cells were grown to an OD_{600} of 0.4, treated with 0.5 mM isopropyl-β-D-thiogalactopyranoside at 37°C for 3 hours.

Protein purification was carried out as described previously [41]

The final supernatant after cell extraction was loaded on a Ni-NTA column (Novagen) and purified according to the Novagen protocol. The purity of the protein preparation was analyzed by SDS-PAGE. The enzyme conferring a single Trp in the active site ($mtDUT^{H145W}$) was used as wild-type in the kinetic measurements [10]. Protein concentration was measured using the Bradford method (Bio-Rad Protein Assay) and by UV absorbance ($\lambda_{280} = 8480\ M^{-1}cm^{-1}$ for $mtDUT^{H145W}$and for $mtDUT^{\Delta\text{-loop}}$) and is given in monomers. All measurements were carried out in the dialysis buffer comprising 20 mM HEPES pH 7.5, 100 mM NaCl, 2 mM $MgCl_2$ and 1 mM DTT if not stated otherwise.

Steady-state colorimetric dUTPase assay

Protons released in the dUTPase reaction were detected by phenol red pH indicator in 1 mM HEPES pH 7.5 buffer also containing 100 mM KCl, 40 μM phenol red (Merck) and 5 mM $MgCl_2$. A Specord 200 (Analytic Jena, Germany) spectrophotometer and 10 mm path length thermostatted cuvettes were used at 20°C. Absorbance was recorded at 559 nm. The Michaelis-Menten equation was fitted to the steady-state curves using Origin 7.5 (OriginLab Corp., Northampton, MA).

Fluorescence intensity titrations

Fluorescence was measured in a Jobin Yvon Spex Fluoromax-3 spectrofluorometer at 20°C, with excitation at 295 nm (slit 1 nm) and emission at 347 nm (slit 5 nm). 4 μM protein was titrated by the addition of 1–2 μl aliquots from concentrated dUPNPP solutions (purchased from Jena Bioscience, Germany). Because large concentrations of nucleotides were used, care was taken to correct for any additional fluorescence or inner filter effect imposed on the measured intensities by the nucleotide stock solutions.

Circular dichroism intensity titrations

CD spectra were recorded at 20°C on a JASCO 720 spectropolarimeter using a 10 mm path length cuvette. 50 μM protein was titrated by stepwise addition of the non-hydrolysable substrate analogue dUPNPP, in a buffer containing 20 mM HEPES pH 7.5, 50 mM NaCl and 2 mM $MgCl_2$. A spectrum between $\lambda = 240$–350 nm was recorded at each nucleotide concentration. Differential curves were obtained by subtracting the signal of dUPNPP alone from that of the corresponding complex. Differential ellipticity at $\lambda_{max} = 269$ nm was plotted against the dUPNPP concentration to obtain the binding curves. The following quadratic equation was fitted to the experimental curves:

$$y = s + A * \left((c + x + K) - \sqrt{(c + x + K)^2 - 4 * c * x} \right) / 2 * c$$

s = y at x = 0; A = amplitude; c = protein concentration; $K = K_d$.

Statistical analysis

Spectroscopy and kinetics measurements were carried out at least 3 times. Error bars represent standard deviations. In case of no error bars shown, a representative curve is displayed and the relevant table shows the standard deviations of a certain parameter obtained from several different measurements. In case of experiments carried out in the whole bacterium the Fischer's Exact Test was applied to determine the *p* value.

Supporting Information

Figure S1 Key plasmids used in the generation of *dut* deletion mutant *M. smegmatis*. (**A**) p2Nbk-*dut*h delivery vector used to generate mutant SCOs. The 2.1 kb HindIII *M. smegmatis* fragment indicated in Figure 3 was inserted into the p2NIL vector to construct the delivery vector. The *dut* allele was disrupted with a 1.8 kb fragment encoding hygromycin resistance, resulting in a non-functional *dut* gene. (**B**) The plasmid pGem-*dut* was used to complement the gene-disruption mutation. The wild-type *dut* allele together with its own promoter (337 bp upstream of the *dut* coding region) was cloned into an L5-based integrating vector to produce pGem-*dut*. Detailed cloning procedures are given in Materials and Methods. C*dut*, WT *dut* gene with its own promoter; *kan*, kanamycin resistance gene; *hyg*, hygromycin resistance gene; *lacZ*, β – galactosidase; *sacB*, sucrose sensitivity gene; *amp*, ampicillin resistance gene; *aacC1*, gentamycin resistance gene.
(TIF)

Table S1 Primers used in the present study.
(DOCX)

Acknowledgments

We thank Dr. Paul Carroll for constructive advice on the work with *M. smegmatis* and Melanie Ikeh for technical help. We thank Prof. Valerie Mizrahi and Dr. Bhavna G. Gordhan for mycobacterial vectors and for advice on experimental design. We also thank Judit E. Szabo for her comments and suggestions on the manuscript.

Author Contributions

Conceived and designed the experiments: IP RH ACB AL TP BGV JT. Performed the experiments: IP RH AL ACB. Analyzed the data: IP RH ACB AL JT. Contributed reagents/materials/analysis tools: ACB TP. Wrote the paper: IP RH AL JT.

References

1. Furlow B (2010) Tuberculosis: a review and update. Radiol Technol 82: 33–52.
2. Jagielski T, Augustynowa-Kopec E, Zwolska Z (2010) Epidemiology of tuberculosis: a global, European and Polish perspective. Wiad Lek 63: 230–246.
3. WHO (2010) Global Tuberculosis Control: World Health Organization.
4. Chakroborty A Drug-resistant tuberculosis: an insurmountable epidemic? Inflammopharmacology).
5. Jassal M, Bishai WR (2009) Extensively drug-resistant tuberculosis. Lancet Infect Dis 9: 19–30.
6. Harries AD, Dye C (2006) Tuberculosis. Ann Trop Med Parasitol 100: 415–431.
7. Koul A, Arnoult E, Lounis N, Guillemont J, Andries K (2011) The challenge of new drug discovery for tuberculosis. Nature 469: 483–490.
8. Chernyshev A, Fleischmann T, Kohen A (2007) Thymidyl biosynthesis enzymes as antibiotic targets. Appl Microbiol Biotechnol 74: 282–289.
9. Vertessy BG, Toth J (2009) Keeping uracil out of DNA: physiological role, structure and catalytic mechanism of dUTPases. Acc Chem Res 42: 97–106.
10. Varga B, Barabas O, Takacs E, Nagy N, Nagy P, et al. (2008) Active site of mycobacterial dUTPase: structural characteristics and a built-in sensor. Biochem Biophys Res Commun 373: 8–13.
11. Takacs E, Nagy G, Leveles I, Harmat V, Lopata A, et al. (2010) Direct contacts between conserved motifs of different subunits provide major contribution to active site organization in human and mycobacterial dUTPases. FEBS Lett 584: 3047–3054.
12. Chan S, Segelke B, Lekin T, Krupka H, Cho US, et al. (2004) Crystal structure of the Mycobacterium tuberculosis dUTPase: insights into the catalytic mechanism. J Mol Biol 341: 503–517.
13. Ladner RD (2001) The role of dUTPase and uracil-DNA repair in cancer chemotherapy. Curr Protein Pept Sci 2: 361–370.
14. Whittingham JL, Leal I, Nguyen C, Kasinathan G, Bell E, et al. (2005) dUTPase as a platform for antimalarial drug design: structural basis for the selectivity of a class of nucleoside inhibitors. Structure 13: 329–338.
15. Wilson PM, Fazzone W, LaBonte MJ, Lenz HJ, Ladner RD (2009) Regulation of human dUTPase gene expression and p53-mediated transcriptional repression in response to oxaliplatin-induced DNA damage. Nucleic Acids Res 37: 78–95.
16. Wilson PM, Fazzone W, LaBonte MJ, Deng J, Neamati N, et al. (2008) Novel opportunities for thymidylate metabolism as a therapeutic target. Mol Cancer Ther 7: 3029–3037.
17. Nyman PO (2001) Introduction. dUTPases. Curr Protein Pept Sci 2: 277–285.
18. Mustafi D, Bekesi A, Vertessy BG, Makinen MW (2003) Catalytic and structural role of the metal ion in dUTP pyrophosphatase. Proc Natl Acad Sci U S A 100: 5670–5675.
19. Fiser A, Vertessy BG (2000) Altered subunit communication in subfamilies of trimeric dUTPases. Biochem Biophys Res Commun 279: 534–542.
20. Kovari J, Barabas O, Takacs E, Bekesi A, Dubrovay Z, et al. (2004) Altered active site flexibility and a structural metal-binding site in eukaryotic dUTPase:

kinetic characterization, folding, and crystallographic studies of the homotrimeric Drosophila enzyme. J Biol Chem 279: 17932–17944.
21. Horvath A, Vertessy BG (2010) A one-step method for quantitative determination of uracil in DNA by real-time PCR. Nucleic Acids Res 38: e196.
22. Lari SU, Chen CY, Vertessy BG, Morre J, Bennett SE (2006) Quantitative determination of uracil residues in Escherichia coli DNA: Contribution of ung, dug, and dut genes to uracil avoidance. DNA Repair (Amst) 5: 1407–1420.
23. Merenyi G, Kovari J, Toth J, Takacs E, Zagyva I, et al. (2011) Cellular response to efficient dUTPase RNAi silencing in stable HeLa cell lines perturbs expression levels of genes involved in thymidylate metabolism. Nucleosides Nucleotides Nucleic Acids 30: 369–390.
24. Huffman JL, Li H, White RH, Tainer JA (2003) Structural basis for recognition and catalysis by the bifunctional dCTP deaminase and dUTPase from Methanococcus jannaschii. J Mol Biol 331: 885–896.
25. Johansson E, Bjornberg O, Nyman PO, Larsen S (2003) Structure of the bifunctional dCTP deaminase-dUTPase from Methanocaldococcus jannaschii and its relation to other homotrimeric dUTPases. J Biol Chem 278: 27916–27922.
26. Helt SS, Thymark M, Harris P, Aagaard C, Dietrich J, et al. (2008) Mechanism of dTTP inhibition of the bifunctional dCTP deaminase: dUTPase encoded by Mycobacterium tuberculosis. J Mol Biol 376: 554–569.
27. Bjornberg O, Neuhard J, Nyman PO (2003) A bifunctional dCTP deaminase-dUTP nucleotidohydrolase from the hyperthermophilic archaeon Methanocaldococcus jannaschii. J Biol Chem 278: 20667–20672.
28. el-Hajj HH, Zhang H, Weiss B (1988) Lethality of a dut (deoxyuridine triphosphatase) mutation in Escherichia coli. J Bacteriol 170: 1069–1075.
29. Gadsden MH, McIntosh EM, Game JC, Wilson PJ, Haynes RH (1993) dUTP pyrophosphatase is an essential enzyme in Saccharomyces cerevisiae. EMBO J 12: 4425–4431.
30. Guillet M, Van Der Kemp PA, Boiteux S (2006) dUTPase activity is critical to maintain genetic stability in Saccharomyces cerevisiae. Nucleic Acids Res 34: 2056–2066.
31. Sassetti CM, Boyd DH, Rubin EJ (2003) Genes required for mycobacterial growth defined by high density mutagenesis. Mol Microbiol 48: 77–84.
32. Griffin JE, Gawronski JD, Dejesus MA, Ioerger TR, Akerley BJ, et al. (2011) High-resolution phenotypic profiling defines genes essential for mycobacterial growth and cholesterol catabolism. PLoS Pathog 7: e1002251.
33. Pecsi I, Leveles I, Harmat V, Vertessy BG, Toth J (2010) Aromatic stacking between nucleobase and enzyme promotes phosphate ester hydrolysis in dUTPase. Nucleic Acids Res 38: 7179–7186.
34. Barabas O, Pongracz V, Kovari J, Wilmanns M, Vertessy BG (2004) Structural insights into the catalytic mechanism of phosphate ester hydrolysis by dUTPase. J Biol Chem 279: 42907–42915.
35. Johansson E, Fano M, Bynck JH, Neuhard J, Larsen S, et al. (2005) Structures of dCTP deaminase from Escherichia coli with bound substrate and product: reaction mechanism and determinants of mono- and bifunctionality for a family of enzymes. J Biol Chem 280: 3051–3059.
36. Parish T, Stoker NG (2000) Use of a flexible cassette method to generate a double unmarked Mycobacterium tuberculosis tlyA plcABC mutant by gene replacement. Microbiology 146 (Pt 8): 1969–1975.
37. Toth J, Varga B, Kovacs M, Malnasi-Csizmadia A, Vertessy BG (2007) Kinetic mechanism of human dUTPase, an essential nucleotide pyrophosphatase enzyme. J Biol Chem 282: 33572–33582.
38. Dos Vultos T, Mestre O, Tonjum T, Gicquel B (2009) DNA repair in Mycobacterium tuberculosis revisited. FEMS Microbiol Rev 33: 471–487.
39. Springer B, Sander P, Sedlacek L, Hardt WD, Mizrahi V, et al. (2004) Lack of mismatch correction facilitates genome evolution in mycobacteria. Mol Microbiol 53: 1601–1609.
40. Boshoff HI, Reed MB, Barry CE 3rd, Mizrahi V (2003) DnaE2 polymerase contributes to in vivo survival and the emergence of drug resistance in Mycobacterium tuberculosis. Cell 113: 183–193.
41. Varga B, Barabas O, Kovari J, Toth J, Hunyadi-Gulyas E, et al. (2007) Active site closure facilitates juxtaposition of reactant atoms for initiation of catalysis by human dUTPase. FEBS Lett 581: 4783–4788.
42. Pecsi I, Szabo JE, Adams SD, Simon I, Sellers JR, et al. (2011) Nucleotide pyrophosphatase employs a P-loop-like motif to enhance catalytic power and NDP/NTP discrimination. Proc Natl Acad Sci U S A 108: 14437–14442.
43. Raghunand TR, Bishai WR (2006) Mapping essential domains of Mycobacterium smegmatis WhmD: insights into WhiB structure and function. J Bacteriol 188: 6966–6976.
44. Sinha KM, Glickman MS, Shuman S (2009) Mutational analysis of Mycobacterium UvrD1 identifies functional groups required for ATP hydrolysis, DNA unwinding, and chemomechanical coupling. Biochemistry 48: 4019–4030.
45. Tormo-Mas MA, Mir I, Shrestha A, Tallent SM, Campoy S, et al. (2010) Moonlighting bacteriophage proteins derepress staphylococcal pathogenicity islands. Nature 465: 779–782.
46. Sassetti CM, Rubin EJ (2003) Genetic requirements for mycobacterial survival during infection. Proc Natl Acad Sci U S A 100: 12989–12994.
47. Sampathkumar P, Turley S, Sibley CH, Hol WG (2006) NADP+ expels both the co-factor and a substrate analog from the Mycobacterium tuberculosis ThyX active site: opportunities for anti-bacterial drug design. J Mol Biol 360: 1–6.
48. Fivian-Hughes AS, Houghton J, Davis EO (2012) Mycobacterium tuberculosis thymidylate synthase gene thyX is essential and potentially bifunctional, while thyA deletion confers resistance to p-aminosalicylic acid. Microbiology 158: 308–318.
49. Jarmula A (2010) Antifolate inhibitors of thymidylate synthase as anticancer drugs. Mini Rev Med Chem 10: 1211–1222.
50. Cosma CL, Sherman DR, Ramakrishnan L (2003) The secret lives of the pathogenic mycobacteria. Annu Rev Microbiol 57: 641–676.
51. Mustafa AS, Cockle PJ, Shaban F, Hewinson RG, Vordermeier HM (2002) Immunogenicity of Mycobacterium tuberculosis RD1 region gene products in infected cattle. Clin Exp Immunol 130: 37–42.
52. Arnold K, Bordoli L, Kopp J, Schwede T (2006) The SWISS-MODEL workspace: a web-based environment for protein structure homology modelling. Bioinformatics 22: 195–201.
53. Melo F, Feytmans E (1998) Assessing protein structures with a non-local atomic interaction energy. J Mol Biol 277: 1141–1152.
54. Benkert P, Biasini M, Schwede T (2011) Toward the estimation of the absolute quality of individual protein structure models. Bioinformatics 27: 343–350.
55. Laskowski R A MMW, Moss D, Thornton J M (1993) PROCHECK: a program to check the stereochemical quality of protein structures. J Appl Cryst 26, 283–291.
56. Snapper SB, Melton RE, Mustafa S, Kieser T, Jacobs WR Jr. (1990) Isolation and characterization of efficient plasmid transformation mutants of Mycobacterium smegmatis. Mol Microbiol 4: 1911–1919.
57. Roberts G, Muttucumaru DG, Parish T (2003) Control of the acetamidase gene of Mycobacterium smegmatis by multiple regulators. FEMS Microbiol Lett 221: 131–136.
58. Mahenthiralingam E, Marklund BI, Brooks LA, Smith DA, Bancroft GJ, et al. (1998) Site-directed mutagenesis of the 19-kilodalton lipoprotein antigen reveals No essential role for the protein in the growth and virulence of Mycobacterium intracellulare. Infect Immun 66: 3626–3634.
59. Parish T, Stoker NG (1998) Electroporation of mycobacteria. Methods Mol Biol 101: 129–144.
60. Goude R, Parish T (2008) Electroporation of mycobacteria. J Vis Exp.
61. Silhavy. TJ, Berman, M. L, Enquist, W L (1984) Experiments with gene fusions; Laboratory. CSH, editor: Cold Spring Harbor, N.Y.

SUPPLEMENTARY MATERIAL

The dUTPase enzyme is essential in *Mycobacterium smegmatis*

running title: *Dut* is required for mycobacterial viability

Ildiko Pecsi[a,b], Rita Hirmondo[a], Amanda C.Brown[b], Anna Lopata[a], Tanya Parish[b], Beata G. Vertessy [a,c,*] and Judit Toth[a,*]

[a]Institute of Enzymology, RCNS, Hungarian Academy of Sciences, Budapest, Hungary

[b]Queen Mary University of London, Barts and the London School of Medicine and Dentistry, London, E1 2AT, United Kingdom

[c]Department of Applied Biotechnology and Food Sciences, Budapest University of Technology and Economics, Budapest, Hungary

Keywords: tuberculosis/ essential gene/ drug target/ *Mycobacterium smegmatis* / thymidylate synthesis

* Corresponding authors:

Judit Toth
Institute of Enzymology
Karolina út 29, H-1113, Budapest, Hungary
Phone: +36 1 2793142
fax: +36 1 4665465
e-mail: tothj@enzim.hu

Beata G. Vertessy
Institute of Enzymology
Karolina út 29, H-1113, Budapest, Hungary
Phone: +36 1 2793116
fax: +36 1 4665465
e-mail: vertessy@enzim.hu

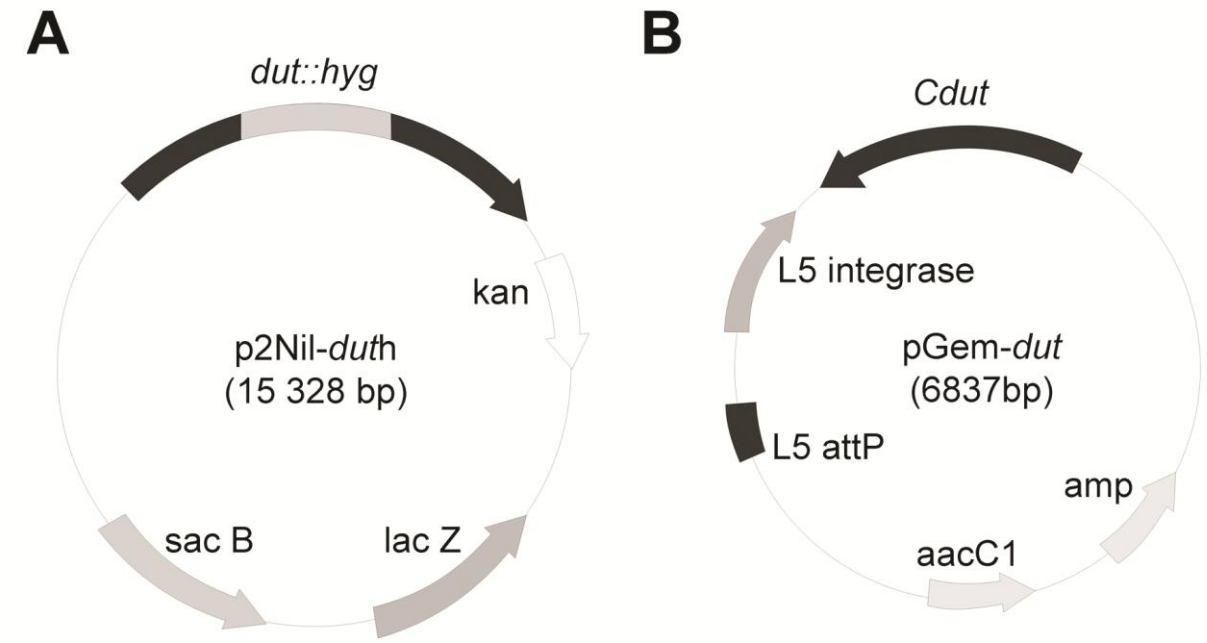

Figure S1. Key plasmids used in the generation of *dut* deletion mutant *M. smegmatis*. (**A**) p2Nbk-*dut*h delivery vector used to generate mutant SCOs. The 2.1 kb HindIII *M. smegmatis* fragment indicated in Figure 3 was inserted into the p2NIL vector to construct the delivery vector. The *dut* allele was disrupted with a 1.8 kb fragment encoding hygromycin resistance, resulting in a non-functional *dut* gene. **(B)** The plasmid pGem-*dut* was used to complement the gene-disruption mutation. The wild-type *dut* allele together with its own promoter (337 bp upstream of the *dut* coding region) was cloned into an L5-based integrating vector to produce pGem-*dut*. Detailed cloning procedures are given in Materials and Methods. C*dut*, WT *dut* gene with its own promoter; *kan*, kanamycin resistance gene; *hyg*, hygromycin resistance gene; *lacZ*, β – galactosidase; *sacB*, sucrose sensitivity gene; *amp*, ampicillin resistance gene; *aacC1*, gentamycin resistance gene.

Table S1.

Name	Cloning primer sequences (5'→3')	Function
MSM dut For	ctacgaagctaccctgatcttggtctcggc	amplify dut gene + flanking regions for cloning p2NIL-duth (HindIII site)
MSM dut Rev	ctacgaagcttaccgagccgcgcgtgaccgg	
hyg cloning For	cgtcaccggtgcagtcctccacgggcagctcgt	amplify hyg marker gene for disrupting dut (AgeI site)
hyg cloning Rev	cgtcaccggtctgaaggtggcatttccgcag	
MSM dut C WT For	cgccgatttcggcacctcgg	amplify dut gene with promoter region to cloning pGEM-dut (HindIII site)
MSM dut C WT Rev	cgtcaagcttcacaaactcgcatgtccgcc	
MSM dut C Δ-loop For	cctcgttcgacgagacaacccgtggcg	quick-change mutagenezis primers for Δ-loop pGEM-dut
MSM dut C Δ-loop Rev	cgccacgggttgtctcgtcgaacgagg	
Flag-tag For	ctagctagctcac*ttgtcatcgtcgtccttgtagtc* caaactcgcatgtc	flag-tag coding cloning primers for flag-tagged complement vectors (NheI site, *flag-tag*)
Flag-tag Rev	tactagctagctcgaccaagacgatcacc	
MTB dut For	gtgtcgaccactctggccg	amplify Mtb dut coding sequence for cloning pGEM-Mtbdut (NheI site, *flag-tag*)
MTB dut Rev	ctagctagctcac*ttgtcatcgtcgtccttgtagtc* caaactcgcatgtc	
MTB dut C For	tactagctagctcgaccaagacgatcacc	amplify pGEM-dut vector without dut coding region (NheI site)
MTB dut C Rev	gacgtcacagattactctgaggccg	
mtDUT$^{\Delta\text{-loop}}$ For	cgtcgttcgacgagacatcccgcggcgac	quick-change mutagenezis primers for Mtb Δ-loop dut protein expression vector
mtDUT$^{\Delta\text{-loop}}$ Rev	gtcgccgcgggatgtctcgtcgaacgacg	
	***Screening primer sequences (5'→3')**	
S probe For	ggcggaccttccggagagg	amplify the region of the probe of the Southern blot
S probe Rev	cgggggccagttcgacgttc	
dut SCO For	acggcatacggaacccaggcc	SCO/DCO screening primers
dut DCO For	gaaccaccagaaccatcgggg	
hyg Rev	cacctcctgcacgacttcg	
dut Rev	cgtctgcggatccaggttg	
dut For	caacctggatccgcagacg	confirmation of integration of complement vector to the genome
Gm-Int cassette Rev	ggctacgtctccgaactcacg	

SCIENTIFIC REPORTS

OPEN

Differential control of dNTP biosynthesis and genome integrity maintenance by the dUTPase superfamily enzymes

Received: 6 November 2015
Accepted: 12 June 2017
Published online: 20 July 2017

Rita Hirmondo[1], Anna Lopata[1], Eva Viola Suranyi[1,2], Beata G. Vertessy[1,2] & Judit Toth[1]

dUTPase superfamily enzymes generate dUMP, the obligate precursor for *de novo* dTTP biosynthesis, from either dUTP (monofunctional dUTPase, Dut) or dCTP (bifunctional dCTP deaminase/dUTPase, Dcd:dut). In addition, the elimination of dUTP by these enzymes prevents harmful uracil incorporation into DNA. These two beneficial outcomes have been thought to be related. Here we determined the relationship between dTTP biosynthesis (dTTP/dCTP balance) and the prevention of DNA uracilation in a mycobacterial model that encodes both the Dut and Dcd:dut enzymes, and has no other ways to produce dUMP. We show that, in *dut* mutant mycobacteria, the dTTP/dCTP balance remained unchanged, but the uracil content of DNA increased in parallel with the *in vitro* activity-loss of Dut accompanied with a considerable increase in the mutation rate. Conversely, *dcd:dut* inactivation resulted in perturbed dTTP/dCTP balance and two-fold increased mutation rate, but did not increase the uracil content of DNA. Thus, unexpectedly, the regulation of dNTP balance and the prevention of DNA uracilation are decoupled and separately brought about by the Dcd:dut and Dut enzymes, respectively. Available evidence suggests that the discovered functional separation is conserved in humans and other organisms.

Proper control of the intracellular concentration of deoxyribonucleoside-5-triphosphates (dNTPs), the building blocks of DNA, is critically important for efficient and high-fidelity DNA replication and genomic stability[1,2]. Three of the four canonical dNTPs are synthesized from their respective ribonucleoside diphosphate (NDP) counterparts[3]. The direct precursor for dTTP, however, is missing from the ribonucleoside pool and is synthesized via separate routes (Fig. 1).

The *de novo* synthesis of dTTP occurs through uracil base-containing precursors: dUMP is the direct input into the thymidylate synthase reaction (Fig. 1). In most organisms, the main dUMP supply is provided by the deamination of a cytosine deoxyribonucleotide (dCMP or dCTP) while other possible routes, e.g. the dephosphorylation of dUDP, are considered to be minor supplements[4–6]. When cytosine deamination occurs at the triphosphate level, the resulting dUTP is then converted into dUMP. The enzymes that catalyze these conversions belong to the dUTPase superfamily comprising dCTP deaminase (Dcd), dUTPase (Dut) and the bifunctional dCTP deaminase/dUTPase (Dcd:dut) (Fig. 1). These enzymes share the same quaternary structure as shown in Fig. 2A.

In addition to dUMP production, the dUTPase reaction also serves to eliminate excess dUTP to prevent uracil incorporation into DNA in place of thymine[7,8]. Although not mutagenic when replacing thymine, the uracil in DNA is considered to be an error and induces uracil-excision repair mechanisms[9]. In high dUTP/dTTP ratios, however, DNA polymerases keep re-incorporating dUTP and the repair process becomes overwhelmed. Dut is ubiquitous and essential in most investigated cases[10–16]. Recently, novel functions of Dut emerged in gene expression regulation as well[15,17–20]. Our genetic experiments also suggested that the mycobacterial Dut has a yet unknown but essential moonlighting function[11].

In summary, Dut catalyzes the break-down of dUTP to dUMP and with this action it potentially takes part i) in dTTP biosynthesis, ii) in the maintenance of low dUTP/dTTP ratio to prevent uracil incorporation into DNA

[1]Institute of Enzymology, RCNS, Hungarian Academy of Sciences, Budapest, Hungary. [2]Department of Applied Biotechnology, Budapest University of Technology and Economics, Budapest, Hungary. Rita Hirmondo, Anna Lopata and Eva Viola Suranyi contributed equally to this work. Correspondence and requests for materials should be addressed to J.T. (email: toth.judit@ttk.mta.hu)

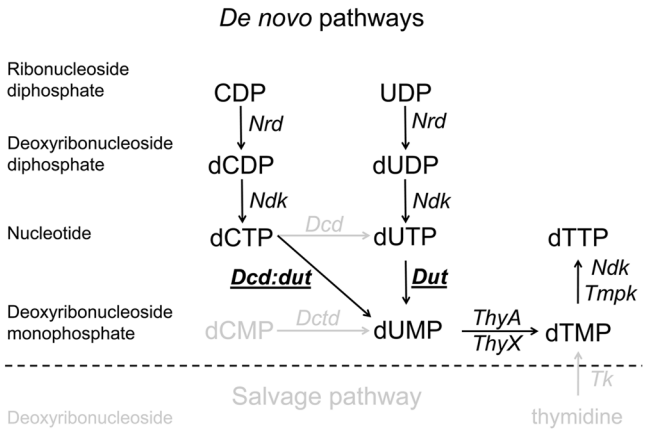

Figure 1. dTTP biosynthesis pathways and enzymes. Processes present in Mycobacteria are shown in black. Most organisms encode for additional de novo and salvage pathways that are shown in grey. Abbreviations: *Dcd* – dCTP deaminase, *Dut* – dUTPase, *Dctd* – dCMP deaminase, *Dcd:dut* – bifunctional dCTP deaminase: dUTPase, *Nrd* – Nucleoside diphosphate reductase, *Ndk* – Nucleoside diphosphate kinase, *Tmpk* – dTMP kinase, *Tk* – Thymidine kinase, *ThyA, ThyX* – thymidylate synthases.

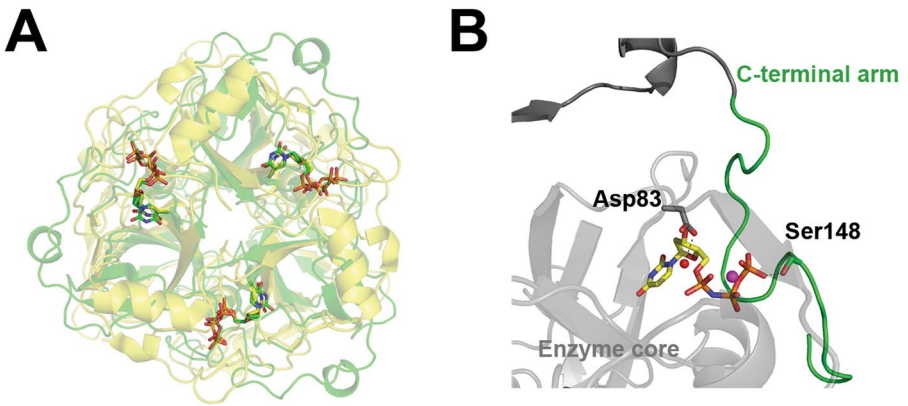

Figure 2. (**A**) Superposition of the quaternary structures of the *M. tuberculosis* dUTPase (Dut) depicted in green (PDB ID:2PY4) and the *M. tuberculosis* bifunctional dCTP deaminase/dUTPase enzymes (Dcd:dut) depicted in yellow (PDB ID:2QLP). Note the identical organization of the enzyme core of the homotrimers. Both structures contain the non-hydrolysable substrate analog α-β-imido-dUTP (dUPNPP) in the active sites. (**B**) Enlarged view of the active site of *M. tuberculosis* Dut showing the C-terminal arm in green. The side chains of the amino acids in case of point mutations and C-terminal arm truncation are shown with atomic colored stick representation similarly to the dUPNPP molecule and with green cartoon representation, respectively. The catalytic water is shown as a red sphere while the yellow sphere denotes the Mg^{2+} ion that coordinates the nucleotide.

and iii) in interactions with regulatory proteins. The various roles now attributed to Dut and the large amount of knock-out and knock-down data on the dUTPase superfamily enzymes in various genetic backgrounds create a confusing picture of the contribution of Dut to the physiological processes in which it may be involved. As dTTP biosynthesis is an essential process and a major target in several current drug therapies, it is important to pinpoint those pathways in which Dut is a key contributing enzyme.

We therefore set-out to dissect the contributions of dUTP-hydrolyzing enzymes, Dut and Dcd:dut, to dTTP biosynthesis and to the prevention of DNA uracilation. For this reason, we searched for a simple model in which the obligatory dTTP precursor, dUMP, is produced exclusively by Dut and Dcd:dut in lack of salvage pathways and dCMP deamination (Fig. 1). This favorable set of conditions naturally occurs in the genus *Mycobacteria*[11,21]. Due to the exclusive biosynthetic role of Duts in these organisms, they present potential targets for drug development, as well. Earlier mutagenesis studies found the presence of the bifunctional Dcd:dut to be dispensable for growth in *M. tuberculosis*[10,22] while the intact Dut protein is essential in *Mycobacteria*[10,11,22].

In the present study, we created *M. tuberculosis* Dut mutant proteins in which the enzyme activity is gradually tuned down. We then carried out genetic experiments in the fast-growing *M. smegmatis* in which we created the same Dut mutations and also included an inactive *dcd:dut* mutant strain in the experiments. We found that the dUTPase activity of either Dut or Dcd:dut can support cell growth. The double mutant *M. smegmatis* strain lacking the complete dUTPase activity, however, is inviable. We investigated the mutation-induced effects including

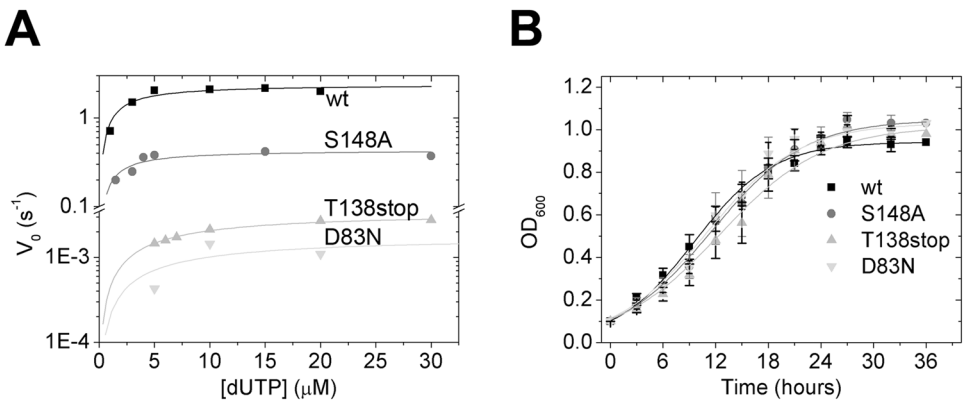

Figure 3. (**A**) Steady-state activity of wt and mutant Duts. Michaelis-Menten curves were measured using the phenol red pH indicator assay. Fitting the Michaelis-Menten equation to the curves yielded the following kcat and KM values: $1.22 \pm 0.06\ s^{-1}$ and $1.7 \pm 0.5\,\mu M$ for WT, $0.43 \pm 0.04\ s^{-1}$ and $1.5 \pm 0.6\,\mu M$ for S148A, $0.0035 \pm 0.0001\ s^{-1}$, $6.7 \pm 0.4\,\mu M$ for T138stop and $0.0013 \pm 0.0005\ s^{-1}$, $7.7 \pm 6.7\,\mu M$ for D83N mutant Dut. (**B**) *In vitro* growth analysis of wt and dut mutant *M. smegmatis* strains. The strains were grown in Lemco broth in shaking cultures for 2 days at 37 °C. Growth curves were prepared from (3*3) independent colonies from each mutation; means ± SD are plotted. Fitting the $y = a/(1 + \exp(-k*(x - xc)))$ equation to the curves yielded the following a, xc and k values: 0.94, 9.5 and 0.22 for WT, 1.04, 11.5 and 0.19 for S148A, 1.02, 12.4 and 0.17 for T138stop and 1.03, 11.0 and 0.19 for D83N Dut mutant strains.

Enzyme	k_{cat} (s^{-1})	K_M (μM)	K_d.dUPNPP (μM)	k_{cat}/K_M ($M^{-1}\,s^{-1}$)	Efficiency
wt Dut	1.22 ± 0.06	1.7 ± 0.5	0.9 ± 0.5	7.18E + 05	1
S148A Dut	0.43 ± 0.04	1.5 ± 0.6	1.8 ± 1.0	2.87E + 05	0.4
T138stop Dut	0.0035 ± 0.0001	6.7 ± 0.4	3.9 ± 1.3	5.22E + 02	0.0007
D83N Dut	0.0013 ± 0.0005	7.7 ± 6.7*	1.5 ± 0.1	1.69E + 02*	0.0002
wt Dcd:dut dUTPase	0.033 ± 0.008	12 ± 3	—	2.75 E + 03	0.004
wt Dcd:dut dCTP deaminase	0.022 ± 0.005	20 ± 12		1.10 E + 03	NA
A115F Dcd:dut	no activity	—	—	—	—

Table 1. Kinetic parameters of the *M. tuberculosis* Dut and Dcd:dut enzymes. *Data not reliable due to the limitations of the activity measurement. NA: not applicable.

dNTP pool changes, the mutation rate and the uracil content of DNA in *M. smegmatis* strains conferring various Dut and Dcd:dut mutants. Unexpectedly, the lack of Dut activity did not influence the biosynthesis of dTTP. We arrived to the conclusion that dTTP biosynthesis and the maintenance of genomic integrity by dUTP elimination are under differential control.

Results

Tuning down the activity of *M. tuberculosis* Dut. On the basis of our previous investigations on the human and *Escherichia coli* (*E. coli*) Duts[23,24], we planned and created three mutants of the *M. tuberculosis* Dut enzyme by site-directed mutagenesis. These mutants were chosen to represent enzymatic activity loss from one order of magnitude to the practical inactivity.

The D83N substitution aims at compromising the coordination of the catalytic water by mutating the catalytic aspartate residue (Asp90 in *E. coli* Dut) (Fig. 2B). In effect, this mutant presents an extremely low catalytic activity (Fig. 3A, Table 1) similarly to what was observed in the *E. coli* enzyme[24]. The determination of the Michaelis constant (K_M), however, is uncertain due to the limitations of the activity measurements at such low activities. The K_M could be better estimated in this case from the dissociation constant (K_d) of the protein complexed with the non-hydrolysable substrate analog α, β-imido-dUTP (dUPNPP). We measured the K_d of the D83N.dUPNPP complex to be similar to that of the WT.dUPNPP complex (Table 1, Fig. S1B). Its catalytic efficiency being 0.0002 compared to the wt means that the D83N Dut is a practically inactive mutant.

The efficient dUTPase catalysis requires conserved sequence motifs I-V from all three monomers of the Dut homotrimer[7]. Motifs I-IV constitute the active sites at the intermonomer clefts while motif V, located at the C-terminal arm, leaves the globular core of its monomer to associate with the neighboring active site and shield it from the solvent (C-terminal arm shown in green in Fig. 2B). This P-loop-like motif V changes conformation upon substrate binding and positions the phosphate chain of the nucleotide for efficient hydrolysis. The lack of this motif results in a nearly inactive enzyme in all investigated species[23,25–33]. We created a mutant lacking conserved motif V by the truncation of the 154 amino acid long protein at position 138 (T138Stop). The T138Stop mutant exhibits 3-fold higher enzymatic activity than that of the D83N mutant the catalytic efficiency still being

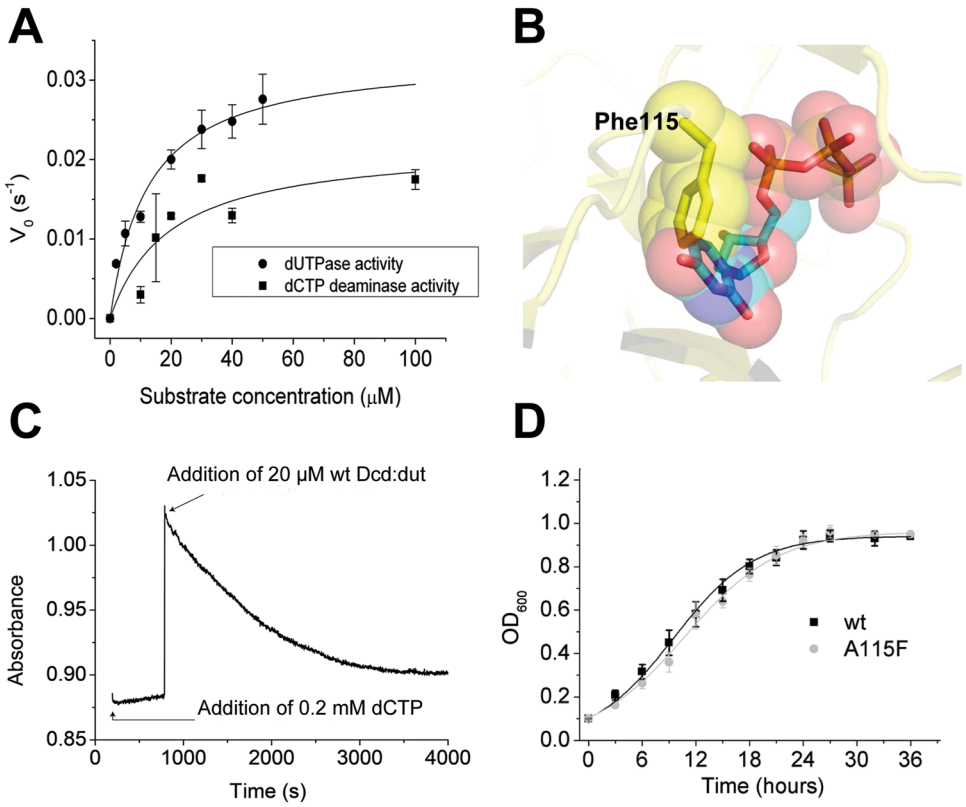

Figure 4. (**A**) Steady-state dUTPase and dCTP deaminase activity of wt Dcd:dut. The parameters yielded by fitting the Michaelis-Menten equation are shown in Table 1. The error represents the SD of 3 measurements. (**B**) The structural model of the active site of the *M. tuberculosis* Dcd:dut showing the steric conflict of the Phe115 side chain with the uracil ring of the substrate dUTP. (**C**) dCTP deaminase time course demonstrating the inactivity of the A115F Dcd:dut mutant. At t = 0, dCTP was added to a premix containing 0.02 mM A115F Dcd:dut. During ~500 s incubation time, no reaction (i.e. absorbance decrease) was detectable. The time course obtained upon the addition of the wt Dcd:dut enzyme confirmed that the assay was functional. (**D**) *In vitro* growth analysis of wt and Dcd:dut mutant *M. smegmatis* strains. The strains were grown in Lemco broth in shaking cultures for 2 days at 37 °C. Growth curves were prepared from (3*3) independent colonies from each mutation; means ± SD are plotted. Fitting the $y = a/(1 + \exp(-k*(x - xc)))$ equation to the curves yielded the following a, xc and k values: 0.94, 9.5 and 0.22 for the wt and 0.96, 10.8 and 0.19 for the A115F dcd:dut mutant strains.

extremely low compared to the WT (Fig. 3A, Table 1). Both the K_d of the enzyme.dUPNPP complex (Fig. S1A) and the K_M are 4-fold higher than that of the WT complex (Table 1).

We created the S148A mutation to distort one of the hydrogen bonding interactions between the P-loop-like motif and the γ–phosphate of the substrate dUTP (Fig. 2B). The S148A mutant showed one order of magnitude loss in the enzyme activity (Fig. 3A, Table 1) similarly to an analogous mutant in the human Dut[23]. The K_M, in concert with the K_d, increased only 2-fold (Table 1, Fig. S1A).

The A115F mutation inactivates the Dcd:dut enzyme. We cloned and expressed the *M. tuberculosis* and *M. smegmatis* Dcd:dut enzymes and determined their steady-state kinetic parameters. In lack of significant difference between the behaviors of the *M. tuberculosis* and *M. smegmatis* Dcd:duts, we report the parameters for the *M. tuberculosis* enzyme for comparison with *M. tuberculosis* Dut constructs (Fig. 4A, Table 1). As expected[21], the bifunctional enzyme is a relatively low-efficiency dUTPase compared to the monofunctional Dut (Table 1). In order to inactivate Dcd:dut without perturbing the overall structure of the enzyme, we introduced a bulky Phe into amino acid position 115 in place of an Ala (A115F) to prevent substrate binding to the active site. The Phe side chain in position 115 can only be accommodated within the active site cavity where it occupies the binding site of the uracil base (Fig. 4B). This mutant has the advantage that the cells keep synthetizing a structurally intact Dcd:dut protein. Fig. 4C shows that the Dcd:dut A115F does not exhibit enzyme activity. We have previously created this mutation in the structurally homologous human Dut and obtained an inactive but structurally intact mutant, as well[34].

The hydrolysis activity of either Dut or Dcd:dut supports the growth of *M. smegmatis*. We aimed to investigate the effect of dUTPase activity loss in the living cell. We therefore created the above mutations (S148A, T138Stop and D83N) within the genome of *M. smegmatis*. The *M. tuberculosis* and *M. smegmatis* Duts share 85% amino acid sequence identity (100% within the conserved motifs)[11] and thus it is expected that the two

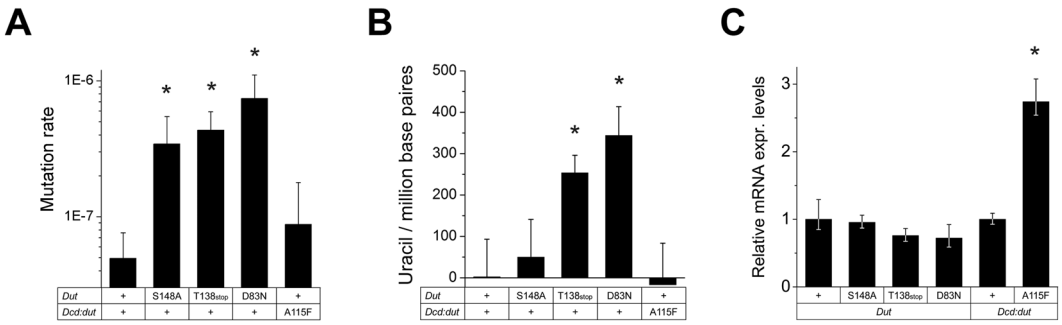

Figure 5. The effect of *dut* and *dcd:dut* mutations on the mutation rate, DNA uracilation and gene expression. (**A**) Mutation rates of mutant *M. smegmatis* strains. Means ± SE are calculated from (3*3) independent colonies from each mutation. Note that mutation rates of dut mutant strains directly correlate with the *in vitro* activity-loss of the corresponding mutant enzyme. Significance levels: P = 0.000115 for S148A, P = 0.000034 for T138stop and P =0.000004 for D83N. "+" denotes the wt enzyme. (**B**) Genomic uracil content of the mutant strains compared to the wt strain. Uracil contents were calculated from three independent strains from each mutant and normalized to the wt strain; means ± SE are plotted. Note that the genomic uracil content of dut mutant strains directly correlates with the *in vitro* activity-loss of the corresponding mutant enzyme. Significance levels: P = 0.074 for T138stop, P = 0.018 for D83N. (**C**) Quantitation of *dut* and *dcd:dut* expression levels in the wt and mutant *M. smegmatis* strains. mRNA levels were calculated from three independent strains from each mutant and normalized to their respective wt strain; means ± SE are plotted. Significance level: P = 0.029 for the A115F mutant.

enzymes behave similarly. In a previous paper, we established a method in which the disruption of the endogenous *dut* was rescued by a functional (complementing) copy of *dut* inserted into the genome on an integrating vector[11]. We used this scheme and introduced the mutations into the complementing copy of *M. smegmatis dut*. We obtained *M. smegmatis* strains that carried the mutant *dut* in a *dut* knock-out background (i.e. no wt copy present). Successful allele exchange was verified by Southern blot analysis (Fig. S2) and the mutations on the complementing *dut* copy were verified by sequencing of the appropriate genome region.

All three *dut* mutant strains were viable and unexpectedly, showed no growth defects when grown in liquid culture under stress-free conditions (Fig. 3B). This result suggests that the fully functional Dcd:dut in these *dut* mutant strains produces enough dUMP for the synthesis of more than limiting amounts of dTTP.

We also created a *M. smegmatis* strain carrying the non-functional A115F *dcd:dut* in a wt *dut* background. We constructed the A115F *dcd:dut* strain by allele exchange of the endogenous *dcd:dut* gene to a GFP-tagged copy carrying a point mutation. The A115F mutation was introduced either in wt or in inactive *dut* (D83N) background. Successful allele exchange was verified by Southern blot analysis (Fig. S2), and the mutation was verified by the sequencing of the appropriate genome region. The A115F *dcd:dut* strain encoding wt *dut* was viable and its growth rate was similar to that of the wt when grown in liquid culture (Fig. 4D). In contrast, we could not obtain any double mutant strains carrying both the *dut* D83N and the *dcd:dut* A115F mutations. In these cells, the dUTPase activity is completely abolished due to the fact that only inactive Duts are encoded. However, these inactive proteins are structurally intact and could still potentially mediate functions that are independent from their enzymatic activity or can operate in an inactive state (e.g. the essential surface loop in Dut[11] and examples from other species[15,18–20,35]). This implies that the dUTPase activity is essential for viability and reinforces that the dUTPase activity has exclusive role in dTTP biosynthesis in *Mycobacteria* (cf. Fig. 1).

Mutator phenotype of the dut and dcd:dut mutant strains. As we could not reveal any obvious defects in the enzymatically compromised *dut* or *dcd:dut* mutant *M. smegmatis* strains, we investigated possible long term effects of these mutations. We measured the mutation rates in each of the mutant strains[36,37]. We found that the mutation rates increased remarkably in the *dut* mutant strains (7-fold, 9-fold and 15-fold in the S148A, T138stop and D83N *dut* mutant strains, respectively). The mutation rate of the *dcd:dut* A115F strain appeared two-fold higher than the wt, however, the difference did not prove to be significant (Fig. 5A).

Dut mutant strains accumulate uracil in their genome. We also measured the genomic uracil content of the mutant strains by a q-PCR based method developed in our laboratory[38]. This assay is based on the fact that the Pfu polymerase does not amplify uracil-containing template DNA while other polymerases do (e.g. Taq). It is therefore possible to calculate the relative uracil content of the sample on the basis of PCR efficiencies driven parallel by Pfu and by Taq polymerases. We found that *dut* mutants have elevated genomic uracil content compared to the wt strain and that the increase in uracil content correlates with the *in vitro* measured activity loss (50, 250 and 340 uracil/million base pairs in the S148A, T138stop and D83N *dut* mutant strains, respectively.) (Fig. 5B). For comparison, the 340 uracil/million base pairs genomic uracil content matches that measured in the *ung- E. coli* and the *ung-* MEF cells deficient in uracil misincorporation repair. The *dut-/ung- E. coli* strain contains even 20-times more uracils in its genome[38]. We could not detect any change in the genomic uracil content in the A115F *dcd:dut* mutant strain compared to the wt (Fig. 5B).

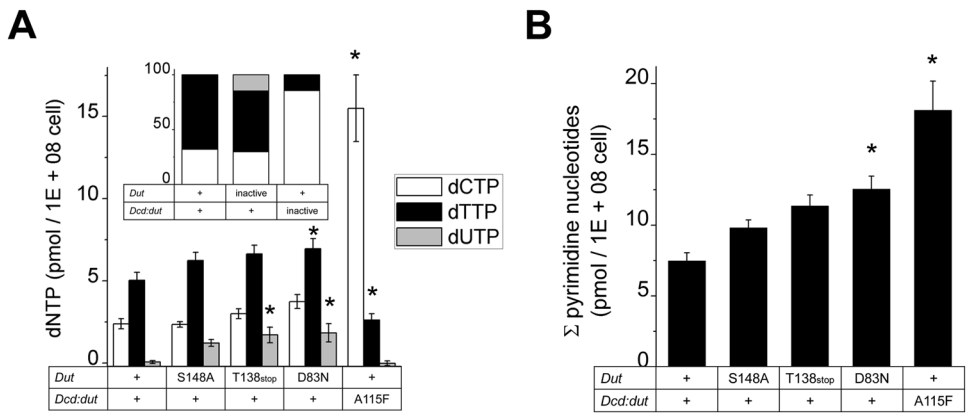

Figure 6. The effect of *dut* and *dcd:dut* mutations on the pyrimidine nucleotide pool. (**A**) dTTP, dCTP and dUTP concentrations were measured using a DNA polymerase-based method in all mutant strains. Mutant enzymes are indicated, "+" denote the wt enzyme. Means ± SE are calculated from 12 data points for each mutation. The dUTP concentration in the wt and in the A115F mutant falls out of the measurement range (<0.5 pmol/108 cells). Significance levels: P = 0.063 for the T138stop dUTP level, P = 0.095 for the D83N dTTP level, P = 0.047 for the D83N dUTP level, P = 0.000012 for the A115F dCTP level, P = 0.066 for the A115F dTTP level. The inset shows a comparison of the ratios of pyrimidine nucleotides within the wt and inactive mutant strains. (**B**) The change in total pyrimidine concentration in function of the mutation carried by each strain. Means ± SE are plotted. Significance levels: P = 0.05959 for D83N and P = 0.0028 for A115F.

To investigate if these marked effects are not simply due to an underlying difference in gene expression, we measured the mRNA levels of the various constructs. The expression of the T138stop and D83N *dut* constructs in the *M. smegmatis* cells seems to decrease compared to the wt, however, the difference proved not to be significant (Fig. 5C). On the other hand, the expression level of the A115F *dcd:dut* construct increased significantly compared to the wt (Fig. 5C). This finding emphasizes the differential effects in DNA uracilation and mutagenicity between the *dut* and *dcd:dut* mutations even more.

Pyrimidine nucleotide pool changes in the dut and dcd:dut mutant strains. To reveal the mechanism of uracil accumulation and mutation rate changes in our mutant strains, we measured the pyrimidine nucleotide pools in each strain. We used a DNA polymerase-based method to determine the concentration of dUTP, dTTP and dCTP in cell extracts[39,40]. The method is based on the incorporation of radiolabeled dATP into a nucleotide-specific template limited by the concentration of the quantifiable dNTP. The concentration of dUTP in the wt strain proved to be too low to be accurately quantified in our assay (<0.5 pmol/10^8 cells). We found that the concentration of dUTP became significantly elevated in the T138stop and D83N *dut* mutants (Fig. 6A). The dTTP:dUTP ratio changed from the >>10:1 ratio in the wt to 5:1 in the S148A *dut* mutant strain and to 4:1 in the T138stop and D83N *dut* mutant strains. The dTTP and dCTP concentrations remained quasi unchanged and consequently, the dTTP:dCTP ratio also remained in the wt range. However, the total pyrimidine content increased moderately but significantly in the D83N *dut* strain (Fig. 6, dCTP and dTTP concentrations increased 1.6- and 1.4-fold, respectively). Interestingly, however, the A115F *dcd:dut* strain had a normal low concentration of dUTP in its nucleotide pool while the dTTP:dCTP ratio became greatly imbalanced (Fig. 6 inset). The dCTP concentration of the A115F cell extract increased more than 6-fold while the dTTP concentration decreased to half of the wt (Fig. 6A).

These results clearly suggest two different roles for *dcd:dut* and *dut* in the regulation of pyrimidine nucleotide concentration and in the maintenance of genome integrity, respectively.

Discussion

Previous knock-out studies found *dut* essential and *dcd:dut* dispensable for *Mycobacteria*[10,11,22]. We reported that a complete knockout of *dut* is lethal[11]. We also reported that lethality is not due to the loss of the catalytic function but is mediated by a surface loop of unknown function independently of the dUTPase activity[11]. A well-folded and enzymatically active Dut enzyme lacking only this 5 amino acid long mycobacterium-specific surface loop does not support growth[11]. These previous studies did not provide information about the *in vivo* function of the enzymes bearing dUTPase activity, *dut* and *dcd:dut*. It was not clear, for example, how dUTPase activity affects the dNTP pool and downstream genomic processes. In the present study, we combined enzymology with genetics to address the role of dUTPase activity within the mycobacterial cell.

The mutant enzymes we created to tune down enzyme activity behaved in a well predictable manner in our *in vitro* experiments. The S148A and the T138stop *dut* mutations that compromised one or all interactions of the P-loop-like motif with the phosphate chain of the substrate resulted in small or severe activity loss, respectively, accompanied by weaker binding of the substrate (proportionally increased K_d and K_M, Table 1). The D83N mutation impaired the coordination of the catalytic water which left the binding of the substrate unaffected (Table 1). However, the subsequent catalytic reaction was compromised resulting in practical inactivity (Table 1).

The activity-compromised *dut* point mutant *M. smegmatis* strains exhibit an increased mutation rate that accompanies the increase in the genomic uracil content (20–150 folds, Fig. 5). *Mycobacteria* encode three uracil

DNA glycosylase enzymes (*ung, udgB and udgX*)[41–43] enabling effective uracil excision repair in these organisms[42]. This functional redundancy reinforces that the accumulation of uracil in DNA is an unwanted process. The potential reason why uracil could still accumulate in the DNA of our *dut* mutants is that DNA polymerases re-incorporate uracil despite the excision repair mechanism constantly excising it from the mycobacterial DNA. Polymerases usually do not distinguish between dTTP and dUTP and thus, they will likely incorporate dUTP from a nucleotide pool containing highly elevated dUTP concentrations (Fig. 6). Uracils (U·A pairs) are generally not considered as mutagenic compounds[44] while there is a controversy in the literature about the mutagenicity of abasic sites[44–46]. However, constantly excised and re-incorporated uracils probably cause stress and genome instability in the bacteria. In an *ndk, dut* double mutant *E. coli* strain, increased dUTP levels and replication intermediates from the uracil excision process caused several thousand-fold elevations in the mutation rate. The *Ung* mutation, which enables stable incorporation of uracil into DNA, could only partially alleviate the mutagenic effect[47]. This suggests that among other possible mechanisms, an increased frequency of uracil repair processed by either short patch or long patch base excision repair (BER) mechanism[48] may be responsible for the observed elevation in the mutation rates. In addition, the *dut* mutation had a modest effect on dCTP and dTTP levels[47]. In our experiments, the most severe D83N *dut* mutation also resulted in a modest increase of cellular pyrimidine levels. The overproduction of dNTPs in response to endogenous DNA damage is a general stress response[3,49,50] and most likely serves to promote tolerance against genotoxic stress. The elevated dNTP levels, in turn, increase the mutation rate[50–53] as the activity balance of DNA polymerases is transiently altered allowing the proofreading activity to decrease for the benefit of the nucleotide incorporating function (i.e. next nucleotide effect)[52]. These considerations are in agreement with our observations as well. The equally large increase in the mutation rates of the various *dut* mutants also suggests that this phenomenon is part of a general stress response and not specific to dUTPase activity loss. Interestingly, although the dTTP:dCTP ratio was highly imbalanced in the *dcd:dut* mutant strain, it displayed only two-fold increase in the mutation rate possibly indicating that dCTP is a relatively poor mutagenic precursor (Figs 5, 6). These results are in good accordance with previous literature data also reporting 2-fold increase in the mutation rate using the rifampicin resistance method in *dcd* mutant *E. coli*[46]. However, Schaaper and Matthews also found that the experimental system greatly affects the observation of mutagenicity. In their study, the 2-fold increase in the mutation rate observed using the rifampicin resistance assay appeared much higher (<42-fold) using a different assay (only available for *E. coli* for the moment)[46]. Moreover, Kumar and his colleagues found that even mild dNTP pool imbalances were mutagenic in *Saccharomyces cerevisiae*. However, the mutagenic potential of different imbalances did not directly correlate with their extent[53]. Nordman and Wright proposed that dNTP imbalances were not responsible for increased mutation rate in the *ndk, dut* mutant *E. coli*[47]. Our findings suggest that the dCTP:dTTP imbalance results in lower mutagenic potential than that of DNA uracilation.

Unexpectedly, the reduced dTTP concentration in the *dcd:dut* mutant strain did not limit the proliferation rate of the bacteria (Fig. 4D). This indicates that the activity of either of the two dUTPases is sufficient to support dTTP synthesis for the efficient growth of *M. smegmatis*. Our further results shown in Fig. 6 suggest, however, that dUMP production and dTTP biosynthesis are mainly under the control of the bifunctional Dcd:dut enzyme. The fact that Dcd:dut is a hundred-fold less efficient dUTPase than Dut (Table 1 and ref 21, 54) suggests that the mechanistic differences between the two dUTPase enzymes are more important than simply is their catalytic efficiency. Dcd:dut is able to bind dTTP which inhibits its activity[55]. This negative feedback inhibition allows for the regulation of the cellular dCTP:dTTP concentration ratio. Dut, however, can only accommodate dUTP and does not show any allosteric features[56]. Based on our results shown in Figs 5, 6, we propose that Dut is responsible for the efficient elimination of dUTP, while the role of the bifunctional Dcd:dut is to maintain the proper dCTP:dTTP ratio. There are clear advantages to such functional diversion. dUTP is constantly generated from dUDP by the nucleoside diphosphate kinase (*Ndk*) and also by spontaneous dCTP deamination in mycobacteria (and by other enzymatic pathways in eukaryotes and in some prokaryotes (Table 2). The accumulation of dUTP is efficiently prevented by the monofunctional Dut. The purpose here is to sanitize the dNTP pool from dUTP to prevent genome uracilation. The regulatory capabilities are built in the other, closely related, Dcd:dut enzyme that proved to be an inefficient dUTP sanitizer but keeps the pyrimidine DNA building blocks in a correct concentration ratio (Fig. 6). The preventive aspect of the bifunctional enzyme may be that dangerous dUTP is not released following the dCTP deamination reaction but is converted to dUMP on the same enzyme[21,57].

We compiled the available literature data on the *in vivo* effects of dUTPase activity loss in various organisms in Table 2. This comprehensive data set supports a similar partition between the dUTP eliminating and the dNTP balancing functions in other organisms that bear additional dTTP producing pathways, as well. In *Saccharomyces cerevisiae* and *Caenorhabditis elegans* (bearing dCMP deaminase and a salvage pathway), the inactivation of *dut* is lethal. The inhibition of *ung*, however, can rescue the observed phenotype in these organisms[14,58] indicating the deleterious effect of genome uracilation in the *dut* mutant. The numerous reports on *E. coli dut* mutants also indicate that the major effect of Dut inactivation is genome instability and not a short supply of dTTP (Table 2). While the *dut*-1/*ung*-1 mutant *E. coli* strain can be maintained, the *dut-1* phenotype is lethal[59]. However, in *Trypanosoma brucei*, in which there is no dCTP/dCMP deaminase and dUMP production strongly depends on dUDP/dUTP hydrolysis, the inactivation of *ung* could not rescue *dut* silencing but instead increased the cytotoxic effects conveyed by the low dUMP levels[13]. Efficient *dut* silencing in human cell lines resulted in a decline in clonogenic survival due to genome instability (Table 2). All these literature data support the major role of *dut* in dNTP sanitizing. The regulation of dTTP concentration, however, seems to be exclusively committed to dCTP and/or dCMP transforming enzymes (Dcd, Dcd:dut, Dctd) which may be structurally unrelated from each other but are all allosterically regulated[55,57,60–62]. A further in-depth investigation of the de-coupling of these functions may shine light on mechanisms supporting the appearance of T in and the exclusion of U from DNA.

Organism	Pathways	Phenotype	Rescue	dNTP pool/ Mutagenicity	Ref.
E. coli	Dcd, Dut, Tk	KO lethal; Mutants: thymidine auxotroph, filamentous, hyperrec (nicks in DNA), prolonged generation time, increased sensitivity to 5′- FUs	Dcd-, ung- rescues synthetic lethality with pyrE, xth, recA, recBC but not with Tk	dUTP 10x up, dTTP 3x up, mutagenicity 5–15x up	12, 59, 68–70
M. smegmatis	Dcd:dut, Dut	Dut KO lethal; Mutants: normal generation time, high genomic U content	No rescue with active but loop(−) Dut	dUTP 20x up, mutagenicity ~15 × up	11, this study
T. brucei	Dut, Tk	KO lethal; Mutants: cell cycle alterations, chromosome fragmentation, sensitive to MTX	Thymidine supply (ung- increases cytotoxicity)	dUTP 9x up, mutagenicity 9x up	13, 71, 72
C. elegans	Dctd, Dut, Tk	embrionic lethality; ATL1, RAD51 foci –> S-phase checkpoint activation	ung1, clk2 rescues, thymidine supplemented medium only partially	n.d.	14
D. melanogaster	Dctd, Dut, Tk?	lethality in early pupal stage, DNA strand breaks, U in DNA	n.d.	n.d.	15
S. cerevisiae	Dctd, Dut	dTMP auxotrophs (no Tk!), growth delay, cell cycle abnormalities	exogenous dTMP, ung inactivation rescues, APE inactivation does not	mostly AT –> CG mutations	58, 73
Human cell lines	Dctd, Dut, Tk	sensitization for FdUrd, even more with Tmk double silencing; decline in clonogenic survival, increase in DNA double strand breaks and in Tmk, Tk expression levels; genome instability, tumorigenesis; apoptosis in pancreatic beta cells	n.d.	variable, no significant change or n.d.	67, 74–77
Arabidopsis	Dctd, Dut, Tk	lethality or sterility, sensitive to 5FUs, 7-fold increase in homologous recombination events	critical partners unknown	n.d.	16, 78

Table 2. The effects of dUTPase modification in various organisms.

Methods

Bacterial strains, media and growth conditions. *M. smegmatis mc²155* was grown in Lemco medium (broth) or in Lemco with the addition of 15 g L^{-1} Bacto agar (solid). Kanamycin was added at 20 μg/ml, hygromycin B at 100 μg/ml, gentamicin at 10 μg/ml, and streptomycin at 20 μg/ml final concentration. For sucrose selection, 5% (wt/v) sucrose was included in the medium. X-Gal (5-bromo-4-chloro-3-indolyl-b- D- galactopyranoside) was used at 40 μg/ml.

Mutagenesis, cloning and gene expression. All recombinant proteins were expressed in *E. coli* BL21(DE3)pLysS cells using the *M. tuberculosis dut* gene (Rv2697c) and the *M. smegmatis* and *M. tuberculosis dcd:dut* genes (MSMEG_0678 and Rv0321 respectively). The *M. tuberculosis* pTBdcd7 Dcd:dut expression plasmid was kindly provided by Martin Willemoes. The site-directed mutagenesis of Dut was carried out according to the Stratagene QuikChange site-directed mutagenesis instructions and verified by sequencing of both strands. The recombinant Dut carrying an N-terminal hexa-His tag was cloned into pET19-b vector, and the recombinant *M. smegmatis* Dcd:dut amplified from p2NIL_dcdWT and p2NIL_dcdA115F (created in this study) was cloned into pET45-b vector with restriction sites BamHI and HindIII (Table S1). Both proteins were expressed in *E. coli* BL21(DE3)pLysS cells. For protein overexpression, the cells were grown to an OD_{600} of 0.4, treated with 0.5 mM isopropyl-b-D-thiogalactopyranoside (IPTG) at 37 °C for 3 hours for Dut and at 30 °C for 6 hours for Dcd:dut expression.

Protein purification. Pellets of cells expressing Dut were lysed in a buffer containing 50 mM TRIS pH 7.5, 100 mM NaCl, 0.5 mM EDTA, 1 mM DTT, 0.1 mM PMSF and EDTA-free protease inhibitor (Roche). Dcd:dut expressing cells were lysed in a buffer containing 20 mM HEPES pH 7.5, 100 mM NaCl, 5 mM $MgCl_2$, 10 mM ß-ME, 0.1% v/v TRITON-X-100, ca. 10 μg/ml RNase, ca. 100 μg/ml DNase, 5 mM benzamidine, 0.1 mg/ml lysozyme and EDTA-free protease inhibitor (Roche). Cell suspensions were sonicated (3 × 60 s) and centrifuged (15550g, 30 min). The final Dut and *M. smegmatis* Dcd:dut supernatant after cell extraction was loaded onto a Ni-NTA column (Novagen) and purified according to the Novagen protocol. The *M. tuberculosis* Dcd:dut was purified on Q-Sepharose (GE Healthcare) anion-exchange column, followed by gel filtration on a Superdex 75 column (GE Healthcare) using an AKTA Explorer purifier. The purity of the protein preparation was analyzed by SDS-PAGE. Protein concentration was measured using the Bradford method (Bio-Rad Protein Assay) and by UV absorbance ($\lambda_{280} = 8480\ M^{-1}\,cm^{-1}$ for H145W *M. tuberculosis* Dut and its mutant enzymes, and $\lambda_{280} = 9970\ M^{-1}\,cm^{-1}$ for the *M. smegmatis* Dcd:dut and the A115F mutant enzyme, $\lambda_{280} = 11460\ M^{-1}\,cm^{-1}$ for the *M. tuberculosis* Dcd:dut and the A115F mutant enzyme) and is given in monomers.

Steady-state colorimetric dUTPase assay. Protons released in the dUTPase reaction were detected by phenol red pH indicator in 1 mM HEPES pH 7.5 buffer also containing 100 mM KCl, 40 μM phenol red (Merck) and 5 mM $MgCl_2$. A Specord 200 (Analytic Jena, Germany) spectrophotometer and 10 mm path length thermostatted cuvettes were used at 20 °C for measuring dUTPase activity of the wt and mutant enzymes. The absorbance was recorded at 559 nm. V_0 was extracted from the raw absorbance vs. time curves followed by fitting the

Michaelis-Menten equation to the V_0 vs. substrate concentration steady-state curves using Origin 7.5 (OriginLab Corp., Northampton, MA).

dCTP deaminase activity measurements. The dCTP deaminase activity was measured in a continuous spectrophotometric assay using the difference in the molar extinction coefficients between deoxycytidine and deoxyuridine ($\Delta\varepsilon_{286} = 3240\ M^{-1}\,cm^{-1}$). The absorbance was recorded at 286 nm. The assay was buffered with 20 mM HEPES pH 7.5 also containing 100 mM NaCl and 5 mM $MgCl_2$. The reaction was initiated by the addition of deoxicitidine triphosphate into the enzyme containing premix. A Specord 200 (Analytic Jena, Germany) spectrophotometer and 10 mm path length thermostatted quartz cuvettes were used at 20 °C. V_0 was extracted from the row absorbance vs. time curves followed by fitting the Michaelis-Menten equation to the V_0 vs. substrate concentration steady-state curves using Origin 7.5 (OriginLab Corp., Northampton, MA).

Construction of the *dut* mutant strains. All genetic experiments were carried out in *M. smegmatis mc²155* using *M. smegmatis* genes (MSMEG_2765 *dut* and MSMEG_0678 *dcd:dut*) for complementation. *Dut* KO SCO cells were used[11] to construct our *dut* mutant strains. The mutant *dut* containing complementing vectors were created by the QuikChange method (Stratagene) using the vector pGem-dut[11] as template. Mutant strains were constructed by electroporating the *Dut* KO SCO strains with the appropriate complementing plasmids. Double crossovers (DCOs) carrying the mutant *dut*s were selected by colony PCR (Table S1) and verified by Southern blot (Fig. S2) and by sequencing the appropriate genome region. Three parallel strains from each mutant were chosen and used for forward experiments. Primers used for cloning, mutagenesis and screening are compiled in Table S1.

Construction of the *dcd:dut* mutant strains. *Dut* KO strains carrying the wt[11] or the D83N mutant complementing *dut* copy were used to construct the A115F *dcd:dut* mutant and the D83N *dut*/A115F *dcd:dut* double mutant strains, respectively. A 3.5 kb fragment containing the *dcd:dut* gene and its flanking regions was cloned into p2NIL using HindIII restriction sites (Table S1) generating p2NIL_dcdWT. The A115F mutant *dcd:dut* containing vector was created by a modified QuikChange method[63]. A green fluorescent protein from pLL192[64] was C-terminally fused to the *dcd:dut*. The 6.1 kb PacI cassette carrying the *lacZ* and *sacB* selection markers from pGOAL17 was cloned into the sole PacI site of p2NIL to yield p2NIL_dcdA115F. p2NIL_dcdA115F was electroporated into electrocompetent cells. DCOs carrying the mutant *dcd:dut* were selected by colony PCR and verified by Southern blot (Fig. S2), then finally by sequencing the appropriate genome region. Three parallel strains were chosen and used for forward experiments. While the *dcd:dut* allele exchange worked in the wt *dut* background, it did not work in the D83N *dut* background even after several trials. Primers used for cloning, mutagenesis and screening are compiled in Table S1.

Growth assays. *M. smegmatis* mutant strains were grown in liquid media. OD_{600} was measured every 3 hours. Three parallel strains were used from each investigated strain (9 parallel from each mutation) in these experiments. For quantitative comparison, growth curves were fitted with the $y = a/(1 + \exp(-k^*(x - x_c)))$ equation that yielded the best fit keeping the function as simple as possible.

Determination of the spontaneous mutation rate. To determine the spontaneous mutation rates, three rifampicin sensitive independent colonies of each of the three strains/applied mutations were used to inoculate cultures that were grown at 37 °C, 150 rpm. Saturated cultures were serially diluted in sterile broth and plated onto agar plates to determine total CFUs or onto agar plates supplemented with 100 μg/ml rifampicin. The mutation rate for each of the 9 (3×3) independent cultures/applied mutation was determined as follows,

$$\mu = [(m_t/N_t) - (m_0/N_0)] \times \ln(N_t/N_0)$$

where m_0 is the observed number of mutants at time point 0, m_t is the observed number of mutants at the next time point, and N_0 and N_t are the numbers of cells at time points 0 and t, respectively. The mean mutation rate was calculated for each mutant[36].

Genomic DNA isolation. 10 ml liquid culture was grown until $OD_{600} = 0.5$ and harvested. The cells were resuspended in 1 ml 10 mM Tris, pH 7.5 and 0.1 mm glass beads were added to 2 ml volume. The cells were disrupted by vortex and incubation on ice by turn. After centrifugation, the supernatant was manipulated routinely to purify DNA by phenol:chloroform:IAA (25:24:1) extraction followed by isopropanol precipitation.

Determination of the genomic uracil content. In order to quantify the uracil content of DNA, a real-time quantitative PCR-based assay was used[38]. Genomic DNA was isolated and digested with BamHI. DNA fragments of 5 kb were purified from gel. Real-time PCR was performed on a Mx3000P qPCR System (Agilent Technologies) using EvaGreen dye (Biotium) and PfuTurbo Hotstart DNA polymerase (Stratagene) and Mytaq Hotstart DNA polymerase (Bioline). A segment with 1017 base length defined by the primers (Table S41) was amplified during the PCR reaction. Two-fold dilution series were prepared from the DNA samples. Three parallel strains were used for each mutation in the experiments.

dNTP extraction. Exponential phase cells were grown with appropriate antibiotics until $OD_{600} = 0.6$. The total CFUs were determined for each culture, and cells were centrifuged for extraction. Washed pellets were extracted in 0.5 ml ice-cold 60% methanol overnight at −20 °C. Cells were removed by centrifugation (15–20 min, 13.000 rpm) the methanolic supernatant was boiled for 5 min and centrifuged. The supernatant containing

the soluble dNTP fraction was vacuum-dried (Eppendorf) at 45 °C, 1h. Extracted dNTPs were dissolved in 50 μl dUTPase buffer (30 mM Tris-HCL, pH 7.5, 10 mM $MgCl_2$, 50 mM NaCl, 1 mM EDTA) and stored at −80 °C.

The quantitation of *dcd:dut* and *dut* expression levels. Cells were grown in 50 ml liquid culture until saturation, washed in ice cold PBS and harvested by centrifugation (3100 g, 20 min). Bacterial pellets were resuspended in 1 ml Trizol (Life Technologies), and the cell wall was disrupted by repetitive vortexing with glass beads (6 × 1min). Nucleic acid recovered in the aqueous phase after addition of 0.2 ml chloroform was precipitated with the addition of 0.5 ml isopropanol. The RNA preparations were DNase-treated (10 min, 37 °C) and purified with the Nucleospin RNA Clean-up kit according to the instructions of the manufacturer. Mycobacterial RNA yield were assayed using the Nano-Drop ND-2000 Spectrophotometer (NanoDrop Technologies). RNA samples were amplified from 1 μg total RNA by random hexamer primers using the Transcriptor First Strand cDNA Synthesis Kit (Roche). The resulting cDNA was quantified by Quantitative PCR using EvaGreen (Bioline) and MyTaq PCR master mix (Bioline) in a Stratagene Mx3000P instrument. *sigA* (MSMEG_2758), an endogenous reference gene was used to normalize input cDNA concentration[65]. The relative expression ratios of the examined genes were calculated using the comparative Ct method (ΔΔCt). Primers used to measure cDNA of *sigA, dcd* and *dut* are compiled in Table S1.

Determination of the pyrimidine nucleotide pool size. The determination of the pyrimidine nucleotide pool size in each extract was based on DNA polymerase-catalyzed incorporation of radioactive dNTP into the synthetic oligonucleotide template method described in ref. 66. The reaction mixture (50 μl) contained *Klenow* buffer, 0.5 unit exonuclease negative *Klenow*-fragment (Fermentas), 0.25 μM dTTP/dCTP specific template, 0.25 μM primer (Table S1), 2.5 μM [3H] dATP (1,5 Ci/mmol) (American Radiolabeled Chemicals, Inc.) and 8 μl dNTP-extract or premixed dNTP for calibration. Calibration curve was prepared using 0, 0.1, 0.5, 1, 2, 4 and 8 pmol of each dNTPs/reaction mixture. Incubation was carried out for 60 min at 37 °C and the reaction mix was spotted onto DE81 paper. The papers were dried, washed (3 × 10 min) with 5% Na_2HPO_4, and rinsed once with distilled water and once with 95% ethanol. After drying, radioactivity on the papers was measured in a liquid scintillation counter (Beckman). In case of the dCTP measurement, we used Taq polymerase (RedTaq, Sigma), the incubation was carried out at 48 °C for 1 hour, as Klenow polymerase is capable of incorporating CTP and GTP from nucleotide extracts[39].

dUTP concentration was measured according to Koehler *et al.*[67]. Half of the samples for dTTP measurement were treated with 40 ng recombinant Dut at 37 °C, 45 min. The Dut enzyme was precipitated with 60% methanol. The dUTP in half of the extract was enzymatically hydrolyzed while in the parallel sample it was not. Then dUTP concentration was measured using the same protocol as for dTTP determination.

Two-fold dilution series were prepared from cell extracts in the polymerase reactions. Four samples for each of the three parallel strains were used for each mutation in the experiments (i.e. 12 data points).

Statistical analysis. Statistical analysis was carried out using the STATISTICA.13 software. The non-parametric Kruskal–Wallis test or the one-way ANOVA test with Student-Newman-Keuls multiple comparison post-hoc test was used when samples passed the equal variance (Bartlett's) criterion.

References

1. Mathews, C. K. Deoxyribonucleotides as genetic and metabolic regulators. *FASEB J.* 1–9, doi:10.1096/fj.14-251249 (2014).
2. Kunz, B. A. Mutagenesis and deoxyribonucleotide pool imbalance. *Mutat. Res.* **200**, 133–47 (1988).
3. Nordlund, P. & Reichard, P. Ribonucleotide reductases. *Annu. Rev. Biochem.* **75**, 681–706 (2006).
4. Bianchi, V., Pontis, E. & Reichard, P. Regulation of pyrimidine deoxyribonucleotide metabolism by substrate cycles in dCMP deaminase-deficient V79 hamster cells. *Mol. Cell. Biol.* **7**, 4218–24 (1987).
5. Neuhard, J. & Thomassen, E. Deoxycytidine triphosphate deaminase: identification and function in Salmonella typhimurium. *J. Bacteriol.* **105**, 657–65 (1971).
6. Mollgard, H. & Neuhard, J. Deoxycytidylate Deaminase from Bacillus subtilis. *J. Biol. Chem.* (1978).
7. Vértessy, B. G. & Tóth, J. Keeping uracil out of DNA: physiological role, structure and catalytic mechanism of dUTPases. *Acc. Chem. Res.* **42**, 97–106 (2009).
8. Lari, S.-U., Chen, C.-Y., Vertéssy, B. G., Morré, J. & Bennett, S. E. Quantitative determination of uracil residues in *Escherichia coli* DNA: Contribution of ung, dug, and dut genes to uracil avoidance. *DNA Repair (Amst).* **5**, 1407–20 (2006).
9. Visnes, T. *et al.* Uracil in DNA and its processing by different DNA glycosylases. *Philos. Trans. R. Soc. Lond. B. Biol. Sci.* **364**, 563–8 (2009).
10. Sassetti, C. M., Boyd, D. H. & Rubin, E. J. Genes required for mycobacterial growth defined by high density mutagenesis. *Mol. Microbiol.* **48**, 77–84 (2003).
11. Pecsi, I. *et al.* The dUTPase enzyme is essential in Mycobacterium smegmatis. *PLoS One* **7**, e37461 (2012).
12. el-Hajj, H. H., Zhang, H. & Weiss, B. Lethality of a dut (deoxyuridine triphosphatase) mutation in *Escherichia coli*. *J. Bacteriol.* **170**, 1069–75 (1988).
13. Castillo-Acosta, V. M. *et al.* Pyrimidine requirements in deoxyuridine triphosphate nucleotidohydrolase deficient Trypanosoma brucei mutants. *Mol. Biochem. Parasitol.* **187**, 9–13 (2013).
14. Dengg, M. *et al.* Abrogation of the CLK-2 checkpoint leads to tolerance to base-excision repair intermediates. *EMBO Rep.* **7**, 1046–51 (2006).
15. Muha, V. *et al.* Uracil-containing DNA in Drosophila: stability, stage-specific accumulation, and developmental involvement. *PLoS Genet.* **8**, e1002738 (2012).
16. Siaud, N. *et al.* The SOS screen in Arabidopsis: a search for functions involved in DNA metabolism. *DNA Repair (Amst).* **9**, 567–78 (2010).
17. Tormo-Más, M. A. *et al.* Moonlighting bacteriophage proteins derepress staphylococcal pathogenicity islands. *Nature* **465**, 779–82 (2010).
18. Ariza, M.-E. & Williams, M. V. A human endogenous retrovirus K dUTPase triggers a TH1, TH17 cytokine response: does it have a role in psoriasis? *J. Invest. Dermatol.* **131**, 2419–27 (2011).
19. Szabó, J. E. *et al.* Highly potent dUTPase inhibition by a bacterial repressor protein reveals a novel mechanism for gene expression control. *Nucleic Acids Res.* **42**, 11912–20 (2014).

20. Leveles, I. *et al*. Structure and enzymatic mechanism of a moonlighting dUTPase. *Acta Crystallogr. D. Biol. Crystallogr.* **69**, 2298–308 (2013).
21. Helt, S. S. *et al*. Mechanism of dTTP inhibition of the bifunctional dCTP deaminase:dUTPase encoded by Mycobacterium tuberculosis. *J. Mol. Biol.* **376**, 554–69 (2008).
22. Griffin, J. E. *et al*. High-resolution phenotypic profiling defines genes essential for mycobacterial growth and cholesterol catabolism. *PLoS Pathog.* **7**, e1002251 (2011).
23. Pécsi, I. *et al*. Nucleotide pyrophosphatase employs a P-loop-like motif to enhance catalytic power and NDP/NTP discrimination. *Proc. Natl. Acad. Sci. USA* **108**, 14437–42 (2011).
24. Barabás, O., Pongrácz, V., Kovári, J., Wilmanns, M. & Vértessy, B. G. Structural insights into the catalytic mechanism of phosphate ester hydrolysis by dUTPase. *J. Biol. Chem.* **279**, 42907–15 (2004).
25. Vertessy, B. G. Flexible glycine rich motif of *Escherichia coli* deoxyuridine triphosphate nucleotidohydrolase is important for functional but not for structural integrity of the enzyme. *Proteins* **28**, 568–79 (1997).
26. Nord, J., Kiefer, M., Adolph, H. W., Zeppezauer, M. M. & Nyman, P. O. Transient kinetics of ligand binding and role of the C-terminus in the dUTPase from equine infectious anemia virus. *FEBS Lett.* **472**, 312–6 (2000).
27. Shao, H. *et al*. Characterization and mutational studies of equine infectious anemia virus dUTPase. *Biochim. Biophys. Acta* **1339**, 181–91 (1997).
28. Freeman, L. *et al*. The flexible motif V of Epstein-Barr virus deoxyuridine 5′-triphosphate pyrophosphatase is essential for catalysis. *J. Biol. Chem.* **284**, 25280–9 (2009).
29. Mol, C. D., Harris, J. M., McIntosh, E. M. & Tainer, J. A. Human dUTP pyrophosphatase: uracil recognition by a beta hairpin and active sites formed by three separate subunits. *Structure* **4**, 1077–92 (1996).
30. Pecsi, I., Leveles, I., Harmat, V., Vertessy, B. G. & Toth, J. Aromatic stacking between nucleobase and enzyme promotes phosphate ester hydrolysis in dUTPase. *Nucleic Acids Res.* **38**, 7179–86 (2010).
31. Takács, E., Grolmusz, V. K. & Vértessy, B. G. A tradeoff between protein stability and conformational mobility in homotrimeric dUTPases. *FEBS Lett.* **566**, 48–54 (2004).
32. Németh-Pongrácz, V. *et al*. Flexible segments modulate co-folding of dUTPase and nucleocapsid proteins. *Nucleic Acids Res.* **35**, 495–505 (2007).
33. Mustafi, D., Bekesi, A., Vertessy, B. G. & Makinen, M. W. Catalytic and structural role of the metal ion in dUTP pyrophosphatase. *Proc. Natl. Acad. Sci. USA* **100**, 5670–5 (2003).
34. Szabó, J. E., Takács, E., Merényi, G., Vértessy, B. G. & Tóth, J. Trading in cooperativity for specificity to maintain uracil-free DNA. *Sci. Rep.* **6**, 24219 (2016).
35. Maiques, E. *et al*. Another look at the mechanism involving trimeric dUTPases in *Staphylococcus aureus* pathogenicity island induction involves novel players in the party. *Nucleic Acids Res.* **44**, 5457–5469 (2016).
36. David, H. L. Probability distribution of drug-resistant mutants in unselected populations of Mycobacterium tuberculosis. *Appl. Microbiol.* **20**, 810–814 (1970).
37. Pope, C. F., O'Sullivan, D. M., McHugh, T. D. & Gillespie, S. H. A practical guide to measuring mutation rates in antibiotic resistance. *Antimicrob. Agents Chemother.* **52**, 1209–14 (2008).
38. Horváth, A. & Vértessy, B. G. A one-step method for quantitative determination of uracil in DNA by real-time PCR. *Nucleic Acids Res.* **38**, e196 (2010).
39. Ferraro, P., Franzolin, E., Pontarin, G., Reichard, P. & Bianchi, V. Quantitation of cellular deoxynucleoside triphosphates. *Nucleic Acids Res.* **38**, e85 (2010).
40. Martí, R., Dorado, B. & Hirano, M. Measurement of Mitochondrial dNTP Pools. *Methods Mol. Biol.* **837**, 135–148 (2012).
41. Kumar, P., Bharti, S. K. & Varshney, U. Uracil excision repair in Mycobacterium tuberculosis cell-free extracts. *Tuberculosis (Edinb).* **91**, 212–8 (2011).
42. Srinath, T., Bharti, S. K. & Varshney, U. Substrate specificities and functional characterization of a thermo-tolerant uracil DNA glycosylase (UdgB) from Mycobacterium tuberculosis. *DNA Repair (Amst).* **6**, 1517–28 (2007).
43. Sang, P. B., Srinath, T., Patil, A. G., Woo, E.-J. & Varshney, U. A unique uracil-DNA binding protein of the uracil DNA glycosylase superfamily. *Nucleic Acids Res.* **43**, 8452–8463 (2015).
44. Duncan, B. K. & Weiss, B. Specific mutator effects of ung (uracil-DNA glycosylase) mutations in *Escherichia coli*. *J. Bacteriol.* **151**, 750–5 (1982).
45. Glassner, B. J., Rasmussen, L. J., Najarian, M. T., Posnick, L. M. & Samson, L. D. Generation of a strong mutator phenotype in yeast by imbalanced base excision repair. *Proc. Natl. Acad. Sci. USA* **95**, 9997–10002 (1998).
46. Schaaper, R. M. & Mathews, C. K. Mutational consequences of dNTP pool imbalances in *E. coli* Roel. *DNA Repair (Amst)*. DNA Repair 12 (2013) 73–79, doi:10.1016/j.dnarep.2012.10.011 (2013).
47. Nordman, J. & Wright, A. The relationship between dNTP pool levels and mutagenesis in an *Escherichia coli* NDP kinase mutant. *Proc. Natl. Acad. Sci. USA* **105**, 10197–202 (2008).
48. Sung, J. S. & Mosbaugh, D. W. *Escherichia coli* uracil- and ethenocytosine-initiated base excision DNA repair: Rate-limiting step and patch size distribution. *Biochemistry* **42**, 4613–4625 (2003).
49. Gon, S. & Beckwith, J. Ribonucleotide Reductases: Influence of Environment on Synthesis and Activity. *Antioxidants Redox Signal.* **8** (2006).
50. Davidson, M. B. *et al*. Endogenous DNA replication stress results in expansion of dNTP pools and a mutator phenotype. *EMBO J.* **31**, 895–907 (2012).
51. Ahluwalia, D., Bienstock, R. J. & Schaaper, R. M. Novel mutator mutants of *E. coli* nrdAB ribonucleotide reductase: Insight into allosteric regulation and control of mutation rates. *DNA Repair (Amst).* **11**, 480–487 (2012).
52. Gon, S., Napolitano, R., Rocha, W., Coulon, S. & Fuchs, R. P. Increase in dNTP pool size during the DNA damage response plays a key role in spontaneous and induced-mutagenesis in *Escherichia coli*. *Proc. Natl. Acad. Sci.* **108**, 19311–19316 (2011).
53. Kumar, D., Viberg, J., Nilsson, A. K. & Chabes, A. Highly mutagenic and severely imbalanced dNTP pools can escape detection by the S-phase checkpoint. *Nucleic Acids Res.* **38**, 3975–83 (2010).
54. Varga, B. *et al*. Active site of mycobacterial dUTPase: structural characteristics and a built-in sensor. *Biochem. Biophys. Res. Commun.* **373**, 8–13 (2008).
55. Johansson, E. *et al*. Regulation of dCTP deaminase from *Escherichia coli* by nonallosteric dTTP binding to an inactive form of the enzyme. *FEBS J.* **274**, 4188–98 (2007).
56. Tóth, J., Varga, B., Kovács, M., Málnási-Csizmadia, A. & Vértessy, B. G. Kinetic mechanism of human dUTPase, an essential nucleotide pyrophosphatase enzyme. *J. Biol. Chem.* **282**, 33572–82 (2007).
57. Siggaard, J. H. B. *et al*. Concerted bifunctionality of the dCTP deaminase-dUTPase from Methanocaldococcus jannaschii: a structural and pre-steady state kinetic analysis. *Arch. Biochem. Biophys.* **490**, 42–9 (2009).
58. Guillet, M., Van Der Kemp, P. A. & Boiteux, S. dUTPase activity is critical to maintain genetic stability in Saccharomyces cerevisiae. *Nucleic Acids Res.* **34**, 2056–66 (2006).
59. Warner, H. R., Duncan, B. K., Garrett, C. & Neuhard, J. Synthesis and metabolism of uracil-containing deoxyribonucleic acid in *Escherichia coli*. *J. Bacteriol.* **145**, 687–95 (1981).
60. Hou, H. F., Liang, Y. H., Li, L. F., Su, X. D. & Dong, Y. H. Crystal Structures of Streptococcus mutans 2′-Deoxycytidylate Deaminase and Its Complex with Substrate Analog and Allosteric Regulator dCTP × Mg2+. *J. Mol. Biol.* **377**, 220–231 (2008).

61. Marx, A. & Alian, A. The First Crystal Structure of a dTTP-bound Deoxycytidylate Deaminase Validates and Details the Allosteric-Inhibitor Binding Site. *J. Biol. Chem.* **290**, 682–690 (2015).
62. Kadirvelraj, R., Sennett, N. C., Polizzi, S. J., Weitzel, S. & Wood, Z. A. Role of packing defects in the evolution of allostery and induced fit in human UDP-glucose dehydrogenase. *Biochemistry* **50**, 5780–5789 (2011).
63. Liu, H. & Naismith, J. H. An efficient one-step site-directed deletion, insertion, single and multiple-site plasmid mutagenesis protocol. *BMC Biotechnol.* **8**, 91 (2008).
64. Srivastava, V. *et al*. Macrophage-specific Mycobacterium tuberculosis genes: identification by green fluorescent protein and kanamycin resistance selection. *Microbiology* **153**, 659–66 (2007).
65. Milano, A. *et al*. The Mycobacterium tuberculosis Rv2358–furB operon is induced by zinc. *Res. Microbiol.* **155**, 192–200 (2004).
66. Sherman, P. A. & James, A. Fyfe. Enzymatic Assay for Deoxyribonucleoside Triphosphates Using Synthetic Oligonucleotides as Template. Primers. *Anal. Biochem.* **226**, 222–226 (1989).
67. Koehler, S. E. & Ladner, R. D. Small interfering RNA-mediated suppression of dUTPase sensitizes cancer cell lines to thymidylate synthase inhibition. *Mol. Pharmacol.* **66**, 620–6 (2004).
68. Hochhauser, S. J. & Weiss, B. *Escherichia coli* mutants deficient in deoxyuridine triphosphatase. *J. Bacteriol.* **134**, 157–66 (1978).
69. Taylor, A. F. & Weiss, B. Role of exonuclease III in the base excision repair of uracil-containing DNA. *J. Bacteriol.* **151**, 351–7 (1982).
70. Kouzminova, E. A. & Kuzminov, A. Chromosomal fragmentation in dUTPase-deficient mutants of *Escherichia coli* and its recombinational repair. *Mol. Microbiol.* **51**, 1279–95 (2004).
71. Castillo-Acosta, V. M. *et al*. Increased uracil insertion in DNA is cytotoxic and increases the frequency of mutation, double strand break formation and VSG switching in Trypanosoma brucei. *DNA Repair (Amst).* **11**, 986–95 (2012).
72. Castillo-Acosta, V. M., Estévez, A. M., Vidal, A. E., Ruiz-Perez, L. M. & González-Pacanowska, D. Depletion of dimeric all-alpha dUTPase induces DNA strand breaks and impairs cell cycle progression in Trypanosoma brucei. *Int. J. Biochem. Cell Biol.* **40**, 2901–13 (2008).
73. Gadsden, M. H., McIntosh, E. M., Game, J. C., Wilson, P. J. & Haynes, R. H. dUTP pyrophosphatase is an essential enzyme in Saccharomyces cerevisiae. *EMBO J.* **12**, 4425–31 (1993).
74. Studebaker, A. W., Lafuse, W. P., Kloesel, R. & Williams, M. V. Modulation of human dUTPase using small interfering RNA. *Biochem. Biophys. Res. Commun.* **327**, 306–10 (2005).
75. Merényi, G. *et al*. Cellular response to efficient dUTPase RNAi silencing in stable HeLa cell lines perturbs expression levels of genes involved in thymidylate metabolism. *Nucleosides. Nucleotides Nucleic Acids* **30**, 369–90 (2011).
76. Dos Santos, R. S. *et al*. dUTPase (*DUT*) Is Mutated in a Novel Monogenic Syndrome With Diabetes and Bone Marrow Failure. *Diabetes* **66**, 1086–1096 (2017).
77. Chen, C.-W. *et al*. The Impact of dUTPase on Ribonucleotide Reductase-Induced Genome Instability in Cancer Cells. *Cell Rep.* **16**, 1287–1299 (2016).
78. Dubois, E. *et al*. Homologous recombination is stimulated by a decrease in dUTPase in Arabidopsis. *PLoS One* **6**, e18658 (2011).

Acknowledgements

We thank Drs Ildikó Pécsi, András Horváth and Gábor Merényi for constructive advice on mycobacterial strain construction and genomic uracil and dNTP pool measurements. We thank Prof. Camille Locht for mycobacterial vector pLL192. We also thank Judit E. Szabó and Prof. Mihály Kovács for their constructive comments and suggestions on the manuscript. This work was supported by the National Research, Development and Innovation Office, Hungary [OTKA K115993; K109486; K119493; NVKP_16-1-2016-0020], ICGEB CRP/HUN14-01, the European Commission FP7 Biostruct-X project [contract No. 283570]. RH is the recipient of a Postgraduate Research Fellowship of Gedeon Richter Plc. Hungary. JT is the recipient of the János Bolyai Research Scholarship of the Hungarian Academy of Sciences. The funders had no role in study design, data collection and analysis, decision to publish, or preparation of the manuscript.

Author Contributions

Conceived and designed the experiments: R.H., A.L., E.V.S., B.G.V., J.T. Performed the experiments: R.H., A.L., E.V.S. Analyzed the data: R.H., A.L., E.V.S., J.T. Wrote the paper: R.H., A.L., E.V.S., B.G.V., J.T. All authors reviewed the manuscript.

Additional Information

Supplementary information accompanies this paper at doi:10.1038/s41598-017-06206-y

Competing Interests: The authors declare that they have no competing interests.

Publisher's note: Springer Nature remains neutral with regard to jurisdictional claims in published maps and institutional affiliations.

Open Access This article is licensed under a Creative Commons Attribution 4.0 International License, which permits use, sharing, adaptation, distribution and reproduction in any medium or format, as long as you give appropriate credit to the original author(s) and the source, provide a link to the Creative Commons license, and indicate if changes were made. The images or other third party material in this article are included in the article's Creative Commons license, unless indicated otherwise in a credit line to the material. If material is not included in the article's Creative Commons license and your intended use is not permitted by statutory regulation or exceeds the permitted use, you will need to obtain permission directly from the copyright holder. To view a copy of this license, visit http://creativecommons.org/licenses/by/4.0/.

© The Author(s) 2017

Supplementary Information

Differential control of dNTP biosynthesis and genome integrity maintenance by the dUTPase superfamily enzymes

Rita Hirmondó*[1], Anna Lopata*[1], Éva Viola Surányi*[1,2], Beáta G. Vértessy[1,2] and Judit Tóth[#1]

1 Institute of Enzymology, RCNS, Hungarian Academy of Sciences, Budapest, Hungary,

2 Dept of Applied Biotechnology, Budapest University of Technology and Economics, Budapest, Hungary

*equal contribution

[#] Corresponding author:

Judit Toth

Institute of Enzymology, Res Cent for Nat Sci, HAS

Magyar tudósok körútja 2, H-1117, Budapest, Hungary

Phone: +36 1 382 6707

e-mail: toth.judit@ttk.mta.hu

Figure S1 Effect of the created mutations on the substrate binding of *M. tuberculosis* dUTPase (**A**) CD equilibrium titrations. Comparison of ligand (dUPNPP) binding to the WT, S148A and to the T138stop mutant dUTPase. Solid lines represent quadratic fits to the data yielding the following K_d values: 0.9 ± 0.5 μM for the wt, 1.8 ± 1.0 μM for the S148A and 3.9 ± 1.3 μM for the T138stop mutant. (**B**) Fluorescence intensity titration of the single Trp in the D83N mutant upon dUPNPP binding. The smooth line through the data is a quadratic fit yielding the K_d value of 1.5 ± 0.6 μM. Errors represent S.D. for n = 3. For more parameters see Table 1.

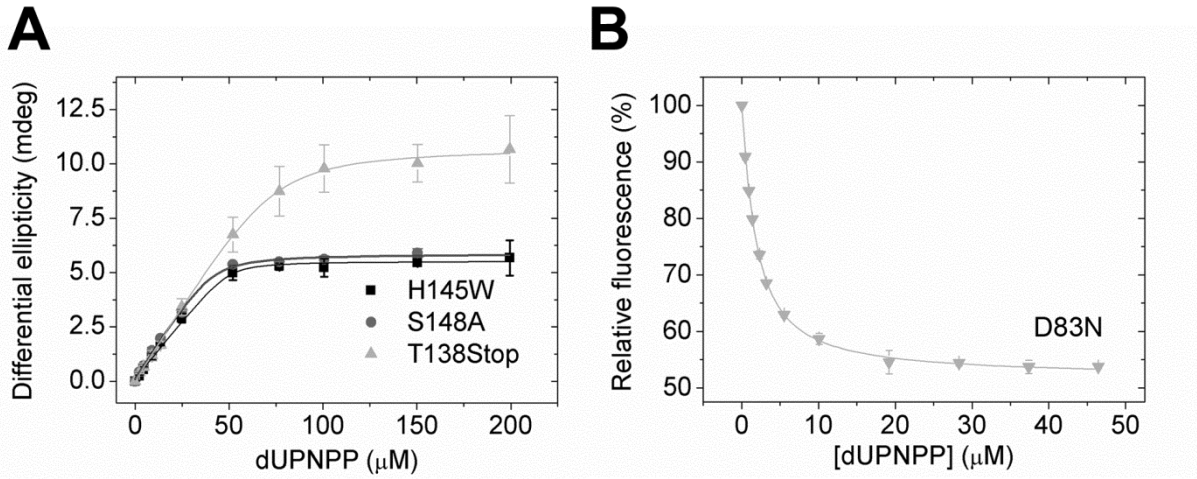

Materials and Methods

Fluorescence intensity titrations. Fluorescence was measured in a Jobin Yvon Spex Fluoromax-3 spectrofluorometer at 20 °C, with excitation of the single Trp at 295 nm (slit 1 nm) and emission at 347 nm (slit 5 nm). 4 μM protein was titrated by the addition of 1-2 μl aliquots from concentrated dUPNPP solutions (purchased from Jena Bioscience, Germany). Because large concentrations of nucleotides were used, care was taken to correct for any additional fluorescence or inner filter effect imposed on the measured intensities by the nucleotide stock solutions.

Circular dichroism intensity titrations. CD spectra were recorded at 20 ^{o}C on a JASCO 720 spectropolarimeter using a 10 mm path length cuvette. 50 μM protein was titrated by stepwise addition of the non-hydrolysable substrate analogue dUPNPP, in a buffer containing 20mM HEPES pH 7.5, 50mM NaCl and 2 mM $MgCl_2$. A spectrum between λ = 240-350 nm was recorded at each nucleotide concentration. Differential curves were obtained by subtracting the signal of dUPNPP alone from that of the corresponding complex. Differential ellipticity at λ_{max} = 269 nm was plotted against the

dUPNPP concentration to obtain the binding curves. The following quadratic equation was fitted to the experimental curves:

$$y = s + A*\left((c + x + K) - \sqrt{(c + x + K)^2 - 4*c*x} \right) / 2*c$$

s = y at x = 0; A = amplitude; c = protein concentration; K = K_d

Figure S2 Southern blot analysis of the mutant strains

Southern blot analysis resulted in 1.5 kb and 3.3 kb bands in the case of wt *dut* and the S148A, T138stop and D83N mutant *dut* strains, and 5.4 kb and a 2.1 kb bands in the case of wt *dcd:dut* and A115F *dcd:dut* mutant strains, respectively.

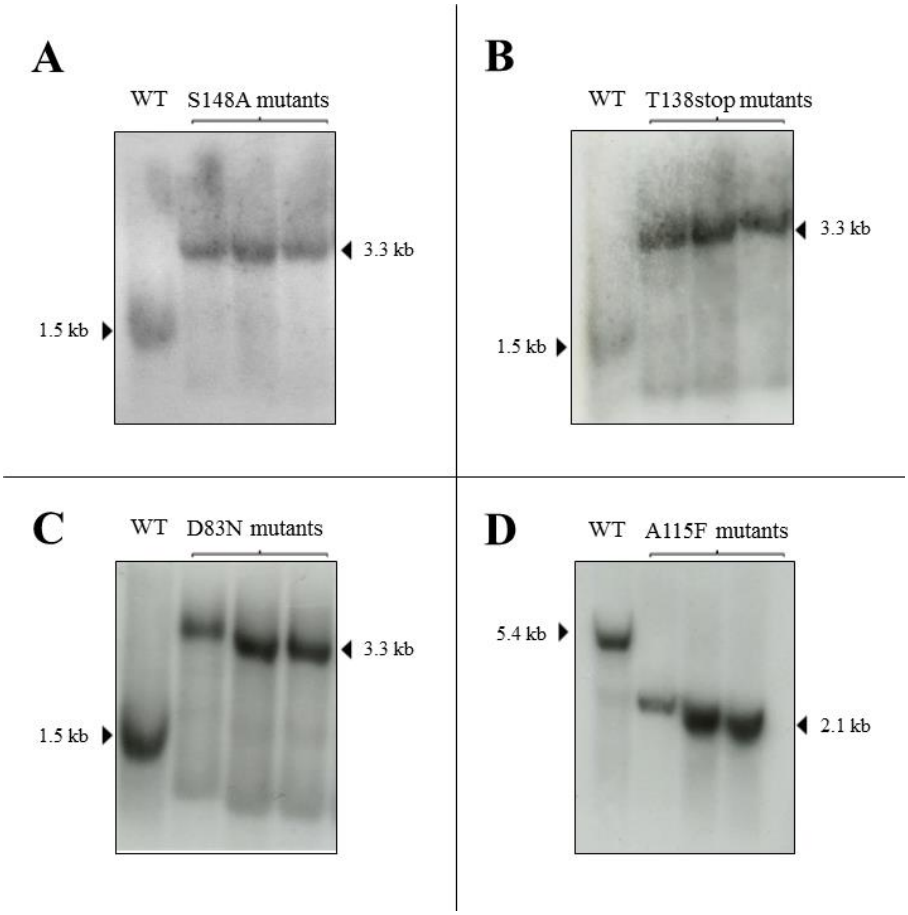

Materials and Methods

Southern-blot analysis. Southern-blot analysis was carried out using the DecaLabel TM DNA Labeling Kit (Fermentas) according to the manufacturer's instruction. Restriction digestion of the genomic DNA was performed using NcoI and PstI resulting in 1.5 kb and 3.3 kb fragments in the case of WT and *dut*-disrupted mutant strains, respectively. The probe was a 0.7 kb fragment encompassing the *dut* gene (for primers see Table S2). Restriction digestion of the genomic DNA was performed using NcoI resulting in 5.4 kb and 2.1 kb fragments in the case of WT and A115F *dcd:dut* mutant strains, respectively. The probe was a 0.5 kb fragment following the coding region of the *dcd:dut* gene (for primers see Table S2).

Table S1. Oligonucleotide sequences used in this study

Primer sequence	Application	
5’- GGTGGCTGGGGTTCCGCCGGCGGACATGCG -3’	S148A mutant	QuikChange mutagenesis to create mutant Mtb dut enzymes
5’- CGCATGTCCGCCGGCGGAACCCCAGCCACC -3’		
5’- GGGCTGGCCTCGTGATCCCGCGGCGACGG -3’	T138stop mutant	
5’- CCGTCGCCGCGGGATCACGAGGCCAGCCC -3’		
5’- CCGGGCACCATCAACGCGGGTTATCGTGGGG -3’	D83N mutant	
5’- GGCCCGTGGTAGTTGCGCCCAATAGCACCCC -3’		
5’- CGGTCACGGTTCCGCCGGCGGACATGCG -3’	S148A mutant	QuikChange mutagenesis to create complementing *dut* mutant pGem vectors
5’- CGCATGTCCGCCGGCGGAACCGTGACCG -3’		
5’- GCCGGTTTGGCGGACTGAACCCGTGGCG -3'	T138stop mutant	
5’- CGCCACGGGTTCAGTCCGCCAAACCGGC -3'		
5’- CCGGCACGATCAACGCCGGCTACCG -3'	D83N mutant	
5’- CGGTAGCCGGCGTTGATCGTGCCGG -3'		
5’- CAACCTGGATCCGCAGACG -3'	SCO, DCO screening for *dut* mutant *M. smegmatis* strains	
5’- CACCTTCCTGCACGACTTCG -3'		
5’- CGTCTGCGGATCCAGGTTG -3'		
5’- GAACCACCAGAACCATCGGG -3'	Confirmation of the integration of the complement vector into the genome	
5’- CAGTACGCGAAGAACCACGCC -3'		
5’- GGCGGACCTTTCCGGAGAGG -3'	*dut* probe amplification for Southern blot	
5’- CGGGGGCCAGTTCGACGTTC -3'		
5’- TTCCTGAGCACACCGTGACC -3'	SCO, DCO screening for *dcd:dut* mutant *M. smegmatis* strains	
5’- GTTCCGAGAATTGCTGCGACG -3'		
5'- CGCCAATTCACTTGCGTCTCAC -3'	A115F *dcd:dut* probe amplification for Southern blot	
5’- ACGTGACACCGATCGACTTGAGAT -3'		
5'- GCTGACGCACTCGACCTTCGGCTTCATCGATCCGGG -3'	QuikChange mutagenesis to create the A115F mutant Dcd:dut	
5'- CCCGGATCGATGAAGCCGAAGGTCGAGTGCGTCAGC -3'		
5’- TACTAAGATCTGCCCCGCCGGAAGGAGATATACATATGAGTAAAGGAG -3'	Cloning the C-terminal GFP fusion A115F *dcd:dut*	
5’- TAGTAAGATCTTCATTTGTATAGTTCATCCATGCC -3'		
5'- TCTCAACCGAAGAGTTCACC -3'	Primers for genomic uracil quantification	
5'- ATTCCGTAGTCATCCTGTGG -3'		
5'- GTACCTGGTGCGTCTGC -3'	Amplification of 1 kbp of *rpoB*	
5'- AGGCGGTAGGACTGACG -3'		
5'- TTTGTTTGTTTGTTTGTTTGGGCGGTGGAGGCGG -3'	Primers for dNTP pool measurements	
5'- TTATTATTATTATTATTAGGCGGTGGAGGCGG -3'		
5'- CCGCCTCCACCGCC -3'		
5’- CGTCGCCGATGGTCT G -3’	*sigA* cDNA amplification primers	
5’- CCACGCCCGAAGAGC -3’		
5’- CATACCGCACGGAATGGT -3’	*dut* cDNA amplification primers	
5’- TGATCAGCGAAACCTTGATCTC -3’		
5’- CTTCATCGATCCGGGCTTC -3’	*dcd:dut* cDNA amplification primers	
5’- CAGCTGCCCGATCTTCAT -3’		

5’- ATTAGGATCCAGTGCTGCTTTCCGATCGTGACATCC -3’	*M. smegmatis* Dcd:dut cloning primers
5'- ATTAAAGCTTTCAGGACTTGATGAAGTTGAGGTGCG -3'	

11912–11920 *Nucleic Acids Research, 2014, Vol. 42, No. 19* *Published online 1 October 2014*
doi: 10.1093/nar/gku882

Highly potent dUTPase inhibition by a bacterial repressor protein reveals a novel mechanism for gene expression control

Judit E. Szabó[1,2,*], Veronika Németh[1], Veronika Papp-Kádár[1,2], Kinga Nyíri[1,2], Ibolya Leveles[1,2], Ábris Á. Bendes[1,2], Imre Zagyva[1,2], Gergely Róna[1,2], Hajnalka L. Pálinkás[1,2,3], Balázs Besztercei[1], Olivér Ozohanics[1], Károly Vékey[1], Károly Liliom[1], Judit Tóth[1,*] and Beáta G. Vértessy[1,2,*]

[1]Institutes of Enzymology and Organic Chemistry, RCNS, Hungarian Academy of Sciences, Budapest, Hungary, [2]Department of Applied Biotechnology and Food Sciences, Budapest University of Technology and Economics, Budapest, Hungary and [3]Doctoral School of Multidisciplinary Medical Science, University of Szeged, Szeged, Hungary

Received July 12, 2014; Revised September 11, 2014; Accepted September 12, 2014

ABSTRACT

Transfer of phage-related pathogenicity islands of *Staphylococcus aureus* (SaPI-s) was recently reported to be activated by helper phage dUTPases. This is a novel function for dUTPases otherwise involved in preservation of genomic integrity by sanitizing the dNTP pool. Here we investigated the molecular mechanism of the dUTPase-induced gene expression control using direct techniques. The expression of SaPI transfer initiating proteins is repressed by proteins called Stl. We found that Φ11 helper phage dUTPase eliminates SaPIbov1 Stl binding to its cognate DNA by binding tightly to Stl protein. We also show that dUTPase enzymatic activity is strongly inhibited in the dUTPase:Stl complex and that the dUTPase:dUTP complex is inaccessible to the Stl repressor. Our results disprove the previously proposed G-protein-like mechanism of SaPI transfer activation. We propose that the transfer only occurs if dUTP is cleared from the nucleotide pool, a condition promoting genomic stability of the virulence elements.

INTRODUCTION

Staphylococcus aureus (*S. aureus*) is one of the most important opportunistic pathogens causing nosocomial and community acquired infections, including several toxinoses, such as food poisoning, toxic shock syndrome (TSS), necrotizing pneumonitis and necrotizing fasciitis. Mobile genetic elements of *S. aureus* contribute largely to pathogenesis and to the spread of virulence factors and antibiotic resistance (1,2).

Major superantigenes (e.g. TSS toxin 1 (TSST-1), Enterotoxin B (SEB)) responsible for the different toxinoses are encoded as accessory genes by phage-related *S. aureus* pathogenicity islands (SaPIs) of diverse size (2–17 kb). SaPIs themselves do not encode any machinery for horizontal gene transfer, they take advantage of phage reproduction instead (2). In the absence of a helper phage, the expression of SaPI-encoded transfer initiating proteins (integrase and excisionase (3)) is repressed by SaPI-encoded repressor proteins called Stl. Helper phage infection or prophage activation relieves Stl repression and leads to the excision and extensive replication of SaPI. The resulting SaPI DNA is packaged into phage capsids (2). The helper phage proteins responsible for the de-repression are identified only in a few cases: SaPI1 is de-repressed by Sri, a DNA-binding protein, Sapibov2 is de-repressed by a small protein of unknown function, while SaPIbov5 and SaPIbov1 are de-repressed by dUTPases from phage 80α (for both) and phage Φ11 (for SapiBov1)) (4,5). In the latter case, it was shown also that phage Φ11 dUTPase disrupts the preformed Stl-DNA interaction, relieving the transcription of the repressed protein responsible for the initiation of the transfer (5).

The discovery of new 'moonlighting' functions of metabolic enzymes in gene expression regulation is of much current interest. In this specific case, dUTPase, a well characterized enzyme in pyrimidine biosynthesis and genome integrity maintenance, was found to regulate the transfer of mobile genetic elements. dUTPase is responsible for hy-

*To whom correspondence should be addressed. Tel: +36 1 382 6707; Email: vertessy@mail.bme.hu, vertessy.beata@ttk.mta.hu
Correspondence may also be addressed to Judit Tóth. Tel: +36 1 382 6707; Email: toth.judit@ttk.mta.hu
Correspondence may also be addressed to Judit E. Szabó. Tel: + 36 1 382 6731; Email: szabo.judit.eszter@ttk.mta.hu

© The Author(s) 2014. Published by Oxford University Press on behalf of Nucleic Acids Research.
This is an Open Access article distributed under the terms of the Creative Commons Attribution License (http://creativecommons.org/licenses/by/4.0/), which permits unrestricted reuse, distribution, and reproduction in any medium, provided the original work is properly cited.

Downloaded from https://academic.oup.com/nar/article/42/19/11912/2902985 by guest on 04 November 2021

drolyzing dUTP, thereby providing dUMP and regulating the cellular dUTP: dTTP ratio (6–10).

A recent study showed that dUTPase mutants that are defective in dUTPase activity are also defective in SaPI activation (4). Based on indirect cellular experiments and the crystal structures of wild type and mutant phage dUTPases in complex with a dUTP analog, the authors also suggested that a specific conformational shift of the C-terminal arm of dUTPase, induced by dUTP binding is indispensable for the dUTPase:Stl interaction (4). The conformational shift of the C-terminal segment of trimeric dUTPases (such as dUTPases in phages 80α and Φ11) has been characterized in-depth in the literature as the single major conformational change occurring upon substrate binding and required for efficient catalysis (11–14). The dUTPase-regulated gene transfer was further proposed to adopt a mechanism highly reminiscent of G protein-mediated signaling, where the switching conformational change occurs upon GTP binding to the G protein (4). However, such a mechanism is in disagreement with the kinetic properties of the dUTPase enzyme cycle, which is fundamentally different from that of G proteins (15–20).

To resolve this contradiction, we aimed at a quantitative in-depth characterization of the dUTPase-induced derepression mechanism. Our results from numerous biophysical methods disprove the previously suggested G protein-like mechanism and suggest an alternative regulation model that fits into a broad physiological context, as well.

MATERIALS AND METHODS

Cloning, protein expression and purification

$Stl_{SaPIbov1}$ protein (GenBank ID AAG29617.1) supplemented with an N-terminal HIS-tag was cloned into the pGEX-4T-1 vector to allow glutathione-S-transferase fusion expression and purification (details are given in the Supplementary Material). In this study we used tag-free Φ11 dUTPases, that were expressed from pETDuet-1 (Novagen) vector as was described previously for $\Phi11DUT^{WT}$ (21). Purification was performed on a Q-sepharose ion-exchange chromatography, followed by gel filtration on a Superdex 75 column (GE Healthcare) using an AKTA Explorer purifier. For purification details see the Supplementary Material. Protein concentrations are given in monomers.

Isothermal titration calorimetry (ITC)

ITC experiments were carried out at 293 K on a Microcal ITC_{200} instrument. Proteins were dialyzed into 20 mM HEPES (pH = 7.5), 300 mM NaCl, 5 mM $MgCl_2$, 1 mM TCEP and were used at 36 μM (Stl, in the cell) and 230 μM ($\Phi11dUTPase^{WT}$, in the syringe) concentration. Both protein concentrations correspond to subunits. As a control, Φ11 dUTPase was also injected into the buffer to allow for considering mixing and dilution heat effects. The binding isotherms were fitted with an independent binding sites model 'One Set of Sites' (ORIGIN 7.5 software Microcal). This model is appropriate for any number of sites n if all sites have the same K and ΔH.

Native gel electrophoresis

Native gel electrophoresis was performed in 8% polyacrylamide gels. After 2 h pre-electrophoresis with constant voltages of 100 V, the electrophoresis was performed for 2.5 h at 150 V in pH 8.7 Tris-HCl buffer. During electrophoresis the apparatus was cooled on ice. Note that 10 μl of a sample was added to each well. The gel was stained with Coomassie-Brilliant Blue dye.

Quartz crystal microbalance (QCM) measurements

Stl was immobilized on sensor chips (Attana AB, Stockholm) (for details see the Supplementary Material). Binding experiments were performed with a continuous flow (25 μl/min) of running buffer (10 mM HEPES, 150 mM NaCl, 0.005% Tween 20, pH 7.4) allowing for a contact time of 90 s. Analyte samples were prepared in running buffer for $\Phi11$ $dUTPase^{WT}$ and $\Phi11$ $dUTPase^{F164W}$ (0.46 μM) in the absence and presence of 0.5 mM dUTP or 2 mM dUMP at 298 K. In the case of measurements with dUTP care was taken to ensure steady-state dUTP hydrolysis state during the experiment. The frequency response curves were analyzed by the BIAevaluation 4.1 software.

Steady-state fluorescent measurements

For steady-state measurements of Trp fluorescence a Perkin Elmer EnSpire Multimode Plate Reader was used (details in Supplementary Material). For titration the binding partner was pre-incubated in assay buffer (phosphate buffered saline (PBS) (pH 7.3), 5 mM $MgCl_2$, 400 mM NaCl) for 20 min. Titration results were fitted to the quadratic binding equation describing 1:1 stoichiometry for the dissociation equilibrium with no cooperativity:

$$y = s + \frac{A\left[(c + x + K) - \sqrt{(c + x + K)^2 - 4cx}\right]}{2c}, \quad (1)$$

where x is the concentration of titrant and y is the fluorescence intensity, $s = y$ at $x = 0$, A is the total amplitude of the fluorescence intensity change, c is the enzyme concentration, K is the half-saturation coefficient. The concentrations of titrands are given in the figure legends. All measurements were done at 293 K.

Transient kinetics experiments

Stopped-flow measurements were carried out using an SX-20 (Applied Photophysics, UK) stopped-flow instrument, following Trp fluorescence at 293 K, as described previously (17,18). Typically 5–8 traces were collected and averaged. The mixed species and their concentrations (post-mixing) are indicated in the figure legends.

Enzyme activity assay

Proton release during the transformation of dUTP into dUMP and PPi was followed continuously at 559 nm at 293 K (19) using a JASCO-V550 spectrophotometer. Reaction mixtures contained 10 nM enzyme and varying concentrations of Stl in activity buffer (1 mM Hepes (pH 7.5), 5 mM

Downloaded from https://academic.oup.com/nar/article/42/19/11912/2902985 by guest on 04 November 2021

$MgCl_2$, 150 mM KCl and 40 μM Phenol Red indicator). The reaction was started with the addition of 30 μM dUTP after 5 min pre-incubation of the two proteins. Initial velocity was determined from the slope of the first 10% of the progress curve.

Electrophoretic mobility shift assay (EMSA)

EMSA experiments were done using an 183mer oligonucleotide (Stl binding $site_{183}$) derived from the 171mer oligonucleotide described previously (5). Stl binding $site_{183}$ (75 ng) and the investigated proteins were mixed in EMSA buffer (PBS (pH 7.3), 5 mM $MgCl_2$, 75 mM NaCl, 0.5 mM ethylenediaminetetraacetic acid) in the presence or absence of α,β-imido-dUTP (dUPNPP) in 20 μl total volume. Before loading onto 8% polyacrylamide gel the samples were incubated for 15 min at room temperature. Electrophoresis was performed in Tris- Borate- EDTA (TBE) buffer for about 60 min at room temperature, after 1 h pre-electrophoresis. Gels were detected with a Uvi-Tec gel-documentation system (Cleaver Scientific Ltd., Rugby, UK) using GelRed staining (Biotium).

S. aureus genome analysis

Completed genomes (to date 03/05/2014; http://www.ncbi.nlm.nih.gov/genome/genomes/154) of different *S. aureus* strains were searched in the REFSEQ database with trimeric dUTPase (Φ11 dUTPase, GeneID: 1258034) and with dimeric dUTPase (Φeta3 dUTPase, GeneID:927341) sequences using tblastn (http://blast.ncbi.nlm.nih.gov/Blast.cgi?PROGRAM=tblastn&PAGE_TYPE=BlastSearch&LINK_LOC=blasthome). The search was performed with the basic parameter settings offered by the software. Prophage regions were identified based on the publications describing the genomic sequence or by PHAST software (22).

RESULTS AND DISCUSSION

Complex formation between Stl and dUTPase

The physical interaction between Φ11 dUTPase and SaPIbov1 Stl was proposed to result in the release from Stl repression observed in cellular systems (5). However, no quantitative description of a dUTPase-Stl protein complex was available. To provide such data indispensable for mechanistic insights, we cloned and purified both protein components of the putative complex. ITC data indicated that the Φ11 dUTPase and Stl form a considerably strong complex (dissociation constant is 0.10 ± 0.03 μM) (Figure 1A, Table 1)). A variety of additional methods confirmed this complex equilibrium: native gel electrophoresis (Figure 1B), soft-ionization mass spectrometry (Supplementary Figure S1A and B) and size-exclusion chromatography (Supplementary Figure S1C). As seen in the native gel, at stoichiometric amounts of Stl and Φ11dUTPase (1:1 with respect to monomeric species or subunits), no band is observable at the positions of the free proteins, arguing that complexation is maximal at this concentration ratio (complex 'A' in Figure 1B). It is also evident that at substoichiometric amounts of Stl another complex form is observed (complex 'B' in Figure 1B), probably reflecting an altered composition within the heterooligomer of the two proteins (see also Supplementary Results and Discussion).

Kinetics of complex formation was analyzed by QCM and stopped-flow measurements. QCM results showed that both the association and dissociation rate constant of the dUTPase:Stl complexation are approximately two orders of magnitudes lower than those data for the dUTPase:dUTP complexation (Table 1, Supplementary Figure S1D, cf. also (18,20)). The equilibrium dissociation constants, calculated from the association and dissociation rate constants ($K_d = k_{off}/k_{on}$), is in good agreement with the ITC data (Table 1). The QCM data also indicate that dUTPase and Stl complex formation may involve a conformational change also, although this suggestion needs further experimental investigation (see Supplementary Results and Discussion and Supplementary Table S1).

The slow and tight binding character of the complex formation between Stl and dUTPase was also confirmed by fluorescent experiments (Figure 1C and Supplementary Figure S1E and F) exploiting the useful tryptophan label within the active site of dUTPase that does not change the enzymatic properties (Φ11 dUTPaseF164W (20)). We repeated the QCM experiments with the Φ11 dUTPaseF164W protein and Stl, and found that the measured parameters did not show any significant change as compared to the wild-type dUTPase (Table 1). Hence, we conclude that the Φ11 dUTPaseF164W shows wild-type behavior in both enzyme kinetics and Stl-interaction, allowing us to use this useful mutant in stopped-flow and other experiments as well. As shown on Supplementary Figure S1E, Stl binding to Φ11 dUTPaseF164W enhances the fluorescent intensity. Using this fluorescence intensity change to detect Stl binding to dUTPase (Supplementary Figure S1F) one binding step was observed that was identified as the bimolecular complex formation (Figure 1C). The rate constants yielded from these experiments are in good agreement with QCM data (Table 1).

Our experiments clearly indicate that a strong physical interaction takes place between dUTPase and Stl in the absence of dUTP. This finding does not support the earlier suggestion that this interaction require the presence of dUTP (4). To gain insight into how substrate and product (dUTP and dUMP) may modulate the dUTPase-Stl interaction, we performed further experiments.

dUTPase:Stl complex formation abolishes the known physiological function of both proteins

We measured the enzymatic activity of dUTPase in the dUTPase:Stl complex and found that Stl exerts highly potent inhibition of dUTPase activity with an IC_{50} value that approximates the K_d of the protein–protein complex (Figure 2A, Table 1). This inhibition is only observed if dUTPase is pre-incubated with Stl prior to dUTP addition. Such behavior is typical for a slow and tight binding inhibitor (23) and is in excellent agreement with data obtained for the formation of the dUTPase:Stl complex (Figure 1, Table 1) as well as with the previously published kinetics of dUTP binding (20).

Downloaded from https://academic.oup.com/nar/article/42/19/11912/2902985 by guest on 04 November 2021

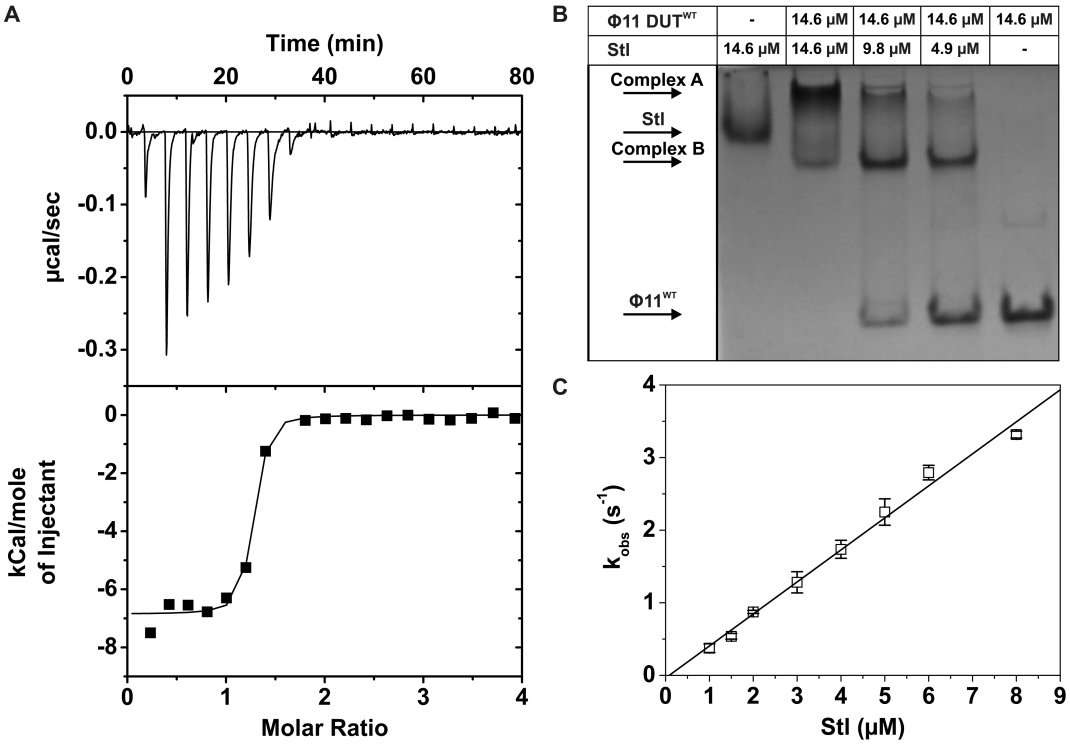

Figure 1. Φ11 dUTPaseWT and Stl form a tight complex with slow kinetics. **(A)** ITC measurement of dUTPase:Stl complex formation. The smooth line represents the fitted model, assuming one binding site. For the fitted parameters see Table 1. **(B)** Shows the result of native gel electrophoresis. Species and concentrations are indicated on the figure. **(C)** Shows the concentration dependence of the pseudo-first-order rate constant (k_{obs}) observed upon Φ11 DUT^{F164W}:Stl complex formation. Error bars represent SD for $n = 2$. Linear fit to the data ($r^2 = 0.99$) yielded the association rate constant $k_{on} = 0.41 \pm 0.014\ \mu M^{-1}s^{-1}$. The y intercepts of the fitted line was too small for the exact determination of the k_{off} value. However, the k_{off} value is small and indicate submicromolar K_d.

Stl stands as the first and single potent and directly identified protein inhibitor of dUTPase. Earlier suggestions for Drosophila and phage PBS2 proteins remained elusive (24,25). The regulation of the uracil content of DNA primarily depends on dUTPase and on uracil-DNA glycosylases (UDG-s) (26–31). It is therefore relevant to note that a similarly tight binding protein inhibitor (UGI–Uracil Glycosylase Inhibitor) of the main UDG, UNG is encoded in phage PBS1 and PBS2 (32). Interestingly, UGI was shown to be capable of inhibiting UNG-s from other species as well (33). It remains to be seen if Stl may prove to be a general dUTPase inhibitor, as well.

In order to better understand the mechanism of the dUTPase:Stl interaction and its functional consequences, we investigated the binding of Stl to dUTPase in the presence of the substrate, dUTP (or the substrate analogue dUPNPP) and in the presence of the product, dUMP. Both in equilibrium fluorescence titration (Figure 2B and Supplementary Figure S2A) and QCM experiments (Supplementary Figure S2B) we found that the presence of dUTP or dUPNPP strongly interferes with Stl:dUTPase complex formation. The fluorescence titration of the dUTPase:dUPNPP complex with Stl (Figure 2B) resulted in an equlibrium fluorescence intensity that was identical to that of the dUTPase:Stl complex implying that Stl displaced all dUPNPP. Hence, Stl and dUPNPP compete for binding to dUTPase (cf. also limited proteolysis results reported in Supplementary Figure S2C). The presence of Stl in turn inhibited the formation of the dUTPase:dUPNPP complex (Supplementary Figure S2A). On the other hand, dUMP, the product of the dUTPase reaction, and Stl do not influence the binding of each other (Figure 2B). The formation of a dUTPase:dUMP:Stl ternary complex is indicated by a distinct fluorescence state characterized with lower fluorescence intensity than that of the dUTPase:Stl complex (Supplementary Figure S1E and Table 1).

Transient kinetic experiments also showed that preincubation of dUTPase and Stl fully prevented any enzymatic reaction on the time scale used to observe the reaction in the absence of Stl (Figure 2C, compare curves 1 and 2, cf. also with the controls (curves 5 and 6)). At longer time scales, a slow decrease in fluorescence intensity followed by a fluorescent increase, reminiscent of dUTP binding and product release (cf. (18,20)), was observed (Supplementary Figure S2D). In agreement with the competition between Stl and dUTP for dUTPase binding, single exponentional fit to decreasing phase yielded a dUTP concentration (500–2300 µM) independent $k_{obs} = 0.00303 \pm 0.00008\ s^{-1}$, which is in agreement with the rate constant of Stl dissociation from dUTPase. We therefore propose that when dUTP is added to the pre-formed Stl:dUTPase complex, dUTP binding and hydrolysis requires Stl dissociation. On the other hand, if the mixture of dUTP and Stl are added together to dUTPase, the fluorescence time course (Figure 2C, curve 3) is analogous to the curve observed in the absence of Stl (curve 2) except that the equilibrium fluorescence in-

Downloaded from https://academic.oup.com/nar/article/42/19/11912/2902985 by guest on 04 November 2021

Table 1. Kinetic and thermodynamic parameters of Φ11 dUTPase: $Stl_{SaPIbov1}$ interaction in the presence and absence of uracil nucleotides

Experiment type	**Investigated parameters**			
ITC*	**K_d (μM)**	**n**	**ΔH (cal/mol)**	**ΔS (cal/mol/deg)**
Φ11 dUTPase^{WT}: Stl	0.10 ± 0.03	1.19 ± 0.12	-6852 ± 117	8.61
QCM[1, **]	**k_{on} (μM^{-1} s^{-1})**	**k_{off} (s^{-1})**		**k_{off} / k_{on} (μM)**
Φ11 dUTPase^{WT} binding to Stl	0.108 ± 0.005	0.0066 ± 0.0010		0.062 ± 0.012
Φ11 dUTPase^{F164W} binding to Stl	0.131 ± 0.013	0.0088 ± 0.0001		0.067 ± 0.008;
Φ11 dUTPase^{F164W} : dUTP binding to Stl	0.026 ± 0.002	0.0130 ± 0.0008		0.509 ± 0.062;
Φ11 dUTPase^{F164W}: dUMP binding to Stl	0.114 ± 0.004	0.0105 ± 0.0009		0.092 ± 0.001;
Fluorescent stopped-flow*	**k_{on} (μM^{-1} s^{-1})**	**k_{off} (s^{-1})**		**$k_{off\,obs}$ (s^{-1})+**
Stl binding to Φ11 dUTPase^{F164W}	0.41 ± 0.01	ND		0.00303 ± 0.00008
dUTP binding to Φ11 dUTPase^{F164W}	21.4 ± 0.7#	17.7 ± 7.5#		-
Steady-state inhibition by Stl*	**K_i (μM)**		**Inhibition**	
Φ11 dUTPase^{WT}	0.027± 0.005		100%	
Equlibrium fluorescence*	K_d (μM)			
	No nucl.	**+ dUMP**		**+ dUPNPP**
Φ11 dUTPase^{F164W}: Stl	0.031 ± 0.062	0.026 ± 0.048		3.17 ± 1.17
	No Stl		**+ Stl**	
Φ11 dUTPase^{F164W}: dUPNPP	0.3 ± 02#		655 ± 229	

*The reliabilities of the fits are shown by the error values.

**Errors represent SEM for n=2–6.

+Observed upon mixing preincubated complex of dUTPase and Stl with excess dUPNPP (cf. Supplementary Figure S2D).

#data from (20).

[1]The QCM data indicated another process in addition to the second order binding for the dUTPase:Stl complex formation (see Supplementary Results and Discussion and Supplementary Table I.).

ND: Not determined.

tensity approaches that of the dUTPase:Stl complex (curve 4). Stl binding, reflected in fluorescence increase (paralleled with product release, that also causes fluorescence increase, cf. arrow on curve 3), may only occur when the concentration of the dUTPase:dUTP Michaelis complex starts to decrease. This is in agreement with the steady-state results and reinforces the conclusion that Stl is a competitive, slow and tight binding inhibitor of dUTPase.

Based on the direct experimental data of numerous independent assays (Figure 2A–C and Supplementary Figure S2), we suggest that dUTP and Stl compete for dUTPase binding and that the dUTPase:dUTP complex is inaccessible for Stl. Therefore, the previously suggested model stating that dUTP mediates the dUTPase:Stl interaction (4) remains unsubstantiated.

It was also of immediate interest whether the de-repression activity (i.e. the physiological function) of the dUTPase:Stl complex is also modulated by dUTP. To this end, we performed EMSA experiments (Figure 2D). We observed that dUTPase inhibits the binding of Stl to its cognate DNA sequence only in the absence of the dUTP analog. This suggests that dUTP counteracts the de-repression event by preventing dUTPase:Stl complex formation.

The EMSA results again disagree with the previous model in which dUTP was suggested to enhance de-repression and the ensuing horizontal transfer of mobile

Downloaded from https://academic.oup.com/nar/article/42/19/11912/2902985 by guest on 04 November 2021

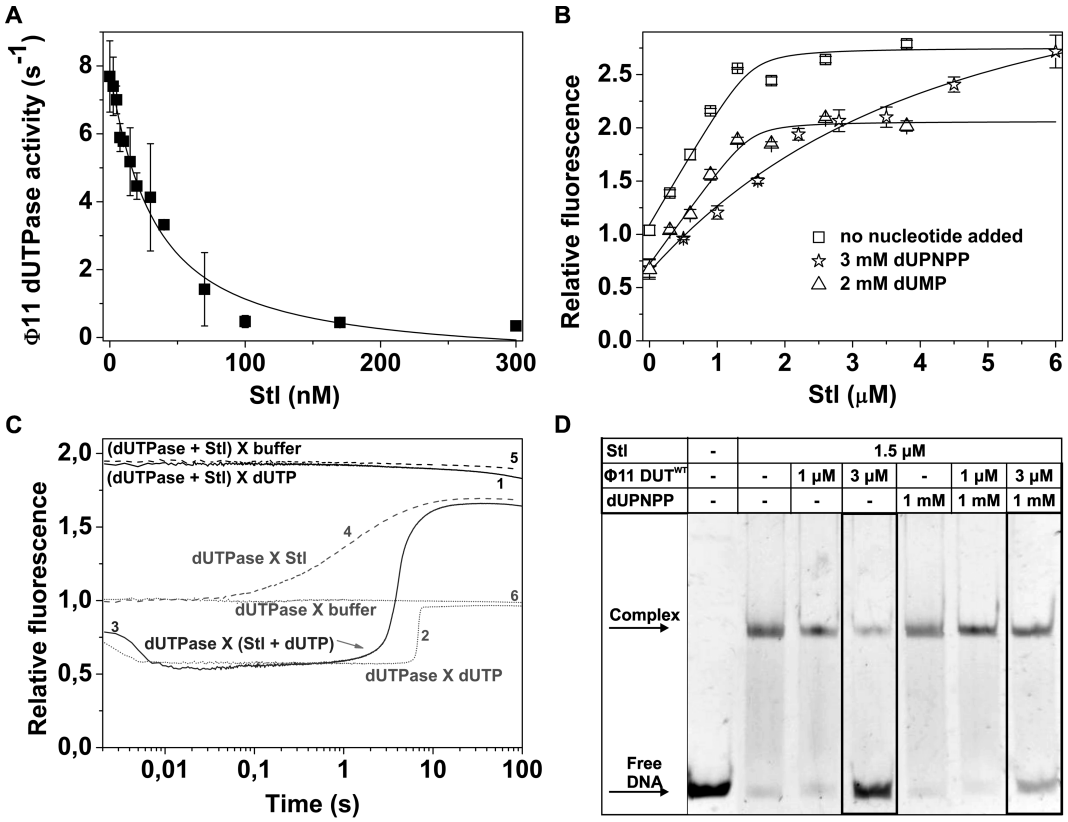

Figure 2. dUTPase:StI complex formation eliminates the physiological function of both proteins. **(A)** Inhibitory effect of StI on Φ11DUT^{WT} (10 nM) catalytic activity. Data represent average and error of three parallel measurements. Solid line represents fit of quadratic binding equation to the data, yielding IC_{50} 26.64 $\pm$ 5.07 nM. **(B)** Shows titration of Φ11DUT^{F164W} (1.5 μM) and Φ11DUT^{F164W} (1.5 μM): dUPNPP (3 mM)/dUMP (2 mM) complex with StI. Error bars represents SD for $n = 3$. Solid lines represent quadratic fits to the data (see Equation (1)). Dissociation constants from the fitted model are shown in Table 1. **(C)** Shows transient kinetic investigation of the mixing order dependency of StI inhibition. 2 μM d Φ11DUT^{F164W}, 3 μM StI and 50 μM dUTP was mixed (post-mixing concentrations: X indicates the mixing of species in syringe A and B (syringe A X syringe B), parenthesis indicates that the components were pre-mixed. The curves are shown from 0.002 s (after the dead time). **(D)** Effect of dUPNPP on dUTPase derepression activity characterized by EMSA.

genetic elements. Our results support instead that dUTP counteracts de-repression. Another key point of the previous model concerned the role of the C-terminal arm of dUTPase: it was suggested, based on indirect experiments, that de-repression may only occur if the C-terminal arm of dUTPase adopts a predominantly ordered conformation as it does in the dUTP-bound form. The present direct EMSA experiments, however, clearly show that a C-terminal arm-truncated dUTPase may also disrupt StI binding to DNA, very similarly to the wild type (Supplementary Figure S3). Hence, the dUTPase:StI interaction does not seem to require the presence of the C-terminal arm.

Staphyloccus aureus strains do not encode genomic dUTPase

To consider the physiological relevance of the regulatory role of dUTP, we need to take cellular nucleotide concentrations into account. It is known that the general cellular concentrations of dNTPs are in the order of 5–40 μM (34), with the exception of dUTP which is under control by dUTPase (35) and normally, its concentration is around 0.2 μM only (34). dUTPase is considered to be a ubiquitous enzyme, due to its important role in nucleotide pool control. Accordingly, knock down of dUTPase results in significant increase of the dUTP level gaining up to the level of the canonical dNTPs, as it was shown in several human cell lines (36–38). According to our results an elevated cellular dUTP concentration probably interferes with the dUTPase:StI interaction and consequently inhibits the activation of SaPI transfer.

To investigate if dUTPase, the major regulator of dUTP levels, is also present in *S. aureus*, we analyzed the genome data available for different *S. aureus* strains. Interestingly, neither of these strains encode an endogenous dUTPase gene. However, in most cases the chromosome contained integrated prophages carrying dUTPase genes (Supplementary Table S2). Importantly, the expression of proteins located in the replication module of prophages are probably under repression in the lysogenic phase and dUTPase expression is upregulated only after prophage induction (39).

Such an expression pattern of dUTPase is expected to be paralleled with an increased dUTP level within *S. aureus*. Interestingly, it was also found recently that a conserved *S. aureus* protein (SaUGI) has an UNG inhibitory effect (40). Lack of dUTPase and UNG activity may lead to the accumulation of uracil in genomic DNA (26,41) and to an increased mutagenic rate in this biomedically challenging pathogenic microorganism (c.f. (30,42–43)).

Downloaded from https://academic.oup.com/nar/article/42/19/11912/2902985 by guest on 04 November 2021

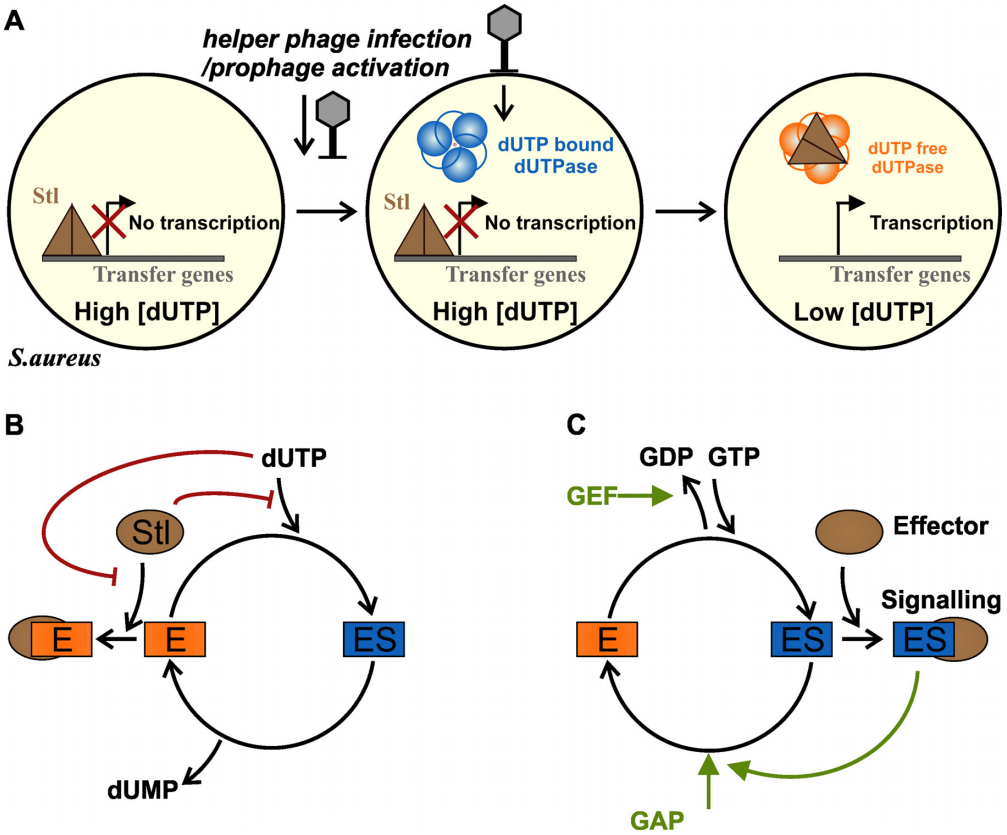

Figure 3. Model of the mechanism of dUTPase-controlled SaPI activation. **(A)** Shows our novel model for dUTPase-based SaPI activation. **(B)** Molecular mechanism of dUTP controlled dUTPase:Stl interaction. **(C)** Molecular mechanism of G-protein-based switch. On panels B and C ES represents substrate bound, while E represents substrate-free enzyme (free enzyme or product bound enzyme). Red and green arrows represent inhibition and activation, respectively.

A novel mechanism for the dUTPase-regulated molecular switch

Figure 3A shows our model for the regulation of horizontal gene transfer by dUTP. We propose that in the absence of genomic dUTPase, *S. aureus* strains may contain a relatively high dUTP concentration. Upon helper phage infection or prophage activation, phage dUTPase is expressed and hydrolyses dUTP in a fast and efficient process. dUTPase and Stl do not interact efficiently if dUTP is present, therefore, dUTPase becomes available for binding to the Stl repressor protein only after the dNTP pool is cleared from dUTP. In our proposed mechanism, the helper phage dUTPase breaks down dUTP and subsequently activates the transcription of the transfer initiating proteins within the pathogenicity island.

Our data leaves an earlier G protein-like hypothesis unsubstantiated (4). The fundamental differences between G protein regulation and the dUTPase:Stl interaction-based regulation are displayed in Figure 3B and C, and in Supplementary Table S3. dUTPases are responsible for fast and efficient clearance of dUTP from the cellular pool, facilitated by fast release of the products. dUTPases are predominantly dUTP-bound while the level of dUTP is high, and the hydrolysis product dUMP is quickly released (cf. (18,20)). G proteins, however, are very slow hydrolases and exist predominantly in ligand-bound states. For both hydrolysis and product release, G proteins require additional protein regulators (GAPs (G-protein Activating Protein) and GEFs (Guanoside Exchange Factor)). The multistep regulatory pattern relying on various factors allows G proteins to fulfill widespread finely tuned signaling processes. dUTPases, on the other hand, are simple and fast catalysts of dUTP cleavage.

For the dUTPase-dependent molecular switch, the dUTPase:Stl interaction is the only yet described example, and it remains to be seen if further such dUTPase-binding proteins may be identified. It is important to emphasize that while our model of the dUTP-regulated dUTPase:Stl interaction contradicts the earlier proposed G protein-like scheme, it is still fully consistent with the experimental observations reported in the same study (4), as demonstrated in Supplementary Table S4. Importantly, these *in vivo* results also show that the extent of SaPI activation correlates with dUTPase activity.

CONCLUSION

We described a molecular mechanism that connects the regulation of gene expression to the regulation of the enzymatic activity of trimeric dUTPase, a nucleoside triphosphate hydrolase that is responsible for genome integrity. Our data show that dUTPase strongly binds to the Stl repressor protein in the absence of substrate and this complex disrupts

Downloaded from https://academic.oup.com/nar/article/42/19/11912/2902985 by guest on 04 November 2021

the capability of Stl binding to its cognate DNA element. We also found that the presence of dUTP precludes Stl binding to dUTPase. Despite being considered to be ubiquitous, several *S. aureus* strains do not encode endogenous dUTPase, suggesting high intracellular dUTP level. We propose that helper phage dUTPases may be responsible for sanitizing the dUTP pool. Once dUTP is hydrolyzed, dUTPase switches function and becomes quantitatively available for driving the gene expression that initiates the horizontal transfer of SaPI. The countereffect of dUTP suggests that the excision and extensive replication of SaPI occurs under dUTP-cleaned, sanitized nucleotide pool conditions, ensuring uracil-free replication of the subsequently transferred mobile genetic element. The presence of uracil in SaPI DNA is probably unfavorable, as the uracil content of a mobile genetic element may negatively influence its integration into the DNA of the new host, as it was recently shown for HIV (44,45). In case of HIV, if the new host cell contains an active UNG, the uracilated viral DNA may be degraded before its integration into the genome could happen (44).

The presently discovered specific and efficient inhibition of dUTPase, not described before, will greatly contribute to the understanding of the communication between pathways responsible for maintaining nucleotide pools, DNA damage recognition, repair and genome integrity.

SUPPLEMENTARY DATA

Supplementary Data are available at NAR Online.

FUNDING

Hungarian Scientific Research Fund OTKA [NK 84008, K109486]; Baross Program of the New Hungary Development Plan [3DSTRUCT, OMFB-00266/2010 REG-KM-09-1-2009-0050]; Hungarian Academy of Sciences ([TTK IF-28/ 2012]; MedinProt program); European Commission FP7 Biostruct-X project [283570]. Funding for open access charge: Hungarian Academy of Sciences.
Conflict of interest statement. None declared.

REFERENCES

1. Lindsay,J.A. and Holden,M.T.G. (2004) Staphylococcus aureus: superbug, super genome? *Trends Microbiol.*, **12**, 378–385.
2. Novick,R.P., Christie,G.E. and Penadés,J.R. (2010) The phage-related chromosomal islands of Gram-positive bacteria. *Nat. Rev. Microbiol.*, **8**, 541–551.
3. Mir-Sanchis,I., Martínez-Rubio,R., Martí,M., Chen,J., Lasa,Í., Novick,R.P., Tormo-Más,M.Á. and Penadés,J.R. (2012) Control of Staphylococcus aureus pathogenicity island excision. *Mol. Microbiol.*, **85**, 833–845.
4. Tormo-Más,M.Á., Donderis,J., García-Caballer,M., Alt,A., Mir-Sanchis,I., Marina,A. and Penadés,J.R. (2013) Phage dUTPases control transfer of virulence genes by a proto-oncogenic G protein-like mechanism. *Mol. Cell*, **49**, 947–958.
5. Tormo-Más,M.A., Mir,I., Shrestha,A., Tallent,S.M., Campoy,S., Lasa,I., Barbé,J., Novick,R.P., Christie,G.E. and Penadés,J.R. (2010) Moonlighting bacteriophage proteins derepress staphylococcal pathogenicity islands. *Nature*, **465**, 779–782.
6. Vértessy,B.G. and Tóth,J. (2009) Keeping uracil out of DNA: physiological role, structure and catalytic mechanism of dUTPases. *Acc. Chem. Res.*, **42**, 97–106.
7. Nyman,P.O. (2001) Introduction. dUTPases. *Curr. Protein Pept. Sci.*, **2**, 277–285.
8. Vertessy,B.G., Persson,R., Rosengren,A.M., Zeppezauer,M. and Nyman,P.O. (1996) Specific derivatization of the active site tyrosine in dUTPase perturbs ligand binding to the active site. *Biochem. Biophys. Res. Commun.*, **219**, 294–300.
9. Fiser,A. and Vértessy,B.G. (2000) Altered subunit communication in subfamilies of trimeric dUTPases. *Biochem. Biophys. Res. Commun.*, **279**, 534–542.
10. Mustafi,D., Bekesi,A., Vertessy,B.G. and Makinen,M.W. (2003) Catalytic and structural role of the metal ion in dUTP pyrophosphatase. *Proc. Natl. Acad. Sci. U.S.A.*, **100**, 5670–5675.
11. Kovári,J., Barabás,O., Takács,E., Békési,A., Dubrovay,Z., Pongrácz,V., Zagyva,I., Imre,T., Szabó,P. and Vértessy,B.G. (2004) Altered active site flexibility and a structural metal-binding site in eukaryotic dUTPase: kinetic characterization, folding, and crystallographic studies of the homotrimeric Drosophila enzyme. *J. Biol. Chem.*, **279**, 17932–17944.
12. Németh-Pongrácz,V., Barabás,O., Fuxreiter,M., Simon,I., Pichová,I., Rumlová,M., Zábranská,H., Svergun,D., Petoukhov,M., Harmat,V. *et al.* , (2007) Flexible segments modulate co-folding of dUTPase and nucleocapsid proteins. *Nucleic Acids Res.*, **35**, 495–505.
13. Kovári,J., Barabás,O., Varga,B., Békési,A., Tölgyesi,F., Fidy,J., Nagy,J. and Vértessy,B.G. (2008) Methylene substitution at the alpha-beta bridging position within the phosphate chain of dUDP profoundly perturbs ligand accommodation into the dUTPase active site. *Proteins*, **71**, 308–319.
14. Varga,B., Barabás,O., Takács,E., Nagy,N., Nagy,P. and Vértessy,B.G. (2008) Active site of mycobacterial dUTPase: structural characteristics and a built-in sensor. *Biochem. Biophys. Res. Commun.*, **373**, 8–13.
15. Neal,S.E., Eccleston,J.F., Hall,A. and Webb,M.R. (1988) Kinetic analysis of the hydrolysis of GTP by p21N-ras. The basal GTPase mechanism. *J. Biol. Chem.*, **263**, 19718–19722.
16. Larsson,G., Nyman,P.O. and Kvassman,J.O. (1996) Kinetic characterization of dUTPase from Escherichia coli. *J. Biol. Chem.*, **271**, 24010–24016.
17. Pécsi,I., Szabó,J.E., Adams,S.D., Simon,I., Sellers,J.R., Vértessy,B.G. and Tóth,J. (2011) Nucleotide pyrophosphatase employs a P-loop-like motif to enhance catalytic power and NDP/NTP discrimination. *Proc. Natl. Acad. Sci. U.S.A.*, **108**, 14437–14442.
18. Tóth,J., Varga,B., Kovács,M., Málnási-Csizmadia,A. and Vértessy,B.G. (2007) Kinetic mechanism of human dUTPase, an essential nucleotide pyrophosphatase enzyme. *J. Biol. Chem.*, **282**, 33572–33582.
19. Vertessy,B.G. (1997) Flexible glycine rich motif of Escherichia coli deoxyuridine triphosphate nucleotidohydrolase is important for functional but not for structural integrity of the enzyme. *Proteins*, **28**, 568–579.
20. Leveles,I., Németh,V., Szabó,J.E., Harmat,V., Nyíri,K., Bendes,Á.Á., Papp-Kádár,V., Zagyva,I., Róna,G., Ozohanics,O. *et al.* , (2013) Structure and enzymatic mechanism of a moonlighting dUTPase. *Acta Crystallogr. D. Biol. Crystallogr.*, **69**, 2298–2308.
21. Leveles,I., Róna,G., Zagyva,I., Bendes,Á., Harmat,V. and Vértessy,B.G. (2011) Crystallization and preliminary crystallographic analysis of dUTPase from the φ11 helper phage of Staphylococcus aureus. *Acta Crystallogr. Sect. F. Struct. Biol. Cryst. Commun.*, **67**, 1411–1413.
22. Zhou,Y., Liang,Y., Lynch,K.H., Dennis,J.J. and Wishart,D.S. (2011) PHAST: a fast phage search tool. *Nucleic Acids Res.*, **39**, W347–W352.
23. Morrison,J.F. (1982) The slow-binding and slow, tight-binding inhibition of enzyme-catalysed reactions. *Trends Biochem. Sci.*, **7**, 102–105.
24. Nation,M.D., Guzder,S.N., Giroir,L.E. and Deutsch,W.A. (1989) Control of Drosophila deoxyuridine triphosphatase. Existence of a developmentally expressed protein inhibitor. *Biochem. J.*, **259**, 593–596.
25. Price,A.R. and Frato,J. (1975) Bacillus subtilis deoxyuridinetriphosphatase and its bacteriophage PBS2-induced inhibitor. *J. Biol. Chem.*, **250**, 8804–8811.
26. Muha,V., Horváth,A., Békési,A., Pukáncsik,M., Hodoscsek,B., Merényi,G., Róna,G., Batki,J., Kiss,I., Jankovics,F. *et al.* , (2012) Uracil-containing DNA in Drosophila: stability, stage-specific accumulation, and developmental involvement. *PLoS Genet.*, **8**, e1002738.

Downloaded from https://academic.oup.com/nar/article/42/19/11912/2902985 by guest on 04 November 2021

27. Dengg,M., Garcia-Muse,T., Gill,S.G., Ashcroft,N., Boulton,S.J. and Nilsen,H. (2006) Abrogation of the CLK-2 checkpoint leads to tolerance to base-excision repair intermediates. *EMBO Rep.*, **7**, 1046–1051.
28. Tye,B.K., Chien,J., Lehman,I.R., Duncan,B.K. and Warner,H.R. (1978) Uracil incorporation: a source of pulse-labeled DNA fragments in the replication of the Escherichia coli chromosome. *Proc. Natl. Acad. Sci. U.S.A.*, **75**, 233–237.
29. Dubois,E., Córdoba-Cañero,D., Massot,S., Siaud,N., Gakière,B., Domenichini,S., Guérard,F., Roldan-Arjona,T. and Doutriaux,M.-P. (2011) Homologous recombination is stimulated by a decrease in dUTPase in Arabidopsis. *PLoS ONE*, **6**, e18658.
30. Castillo-Acosta,V.M., Aguilar-Pereyra,F., Bart,J.-M., Navarro,M., Ruiz-Pérez,L.M., Vidal,A.E. and González-Pacanowska,D. (2012) Increased uracil insertion in DNA is cytotoxic and increases the frequency of mutation, double strand break formation and VSG switching in Trypanosoma brucei. *DNA Repair (Amst).*, **11**, 986–995.
31. Castillo-Acosta,V.M., Estévez,A.M., Vidal,A.E., Ruiz-Perez,L.M. and González-Pacanowska,D. (2008) Depletion of dimeric all-alpha dUTPase induces DNA strand breaks and impairs cell cycle progression in Trypanosoma brucei. *Int. J. Biochem. Cell Biol.*, **40**, 2901–2913.
32. Wang,Z. and Mosbaugh,D.W. (1989) Uracil-DNA glycosylase inhibitor gene of bacteriophage PBS2 encodes a binding protein specific for uracil-DNA glycosylase. *J. Biol. Chem.*, **264**, 1163–1171.
33. Mol,C.D., Arvai,A.S., Sanderson,R.J., Slupphaug,G., Kavli,B., Krokan,H.E., Mosbaugh,D.W. and Tainer,J.A. (1995) Crystal structure of human uracil-DNA glycosylase in complex with a protein inhibitor: protein mimicry of DNA. *Cell*, **82**, 701–708.
34. Traut,T.W. (1994) Physiological concentrations of purines and pyrimidines. *Mol. Cell. Biochem.*, **140**, 1–22.
35. Lari,S.-U., Chen,C.-Y., Vertéssy,B.G., Morré,J. and Bennett,S.E. (2006) Quantitative determination of uracil residues in Escherichia coli DNA: contribution of ung, dug, and dut genes to uracil avoidance. *DNA Repair (Amst).*, **5**, 1407–1420.
36. Studebaker,A.W., Lafuse,W.P., Kloesel,R. and Williams,M.V. (2005) Modulation of human dUTPase using small interfering RNA. *Biochem. Biophys. Res. Commun.*, **327**, 306–310.
37. Koehler,S.E. and Ladner,R.D. (2004) Small interfering RNA-mediated suppression of dUTPase sensitizes cancer cell lines to thymidylate synthase inhibition. *Mol. Pharmacol.*, **66**, 620–626.
38. Wilson,P.M., LaBonte,M.J., Lenz,H.-J., Mack,P.C. and Ladner,R.D. (2012) Inhibition of dUTPase induces synthetic lethality with thymidylate synthase-targeted therapies in non-small cell lung cancer. *Mol. Cancer Ther.*, **11**, 616–628.
39. Cirz,R.T., Jones,M.B., Gingles,N.A., Minogue,T.D., Jarrahi,B., Peterson,S.N. and Romesberg,F.E. (2007) Complete and SOS-mediated response of Staphylococcus aureus to the antibiotic ciprofloxacin. *J. Bacteriol.*, **189**, 531–539.
40. Wang,H.-C., Hsu,K.-C., Yang,J.-M., Wu,M.-L., Ko,T.-P., Lin,S.-R. and Wang,A.H.-J. (2014) Staphylococcus aureus protein SAUGI acts as a uracil-DNA glycosylase inhibitor. *Nucleic Acids Res.*, **42**, 1354–1364.
41. Békési,A., Zagyva,I., Hunyadi-Gulyás,E., Pongrácz,V., Kovári,J., Nagy,A.O., Erdei,A., Medzihradszky,K.F. and Vértessy,B.G. (2004) Developmental regulation of dUTPase in Drosophila melanogaster. *J. Biol. Chem.*, **279**, 22362–22370.
42. Sedwick,W.D., Brown,O.E. and Glickman,B.W. (1986) Deoxyuridine misincorporation causes site-specific mutational lesions in the lacI gene of Escherichia coli. *Mutat. Res.*, **162**, 7–20.
43. Guillet,M., Van Der Kemp,P.A. and Boiteux,S. (2006) dUTPase activity is critical to maintain genetic stability in Saccharomyces cerevisiae. *Nucleic Acids Res.*, **34**, 2056–2066.
44. Weil,A.F., Ghosh,D., Zhou,Y., Seiple,L., McMahon,M.A., Spivak,A.M., Siliciano,R.F. and Stivers,J.T. (2013) Uracil DNA glycosylase initiates degradation of HIV-1 cDNA containing misincorporated dUTP and prevents viral integration. *Proc. Natl. Acad. Sci. U.S.A.*, **110**, E448–E457.
45. Yan,N., O'Day,E., Wheeler,L.A., Engelman,A. and Lieberman,J. (2011) HIV DNA is heavily uracilated, which protects it from autointegration. *Proc. Natl. Acad. Sci. U.S.A.*, **108**, 9244–9249.

Downloaded from https://academic.oup.com/nar/article/42/19/11912/2902985 by guest on 04 November 2021

Highly potent dUTPase inhibition by a bacterial repressor protein reveals a novel mechanism for gene expression control
Running title: dUTP level controls horizontal gene transfer

Judit E. Szabó[1]*, Veronika Németh[1], Veronika Papp-Kádár[1], Kinga Nyíri1, Ibolya Leveles[1], Ábris Á. Bendes[1], Imre Zagyva[1], Gergely Róna[1], Hajnalka Pálinkás[1], Balázs Besztercei[1], Olivér Ozohanics [1], Károly Vékey[1], Károly Liliom[1], Judit Tóth[1]* and Beáta G. Vértessy[1,2]*

[1] Institutes of Enzymology and Organic Chemistry, RCNS, Hungarian Academy of Sciences
[2] Dept. Biotechnology, Budapest University of Technology and Economics

* To whom correspondence should be addressed. Beáta G. Vértessy (Email: vertessy.beata@ttk.mta.hu) Correspondence may also be addressed to Judit Tóth (Email: toth.judit@ttk.mta.hu) and Judit E. Szabó (Email: szabo.judit.eszter@ttk.mta.hu)

Supplemental Results and Discussion

Oligomerization of Stl

The electrospray mass spectrum of Stl presented in (Suppl. Fig. 1A) shows the presence of two abundant species in the 1500-3500 and in the 3500-6000 m/z range. Molecular mass of these species are 32910 ±40 Da and 65860 ±80 Da, corresponding to the monomer (S_1) and dimer (S_2) form of Stl, respectively (in good agreement with the monomer molecular mass of 32,896 calculated from the amino acid sequence (http://web.expasy.org/protparam/). Based on the integrated peak intensities the S_1 : S_2ratio is 10:9 (rough estimation, due to the overlapping peaks). Other oligomers were not detected. Size-exclusion chromatography (Suppl. Fig. 1C) also showed that Stl exists in an equilibrium between monomer and dimer forms. The oligomeric status of Stl has never been addressed before. However, dimerization of DNA binding proteins is a frequently occurring phenomenon.

Stochiometry of dUTPase Stl complex

The electrospray mass spectrum of Φ11 dUTPase^{WT}: Stl mixture presented in Suppl. Fig. 1B shows the existence of different species in the sample. Below 3600 m/z different various charge states of the of Φ11 dUTPase^{WT} monomer (Φ_1) are visible in low amount, while in the range of 3700 – 5000 m/z the trimer form (Φ_3) of Φ11 dUTPase^{WT} is observable with low intensity (59660 ±20 Da), as also described in (1). Note, that the dimer form of dUTPase (Φ_2) is not observed – this strongly suggests that the well-observable Φ_3 form is indeed the stable, native complex. An abundant species in the 4800-6000 m/z range is observable. The molecular mass of this species (125500 ±80 Da) corresponds to the Φ_3S_2 complex (consisting of Φ_3 and S_2 or 2 * S_1). Free Stl molecules (S_2 or S_1) and other complex forms were not observed in this mass/charge range. As shown by native gel results Suppl. Fig. 1B Φ11 dUTPase^{WT} and Stl form more types of complexes. Based on the mass spectrometry (MS) and analytical gel filtration Stl is in equilibrium between monomers and dimers (see Suppl. Fig. 1B and suppl. Fig 1C), while Φ11 dUTPase^{WT} is present as a trimer (Φ_3) at least in 90% (1). Therefore it is straightforward to assume that the different species are the complexes of Φ_3 plus different number of Stl molecules (monomers and dimers). If Stl and Φ11 dUTPase^{WT} are in

stoichiometric concentration neither the distinct band of free Φ11 dUTPase^{WT} nor the distinct band of free Stl are observable (see Suppl. Fig. 1B lane 4). Therefore complex A is probably equivalent to the Φ_3S_3 complex consisting of Φ_3 and three Stl molecules (3 * S_1 or S_2 + S_1). If the concentration of Stl is substoichiometric to Φ11 dUTPase^{WT} (see Suppl. Fig. 1B lane 2 and 3) another complex species, complex B also appears. The appearance of complex B at substoichiometric Stl concentrations indicates that this complex may contain Φ_3 and fewer than 3 Stl molecules. If this complex consisted of Φ_3 and one S_1, then at 3:1 Φ11 dUTPase^{WT}: Stl ratio (see Suppl. Fig. 1B B lane 2) the concentration of complex forming species would be stoichiometric and neither free Stl nor free Φ11 dUTPase^{WT} would be present (used protein concentrations were high above the K_d of complex formation). However free Φ11 dUTPase^{WT} is present, indicating that complex B corresponds to the Φ_3S_2 complex (consisting of Φ_3 and S_2 or 2 * S_1), observed also by MS.

In MS we could not observe the Φ_3S_3 complex. Assuming that this complex exists (based on native gel), there are two different explanation for the lack of this complex in MS: *i,* the stabilities of the different complexes are different under the different conditions of native gel and MS; *ii,* Stl is present in substoichiometric concentration in MS due to stability problems in lack of high salt concentration. Since Φ11 dUTPase^{WT} and Stl were mixed stoichiometrically in the MS measurement, the absence of free Stl species from the mass spectra argues for the second explanation.

Kinetics of the complex formation between dUTPase and Stl

The kinetics of the dUTPase-Stl interaction was investigated by two independent methods. One of the methods, Quartz Crystal Microbalance (QCM) yielded the best fit to the data when a two state reaction model was applied (Suppl. Fig. 1D, Table I and Suppl. Table I). This model assumes bimolecular complex formation, followed by a conformational change. It is important to highlight that QCM is actually refractory to conformational changes, since it only reflects mass changes. However, according to the manufacturer's manual, a good fit of experimental data to a multi-state model might be taken as an indication for a putative conformational change. Using the other, fluorescence detection-based method however, we did not find evidence for a conformational change within the Φ11 dUTPase:Stl complexes. The K_d values calculated from the k_{off}/ k_{on} ratio, determined in the QCM experiments, are in good agreement with the K_d values obtained by equlibrium methods, therefore only the kinetic properties of bimolecular complex formation were analyzed in detail (see Table I). The data on the putative conformational change observed by QCM are summarized in Suppl. Table I. The two state reaction model fitted to the QCM data may be the result of the formation of more than one type of Φ11 dUTPase:Stl complex. To elucidate this issue, a further detailed kinetic analysis of the complex formation is necessary, that will be the subject of another paper.

Supplemental Experimental Procedures

Reagents

Molecular biology products were from New England Biolabs (US) and Fermentas (Canada), electrophoresis and chromatography reagents were from Bio-Rad (US) and Qiagen (Netherland). Phenol red was from Merck (Germany), dUDP and dUPNPP were from Jena Bioscience (Germany), dUTP and other chemicals were from Sigma-Aldrich (US), if not indicated otherwise

Cloning of Stl

The cDNA of the $Stl_{SaPIbov1}$ protein (GenBank ID AAG29617.1) from *Staphylococcus aureus* was synthesized as a codon-optimized (EnCor Biotechnology Inc.) construct. The codon-optimized construct was cloned into the vector pETDuet-1 from Novagen with EcoRI and NotI restriction sites using the services of Eurofins MWG Operon. Thus, a His-tag and a thrombin cleavage site were attached to the N-terminal protein sequence. For glutathione-S-transferase (GST) fusion expression, Stl was further amplified from this expression vector, and was cloned into the EcoRI/XhoI restriction sites of the pGEX-4T-1 vector in frame with the N-terminal GST tag, as well as with a thrombin cleavage site and a 6xHis tag between the GST and the dUTPase sequence. For the amplification of Stl the $Stl_{pETDuet-1}$-F (5'-TATTGAATTCCATCATCATCATCATCACGGCAGCATGGAAGGCGCGGGCCAGATG-3') and the $Stl_{pETDuet-1}$-R (5'-GGTCCTCGAGTTAGTTGGTATCTTTTTCCAGAATAATTTTTTTCTGATG-3') primers were used. The resulting constructs were verified by DNA sequencing at Eurofins MWG Operon.

Expression of Stl

For expression of Stl,cells transformed with respective plasmids were propagated in 500 ml LB till exponential growth, then the culture was cooled to 303 K and then induced with 0.5 mM iso-propyl- β -D-thiogalactoside. After induction, the cell cultures were grown for a further 4 h at 293 K. Finally the cells were harvested by centrifugation and stored at 193 K. Subsequent manipulations were carried out on ice.

Purification of Stl

For purification of Stl protein, cell pellets were solubilized in 15 ml of buffer A (PBS (pH 7.3), 5 mM $MgCl_2$) supplemented with 400 mM NaCl, 2 mM dithiothreitol (DTT), 1% Triton X-100, 2 µg/ml RNase and Dnase. One tablet of Complete ULTRA Tablets, Mini, EDTA-free protease inhibitor preparation was added to every 100 ml of the solution. Cell suspensions were stirred for 10 min, sonicated (4 x 60 s), and centrifuged (16000g for 30 min). Supernatant was diluted in buffer A to contain 200 mM NaCl and loaded on a pre-equlibrated benchtop glutathion-agarose affinity-chromatography column (GE Healthcare). The column was washed with ten volumes of buffer A (200 mM NaCl). After that 80 Cleavage Units thrombin (GE Healthcare) was added to perform on-column cleavage for the removal of GST tag. After overnight cleavage >95% pure Stl protein was eluted from the column. The eluted Stl protein solution was supplemented to contain 400mM NaCl in order to obtain suitable protein stability. The purified preparations appeared as single bands on SDS-PAGE, gel densitometry suggested at least 95% purity**.** The protein preparation was flash-frozen in liquid nitrogen, and stored at 193 K. Before use, aliquots of the enzyme were dialyzed against respective buffers.

Cloning of tag-free Φ11 dUTPase mutants

The tag free versions of Φ11 dUTPase^{F164W} and Φ11 dUTPase^{E158STOP} proteins were created by QuickChange site-directed mutagenesis (Stratagene) from the pETDuet-Φ11DUT^{WT} construct with the mutagenic primers that were used to create the same Φ11DUT variants with the GST tag (1).

Purification of tag-free Φ11 dUTPases

For purification of dUTPase proteins cell pellets were solubilized in buffer B (20 mM HEPES (pH 7.5), 100 mM NaCl, 5 mM $MgCl_2$,10 mM ß-mercaptoethanol) supplemented with 2 µg/ml RNase and Dnase. One tablet of Complete ULTRA Tablets, Mini, EDTA-free protease inhibitor preparation was added to every 100 ml of the solution. Cell suspensions were stirred for 10 min, sonicated (4 x 60 s), and centrifuged (16000g for 30 min). Supernatants were directly loaded on a Q-Sepharose column (5ml) equilibrated in buffer B (supplemented with 0.1 mM PMSF (phenylmethylsulfonyl fluoride)) and developed using 50 ml of a linear gradient up to 1 M NaCl. dUTPase appeared at 0.3–0.5 M NaCl. A second purification step was performed on a size exclusion column (Superdex 200 10/300 GL, GE Healthcare) in buffer B containing 300 mM NaCl and 0.1 mM PMSF with a molecular weight separation range between 10 000-600 000. AKTA Purifier (GE Healthcare) system, with Unicorn software (GE Healtcare) was used for size exclusion chromatography, absorbance of the eluates were monitored at 280 and 260 nm. The purified preparations appeared as single bands on SDS-PAGE, gel densitometry suggested at least 95% purity**.** Enzyme stocks were concentrated on Millipore centrifugal filters (10 kDa cutoff) to a final concentration, flash-frozen in liquid nitrogen, and stored at 193 K. Before use, aliquots of the enzyme were dialyzed against respective buffers.

Protein quantification

Protein concentration was measured by Bradford's assay or spectrophotometrically using $A_{280}^{0.1\%}$ values 1.051, 0.786, 1.083 and 0.84 ml * mg^{-1}* cm^{-1} for Stl, Φ11dUTPase^{WT}, Φ11dUTPase^{F164W}, Φ11dUTPase^{E158STOP} respectively, as calculated from amino acid composition (http://web.expasy.org/protparam/).

Mass spectrometry (MS)

A commercial Waters QTOF Premier instrument equipped with an electrospray ionization source was used in positive ion mode. The ions were generated from 20 mM NH_4HCO_3 buffer solution (pH = 8.0) containing a total protein concentration of 40 µM. These conditions allow transfer of the native protein complexes into the gas phase (2, 3).The capillary voltage was 2600 V, the sampling cone voltage was 128 V and the temperature of the source was kept at 363 K. Mass spectra were recorded in the mass range of 1500 – 6000 m/z.

Analytic gel filtration

Analytical gel filtration was performed as described in the "Purification of tag-free Φ11 dUTPases" part. Calibration curve was plotted after running successively on the column proteins

of well-known molecular weights in order to determine the native oligomerization state of Stl and Φ11 dUTPase, and to determine the complexation of the above mentioned proteins.

Quartz Crystal Microbalance (QCM) measurements

For the immobilization of Stl LNB-carboxyl chips were prewetted with MilliQ water prior to immobilization, inserted in the Attana A100 QCM biosensor instrument (Attana AB, Stockholm, Sweden), and left to stabilize. Immobilization was carried out at a flow rate of 10 µl/min in HBS-T buffer (10 mM HEPES, 150 mM NaCl, 0.005% Tween 20, pH 7.4) at 25°C. Thereafter, 0.4 mM N-(3-dimethylaminopropyl)-N'-ethylcarbodiimide hydrochloride and 0.1 mM Sulfo-NHS were mixed at 1:1 ratio and this solution was injected immediately with 300 s of contact time to activate the chip's surface. After rinsing the injection loop with MilliQ water the ligand solution containing 20 µg/ml of purified Stl in 10 mM CH_3COONa, pH 4.0, was loaded to the chip for 300 s. The injection loop was washed again with MilliQ water, and finally, the remaining activated carboxyl groups on the chip's surface were neutralized by the injection of 1 M ethanolamine, pH 8.5 for 300 s.

After each measurement the chip's surface was regenerated by an injection of 50 mM NaOH for 40 s to remove any remaining analyte. At least three independent experiments were performed.

Steady-state fluorescent measurements

Measurements were done in Greiner 96 Well Black Non-Binding Microplates. Tryptophan residues were excited at 295 nm, emission spectra were recorded between 320-400 nm. For titration, the fluorescence intensities were recorded at 350 nm. Excitation and emission slits were 1nm. Fluorescence was measured in top detection mode, measurement height was optimized for every plate. Additional fluorescence or inner filter effect imposed on the measured intensities during titration experiments were corrected by subtracting the intensity of the assay buffer. The background fluorescence of Stl (Trp:0; Tyr: 24; Phe 6) was subtracted in every case where Stl was present (in these cases buffer was not subtracted).

Fluorescence kinetics experiments

Long time courses were recorded in a Jobin Yvon Spex Fluoromax-3 spectrofluorometer at 293 K. After 5 minutes preincubation of 2 µM Φ11dUTPase^{F164W} with 4 µM Stl in assay buffer, dUTP was added in various concentrations (500-2300 µM) manually. Trp fluorescence was excited at 297 nm (at 1 nm slit width) and emission was monitored continuously in time at 347 nm. Time courses were analyzed using Origin 7.5. (OriginLab Corp., Northampton, MA).

Limited proteolysis

Limited tryptic digestion was carried out at 25 °C, using 4.3 µM Stl, 2.2 µM Φ11dUTPase^{WT}, 1mM dUPNPP concentrations and 1:800 (w/w) trypsin:Stl ratio in 1.8 mM KH_2PO_4, 10mM Na_2HPO_4 buffer , pH 7.3, containing 2.7 mM KCl, 200 mM NaCl and 5mM $MgCl_2$. Aliquots were taken at different time points. After stopping the digestion by the addition of 1 mM PMSF, samples were analyzed by SDS-PAGE.

Production of Stl binding site$_{183}$ for EMSA experiments

The 171mer oligonucleotide, that was used in previously for EMSA experiments (4), and was custom synthetized by Eurofins MWG Operon and cloned into the NotI/NotI sites of the vector pEX-A. The sequence was additionally flanked by an EcoRI site on 5' and BamHI site on the 3' end. The binding site was amplified for EMSA experiments yielding a 183mer oligo (Stl binding site$_{183}$). For amplification Stl_oligo_F (5'-GAATTCATTTCAACATTAAATATTG-3') and Stl_oligo_R (5'-GGATCCTAAATCCTGTCCTTTCAC-3') primers were used. The PCR product was purified with Quiagen PCR clean up KIT.

Supplemental References

1. Leveles, I., Németh, V., Szabó, J.E., Harmat, V., Nyíri, K., Bendes, Á.Á., Papp-Kádár, V., Zagyva, I., Róna, G., Ozohanics, O., et al. (2013) Structure and enzymatic mechanism of a moonlighting dUTPase. *Acta Crystallogr. D. Biol. Crystallogr.*, **69**, 2298–308.

2. Benesch, J.L.P. and Robinson, C. V (2006) Mass spectrometry of macromolecular assemblies: preservation and dissociation. *Curr. Opin. Struct. Biol.*, **16**, 245–51.

3. Grandori, R., Santambrogio, C., Brocca, S., Invernizzi, G. and Lotti, M. (2009) Electrospray-ionization mass spectrometry as a tool for fast screening of protein structural properties. *Biotechnol. J.*, **4**, 73–87.

4. Tormo-Más, M.A., Mir, I., Shrestha, A., Tallent, S.M., Campoy, S., Lasa, I., Barbé, J., Novick, R.P., Christie, G.E. and Penadés, J.R. (2010) Moonlighting bacteriophage proteins derepress staphylococcal pathogenicity islands. *Nature*, **465**, 779–82.

5. Kuroda, M., Ohta, T., Uchiyama, I., Baba, T., Yuzawa, H., Kobayashi, I., Cui, L., Oguchi, a, Aoki, K., Nagai, Y., et al. (2001) Whole genome sequencing of meticillin-resistant Staphylococcus aureus. *Lancet*, **357**, 1225–40.

6. Mwangi, M.M., Wu, S.W., Zhou, Y., Sieradzki, K., de Lencastre, H., Richardson, P., Bruce, D., Rubin, E., Myers, E., Siggia, E.D., et al. (2007) Tracking the in vivo evolution of multidrug resistance in Staphylococcus aureus by whole-genome sequencing. *Proc. Natl. Acad. Sci. U. S. A.*, **104**, 9451–6.

7. Nübel, U., Dordel, J., Kurt, K., Strommenger, B., Westh, H., Shukla, S.K., Zemlicková, H., Leblois, R., Wirth, T., Jombart, T., et al. (2010) A timescale for evolution, population expansion, and spatial spread of an emerging clone of methicillin-resistant Staphylococcus aureus. *PLoS Pathog.*, **6**, e1000855.

8. Holden, M.T.G., Lindsay, J. a, Corton, C., Quail, M. a, Cockfield, J.D., Pathak, S., Batra, R., Parkhill, J., Bentley, S.D. and Edgeworth, J.D. (2010) Genome sequence of a recently emerged, highly transmissible, multi-antibiotic- and antiseptic-resistant variant of methicillin-resistant Staphylococcus aureus, sequence type 239 (TW). *J. Bacteriol.*, **192**, 888–92.

9. Golding, G.R., Bryden, L., Levett, P.N., McDonald, R.R., Wong, A., Graham, M.R., Tyler, S., Van Domselaar, G., Mabon, P., Kent, H., et al. (2012) whole-genome sequence of livestock-associated st398 methicillin-resistant staphylococcus aureus Isolated from Humans in Canada. *J. Bacteriol.*, **194**, 6627–8.

10. Larner-Svensson et al. (2013) Complete genome sequence of Staphylococcus aureus strain M1, a unique t024-ST8-IVa Danish methicillin-resistant S. aureus clone. *Genome Announc.*, **1**, e00336–13.

11. Herron-Olson, L., Fitzgerald, J.R., Musser, J.M. and Kapur, V. (2007) Molecular correlates of host specialization in Staphylococcus aureus. *PLoS One*, **2**, e1120.

12. Zhou, Y., Liang, Y., Lynch, K.H., Dennis, J.J. and Wishart, D.S. (2011) PHAST: a fast phage search tool. *Nucleic Acids Res.*, **39**, W347–52.

13. Vogel, V., Falquet, L., Calderon-Copete, S.P., Basset, P. and Blanc, D.S. (2012) Short term evolution of a highly transmissible methicillin-resistant Staphylococcus aureus clone (ST228) in a tertiary care hospital. *PLoS One*, **7**, e38969.

14. Stegger, M., Price, L.B., Larsen, A.R., Gillece, J.D., Waters, A.E., Skov, R. and Andersen, P.S. (2012) Genome sequence of Staphylococcus aureus strain 11819-97, an ST80-IV European community-acquired methicillin-resistant isolate. *J. Bacteriol.*, **194**, 1625–6.

15. Uhlemann, A.-C., Porcella, S.F., Trivedi, S., Sullivan, S.B., Hafer, C., Kennedy, A.D., Barbian, K.D., McCarthy, A.J., Street, C., Hirschberg, D.L., et al. (2012) Identification of a highly transmissible animal-independent Staphylococcus aureus ST398 clone with distinct genomic and cell adhesion properties. *MBio*, **3**, 1–9.

16. Gill, S.R., Fouts, D.E., Archer, G.L., Mongodin, E.F., Deboy, R.T., Ravel, J., Paulsen, I.T., Kolonay, J.F., Brinkac, L., Beanan, M., et al. (2005) Insights on evolution of virulence and resistance from the complete genome analysis of an early methicillin-resistant Staphylococcus aureus strain and a biofilm-producing methicillin-resistant Staphylococcus epidermidis strain. *J. Bacteriol.*, **187**, 2426–38.

17. Guinane, C.M., Ben Zakour, N.L., Tormo-Mas, M. a, Weinert, L. a, Lowder, B. V, Cartwright, R. a, Smyth, D.S., Smyth, C.J., Lindsay, J. a, Gould, K. a, et al. (2010) Evolutionary genomics of Staphylococcus aureus reveals insights into the origin and molecular basis of ruminant host adaptation. *Genome Biol. Evol.*, **2**, 454–66.

18. Lowder, B. V, Guinane, C.M., Ben Zakour, N.L., Weinert, L. a, Conway-Morris, A., Cartwright, R. a, Simpson, a J., Rambaut, A., Nübel, U. and Fitzgerald, J.R. (2009) Recent human-to-poultry host jump, adaptation, and pandemic spread of Staphylococcus aureus. *Proc. Natl. Acad. Sci. U. S. A.*, **106**, 19545–50.

19. Köser, C.U., Holden, M.T.G., Ellington, M.J., Cartwright, E.J.P., Brown, N.M., Ogilvy-Stuart, A.L., Hsu, L.Y., Chewapreecha, C., Croucher, N.J., Harris, S.R., et al. (2012) Rapid whole-genome sequencing for investigation of a neonatal MRSA outbreak. *N. Engl. J. Med.*, **366**, 2267–75.

20. Chua, K.Y.L., Seemann, T., Harrison, P.F., Monagle, S., Korman, T.M., Johnson, P.D.R., Coombs, G.W., Howden, B.O., Davies, J.K., Howden, B.P., et al. (2011) The dominant Australian community-acquired methicillin-resistant Staphylococcus aureus clone ST93-IV [2B] is highly virulent and genetically distinct. *PLoS One*, **6**, e25887.

21. Harrison, E.M., Paterson, G.K., Holden, M.T.G., Larsen, J., Stegger, M., Larsen, A.R., Petersen, A., Skov, R.L., Christensen, J.M., Bak Zeuthen, A., et al. (2013) Whole genome sequencing identifies zoonotic transmission of MRSA isolates with the novel mecA homologue mecC. *EMBO Mol. Med.*, **5**, 509–15.

22. Huang, T.-W., Chen, F.-J., Miu, W.-C., Liao, T.-L., Lin, A.-C., Huang, I.-W., Wu, K.-M., Tsai, S.-F., Chen, Y.-T. and Lauderdale, T.-L.Y. (2012) Complete genome sequence of Staphylococcus aureus M013, a pvl-positive, ST59-SCCmec type V strain isolated in Taiwan. *J. Bacteriol.*, **194**, 1256–7.

23. Holden, M.T.G., Feil, E.J., Lindsay, J. a, Peacock, S.J., Day, N.P.J., Enright, M.C., Foster, T.J., Moore, C.E., Hurst, L., Atkin, R., et al. (2004) Complete genomes of two clinical Staphylococcus aureus strains: evidence for the rapid evolution of virulence and drug resistance. *Proc. Natl. Acad. Sci. U. S. A.*, **101**, 9786–91.

24. Holt, D.C., Holden, M.T.G., Tong, S.Y.C., Castillo-Ramirez, S., Clarke, L., Quail, M. a, Currie, B.J., Parkhill, J., Bentley, S.D., Feil, E.J., et al. (2011) A very early-branching Staphylococcus aureus lineage lacking the carotenoid pigment staphyloxanthin. *Genome Biol. Evol.*, **3**, 881–95.

25. Baba, T., Takeuchi, F., Kuroda, M., Yuzawa, H., Aoki, K., Oguchi, A., Nagai, Y., Iwama, N., Asano, K., Naimi, T., et al. (2002) Genome and virulence determinants of high virulence community-acquired MRSA. *Lancet*, **359**, 1819–27.

26. Neoh, H., Cui, L., Yuzawa, H., Takeuchi, F., Matsuo, M. and Hiramatsu, K. (2008) Mutated response regulator graR is responsible for phenotypic conversion of Staphylococcus aureus from heterogeneous vancomycin-intermediate resistance to vancomycin-intermediate resistance. *Antimicrob. Agents Chemother.*, **52**, 45–53.

27. Iandolo, J.J., Worrell, V., Groicher, K.H., Qian, Y., Tian, R., Kenton, S., Dorman, A., Ji, H., Lin, S., Loh, P., et al. (2002) Comparative analysis of the genomes of the temperate bacteriophages phi 11, phi 12 and phi 13 of Staphylococcus aureus 8325. *Gene*, **289**, 109–18.

28. Schijffelen, M.J., Boel, C.H.E., van Strijp, J. a G. and Fluit, A.C. (2010) Whole genome analysis of a livestock-associated methicillin-resistant Staphylococcus aureus ST398 isolate from a case of human endocarditis. *BMC Genomics*, **11**, 376.

29. Hung, W.-C., Takano, T., Higuchi, W., Iwao, Y., Khokhlova, O., Teng, L.-J. and Yamamoto, T. (2012) Comparative genomics of community-acquired ST59 methicillin-resistant Staphylococcus aureus in Taiwan: novel mobile resistance structures with IS1216V. *PLoS One*, **7**, e46987.

30. Li, Y., Cao, B., Zhang, Y., Zhou, J., Yang, B. and Wang, L. (2011) Complete genome sequence of Staphylococcus aureus T0131, an ST239-MRSA-SCCmec type III clone isolated in China. *J. Bacteriol.*, **193**, 3411–2.

31. Diep, B.A., Gill, S.R., Chang, R.F., Phan, T.H., Chen, J.H., Davidson, M.G., Lin, F., Lin, J., Carleton, H.A., Mongodin, E.F., et al. (2006) Complete genome sequence of USA300, an epidemic clone of community-acquired meticillin-resistant Staphylococcus aureus. *Lancet*, **367**, 731–9.

32. Highlander, S.K., Hultén, K.G., Qin, X., Jiang, H., Yerrapragada, S., Mason, E.O., Shang, Y., Williams, T.M., Fortunov, R.M., Liu, Y., et al. (2007) Subtle genetic changes enhance virulence of methicillin resistant and sensitive Staphylococcus aureus. *BMC Microbiol.*, **7**, 99.

33. Howden, B.P., Seemann, T., Harrison, P.F., McEvoy, C.R., Stanton, J.-A.L., Rand, C.J., Mason, C.W., Jensen, S.O., Firth, N., Davies, J.K., et al. (2010) Complete genome sequence of Staphylococcus aureus strain JKD6008, an ST239 clone of methicillin-resistant Staphylococcus aureus with intermediate-level vancomycin resistance. *J. Bacteriol.*, **192**, 5848–9.

34. Baba, T., Bae, T., Schneewind, O., Takeuchi, F. and Hiramatsu, K. (2008) Genome sequence of Staphylococcus aureus strain Newman and comparative analysis of staphylococcal genomes: polymorphism and evolution of two major pathogenicity islands. *J. Bacteriol.*, **190**, 300–10.

35. Fraunholz, M., Bernhardt, J., Schuldes, J., Daniel, R., Hecker, M. and Sinha, B. (2013) Complete Genome Sequence of Staphylococcus aureus 6850, a Highly Cytotoxic and Clinically Virulent Methicillin-Sensitive Strain with Distant Relatedness to Prototype Strains. *Genome Announc.*, **1**.

36. Chen, C.-J., Unger, C., Hoffmann, W., Lindsay, J.A., Huang, Y.-C. and Götz, F. (2013) Characterization and comparison of 2 distinct epidemic community-associated methicillin-resistant Staphylococcus aureus clones of ST59 lineage. *PLoS One*, **8**, e63210.

37. Tóth, J., Varga, B., Kovács, M., Málnási-Csizmadia, A. and Vértessy, B.G. (2007) Kinetic mechanism of human dUTPase, an essential nucleotide pyrophosphatase enzyme. *J. Biol. Chem.*, **282**, 33572–82.

38. John, J., Sohmen, R., Feuerstein, J., Linke, R., Wittinghofer, A. and Goody, R.S. (1990) Kinetics of interaction of nucleotides with nucleotide-free H-ras p21. *Biochemistry*, **29**, 6058–65.

39. Rensland, H., John, J., Linke, R., Simon, I., Schlichting, I., Wittinghofer, A. and Goody, R.S. (1995) Substrate and product structural requirements for binding of nucleotides to H-ras p21: the mechanism of discrimination between guanosine and adenosine nucleotides. *Biochemistry*, **34**, 593–9.

40. Haller, M. (1997) Nucleotide Hydrolysis-dependent Conformational Changes in p21ras as Studied Using ESR Spectroscopy. *J. Biol. Chem.*, **272**, 30103–30107.

41. Gideon, P., John, J., Frech, M., Lautwein, A., Clark, R., Scheffler, J.E. and Wittinghofer, A. (1992) Mutational and kinetic analyses of the GTPase-activating protein (GAP)-p21 interaction: the C-terminal domain of GAP is not sufficient for full activity. *Mol. Cell. Biol.*, **12**, 2050–6.

42. Herrmann, C., Martin, G.A. and Wittinghofer, A. (1995) Quantitative analysis of the complex between p21ras and the Ras-binding domain of the human Raf-1 protein kinase. *J. Biol. Chem.*, **270**, 2901–5.

43. Sydor, J.R., Engelhard, M., Wittinghofer, a, Goody, R.S. and Herrmann, C. (1998) Transient kinetic studies on the interaction of Ras and the Ras-binding domain of c-Raf-1 reveal rapid equilibration of the complex. *Biochemistry*, **37**, 14292–9.

44. Tormo-Más, M.Á., Donderis, J., García-Caballer, M., Alt, A., Mir-Sanchis, I., Marina, A. and Penadés, J.R. (2013) Phage dUTPases control transfer of virulence genes by a proto-oncogenic G protein-like mechanism. *Mol. Cell*, **49**, 947–58.

45. Pécsi, I., Szabó, J.E., Adams, S.D., Simon, I., Sellers, J.R., Vértessy, B.G. and Tóth, J. (2011) Nucleotide pyrophosphatase employs a P-loop-like motif to enhance catalytic power and NDP/NTP discrimination. *Proc. Natl. Acad. Sci. U. S. A.*, **108**, 14437–42.

Supplemental Tables

Supplemental Table I. Rate constants of the potential conformational change observed by QCM

	k_2 (s^{-1})	k_{-2} (s^{-1})
Φ11 dUTPase^{WT}	0.0105 ± 0.0021	0.0012 ± 0.0003
Φ11 dUTPase^{F164W}	0.0083 ± 0.0004	0.0011 ± 0.0001
Φ11 dUTPase^{F164W}, dUTP	0.0120 ± 0.0018	0.0046 ± 0.0011
Φ11 dUTPase^{F164W}, dUMP	0.0089 ± 0.0008	0.0016 ± 0.0002

Supplemental Table II. Occurrence of dUTPases in *Staphylococcus aureus* strains

Genome sequence	Organism (NCBI Genome)	Genomic dUTPase[1]	Phage dUTPases			
			Dimer[1]	Trimer[1]	Prophage carrying dUTPase[2]	Reference for prophage detection
NC_002745.2	N315	–	1124674	–	ΦN315	(5)
NC_009632.1	JH1	–	5317510	–	Phage 92 –like	(6)
			–	5317603	ΦSaST5-K	(6, 7)
			5317432	–	$\Phi Sa2_{USA}$-like	(6)
			5317353	–	ΦN315 -like	
NC_017331.1	TW20	–	12862042	–	$\Phi Sa1_{TW20}$	(8)
			12863174	–	$\Phi Sa3_{TW20}$	
NC_017340.1	04-02981	–	–	12865016	ΦSaST5-K	(7)
			12864800	–	ΦN315	
NC_018608.1	08BA02176	–	–	–	–	(9)
NC_021059	M1	–	15299711	–	$\Phi Sa2_{USA}$ –like	(10)
			15300291	–	$\Phi Sa3_{USA}$ –like	
NC_007622.1	RF122	–	3795196	–	ΦSaBov	(11)
NC_020566.1	ST228 isolate 16125	–	14837587	–	P954-like(100/ 1984860)	(12, 13)
NC_020568.1	ST228 isolate 18583	–	14839621	–	ΦNM3-like(60/1984723)	
NC_020564.1	ST228 isolate 10497	–	14835590	–	ΦNM3-like(70/1984906)	
NC_020537.1	ST228 isolate 18412	–	14817523	–	P954-like(70/1984670)	
NC_020536.1	ST228 isolate 18341	–	14815488	–	P954-like(90/1984905)	
NC_020533.1	ST228 isolate 16035	–	14813492	–	P954-like(90/1984851)	
NC_020532.1	ST228 isolate 15532	–	14811453	–	P954-like(60/1985219)	
NC_020529.1	ST228 isolate 10388	–	14809415	–	P954-like(70/1984919)	
NC_017351.1	11819-97	–	–	12424268	ΦSa2	(14)
			12424797	–	ΦSa3,	
			12423395	–	Φ37-like	
NC_017673.1	71193	–	–	12731126	Φ3	(15)
NC_002951.2	Col	–	–	3236924	ΦCol	(16)
NC_017343.1	ECT-R2	–	12336428	–	ΦN315-ike(136/1950872)	(12)
NC_017337.1	ED-133	–	12324986	–	ΦSaov1	(17)
			–	12324459	ΦSaov2	
			–	12323829	ΦSaov3	
NC_013450.1	ED-98	–	–	8613603	ΦAv1	(18)
			8614777	–	ΦAvß	
NC_017763.1	HO 5096 0412	–	–	12799907	ΦSa2	(19)
			–	12801001	ΦSa3	
NC_009487.1	JH9	–	5168136	–	Phage 92 –like	(6)
			–	5169631	ΦSaST5-K	(6, 7)
			5168479	–	$\Phi Sa2_{USA}$-like	(6)
			5168299	–	ΦN315 -like	
NC_017338.1	JKD6159	–	12327664	–	ΦSa2	(20)
			12326670	–	ΦSa3	
NC_017349.1	LGA251	–	–	12907879	ΦSa8	(21)
NC_016928.1	M013	–	11862817	–	ΦPVL	(22)
NC_002952.2	MRSA252	–	2860609	–	ΦSa2	(23)
			–	2861519	ΦSa3	
NC_016941.1	MSHR1132	–	–	11931868	ΦSa3	(24)
NC_002953.3	MSSA476	–	2863935	–	ΦSa4	(23)
NC_003923.1	MW2	–	1003527	–	$\Phi Sa2_{MW}$	(25)

NC_009782.1	Mu3	–	–	5559151	Mu50A$_{Mu3}$	(5, 26)
			5560392	–	Mu50B $_{Mu3}$	
NC_002758.2	Mu50	–	–	1121986	Mu50A	(5)
			1120851	–	Mu50B	
NC_007795.1	NCT8325	–	–	3919744	Φ11	(27)
			–	3920595	Φ12	
			3919570	–	Φ13	
NC_017333.1	ST398	–	12322852	–	ΦSa2$_{S0385}$	(28, 29)
			12323353	–	ΦSa6$_{S0385}$	
NC_017347.1	T0131	–	12338028	–	ΦNM3-like$_{(100/2058773)}$	(12, 30)
NC_017342.1	TCH60	–	–	12333594	Φ7401PVL-like$_{(150/1737832)}$	(12)
NC_007793.1	USA300_FPR3757	–	3913324	–	ΦSa2$_{USA}$	(31)
			–	3913209	ΦSa3$_{USA}$	
NC_010079.1	USA300_TCH1516	–	5776354	–	ΦSLT$_{USA300}$	(32)
			–	5776354	Φß$_{USA300}$	
NC_016912.1	VC40	–	–	–	–	–
NC_017341.1	JKD6008	–	12331190	–	Phage 92 –like$_{(60/1964562)}$	(12, 33)
			12331352	–	ΦNM3$_{(60/2113993)}$	
NC_009641.1	Newman	–	5331083	–	ΦNM1	(34)
			5330616	–	ΦNM2	
			–	5331168	ΦNM3	
			5330123	–	ΦNM4	
NC_022222.1[3]	6850	–	–	–	–	(12, 35)
NC_022113.1[3]	55/2053	–	16643574	–	ΦPVL108-like$_{(90/1971076)}$	(12)
			–	16643031	ΦNM3-like$_{(130/1457369)}$	
NC_021670.1[3]	Bmb9393	–	16042074	–	P954-like$_{(80/2165809)}$	(12)
			–	16041143	StauST398_2-like$_{(150/1165187)}$	
			–	16041551	ΦMR1-like$_{(1130/1632359)}$	
NC_021554.1[3]	CA-347	–	16168865	–	Staphy_2-like$_{(117/2068311)}$	(12)
			16169566	–	ΦNM3-like$_{(150/1517475)}$	
NC_022226.1[3]	CN1	–	16743935	–	ΦNM3-like$_{(113/1973210)}$	(12)
NC_022443.1[3]	SA40	–	–	–	–	(12, 36)
NC_022442.1[3]	SA957	–	17054050	–	Φ5967PVL-like$_{(146/1523591)}$	(12, 36)
NC_022604.1[3]	Z172	–	17370004	–	ΦNM3-like$_{(108/2105565)}$	(12)
			17369075	–	ΦMR11-like$_{(100/1151302)}$	

[1] Gene ID of the hits is given in the indicated columns.

[2] Only the prophages that carry a dUTPase are indicated. In case of PHAST detection the PHAST score of the appropriate hit and the starting site of the prophage region are indicated as subscript (score/starting site). Meaning of PHAST scores: >90 indicates intact and inducible prophage, 60-90 indicates that the inducibility of the prophage is quiestionable, <60 indicates that the prophage is probable not activable anymore.

[3] Provisional REFSEQ

Supplemental Table III. Kinetic comparison of dUTPase and G protein based switches.

	dUTPase*	**$p21^{H\text{-}Ras}$ ****
Properties of nucleotide hydrolase reaction		
d(NTP) k_{on} ($\mu M^{-1}s^{-1}$)	$1.2 * 10^{2}$ (37)	2.1 (38)
d(NTP) k_{off} (s^{-1})	$1.0 * 10^{2}$ (37)	$2.9 * 10^{-5}$ (39)
K_d (μM) (k_{off} / k_{on})	$8.3 * 10^{-1}$ (37)	$1.4 * 10^{-5}$
k_{on} product nucl. ($\mu M^{-1}s^{-1}$)	$3.1 * 10^{1}$ (37)	$8.4 * 10^{-1}$ (38)
k_{off} product nucl. (s^{-1})	$1.0 * 10^{3}$ (37)	$1.8 * 10^{-5}$ (38)
K_d product nucl.(μM) (k_{off} / k_{on})	$3.2 * 10^{1}$ (37)	$2.1 * 10^{-5}$ (38)
k_{cat} (s^{-1})	6.4 (37)	$5.5 * 10^{-3}$ (40)
p120-GAP activated k_{cat} (s^{-1})	NA	10^{5} stimulation (41)
Interaction with the effector		
	Stl	Ras Binding domain of Raf
Effect on activity	total inhibition	none (42)
k_{on} ($\mu M^{-1}s^{-1}$)	$4.1 * 10^{-1}$ (This work)[#]	NA
k_{off} (s^{-1})	$2.8 * 10^{-3}$ (This work) [#]	NA
K_d (μM) (k_{off} / k_{on})	$6.8 * 10^{-2}$ (This work) [##]	NA
protein.d(NTP) k_{on} ($\mu M^{-1}s^{-1}$)	NA	$4.5 * 10^{1}$ (43)
protein.d(NTP) k_{off} (s^{-1})	NA	7.4 (43)
protein.d(NTP) K_d (μM) (k_{off} / k_{on})	NA	$1.6 * 10^{-1}$ (43)
protein.product nucl. K_d (μM) (K_{eqv}).	$9.2 * 10^{-2}$ (This work) [##]	$3.2 * 10^{1}$ (43)

* 20°C; ** 25°C; [#] From stopped-flow experiments, cf. Table I. [##] From QCM experiment

Supplemental Table IV. Our model is consistent with previous *in vivo* results

Protein	K_d (μM)	Activity (%)*	Probable state *in vivo*	SAPI induction	Consistent with our model?
Φ11 dUTPase^{WT}	0.8 [2]	157 [3]	dUTP bound until dUTP is converted into dUMP	Yes (better than 80α)	YES
80α dUTPase^{WT}	0.88 [4]	100 [4]	dUTP bound until dUTP is converted into dUMP	Yes [4]	YES
80α dUTPase^{D81A}	2.63 [4]	0 [4]	dUTP bound	no, only if overexpressed [4]	YES
80α dUTPase^{D81N}	2.64 [4]	0 [4]	dUTP bound	No [4]	YES
80α dUTPase^{Y84A}	3.37 [4]	24 [4]	dUTP bound until dUTP is converted into dUMP	Low [4]	YES
80α dUTPase^{Y84F}	0.88 [4]	77 [4]	dUTP bound until dUTP is converted into dUMP	Yes [4]	YES
80α dUTPase^{Y84I}	>400 [4]	0 [4]	substrate free	No [4]	not enough information
80α dUTPase$^{\Delta V}$	ND, probably similar to dUDP binding[5]	0 [4]	dUTP/dUDP bound[5]	No [4]	YES
C-C	ND	0 [4]	not enough information	Hyperactive [4]	not enough information,
80α dUTPase^{D95E}	ND	66 [3]	dUTP bound until dUTP is converted into dUMP	No [3]	not enough information

* 100% activity relates to the activity of wild type 80α dUTPase, the values of the mutant species are related to this value

[2] (1)

[3] (4)

[4] (44)

[5] (45)

Supplemental figures

Supplemental Figure 1: Φ11 dUTPase^{WT} and Stl form a tight complex with slow kinetics: Supplemental results

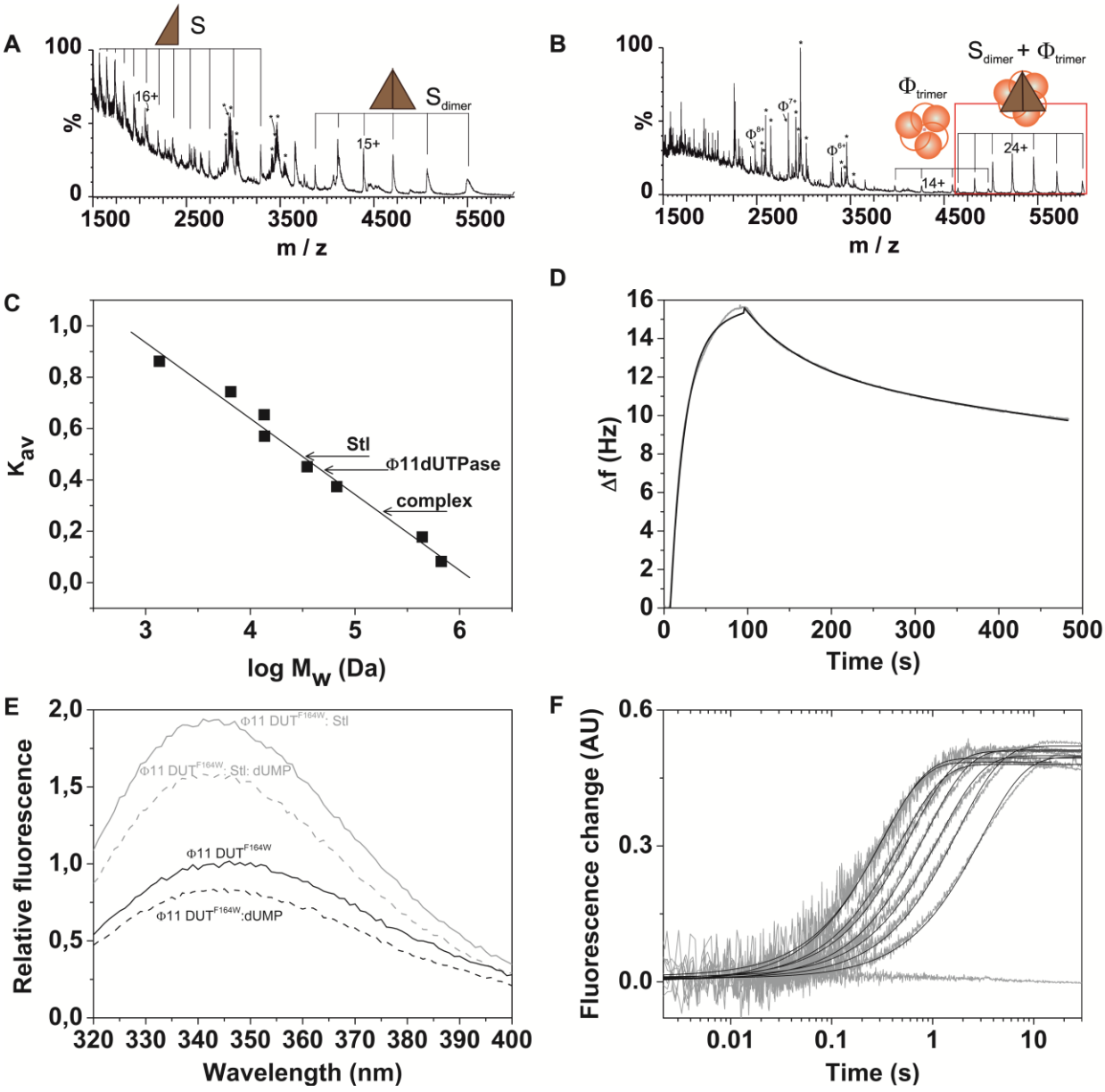

Mass spectra of the Stl protein (**Panel A**) and a 1:1 mixture of the Stl (S) and Φ11 dUTPase^{WT} (Φ) proteins (**Panel B)** measured under native electrospray conditions. Subscripts indicate the oligomerization states of the proteins, while numbers in superscripts and next to the peaks indicate the charge states. The red frame in part B highlights the region of the Φ_3S_2 complex, supporting the specific interaction between the proteins under study. Impurities are marked with asterisk. **Panel C** Size-exclusion chromatography indicates stable complex formation between Stl and dUTPase. **Panel D** shows QCM experiments for complex formation between Stl and wild type Φ11 DUT^{WT} (grey line). A solid black line represents the fit of two state reaction model.

Rate constants from the fitted model are shown in Table I and Suppl. Table I. **Panel E** shows steady-state fluorescence spectra of 3 μM Φ11DUT^{F164W} enzyme with (dashed line) and without (solid line) 2mM dUMP in the presence (grey lines) and absence (black lines) of 3 μM Stl. Data were normalized to the emission peak (346 nm) of the free Φ11DUT^{F164W}. The maximum relative fluorescence of the complexes were: 0.84 at 345 nm for Φ11DUT^{F164W}: dUMP, 1.94 at 341 nm for Φ11DUT^{F164W}: Stl and 1.53 at 341 nm for Φ11DUT^{F164W}: Stl: dUMP. **Panel F** shows the fluorescence time courses observed upon the binding of Stl (1-8 μM) to 0.25 μM Φ11DUT^{F164W}. The curves are shown from 0.002 s (after the deadtime). Smooth lines are single exponential fit to the experimental curves. No further resolvable fluorescence phases were observed.

Supplemental Figure 2: dUTPase:Stl complex formation eliminates the physiological function of both proteins: Supplemental results

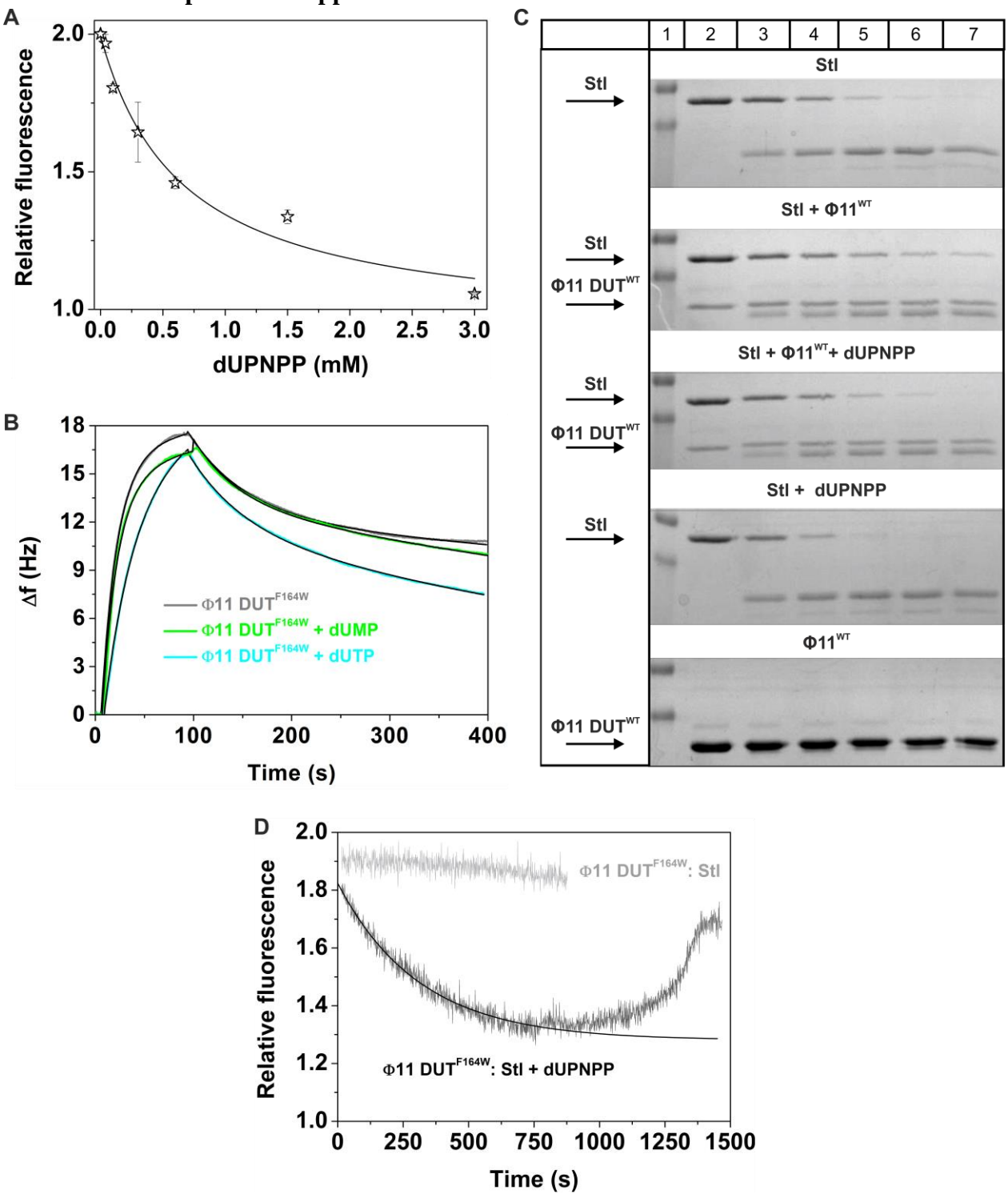

Panel A Fluorescence equilibrium titration of Φ11DUT^{F164W} (2 μM):Stl (3.5 μM) complex with dUPNPP. **Panel B**. shows QCM measurements of Φ11DUT^{F164W} in the absence and presence of dUMP and dUTP. **Panel C.** Limited proteolysis of Stl and Φ11DUT^{WT} complex in absence and in presence of dUPNPP. Trypsin was used for digestion of Stl and Φ11DUT^{WT} proteins. Black

arrows indicate the position of intact Stl or Φ11DUT^{WT}. First lane of each gel corresponds to molecular mass marker with 35 and 25 kDa bands. The following lanes represent the tryptic digestion at different time points (0 min, 5 min, 15 min, 30 min, 45 min and 60 min, respectively). **Panel D** shows the interaction of 2.3 mM dUTP with premixed Φ11DUT^{F164W}(2 μM):Stl(4 μM) complex (red curve). Single exponential fitting to the first phase with fluorescence decreasing (represented as smooth black line) yield observed rate constant 0.00303 ± 0.00008 s^{-1}.

Supplemental Figure 3: dUTPase eliminates Stl binding to its cognate DNA element independently of the presence of its C-terminal segment

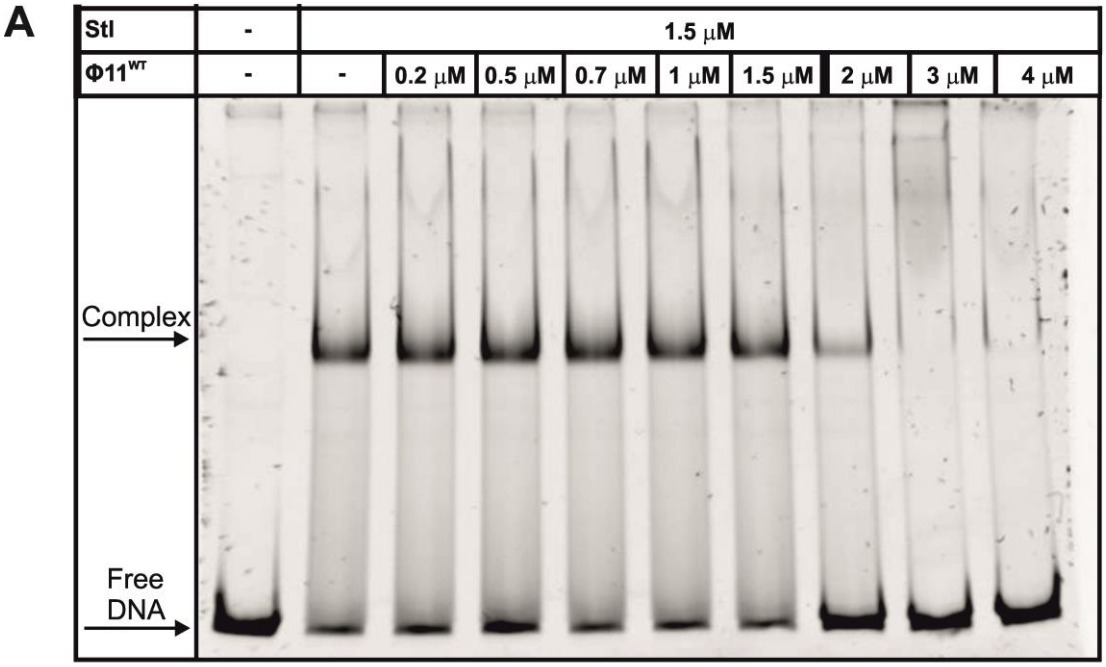

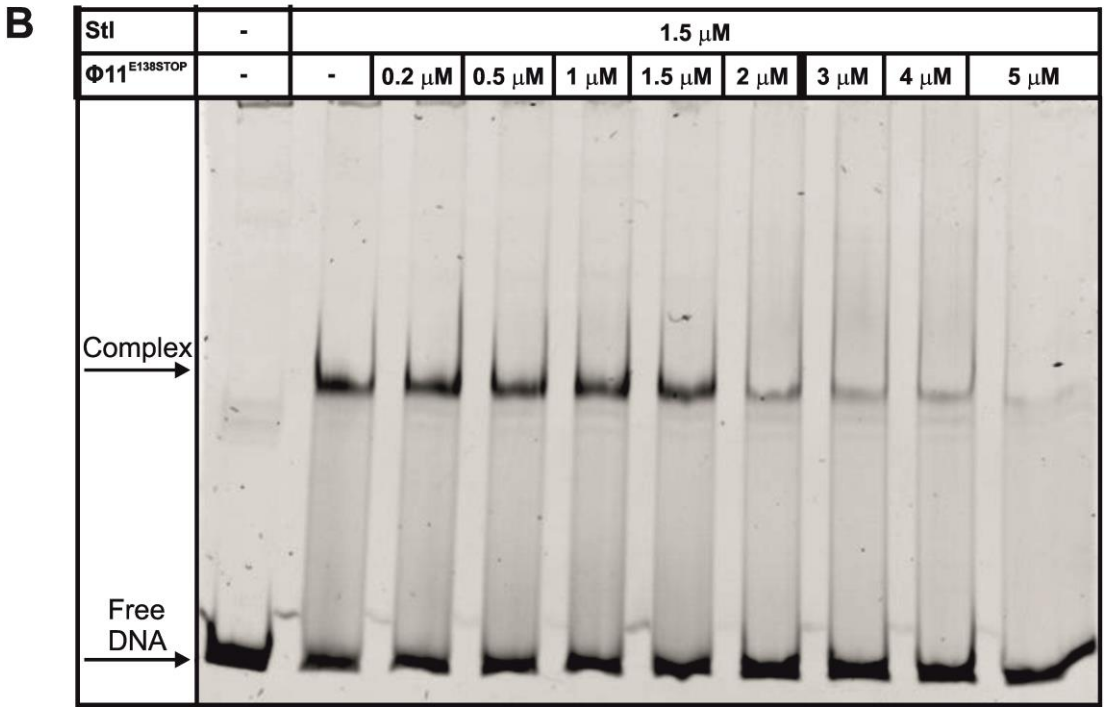

Panel A Φ11 DUT^{WT} prevents Stl from binding to the Stl binding $site_{183}$ shown in EMSA. 1.5 μM Stl was titrated with increasing amounts of Φ11 DUT^{WT} (0.2, 0.5, 0.7 1, 1.5, 2,3,4 μM). **Panel B** Φ11 $DUT^{E158STOP}$ prevents Stl from binding to the Stl binding $site_{183}$ shown in EMSA.

1.5 μM Stl was titrated with increasing amounts of Φ11 $DUT^{E158STOP}$ (0.2, 0.5, 1, 1.5, 2, 3, 4, 5 μM). Arrows on the left show the positions of free oligonucleotide and Stl bound oligonucleotide.

Published online 27 February 2020

Nucleic Acids Research, 2020, Vol. 48, No. 8 ***e45***
doi: 10.1093/nar/gkaa116

A user-friendly, high-throughput tool for the precise fluorescent quantification of deoxyribonucleoside triphosphates from biological samples

Judit Eszter Szabó[1,2,*,†], Éva Viola Surányi[1,2,†], Bence Sándor Mébold[1], Tamás Trombitás[1,2], Mihály Cserepes[1,3] and Judit Tóth[1,*]

[1]Institute of Enzymology, Research Centre for Natural Sciences, Budapest 1117, Hungary, [2]Department of Applied Biotechnology and Food Sciences, Budapest University of Technology and Economics, Budapest 1111, Hungary and [3]Department of Experimental Pharmacology, National Institute of Oncology, Budapest, Hungary

Received August 02, 2019; Revised February 05, 2020; Editorial Decision February 12, 2020; Accepted February 17, 2020

ABSTRACT

Cells maintain a fine-tuned, dynamic concentration balance in the pool of deoxyribonucleoside 5′-triphosphates (dNTPs). This balance is essential for physiological processes including cell cycle control or antiviral defense. Its perturbation results in increased mutation frequencies, replication arrest and may promote cancer development. An easily accessible and relatively high-throughput method would greatly accelerate the exploration of the diversified consequences of dNTP imbalances. The dNTP incorporation based, fluorescent TaqMan-like assay published by Wilson *et al.* has the aforementioned advantages over mass spectrometry, radioactive or chromatography based dNTP quantification methods. Nevertheless, the assay failed to produce reliable data in several biological samples. Therefore, we applied enzyme kinetics analysis on the fluorescent dNTP incorporation curves and found that the Taq polymerase exhibits a dNTP independent exonuclease activity that decouples signal generation from dNTP incorporation. Furthermore, we found that both polymerization and exonuclease activities are unpredictably inhibited by the sample matrix. To resolve these issues, we established a kinetics based data analysis method which identifies the signal generated by dNTP incorporation. We automated the analysis process in the nucleoTIDY software which enables even the inexperienced user to calculate the final and accurate dNTP amounts in a 96-well-plate setup within minutes.

INTRODUCTION

Despite the longstanding need and desire for the precise quantification of cellular levels of deoxyribonucleoside triphosphates (dNTP), none of the existing methods could become routine molecular biology procedure. Besides the general importance of dNTP homeostasis, recent studies have started to unveil its key roles in oncogenic progression (1–7), antiviral defense (8), aging (9–11), cell cycle control (3,4,12,13) and antibody hypermutation (14). To understand the role of dNTP concentration changes in these processes, the most valuable information could be obtained by measuring intracellular dNTP levels directly in the cell. As no method is available to do so, we would need to reliably evaluate the dNTP concentration of cellular lysates, at least. For this, several high performance liquid chromatography (HPLC) based methods and enzymatic assays have been developed. Each method has its advantages and disadvantages but in general, the biggest challenge of dNTP quantitation is that other nucleotides, primarily ribonucleoside triphosphates (rNTPs) are present in much higher concentration in the cell lysate than dNTPs and the separation of the various nucleotides from each other and from the sample matrix is not straightforward.

For HPLC analysis, rNTPs may be removed by boronate chromatograpy (15,16) (compatible only with UV detection (17)) or by specific degradation using chemical or enzymatic methods (17). But even at a 99% efficient removal of rNTP-s, the remaining 1% can interfere with dNTP quantitation (17). HPLC may be coupled with either UV or mass spectrometry (MS) detection. The main advantage of the UV-based HPLC methods is that they can also be used to measure the rNTPs which provides a good control to know whether nucleotide extraction worked properly. UV detection has the disadvantage of the requirement of a large sample size.

*To whom correspondence should be addressed. Tel: +36 1 382 6793; Email: toth.judit@ttk.mta.hu
Correspondence may also be addressed to Judit Eszter Szabó. Email: szabo.judit.eszter@ttk.hu
†The authors wish it to be known that, in their opinion, the first two authors should be regarded as joint First Authors.

© The Author(s) 2020. Published by Oxford University Press on behalf of Nucleic Acids Research.
This is an Open Access article distributed under the terms of the Creative Commons Attribution License (http://creativecommons.org/licenses/by/4.0/), which permits unrestricted reuse, distribution, and reproduction in any medium, provided the original work is properly cited.

Downloaded from https://academic.oup.com/nar/article/48/8/e45/5760754 by guest on 04 November 2021

The HPLC coupled MS detection provides the highest sensitivity, but it has several disadvantages. Generally, the sample extraction and chromatographic separation processes are time-consuming and these methods require specialized labs and high level of expertise in analytics. The optimal separation of nucleotides is commonly achieved using ion paring agents (e.g. the most often used diethylamine). However, these chemicals are incompatible with other standard uses of the MS instrument due to their strong retention inside the mass spectrometer (18). Therefore, the reported HPLC-MS based methods cannot simply be applied on any instrumentation. The mobile phase of the HPLC method, largely responsible for the separation of nucleotides, is needed to be tailored to make it compatible with the available instrumentation and with its other uses. Furthermore, isobaric nucleotide pairs sharing the same mass cannot be distinguished using MS ((deoxy)cytidine vs. (deoxy)uridine isobars (19), deoxyguanosine versus adenosine isobars (17)). A recently published method surmounted the latter difficulties by using an ion-pair-free mobile phase and it is able to detect the eight canonical dNTPs and rNTPs in the biological sample with high sensitivity (20).

Enzyme based methods include the DNA polymerization based radioisotope incorporation technique (21,22), the single nucleotide incorporation based radioisotope technique (23), the TaqMan assay-like fluorescence method by Wilson *et al.* (24), and the most recent DNA polymerase/restriction enzyme based isothermal DNA machine (not yet tested by the scientific community according to the literature) (25). Amongst the enzymatic methods, the most widely used is the DNA polymerization based radioisotope incorporation method. Although this technique is sensitive and reliable, it is labour-intensive and hardly applicable as a high throughput method. This also applies for the single nucleotide incorporation method (23). DNA polymerization based methods may also interfere with the presence of high concentration of rNTPs (22) which can be overcome by the appropriate choice of DNA polymerase and its concentration. These conditions were already considered in the TaqMan assay-like fluorescence method, which relies on similar principles as the polymerization based radioisotope incorporation method using a different detection technique (24). This fluorescence method appeared to revolutionize dNTP concentration measurements with its basic molecular biology requirements and high throughput manner (24).

As we have been interested in dNTP metabolism, we set out to adapt a method for dNTP quantitation for everyday use. Although we applied the radioactive assay successfully before (26), we wished to analyze a high number of samples in a more high throughput manner. We initiated HPLC-MS trials in collaboration, which failed due to the aforementioned incompatibility of the ion pairing organic solvents with other uses of the MS instrument. The fluorescence method by Wilson *et al.* (24) seemed the only option for high-throughput, quantitative dNTP measurements. However, the assay failed in several biological samples, the data analysis method described in the paper yielded negative values. It was particularly difficult to measure dATP. We analyzed the 29 publications citing this paper so far to find out if fellow researchers could apply this method with success. Of the 14 papers that actually applied the dNTP quantification method, detailed method description and exact dNTP quantities are presented in only 3, including a paper from the same authors (27–29). In the other citing publications, the results are presented as relative dNTP levels or extremely raw data (fluorescence intensity) which do not allow the evaluation of the applicability of this method. Matsuura *et al.* mentions that they modified the original method by Wilson *et al.* to 'reduce the background noise caused by polymerase-mediated hydrolysis of the probe' (30). Unfortunately, the modified method was not included in the paper and is still not published. Our own experience and the citing literature indicated that this promising method needed further elaboration in order to become an easily accessible and popular means of dNTP quantification.

Here, we report that the major artefacts hindering the applicability of the Wilson *et al.* method originate from the polymerization independent 5′-3′ exonuclease activity of Taq polymerase and from kinetic inhibition by the biological sample. Both of these disturbing effects can be overcome by our altered assay conditions and by a novel data analysis method. We apply a kinetic treatment of the assay curves which enables the separation of the polymerization dependent and independent processes. We also developed a software offering streamlined data analysis. Using the nucleoTIDY software, the whole analysis process including the kinetic treatment of the assay curves, the construction of the calibration curves and the calculation of the dNTP quantity in the actual biological samples takes just a few minutes for a 96-well-plate. These developments make dNTP quantification widely available to the scientific community in any biological samples.

MATERIALS AND METHODS

Strains and growth conditions

The *Mycobacterium smegmatis* mc^2155 strain used for the experiments was grown in Lemco liquid culture or on solid Lemco plates with the addition of 15 g l^{-1} Bacto agar as described previously (31). MES-SA human uterine sarcoma cell line was obtained from ATCC. The cells were cultured in DMEM (Gibco) supplemented with 10% fetal bovine serum (Gibco), 5 mM L-glutamine (Gibco), and 50 U/ml penicillin/streptomycin solution (Life Technologies). Cell culture flasks were grown up to 90% confluency before harvesting in order to examine monolayer cells.

dNTP pool extraction and sample handling

Bacterial cells. Cells were grown until the culture reached the mid-exponential phase $OD_{600} = 0.7$. The total CFUs were determined for each culture. The cultures were centrifuged (20 min, 3600 g, 4°C) and the cell pellets were extracted in precooled 0.5 ml 60% methanol overnight at −20°C. After 5 minutes boiling at 95°C, cell debris were removed by centrifugation (20 min, 16 000 g, 4°C). The methanolic supernatant containing the soluble dNTP fraction was vacuum-dried (Eppendorf) at 45°C. Extracted dNTPs were dissolved in 50 μl nuclease-free water and stored frozen until use.

Downloaded from https://academic.oup.com/nar/article/48/8/e45/5760754 by guest on 04 November 2021

Human cells. Cultured cells were rinsed with phosphate-buffered saline (PBS) to remove residual media. dNTPs were extracted based on Wilson *et al.* (24) with a few modifications. Briefly, adherent cells were detached by trypsin, resuspended gently in 10 ml of ice-cold PBS and 500 μl aliquot was removed for cell number determination using a hemocytometer. The samples were centrifuged for 10 min at 3000 g at 4°C, cell pellets were resuspended in 500 μl of ice-cold 60% methanol, then placed at -20°C overnight. The sample was afterwards boiled at 95°C for 3 min, then centrifuged (16 000 g for 5 min at 4°C). The supernatant was transferred into a new tube and evaporated under centrifugal vacuum at 45°C. The resultant pellet was resuspended in 50 μl nuclease-free water ready to assay or stored frozen until use.

Handling of the dNTP extracts. dNTP samples, if not properly handled, are prone to degradation. To avoid uncontrolled loss of dNTP within the sample, the extracts should be analysed as soon as they are ready or else should be stored in a deep freezer considering that storage in too small aliquots leads to significant concentration of the samples. Freezing must be done in liquid nitrogen. Repeated freeze-thaw cycles should be avoided and all analyses are best completed in a reasonably short time. The pH of the sample and reaction mix should be well controlled.

Reaction conditions, data acquisition and evaluation

We applied the reaction conditions described in Wilson *et al.* (24) to obtain the results shown in Figures 1–4 and Supplementary Figures S1–S4. Briefly, 10 pmol template, 10 pmol probe and 10 pmol NDP1 primer was present per 25 μl reaction. The concentration of each non-specific dNTP was kept at 100 μM. The AmpliTaq Gold™ DNA Polymerase (Applied Biosystems™, Thermo Fisher Scientific) was used at 0.825 unit/reaction while the VWR® TEMPase Hot Start DNA Polymerase (VWR) was used at 0.9 unit / reaction in the presence of 2.5 mM $MgCl_2$. To record calibration curves, the reaction was supplied with 0–10 pmol or 0–20 pmol specific dNTP depending on the applied dT1 or dT2 template, respectively. The sensitivity of the dNTP quantitation reaction is highly determined by the number of specific dNTPs to be incorporated. The dT1 template allows the incorporation of only one molecule of specific dNTP (Figure 1A), and is applicable in the 0–10 pmol dNTP range, while the dT2 template allows the incorporation of two specific dNTPs, and is applicable up to 20 pmol dNTP with a lower sensitivity. The sequences of the applied primers and probes are presented in Table 2 (24). Fluorescence was recorded every 17 seconds in a CFX96 Touch™ Real-Time PCR Detection System for 25 min, or longer. We used FrameStar® 96-Well Skirted PCR Plates with black wire and white wells and sealed with Eppendorf adhesive PCR films. In a few measurements, the QuantStudio 5, QuantStudio 1 (Thermo Fisher), and the AriaMx (Agilent) instruments were also used with plates recommended by the manufacturers. The choice of instrument did not seem to affect the results. DNA primers were from Sigma (standard purification), while the fluorescence probes were ordered from Integrated DNA Technologies subjected to HPLC purification. The concentration of each stock of the dNTPs and primers were determined by measuring the absorbance at 260 nm. The VWR® TEMPase Hot Start DNA Polymerase catalysed reaction proved to be faster than the AmpliTaq Gold™ polymerase catalyzed reaction, therefore, data were collected for shorter time, and fluorescence was read out earlier than with the AmpliTaq Gold™ polymerase (cf. Supplementary Figure S1). The thermal profile for the AmpliTaq Gold™ polymerase: 95°C 10 minutes, 60°C for varying times (cf. Table 1); and for the VWR® TEMPase Hot Start DNA Polymerase: 95°C 15 min, 60°C 13 s × 260 cycle for dATP measurement. For dCTP, dGTP and dTTP measurements, the polymerization temperature needed to be decreased to 55°C for the VWR® TEMPase Hot Start DNA Polymerase to be able to record the initial fluorescence change. Later, to optimize the reaction conditions for amplitude based dNTP quantification, we varied the template, probe, primer, $MgCl_2$ and polymerase concentrations (Cf. Results, Table 1 and Supplementary Table SI).

Denaturing urea-PAGE gel

To demonstrate the exonuclease activity of the Taq polymerase on the template-probe complex, we used the dTTP assay under the same reaction conditions as described above (10 pmol dTTP-dT1 template, 10 pmol NDP1 primer in 25 μl reaction). We used denaturing 14% polyacrylamide-urea gel (7.5 M urea) to separate oligonucleotides at one base pair precision (23,32). As the probe did not penetrate into the gel in its original form containing the FAM fluorophore and the ZEN and iBFQ quenchers, we used 10 pmol dTTP-probe of identical sequence (5′ AGGACCGAGGCAAG AGCGAGCGA 3′) without these chemical modifications. We incubated the reaction mixtures at 95°C for 15 minutes followed by incubation at 60°C for 0–90 min. Reactions were terminated by adding 25 μl of the 2× formamide gel loading buffer (95% formamide, 0.025 w/v% Bromophenol Blue, 5 mM EDTA). The resulted 50 μl samples were heat denatured for 5 minutes at 95°C. The gel was prerun at 150 V at 45°C in TBE buffer for 1 h. Then 20 μl of each sample were loaded and the run was carried out at 100 V at 45°C in TBE buffer for 1 h 15 min. The gel was stained using 3333x GelRed in 100 mM NaCl solution.

Kinetic analysis

When applying a kinetic analysis approach for dNTP quantitation, fluorescence data was plotted against time (s) and fitted with single or double exponential decay functions, as it is usual in enzyme kinetic analysis (Equations 1 and 2, respectively):

$$F = A{*}e^{-k_{obs}x} + F_0 \quad (1)$$

$$F = A_1{*}e^{-k1_{obs}x} + A_2{*}e^{-k2_{obs}x} + F_0 \quad (2)$$

where F is the observed fluorescence, x is the variable (time), A and $A_{1–2}$ are the amplitudes, k_{obs} and $k_{1–2obs}$ are the rate constants of the observable fluorescence phases, while F_0 is

Downloaded from https://academic.oup.com/nar/article/48/8/e45/5760754 by guest on 04 November 2021

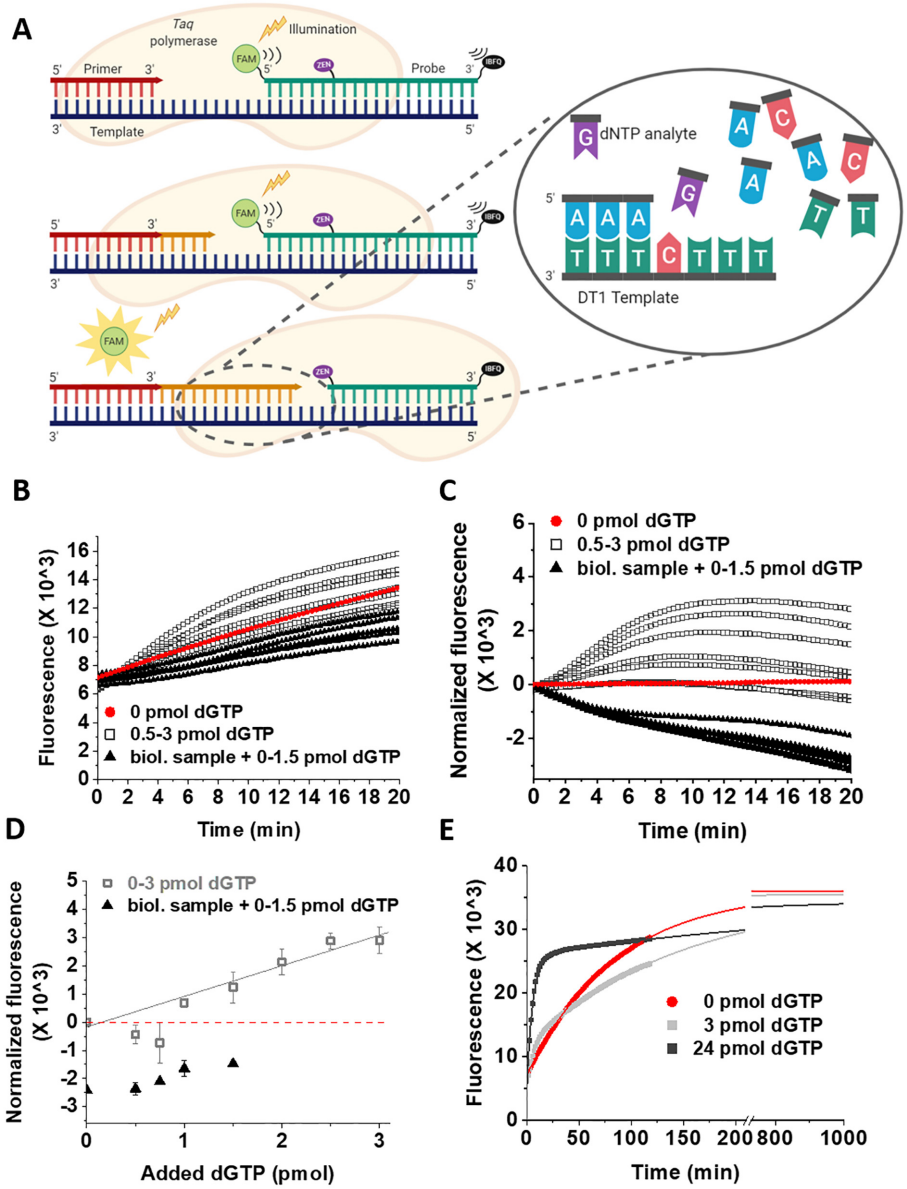

Figure 1. Measurement of cellular dGTP concentration with dT1 template in human sample using the method by Wilson *et al.* (24) (**A**) The schematic representation of the assay. The yellow star symbolizes the release of FAM (light green circle) from the probe (dark green DNA) previously quenched by the ZEN (purple oval) and IBFQ (black oval) quenchers. The light orange shape symbolizes the *Taq* polymerase, while DNA strands are symbolized by comb shapes as follows: dark blue, template; red, primer; orange, newly synthesized DNA; dark green, probe. (**B**) Raw reaction curves in the absence of biological sample (0–3 pmol dGTP /calibration reaction) and in the presence of human sample (0–1.5 pmol dGTP standard addition + dNTP extract from 5×10^5 cells /reaction). Note, that the blank reaction (0 pmol dGTP) also produces signal, which complication was eliminated by Wilson *et al.* via subtracting blank curves from sample curves (shown in panel C). (**C**) Reaction curves normalized according to Wilson *et al.* (**D**) Calibration curve (0–3 pmol dGTP) in the absence of biological sample, and standard addition points in the presence of biological sample derived from reading the fluorescence of panel C at 15 min. Continuous lines are linear fits to the data yielding the following parameters: calibration without biological sample: intercept = −115±145, slope = 1056 ± 113, $R^2 = 0.98$. In case of the calibration points, the negative data points were omitted from the fitting. Data and errors represent the average and standard deviation of technical parallels ($n = 2$). (**E**) Fitting the raw calibration curves (scatter plots) with exponential function (continuous line). In case of the blank reaction (0 pmol dGTP) single exponential equation (Equation 1) could be fitted to the raw reaction curve, while in the presence of the specific dNTP (here dGTP), the reaction could be well described with a double exponential (Equation 2). The parameters yielded from the exponential fits were as follows: 0 pmol dGTP: A = −28 869, $k_{obs} = 2.0 \times 10^{-4}$ s^{-1}, $y_0 = 35\,978$; 3 pmol dGTP: $A_1 = -6393$, $k_{1obs} = 2.5 \times 10^{-3}$ s^{-1}, $A_2 = -23\,485$, $k_{2obs} = 1.1 \times 10^{-4}$ s^{-1}, $y_0 = 35540$; 10 pmol dGTP: $A_1 = -8480$, $k_{1obs} = 2.9 \times 10^{-3}$ s^{-1}, $A_2 = -20\,879$, $k_{2obs} = 5.0 \times 10^{-5}$ s^{-1}, $y_0 = 34\,454$.

Downloaded from https://academic.oup.com/nar/article/48/8/e45/5760754 by guest on 04 November 2021

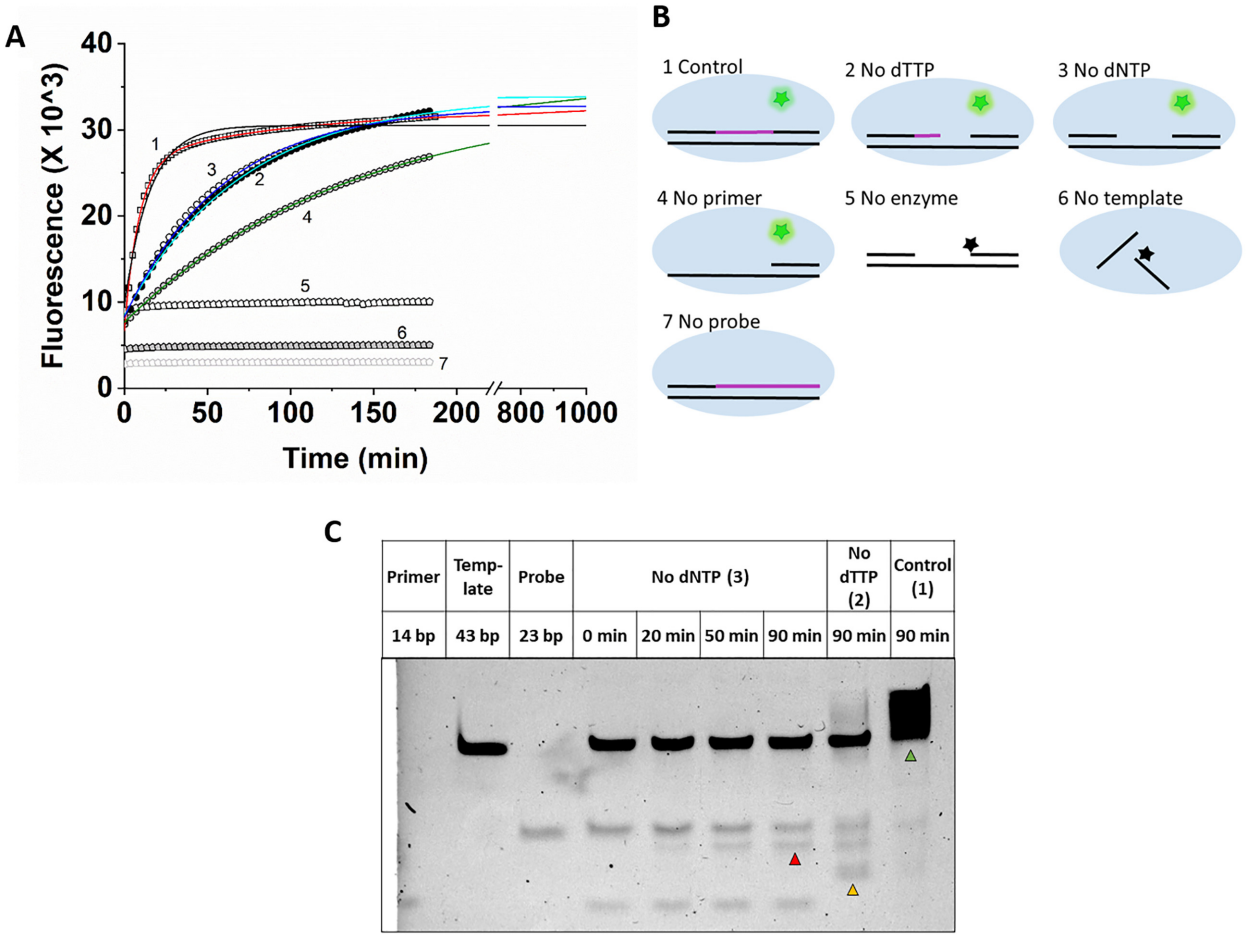

Figure 2. Assay background originates from dNTP incorporation independent 5′-3′ exonuclease activity of AmpliTaq Gold™ polymerase. (**A**) An analysis of the dTTP assay was chosen using the dT1 template. The data presented in Panel A represent the reaction curves obtained under the conditions schematically shown in panel B. Continuous lines represent the exponential fits to the data. Parameters are as follows: 10 pmol dTTP (1), red: $A_1 = -19\,786$, $k_{1obs} = 1.91 \times 10^{-3}$ s^{-1}, $A_2 = -5787$, $k_{2obs} = 1.79 \times 10^{-4}$ s^{-1} $y_0 = 32\,213$; 0 pmol dTTP (2), cyan: $A_1 = -25\,382$, $k_{obs} = 2.37 \times 10^{-4}$ s^{-1}, $y_0 = 33\,832$; No aspecific dNTP added (3), blue: $A_1 = -24\,458$, $k_{obs} = 2.79 \times 10^{-4}$ s^{-1}, $y_0 = 32\,718$; No primer added (4), green: $A = -26\,023$, $k_{obs} = 1.22 \times 10^{-4}$ s^{-1}, $y_0 = 33\,659$. A single exponential function fitted to the '10 pmol dTTP' (1) data is shown as continuous black line. (**B**) Panel B schematically explains the constitution of the different assays. The incorporated dNTP-s are colored magenta. (**C**) Denaturing urea-PAGE gel demonstrating the dNTP incorporation independent 5′-3′ exonuclease activity of Taq polymerase. Numbers in parenthesis correspond to those in panels A and B. Red arrow: hydrolyzed probe; yellow arrow: elongated primer; green arrow: duplicated template.

the y offset. Note, that the polymerase based dNTP quantitation method is not a PCR reaction, only primer elongation occurs without template amplification. Therefore, equations used in qPCR analysis are not applicable here. Also, note that as the fitted equations are decay functions, and we have an increasing signal, the resulting amplitude parameters are negative values. For a more straightforward interpretation, in further analyses we used the additive inverse of the fitted amplitude parameters, and simply referred to them as A, A_1 and A_2.

The resulting values ($A_{1–2}$ and $k_{1–2obs}$) were plotted against the corresponding dNTP concentrations to extract mechanistic information. Amplitude data were then fitted with the quadratic binding equation (Equation 3) describing 1:1 stoichiometry assuming no cooperativity:

$$F = F_0 + A_{quad}\frac{(E_T + L_T + K_d) \pm \sqrt{(E_T + L_T + K_d)^2 - 4 \times E_T \times L_T}}{2 \times E_T} \quad (3)$$

where F is the fluorescence or relative fluorescence of the sample, F_0 is the intercept, A_{quad} is the total change in the amplitudes in the investigated specific dNTP concentration range, E_T is considered as the concentration of the polymerase:template:primer:probe complex, K_d is the apparent equilibrium constant of the specific dNTP dependent fluorophore release, L_T is the independent variable and it stands for the total added specific dNTP concentration.

dNTP quantification based on kinetic analysis

Calibration curves for each specific dNTP were set up in the assay range and assay concentrations optimized for that specific dNTP. Raw fluorescence data was plotted against time and then fitted with Equation (2). As the blank reaction is better fitted by Equations (1) than (2) according to the Akaike information criterion (AIC), it was omitted from the further analysis. AIC is a statistical tool that, by estimating the amount of information lost by a model, allows us to

Downloaded from https://academic.oup.com/nar/article/48/8/e45/5760754 by guest on 04 November 2021

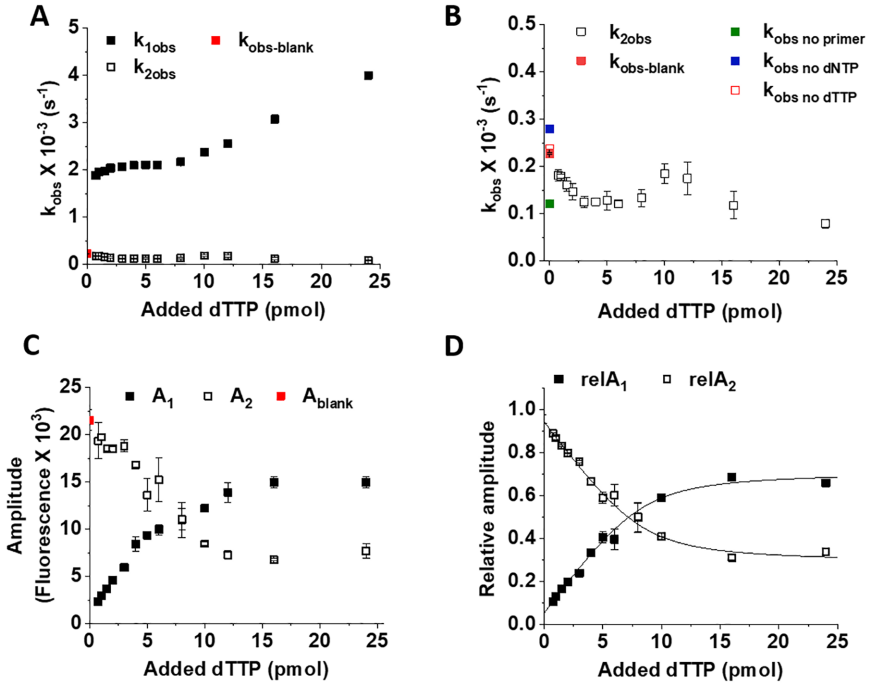

Figure 3. Background exonuclease activity of AmpliTaq Gold™ polymerase competes with specific dNTP incorporation in a concentration dependent manner. Concentration is understood to be pmol dTTP in constant reaction volume. (**A**) Concentration dependence of the observed rate constants of the two kinetic phases in the assay (k_{1obs} and k_{2obs}, respectively). (**B**) Concentration dependence of the observed rate constant of the slower phase (k_{2obs}). The observed rate constants of the background reaction presented in Figure 2A are also shown as $k_{obs\ no\ primer}$, $k_{obs\ no\ dNTP}$, $k_{obs\ no\ dTTP}$ (blank). (**C**) Concentration dependence of the amplitudes of the two phases (A1 and A2, respectively). (**D**) Concentration dependence of the relative amplitudes of the two phases ($relA_1$ and $relA_2$, respectively). The amplitudes were normalized compared to the total amplitude of the reaction (A1 + A2). The relative amplitudes could be fitted with quadratic binding equation (Equation 3) yielding the following parameters: $A_{quad} = 0.660 \pm 0.036$, $S = 0.054 \pm 0.002$, $c = 8.345 \pm 0.453$, $K_{app} = 0.741 \pm 0.290$ for $relA_1$, and $A_{quad} = -0.660 \pm 0.036$, $S = 0.946 \pm 0.002$, $c = 8.345 \pm 0.453$, $K_{app} = 0.741 \pm 0.290$ for $relA_2$. Data represent the average and SD of two technical parallels for each panel.

estimate the risk of overfitting (the increasing number of parameters, the better the fit) and the risk of underfitting. The AIC formula for independent normally distributed random variables is described in Equation (4) (33,34),

$$AIC = \begin{cases} 2k + N * \ln(RSS), & \text{when } \frac{N}{k} \geq 40 \\ 2k + N * \ln(RSS) + \frac{2k(k+1)}{N-k-1}, & \text{when } \frac{N}{k} < 40 \end{cases} \quad (4)$$

where AIC is the indicator upon the AIC calculation, k is the number of parameters of the fit (for single exponential fitting: $k = 3$, for double exponential fitting: $k = 5$), N is the number of data points within the curves, RSS is the residual sum of squares. Those low concentration points that could not be properly fitted with the double exponential function due to a small amplitude of the specific phase were also omitted and considered as data points under the detection limit. To obtain a calibration curve, the A_1 values from the double exponential fits were plotted against the specific dNTP concentration. The appropriate range was fitted with linear function and then the parameters of the fitted linear function were used to quantify dNTP in biological samples. Results were normalized to 10^8 CFU in case of bacterial or to 10^6 cells in case of human samples.

Construction of the nucleoTIDY software

We created a Python-based software termed 'nucleoTIDY', by using the Matplotlib, NumPy, SciPy, xlrd and xlsxwriter free packages without any modification. nucleoTIDY fits single and double exponential equations modified to result in positive amplitude values (Equations 5 and 6, respectively) using non-linear least squares minimization method built in the SciPy package.

$$F = -A*e^{-k_{obs}x} + F_0 \quad (5)$$

$$F = -A_1*e^{-k1_{obs}x} - A_2*e^{-k2_{obs}x} + F_0 \quad (6)$$

where the parameters are the same as in Equations (1) and (2). Further details are described in the Results section.

Analysis of assay performance

Intra- and interassay coefficient of variation (CV), recovery and accuracy parameters were calculated as in Wilson *et al.* (24). Limit of detection (LOD) was calculated using two different methods. Either the lowest dNTP amount at which the progress curve could be fitted was considered as the detection limit. Or LOD = calibration line offset + 3*SD $A1_{low\ calibration\ points}$, where the offset of the calibration line and the standard deviation of the A1 values for parallel measurements were considered at low dNTP concentration. These two methods usually gave similar values. Limit of quantitation was calculated similarly, except that 5*SD was taken into consideration instead of 3*SD.

Downloaded from https://academic.oup.com/nar/article/48/8/e45/5760754 by guest on 04 November 2021

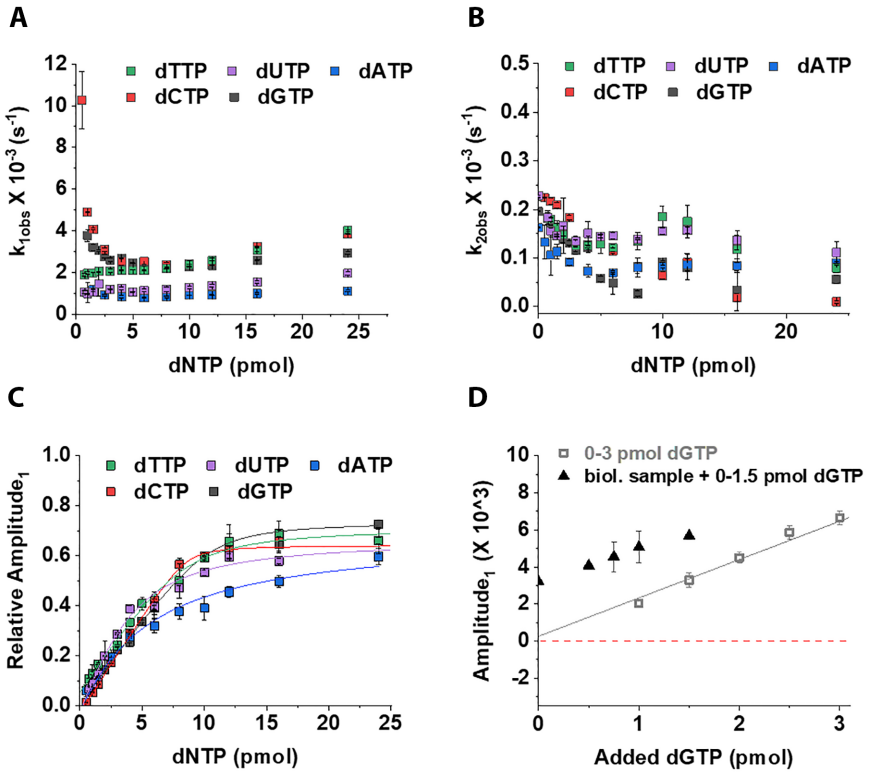

Figure 4. Separation of the reaction phases for dNTP quantitation. (**A**) For each dNTP-s, the dependence on the amount of added specific dNTP is shown for (A) the observed rate constants of the fast, dNTP incorporation associated phase (k_{1obs}); (**B**) the slow, aspecific phase (k_{2obs}); (**C**) the relative amplitudes of the fluorescence change of the fast, dNTP incorporation associated phase. Relative amplitudes could be fitted with the quadratic binding equation (Equation 3) yielding the following parameters: $A_{quad} = 0.70 \pm 0.10$, $S = 0.03 \pm 0.03$, $c = 3.60 \pm 2.10$, $K_{app} = 1.67 \pm 1.48$ for dUTP; $A_{quad} = 0.59 \pm 0.11$, $S = -0.01 \pm 0.03$, $c = 3.94 \pm 3.09$, $K_{app} = 2.29 \pm 2.12$ for dATP, $A_{quad} = 0.77 \pm 0.10$, $S = -0.03 \pm 0.00$, $c = 8.57 \pm 0.31$, $K_{app} = 0.10 \pm 0.13$ for dCTP and $A_{quad} = 0.73 \pm 0.06$, $S = 0.01 \pm 0.00$, $c = 10.41 \pm 0.72$, $K_{app} = 0.39 \pm 0.26$ for dGTP. For dTTP the same curve is presented in panels A–C as in Figure 3. (**D**) Comparison of calibration curves in the presence and absence of biological sample using the A1 parameter. The data points were derived from the measurement presented in Figure 1. The continuous line is a linear fit to the data ($R^2 = 0.98$). Note that using the A_1 parameter, dGTP could be quantified in the biological sample in contrast to the analysis method presented in Figure 1D. Also, the added extra dGTP could be recovered. We calculated the recovery for the presented standard addition points to be 85 ± 4% (mean + SD, note that this measurement was still conducted under the original, suboptimal conditions). Also note that the first three data points of the calibration curve are not presented here, since the contribution of the fast, specific phase to the total amplitude was too small for reliable fitting. Data represent the average and SD of two technical parallels for each panel.

Assay validation using the tritium based polymerase assay

dNTP quantification using the tritium based polymerase assay was done as described previously (21,22,26) with a few modifications. Briefly, the reaction mixture (50 μl) contained 0.5 unit of exonuclease negative Klenow-fragment (Thermo Fischer Scientific) or 1 unit of recombinant Taq polymerase (Thermo Fischer Scientific), Klenow buffer or Taq buffer, 0.25 μM dNTP specific template, 0.25 μM primer, 2.5 μM [3H] dATP/ or [3H] dTTP (3 Ci/mmol) (American Radiolabeled Chemicals, Inc.) and 8 μl dNTP-extract or premixed dNTP for calibration. The calibration curve was prepared using 0, 0.25, 0.5, 1, 2, 4, 8 and 16 pmol dNTP/reaction. Incubation was carried out for 60 min at 37°C, or in case of Taq polymerase at 48°C. Next, the 50 μl reaction mix was spotted onto Whatman Grade 3MM Chr (Sigma) chromatographic disks (d = 24 mm). Disks were dried, washed with 5% Na_2HPO_4 for 3 × 10 min, rinsed once with distilled water and once again with 95% ethanol and then dried. Alternatively, 40 μl samples were spotted onto a prewetted positively charged nylon membrane (Zeta-Probe® Membrane, Bio-Rad) using a vacuum-driven microfiltration apparatus (Bio-Dot, Bio-Rad). After 10 min of air-drying, immobilization of DNA was performed by applying 30 h of incubation at 80°C. The membrane was then washed similarly as described for the paper disks, dried, and cut into equal pieces.

The radioactivity retained by the disks/membrane pieces was measured in a liquid scintillation counter (Beckman). For dCTP and dGTP measurements, recombinant Taq polymerase (Thermo Fisher Scientific) was used, as the Klenow polymerase readily incorporates CTP and GTP from nucleotide extracts thus resulting in the overestimation of dCTP and dGTP concentrations (22).

dUTPase treatment

For the determination of dUTP concentration, half of the sample was treated with dUTPase, then the difference between the dUTPase treated and nontreated parallel samples was considered. For dTTP measurement by the fluorescence method, dUTPase treatment was performed as part of the assay, as suggested by Wilson *et al.* (24) using 10–20 ng re-

Downloaded from https://academic.oup.com/nar/article/48/8/e45/5760754 by guest on 04 November 2021

Table 1. Analysis of assay performance using dT1 templates and AmpliTaq Gold™ polymerase or VWR® TEMPase Hot Start DNA Polymerase

	Assay conditions	qPCR	Data acquisition	T (°C)	Calibration range (pmol)	R^2	LOD[a] (pmol)	LOQ[a] (pmol)	Accuracy low, high (%)	Interassay CV (%)	Intraassay CV (%)	Recovery (%)	Recovery CFU or cell[b] /	Recovery Sample type
dTTP	20 pmol TPP, 0.875 u AmpliTaq Gold™, 5 mM $MgCl_2$	BioRad CFX96	14 s for 600 cycles	60	0.63–12	0.986 ± 0.006	0.41 ± 0.07	0.68 ± 0.12	100 ± 14 100 ± 6	9.6 ± 7.0	7.8 ± 5.3	105	1×10^7	*M. smegmatis*
												100	1×10^8	*S. aureus*
												98	2×10^5	MES-SA
	10 pmol TPP 0.9 unit VWR® TEMPase, 2 mM $MgCl_2$	QuantStudio 1	13 s for 260 cycles	55	0.1–6	0.999	0.05	0.10	102 ± 7 109 ± 4	5.5 ± 6.5	5.3 ± 3.7	101	1×10^5	MES-SA
dCTP	10 pmol TPP, 0.438 u AmpliTaq Gold™, 2.5 mM $MgCl_2$	BioRad CFX96	13 s for 60 s then 80 s for 128 cycles	60	1–8	0.991 ± 0.001	0.70 ± 0.13	1.10 ± 0.03	98 ± 4 100 ± 5	7.4 ± 4.3	6.9 ± 4.6	98	5×10^6	*M. smegmatis*
												76	1×10^7	*M. smegmatis*
												92	1×10^8	*S. aureus*
												94	1×10^6	MES-SA
	10 pmol TPP, 0.9 u VWR® TEMPase, 2 mM $MgCl_2$	QuantStudio 1	13 s for 260 cycles	55	0.6–10	0.992	0.30	0.50	101 ± 3 100 ± 9	6.5 ± 4.4	5.2 ± 2.9	92	6×10^7	*M. smegmatis*
dGTP	10 pmol TPP, 0.438 u AmpliTaq Gold™, 2.5 mM $MgCl_2$	BioRad CFX96	13 s for 60, then 80 s for 128 cycles	60	0.5–10	0.992 ± 0.001	0.50 ± 0.07	0.83 ± 0.11	99 ± 21 99 ± 4	12.6 ± 10.2	9.4 ± 5.7	102	1×10^7	*M. smegmatis*
												109	5×10^5	MES-SA
	10 pmol TPP, 0.438 u AmpliTaq Gold™, 5 mM $MgCl_2$	QuantStudio 1	13 s for 100, then 80 s, for 200cycles	57	0.25–8	0.997	0.18	0.33	99 ± 15 98 ± 6	ND	ND	115	5×10^7	*E. coli*
												91	4×10^7	*S. aureus*
	10 pmol TPP, 0.9 u VWR® TEMPase, 3.5 mM $MgCl_2$	QuantStudio 1	13 s for 260 cycles	55	0.4–10	0.999	0.11	0.19	99 ± 2 101 ± 5	5.6 ± 4.9	4.5 ± 2.5	101	6×10^6	*M. smegmatis*
dATP	20 pmol TPP, 0.875 u AmpliTaq Gold™, 5 mM $MgCl_2$	BioRad CFX96	17 s for 700 cycles	60	1–8	0.991 ± 0.004	0.59 ± 0.26	1.06 ± 0.26	95 ± 7 100 ± 0.1	12.0 ± 0.1	7.9 ± 1.6	92	1×10^6	MES-SA
												73	1×10^8	*S. aureus*
												102	1×10^7	*M. smegmatis*
	15 pmol TPP, 0.9 u VWR® TEMPase, 5 mM $MgCl_2$	BioRad CFX96	13 s for 260 cycles	60	1.5–15	0.977	1.68	2.81	104 ± 3 99 ± 1	10.1 ± 2.4	3.3 ± 1.8	97	1×10^8	*M. smegmatis*

[a]LOD and LOQ were calculated by the two methods presented in the methods sections. If the mathematical calculation of LOD and LOQ gave lower value than the lowest resolvable calibration point, then the lowest calibration point should be considered as the LOD.
[b]dNTP extract from the given number of CFU (for bacteria) or cells (for eukaryotic cells) / well.
TPP: template, probe, primer (NDP1), u: unit.

Downloaded from https://academic.oup.com/nar/article/48/8/e45/5760754 by guest on 04 November 2021

Table 2. Sequences of oligonucleotides used in the assays

Name	Sequence (5′→3′)
NDP-1 primer	CCGCCTCCACCGCC
FAM-dTTP probe	**6-FAM/**AGGACCGAG**/ZEN/**GCAAGAGCGAGCGA**/IBFQ**
FAM-dATP probe	**6-FAM/**TGGTCCGTG**/ZEN/**GCTTGTGCGTGCGT**/IBFQ**
FAM-dGTP probe	**6-FAM/**ACCATTCAC**/ZEN/**CTCACACTCACTCC**/IBFQ**
FAM-dCTP probe	**6-FAM/**AGGATTGAG**/ZEN/**GTAAGAGTGAGTGG**/IBFQ**
dTTP-DT1 template	TCGCTCGCTCTTGCCTCGGTCCTTT**A**TTTGGCGGTGGAGGCGG
dTTP-DT2 template	TCGCTCGCTCTTGCCTCGGTCCTTT**A**TTT**A**TTTGGCGGTGGAGGCGG
dATP-DT1 template	ACGCACGCACAAGCCACGGACCAAA**T**AAAGGCGGTGGAGGCGG
dCTP-DT1 template	CCACTCACTCTTACCTCAATCCTTT**G**TTTGGCGGTGGAGGCGG
dCTP-DT2 template	CCACTCACTCTTACCTCAATCCTTT**G**TTT**G**TTTGGCGGTGGAGGCGG
dGTP-DT1 template	GGAGTGAGTGTGAGGTGAATGGTTT**C**TTTGGCGGTGGAGGCGG
dGTP-DT2 template	GGAGTGAGTGTGAGGTGAATGGTTT**C**TTT**C**TTTGGCGGTGGAGGCGG

combinant human (hDUT), or *Mycobacterium tuberculosis* dUTPase (mtDUT) per reaction. For the tritium method, half of the sample was treated with 10–20 ng recombinant mtDUT at 37°C for 1 h. dUTPase was inactivated by incubation at 95°C for 5 min. Recombinant hDUT and mtDUT were expressed and purified as described earlier in refs (35) and (36), respectively.

Quantitation of dNTP from previously published bar graph

Data from Machon *et al.* (37) were quantified using the Web plot digitizer program (https://automeris.io/WebPlotDigitizer). dNTP values were calculated to 10^6 cells based on the assay description in the article (200 000 cells/10 μl, 10 μl injected).

RESULTS

The polymerase based fluorescence dNTP quantitation assay by Wilson *et al.* fails in certain biological samples

We could well reproduce the assay developed by Wilson *et al.* (24) in water and with all components controlled. The performance including limit of detection, limit of quantification and accuracy we obtained was similar to the one reported in (24). However, when trying to determine dNTP levels in human (Figure 1) or bacterial (Supplementary Figure S1) cell lysates, the analysis failed as we obtained negative values. As this is far more the most attainable method to measure dNTP concentrations in a standard molecular biology laboratory, we set out to explore the background of this phenomenon and modify the assay so that it can be used in any biological samples.

The assay developed by Wilson *et al.* (24) is based on the TaqMan PCR principles. It utilizes a synthetic oligonucleotide template, a single primer and a dual-quenched fluorophore-labeled probe (Figure 1A). The fluorescent signal is generated by the cleavage of the 6-FAM fluorophore off the probe by the 5′-3′ exonuclease activity of the Taq polymerase. The concentration of limiting dNTP is expected to be directly proportional to the fluorescent signal. The calculation method they used assumed that the fluorescence intensity at a given time point should be used to calculate the limiting dNTP concentration in the sample using a linear calibration curve measured in water. We observed, however, that the reaction curves containing biological samples consistently run below the calibration curves obtained in water. Even if the standard dNTP solutions used for calibration were added directly into the biological samples, the same problem arose (Figure 1B). Besides, the kinetics of the reaction curves containing biological samples seemed to be slower compared to the calibration curves measured in water. The latter was also noted by Wilson *et al.* (24) and therefore, they suggested that the fluorescence results should be read out upon the completion of the reaction, approximately at 15 min for dGTP, dCTP, dTTP and at 20 min for dATP. In our repeated experiments, the reaction was not completed within 20 minutes neither for dGTP (Figure 1B), nor for other nucleotides.

We also observed that the reaction curve representing the zero calibration point (i.e. sample not containing the limiting dNTP species, 'blank') appeared kinetically faster than the curves representing the lower concentration calibration range. As a result, the blank curve exhibited higher fluorescence value at 20 min than some of the calibration points (Figure 1B). Upon extraction of the blank reaction suggested by the authors of ref. (24), the reaction curves reached a maximum followed by a fluorescence decrease (Figure 1C). Reading out the fluorescence at 15 min, we obtained the calibration curves presented in Figure 1D.

In conclusion, the suggested calibration method and single point read out cannot be used to obtain quantitative results for dNTP concentrations in biological samples.

Kinetic analysis. Figure 1B and C suggested more than one kinetically separable ongoing processes in the reaction mixture. Indeed, longer records unequivocally reveal that a substantial slow process is present even if the limiting dNTP concentration to be measured is zero (Figure 1E). We observed this phenomenon for all dNTPs in most samples including human (Figure 1) and bacterial ones (Supplementary Figure S1). We applied two different hot-start Taq polymerases with similar results: AmpliTaq Gold™ (Thermo) used by Wilson *et al.* (24) (Figure 1), and VWR® TEMPase Hot Start DNA Polymerase (Supplementary Results and Supplementary Figure S1). The observed phenomenon did not depend on either the used template (dT1 template for 0–10 pmol dNTP and dT2 template for 0–20 pmol dNTP in Figure 1 and Supplementary Figure S1, respectively) or the used qPCR instrument (we used three different ones from Bio-Rad, Thermo Fisher Scientific and Agilent).

Downloaded from https://academic.oup.com/nar/article/48/8/e45/5760754 by guest on 04 November 2021

Background phenomenon originates from the polymerization independent 5′-3′ exonuclease activity of Taq polymerase

To reveal the origin of the substantial slow process in the DNA elongation curve, we eliminated the assay components one by one (Figure 2). Figure 2A shows the resulting reaction curves while Figure 2B schematically indicates the macromolecular complexes formed in each set of conditions. A large fluorescence signal change occurs in all samples that contain polymerase, template and probe together (Figure 2). This indicates that the observed signal change is the result of a polymerase catalyzed reaction on the template-probe complex (TP complex), practically a polymerization independent 5′-3′ exonuclease activity. The presence of the primer seems to accelerate this reaction (cf. curve 2 versus curve 4 in Figure 2A). We came to the same conclusion using the VWR® TEMPase Hot Start DNA Polymerase (Supplementary Figure S2). To confirm the polymerization independent 5′-3′ exonuclease activity of the Taq polymerase on the TP complex, we analysed the different reaction mixtures using denaturing 14% polyacrylamide-urea gel electrophoresis (Figure 2C). We set up reaction mixtures without dNTPs added (equal to condition 3 in Figure 2B) and run a time course (0, 20, 50 and 90 min). Primer (14 bp), template (43 bp) and probe (23 bp) were loaded separately to make the bands in the lanes containing all these three components identifiable. At $t = 0$ min, the primer, the template and the probe run at the height of their respective controls, while at later time points, a band appears below the size of the probe (red arrow) indicating the exonuclease activity of the Taq polymerase. We also applied a reaction condition where only the limiting nucleotide, dTTP was missing from the reaction mixture while all non-limiting dNTPs were added (condition 2 in Figure 2B). In this case, the elongated primer (yellow arrow) indicates the incorporation of the non-limiting dNTPs while the hydrolyzed probe also appears below the intact one. As a control, we performed a reaction with all assay components included (condition 1 in Figure 2B). In this case, the primer is fully elongated generating the complementary strand of the template DNA (green arrow). Note, that the running temperature of the urea gel (45°C) did not allow the complete denaturation of the template-length double stranded DNA ($T_m = 80–22.5 = 57.5$°C in the applied urea concentration (32)) resulting in a wide band. The polymerization independent 5′-3′ exonuclease activity of Taq polymerase was previously reported on substrates consisting of a template and a 5′ hybridized oligonucleotide (38). It was also reported that the presence of a second oligonucleotide annealed upstream to the first oligonucleotide enhances this exonuclease activity 3-fold, even if dNTP-s are not present (38), probably by promoting a more productive conformation of the polymerase-substrate complex. Our fluorescence observations in Figure 2A agree with the previously reported properties of the polymerization independent 5′-3′ exonuclease activity of Taq polymerase. Also supported by the observation of the time dependent hydrolysis of the probe in the gel electrophoresis experiment we identify the polymerization independent 5′-3′ exonuclease activity of Taq polymerase as the source of the slow process in the full reaction curve.

Kinetic analysis of the assay curves enables the separation of the polymerization dependent and independent processes

The fluorescence time curves obtained in the assay describe the elongation of one primer per enzyme. This is ensured by the single thermal cycle setup and also by the slight excess of enzyme over the template, primer and probe added in equal quantities. The dNTP to be measured is substoichiometric compared to the enzyme-template-primer-probe complex (ETPP) in the 0–10 pmol range and superstoichiometric above. The treatment of the obtained progress curves with exponential equations serves as a tool to separate the polymerization—and dNTP—dependent process from the background so that a measure directly proportional to the concentration of the limiting dNTP species could be extracted. The blank reaction and all the other reactions arising from incomplete reaction mixtures shown in Figure 2 could be fitted with single exponential function (Equation 1). The curves obtained at various concentrations of the limiting dNTP could be well described with double exponential fits (Equation 2). We performed the AIC analysis, which indicated that using the double exponential model is justified over the single exponential one for reaction curves arising from the incorporation of any of the dNTP species. The observed rate constant (k_{obs}) of the blank reaction approximated the k_{obs} of the second, slower phase of the specific dNTP containing reaction. Fittings revealed that the reactions go into real completion only around 1000 min by using the AmpliTaq Gold™ polymerase (Figure 1E) and around 400 min by using the VWR® TEMPase Hot Start DNA Polymerase.

We investigated the kinetic parameters of the reaction curves in a broad dNTP concentration range (0–25 pmol specific dNTP/reaction which equals to 0–1 μM specific dNTP) for dTTP using the dT1 template (Figure 3). As shown in Figure 3A, the concentration dependence of the obtained k_{obs} values indicates two kinetically well separated processes. The k_{obs} of the fast phase (k_{1obs}) exhibits strong dTTP concentration dependence (Figure 3A) indicating a dNTP incorporation dependent fluorescence signal change. The concentration dependence of k_{1obs} differs in the substoichiometric and superstoichiometric dNTP ranges (stoichiometric ratio is reached at 10 pmol/0.4 μM dTTP)) (Figure 3A). Below 10 pmol/0.4 μM dTTP, the observed rate constants exhibit a hyperbolic concentration dependence followed by a linear concentration dependence at superstoichiometric dTTP concentrations. The k_{obs} values of the slow phase (k_{2obs}) are in the same order of magnitude as the single k_{obs} of the blank reaction (Figure 3A). A closer look at the concentration dependence of k_{2obs} (Figure 3B) reveals that the k_{2obs} varies between the polymerization independent hydrolysis values exhibited in the presence and in the absence of primer (cf. complexes 3 and 4 in Figure 2B).

The concentration dependence of the raw amplitudes, and the relativized amplitudes of the two phases are shown in Figure 3C and D, respectively. As expected, the amplitude of the polymerization dependent fast phase increases, while the amplitude of the slow phase decreases with increasing dNTP concentration (Figure 3C and D). The polymerization dependent relA1 goes into saturation at 7 pmol

Downloaded from https://academic.oup.com/nar/article/48/8/e45/5760754 by guest on 04 November 2021

dTTP (see quadratic fit analysis in the figure legend of Figure 3D) and reaches a maximum of 0.7 (Figure 3D). 10 pmol template-probe-primer complex is present in the assay and thus, the theoretical maximum of limiting dNTP to be incorporated using the dT1 template is 10 pmol. The saturation of the specific incorporation reaction at 7 pmol dTTP indicates that 30% of this complex is not available for specific dNTP incorporation. This portion of the fluorescence signal is generated in the competing polymerization independent reaction.

Another example of the kinetic characterization of this assay is shown in Supplementary Figure S3 using dCTP as the dNTP to be quantified, a longer template (dT2) and the faster VWR® TEMPase Hot Start DNA Polymerase. Similar conclusions can be drawn from this set of experiments. The relative amplitudes indicate that 20% of the signal is generated in the polymerization independent process (Supplementary Figure S3).

The analysis of the fast phase amplitudes yields reliable readout

By investigating the kinetics of the assay curves for all dNTPs, we obtained different behavior for dCTP and dGTP incorporation into dT1 templates than for dTTP, dUTP and dATP incorporation using the AmpliTaq Gold™ polymerase (Figure 4A). The k_{1obs} hyperbolically decreases with increasing dCTP or dGTP concentration up to reaching stoichiometry with the template. On the other hand, the k_{1obs} hyperbolically increases with the increasing dNTP concentration for the three other dNTPs (Figures 4A and 3A). In superstoichiometric dNTP concentrations, the k_{1obs} of all dNTPs shows linear increase with increasing dNTP concentrations (Figures 4A and 3A). This phenomenon likely indicates conformational selection mechanism (39) for dNTP binding to the enzyme-template-primer-probe complex (ETPP) (Scheme 1). In this case, there exist an equilibrium between two conformers of the ETPP complex only one being competent for dNTP binding. The substoichiometric concentration dependence of k_{1obs} will then depend on the ratio of the constant k_1 and k_{off} for each dNTP (Scheme 1): it will either be a hyperbola with an increasing ($k_1 > k_{off}$) or a decreasing ($k_1 < k_{off}$) slope (for more detailed explanation of conformational selection check ref. (39)). This would explain the different behavior of k_{1obs} in the substoichiometric concentration range of dCTP/dGTP and dTTP/dUTP/dATP. The underlying mechanism of the phenomenon we observe can be explained by the discrete state model of DNA polymerase reaction created on the basis of kinetics data and crystal structures of polymerase–DNA and ternary complexes (40). Based on structural data, two different conformers of the polymerase–DNA complex (equivalent of ETPP here) are distinguished (40). According to the model, there exists an equilibrium between a stacked and an unstacked state of the template base in the polymerase–DNA complex (40). In the stacked conformer, the template base is organized so that it base pairs with the incoming nucleotide while in the unstacked conformer, the incoming nucleotide cannot base pair with the template (40). The incoming dNTP will therefore preferentially bind to the stacked state on the end of the primer strand as if it were already part of a double-stranded DNA. The base pairing and stacking of the incoming dNTP with the complementer nucleotide is a driving force in the polymerase reaction and serves fidelity. We suggest that the conformational selection phenomenon we observe in our kinetics data occurs at the level of this pre-existing equilibrium between the stacked and unstacked template base. The fact that the incorporation kinetics of the nucleotides falls into two categories according to the number of H-bonds present between base pairs (dCTP/dGTP versus dTTP/dUTP/dATP) supports this suggestion. A pre steady-state kinetics study that uses Förster resonance energy transfer (FRET) to investigate the conformational dynamics of Taq DNA polymerase during nucleotide binding and incorporation could also distinguish a rapid conformational equilibrium in the polymerase-DNA complex prior to dNTP binding (11–36 s^{-1}) (41). The authors presumed that only one of these conformations is competent for dNTP binding (41). Moreover, the study showed that this equilibrium remained unchanged using a non-extendable DNA template (41). These experimental findings are in line with our observations.

Figure 4B shows that the dNTP concentration dependence of k_{2obs} is not sensitive to the dNTP species.

Figure 3D indicates that the specific, dNTP incorporation dependent signal release competes with the aspecific, dNTP independent signal release. As the concentration of the specific dNTP increases in the reaction mixture, the amplitude contribution of the specific reaction increases, while that of the aspecific reaction decreases. Figure 4C and D shows that the relative amplitudes and amplitudes of the fast reaction, respectively, exhibit strong and consistent dNTP concentration dependence for all five dNTPs measured. The linear phase of the amplitude curve (Figure 4D) can be used as a reliable readout for dNTP quantification. By using the VWR® TEMPase Hot Start DNA Polymerase, the same conclusions can be drawn for k_{1obs}, k_{2obs} and the A_1 amplitude appropriate for dNTP quantification (Supplementary Figure S4). Due to the differences in the kinetic mechanism of incorporating various dNTP species by DNA polymerase, the assay conditions should be modified to arrive to the largest possible dynamic range in amplitude based dNTP quantitation.

Novel analysis method and altered assay conditions eliminate disturbing effects

The dNTP concentration dependent competition of the dNTP dependent and independent reactions, and the resulting observed rate and amplitude changes explain the disturbing effects in the original method presented in Figure 1. As the amplitude of the dNTP independent reaction is largest in the blank reaction (cf. Figures 1E or 3C) and at low dNTP concentration, the subtraction of the blank reaction at the apparent saturation point (fluorescence read out at 15 min) results in a negative value (cf. the 0.5 pmol, and the 0.75 pmol calibration point in Figure 1D). The sample matrix may cause similar effect by inhibiting the dNTP-independent kinetics more than the dNTP dependent kinetics (latter also observed by Wilson *et al.* (24)). During our hundreds of trials, we observed that the incorporation rates of the various dNTPs are different and are also greatly affected by the biological matrix. The amplitudes of the poly-

Downloaded from https://academic.oup.com/nar/article/48/8/e45/5760754 by guest on 04 November 2021

$$ETPP\ Conformer1 \underset{k_{-1}}{\overset{k_1}{\rightleftharpoons}} ETPP\ Conformer2 \underset{k_{off}}{\overset{k_{on}}{\rightleftharpoons}} ETPP\ Conformer2.dNTP \rightarrow \rightarrow \rightarrow signal\ release$$

Scheme 1. Conformational selection mechanism for dNTP binding to the enzyme-template-primer-probe complex (ETPP).

merization dependent fast phase, however, are reliable and yield high quality calibration curves for dNTP quantitation. Figure 4D shows the result of the kinetic analysis of the same data set as the one shown in Figure 1.

However, as it is observable in Figure 4C and D, few concentration points define the linear range which can be used for the amplitude based analysis. To broaden the dynamic range for amplitude based dNTP quantitation, we varied the template, probe, and NDP1 primer concentration between 10–20 pmol / reaction, the $MgCl_2$ final concentration between 2.5 and 5 mM, and the AmpliTaq Gold™ polymerase concentration between 0.413 and 0.825 units/reaction.

For optimizing data acquisition, different cycle lengths and cycle numbers were applied in the qPCR instrument. 'Split time' data acquisition was also applied: the first half of the cycles was set up with a short cycle length for the optimal detection of the fast reaction phase, while the later cycles were longer for the optimized detection of the slow phase.

We observed that an increase in the primer-template-probe concentration in the reaction broadened the linear range of the calibration curves, while the detection limit of the assay did not change. By optimizing the cycle length, and by introducing split time data acquisition, the detection limit also improved as the quality of the fitting improved. This change in settings prevented overfitting of the slow phase.

In our experiments, we mostly used oligonucleotides ordered with standard desalting purification. We observed that the applicable calibration range varied from batch to batch. This is probably due to the fact that shorter oligonucleotide variants may also be present in the batches. To avoid this variation, we suggest the use of PAGE purified oligonucleotides, as it was also done by Wilson *et al.* (24) However, if cost reduction is a goal, the applicable calibration range should be determined for each batch. Also note that increasing the primer-template-probe concentration (cf. Table 1 dTTP data) will broaden the linear range of the measurement. This proved to be especially important for dATP measurements, where the aspecific reaction can more efficiently compete with the relatively slow dATP incorporation reaction.

In case of dCTP and dGTP, which are incorporated faster by both DNA polymerases than the other dNTPs, the decrease of polymerase concentration and of the assay temperature improved the detection limit as the reaction became slower (cf. Table 1, dGTP data). For dTTP, decreasing the assay temperature improved the detection limit too (cf. Table 1 dTTP data). In contrast, the original, relatively high concentration of polymerase needed to be retained in dTTP measurements. For dATP, decreasing either the polymerase concentration or the assay temperature was disadvantageous, as they decreased the already low rate of dATP incorporation.

We found that an increased $MgCl_2$ concentration counteracted part of the kinetic inhibition always observed in biological samples. Mg^{2+} chelation may result from high pyrophosphate and/or nucleotide concentration in cell lysates. The addition of extra $MgCl_2$ was absolutely necessary for dATP quantitation in samples with low dATP concentrations. In case of dATP, data acquisition had to be much longer even with the addition of extra $MgCl_2$ than for the other nucleotides (cf. Table 1).

In some samples, we also observed a lag phase (100–200 s long) which could be decreased by adding extra $MgCl_2$. Another solution to overcome this disturbing effect is to dilute the sample where it is possible.

In the radioisotope incorporation assay, a large overestimation of dNTP levels was observed in the background of high concentrations of rNTP (22). Under the optimized measurement conditions and using the kinetic data analysis, our method quantifies dNTP reliably even in a large excess of rNTP. dCTP, dTTP, dATP and dGTP recovery in the presence of 1000× excess of CTP, UTP, ATP and GTP was 105.7 ± 4.9%, 95.3 ± 0.7%, 101.3 ± 15.4% and 80.4 ± 0.1%, respectively. The recovery of dGTP in the presence of 500× excess of GTP was 100.3 ± 1.3%. We offer optimized conditions in Table 1 and Supplementary Table SI for AmpliTaq Gold™ and VWR® TEMPase Hot Start DNA polymerases, respectively. Statistical parameters of the improved assay can also be found in Table 1. The detection limits for individual dNTPs are similar to those reported by Wilson *et al.* In average, the recoveries are also similar. However, we observed that the recovery depends on the concentration and on the particular sample (cf. Table 1). Therefore, it is useful to include a standard addition control when measuring a yet untested type of sample.

dUTP concentration determination. Wilson *et al.* suggested to digest the dUTP content of the sample and calculate dUTP concentration as the difference between the non-treated (dTTP + dUTP) and the dUTPase treated (dTTP) measurements. They used human dUTPase which did not work for us in the biological sample. The dUTPase catalysed reaction is accelerated by Mg^{2+} and some dUTPases, including the human dUTPase, contain structural Mg^{2+} binding site(s), as well (42). To hydrolyze dUTP in biological samples, we suggest the use of a dUTPase that does not contain any structural Mg^{2+} binding site (e.g. *Mycobacterium tuberculosis* dUTPase (43)). Even though we could eliminate dUTP in the biological samples using dUTPase digestion, we still not gained reproducible dUTP concentrations. When we created various predetermined dUTP:dTTP ratios in the reaction mixtures, we failed to recover dUTP if the dTTP:dUTP ratio was >1.5. We suggest that the reason behind this phenomenon is the kinetic difference in dTTP and dUTP incorporation into DNA. Although not really emphasized in the literature, dUTP incorporation is significantly slower than dTTP incorporation under the same con-

Downloaded from https://academic.oup.com/nar/article/48/8/e45/5760754 by guest on 04 November 2021

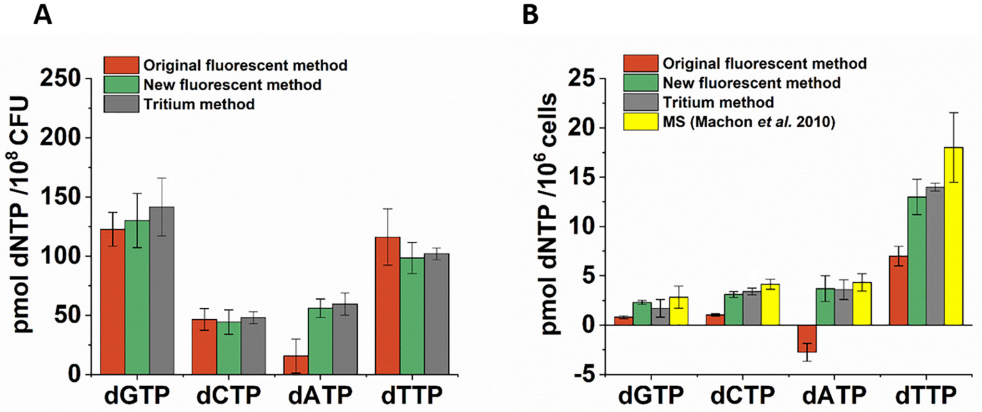

Figure 5. Comparison of the improved dNTP quantification method with the original, the radioactive isotope based and the MS based ones. (**A**) dNTP quantification in *Mycobacterium smegmatis* samples. Data represent mean and standard error of two biological parallels and 3 technical repeats each. The presented dNTP quantities were determined for the same sample using the three different methods. The same raw curves were quantified using the original and our new, improved fluorescent methods. (**B**) dNTP quantitation in human MES-SA samples. Data represent mean and standard error of 4 biological parallels and at least three technical repeats, for dCTP measured using the tritium method three technical repeats. For MS spectrometry, data were extracted from the results published in Machon *et al.* (37).

ditions (cf. Figure 4A). According to our experience, this makes the proper detection of dUTP unmanageable. For quantitative detection of dUTP, we suggest using the radioactive end point assays.

Validation of the assay

For comparison, we subjected the same biological samples to the following measurements: (i) the original Wilson *et al.*, (ii) the here improved fluorescence and iii) the well-established radioactive (21,22) one (Figure 5B). We used cell extracts from logarithmically growing *Mycobacterium smegmatis* culture. The improved fluorescence and the radioactive methods yielded indistinguishable dNTP concentrations for all four canonical dNTPs, while the original fluorescence assay detected dATP with much less certainty (Figure 5A). This bacterial sample contains particularly high concentrations of dNTPs and therefore, the disturbing effects in the original method are manifested only with the most problematic dNTP, dATP. However, when using human cell extracts which contain lower dNTP concentrations, the comparison yields large differences. We chose MES-SA cells as reliable literature data is available on the quantitation of dNTPs by MS for this cell line (37). Figure 5B shows the results of comparing our measurements analysed by i) the original Wilson *et al*. method; ii) the improved fluorescence method and iii) the tritium method with the MS data from (37). Importantly, at low dNTP concentrations, our method permits dNTP quantitation while the original Wilson *et al*. method does not. The result of our novel analysis corresponds well with the tritium and the MS data, considering that the MS experiments were done separately and that these are widely different approaches.

nucleoTIDY, a tool for streamlined kinetic analysis of fluorescent dNTP incorporation curves

The method presented herein is the most accessible and most high-throughput of all existing dNTP quantitation methods. Still a major drawback in using it might be the necessity of kinetic analysis in which most potential users are inexperienced. To overcome this complication, we implemented our evaluation algorithm into the software nucleoTIDY, a Python-based stand-alone executable program able to read and kinetically analyze the exported qPCR runs. nucleoTIDY is a user-friendly software which provides a graphical user interface (Figure 6) displaying the 96-well assay plate as well as the running instructions. The software is made in a way, however, that even the inexperienced user can judge the quality of the kinetic analysis through the process. Several checkpoints were built in to prevent the further use of unreliable results when applying the software to analyse low quality raw data. The cause of failure of the analysis most often is the overfitting of a single exponential curve with double exponential function which results in two inseparable kinetic phases. To avoid that error, the nucleoTIDY software fits all curves with both single (Equation 5) and double exponential functions (Equation 6). The software then compares the single and double exponential fitting parameters using the Akaike information criterion (AIC) (Equation 4) and selects the appropriate fitting method.

If a single exponential fit is more appropriate than a double exponential fit, i.e. AIC (single exponential fit) < AIC (double exponential fit), then those curves will be excluded from further analysis, and nucleoTIDY displays an 'x' in these wells. Following the fitting process, nucleoTIDY sorts out and compiles the fitted parameters. dNTP amounts are calculated based on the A_1 parameter as discussed earlier. The user defines the wells that contain the calibration points (represented as orange wells in Figure 6). Then by hitting the calculate button, the calibration points are calculated, plotted and fitted with a linear equation. The software displays the calibration chart so that the user can evaluate its quality. There is a possibility to refine the calibration curve via excluding outlier data points (grey wells in Figure 6). The calculated result, i.e. the amount of dNTP in each well, is displayed in the graphical representation of the 96-well plate.

Downloaded from https://academic.oup.com/nar/article/48/8/e45/5760754 by guest on 04 November 2021

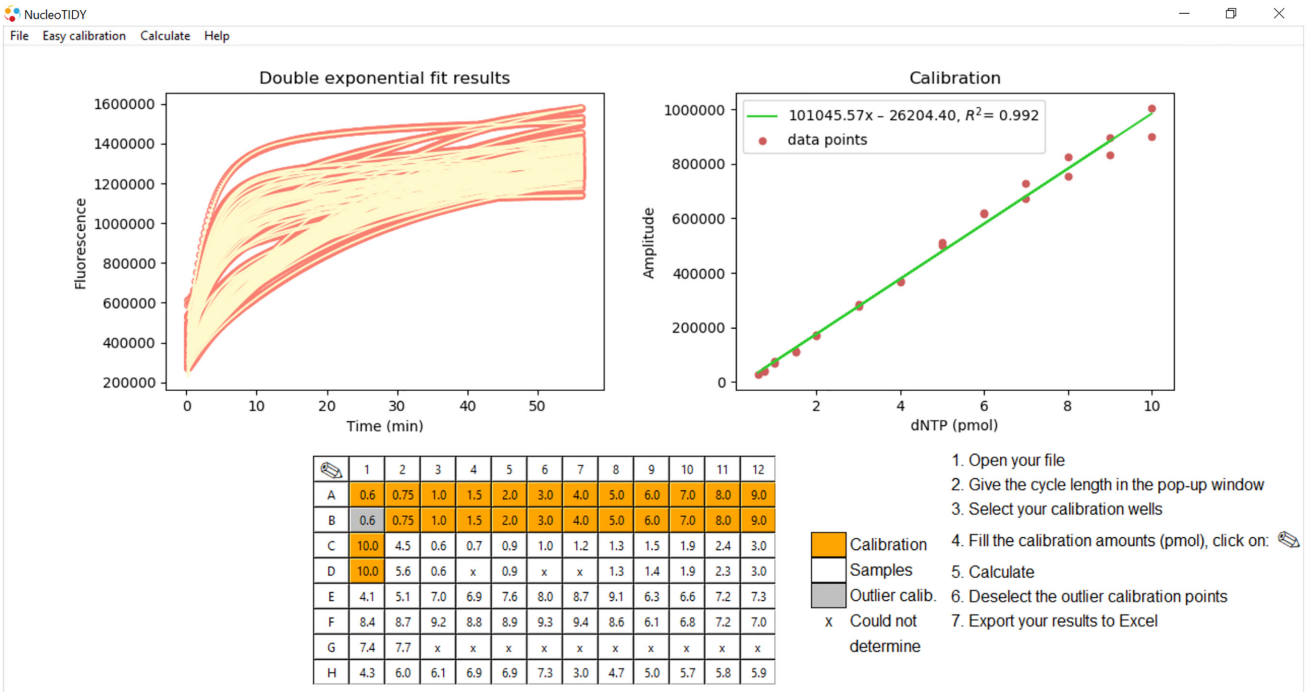

	1	2	3	4	5	6	7	8	9	10	11	12
A	0.6	0.75	1.0	1.5	2.0	3.0	4.0	5.0	6.0	7.0	8.0	9.0
B	0.6	0.75	1.0	1.5	2.0	3.0	4.0	5.0	6.0	7.0	8.0	9.0
C	10.0	4.5	0.6	0.7	0.9	1.0	1.2	1.3	1.5	1.9	2.4	3.0
D	10.0	5.6	0.6	x	0.9	x	x	1.3	1.4	1.9	2.3	3.0
E	4.1	5.1	7.0	6.9	7.6	8.0	8.7	9.1	6.3	6.6	7.2	7.3
F	8.4	8.7	9.2	8.8	8.9	9.3	9.4	8.6	6.1	6.8	7.2	7.0
G	7.4	7.7	x	x	x	x	x	x	x	x	x	x
H	4.3	6.0	6.1	6.9	6.9	7.3	3.0	4.7	5.0	5.7	5.8	5.9

Figure 6. The graphical interface of the nucleoTIDY software displays instructions for use and the results of the kinetic analysis as well. The software fits the raw measurement curves (left panel, salmon data points) with double exponential equations (left panel, yellow lines). Once the user defines the calibration wells and amounts, hitting the Calculate button in the menu bar results in linear regression of the calibration points (shown in the right panel) and the amount of dNTP in the default sample wells are calculated (shown in the 96-well panel). The user can refine the calibration by removing outlier data points (grey wells in the 96-well panel). In case the raw data are not appropriate for converting into results, an x is shown in the 96-well panel. The exported Excel file contains all the results and fitted parameters as well as information on calculation failure, if any. The output file also specifies if the result fell outside of the calibration range. This figure demonstrates a dCTP measurement using dT1 template and VWR® TEMPase Hot Start DNA Polymerase at 55°C.

The in-built analysis checkpoints include the recognition of (i) inseparable kinetic phases discussed above; (ii) a high error (error > value) in the key parameter A_1; (iii) k_{1obs} being within the error range of the average of k_{2obs} values of the entire plate; (iv) k_{2obs} being lower, than 10^{-5} s^{-1}; (v) A_1 being negative (inverse run of the exponential) and (vi) a small signal change, i.e. the total fluorescence signal change of the curve is 50% smaller than the total fluorescent signal change of the lowest calibration point. If the analysis fails at these checkpoints, nucleoTIDY displays an 'x' in the respective wells to prevent further use of low quality data. If the raw curves contain a lag phase, data points of the lag phase are eliminated to improve the quality of fitting. The output of the process can be chosen by the user: results can be exported into Excel or saved in the software for later use. The xlsx report of the analysis contains the explanation of failure for each well and thus makes the kinetic analysis transparent. The software processes one 96-well plate in some seconds saving the user significant time and effort in data analysis. nucleoTIDY is freely available at http://nucleotidy.enzim.ttk.mta.hu/. A tutorial video presents its simple use at the same site.

DISCUSSION

We developed an improved fluorescent dNTP quantification method which performs well in biological samples even at low dNTP concentrations. Although this method requires the rigorous kinetic analysis of the fluorescence time courses recorded by the qPCR instrument, the nucleoTIDY data analysis software we developed (http://nucleotidy.enzim.ttk.mta.hu/) makes the method user friendly and readily applicable in any molecular biology laboratory.

We identified and addressed three major drawbacks in the basically ingenious method published earlier by Wilson *et al.* (24) that hindered the production of reliable results. First of all, due to the slow, nonspecific cleavage of the fluorescent probe by the Taq polymerase, no endpoint of the dNTP incorporation reaction can be reliably detected. Secondly, the rate of incorporation of various nucleotides widely varies, dATP being the slowest and dCTP/dGTP being the fastest of dNTPs. Finally, other components in the biological sample slow down the reaction in an unpredictable and unreproducible way. We efficiently resolved these issues by taking the whole progress curve into consideration and by the optimization of the assay conditions for each dNTP. The kinetic treatment of the qPCR curves allowed us to distinguish the dNTP incorporation process from background reactions. This way, the amplitude of the separated dNTP incorporation process does correlate with the amount of available dNTP in the reaction mixture. The altered kinetic properties of dNTP incorporation in biological samples may originate from the competition of dNTPs with rNTPs, (d)NDPs and (d)NMPs for bind-

Downloaded from https://academic.oup.com/nar/article/48/8/e45/5760754 by guest on 04 November 2021

ing to the polymerase. Although this competition decreases the progress rate, the reaction amplitude is not affected. Another reason for a slower observed dNTP incorporation kinetics can be Mg^{2+} depletion by chelating molecules in the biological sample. Adding extra $MgCl_2$ helped the otherwise extremely slow dATP measurement and increased sensitivity.

We applied two different hot start Taq polymerases throughout the study (AmpliTaq Gold™ and VWR® TEMPase Hot Start DNA Polymerase). Both exhibited background exonuclease activity and were affected by the matrix effect of the biological sample. However, there was a relatively large difference in the incorporation and in the background exonuclease reaction kinetic rates between the two polymerases. AmpliTaq Gold™ proved to be slower than VWR® TEMPase Hot Start DNA Polymerase (both the specific and the background reactions). The faster VWR® TEMPase Hot Start DNA Polymerase is time saving, more cost effective and provides the same sensitivity as AmpliTaq Gold™. Other DNA polymerases can also be used, however, the measurement conditions will probably require optimization.

The reliability of the quantitative detection of dUTP in this assay highly depended on the dUTP:dTTP ratio due to the different incorporation kinetics of these nucleotides. Several pieces of evidence in the literature reinforce that DNA polymerases distinguish dTTP and dUTP (44,45). Commercial PCR protocols also suggest using double concentration of dUTP when replacing dTTP in the dNTP mixture (e.g. the protocol for AmpliTaq Gold™ polymerase). The comparison of the non-treated (comprising dTTP + dUTP) and the dUTPase treated (comprising only dTTP) data points may be suitable for the indication of large amounts of dUTP in a sample. Nevertheless, we suggest that neither the original fluorescence assay nor the present method is applicable for dUTP quantification. Instead, we suggest using the tritium based assay (which is a real endpoint assay) or an MS method for dUTP quantitation. We also strongly suggest that any samples should be treated with dUTPase before dTTP quantitation.

dNTP recoveries depended on sample concentration and cell type (cf. Table 1). Therefore, we strongly suggest to include standard addition as a control, especially when measuring a yet untested type of sample. Adding a known amount of dNTP at the time of extraction is also useful to detect and quantitate possible degradation of dNTPs. Another method to ascertain sample stability is to compare first results to those obtained using HPLC or, HPLC coupled MS methods (e.g. those presented in (17,20,37)). From HPLC, it will be possible to judge the extraction efficiency (since NTPs vary much less than dNTPs in different cells) and if NTPs are degraded to NDPs.

We calculated that we measured 100–500-fold difference in dNTP concentration between mycobacterial and human cells considering that the cell volume of a typical bacterium is 1 μm^3 and that of a typical human cell is 1000 μm^3. When measuring high concentrations of dNTP, the performance of the original method approaches that of the new one. Except that the quantitation of dATP levels remains less reliable. However, the determination of dNTP concentrations from mammalian cells unquestionably requires our assay developments.

This is the first report on the dNTP pool balance of a mycobacterial species. Interestingly, dGTP is the most abundant of dNTPs in *Mycobacterium smegmatis* while in other species it is the least abundant one e.g. in *Escherichia coli* (46) or in yeast (47). This difference may be due to the fact that the GC/TA ratio in the genome of *Mycobacterium smegmatis* is especially high (67%).

We developed the nucleoTIDY software to make the presented assay improvements attainable for users. The software can handle the output files of qPCR instruments from three major worldwide suppliers. We invite users of other types of qPCR instruments to contact us in order to include the capability of handling their output files in the software, as well.

DATA AVAILABILITY

The nucleoTIDY software is available for download at http://nucleotidy.enzim.ttk.mta.hu/.

SUPPLEMENTARY DATA

Supplementary Data are available at NAR Online.

ACKNOWLEDGEMENTS

We thank Olivér Surányi and Tamás Hubai for their guidance and helping instructions for creating the nucleoTIDY software. We thank Bálint Sámuel Szabó and Zsuzsanna Eke for their efforts to tailor a dNTP quantifying HPLC–MS method to the available equipment. We thank Rita Hirmondo, Dóra Füzesi and Gábor Kovács for providing their measurements to be included in the assay performance analysis. We are grateful to Bálint Szeder for his contribution to the tutorial video.

FUNDING

National Research, Development and Innovation Office, Hungary [OTKA K115993, FK124527, PD124330]; J.T. and J.E.S. are the recipient of the János Bolyai Research Scholarship of the Hungarian Academy of Sciences; J.E.S. is the recipient of ÚNKP-18-4-BME-391 and ÚNKP-19-4-BME-420 New National Excellence Program of the Ministry of Human Capacities. The funders had no role in study design, data collection and analysis, decision to publish or preparation of the manuscript. Funding for open access charge: National Research, Development and Innovation Office, Hungary.

Conflict of interest statement. None declared.

REFERENCES

1. Saxena,S., Somyajit,K. and Nagaraju,G. (2018) XRCC2 regulates replication fork progression during dNTP alterations. *Cell Rep.*, **25**, 3273–3282.
2. Somyajit,K., Gupta,R., Sedlackova,H., Neelsen,K.J., Ochs,F., Rask,M., Choudhary,C. and Lukas,J. (2017) Redox-sensitive alteration of replisome architecture safeguards genome integrity. *Science*, **358**, 797–802.

Downloaded from https://academic.oup.com/nar/article/48/8/e45/5760754 by guest on 04 November 2021

3. Garzón,J., Rodríguez,R., Kong,Z., Chabes,A., Rodríguez-Acebes,S., Méndez,J., Moreno,S. and Garciá-Higuera,I. (2017) Shortage of dNTPs underlies altered replication dynamics and DNA breakage in the absence of the APC/C cofactor Cdh1. *Oncogene*, **36**, 5808–5818.
4. Santinon,G., Brian,I., Pocaterra,A., Romani,P., Franzolin,E., Rampazzo,C., Bicciato,S. and Dupont,S. (2018) dNTP metabolism links mechanical cues and YAP/TAZ to cell growth and oncogene-induced senescence. *EMBO J.*, **37**, e97780.
5. Mathews,C.K. (2014) Deoxyribonucleotides as genetic and metabolic regulators. *FASEB J.*, **28**, 3832–3840.
6. Pai,C. and Kearsey,S. (2017) A critical balance: dNTPs and the maintenance of genome stability. *Genes (Basel).*, **8**, 57.
7. Wang,Q., Liu,X., Zhou,J., Huang,Y., Zhang,S., Shen,J., Loera,S., Yuan,X., Chen,W., Jin,M. *et al.* (2013) Ribonucleotide reductase large subunit M1 predicts poor survival due to modulation of proliferative and invasive ability of gastric cancer. *PLoS One*, **8**, e70191.
8. Chen,S., Bonifati,S., Qin,Z., St Gelais,C. and Wu,L. (2019) SAMHD1 suppression of antiviral immune responses. *Trends Microbiol.*, **27**, 254–267.
9. Rotskaya,U.N., Rogozin,I.B., Vasyunina,E.A., Malyarchuk,B.A., Nevinsky,G.A. and Sinitsyna,O.I. (2010) High frequency of somatic mutations in rat liver mitochondrial DNA. *Mutat. Res.*, **685**, 97–102.
10. Maine,I.P., Chen,S.F. and Windle,B. (1999) Effect of dGTP concentration on human and CHO telomerase. *Biochemistry*, **38**, 15325–15332.
11. Gupta,A., Sharma,S., Reichenbach,P., Marjavaara,L., Nilsson,A.K., Lingner,J., Chabes,A., Rothstein,R. and Chang,M. (2013) Telomere length homeostasis responds to changes in intracellular dNTP pools. *Genetics*, **193**, 1095–1105.
12. Ke,P.Y., Kuo,Y.Y., Hu,C.M. and Chang,Z.F. (2005) Control of dTTP pool size by anaphase promoting complex/cyclosome is essential for the maintenance of genetic stability. *Genes Dev.*, **19**, 1920–1933.
13. Hu,C.M. and Chang,Z.F. (2007) Mitotic control of dTTP pool: A necessity or coincidence? *Journal of Biomedical Science*, **14**, 491–497.
14. Thientosapol,E.S., Bosnjak,D., Durack,T., Stevanovski,I., van Geldermalsen,M., Holst,J., Jahan,Z., Shepard,C., Weninger,W., Kim,B. *et al.* (2018) SAMHD1 enhances immunoglobulin hypermutation by promoting transversion mutation. *Proc. Natl. Acad. Sci. U.S.A.*, **115**, 4921–4926.
15. Shewach,D.S. (1992) Quantitation of deoxyribonucleoside 5′-triphosphates by a sequential boronate and anion-exchange high-pressure liquid chromatographic procedure. *Anal. Biochem.*, **206**, 178–182.
16. Jia,S., Marjavaara,L., Buckland,R., Sharma,S. and Chabes,A. (2015) Determination of deoxyribonucleoside triphosphate concentrations in yeast cells by strong anion-exchange high-performance liquid chromatography coupled with ultraviolet detection. *Methods Mol. Biol.*, **1300**, 113–121.
17. Chen,P., Liu,Z., Liu,S., Xie,Z., Aimiuwu,J., Pang,J., Klisovic,R., Blum,W., Grever,M.R., Marcucci,G. *et al.* (2009) A LC-MS/MS method for the analysis of intracellular nucleoside triphosphate levels. *Pharm. Res.*, **26**, 1504–1515.
18. Mičová,K., Friedeckyý,D. and Adam,T. (2017) Mass spectrometry for the sensitive analysis of intracellular nucleotides and analogues. In: Aliofkhazraei,M (ed). *Mass Spectrometry.* InTech, doi:10.5772/68073.
19. Galashevskaya,A., Sarno,A., Vågbø,C.B., Aas,P.A., Hagen,L., Slupphaug,G. and Krokan,H.E. (2013) A robust, sensitive assay for genomic uracil determination by LC/MS/MS reveals lower levels than previously reported. *DNA Repair (Amst).*, **12**, 699–706.
20. Kong,Z., Jia,S., Chabes,A.L., Appelblad,P., Lundmark,R., Moritz,T. and Chabes,A. (2018) Simultaneous determination of ribonucleoside and deoxyribonucleoside triphosphates in biological samples by hydrophilic interaction liquid chromatography coupled with tandem mass spectrometry. *Nucleic Acids Res.*, **46**, e66.
21. Sherman,P.A. and Fyfe,J.A. (1989) Enzymatic assay for deoxyribonucleoside triphosphates using synthetic oligonucleotides as template primers. *Anal. Biochem.*, **180**, 222–226.
22. Ferraro,P., Franzolin,E., Pontarin,G., Reichard,P. and Bianchi,V. (2010) Quantitation of cellular deoxynucleoside triphosphates. *Nucleic Acids Res.*, **38**, e85.
23. Diamond,T.L., Roshal,M., Jamburuthugoda,V.K., Reynolds,H.M., Merriam,A.R., Lee,K.Y., Balakrishnan,M., Bambara,R.A., Planelles,V., Dewhurst,S. *et al.* (2004) Macrophage tropism of HIV-1 depends on efficient cellular dNTP utilization by reverse transcriptase. *J. Biol. Chem.*, **279**, 51545–51553.
24. Wilson,P.M., LaBonte,M.J., Russell,J., Louie,S., Ghobrial,A.A. and Ladner,R.D. (2011) A novel fluorescence-based assay for the rapid detection and quantification of cellular deoxyribonucleoside triphosphates. *Nucleic Acids Res.*, **39**, e112.
25. Dong,J., Wu,T., Xiao,Y., Xu,L., Fang,S. and Zhao,M. (2016) A fuel-limited isothermal DNA machine for the sensitive detection of cellular deoxyribonucleoside triphosphates. *Chem. Commun.*, **52**, 11923–11926.
26. Hirmondo,R., Lopata,A., Suranyi,E.V., Vertessy,B.G. and Toth,J. (2017) Differential control of dNTP biosynthesis and genome integrity maintenance by the dUTPase superfamily enzymes. *Sci. Rep.*, **7**, 6043.
27. Wilson,P.M., LaBonte,M.J., Lenz,H.-J., Mack,P.C. and Ladner,R.D. (2012) Inhibition of dUTPase induces synthetic lethality with thymidylate synthase-targeted therapies in non-small cell lung cancer. *Mol. Cancer Ther.*, **11**, 616–628.
28. Goldstone,D.C., Ennis-Adeniran,V., Hedden,J.J., Groom,H.C.T., Rice,G.I., Christodoulou,E., Walker,P.A., Kelly,G., Haire,L.F., Yap,M.W. *et al.* (2011) HIV-1 restriction factor SAMHD1 is a deoxynucleoside triphosphate triphosphohydrolase. *Nature*, **480**, 379–382.
29. Rehwinkel,J., Maelfait,J., Bridgeman,A., Rigby,R., Hayward,B., Liberatore,R.A., Bieniasz,P.D., Towers,G.J., Moita,L.F., Crow,Y.J. *et al.* (2013) SAMHD1-dependent retroviral control and escape in mice. *EMBO J.*, **32**, 2454–2462.
30. Matsuura,M.F., Shaw,R.W., Moses,J.D., Kim,H.-J., Kim,M.-J., Kim,M.-S., Hoshika,S., Karalkar,N. and Benner,S.A. (2016) Assays to detect the formation of triphosphates of unnatural nucleotides: Application to escherichia coli nucleoside diphosphate kinase. *ACS Synth. Biol.*, **5**, 234–240.
31. Parish,T., Brown,A.C., Rustad,T.R., Roberts,D.M., Liao,R.P. and Sherman,D.R. (2009) In: *Mycobacteria Protocols.* Parish T, and Brown,AC (eds). Humana Press, Totowa, NJ.
32. Summer,H., Grämer,R. and Dröge,P. (2009) Denaturing urea polyacrylamide gel electrophoresis (Urea PAGE). *J. Vis. Exp.*, **32**, 1485.
33. Li,B., Morris,J. and Martin,E.B. (2002) Model selection for partial least squares regression. *Chemom. Intell. Lab. Syst.*, **64**, 79–89.
34. HURVICH,C.M. and TSAI,C.-L. (1989) Regression and time series model selection in small samples. *Biometrika*, **76**, 297–307.
35. Tóth,J., Varga,B., Kovács,M., Málnási-Csizmadia,A., Vértessy,B.G., Toth,J., Varga,B., Kovacs,M., Malnasi-Csizmadia,A. and Vertessy,B.G. (2007) Kinetic mechanism of human dUTPase, an essential nucleotide pyrophosphatase enzyme. *J. Biol. Chem.*, **282**, 33572–33582.
36. Hirmondó,R., Szabó,J.E.J.E., Nyíri,K., Tarjányi,S., Dobrotka,P., Tóth,J. and Vértessy,B.G.B.G. (2015) Cross-species inhibition of dUTPase via the Staphylococcal Stl protein perturbs dNTP pool and colony formation in Mycobacterium. *DNA Repair (Amst).*, **30**, 21–27.
37. Machon,C., Jordheim,L.P., Puy,J.Y., Lefebvre,I., Dumontet,C. and Guitton,J. (2014) Fully validated assay for the quantification of endogenous nucleoside mono- and triphosphates using online extraction coupled with liquid chromatography-tandem mass spectrometry. *Anal. Bioanal. Chem.*, **406**, 2925–2941.
38. Longley,M.J., Bennett,S.E. and Mosbaugh,D.W. (1990) Characterization of the 5′ to 3′ exonuclease associated with thermus-aquaticus DNA polymerase. *Nucleic Acids Res*, **18**, 7317–7322.
39. Vogt,A.D. and Di Cera,E. (2012) Conformational selection or induced fit? A critical appraisal of the kinetic mechanism. *Biochemistry*, **51**, 5894–5902.
40. Keller,D.J. and Brozik,J.A. (2005) Framework Model for DNA Polymerases. *Biochemistry*, **44**, 6877–6888.
41. Xu,C., Maxwell,B.A. and Suo,Z. (2014) Conformational dynamics of thermus aquaticus DNA Polymerase I during catalysis. *J. Mol. Biol.*, **426**, 2901–2917.
42. Mol,C.D., Harris,J.M., McIntosh,E.M. and Tainer,J.A. (1996) Human dUTP pyrophosphatase: uracil recognition by a β hairpin and active sites formed by three separate subunits. *Structure*, **4**, 1077–1092.

Downloaded from https://academic.oup.com/nar/article/48/8/e45/5760754 by guest on 04 November 2021

43. Szabó,J.E.J.E., Takács,E., Merényi,G., Vértessy,B.G.B.G. and Tóth,J. (2016) Trading in cooperativity for specificity to maintain uracil-free DNA. *Sci. Rep.*, **6**, 24219.
44. Bustin,S.A. (2017) How to speed up the polymerase chain reaction. *Biomol. Detect. Quantif.*, **12**, 10–14.
45. Montgomery,J.L., Rejali,N. and Wittwer,C.T. (2014) The influence of nucleotide sequence and temperature on the activity of thermostable DNA polymerases. *J. Mol. Diagn.*, **16**, 305–313.
46. Laureti,L., Selva,M., Dairou,J. and Matic,I. (2013) Reduction of dNTP levels enhances DNA replication fidelity in vivo. *DNA Repair (Amst).*, **12**, 300–305.
47. Buckland,R.J., Watt,D.L., Chittoor,B., Nilsson,A.K., Kunkel,T.A. and Chabes,A. (2014) Increased and imbalanced dNTP pools symmetrically promote both leading and lagging strand replication infidelity. *PLoS Genet.*, **10**, e1004846.

Downloaded from https://academic.oup.com/nar/article/48/8/e45/5760754 by guest on 04 November 2021

Supplementary material to

A user-friendly, high-throughput tool for the precise fluorescent quantification of deoxyribonucleoside triphosphates from biological samples

Judit Eszter Szabó[1,2]*, Éva Viola Surányi[1,2], Bence Sándor Mébold[1], Tamás Trombitás[1,2], Mihály Cserepes[1], Judit Tóth[1]*

[1] Institute of Enzymology, Research Centre for Natural Sciences, Budapest 1117, Hungary
[2] Department of Applied Biotechnology and Food Sciences, Budapest University of Technology and Economics, Budapest 1111, Hungary
* To whom correspondence should be addressed. Tel: +36 1 382 6793; Email: toth.judit@ttk.mta.hu Correspondence may also be addressed to szabo.judit.eszter@ttk.mta.hu.

The authors wish it to be known that, in their opinion, the first two authors should be regarded as joint First Authors.

Supplementary Figures

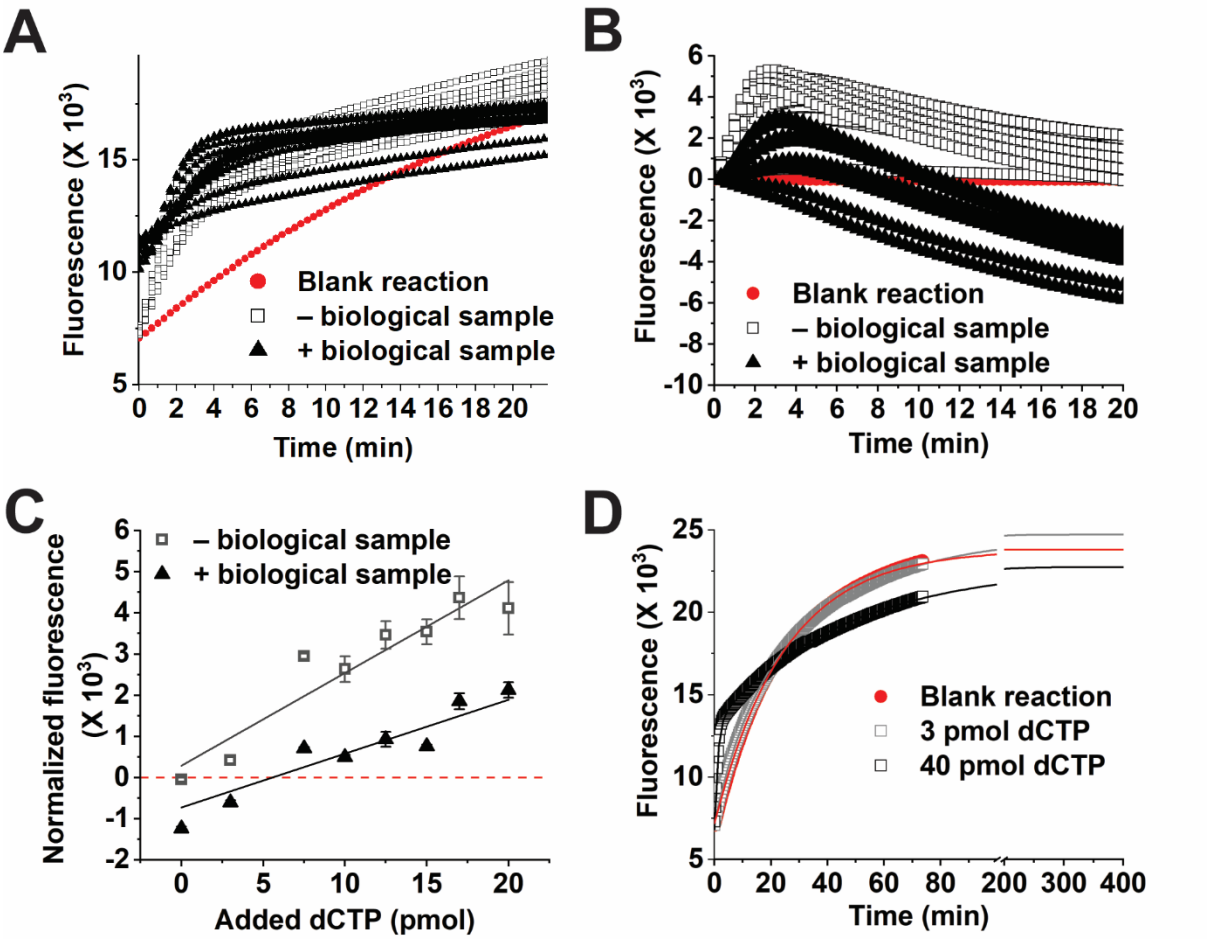

Figure S1 Measurement of cellular dCTP concentration in *Mycobacterium smegmatis* sample using the dCTP-dT2 template and TEMPase Hot Start DNA Polymerase at 55 °C Panel **A)** Raw reaction curves in the absence (hollow squares) and in the presence (black triangles) of *Mycobacterium smegmatis (M. smegmatis)* extract ($1.5*10^8$ cells / reaction). 0-40 pmol dCTP was added to the assays. Note, that the blank reaction (0 pmol dCTP) also produces signal which was corrected for by Wilson *et al.* via subtracting the blank curves from assay curves containing added dCTP or biological sample (shown in Panel B). **B)** Reaction curves corrected for according to Wilson *et al.* **C)** Calibration curve (0-40 pmol dCTP) in the absence of biological sample (hollow squares), and standard addition points in the presence of biological sample (black triangles) derived from reading the fluorescence in Panel C at 4 min. Continuous line is the linear fit to the calibration points yielding the following parameters: slope = 225 ± 32, intercept = 288 ± 396, $R^2 = 0.87$. Data and errors represent the average and standard deviation of technical parallels (n=2). **D)** Fitting the raw calibration curves (scatter plots) with exponential functions (continuous line). In case of the blank reaction (0 pmol dCTP), a single exponential equation (Eq. 1) could be fitted to the reaction curve, while in the presence of the specific dNTP (here, dCTP) the reaction could be well described with a double exponential equation (Eq. 2). The parameters yielded from the exponential fits are as follows: 0 pmol dCTP: A = -16609, $k_{obs} = 6.7 *10^{-4}$ s^{-1}, $y_0 = 23806$; 3 pmol

dCTP: A_1 = - 5446, k_{1obs} = 1.5 * 10^{-3} s^{-1}, A_2 = -12021, k_{2obs} = 4.3 * 10^{-4} s^{-1}, y_0 = 24718; 40 pmol dCTP: A_1 = -6408, k_{1obs} = 1.5 * 10^{-2} s^{-1}, A_2 = -9513, k_{2obs} = 3.7 *10^{-4} s^{-1}, y_0 = 22748.

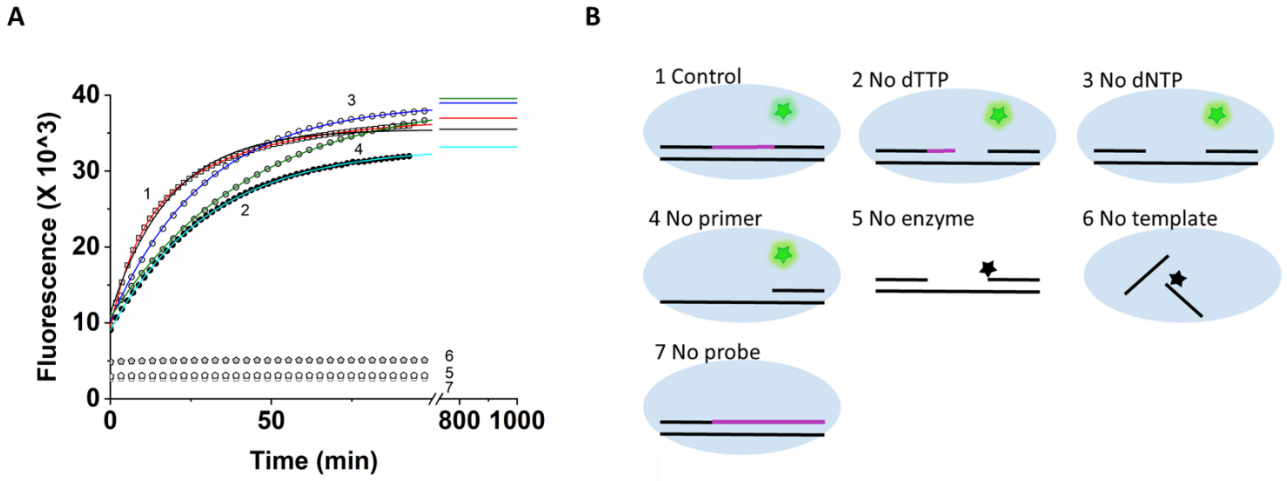

Figure S2 Assay background originates from dNTP incorporation independent 5'-3' exonuclease activity of TAQ polymerase A) To investigate the background of the assay using the TEMPase Hot Start DNA Polymerase, we chose the dTTP assay using the dT2 template. The data presented in Panel A represent the reaction curves obtained under the conditions schematically shown in Panel B. Continuous lines represent the exponential fits to the data. Parameters are as follows: 10 pmol dTTP (1), red : A_1 = -12508, k_{1obs} = 2.05*10^{-3} s^{-1}, A_2 = -15014, k_{2obs} = 4.85*10^{-4} s^{-1} y0 = 36952; 0 pmol dTTP (2), cyan: A_1 = -24118, k_{obs} = 5.45*10^{-4} s^{-1}, y0 = 33165; No aspecific dNTP added (3), blue: A_1 = -28676, k_{obs} = 5.71*10^{-4} s^{-1}, y0 = 38969; No primer added (4), green: A = -28902, k_{obs} = 3.88*10^{-4} s^{-1}, y0 = 39555. A single exponential function fitted to the "10 pmol dTTP" (1) data is shown as continuous black line. Note that the k_{obs} of the aspecific phase is about two times larger than that using AmpliTaq Gold polymerase. However, the observed rate constants relate to each other similarly as in the case of AmpliTaq Gold polymerase under the used conditions. **B)** Panel B schematically explains the constitution of the different assays. The incorporated dNTP-s are colored magenta.

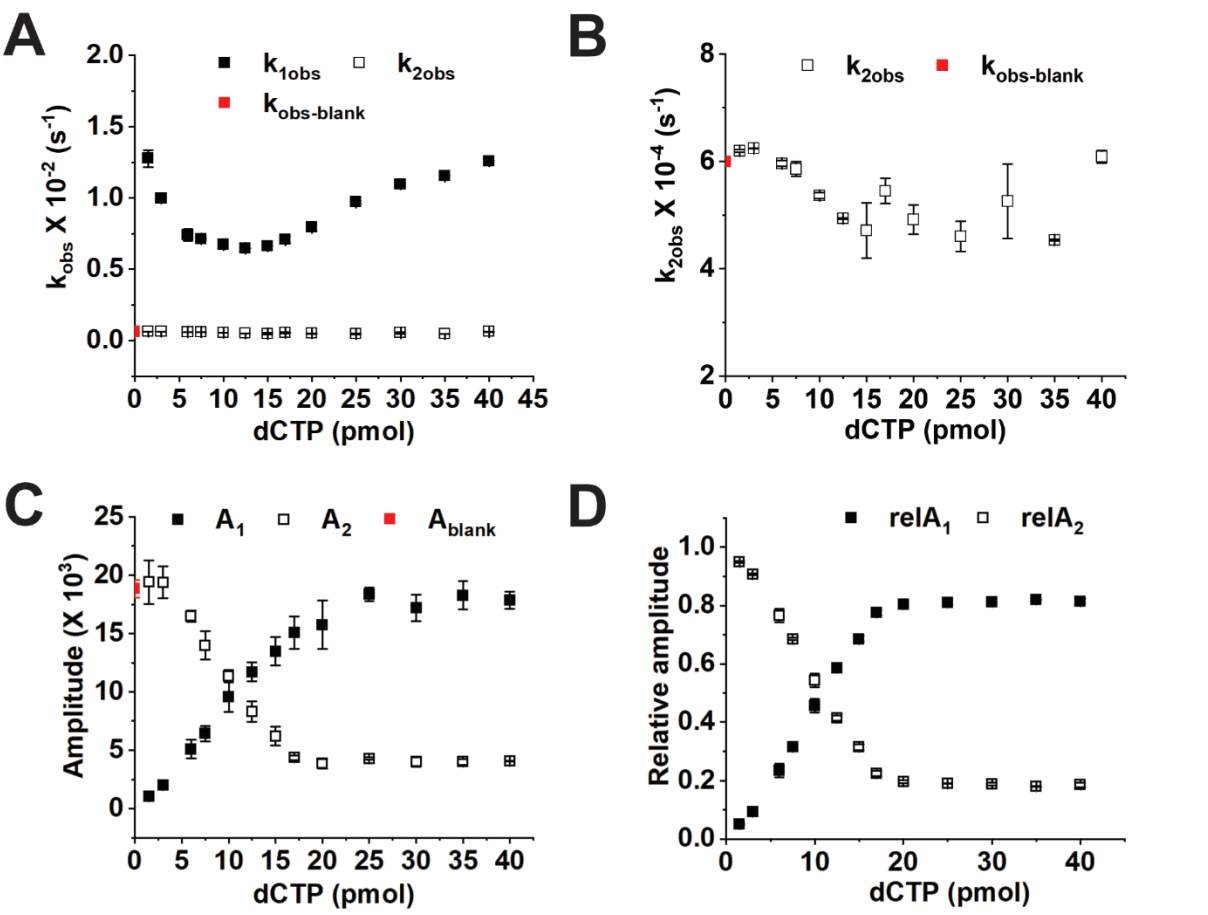

Figure S3 Background exonuclease activity of TEMPase Hot Start DNA Polymerase competes with specific dNTP incorporation in a dNTP concentration dependent manner using the dCTP-dT2 template at 55 °C A) Concentration dependence of the observed rate constants of the two kinetic phases in the assay (k_{1obs} and k_{2obs}, respectively). **B)** Concentration dependence of the observed rate constant of the slower phase (k_{2obs}). **C)** Concentration dependence of the amplitudes of the two phases (A1 and A2, respectively). Note, that the amplitude follows a hyperbola of which the initial linear phase can be used for calibration. **D)** Concentration dependence of the relative amplitudes of the two phases ($relA_1$ and $relA_2$, respectively). The amplitudes were normalized compared to the total amplitude of the reaction (A1+A2). Data and errors represent the average and standard error of the mean of technical parallels (n=2).

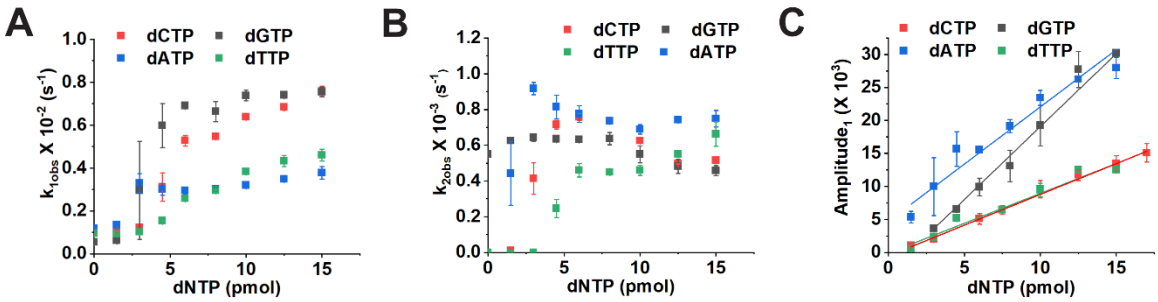

Figure S4 Separation of the reaction phases for precise quantification of dNTP-s using dCTP-dT2, dGTP-dT2, dATP-dT1 and dTTP-dT1 templates and TEMPase Hot Start DNA Polymerase A) Concentration dependence of the observed rate constants of the fast kinetic phases in the assay (k_{1obs}). **B)** Concentration dependence of the observed rate constant of the slower phase (k_{2obs}). **C)** Concentration dependence of the linear phase of the amplitudes of the fast, specific dNTP incorporation associated phase (A_1). Linear fits to the curves yielded the following parameters: dCTP, intercept = -530 ± 141, slope = 932 ± 36, R^2 = 0.99; dGTP, intercept = -3031 ± 127, slope = 2210 ± 32, R^2 = 0.999; dATP, intercept = 4719 ± 959, slope = 1733 ± 100, R^2 = 0.98; dTTP, intercept = -118 ± 734, slope = 906 ± 89, R^2 = 0.95. For dCTP, the same data points are presented in Figure 3. Data and errors represent the average and standard error of the mean of technical parallels (n=2).

Supplementary Table I.

	Template	Assay conditions	qPCR	Data acquisition	T (°C)	Calibration range	R^2	LOD[1] (pmol)	LOQ[2] (pmol)	Accuracy Low, High (%)	Interassay CV (%)	Intrassay CV (%)	Recovery		
													(%)	CFU or cell[3] /reaction	Sample type
dTTP	dT2	10 pmol TPP[4], 0.9 unit VWR® TEMPase 2 mM $MgCl_2$	Quant Studio 1	13 or 15 sec/cycle for 260 cycles	55	2-20 pmol	0.99	1.5	2.5	100 ± 2 99 ± 3	3.7 ± 2.5	3.1 ± 2.6	N.D	N.D	-
dCTP	dT2	10 pmol TPP[4], 0.9 unit VWR® TEMPase 2 mM $MgCl_2$	BioRad CFX96	13 or 17 or 19 sec/cycle for 260 cycles	55	1.5-20 pmol	0.99	0.7	1.2	109 ± 6 99 ± 1	4.3 ± 1.7	3.6 ± 2.0	102 ± 5	1 X 10^8	*Mycobacterium smegmatis*
dGTP	dT2	10 pmol TPP[4], 0.9 unit VWR® TEMPase 3.5 mM $MgCl_2$	BioRad CFX96	13 or 15 s for 260 cycles	55	3-20 pmol	0.999	1.4	2.4	103 ± 3 100 ± 1	6.1 ± 0.3	2.8 ± 1.2	110 ± 9	1 X 10^8	*Mycobacterium smegmatis*

[1]LOD calculated as follows: LOD= calibration line offset + 3*SD $A1_{low\ calibration\ points}$
[2]LOQ calculated as follows: LOQ= calibration line offset + 5*SD $A1_{low\ calibration\ points}$
[3]dNTP extract from the given number CFU (for bacteria) or cells (for eukaryotic cells)
[4]Template-primer-probe (TPP) complex

dNTPpoolDB: a manually curated database of experimentally determined dNTP pools and pool changes in biological samples

Rita Pancsa[1,†], Erzsébet Fichó[1,2,†], Dániel Molnár[1], Éva Viola Surányi[1], Tamás Trombitás[1], Dóra Füzesi[1], Hanna Lóczi[1], Péter Szijjártó[1], Rita Hirmondó[1], Judit E. Szabó[1,*] and Judit Tóth[1,3,*]

[1]Institute of Enzymology, Research Centre for Natural Sciences, Budapest, H-1117, Hungary, [2]Cytocast Kft., Vecsés, Hungary and [3]Department of Applied Biotechnology and Food Sciences, Budapest University of Technology and Economics, Budapest, H-1111, Hungary

Received August 15, 2021; Revised September 13, 2021; Editorial Decision September 21, 2021; Accepted September 28, 2021

ABSTRACT

Stimulated by the growing interest in the role of dNTP pools in physiological and malignant processes, we established dNTPpoolDB, the database that offers access to quantitative data on dNTP pools from a wide range of species, experimental and developmental conditions (https://dntppool.org/). The database includes measured absolute or relative cellular levels of the four canonical building blocks of DNA and of exotic dNTPs, as well. In addition to the measured quantity, dNTPpoolDB contains ample information on sample source, dNTP quantitation methods and experimental conditions including any treatments and genetic manipulations. Functions such as the advanced search offering multiple choices from custom-built controlled vocabularies in 15 categories in parallel, the pairwise comparison of any chosen pools, and control-treatment correlations provide users with the possibility to quickly recognize and graphically analyse changes in the dNTP pools in function of a chosen parameter. Unbalanced dNTP pools, as well as the balanced accumulation or depletion of all four dNTPs result in genomic instability. Accordingly, key roles of dNTP pool homeostasis have been demonstrated in cancer progression, development, ageing and viral infections among others. dNTPpoolDB is designated to promote research in these fields and fills a longstanding gap in genome metabolism research.

INTRODUCTION

DNA is a polymer synthesized from four distinct types of deoxyribonucleotide triphosphate (dNTP) monomers. The genetic code is built upon the sequence of these four types of monomers. Predominantly and most often, DNA is constituted of the so-called canonical dATP, dGTP, dCTP and dTTP nucleotides. In addition to that, non-canonical building blocks mimicking one of the canonical ones can be built in by DNA polymerase enzymes. dNTP incorporation rate and fidelity depends largely on the pool of canonical and non-canonical dNTPs available for a given polymerase (1,2). Mutagenesis has been shown to be greatly stimulated either by unbalanced dNTP pools or, intriguingly, by balanced accumulation of all four dNTPs (3–5). On the other hand, proportional depletion of dNTP pools causes genomic instability, probably through replication stress (6). Therefore, the available concentration of DNA building blocks is maintained in homeostasis for proper DNA replication and repair.

The ever-growing interest in cellular dNTP pools can be accounted to the fact that they influence several core biological processes, including the progression of the cell cycle during development (7) and differentiation (8) as well as DNA damage response (9). dNTP pool alterations lead to genomic instability (10) and have been directly linked to ageing (11) and several human diseases, including mitochondrial disorders (12,13), viral infections and immunity (14–17), and cancer (18). Cancer research is a key field benefitting from the accumulated knowledge on dNTP homeostatic changes. The spontaneous mutation frequencies in tumour tissues are at least 200-fold higher than those in normal tissues from which they were derived (19) and this phenomenon is linked to imbalanced dNTP pools. The importance of balanced dNTP pools is also well supported by

*To whom correspondence should be addressed. Tel: +36 1 382 6793; Fax: +36 1 3826 700; Email: toth.judit@ttk.mta.hu
Correspondence may also be addressed to Judit E. Szabó. Tel: +36 1 382 6707; Fax: +36 1 3826 700; Email: szabo.judit.eszter@ttk.hu
†The authors wish it to be known that, in their opinion, the first two authors should be regarded as joint First Authors.

© The Author(s) 2021. Published by Oxford University Press on behalf of Nucleic Acids Research.
This is an Open Access article distributed under the terms of the Creative Commons Attribution License (http://creativecommons.org/licenses/by/4.0/), which permits unrestricted reuse, distribution, and reproduction in any medium, provided the original work is properly cited.

Downloaded from https://academic.oup.com/nar/advance-article/doi/10.1093/nar/gkab910/6395338 by guest on 04 November 2021

the fact that some of the key metabolic enzymes controlling them are important targets of cancer therapeutics (17,20–23).

dNTP metabolism has been researched for over 50 years. Even though an astonishing amount of measured dNTP pool data have been accumulated in the literature, they have not been systematically identified and extracted from it until now. The great diversity in the applied methodology, data quality and presentation make it complicated to grab, order and structure these data. Here, we introduce a novel database called dNTPpoolDB. Stimulated by the growing interest in the role of dNTP pool changes in physiological and malignant processes, we constructed this resource on hitherto measured cellular dNTP quantities and pools from a wide range of species, experimental and developmental conditions. The database contains quantitative data on the four canonical building blocks of DNA as well as on exotic dNTPs. dNTPoolDB is manually curated, each entry is extracted from the literature by a competent annotator. When constructing the information components of the database entries, emphasis was given to be able to offer more than just a catalogue. Functions such as the user-friendly advanced search, the pairwise comparison of any chosen pools and control-treatment correlations provide users with the possibility to quickly recognize changes in the dNTP pools in function of a given parameter they are interested in. A keen interest to detect changes in dNTP levels upon stress, treatments or in altered genetic backgrounds is obvious from the number of papers dealing with this. This interest is also indicated by the recent development of several new or modified experimental methods to tackle the challenging determination of the absolute or relative levels of dNTPs in biological samples (24–27).

dNTPpoolDB provides a wealth of ordered and unambiguous information on dNTP measurements in biological samples through a user-friendly web interface that meets the standards of modern biological databases, extended with state-of-the-art features such as cross-link references and mobile responsivity. To the best of our knowledge, no resource exists with similar content and therefore, dNTPpoolDB fills a long-standing gap in the nucleotide and genome metabolism research fields. dNTPoolDB is designated to promote research in the fields of DNA replication and repair, cancer research, development and ageing, viral and bacterial infections and in the yet undiscovered aspects of dNTP pool homeostasis, comprising the potential signalling function of dNTPs.

DATA COLLECTION AND DATABASE CONTENT

To find relevant data, a large number of publications with the keywords matching several expressions for dNTPs in the title and abstract was initially retrieved from the PubMed database (28). Then we manually filtered this article pool to obtain the pertinent original publications containing experimentally determined dNTP values. We reviewed the full text of the publications to localize measured dNTP data in tables, figures, and in-text descriptions. Our objective was to retrieve as much information as possible related to the measured dNTP values in a structured way. Whenever possible, we used ontologies and custom-built controlled vocabularies. All information taken from the literature through manual curation is linked to corresponding manuscripts via PubMed (28). Each entry represents a single measured dNTP value.

During data collection, it was a challenge to extract the measured values and their errors from figure diagrams. As shown in Figure 1A, about 70% of the data was graphically presented in the literature. To retrieve graphically presented data, we used WebPlotDigitizer 4.4, a free online tool developed by Ankit Rohatgi (https://automeris.io/WebPlotDigitizer). By converting several thousands of graphical dNTP quantitation points into numerical format, we made these valuable data accessible for subsequent bioinformatic analysis. Graphical to numerical representation conversion is indicated in the entry pages.

Another challenge was the management of dimensions due to the large variety of sample sources, measurement methods and data quality. To increase data comparability within the database, we reduced the number of dimensions used without transforming the data in a subjective way. We only allowed order of magnitude conversion, the conversion of fractional representation to percentage, and the conversion of expressions of relative changes into fold change. We created an 'other dimension' category for rarely occurring dimensions. dNTP quantification data are often presented in the literature as relative values compared to a non-treated control or to other nucleotides (ATP, dNTP or NTP content typically). In these cases, we indicated the basis for the comparison. We found it particularly important to identify control-treatment pairs in case of the relative data to increase the information content of the database.

Error values were also extracted from the papers, where available. Error values and error types are also given in the database to provide information on the reliability of the presented values.

We intended to unambiguously describe the source of the measured biological sample at different levels from organism to subcellular compartment. The Taxonomy Browser ID of NCBI is cross-referenced for each organism. Where possible, we included as a cross-reference the Cell Line Ontology (CLO) number with links to the corresponding EMBL-EBI Ontology Search (OLS) entry.

As method developers ourselves, we found it important to identify and indicate the conditions for sample extraction and the measurement methods. dNTP measurement methods all have their biases and limitations and therefore, the included methodological information may come useful when considering the robustness of the data, or when comparing data.

dNTPpoolDB also describes relevant experimental conditions. Most studies inquire about dNTP pool changes emerging as a result of some treatment or naturally occurring genetic or environmental alterations. Therefore, we indicate the fact of treatment and its nature. If it is a drug treatment, we identify the drug using cross-reference to its PubChem ID (29). If the treatment is genetic manipulation, we identify the affected genes and proteins using cross-references to NCBI's Gene IDs and to the UniProt IDs, respectively, together with information on their mutations. When more than one gene is affected, or more than one type of genetic manipulation was done in a sample, these are shown in subsequent sections (e.g. consult

Downloaded from https://academic.oup.com/nar/advance-article/doi/10.1093/nar/gkab910/6395338 by guest on 04 November 2021

Figure 1. Statistics and customizable statistical analysis of the collected data. (**A**) Distribution of the graphical and numerical representations of the data in the source literature. By scrolling over a pie, the number represented by the pie shows up. (**B**) Using the customizable pie charts: deselecting can be done by clicking on the legend. (**C**) Distribution of the number of dNTPs in the pool. (**D**) Source organisms represented in the database. (**E**) Time distribution of the number of papers annotated so far.

entry DNTP000512). Other details of the applied treatments are provided as free text. Within the free text, we intended to yield information about the pathways or processes affected by the drug treatment or genetic manipulation (e.g. thymidylate synthesis, dNTP biosynthesis, oxidative stress). These free text additions are searchable.

dNTP pools are reconstructed from single entries. Those entries that differ only in the type of measured dNTP belong to the same pool. Each dNTP pool has a pool ID. Pools are further related to each other by the definition of control-treatment pairs, where applicable. In addition to the possibility to compare and graphically represent control-

Downloaded from https://academic.oup.com/nar/advance-article/doi/10.1093/nar/gkab910/6395338 by guest on 04 November 2021

treatment pairs, any two pools can be compared, as well (Figure 2).

USER INTERFACE

Overview of functions

dNTPpoolDB provides a simple and intuitive interface to browse, search, visualize, compare, and download detailed information about dNTP measurements (Figure 2). Care was taken to use the same colour code for consistency throughout the pages. The tool bar on the Home page offers access to each of the functions of the database. The Browser page is organized as an interactive and sortable table that allows users to quickly browse through the entire or a subset of the entries. Column headers contain options that help to quickly make a complex selection of entries. Clicking on any row inside the Browser table directs the user to the relevant entry page.

The Advanced search page can be reached from the Browser page or from the constantly available tool bar. It allows free text search using multiple keywords as well as search by structured, predefined parameters. These parameters are organised into tabs that contain a drop-down menu (Figure 2). The user can make multiple choices in each of the drop-down menus thus making a complex selection possible (Figure 2). The result of the selection can be downloaded from here.

The pairwise comparison function is useful for quickly assessing differences between two entries and to detect dNTP pool changes in function of a desired parameter. This function can be reached (i) through the Browser page, (ii) through the Advanced search page, (iii) from the Entry page and (iv) directly in the dedicated Pairwise comparison page. In the Browser and Advanced search pages, one can select two entries to be compared using the selection box on the left (Figure 2). Then by hitting the Compare button on the upper right, the Pairwise comparison page shows up with the result. Although individual entries are selected, the entire pools are compared if applicable (Figure 2). If the dimensions of the measured dNTP values match, the comparison is done in a single bar chart (Figure 2). We alert users whenever datasets are not directly comparable. Below the graphical comparison, the user finds all information available in the Entry pages in a transparent comparison layout. A useful workflow is shown in Figure 2, whereby the user performs a narrow selection of entries using the predefined parameters of the Advanced search function, then chooses two entries from the results list and compare them. Alternatively, the user has the option to introduce two entry or pool identifiers into the relevant query boxes in the Pairwise comparison page and hit the compare button. The discussion of using the compare function from the Entry pages brings us to control-treatment pairing. Whenever we could identify control and treatment measurements in the source publication, we aimed to pair these data. We believe that providing these relationships between different entries will largely facilitate all future analyses of the collected data. When control-treatment pairs are available, the compare button is offered directly below the related pool in the Entry pages to make the graphical comparison of the cohesive pools effortlessly feasible.

The Statistics page provides useful summaries of dNTPpoolDB data from different aspects to provide a quick overview and to facilitate the planning of future data analyses by users, relying on the entirety or any subset of the available data. The pie charts of the Statistics page are customizable. The user may choose the option to visualize a subset of the categories in the pie charts (Figure 1B). Selecting and deselecting a category can be done by clicking on the legend. For example, if the user is interested in visualizing the distribution of the number of dNTP measurements between the cytosol and the nucleus, it can be done by deselecting the other two categories, i.e., the whole cell and the mitochondrion (Figure 1B). That way, the information practically lost in the entire set of these four statistical categories due to the dominance of the large number of entries originating from whole cells can be retrieved. Also, by scrolling over a pie in the pie chart, the user can visualize the number represented by that specific pie (Figure 1A). dNTPpoolDB allows users to download all the obtained data in the Download page in three different formats: TSV (tab-separated version), standard XML and JSON format. In addition, single data points can be downloaded directly from the Entry pages and a selected subset of data from the Advanced search page. A comprehensive online documentation about the use and functionalities of dNTPpoolDB is available in the About page. To encourage users to help in complementing the database, dNTPpoolDB offers a Contact page that enables researchers to submit publication IDs and other information pertinent to the dNTP data content of the proposed source literature.

Entry pages

Each entry in dNTPpoolDB corresponds to a single dNTP measurement with a dedicated entry page containing all relevant information collected manually from the literature. The header of the entry page displays the ID of the entry and the type of dNTP measured. Within the same header, one can also jump to the previous or the following entries by clicking on the displayed IDs. The top right green bar provides the option of downloading the annotation of the given entry in JSON, TSV and XML formats. On the left, the chemical structure of the measured dNTP(s) can be seen (retrieved from PubChem (29)).

The Results section of the entry page contains the actual measured value, its error and dimension. If the value is a relative one, the basis of comparison is indicated in the 'Relative compared to' row. Whether the data point was presented numerically or graphically is also indicated here. This section contains two cross-references to PubMed and PMCID to reach the source article in a new browser page.

The Source section serves to identify the origin of the biological sample in which the measurement was done. Here, we provide a link to the taxonomic identification of the organism and specify further at subsequent organisational levels the origin of the biological sample. In each case, we use the name of the bacterial, fungal and animal strains, that of the cell lines or primary cells, tissues as given in the source article. In addition, if it is possible, we provide the CLO link for cell lines, e.g. Tango cell (CLO:0037271), for HEK 293T.

Downloaded from https://academic.oup.com/nar/advance-article/doi/10.1093/nar/gkab910/6395338 by guest on 04 November 2021

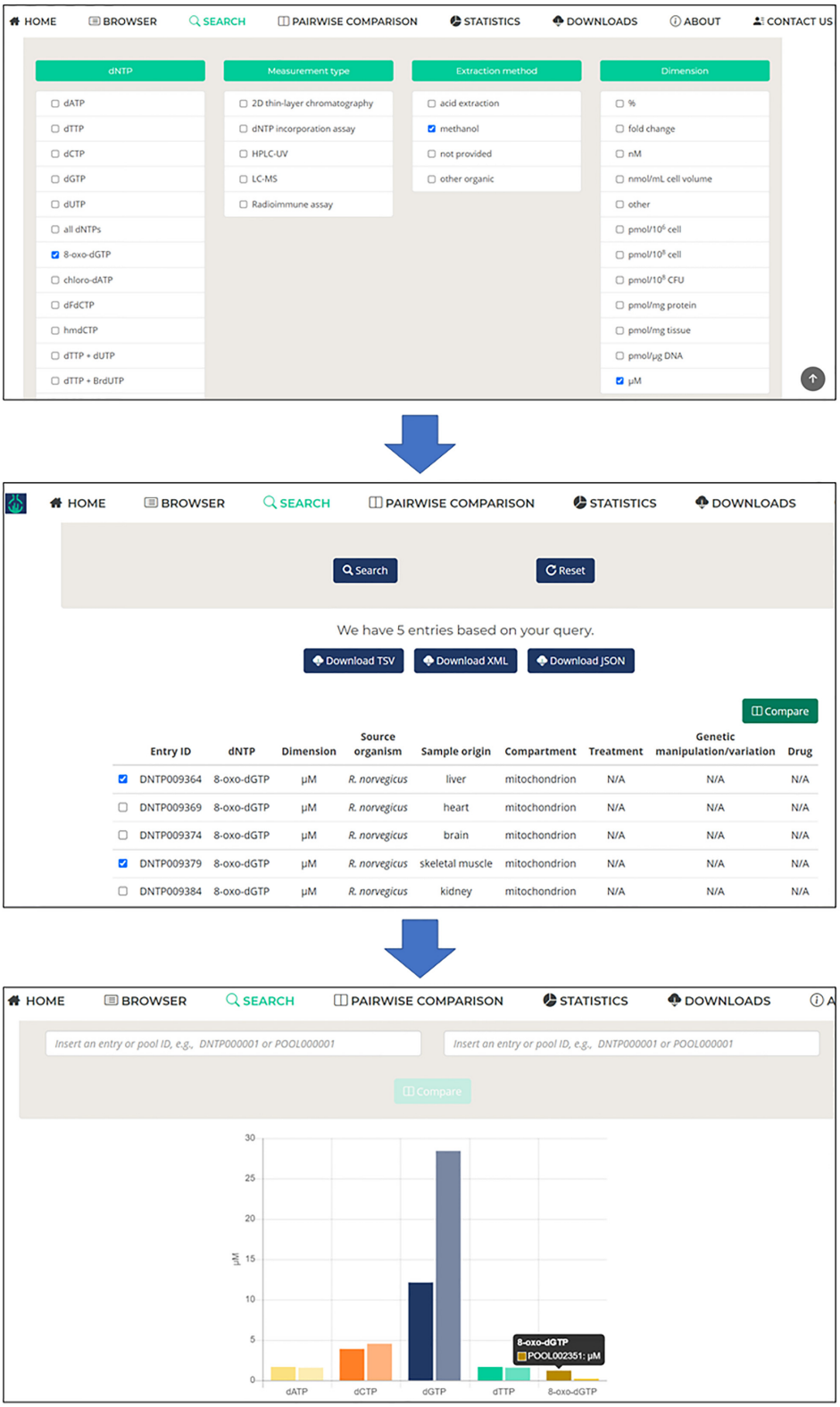

Figure 2. Featured functions of the user interface of dNTPpoolDB. The Advanced search function offers multiple choices of a predefined set of parameters to narrow down data selection in response to a precise query. Upon selecting any two of the search results from the list, one can compare the dNTP pools that belong to the two selected entries by hitting the Compare button. Then, the compared data will graphically appear in a new window. If dimensions match, data will be presented in a single chart. If dimensions are different, two charts will be shown with an alert not to compare these data directly. Below the chart, all the information contained by the two compared entry pages will be displayed side-by-side.

Downloaded from https://academic.oup.com/nar/advance-article/doi/10.1093/nar/gkab910/6395338 by guest on 04 November 2021

The Experimental details section indicates the major type of dNTP quantitation. We defined five main methods comprising the enzymatic dNTP incorporation assay, HPLC–UV, LC–MS, radioimmune assay, and thin layer chromatography. Here, we also indicate the method of dNTP extraction from the biological sample. Any alterations from the predefined methods are indicated in the Remarks to measurement type row. The most often used subtypes of dNTP measuring methods are also referred to in this section (e.g. the method of Sherman and Fyfe is commonly used for dNTP incorporation-based measurements (30).

In the Treatment section, we classified treatments into drug and/or stress treatments and genetic manipulation. Some stress treatments are described in free words as standardization was not always an option. However, in case a chemical was applied on the source organism, we unambiguously specified it using its PubChem link in addition to indicating the drug name as used in the publication. In case the measurement was done following a genetic modification, we indicated the details of this in the Genes and Proteins section. Here, the type of genetic modification/variation (e.g. silencing, overexpression, mutation) and all reported affected genes and proteins are identified using Gene and UniProt IDs, respectively, in addition to indicating the gene and protein names given in the article. If mutated forms of the proteins were applied in the measurement, those are also described. The Treatment details/effects comment potentially also contains information on the effects of the applied mutations or drugs. This and other comments section may be useful when users search the database using the free word finder.

Entries are grouped into identifiable pools whenever the levels of at least two different dNTPs have been measured in the same study under the same conditions. Where available, pool information is also included into the entry pages in the dNTP Pool section on the left-hand side. Here, all linked measurements can be reached via a link to the relevant entry page. The reconstituted pool is graphically represented in a colour coded bar chart. Scrolling over the bars will show the represented value with its dimension. If the presented data is part of a control-treatment pair within the database, then the corresponding control or treatment pool will also be shown in the panel right below the linked pool members. In this case, the compare button will also show up. By hitting the Compare button, control-treatment pairs will be automatically compared.

DATABASE STATISTICS

The current version of dNTPpoolDB contains 11895 individual entries incorporated into 2968 pools, annotated from 283 publications. 78% of the pools contain the four canonical dNTPs (Figure 1C). The number of dNTPs in a pool may be larger, typically five if dUTP is also measured. Exotic dNTPs are often measured separately. It is not rare that authors are interested in measuring only two dNTPs (Figure 1C).

In some cases, the number of data represented by the pie charts are greater than the total number of entries in the database. This only means that non-exclusive categories are involved and thus one entry may fall into more than one category.

More than half of the data comes from human samples, followed in abundance by mice, yeast and *E. coli* samples (Figure 1D). We counted the number of publications that contain dNTP measurements each year from 1970 to 2020 and found that the number of dNTP-related studies steadily grow until the 2010's, when a burst is observed (Figure 1E).

SYSTEM DESIGN AND IMPLEMENTATION

dNTPpoolDB can be accessed through a user-friendly, appealing DJANGO (version 3.2.6) based web interface, backed by a highly efficient multi-layer SQL database. dNTPpoolDB is compatible with the various devices and browsing options users usually use (the front-end is implemented in a combination of Bootstrap (version 3.1.0) and JQuery (version 3.5.1)). Besides providing access to the data through the online interface, those can also be downloaded in JSON, XML or TSV formats.

CONCLUSIONS

dNTPpoolDB is a unique resource with its purpose and content. Our effort to establish dNTPpoolDB was prompted by the need of researchers to access a comprehensive dataset on dNTP quantitation accumulating for a long time. We believe that it fills a long-standing gap in the nucleotide and genome metabolism research fields and will hopefully help answering basic questions related to the diverse roles of dNTP homeostasis. Having overcome the technical difficulties imposed by the diversity in quality, methodology and presentation of published dNTP measurements, we created a reliable manually curated resource. dNTPpoolDB is intended to benefit the scientific community by providing (i) a freely accessible, easy-to-use, efficiently organized resource with relevant data on published cellular dNTP levels and pools, (ii) a good basis for objective comparisons between and assessment of widely applied dNTP measurement methodologies, potentially leading to improved standardization, (iii) ample data for identifying and understanding the species-specific features of dNTP pools, their changes upon different treatments and their role in the development of pathological conditions, 4) clues to the potential non-canonical functions of dNTPs, e.g. in cell signalling and epigenetics.

DATA AVAILABILITY

dNTPpoolDB is an open resource database available at https://dntppool.org/.

Our aim is to maintain a regularly updated online resource by continuously incorporating published dNTP data. To successfully accomplish this goal, we kindly encourage the scientific community to draw our attention to not yet annotated data via the Contact form (https://dntppool.org/contact/). Data collection from users and submitters through the server is executed via a secure interface using HTTPS, and fully adheres to the General Data Protection Regulation (GDPR) of the EU.

The article refers to the following online tools and resources:

Downloaded from https://academic.oup.com/nar/advance-article/doi/10.1093/nar/gkab910/6395338 by guest on 04 November 2021

https://automeris.io/WebPlotDigitizer
https://pubmed.ncbi.nlm.nih.gov/
https://europepmc.org/
https://www.ncbi.nlm.nih.gov/taxonomy
https://pubchem.ncbi.nlm.nih.gov/
https://www.ncbi.nlm.nih.gov/gene/
https://www.uniprot.org/
https://www.ebi.ac.uk/ols/index

ACKNOWLEDGEMENTS

The authors thank István Reményi and Gergő Csókás for their help in server setup, and for their insights to create the website of the database.

FUNDING

National Research, Development and Innovation Office, Hungary [FK124527 and K138318 to J.T., FK128133 to R.P., PD128254 to R.H.]. Funding for open access charge: National Research, Development and Innovation Office.
Conflict of interest statement. None declared.

REFERENCES

1. Watt,D.L., Buckland,R.J., Lujan,S.A., Kunkel,T.A. and Chabes,A. (2016) Genome-wide analysis of the specificity and mechanisms of replication infidelity driven by imbalanced dNTP pools. *Nucleic Acids Res.*, **44**, 1669.
2. Martomo,S.A. and Mathews,C.K. (2002) Effects of biological DNA precursor pool asymmetry upon accuracy of DNA replication in vitro. *Mutat. Res.*, **499**, 197–211.
3. Chabes,A., Georgieva,B., Domkin,V., Zhao,X., Rothstein,R. and Thelander,L. (2003) Survival of DNA damage in yeast directly depends on increased dNTP levels allowed by relaxed feedback inhibition of ribonucleotide reductase. *Cell*, **112**, 391–401.
4. Wheeler,L.J., Rajagopal,I. and Mathews,C.K. (2005) Stimulation of mutagenesis by proportional deoxyribonucleoside triphosphate accumulation in *Escherichia coli*. *DNA Repair*, **4**, 1450–1456.
5. Davidson,M.B., Katou,Y., Keszthelyi,A., Sing,T.L., Xia,T., Ou,J., Vaisica,J.A., Thevakumaran,N., Marjavaara,L., Myers,C.L. *et al.* (2012) Endogenous DNA replication stress results in expansion of dNTP pools and a mutator phenotype. *EMBO J.*, **31**, 895–907.
6. Bester,A.C., Roniger,M., Oren,Y.S., Im,M.M., Sarni,D., Chaoat,M., Bensimon,A., Zamir,G., Shewach,D.S. and Kerem,B. (2011) Nucleotide deficiency promotes genomic instability in early stages of cancer development. *Cell*, **145**, 435–446.
7. Liu,B. and Großhans,J. (2019) The role of dNTP metabolites in control of the embryonic cell cycle. *Cell Cycle*, **18**, 2817.
8. Pajalunga,D., Franzolin,E., Stevanoni,M., Zribi,S., Passaro,N., Gurtner,A., Donsante,S., Loffredo,D., Losanno,L., Bianchi,V. *et al.* (2017) A defective dNTP pool hinders DNA replication in cell cycle-reactivated terminally differentiated muscle cells. *Cell Death Differ.*, **24**, 774–784.
9. Maslowska,K.H., Makiela-Dzbenska,K., Fijalkowska,I.J. and Schaaper,R.M. (2015) Suppression of the E. coli SOS response by dNTP pool changes. *Nucleic Acids Res.*, **43**, 4109–4120.
10. Shui,B., Wang,Q., Lee,F., Byrnes,L.J., Chudakov,D.M., Lukyanov,S.A., Sondermann,H. and Kotlikoff,M.I. (2011) Circular permutation of red fluorescent proteins. *PLoS One*, **6**, e20505.
11. Hämäläinen,R.H., Landoni,J.C., Ahlqvist,K.J., Goffart,S., Ryytty,S., Rahman,M.O., Brilhante,V., Icay,K., Hautaniemi,S., Wang,L. *et al.* (2019) Defects in mtDNA replication challenge nuclear genome stability through nucleotide depletion and provide a unifying mechanism for mouse progerias. *Nat. Metab.*, **1**, 958–965.
12. Rampazzo,C., Gallinaro,L., Milanesi,E., Frigimelica,E., Reichard,P. and Bianchi,V. (2000) A deoxyribonucleotidase in mitochondria: Involvement in regulation of dNTP pools and possible link to genetic disease. *Proc. Natl. Acad. Sci. U.S.A.*, **97**, 8239.
13. Nikkanen,J., Forsström,S., Euro,L., Paetau,I., Kohnz,R.A., Wang,L., Chilov,D., Viinamäki,J., Roivainen,A., Marjamäki,P. *et al.* (2016) Mitochondrial DNA replication defects disturb cellular dNTP pools and remodel one-carbon metabolism. *Cell Metab.*, **23**, 635–648.
14. Ryoo,J., Choi,J., Oh,C., Kim,S., Seo,M., Kim,S.-Y., Seo,D., Kim,J., White,T.E., Brandariz-Nuñez,A. *et al.* (2014) The ribonuclease activity of SAMHD1 is required for HIV-1 restriction. *Nat. Med.*, **20**, 936–941.
15. Morris,E.R., Caswell,S.J., Kunzelmann,S., Arnold,L.H., Purkiss,A.G., Kelly,G. and Taylor,I.A. (2020) Crystal structures of SAMHD1 inhibitor complexes reveal the mechanism of water-mediated dNTP hydrolysis. *Nat. Commun.*, **11**, 3165.
16. Powell,R.D., Holland,P.J., Hollis,T. and Perrino,F.W. (2011) Aicardi-Goutieres syndrome gene and HIV-1 restriction factor SAMHD1 is a dGTP-regulated deoxynucleotide triphosphohydrolase. *J. Biol. Chem.*, **286**, 43596–43600.
17. Goldstone,D.C., Ennis-Adeniran,V., Hedden,J.J., Groom,H.C.T., Rice,G.I., Christodoulou,E., Walker,P.A., Kelly,G., Haire,L.F., Yap,M.W. *et al.* (2011) HIV-1 restriction factor SAMHD1 is a deoxynucleoside triphosphate triphosphohydrolase. *Nature*, **480**, 379–382.
18. Mathews,C.K. (2015) Deoxyribonucleotide metabolism, mutagenesis and cancer. *Nat. Rev. Cancer*, **15**, 528–539.
19. Bielas,J.H., Loeb,K.R., Rubin,B.P., True,L.D. and Loeb,L.A. (2006) Human cancers express a mutator phenotype. *Proc. Natl. Acad. Sci. U.S.A.*, **103**, 18238–18242.
20. Greene,B.L., Kang,G., Cui,C., Bennati,M., Nocera,D.G., Drennan,C.L. and Stubbe,J. (2020) Ribonucleotide reductases: structure, chemistry, and metabolism suggest new therapeutic targets. *Annu. Rev. Biochem.*, **89**, 45–75.
21. Aye,Y., Li,M., Long,M.J.C. and Weiss,R.S. (2015) Ribonucleotide reductase and cancer: biological mechanisms and targeted therapies. *Oncogene*, **34**, 2011–2021.
22. Kohnken,R., Kodigepalli,K.M. and Wu,L. (2015) Regulation of deoxynucleotide metabolism in cancer: novel mechanisms and therapeutic implications. *Mol. Cancer*, **14**, 176.
23. Gad,H., Koolmeister,T., Jemth,A.-S., Eshtad,S., Jacques,S.A., Ström,C.E., Svensson,L.M., Schultz,N., Lundbäck,T., Einarsdottir,B.O. *et al.* (2014) MTH1 inhibition eradicates cancer by preventing sanitation of the dNTP pool. *Nature*, **508**, 215–221.
24. Dong,J., Wu,T., Xiao,Y., Xu,L., Fang,S. and Zhao,M. (2016) A fuel-limited isothermal DNA machine for the sensitive detection of cellular deoxyribonucleoside triphosphates. *Chem. Commun.*, **52**, 11923–11926.
25. Kong,Z., Jia,S., Chabes,A.L., Appelblad,P., Lundmark,R., Moritz,T. and Chabes,A. (2018) Simultaneous determination of ribonucleoside and deoxyribonucleoside triphosphates in biological samples by hydrophilic interaction liquid chromatography coupled with tandem mass spectrometry. *Nucleic Acids Res.*, **46**, e66.
26. Szabó,J.E., Surányi,É.V., Mébold,B., Trombitás,T., Cserepes,M. and Tóth,J. (2020) A user-friendly, high-throughput tool for the precise quantitation of deoxyribonucleoside triphosphates from biological samples. *Nucleic Acids Res.*, **48**, e45.
27. Purhonen,J., Banerjee,R., McDonald,A.E., Fellman,V. and Kallijärvi,J. (2020) A sensitive assay for dNTPs based on long synthetic oligonucleotides, EvaGreen dye and inhibitor-resistant high-fidelity DNA polymerase. *Nucleic Acids Res.*, **48**, e87.
28. Sayers,E.W., Agarwala,R., Bolton,E.E., Brister,J.R., Canese,K., Clark,K., Connor,R., Fiorini,N., Funk,K., Hefferon,T. *et al.* (2019) Database resources of the National Center for Biotechnology Information. *Nucleic Acids Res.*, **47**, D23–D28.
29. Kim,S., Chen,J., Cheng,T., Gindulyte,A., He,J., He,S., Li,Q., Shoemaker,B.A., Thiessen,P.A., Yu,B. *et al.* (2021) PubChem in 2021: new data content and improved web interfaces. *Nucleic Acids Res.*, **49**, D1388–D1395.
30. Sherman,P.A. and Fyfe,J.A. (1989) Enzymatic assay for deoxyribonucleoside triphosphates using synthetic oligonucleotides as template primers. *Anal. Biochem.*, **180**, 222–226.

Downloaded from https://academic.oup.com/nar/advance-article/doi/10.1093/nar/gkab910/6395338 by guest on 04 November 2021